CHARLES UNIVERSITY IN PRAGUE
Faculty of Science

PhD study program: Biochemistry

Mgr. Lucie Potůčková

Regulatory roles of PAG and CSK in FcεRI signaling of mast cells
Regulační úlohy proteinů PAG a CSK v FcεRI signalizaci žírných buněk

PhD. Dissertation in Biochemistry

Supervised by RNDr. Petr Dráber, DrSc.
Institute of Molecular Genetics
Academy of Sciences of the Czech Republic

Prague 2017

This thesis was prepared at the Institute of Molecular Genetics, Academy of Sciences of the Czech Republic in Laboratory of Signal Transduction. Experimental data were compiled into eight original papers, seven of them published in peer-reviewed journals and one original manuscript.

I hereby declare, that I have elaborated this thesis independently, and all the resources as well as co-autors are indicated. I further declare, that I did not submit this thesis, or an essential part of it, to obtain other, or the same university degree.

Prague, February 2017

Mgr. Lucie Potůčková

First of all, I would like to thank my supervisor, Petr Dráber, for his support, motivation and exceptional help during the whole thesis period. Many thanks belong to all my colleagues, from Laboratory of Signal Transduction at Institute of Molecular Genetics in Prague, for their support and great work environment, particularly to Tomáš Paulenda, Ivana Hálová, Monika Bambousková, Viktor Bugajev, Lubica Dráberová, Iva Polakovičová, Magda Tůmová, Hana Mrázová, Oleksij Redčenko, Pavol Utěkal, Romana Budovičová, Michal Šimíček and Filip Franko.

Further, I would like to thank to all co-authors and collaborators from Laboratory of Biology of Cytoskeleton at Institute of Molecular Genetics in Prague, particularly to Pavel Dráber, Eduarda Dráberová and Irena Mlchová as well as to all collaborators from Laboratory of Biochemistry and Brain Pathophysiology, Prague Psychiatric Center, National Institute of Mental Health.

I would like to express my sincere gratitude to my parents and my sister for their kind and endless support during my studies and many thanks go also to my friends for their patience and understanding.

Declaration of co-authors:

This thesis contains eight original papers, seven of them published in peer-reviewed journals and one original manuscript. I, as a corresponding author of all these papers, hereby declare, that Lucie Potůčková/Stegurová, a first author or co-author of the publications, substantially contributed to all of them. The studies were performed in our research team and she actively participated at all stages of the work from study design, performing experiments, and writing manuscript. Her contribution in the experimental part of the first publication "**Transmembrane adaptor protein PAG/CBP is involved in both positive and negative regulation of mast cell signaling**" published in Molecular and Cellular Biology, 2014, consisted of performing all experiments on quantification of proinflammatory cytokines released from mast cell and quantification of IgE levels in serum from mice. Experience she obtained during preparing this article she used in the second article "**C-terminal Src kinase regulates FcεRI activation leading to degranulation and cytokines/chemokines production in opposite ways, independently of the transmembrane adaptor protein PAG**", in which she is the first author. In this project she contributed to determination of the role of C-terminal Src kinase (CSK) in FcεRI-mediated mast cells signaling and thus to deeper understanding of the cross-talk of CSK and PAG in such cells. Particularly, she determined the role of CSK in FcεRI-mediated degranulation by enzymatic assay and flow cytometry in cells with decreased or increased expression of CSK in wild-type or in PAG-deficient cells in which CSK was silenced with shRNA-possesing lentiviral vectors; she investigated the role of CSK in proinflammatory cytokines production, calcium signaling, phosphorylation of selected signal-transduction proteins, IgE internalization and function of CSK in adhesion on fibronectin. In the third article "**Negative regulatory roles of ORMDL3 in the FcεRI-triggered expression of proinflammatory mediators and chemotactic response in murine mast cells**", published in Cellular and Molecular Life Sciences, 2016, she was responsible for quantification of proinflammatory cytokines released from mast cells with reduced or enhanced expression of ORMDL3; she prepared lentiviral constructs for overexpression of ORMDL3 in rescue experiments. In the fourth article "**Ethanol inhibits high-affinity immunoglobulin E (FcεRI) signaling in mast cells by suppressing the function of FcεRI-cholesterol signalosome**", published in PLoS One, 2015, she was responsible for examination of the effect of ethanol on FcεRI-mediated mast cells degranulation under *in vivo* conditions as determined by passive cutaneous anaphylaxis in mice. In the fifth article "**Cross-talk between tetraspanin CD9 and**

transmembrane adaptor protein non-T cell activation linker (NTAL) in mast cell activation and chemotaxis", published in Journal of Biological Chemistry, 2010, she contributed by purification of anti-CD9 monoclonal antibody and generation of CD9 knockdown mast cells by lentiviral transduction strategy. Remaining 3 articles are methodological in nature and reflect her efforts in development and use of new ultrasensitive methods, nano-iPCR for quantification of proteins in complex biological fluids. Her contribution in experimental part of the sixth article "**Gold nanoparticle-based immuno-PCR for detection of tau protein in cerebrospinal fluid**", published in Journal of Immunological Methods, 2014, in which she is the first author, consisted of performing all studies of detection of human tau protein in cerebrospinal fluid samples by nano-iPCR and statistical analysis of the data. In the seventh article "**Quantification of α-tubulin isotypes by sandwich ELISA with signal amplification through biotinyl-tyramide or immuno-PCR**", published in Journal of Immunological Methods, 2013, in which she is the first co-author, she was responsible for all data on quantification of α-tubulin by nano-iPCR method including experiments with mast cells activated with thapsigargin. In the eight article "**Rapid and sensitive detection of cytokines using functionalized gold nanoparticle-based immuno-PCR, comparison with immuno-PCR and ELISA**", published in Journal of Immunological Methods, 2011, in which she is the first author, she developed and optimized nano-iPCR and immuno-PCR methods for quantification of mast cell growth factors.

Prague, February 3rd, 2017

_____

RNDr. Petr Dráber, DrSc.

CONTENTS

1 ABSTRACT (EN) 8

2 ABSTRAKT (CZ) 9

3 ABBREVIATIONS 10

4 INTRODUCTION 14

4.1 MAST CELL 14

4.1.1 Origin and development 14

4.1.2 Diversity in phenotype and tissue localization 16

4.1.3 Growth factors 17

4.2 MAST CELL FUNCTIONS 18

4.3 SIGNAL TRANSDUCTION 21

4.3.1 Receptors 21

4.3.2 Adaptor proteins 23

4.3.3 Src family protein tyrosine kinases 25

4.3.4 Regulation of SFKs 29

4.4 FcεRI-MEDIATED SIGNALING PATHWAYS 33

4.4.1 Initiation of FcεRI signaling 33

4.4.2 Signaling pathways leading to degranulation 35

4.4.3 Signaling pathways leading to cytokine production 37

4.4.4 Signaling pathways leading to chemotaxis 38

5 AIMS 40

6 SUMMARY OF METHODS 42

7 RESULTS 47

7.1 LIST OF PUBLICATIONS 47

7.2 TRANSMEMBRANE ADAPTOR PROTEIN PAG/CBP IS INVOLVED IN BOTH POSITIVE AND NEGATIVE REGULATION OF MAST CELL SIGNALING. 49

7.3 C-TERMINAL SRC KINASE REGULATES FcεRI ACTIVATION LEADING TO DEGRANULATION AND CYTOKINES/CHEMOKINES PRODUCTION IN OPPOSITE WAYS, INDEPENDENTLY OF THE TRANSMEMBRANE ADAPTOR PROTEIN PAG. 66

7.4 NEGATIVE REGULATORY ROLES OF ORMDL3 IN THE FcεRI-TRIGGERED EXPRESSION OF PROINFLAMMATORY MEDIATORS AND CHEMOTACTIC RESPONSE IN MURINE MAST CELLS. 117

7.5 ETHANOL INHIBITS HIGH-AFFINITY IMMUNOGLOBULIN E RECEPTOR (FcεRI) SIGNALING IN MAST CELLS BY SUPPRESSING THE FUNCTION OF FcεRI -CHOLESTEROL SIGNALOSOME. 139

7.6 CROSS-TALK BETWEEN TETRASPANIN CD9 AND TRANSMEMBRANE ADAPTOR PROTEIN NON-T CELL ACTIVATION LINKER (NTAL) IN MAST CELL ACTIVATION AND CHEMOTAXIS…….. 164

7.7 GOLD NANOPARTICLE-BASED IMMUNO-PCR FOR DETECTION OF TAU PROTEIN IN CEREBROSPINAL FLUID. 179

7.8 QUANTIFICATION OF α-TUBULIN ISOTYPES BY SANDWICH ELISA WITH SIGNAL AMPLIFICATION THROUGH BIOTINYL-TYRAMIDE OR IMMUNO-PCR. 186

7.9 RAPID AND SENSITIVE DETECTION OF CYTOKINES USING FUNCTIONALIZED GOLD NANOPARTICLE-BASED IMMUNO-PCR, COMPARISON WITH IMMUNO-PCR AND ELISA. 195

8 GENERAL DISCUSSION 206

9 CONCLUSIONS 215

10 REFERENCES 218

1 ABSTRACT (EN)

This thesis is focused mainly on understanding mechanisms of regulatory roles of C-terminal Src kinase (CSK) and phosphoprotein associated with glycosphingolipid-enriched microdomains (PAG) in the high-affinity IgE receptor (FcεRI)-mediated signaling of murine mast cells. FcεRI activation is initiated by aggregation of the receptor by complexes of multivalent antigen with IgE, followed by activation and enhanced activities of protein tyrosine kinases, phosphatases, adaptor proteins and number of other signal transduction molecules. The signaling events result in mast cell degranulation and release of variety of proinflammatory mediators, responsible for initiation of allergy and other inflammatory diseases. Understanding the function of key regulatory molecules controlling FcεRI-mediated mast cell activation, degranulation, and cytokines production could have therapeutic impact.

CSK is a major negative regulator of Src family tyrosine kinases (SFKs) that play a critical role in various immunoreceptor signaling events. However, its function in mast cell activation has not been completely understood. Because of its cytoplasmic localization, CSK was assumed to be brought to the vicinity of the plasma membrane-bound SFKs via binding to membrane-bound adaptors and PAG was a major candidate. To determine the roles of CSK and PAG in FcεRI signaling, we used as a model bone marrow-derived mast cells (BMMCs) from wild-type or PAG knockout (PAG-KO) mice with reduced amount of CSK (CSK-KD) or with reduced amount of both proteins (CSK-KD/PAG-KO). We found that antigen-activated cells with CSK-KD exhibited significantly higher degranulation, calcium response and chemotaxis. Unexpectedly, PAG played an opposite role in these processes and cells with CSK-KD, similarly as PAG-KO, displayed impaired phosphorylation of the transcription factor STAT5. This was probably caused by enhanced enzymatic activity of Src homology region 2 domain-containing phosphatase-1 (SHP-1), which resulted in inhibition of proinflammatory cytokines and chemokines production. Our data also showed distinct involvement of adaptor proteins LAT and NTAL in CSK- or PAG-dependent signaling in BMMCs. Several lines of evidence suggested, that CSK binds not only to PAG, but also to some other anchors, which could serve better than PAG for positioning of CSK in the vicinity of SFKs and thus more efficiently contribute to their inactivation. Based on these data we postulated a new model of CSK-PAG interplay in mast cell activation.

Since these studies required sensitive detection of various cytokines released or utilized by mast cells, part of the thesis was dedicated to development of such assay. In collaborative studies we used this method, called nano-iPCR, for detection of clinically relevant markers in cerebrospinal fluid of patients and compared it with routinely used enzyme-link immunosorbent assays (ELISAs).

We also used this method for elucidating the role of ORMDL3 protein in mast cell signaling. The key finding was determination of ORMDL3 as a negative regulator of proinflammatory cytokines production, mediated via AKT and NF-κB-directed signaling pathways. Our results also showed that mast cell chemotaxis is regulated by ORMDL3 and CD9. Furthermore, we examined mode of action of widely used dissolving agent, ethanol, and cellular cholesterol remover, methyl-β-cyclodextrin, on FcεRI activation. Our data indicated that ethanol has an inhibitory effect on function of FcεRI signalosomes in which cholesterol plays an indispensable role. These data were corroborated in mice *in vivo* using passive cutaneous anaphylaxis.

2 ABSTRAKT (CZ)

Tato disertační práce je zaměřena především na pochopení regulační úlohy C-terminální Src kinázy (CSK) a proteinu asociovaného s mikrodoménami bohatými na glykosfingolipidy (PAG) v FcεRI zprostředkované signalizaci myších žírných buněk. FcεRI aktivace je zahájena agregací receptoru komplexem multivalentního antigenu s IgE a následnou aktivací protein tyrozin kináz, protein tyrozin fosfatáz a dalších molekul signální transdukce. Signalizační děje vedou k degranulaci žírných buněk a uvolnění prozánětlivých mediátorů zodpovědných za vznik alergických onemocnění. Poznání funkce klíčových regulačních molekul, které kontrolují FcεRI zprostředkovanou aktivaci, degranulaci a cytokinovou produkci žírných buněk, může mít terapeutický dopad.

CSK je hlavním negativním regulátorem protein tyrozin kináz z rodiny Src (SFK), které hrají kritickou úlohu v různých imunoreceptorových dějích. Funkce CSK v žírných buňkách však není zcela objasněna. Předpokládá se, že CSK lokalizovaná v cytoplazmě je translokována do blízkosti membránově vázaných SFK s využitím membránových adaptorových proteinů a PAG byl hlavním kandidátem. Pro určení úlohy proteinů CSK a PAG v FcεRI signalizaci jsme jako model použili žírné buňky odvozené z kostní dřeně (BMMC) myší divokého typu nebo myší deficientních v proteinu PAG (PAG-KO) nebo myší se sníženou expresí CSK (CSK-KD) nebo se sníženou expresí obou těchto proteinů (CSK-KD/PAG-KO). Konkrétně jsme ukázali, že antigenem aktivované buňky s CSK-KD vykazují významně vyšší degranulaci, vápníkovou odpověď a chemotaxi. Překvapivě, PAG měl v těchto dějích opačnou úlohu a buňky s CSK-KD, stejně jako PAG-KO, vykazovaly narušenou fosforylaci transkripčního faktoru STAT5. To bylo pravděpodobně způsobeno zvýšenou enzymatickou aktivitou fosfatázy SHP-1, čímž docházelo k inhibici produkce prozánětlivých cytokinů a chemokinů. Naše výsledky také ukázaly odlišné zapojení adaptorových proteinů LAT a NTAL v CSK- nebo PAG-závislé signalizaci BMMC. Získané výsledky podporují hypotézu, že se CSK váže nejenom na PAG, ale také na jiné adaptorové proteiny, které mohou fungovat lépe než PAG pro lokalizaci CSK v blízkosti SFK, a tím efektivněji přispět k jejich inaktivaci. Na základě těchto výsledků jsme navrhli nový model souhry proteinů CSK a PAG v signalizaci žírných buněk.

Protože tyto studie vyžadovaly citlivou detekci různých cytokinů uvolněných z žírných buněk nebo jimi spotřebovávaných, byla část práce věnována vývoji takové metody. Ve spolupráci s dalšími laboratořemi, jsme tuto metodu, nazvanou nano-iPCR, použili pro detekci klinicky významných reportérů v mozkomíšním moku pacientů a srovnali ji s běžnými imunotesty využívající enzymově značené komplexy antigen-protilátka ukotvené na pevných nosičích (ELISAs).

Tuto metodu jsme také použili pro určení úlohy ORMDL3 proteinu v signalizaci žírných buněk. Klíčovým zjištěním bylo, že ORMDL3 je negativní regulátor produkce prozánětlivých cytokinů, přes AKT- NF-κB řízenou signální dráhu. Naše výsledky také ukázaly, že chemotaxe žírných buněk je regulována proteiny ORMDL3 a CD9. Dále jsme zkoumali vliv běžně používaného rozpouštědla etanolu a látky odstraňující membránový cholesterol, methyl-β-cyclodextrinu, na FcεRI signalizaci. Naše výsledky ukázaly, že etanol inhibuje funkci FcεRI signalozomu, a že cholesterol zde hraje nezastupitelnou úlohu. Tyto výsledky jsme potvrdili na myších *in vivo* s využitím testu pasivní kožní anafylaxe.

3 ABBREVIATIONS

AA	amino acid
AF	Alexa Fluor
ATP	adenosine triphosphate
BCR	B cell receptor
BLK	B-lymphoid tyrosine kinase
BMCP	basophil/mast cell progenitor
BMMC	bone marrow-derived mast cell
BSA	bovine serum albumin
C/EBP	CCAAT-enhancer-binding proteins
CAP	cytoplasmic adaptor protein
CD	cluster of differentiation
CHO	Chinese hamster ovary cell
CMML	chronic myelomonocytic leukemia
CMP	common myeloid progenitor
CSK	C-terminal Src kinase
Ct	cycle threshold
DOK	downstream of tyrosine kinase
ELISA	enzyme-linked immuno sorbent assay
ERK	extracellular regulated kinase
ERM	ezrin, radixin, moesin protein family
FcεRI	high-affinity IgE receptor
FcγRII	Fc receptor for IgG
FGR	Gardner-Rasheed feline
FITC	fluorescein isothiocyanate
GADS	Grb2-related adaptor downstream of Shc
GATA	GATA-binding transcription factor
GMP	granulocyte-macrophage progenitor
GPCR	G-protein-coupled receptor
GRB2	growth factor receptor-bound protein 2
HCK	hematopoietic cell kinase
HEK	human embryonic kidney 293 cells

HRP	horseradish peroxidase
HSC	hematopoietic stem cell
Ig	immunoglobulin
IL	interleukin
IL3R	receptor for IL-3
iPCR	immuno-PCR
ITAM	immunoreceptor tyrosine-based activation motif
ITIM	immunoreceptor tyrosine- based inhibitory motif
IκB	inhibitor of κB
JAK	Janus kinase
KD	knockdown
kDa	kilodalton
KO	knockout
KTIM	kinase tyrosine-based inhibitory motif
LAMP1	lysosomal-associated membrane protein 1
LAT	linker for activation of T cells
LAX	linker for activation of X cells
LCK	leukocyte C-terminal Src kinase
LPS	lipopolysaccharide
LPS	lipopolysaccharide
LTC	leukotriene C
LYP	lymphoid-tyrosine phosphatase
mAb	monoclonal antibody
MAPK	mitogen-activated protein kinase
MCP	mast cell progenitor
MEM	minimal essential medium
MIRR	multichain immune recognition receptor
MITF	microphthalmia-associated transcription factor
MPP	multi-potent progenitor
MβCD	methyl-β-cyclodextrine
Nano-iPCR	gold nanoparticle-based-iPCR
NCBI	National Center for Biotechnology Information
NFAT	nuclear factor of activated T-cells

NF-κB	nuclear factor kappa-light-chain-enhancer of activated B cells
NRTK	non-receptor tyrosine kinase
NTAL	non-T-cell activation linker
OE	overexpressor
OPD	o-phenylenediamine
ORMDL	ORM-like
PAG	phosphoprotein associated with glycosphingolipid-enriched microdomains
PAGE	polyacrylamide gel
PBS	phosphate buffer solution
PCA	passive cutaneous anaphylaxis
PDZ	post-synaptic density protein 95
PGD	prostaglandin D
PI3	inositol-1,4,5-triphosphate
PI3K	phosphatidylinositol-3 kinase
PIP3	phosphatidylinositol-3,4,5-trisphosphate
PKC	protein kinase C
PLC	phospholipase C
PSA	passive systemic anaphylaxis
PTK	protein tyrosine kinase
PTP	protein tyrosine phosphatase
PY20	phospho-tyrosine specific monoclonal antibody
RBL	rat basophilic leukemia
RNA	ribonucleic acid
RNAi	RNA interference
RTK	receptor tyrosine kinase
SCF	stem cell factor
SDS	sodium dodecyl sulphate
SFK	Src family kinase
SH	Src-homology
SHIP	SH2 domain-containing inositol 5-phosphatase
SHP	SH2 domain containing phosphatase
shRNA	short hairpin RNA
siRNA	small interference RNA

SLP-76	SH2 domain-containing leukocyte protein of 76 kDa
STAT	signal transducer and activator of transcription
SYK	spleen tyrosine kinase
TBS	tris buffer solution
TBST	tris buffer tween solution
TCR	T-cell receptor
Th	T helper
TNF	tumor necrosis factor
TPBS	phosphate buffer tween solution
TRAP	transmembrane adaptor protein
VAV	guanine nucleotide exchange factor
WT	wild type

4 INTRODUCTION

4.1 MAST CELL

4.1.1 Origin and development

Mast cells origin and details regarding their differentiation and maturation are still incompletely understood [1]. Mast cells are hematopoietic cells of the myeloid linage originated in bone marrow. In human beings, mast cells develop from $CD^{34+}/CD^{117+}/CD^{13+}$ multipotent hematopoietic progenitors, while mouse mast cells originate from CD^{34+}/CD^{117+} pluripotent hematopoietic progenitors. Majority of other hematopoietic cells are released into the bloodstream primarily in a mature state, however mast cells progenitors enter to the blood circulation in an immature state and migrate through blood vessels to peripheral tissues where maturate under the influence of local environment [2]. Despite of the growing understanding of hematopoiesis, the origin of mast cells is a subject of controversy [3-5].

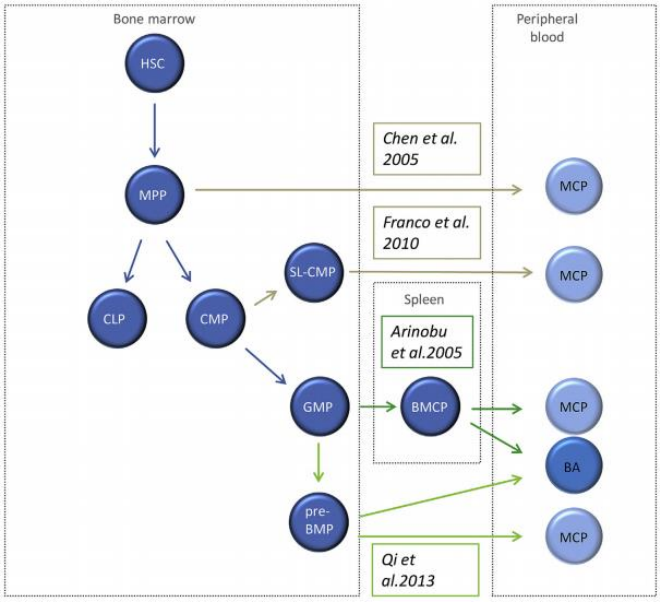

Figure 1. Current models describing the origin of murine mast cells and their differentiation. In adult mice, mast cells originate and develop from hematopoietic stem cells in bone marrow. Mast cell progenitors (MCPs) are currently thought to develop from multi-potent progenitors (MPPs) or common myeloid progenitors (CMPs) in the bone marrow. On the other hand, they also might differentiate from

granulocyte/monocyte progenitors (GMPs) via a common basophil/mast cell progenitor (BMCP), only found in the spleen, or a pre-basophil/mast cell progenitor (pre-BMP). Adapted from [6].

To what lineage the mast cells belong and whether they have their own progenitors or share them with basophils is still debated [6]. Advances in multicolor flow cytometry techniques enabled extensive studies of mast cells origin and thus to understand their relationship to other cells. In Figure 1, the current models of mast cell origin and development are summarized [6]. In mice, bone marrow derived hematopoietic stem cell (HSC) give arise to multi-potent progenitor (MPP), which is capable directly differentiate into mast cell progenitor (MCP) [7] or common myeloid progenitor (CMP) with potential to give arise MCP via Sca-1 low fraction of CMP (SL-CMP) population. This progenitor is more closely related to megakaryocyte/erythrocyte specification [8]. On the other hand, granulocyte/monocyte progenitor (GMP) can develop to the common basophil/mast cell progenitor (BMCP), present only in mouse spleen, which can progress to MCP or basophil progenitor (BA) [4], suggesting a close developmental relationship between basophil and the mast cell lineage. In contrast, more recent study described that BMCP exhibit very low potential to give arise to BA [9]. Subsequent studies identified phenotypically different progenitor called pre-basophil/mast cell progenitor (pre-BMP), which can develop to both MCP and BA progenitor [5].

Mast cells progenitor population has been extensively characterized in terms of its surface markers. After commitment, both mast cells and basophils express high affinity receptor for IgE (FcεRI). In contrast, basophils typically mature in bone marrow and enter blood as a fully mature cells. Identification of mast cell progenitors is crucial for understanding the mechanisms of allergy diseases and various type of mastocytosis, characterized by uncontrolled mast cell proliferation and accumulation within various organs [10]. Recently, Dahlin et al. identified a novel circulating human mast cell progenitor population present in bloodstream in immature state of healthy individuals that can only develop into MCP. Importantly, it has been shown that this progenitor significantly increase in asthma patients with reduced lung function [11].

Differentiation of mast cells from CMP, GMPs or BMCP progenitors is tightly regulated by CCAAT/enhancer binding protein α (C/EBPα), microphthalmia-associated transcription factor (MITF), signal transducer and activator of transcription (STAT5), GATA-1 and GATA-2 transcription factors.

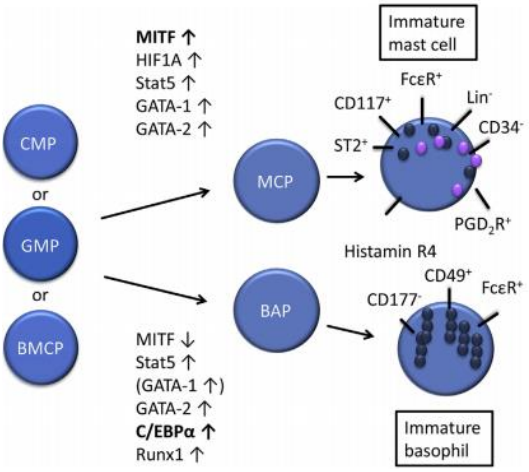

Figure 2. Transcription factors involved in putative pathways of mast cell development. Adapted from [6].

As shown Figure 2, absence of transcription factor C/EBPα result in development of mast cells, but not basophils [12, 13]. Thus, for mast cell progenitors commitment, MITF is upregulated and C/EBPα is further downregulated, whereas for BA commitment, MITF is downregulated and C/EBPα is upregulated [13].

4.1.2 Diversity in phenotype and tissue localization

Although all mast cells can be identified by their receptor expression profile, mature mast cells exhibit great histochemical, biochemical and functional heterogeneity [14]. The plasticity of mast cells phenotype leads to development of phenotypically distinct populations based on animal species, anatomical localizations and processes which physiologically change tissue microenvironment such as hormones, cytokines and chemokines or pathological alteration such as reactive oxygen and nitrogen species, and divers mediators released during inflammation and numerous diseases. Heterogeneity among mast cells populations allow greater flexibility of immunological responsiveness in host defense, allergic reactions and communication with adjacent immune cells [15]. Apart of this, mast cell phenotype is dynamically changed in accordance with current conditions. Mast cells can be find in all blood vessels and peripheral connective tissues, such as skin, joints, lung, nasal mucosa and intestine. In rodents, mast cells are also present in peritoneal cavity and can be easily isolated in contrast to mast cells located in solid tissue. Tissue-resident mast cells are very long-

lived and even after degranulation they are still alive. In rodents, two mast cell populations have been described, mucosal-type and connective tissue-type mast cells, which differ in content of the secretory granules [16].

Majority of proteins found in rodent and human mast cell granules are proteases. In mice, mucosal-type mast cells preferentially express mast cell protease-1 and -2, whereas connective tissue-type mast cells express mast cell protease -4, -5 and -6 and carboxypeptidase. Another difference between these two mast cell types is in the presence or absence of proteoglycan heparin, which is only found in connective tissue-type mast cells. In contrast, all human mast cells contain heparin, but exhibit heterogeneity in content of serine proteases. According to the content of proteases, human mast cells are classified as tryptase-only, chymase-only or both type tryptase and chymase-positive mast cells [2].

4.1.3 Growth factors

Although mast cells are widely distributed among tissues, they represent a minor cell population [17, 18]. Sources of homogenous mast cells and appropriate isolation techniques have therefore been searched for experimental studies [19-21]. The major limitation of these techniques is their poor yield, making biochemical analyses difficult [18]. For this reason, mast cell lines of mouse, rat and human origin, such as rat basophilic leukemia (RBL), have been extensively used; however it has been shown that stable cell lines are not very useful for some biochemical studies [22, 23]. On the other hand, cultured mast cells from pluripotent hematopoietic precursors from bone marrow permitted such studies. Considerable numbers of pure primary mouse mast cells can indeed be generated and kept in culture for several months. Development of murine mast cells is dependent on the presence of two growth factors, interleukin (IL)-3 and stem cell factor (SCF). Therefore, these components need to be added into culture media used for production of bone marrow-derived mast cell (BMMCs).

SCF (also known as c-KIT-ligand or steel factor) is produced by fibroblasts and endothelial cells throughout the body, promoting proliferation, migration, survival, and differentiation of hematopoietic progenitors, melanocytes, and germ cells. Soluble SCF, which has molecular size of 18.5 kDa, binds to its plasma membrane receptor, c-KIT, and thereby enhances mast cell development, potentiates antigen-mediated activation, degranulation and cytokines/chemokines production in mast cells [24, 25]. Importance

of c-KIT and its ligand for mast cells development is demonstrated by phenotype of mice, with loss-of-function mutations in this receptor or its ligand SCF, which are virtually mast cell deficient [26].

Interleukin (IL)-3 was found to be one of the factors in conditioned media of activated lymphocytes, which was responsible for mast cell survival, development, and maturation. Although IL-3 contributes in increasing of murine BBMCs *in vitro*, its effect *in vivo* is not essential [27]. Screening of various cell lines revealed that WEHI-3, a myelomonocytic leukemia B cell line, constitutively produced large amount of IL-3 and Chinese hamster ovarian (CHO) cell line are source of SCF suitable for *in vitro* BMMCs cultivation [28-30].

Bone marrow progenitors cultured in SCF- and IL-3-supplemented media undergo optimal proliferation and maturation *in vitro* and therefore quality of the media is a presumption for preservation of the homogeneous population. Differences in the concentration of SCF and other cytokines such as IL-3 can determine number and phenotype of mast cells. For instance, IL-3 in rodents induce histamine secretion [2] and activates STAT5 pathway, which regulates apoptosis and cytokines production [31]. Mast cell heterogeneity causes by suboptimal concentration of growing factors makes experiments difficult due to inaccurate response to stimulatory signals [32].

4.2 MAST CELL FUNCTIONS

Mast cells can function as a both effector and immunomodulatory cells during innate and adaptive immune responses [15]. Effector functions include several physiological and pathological processes, such as IgE-mediated allergic diseases, asthma, autoimmune disorders, inflammation, homeostatic responses, angiogenesis, wound healing and tissue remodeling. On the other hand, mast cells have also anti-inflammatory and immunosuppressive functions, because they promote clearance of pathogens by phagocytosis and/or by secretion of anti-microbial peptides and degrade toxic endogenous peptides or components of venoms [33].

Mast cells are characteristic by a large amount of cytoplasmic granules containing biologically active compounds which are released upon cell activation [15]. Activation of mast cells by antigen-specific IgE binding and crosslinking FcεRI, the

high-affinity IgE receptor, results in downstream event that lead to the rapid secretion of large amount of preformed and newly synthetized mediators, by process called degranulation. As shown in Figure 3, during early stage of degranulation mast cells release biogenic amines (histamine, serotonin), lysosomal enzymes (β-glucuronidase, β-hexosaminidase), several serine and other proteases (chymases, tryptases), proteoglycans (heparin, chondroitin sulphate), and cytokines, such as tumor necrosis factor-α (TNF-α) [32].

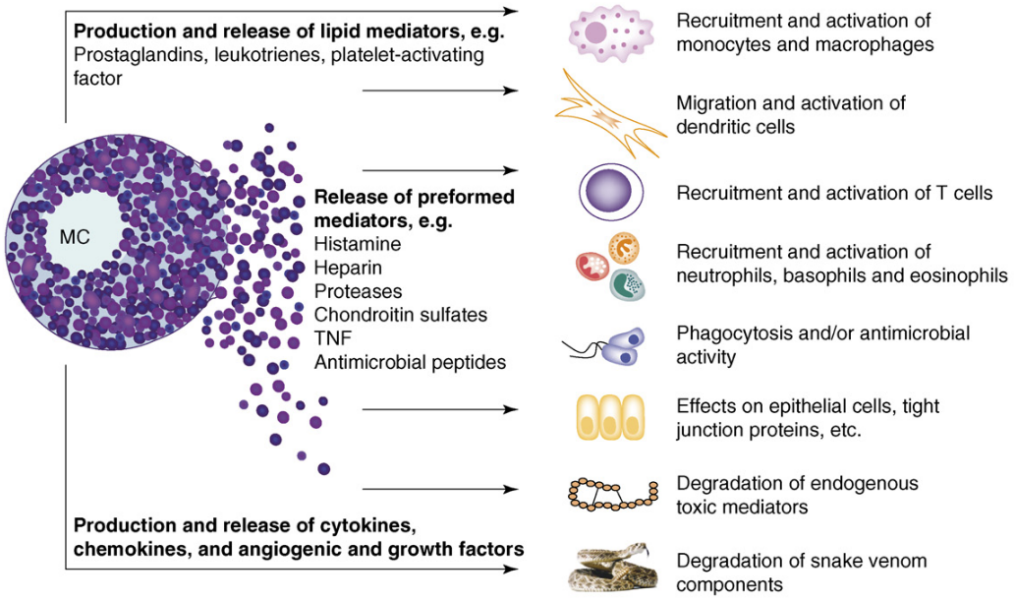

Figure 3. Mast cells can be activated to release preformed and/or de novo-generated products. The secretion of mast cell products can have numerous effects on other cell types and on pathogens and endogenous and exogenous peptides, which can lead to improved innate and/or acquired immune responses. Adapted from [32].

Thus, mast cells have a potential to be the first responders following recognition of an invading pathogens, including parasites, bacteria and probably viruses. Releasing of these mediators by mast cells is signal for recruitment of neutrophils, eosinophils and basophiles accompanied by immediate effect on epithelial, endothelial and nerves, result in increased epithelial permeability, production of mucus, smooth muscle contraction and vasodilation. Late phase of degranulation is characteristic not only by continued mediator release, but also *de novo* synthetized compounds which mediate sustained inflammatory response long after the effect of histamine has fade away. These mediators occur though activation of arachidonic acid metabolic pathways, involving leukotriene

C_4 (LTC_4), prostaglandin D_2 (PGD_2), and other products, such as chemokines and cytokines which drive activation of leukocytes and another tissue resident cells. These early and late phase of degranulation results in allergic and/or inflammatory responses accompanied by characteristic symptoms [2, 32-34]. Generally, histamine and nitric oxide stimulates vasodilatation, heart rate, and together with LTC_4 increase vascular permeability, PGD_2 is responsible for bronchoconstriction and TNF-α activates neutrophils and promote synthesis of chemokines [33, 35].

In certain cases, mast cells and basophiles mediate anaphylaxis, a severe allergy reaction, which can result in airway obstruction, cardiovascular collapse and sometimes death. Generally believed mechanism of anaphylaxis is based on crosslinking of IgE and aggregation of FcεRI, following by activation the signaling pathways result in massive and rapid degranulation within seconds or minutes. Molecular mechanism of degranulation is described later in Chapter 4.4.2, at page 35. Anaphylaxis is also induced by activation of phospholipase A_2, cyclooxygenases and lipoxygenases, arachidonic acid metabolites and proinflammatory cytokines [35].

A number of cytokines (e.g. IL-1, 2, 5, 6, 8, 9, 13, TNF) are synthesized *de novo* and released several hours upon mast cell activation. Of particular interest in humans is the production of tumor necrosis factor (TNF-α, β), and interleukin (IL)-4, IL-5, IL-6, IL-1β and IL-13 [36]. For instance, mast cell derived TNF-α and IL-4 modulate adhesion molecules on endothelial cells and thereby allow other circulating inflammatory cells to adhere to the endothelium and to migrate into the surrounding tissue during inflammation. Moreover, TNF-α also promote activation and antigen presentation of dendritic cells and mast cell derived IL-6 stimulates the proliferation and differentiation of activated B-cells, and can enhance neutrophil activity against some bacteria. Different mechanisms could contribute to the increase in the number of mast cells at the sites of inflammation: resident mast cell precursors could proliferate, released compounds and/or their progenitors could migrate to the site of inflammation [37, 38]. A potent mast cell chemoattractant acting in autocrine/paracrine fashion is SCF which recognize c-KIT receptor, antigen, which binds to IgE recognized by FcεRI, leukotrienes and eicosanoids (LTC_4, PGD_2), and chemokines, which bind to various G-protein-coupled receptors (GPCRs) [39].

4.3 SIGNAL TRANSDUCTION

4.3.1 Receptors

Mast cells expressed on its surface array of receptors that recognized wide variety of stimuli, such as receptor for stem cell factor (c-KIT), receptor for IL-3, lipopolysaccharide (LPS), certain products of complement activation and some neuropeptides. However, the best-studied mechanism for the mast cell activation is via FcεRI. Immunologically specific function of this receptor is interaction with complex of IgE-antigen [15].

FcεRI on mast cells and basophils is a member of a family related antigen/Fc receptors, called Multichain Immune Recognition Receptors (MIRRs), which have conserved structural features and similar roles in initiating intracellular signaling cascades. The FcεRI has a heterotetrameric structure consist of one α-subunits, one membrane-tetraspanning β-subunits, and two identical γ-subunits linked with disulphide bound (Figure 4) [23, 40, 41]. The α-subunit has a short intracellular tail that does not contribute to transduction events, however consist of binding site for IgE [23, 40]. The α-subunit of FcεRI is responsible for binding to the Fc part of monomeric IgE at a very high affinity ($K_d=10^{-9}$-10^{-10}) [23].

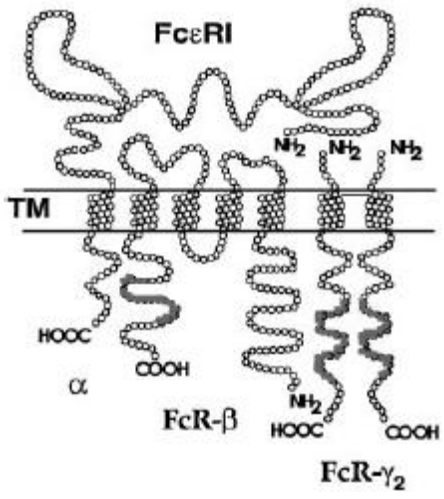

Figure 4. FcεRI structure. The FcεRI is transmembrane (TM) tetrameric receptor composed of 3 chains: one α chain with 2 domains, the second domain is capable of binding to the two IgE Cε3 domain heavy chains. One β chain which amplifies the downstream signal, and two γ chains bound together by a disulphide bridge, they are the site where the downstream signal initiates. Adapted from [40].

The cytoplasmic part of β and γ chains is important for initiation and downstream of signal transduction cascade, since they each contain an immunoreceptor tyrosine-based activation motifs (ITAMs), that serves as a docking sites for Src family kinases possessing phosphotyrosine-binding Src homology (SH)2-domains [22]. The rapid phosphorylation leads to the receptor aggregation and induction multiple signaling pathways that regulates diverse effector responses. These include the secretion of allergic mediators and induction of cytokine gene transcription, resulting in secretion of proinflammatory mediators [42]. Therefore, FcεRI is central to the induction and maintenance of an allergic response and also may confer physiological protection in parasitic infections [23]. FcεRI receptor is the most important receptor on mast cells and its expression on the surface of mast cells, together with c-KIT, a receptor for SCF, is a characteristic hallmark for mature mast cells population.

c-KIT (CD117) is a type III tyrosine kinase and belongs to superfamily of the transmembrane receptors with intrinsic tyrosine kinase activity and is highly, but not exclusively, expressed in hematopoietic lineage [43, 44]. The extracellular part of the receptor contains 5 Ig-like motifs, which regulate binding of the SCF to the receptor. Ligand binding is followed by receptor dimerization and activation of the inherent catalytic activity associated with tyrosine kinase domain present at the cytosolic region of the receptor [45].

SCF-mediated activation of the c-KIT, both directly and indirectly, leads to the downstream of the signaling molecules such as LYN and FYN kinases that activates phosphatidylinositol-3 kinase and serine-threonine kinase AKT (PI3K-AKT) pathway, Janus kinase (JAK)/signal transducer and activator of transcription (STAT) pathway and mitogen-activated protein kinase (MAPK) pathway [43, 44]. Downstream signaling events of c-KIT leads to regulation of transcription activity to prevent mast cells from undergoing apoptosis. On the other hand, mast cells without present of SCF exhibit manifestations of apoptosis and die approximately within 2 days [46]. As was mentioned above, mice defective in functional KIT or SCF are deficient in mast cells [47, 48]. This showing that SCF-induced KIT activation is crucial for maturation of mast cells from their progenitors, homing in the site of residence in vivo, as well as chemotactic properties of SCF for both human and mouse mast cells [39].

4.3.2 Adaptor proteins

Adaptor proteins play an essential role in downstream of the receptor-mediated signals into an appropriate cellular response. They are lacking any enzymatic and transcriptional activity, but instead of this they possess multiple motifs capable mediated protein-protein and/or protein-lipid interaction with other signaling molecules and serves as a docking site for cytoplasmic signaling molecules. There are two major group of adaptor proteins: transmembrane adaptor proteins (TRAPs) and cytoplasmic adaptor proteins (CAPs) [49, 50]. In mast cells five TRAPs have been identified: PAG (phosphoprotein associated with glycosphingolipid-enriched microdomains), LAT (linker for activation of T cells), NTAL (non-T cell activation linker), LAX (linker for activation of X cells) and growth factor receptor-bounded protein 2 (GRB2)-binding adaptor protein [51-53]. In the following chapters, some of the adaptor proteins most relevant for this work is described.

4.3.2.1 LAT and NTAL

Transmembrane adaptor protein, LAT, is present in several cell types, whereas NTAL is mainly expressed in B cells, natural killer cells, monocytes and mast cells, but not in T cells in comparison with LAT. Several studies showed, that LAT could be phosphorylated by spleen tyrosine kinase (SYK) and thus phosphorylated LAT associates directly or indirectly with numerous signaling molecules, such as GRB2, PLCγ, guanine nucleotide exchange factor (VAV), CBL, SH2 domain-containing leukocyte protein of 76 kDa (SLP-76), and Grb2-related adaptor downstream of Shc (GADS) [50].

As other TRAPs, LAT possess a very short extracellular part (four amino acid), a single transmembrane domain with dual palmitoylation, and a long cytoplasmic region, without any enzymatic activity, but composed of various binding motives (Figure 5). The more distal tyrosine on cytoplasmic tail of LAT serve as a binding site for SH2 domain-containing inositol 5-phosphatase 1 (SHIP1), which negatively regulates FcεRI signaling by inhibiting PI3K-dependent pathway. Although LAT and NTAL have structural similarities, the amino-acid sequences differ to each other. NTAL possesses 10 tyrosines within the cytosolic tail: five of them within the putative Grb2-binding sites and one within the putative SH2 domain containing phosphatase (SHP-1)/Src kinase-

binding site (YIDP). In contrast to LAT, NTAL is lacking the PLCγ1 binding motif. In FcεRI stimulated mast cells, NTAL was rapidly phosphorylated by SYK and LYN kinase. Interestingly, these kinases are produced entirely different pattern of phosphorylation of the individual tyrosines [54].

4.3.2.2 PAG

PAG (also known as CSK-binding protein; CBP) was simultaneously described in 2000 by two groups, one in Prague [55] and another in Japan [56] . PAG is ubiquitously expressed transmembrane adaptor protein with relatively highest expression in the immune cells, lungs, heart and placenta. PAG is a major phosphoprotein in resting T cells and its expression correlates with the proliferative capacity of this cells. PAG is also well expressed in B cells and mast cells. Interestingly, different expression of PAG was found in several of cancer cells [57]. PAG is consist of a short extracellular domain, a transmembrane domain for localizing PAG to the lipid raft, and a long cytoplasmic tail with multiple tyrosine-based motifs (Figure 5).

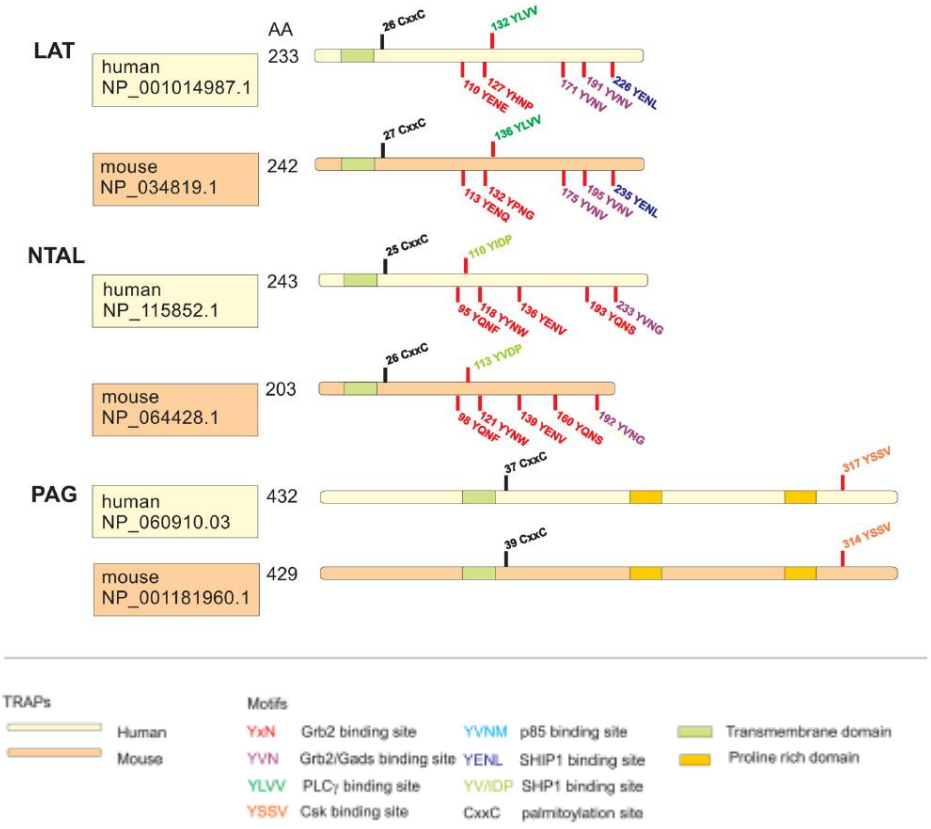

Figure 5. Schematic illustration of TRAPs studied in human and mouse mast cells. TRAPs are characterized by a short extracellular domain, a transmembrane domain, and a cytoplasmic domain with

various motifs. LAT, NTAL, and PAG possess juxtamembrane CxxC palmitoylation site for their interactions with lipids and localization in detergent-resistant membranes. All TRAPs have a various tyrosine-based motif which after phosphorylation serve as binding sites for the indicated SH2-containing proteins. PAG also contains proline-rich domains serving as anchor for SH3-containingnproteins. Number of amino acids (AA) in each TRAP as well as accession numbers in the GenBank sequence database provided by National Center for Biotechnology Information (NCBI) are also shown. Adapted from [50].

Nine of these motifs preferred phosphorylation by Src family kinases (SFKs). In resting T-cells, PAG is phosphorylates mainly by FYN kinase and thus binding site for SH2 domain of C-terminal Src kinase (CSK) is creates. Phosphorylated Tyr 314 in mouse PAG has been shown to be essential for CSK binding [56]. Following T-cell receptor (TCR) activation, SFKs are activated and they phosphorylate their target proteins including PAG. Phosphorylated PAG then recruits CSK to plasma membrane to the vicinity of active SFKs, as described in Chapter 4.3.4.1, page 30. After inactivation of SFKs by CSK, phosphorylation of PAG returns to the basal level and CSK simultaneously dissociate from the membrane. A negative regulatory role of PAG in T cell signaling was shown in experiments with PAG knockdowns (KDs) [58], and very recently this model was validated in PAG-knockout (KO) mice [59], confirming negative regulatory role of PAG in vitro and in vivo. Interestingly, in T cells from PAG-KO mice, CSK becomes more associated with alternative partners such as PTPN22 and adaptor protein DOK; downstream of tyrosine kinases [59]. PAG also possesses two proline-rich sequences that serve as binding sites for proteins with SH3 domains and a VTRL motif at the C-terminus for interaction with the post-synaptic density protein 95 (PDZ) domain of the cytoskeletal linker ezrin/radixin/moesin-binding protein, EBP50. In mast cells, PAG regulates FcεRI signaling by a mechanism more similar to B cell, than T cells. Following FcεRI triggering PAG is phosphorylated by LYN kinase instead of FYN kinase as in case of T cell, which results in recruitment of CSK to lipid raft and negative regulation of SFKs activity by phosphorylation of its C-terminal regulatory tyrosines [57].

4.3.3 Src family protein tyrosine kinases

Phosphorylation plays a pivotal role in many cellular and extracellular processes [60]. Protein tyrosine kinases (PTKs) carry out the phosphorylation reactions by

transferring the γ-phosphates of adenosine triphosphate (ATP) onto hydroxyl groups of tyrosine residues in various substrates including lipids, sugars or amino acids. PTKs, which are exclusively present only in animals, are involved in controlling animal-specific cellular functions such as rapid cell-cell communication via plasma membrane.

PTKs are classified into two major groups: receptor tyrosine kinases (RTKs) and non-receptor tyrosine kinases (NRTKs). RTKs are various cell surface receptors and are autophosphorylated upon binding of the ligand to the extracellular part of the molecule. In mast cells, accumulated evidence suggests that RTKs play a role in both a positive and negative manner to control cell activation [45, 61]. In mast cell, one the most important and extensively studied RTK is c-KIT, the receptor for stem cell factor (SCF). The second group of PTKs, the cytoplasmic NRTKs, are also activated in response to extracellular stimuli via physical and functional interactions with particular transmembrane receptors, thereby activate specific signaling pathways in cells.

The SFKs are the major family of NRTKs expressed in multiple types of mammalian cells. The discovery of SFKs was based on breakthrough finding that a virus could cause cancer. This responsible oncogene was called viral (v)-SRC (Rous sarcoma virus) and related gene found in chickens, as a normal cellular counterpart, was termed cellular (c)-SRC or simply SRC. SRC was identified as a first proto-oncogene and first protein with intrinsic tyrosine kinase activity, respectively. Since the discovery of their biochemical activity and involvement in signaling pathways, SFKs have been the subject of intensive investigation over the several decades [62]. To the family of SFKs belongs eight members, SRC, LYN, YES, FYN, FGR, HCK, LCK and B-lymphoid tyrosine kinase (BLK), that regulate wide range of fundamental cellular processes, including cell growth, differentiation, survival, migration, adhesion, division and specialized cell function such as immune response. [62-66]. Some of these SFKs such as LYN, FGR, HCK, LCK, BLK, are mainly expressed in hematopoietic cells, whereas SRC, FYN, YES are widely distributed in various cells of the body [67].

Structure of SFKs is consists of four Src homology (SH) domains: SH1, SH2, SH3 and SH4 (Figure 6A) [68]. SFKs are highly conserved among the family members, with the exception of the N-terminal SH4 unique region (~50 residues) possessing the lipid modification [69, 70]. Lipid modification such as myristoylation occurs as a co-translational modification, in which N-terminal methionine is removed and the resulting N-terminal glycine is myristoylated by myristoyl-coenzyme A. All members of the Src

family are co-translationally myristoylated, and with the exception of SRC and BLK, are also post-translationally palmitoylated (Figure 6B) [66]. Different state of palmitoylation regulates cellular localization and mechanism of cellular trafficking of the each SFKs. For instance, LYN and FYN, the crucial SFKs, promoting signaling from FcεRI, possess distinct state of palmitoylation. In contrast to mono-palmitoylated LYN which is transported to the plasma membrane via secretory pathway of Golgi, the dually-palmitoylated FYN is directly target to the plasma membrane [71], while SRC kinase is rapidly exchanged between late endosomes or lysosomes and the plasma membrane due to myristoylation alone [72].

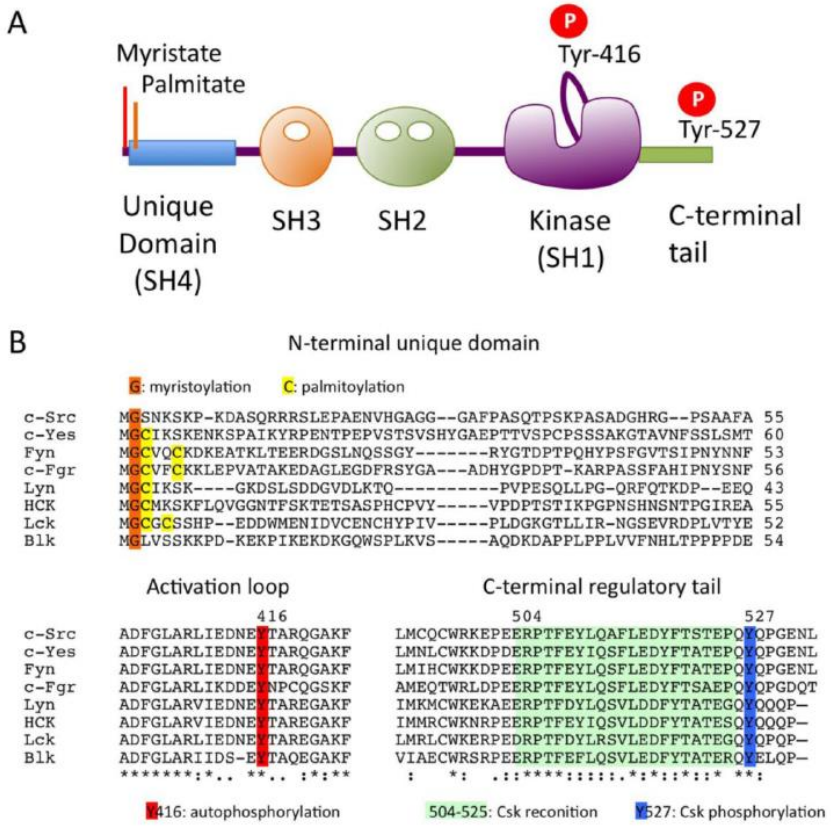

Figure 6. The Src family kinases (SFKs). (A) Domain organization of SFKs. (B) Amino acid alignments of N-terminal unique domain, activation loop and C-terminal regulatory tail in SFKs. Adapted from [66].

Palmitoylation has been implicated in localization of SFKs in the cholesterol-enriched membrane microdomains and recruitment of activated SFKs via transmembrane adaptor PAG/CBP to this microdomain leading to efficient suppression

of SFK-induce transforming potential of fibroblasts [73]. This poorly conserved domain is believed to provide unique functions and is specific to each SFK member [74].

SFKs possess domains that mediate protein-protein, protein-lipid, and protein-DNA interactions. The main function of SH3 domain (~60 residues) is regulation of its own kinase activity through an intermolecular interaction and direct binding to the specific adaptor proteins, many of which are also their substrates [68]. SH3 domain is able to bind proline-rich sequences of various signaling proteins, such as PI3K or CAS. The SH2 domain is compact domain of ~100 residues that binds phosphotyrosine residues in a sequence-specific manner. The SH1 domain corresponds to the kinase domain and contains the autophosphorylation site responsible for activation of SFKs. One of the hallmarks of the SFKs is their possession of two important regulatory tyrosine phosphorylation sites, which regulate kinase activity in opposite way. Phosphorylation of Tyr-527 (in human SRC), located in the carboxy-terminal tail, negatively regulate SFK activity, while phosphorylation of a second regulatory site Tyr-416 (in human SRC), an autophosphorylation site present in the activation loop of SH1 domain, leads to increase in enzymatic activity of SFKs.

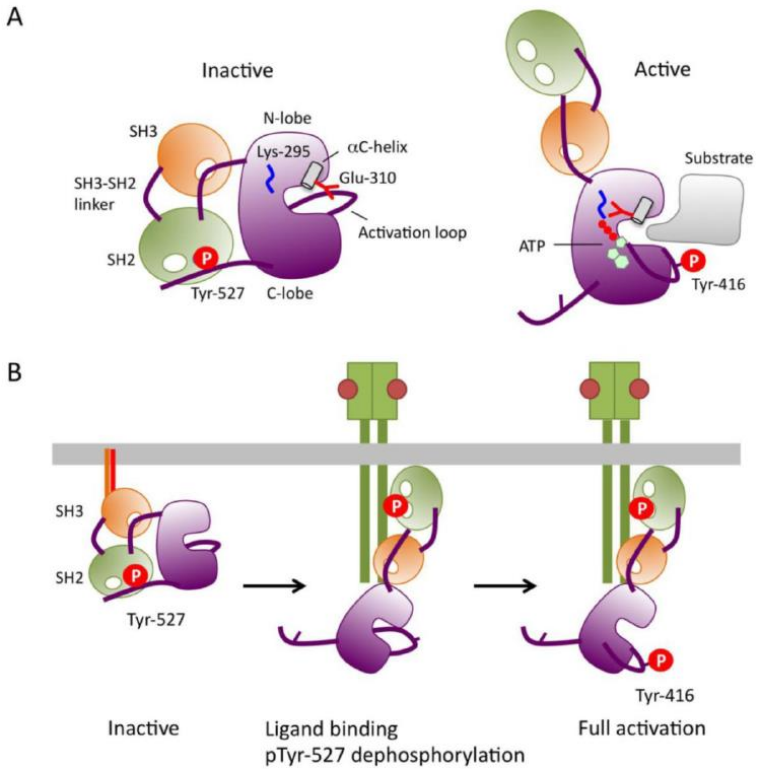

Figure 7. Mechanism of SFK activation. (A) Schematic models of inactive and active forms of c-Src (B) A predicted mechanism of SFK activation. Adapted from [66].

The importance of phosphorylation sites is underscored by oncogenic v-SRC, which lacks the negative regulatory site Tyr-527, results in constitutive activation and uncontrolled growth of infected cells [75-77].

Structural similarities of SFKs allows for common mechanism of their regulation based on the phosphorylation of regulatory tyrosines (Tyr-527 and Tyr-416) and the intramolecular interactions among the SH2 and SH3 domains. Detailed mechanism of SFKs regulation was resolved by analysis of their crystal structure. As indicated in Figure 7, in resting cells, the SFKs are mostly in inactive conformation and Tyr-527 is phosphorylated. This closed conformation is stabilized by binding of phosphorylated Tyr-527 to its own SH2 domain and by the simultaneous binding of SH2 linker to the SH3 domain. Both intramolecular interaction affect the configuration of catalytic pocket leading to disruption of Mg-ATP binding site [66]. Dephosphorylation of Tyr-527 leads to conformational changes in the SH2 and kinase domain resulting in trans-autophosphorylation of Tyr-416 in the activation loop. This autophosphorylation events keep catalytic domain in active conformation and facilitates access of the substrates to the active site [66].

Molecular mechanism of SFKs activation may vary depending on cell types, but in general, is achieved by following events: Firstly, activated receptor or adaptor or effector molecule interact with SH2/SH3 domains of inactive SFKs leading to open up conformation and keeping SFKs in appropriate cellular localization. Next, phosphorylated tyrosine 527 (pTyr-527) is dephosphorylated by protein tyrosine phosphatase, whereby stabilize active conformation of SFKs. Then, activated SFKs undergo intermolecular auto-phosphorylation on Tyr-416 and thus achieved fully active conformation, which in turn phosphorylate substrate proteins and at the same time create binding site for another SFKs. This events represent a positive-feedback loop of SFKs activation [66].

4.3.4 Regulation of SFKs

4.3.4.1 C-terminal Src kinase

CSK is a negative regulator of the SFKs that play pivotal role in various cell signaling [78]. Key function of CSK is specific phosphorylation of tyrosine residues located in the C-terminal tails of SFKs (Tyr-527), thereby inducing an intramolecular

interaction between the C-terminal phosphotyrosine and the SH2 domain and allows them to fold in an inactive conformation (Figure 7). This interaction renders the catalytic domain of SFKs inaccessible to substrates [79-81].

The negative regulatory role and indispensableness of CSK was demonstrated *in vivo* by mice deficient in CSK. These mutant embryos died in early embryonic stages and embryonic tissue exhibited constitutively phosphorylated SFKs [82]. Loss of CSK induced defects in T cell development [83], hyperplasia of epidermis [84], acute inflammation of the skin and lungs, adhesiveness and chemotaxis [85]. Granulocytes isolated from these mice exhibit increase in both spontaneous and ligand-induced degranulation and production of TNF-α [85]. In rat basophil leukemia cells (RBL) with overexpressed CSK were observed decreased in LYN kinase activity at the resting cells suggested that CSK negatively regulates FcεRI-mediated signaling [86].

CSK is highly conserve across the animal kingdom and possess similar primary structure of SH2 and SH3 functional domains with SFKs. But differ from the structure of SFKs in several striking features: the absence of autophosphorylation site in the activation loop as well as absence of inhibitory tyrosine residue close to C-terminal tail, N-terminal fatty acid modification and the different orientation of SH2 and SH3 domain, enabling interaction with others molecules. Because of the lack of transmembrane domain, CSK is localized predominantly in cytoplasm, whereas its substrate SFKs are anchored to the membrane via N-terminal myristoylation and/or palmitoylation moieties. Thus, recruitment of cytosolic CSK to the membrane-associated SFKs is crucial for its regulatory function.

An important regulator of CSK function is a transmembrane adaptor protein PAG, which specifically binds the CSK SH2 domain when phosphorylated. PAG anchored to lipid rafts recruits CSK to lipid raft-associated SFKs, mediates a link to actin cytoskeleton and interacts with several other important cytoplasmic and plasma membrane-associated proteins (Figure 8) [57]. Further, CSK also associates through its SH3 domain with the protein tyrosine phosphatase PTP-PEST and lymphoid-tyrosine phosphatase LYP (mouse orthologue PEP). As these phosphatases dephosphorylate the positive regulatory tyrosine residue in Src family kinases, it is thought that they synergize with CSK by jointly targeting and suppressing these kinases.

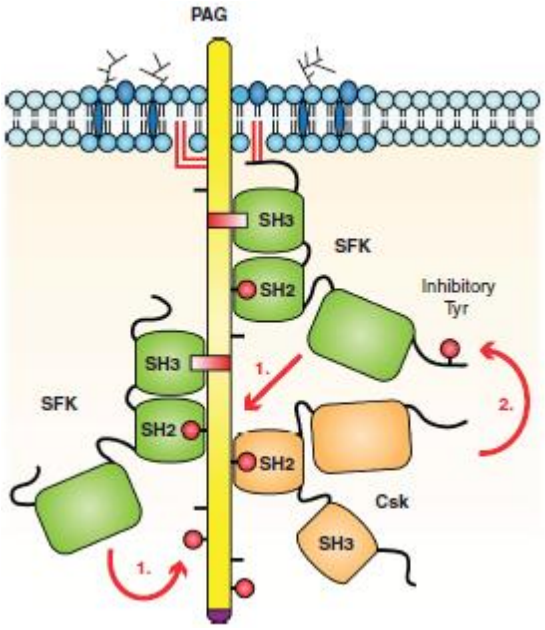

Figure 8. Model of negative regulation loop in SFK signaling mediated by PAG-CSK. PAG present in lipid rafts can associate with and become phosphorylated by SFKs (1). Phosphorylation of PAG creates docking sites for SH2 domains of SFKs and their negative regulator CSK. CSK bound to PAG then phosphorylates the inhibitory tyrosine residue at the C termini of SFKs (2) and inactivates them. Adapted from [57].

Accumulating evidence suggest that CSK may play role in tumor suppression by inhibiting the oncogenic activity of SFKs. Indeed, overexpression of CSK can inhibit tumor growth of human colon cancer cells [87]. However, there is no convincing evidence that supports the direct involvement of CSK in human cancer. Although CSK is downregulated in some cancers, it is likely that CSK is expressed at normal levels in many types of cancer cells, and there have been no reports of somatic mutation in the csk gene, as well as mutation in SFKs genes has not been detected. Therefore, molecular mechanism underlying the causes of SFKs dysregulation in various diseases remain unclear [66].

4.3.4.2 Phosphatases

Although the CSK has been consider as a major negative regulator of SFKs, the little is known about precise protein tyrosine phosphatases (PTPs) responsibility to dephosphorylate activation loop or C-terminal inhibitory site of the SFKs, although numerous have been involved in this processes [68]. In FcεRI-mediated activation of

mast cells and basophils, the protein tyrosine phosphorylation is critical early signaling events reflects the balance between the action of PTKs and PTPs.

One of the extensively studied PTPs involved in mast cell signaling are Src homology 2 (SH2) domain-containing nonreceptor phosphatases SHP-1. SHP-1 is a cytoplasmic PTPs expressed in hematopoietic and epithelial cells [88-90]. The major function of SHP-1 is to limit extend of activation and cellular response by dephosphorylation its target molecules. SHP-1 is generally considered as a negative regulator of various immuno-receptor mediated signaling, including TCR-, B cell receptor, (BCR-) , FcεRI-, c-KIT- and IL3R- mediated signaling [91-93].

Mice with the recessive *motheaten* or allelic viable *motheaten* mutations suffer from severe autoimmune diseases. Mice homozygous for these mutations do not expressed any SHP-1 or expressed catalytic inactive form of SHP-1, which results in autoantibody production with early mortality due to pneumonitis and inflammatory lesion found in various organs. In contrast, heterozygous mice live longer and exhibits an increased incident of lymphoma development with minimal symptoms of autoimmune disease. Using bone marrow-mast cells isolated from *motheatean* mice was shown, that SHP-1 plays a negative regulatory role in FcεRI-induced activation of mitogen-activated protein kinases (MAPKs), cytokine gene transcription and production of cytokines, whereas the phosphorylation of phospholipase C, calcium mobilization and degranulation are positively regulated by SHP-1 [94]. Moreover, SHP-1-defficient mice exhibit enhanced ovalbumin-induced airway inflammation and anaphylactic response including hypothermia. This data suggest a direct role of SHP-1 in regulating Th2 immune response in the lung and inhibitory role in regulation of allergic inflammation and allergen-induced anaphylaxis in mice [95, 96]. However, there is inconsistent report investigated rat basophil leukemia cells, where function of SHP-1 seems to be rather a positive regulator of TNF-α production via JNK activation, although in vivo studies shows the opposite effect. SHP-1 expressed in mast cells interacts with ITAMs of FcεRI β and γ subunits, SYK kinase, SLP-76-related adaptors, VAV and PI3´kinase [97-101].

In humans, reduced expression of SHP-1 is associated with some leukemia and lymphoma cell lines, due to inability of SHP-1 antagonized activity of transcription factor STAT5 which becomes hyperphosphorylated. This raises the question about the molecular mechanism and exact role of SHP-1 and STAT5 in the pathogenesis of leukemia. Studies on phospholipase Cβ3 knockout (PLCβ3-KO) mice, which suffer

with chronic myelomonocytic leukemia (CMML)-like disease shows, that PLCβ3 functions as a scaffolding protein for STAT5 and SHP-1 molecules and thus allows SHP-1 dephosphorylates and inactivates STAT5 [1, 102]. In mast cells, function of PLCβ3-SHP-1-STAT5 signalosome was studied in respect with FcεRI-dependent immune response. It was shown, that PLCβ3-KO mice exhibits mast cell dependent late-phase, but not acute, anaphylactic reaction accompanied by elevated cytokine production, but normal degranulation. Molecular mechanism of this events based on abrogated phosphorylation of SHP-1 at Y536 and Y564, resulting in constitutive activation of STAT5. Furthermore, LYN kinase, the only one member of SFKs possessing KTIM motive, which is recognized by SHP-1 [103], was identified as an indispensable kinase for maximal SHP-1 phosphatase activity [104].

Activation signals in mast cells are strictly counterbalanced by another negative signaling molecules such as SHIP1. SHIP1 (SH2-containing inositol polyphosphate 5´-phosphatase specific for hematopoietic cells) is a lipid phosphatase playing crucial role in mast cells, B cells and macrophages signaling [105]. In mast cells, SHIP1 is well known as a master negative regulator of degranulation and cytokines production through FcεRI-mediated activation. This is attributed to its ability to hydrolyze the 5´phosphate of PIP3, a second messenger generated in activated cells by PI3K. SHIP1 binds via its SH2 domain to the tyrosine phosphorylated ITIM of FcγRII. B cells deficient in SHIP-1 were enhanced antigen receptor activation, elicited calcium fluxes and activation ERK and AKT pathway [106].

Phosphatases play an important role not only in setting activation threshold of mast cells by removal of aggregated FcεRI but also in the regulation of several signal transduction molecules. Numerous PTPs have recently been found in mast cell signaling and may explain some of the pending questions in mast cell signaling [104].

4.4 FcεRI-MEDIATED SIGNALING PATHWAYS

4.4.1 Initiation of FcεRI signaling

In mast cell, LYN the major SFK, is involved in the initial stages of FcεRI-mediated signaling. Several model have been proposed to explain mechanistically how the FcεRI becomes phosphorylated by LYN (Figure 9). The first, transphosphorylation

model assumes, that in resting cells non-phosphorylated FcεRI β subunits is non-covalently associate with LYN which is unable phosphorylate its carrier receptor. Aggregation of the IgE-FcεRI complexes with multivalent antigen initiates LYN-dependent phosphorylation of the neighboring receptor within the aggregate. This process is called transphosphorylation. This model was supported by several experimental finding [107-110], however, in conflict with this theory was shown, that aggregated FcεRI is becomes phosphorylated, even in the absence of β subunits [111] and next, that chimeric receptor possess only γ subunit of the FcεRI becomes phosphorylated upon activation [112]. Therefore, the next model takes into consider the observation that biological membranes are composed of microdomains having a lipidic cholesterol- and sphingomyelin-rich structure with the presence of limited set of proteins.

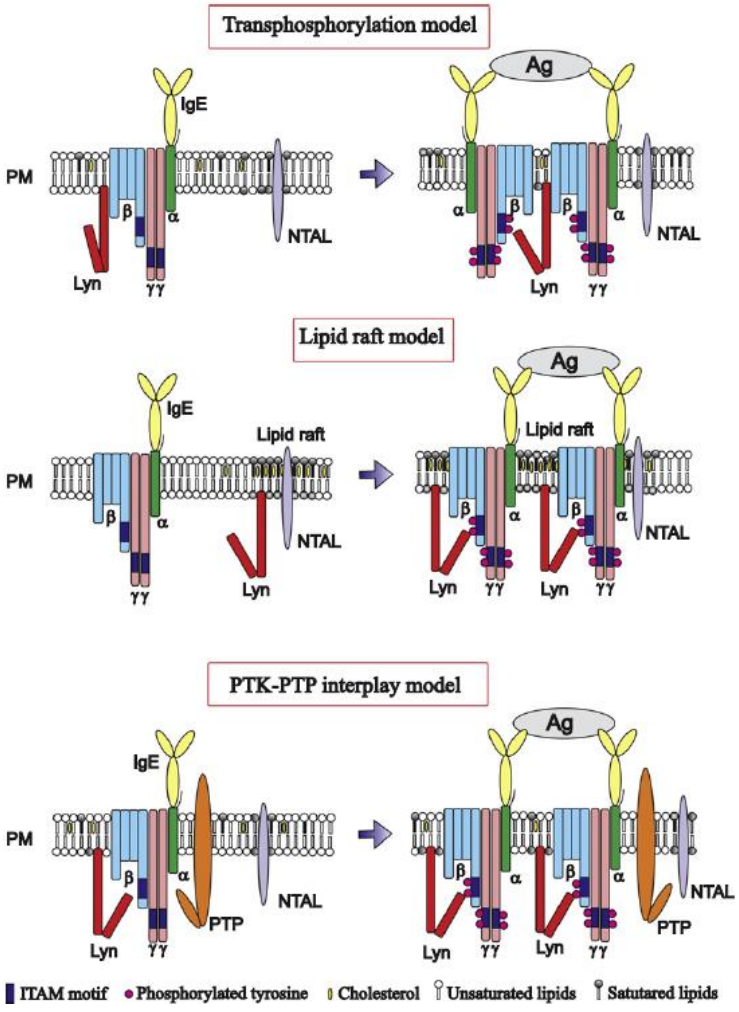

Figure 9. Models of FcεRI phosphorylation. Transphosphorylation model presumes that active Lyn is constitutively associated with non-phosphorylated FcεRI; upon FcεRI aggregation, Lyn phosphorylates

adjacent receptors in the aggregate. Lipid raft model postulates that FcεRI and Lyn are localized in different plasma membrane microdomains; after aggregation FcεRI is translocated to lipid rafts where it is phosphorylated by lipid raft-associated Lyn kinase. PTK–PTP interplay model assumes that PTPs set the threshold of FcεRI tyrosine phosphorylation; after FcεRI triggering there is a shift in the PTK–PTP steady state in favor of PTKs Adapted from [113].

In this lipid raft model was postulated that FcεRI in resting cells is physically separated from active LYN kinase present in lipid raft domains. After aggregation, the FcεRI translocated to the lipid raft microdomain and then LYN associates with its β subunits, which in turn leads to the receptor phosphorylation. In attempt to explain some conflicting experimental data of lipid raft model, the third PTK-PTPs-interplay model was postulated. This model raised from experimental data on B cells, where extent of immunoreceptor phosphorylation is not depend only on PTKs but, at least, partly also on the activity of PTPs [113].

4.4.2 Signaling pathways leading to degranulation

Cross-linking of the IgE-FcεRI complexes by multivalent antigen result in phosphorylation of the immunoreceptor tyrosine-based motifs (ITAMs) in the cytoplasmic tails of the FcεRI β and γ subunits by LYN kinase. When phosphorylated, ITAM of β and γ subunits provide high-affinity docking site for binding another molecules of LYN and SYK through their Src homology SH2 domains. SYK upon binding to receptor changed its conformation to active and became phosphorylated by LYN. As shown in Figure 10, SYK and LYN then phosphorylated several targets molecules, including adaptor proteins LAT and NTAL, which is crucial for coordination of the downstream signal pathways that are required for calcium release, degranulation and activation of transcription factors. Phosphorylated LAT serve as a direct binding partners for various signaling molecules possessing SH2-binding domain, including PLCγ, GRB2, GADS, and SHIP1. Activated PLCγ then catalyze hydrolysis of the membrane phosphatidylinositol-4,5-bisphosphate to generate two second messengers, soluble inositol-1,4,5-trisphosphate and the membrane bound diacylglycerol, which induced intracellular calcium mobilization and protein kinase C (PKC) activation, respectively. Formation of GRB2-SOS-VAV signalosomes is accompanied by activation of the small GTPases, Ras, Rac, Rho and ERK that control activation of transcription factors. Studies carried out in mast cells isolated from LAT-KO mice

showed decreased calcium mobilization, degranulation and production of transcription factors due impaired LAT-regulated PLCγ activation [50]. However, LAT deficiency in T cells results in absolutely impaired immunoreceptor signaling, in mast cells was still observable residual calcium mobilization, degranulation and cytokine production. This residual signal is based on NTAL-dependent signalization which partially compensate loss of LAT. On the other hand, NTAL possess tyrosines which are directly phosphorylated by LYN and as well as by SYK. In contrast to LAT, NTAL did not possess direct binding site for PLCγ, however could modulate calcium signaling indirectly via PI3 signaling pathway. When NTAL is missing, LAT becomes more phosphorylated, which results in enhanced binding of PLCγ and activation of various PLCγ-dependent pathways [15, 52].

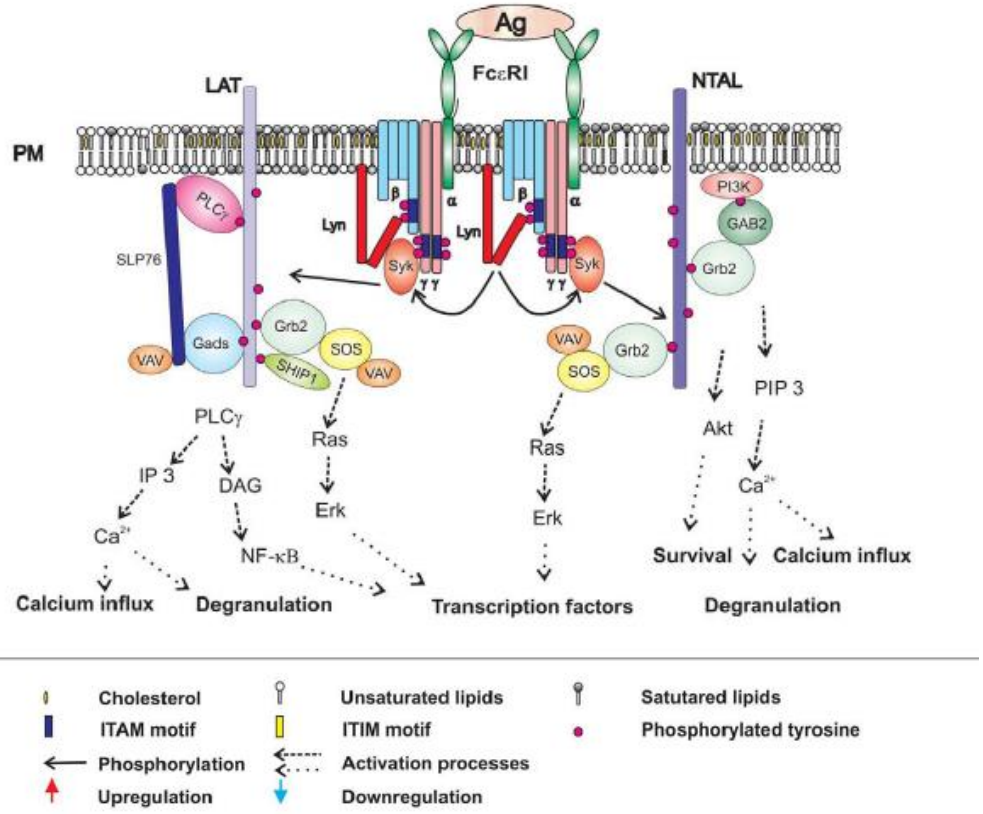

Figure 10. FcεRI-mediated signaling events in WT mast cells. Downstream signaling pathway in antigen-mediated signaling include activation of SFKs, such as LYN and SYK, which phosphorylates adaptor proteins LAT and NTAL. Phosphorylated LAT directly binds PLCγ and GADS, which formed complex with SLP-76 and VAV. On the other hand, NTAL binds GRB2 and several another signaling molecules with exception of PLCγ. These events regulate complex signaling networks leading to calcium mobilization, degranulation and activation of transcription factors [50].

NTAL-KO cells exhibited enhanced phosphorylation of LAT, PLCγ1, PLCγ2, extracellular signal-regulated kinase (ERK), calcium mobilization, degranulation, and cytokines production. Interestingly, mast cells lacking both LAT and NTAL exhibited a stronger block in FcεRI signaling than LAT-KO mast cells, demonstrating that NTAL could play both positive and negative roles in FcεRI signaling [114, 115].

4.4.3 Signaling pathways leading to cytokine production

Cross-linking of the IgE-FcεRI complexes by multivalent antigen leads to activation of numerous PTKs, PTPs, adaptor proteins and other signaling molecules results in the formation of a macromolecular signaling complexes, which allows the diversification of downstream signaling that is required for the production of the numerous pro-inflammatory mediators. As in degranulation, production of cytokines is reduced in mast cells with LAT-KO, however the exact mechanism that leads from LAT to cytokine production has been less defined as in degranulation. It was reported, that gene expression and production of cytokines and eicosanoids, including LTC_4 and PGD_2, initiate by activation of VAV and SOS follows the activation of RAS, which positively regulates RAF signaling pathway and subsequently activate ERK1, ERK2, JNK, and P38 [52]. These molecules, in turn, activates various transcription factors, including activator protein 1 (AP1), FOS and JUN, nuclear factor of activated T cells (NFAT) and nuclear factor-κB (NF-κB). This pathway is directed by PLCγ-dependent calcium signalization. In this connection, parallel signaling pathway initialize by activation of PI3K and AKT is involved in regulation of cytokine production. AKT positively regulates the function of transcription factor NF-κB by phosphorylating inhibitor of NF-κB (IκB) [116]. However, exact mechanism of activation specific signaling factors for cytokine gene expression require further study. Another recent mast cells study showed, that PLCβ3 can form multimolecular complex together with SHP-1 and STAT5 and in LYN-dependent manner regulate cytokines production, but interestingly, not degranulation [102, 104]. In mast cell, STAT5 pathway could be positively regulated by FYN kinase after FcεRI engagement which leads to selectively dependent production of cytokines via STAT5B, but not through STAT5A isoform [117].

4.4.4 Signaling pathways leading to chemotaxis

The crucial signal for mast cells progenitors homing and mature mast cell recruitment into peripheral tissue where the inflammation takes place is directed by several chemical compounds named chemoattractant [118]. A potent mast cell chemoattractant acting in autocrine/paracrine fashion is antigen, which binds to IgE recognized by FcεRI (Figure 11) [119].

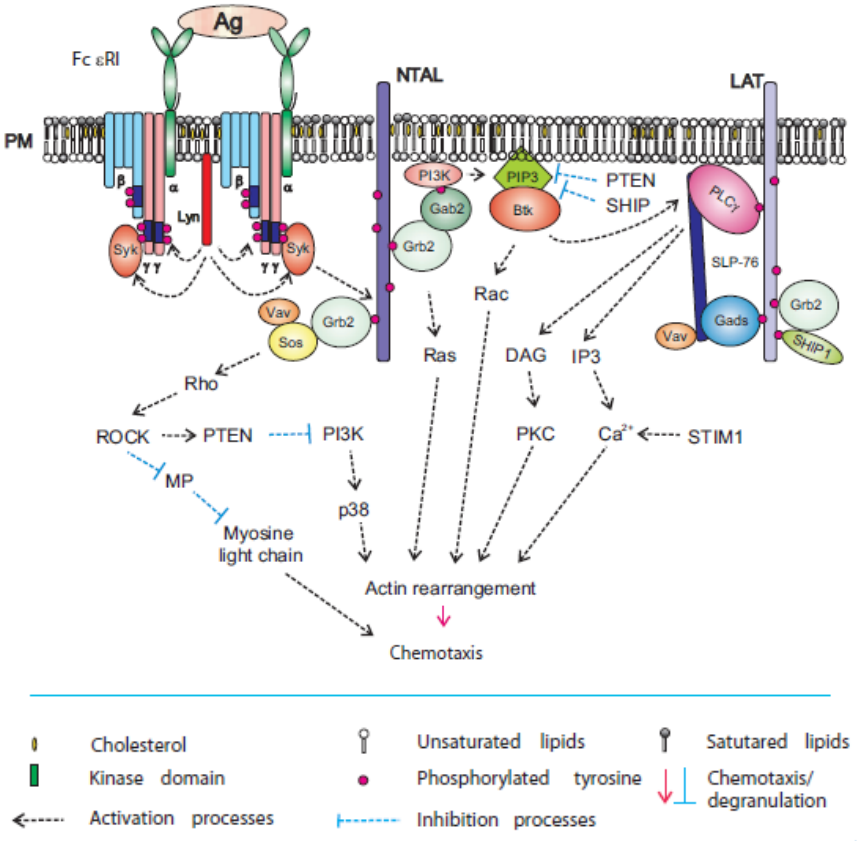

Figure 11. FcεRI-mediated chemotaxis. Adapted from [39].

Antigen-induced chemotaxis is initialized by aggregation of the FcεRI by multivalent antigen. This leads to rapid Lyn kinase-mediated phosphorylation of tyrosine residues in ITAM motifs of the FcεRI β and γ subunits and is followed by anchoring of SYK to FcεRI γ through interaction of SYK SH2 domains with phosphorylated ITAMs. SYK then phosphorylates transmembrane adaptor proteins NTAL and LAT and creates binding sites for various SH2-containing proteins like

GRB2. In this way it brings PI3K and GAB2 to the plasma membrane. Activated PI3K generates PIP3, a binding site for PH-domain containing protein BTK [119].

This leads to further propagation of the signal through activation of PLCγ, resulting in Ca^{2+} release and actin rearrangement. Levels of free intracellular Ca^{2+} are positively regulated by aggregated STIM1. Another PI3K-dependent pathway contributes to activation of p38 and consequently to enhanced chemotactic response. GRB2 orchestrates activation of Ras by recruiting small GTPases Ras and Rho family, SOS, VAV, and other signaling molecules, resulting in actin rearrangement and chemotaxis. NTAL could play a negative regulatory role in chemotaxis through activation of Rho/ROCK pathway that is responsible for controlling cell migration. ROCK could also activate the PTEN phosphatase which inhibits activity of PI3K and in this way decreases the PIP3 levels [39].

5 AIMS

The aim of this thesis was to contribute to deeper understanding, in molecular terms, of the FcεRI-mediated signaling pathways leading to mast cell activation, degranulation and cytokines production. Particularly, we aimed to comprehend the role of PAG and CSK at the earliest stages of mast cell activation and their impact on inflammation and/or anaphylaxis. The second challenge of this thesis was to investigate the role of selected proteins (ORMDL3, CD9) or chemical compounds on mast cell activation *in vitro* as well as *in vivo*. Integral part of these studies, at initial period, was to develop a new method for simplified and sensitive detection of biologically important molecules, and use this method subsequently through these studies.

The specific objectives of this thesis were:

1. **To determine the role of PAG in production of cytokines in activated mast cells *in vitro* and *in vivo***
    a. To determine the role of PAG in production of TNF-α, IL-13 and IL-6
    b. To quantify the level of IgE in serum of PAG-KO mice

2. **To determine the regulatory roles of CSK in antigen-induced mast cell signaling**
    a. To produce BMMCs with CSK-KD or CSK-OE
    b. To determine the role of CSK in FcεRI-mediated degranulation
    c. To elucidate the role of CSK in FcεRI -mediated Ca^{2+} response
    d. To determine the role of CSK in FcεRI -mediated production of proinflammatory cytokines and chemokines
    e. To examine the role of CSK in internalization of Ag-IgE-FcεRI complexes
    f. To elucidate the role of CSK in chemotaxis and adhesion on fibronectin
    g. To determine the role of CSK in FcεRI -induced tyrosine phosphorylation of early signaling proteins
    h. To determine the role of CSK-PAG cross-talk in FcεRI-mediated mast cell activation

3. To contribute to understanding of the role of ORMDL3 in FcεRI-mediated activation

a. To prepare BMMCs with ORMDL3-KD using short hairpin (sh)RNA lentiviral strategy
b. To produce ORMDL3-myc constructs for generation of ORMDL-OE
c. To determine the role of ORMDL3 in production of proinflammatory cytokines

4. To contribute to understanding the role of FcεRI-cholesterol signalosome under *in vivo* conditions

To determine effect of ethanol on FcεRI-mediated degranulation under *in vivo* conditions using PCA

5. To contribute to understanding the role of CD9 in FcεRI-mediated activation

a. To purify a CD9-specific monoclonal antibody (mAb)
b. To prepare BMMCs with CD9-KD using shRNA lentiviral strategy

6. To develop a new method for detection of cytokines and other proteins in complex biological samples

a. To find conditions for production of gold nanoparticles functionalized with antibodies and oligonucleotides and to set the protocols for sensitive detection of various proteins
b. To compare the sensitivity of newly developed gold nanoparticle-based-iPCR (nano-iPCR) with standard enzyme-linked immuno-sorbent assays (ELISAs) and immuno-PCR (iPCR).
c. To verify the nano-iPCR for detection of biologically important proteins, such as pro-inflammatory cytokines or tau protein in complex biological fluids.

6 SUMMARY OF METHODS

All methods used to solve the particular aims of this study are described in more details in the Materials and Methods section of the relevant publications (Chapter 7).

BMMCs generation and cultivation

Bone marrow cells were isolated from the femurs and tibias of 6- to 8-week-old PAG-KO mice or their WT littermates. Cells were cultured in RPMI 1640 medium supplemented with 100 U/ml penicillin, 100 μg/ml streptomycin, 71 μM 2-mercaptoethanol, minimum essential medium (MEM) nonessential amino acids, 0.7 mM sodium pyruvate, 2.5 mM l-glutamine, 12 mM d-glucose, recombinant mouse SCF (15 ng/ml), mouse recombinant IL-3 (15 ng/ml), and 10% fetal bovine serum. In some experiments 5% WEHI supernatant and 5% CHO supernatant were used insted of recombinant proteins.

BMMCs sensitization and activation

BMMCs were cultured for 48 h in medium without SCF (only for PAG study), followed by incubation for 4-12 h in SCF- and IL-3-free medium supplemented with IgE (1 μg/ml). Sensitized cells were washed in buffered salt solution (BSS; 20 mM HEPES, pH 7.4, 135 mM NaCl, 5 mM KCl, 1.8 mM $CaCl_2$, 5.6 mM glucose, 1 mM $MgCl_2$, 0.1% BSA).

Degranulation (β-glucuronidase) assay

To quantify degranulation, the cells (0.2×10^6) in 30-μl aliquots were transferred into the wells of a 96-well plate and challenged with 30 μl of antigen, thapsigargin, or SCF at the various concentrations. Degree of degranulation was quantified as amount of β-glucuronidase released into the supernatant. Briefly, 40-μl aliquots of the cell supernatants were mixed in white wells of a 96-well plate (Nunc) with 40 μl of β-glucuronidase substrate (40 μM 4-methylumbelliferyl-β-d-glucuronide hydrate). After incubation, the reaction was stopped by adding 0.2 M glycine buffer, pH 10.0, and fluorescence was determined in an Infinite M200 microtiter plate reader (Tecan) with 355-nm excitation and 460-nm emission filters. The total content of the enzyme in the

cells was evaluated by measuring the levels of enzyme in the supernatant from cells lysed in 1% Triton X-100.

Calcium release assay

Calcium response was analyzed in IgE-sensitized BMMCs using Fura-2-AM cytoplasmic reporter. Levels of intracellular Ca^{2+} were determined by spectrofluorometry using the Infinite 200 M plate reader with excitation wavelengths at 340 and 380 nm and with a constant emission at 510 nm.

Cell adhesion

Adhesion to fibronectin was quantified in 96-well plates coated overnight with fibronectin (10 µg/ml in PBS), blocked with 4% BSA in PBS and washed twice with PBS. IgE-sensitized BMMCs were loaded with Calcein-AM for 30 min at 37°C, washed and transferred into the fibronectin-coated wells. After activation with antigen or SCF, unbound cells were washed out using microplate washer (HydroSpeed, TECAN) and bound cells were determined using an Infinite 200M Fluorimeter with excitation and emission filters at 485 nm and 538 nm, respectively.

Flow cytometry

To quantify the surface expression of FcεRI and c-KIT, BMMCs were double-stained with anti-mouse FcεRI-FITC and anti-mouse c-KIT-allophycocyanin antibodies for 30 min on ice. After labeling, the cells were washed with ice-cold PBS and analyzed with an LSRII flow cytometer and further processed using FlowJo software. For analysis of surface LAMP1, BMMCs were activated or not with various concentrations of antigen. Activation was stopped by centrifugation at 4°C. The cells were then resuspended in PBS-1% BSA containing 200-fold-diluted V450-conjugated rat anti-mouse CD107a and stained on ice for 30 min. To analyze IgE internalization, IgE-sensitized cells were activated with antigen and fixed by 4% paraformaldehyde. IgE was stained using AF488-conjugated anti-mouse IgG (cross-reacting with IgE) and analyzed as described above.

Immunoblotting

Whole-cell extracts from nonactivated or Ag-activated BMMCs were prepared by solubilizing of cell pelletes in sodium dodecyl sulphate (SDS) sample buffer, followed

by sonication and boiling. Proteins were size fractionated on 10% SDS-polyacrylamide (PAGE) gel electrophoresis, electrophoretically transferred onto nitrocellulose membrane, and analyzed by immunoblotting with protein- or phosphoprotein-specific antibodies and detected with HRP-conjugated secondary antibodies. The HRP signal was detected with chemiluminescence reagent and quantified by a Luminescent Image Analyzer LAS 3000. Aida software was used for signal quantification. Protein levels were normalized to the corresponding controls and/or GRB2 loading control protein after stripping of the membrane in stripping buffer.

Immunoprecipitation

For FcεRI immunoprecipitation, cells were solubilized in ice-cold immunoprecipitation buffer supplemented with 0.2% Triton X-100. After incubation on ice for 30 min, the lysates were centrifuged and postnuclear supernatants were immunoprecipitated with rabbit anti-IgE antibody prebound to UltraLink-immobilized protein A. The immunoprecipitated proteins were size-fractionated by SDS-PAGE as described above, transferred to nitrocellulose membrane and immunoblotted with phosphotyrosine-specific mAb PY20 conjugate or with FcεRI-β chain-specific antibody followed by HRP-conjugated anti-mouse IgG.

Cloning

Several mammalian expression vectors were prepared in the course of these studies using standard cloning techniques. cDNA of proteins of interest were purchase from various vendors or were kindly provided by other researchers from Institute of Molecular Genetics in Prague. cDNA containing mCherry or myc-tag was then inserted into pCDH-based lentiviral vectors. All constructs were verified by sequencing.

Lentiviral vectors and gene transduction

Lentiviral transductions were done using HEK 293 T/17 packaging cells for virus preparation. A set of four murine CSK-specific shRNAs constructs based on pLKO.1 vector were purchased from Open Biosystems. Cells were transduced with individual shRNAs or with a pool of shRNAs prepared by mixing shRNAs in equimolar ratios. Individual constructs or pool of the constructs (14 µg) was mixed with OptiMEM, 21 µl of lentiviral packaging mix (Invitrogen), and 105 µl polyethyleneimine. Then, supernatant containing virus was collected in 48h and 72h of HEK 293 T/17 cultivation,

filtered in 0.2 membranes, and added to BMMCs. Positive selection of BMMCs were achieved by incubation with 4μg/ml puromicin.

Detection of cytokines by Nano-iPCR

Briefly, anti-TNF-α, anti-IL-6, or anti-IL-13 in 100 mM borate buffer (pH 9.5) was dispensed in 50-μl aliquots into the wells of a real-time PCR 96-well plate. After overnight incubation at 4°C, each well was washed and the remaining binding sites were blocked by 2 h of incubation at 37°C with TBST supplemented with 2% BSA. After washing, serial dilutions of recombinant TNF-α, IL-6, or IL-13 (used for construction of calibration curves) or the tested samples diluted in PBS–1% BSA was added. The samples were incubated for 1 h at 37°C, and after washing with TBST, 50 μl of Au-NPs armed with thiolated DNA oligonucleotide template and with the corresponding cytokine-specific antibody was applied into each well. Fifty-microliter aliquots of qPCR master mix solution supplemented with the corresponding oligonucleotide primers were then dispensed into each well. The plates were sealed, and the amount of template DNA bound to antigen-anchored functionalized gold nanoparticles was evaluated by real-time PCR. For calculation of cytokines concentrations, the corresponding Ct values of the cytokines were substituted into the regression equations obtained from the calibration curves constructed from the concentration series of appropriate recombinant proteins.

Detection of cytokines and α-tubulin by iPCR

Twenty-five microliter aliquots of capture anti-tubulin antibody DM1A (5 μg/ml) in 100 mM borate buffer (pH 9.5) were dispensed into each well of TopYield strips. The wells were incubated for 2 h at 37 °C and washed with TBST. Free binding sites were blocked with BSA/TBS. After 2 h at 37 °C, the strips were washed, followed by adding of standards or tested samples diluted in 1% BSA in PBS. The strips were further incubated for 1 h at 37 °C and then overnight at 4 °C, followed by four washings. Subsequently, 25 μl aliquots of biotinylated anti-tubulin antibody TU-07 (1 μg/ml in TBS–1% BSA) were added and the samples were incubated for 1 h at 37 °C. After washing, the wells were filled with extravidin (0.1 μg/ml) in TBS–1% BSA, incubated for 1 h at 37 °C and then washed as before. The next step consists in the addition of 25 μl of biotinylated DNA template (0.27 pg/ml). The strips were then incubated for 1 h at 37 °C followed by washing with TBST and with MilliQ water. Template DNA immobilized on antigen in the wells was quantified by real-time PCR using Realplex4 Mastercycler.

Detection of SCF and IL-3 by ELISA

Wells of the TopYield or NUNC strips were coated with Ag-specific polyclonal antibody, blocked with TPBS-2% BSA and then mixed with antigen as described above for iPCR. The wells were then washed with TPBS, followed by addition of biotinylated antibody (1 μg/ml, in TPBS-1% BSA), incubation for 1 h at 37 °C and washing with TPBS. One hundred microliters of streptavidin-horseradish peroxidase (HRP) conjugate was then added. After incubation for 1 h at 37 °C the wells were washed with TPBS. Finally, 100 μl PBS containing o-phenylenediamine (OPD) and H_2O_2 (0.015%) was dispensed into each well. After 10 min at 37 °C, the reaction was stopped by adding 100 μl of H_2SO_4 (4 M). The absorbance was determined at 492 nm using Infinite M200 plate reader.

Detection of IgE in mouse serum by ELISA

96-wells plate were coated with rat antibody specific for mouse IgE (1 μg/ml in PBS). Wells were washed and blocked by TBST–2% BSA. After 2 h, the plates were washed and incubated with various concentrations of mouse IgE standard or mouse serum samples. Then, the wells were washed and the captured IgE was detected with biotinylated rat anti-mouse IgE antibody (2 μg/ml in PBS–1% BSA), then washed, and incubated for 30 min with streptavidin-HRP conjugate. Peroxidase substrate solution was used for colorimetric reaction. The reaction was stopped by adding 4 M H_2SO_4, and the absorbance at 492 nm was determined using an Infinite M200 plate reader (Tecan).

PCA

Mice were anesthetized by intraperitoneal injection of a cocktail containing ketamine xylazine and atropine and then sensitized by intradermal injection of anti-TNP-specific IgE in PBS into the left ear; the right ear was injected with PBS alone. Twenty-four hours later, dilution series of ethanol in PBS was injected intraperitoneally (0.5 ml per mouse weighing 20 g). One hour after ethanol in PBS or PBS alone injection, each mouse was challenged with an intravenous injection of antigen containing 1% Evans blue. The mice were sacrificed 30 min later and their ears were removed for measurement of the amount of the Evans blue extravasated. The dye was extracted from tissue with formamide and absorbance of supernatants was determined at 620 nm.

7 RESULTS

7.1 LIST OF PUBLICATIONS

Publication included as a part of this doctoral thesis

1. Dráberová L., Bugajev V., **Potůčková L**., Hálová I., Bambousková M., Polakovičová I., Xavier R. J., Seed B., Dráber P.: Transmembrane adaptor protein PAG/CBP is involved in both positive and negative regulation of mast cell signaling. *Mol. Cell. Biol*. **34**(23):4285-300, 2014.

2. **Potuckova L**., Draberova L., Halova I., Paulenda T., Draber P.: C-terminal Src kinase regulates FcεRI activation leading to degranulation and cytokines/chemokines production in opposite ways, independently of the transmembrane adaptor protein PAG. Manuscript, 2017.

3. Bugajev V., Hálová I., Dráberová L., Bambousková M., **Potůčková L**., Dráberová H., Paulenda T., Junyent S., Dráber P.: Negative regulatory roles of ORMDL3 in the FcεRI-triggered expression of proinflammatory mediators and chemotactic response in murine mast cells. *Cell. Mol. Life Sci.* **73**(6):1265-85, 2016.

4. Dráberová L., Paulenda T., Hálová I., **Potůčková L**., Bugajev V., Bambousková M., Tůmová M., Dráber P.: Ethanol inhibits high-affinity immunoglobulin E receptor (FcεRI) signaling in mast cells by suppressing the function of FcεRI - cholesterol signalosome. *Plos One*. **10**(12):e0144596, 2015.

5. Hálová I., Dráberová L., Bambousková M., Machyna M., **Stegurová L**., Smrž D., Dráber P.: Cross-talk between tetraspanin CD9 and transmembrane adaptor protein non-T cell activation linker (NTAL) in mast cell activation and chemotaxis. *J Biol. Chem*., **288**(14):9801-14, 2013.

6. **Stegurová L**., Dráberová E., Bartos A., Dráber P., Rípová D., Dráber P.: Gold nanoparticle-based immuno-PCR for detection of tau protein in cerebrospinal fluid. *J. Immunol. Methods*, **406**:137-42, 2014.

7. Dráberová E., **Stegurová L**., Sulimenko V., Hájková Z., Dráber P., Dráber P.: Quantification of α-tubulin isotypes by sandwich ELISA with signal amplification through biotinyl-tyramide or immuno-PCR. *J. Immunol. Methods*, **395**(1-2):63-70, 2013.

8. **Potůčková L**., Franko F., Bambousková M., Dráber P.: Rapid and sensitive detection of cytokines using functionalized gold nanoparticle-based immuno-PCR, comparison with immuno-PCR and ELISA. *J Immunol. Methods*, **371**(1-2):38-47, 2011.

7.2 TRANSMEMBRANE ADAPTOR PROTEIN PAG/CBP IS INVOLVED IN BOTH POSITIVE AND NEGATIVE REGULATION OF MAST CELL SIGNALING.

Dráberová L., Bugajev V., **Potůčková L.**, Hálová I., Bambousková M., Polakovičová I., Xavier R. J., Seed B., Dráber P.

Mol. Cell. Biol., 34(23):4285-4300, 2014

MCB
Journals.ASM.org

Transmembrane Adaptor Protein PAG/CBP Is Involved in both Positive and Negative Regulation of Mast Cell Signaling

Lubica Draberova,[a] Viktor Bugajev,[a] Lucie Potuckova,[a] Ivana Halova,[a] Monika Bambouskova,[a] Iva Polakovicova,[a] Ramnik J. Xavier,[b,c] Brian Seed,[b] Petr Draber[a]

Department of Signal Transduction, Institute of Molecular Genetics, Academy of Sciences of the Czech Republic, Prague, Czech Republic[a]; Center for Computational and Integrative Biology, Massachusetts General Hospital, Harvard Medical School, Boston, Massachusetts, USA[b]; Broad Institute of Harvard University and Massachusetts Institute of Technology, Cambridge, Massachusetts, USA[c]

The transmembrane adaptor protein PAG/CBP (here, PAG) is expressed in multiple cell types. Tyrosine-phosphorylated PAG serves as an anchor for C-terminal SRC kinase, an inhibitor of SRC-family kinases. The role of PAG as a negative regulator of immunoreceptor signaling has been examined in several model systems, but no functions *in vivo* have been determined. Here, we examined the activation of bone marrow-derived mast cells (BMMCs) with PAG knockout and PAG knockdown and the corresponding controls. Our data show that PAG-deficient BMMCs exhibit impaired antigen-induced degranulation, extracellular calcium uptake, tyrosine phosphorylation of several key signaling proteins (including the high-affinity IgE receptor subunits, spleen tyrosine kinase, and phospholipase C), production of several cytokines and chemokines, and chemotaxis. The enzymatic activities of the LYN and FYN kinases were increased in nonactivated cells, suggesting the involvement of a LYN- and/or a FYN-dependent negative regulatory loop. When BMMCs from PAG-knockout mice were activated via the KIT receptor, enhanced degranulation and tyrosine phosphorylation of the receptor were observed. *In vivo* experiments showed that PAG is a positive regulator of passive systemic anaphylaxis. The combined data indicate that PAG can function as both a positive and a negative regulator of mast cell signaling, depending upon the signaling pathway involved.

Mast cells are widely distributed in the body, where they play important roles in innate as well as adaptive immune responses (1). To fulfill their role in adaptive immune responses, the cells express the high-affinity IgE receptor FcεRI on their plasma membranes. Aggregation of this tetrameric immunoreceptor, αβγ2, induces cell signaling events leading to the release of preformed inflammatory mediators and the *de novo* synthesis and release of leukotrienes, cytokines, and chemokines. The first well-defined biochemical step after FcεRI triggering is tyrosine phosphorylation of the immunoreceptor tyrosine-based activation motifs in the cytoplasmic tail of the FcεRI β and γ subunits by the SRC family protein tyrosine kinase (PTK) LYN (2, 3). The phosphorylated β and γ subunits then serve as binding and activation sites for LYN kinase and spleen tyrosine kinase (SYK), respectively. These two enzymes, together with FYN and other kinases, then phosphorylate various adaptor proteins and enzymes with a variety of functions in signal transduction pathways. The exact molecular events preceding LYN-mediated tyrosine phosphorylation of the FcεRI β subunit are not clear, and several models have been proposed, including the transphosphorylation model (4), the lipid raft model (5), and the PTK-protein tyrosine phosphatase (PTP) interplay model (6).

Our previous study with murine bone marrow-derived mast cells (BMMCs) showed that FcεRI triggering induced transient hyperphosphorylation of LYN kinase on its C-terminal regulatory tyrosine (Tyr 487), leading to the formation of a closed inactive conformation where the SRC homology 2 (SH2) domain interacts with phospho-Tyr 487 and transiently decreases LYN enzymatic activity (7). This finding was surprising because in T cells the corresponding SRC family kinase (SFK), LCK, showed decreased tyrosine phosphorylation of the C-terminal regulatory tyrosine and enhanced enzymatic activity after activation through T cell immunoreceptors (8, 9). Phosphorylation of the C-terminal inhibitory tyrosine in SFKs is catalyzed by the C-terminal SRC kinase (CSK) (10), a cytoplasmic PTK that can be anchored through its SH2 domain to PAG (11), also termed CBP (12). PAG/CBP (here, PAG) is a ubiquitously expressed transmembrane adaptor protein containing a short extracellular domain, a transmembrane domain, and a long cytoplasmic tail with multiple tyrosine-based motifs. Phosphorylated Tyr 314 in mouse PAG has been shown to be essential for CSK binding. PAG also possesses two proline-rich sequences that serve as binding sites for proteins with SH3 domains and a C-terminal VTRL motif for interaction with the PDZ domain of the cytoskeletal linker ezrin/radixin/moesin-binding protein of 50 kDa (13). Similar to some other transmembrane adaptor proteins, such as the non-T cell activation linker and linker for activation of T cells (LAT), PAG has two conserved cysteine residues, located in the vicinity of the transmembrane domain, which are the subject of posttranslational palmitoylation and which contribute to the poor solubility of the proteins in nonionic detergents and their presumed localization in membrane microdomains called lipid rafts (14, 15).

PAG in resting T cells associates with FYN kinase, which constitutively phosphorylates PAG on Tyr 314 to create a docking site for the CSK SH2 domain. This binding brings CSK to the vicinity of its substrate, SFK LCK, and enhances CSK catalytic activity, leading to phosphorylation of the LCK-inhibitory C-terminal tyrosine. Upon T cell receptor activation, PAG is rapidly dephospho-

Received 25 July 2014 **Accepted** 13 September 2014
Published ahead of print 22 September 2014
Address correspondence to Petr Draber, draberpe@img.cas.cz.

doi:10.1128/MCB.00983-14

rylated, CSK is released from PAG, and LCK is dephosphorylated on its C-terminal tyrosine. This modification increases the activity of LCK, leading to increased tyrosine phosphorylation of T cell receptor subunits and other substrates. A negative regulatory role of PAG in T cell signaling was confirmed in experiments with PAG knockdowns (KDs) (16) but not with PAG knockouts (KOs) (17, 18), suggesting that developmental compensatory mechanisms are involved.

In mast cells, PAG is phosphorylated by LYN kinase instead of FYN kinase, and following FcεRI triggering, the decrease in PAG phosphorylation is replaced by an increase (19, 20). Overexpression of PAG has been reported to inhibit FcεRI-mediated degranulation in rat basophilic leukemia (RBL) cells (21). Further experiments showed that FcεRI activation of BMMCs from LYN-deficient mice resulted in enhanced degranulation, whereas FYN-deficient cells showed the opposite effect (22–24). This finding supports the concept that SFKs are tightly regulated in the course of mast cell activation and important differences exist between early regulatory events induced by engagement of the T cell receptors and FcεRI. The exact role of PAG in mast cell activation remains to be determined.

Herein we present data on FcεRI-mediated activation events in BMMCs derived from mice deficient in PAG (PAG-KO mice) and from the corresponding wild-type (WT) mice (PAG-WT mice). We also attempted to determine whether any differences in activation are detectable between BMMCs in which PAG is downregulated by RNA interference and the corresponding control cells. Furthermore, we examined the role of PAG in cells activated through another important mast cell surface receptor, KIT. The combined data indicate that PAG functions as a positive or negative regulator of mast cell signaling and that the specific effect depends on the particular signaling pathway. We also show that PAG-deficient mice have a distinct phenotype *in vivo*, as assessed by induction of a passive systemic anaphylaxis response.

MATERIALS AND METHODS

Mice and cells. Mice deficient in PAG were generated by use of a modified bacterial artificial chromosome technology as previously described (25, 26). Briefly, the bacterial artificial chromosome clones were electroporated into strain 129Sv/J embryonic stem cells. Targeting in clone 7 was confirmed by fluorescence *in situ* hybridization. PAG-KO mice derived from clone 7 were born in the expected Mendelian frequency and were healthy. Transgenic founders were backcrossed to C57BL/6 mice for more than eight generations. For experiments, PAG-KO mice were mated with C57BL/6 mice, and their F1 descendants were genotyped by PCR using the following primers: PAG 1 F (5′-GAC AGC ACA GGA AAG GCC AAG-3′), PAG 2 R (5′-GTG TCC ACC GGT CCC TTC TG-3′), and PAG ZEO R (5′-CCA GGG TGT TGT CCG GCA C-3′), giving PCR products of 498 and 390 bp for the WT and PAG-KO alleles, respectively. Bone marrow cells were isolated from the femurs and tibias of 6- to 8-week-old PAG-KO mice or their WT littermates (PAG-WT mice). All animal studies were performed in compliance with the *Guide for the Care and Use of Laboratory Animals* (27) and were approved by the Animal Care and Usage Committee of the Institute of Molecular Genetics. Cells were cultured in RPMI 1640 medium supplemented with 100 U/ml penicillin, 100 μg/ml streptomycin, 71 μM 2-mercaptoethanol, minimum essential medium (MEM) nonessential amino acids, 0.7 mM sodium pyruvate, 2.5 mM L-glutamine, 12 mM D-glucose, recombinant mouse stem cell factor (SCF; 20 ng/ml; PeproTech EC), mouse recombinant interleukin-3 (IL-3; 20 ng/ml; PeproTech EC), and 10% fetal calf serum (FCS).

Antibodies and reagents. The following monoclonal antibodies (MAbs) were used: anti-LAT (28), anti-LYN (29), anti-FcεRI β chain (30), trinitrophenol (TNP)-specific immunoglobulin E (IgE) (IGEL b4.1) (31), and anti-hypoxanthine guanine phosphoribosyltransferase (anti-HPRT; Santa Cruz Biotechnology Inc.). Antipaxillin was obtained from BD Transduction Laboratories. Polyclonal antibodies specific for LYN and LAT were prepared in the Department of Signal Transduction, Prague, Czech Republic, by immunization of rabbits with the corresponding recombinant proteins or their fragments (32). Rabbit anti-IgE was prepared by immunization with whole IGEL b4.1. Polyclonal antibodies specific for FYN, actin, phospholipase C γ1 (PLCγ1), PLCγ2, GRB2, CSK, KIT, STAT5, SHIP1, phospho-KIT (Y568/570), and phospho-focal adhesion kinase (phospho-FAK; Y925), as well as horseradish peroxidase (HRP)-conjugated donkey anti-goat IgG, goat anti-mouse IgG, and goat anti-rabbit IgG, were obtained from Santa Cruz Biotechnology Inc. Antibodies specific for phospho-SYK (Y525/Y526), phospho-STAT5 (Y694), phospho-SH2-containing inositol 5′-phosphatase 1 (SHIP1; Y1020), and the Myc tag were obtained from Cell Signaling. PAG-specific rabbit polyclonal antibody was from Exbio. HRP-conjugated antiphosphotyrosine MAb (PY-20) was obtained from BD Biosciences. Antibodies specific for tumor necrosis factor alpha (TNF-α), IL-6, and IL-13 were purchased from PeproTech EC. Anti-mouse FcεRI labeled with fluorescein isothiocyanate (FITC) and anti-mouse KIT–allophycocyanin (APC) conjugates were obtained from eBiosciences. ^{45}Ca (specific activity, 773 MBq/mg Ca^{2+}) and [γ-^{32}P]ATP (specific activity, 222 TBq/mmol) were purchased from the Institute of Isotopes Co., Ltd. (Budapest, Hungary). A donkey anti-rabbit IgG–Alexa Fluor 488 conjugate and thapsigargin were obtained from Invitrogen. Mowiol 4-88 mounting solution was from Merck. Colloidal gold nanoparticles (Au-NPs; diameter, 30 nm), consisting of approximately 2×10^{11} Au-NPs/ml, were obtained from BBInternational. All other reagents were from Sigma-Aldrich.

Lentivirus shRNA constructs and cell transduction. A set of four murine Pag1 (Swiss-Prot accession number Q3U1F9) short hairpin (shRNA) constructs based on the pLKO.1 vector (TRCN0000124814 [shRNA14], TRCN0000124815 [shRNA15], TRCN0000124816 [shRNA16], and TRCN0000124817 [shRNA17]) were obtained from Open Biosystems. Each of the Pag1 shRNA constructs (14 μg) was mixed with Opti-MEM (1 ml; Invitrogen), 21 μl of ViraPower lentiviral packaging mix (Invitrogen), and 82 μl of Lipofectamine 2000 (Invitrogen). The mixture was homogenized by vortexing for 10 s and then incubated at room temperature for 20 min before it was added to semiconfluent (70%) HEK-293FT packaging cells growing in 20 ml of freshly added Dulbecco's medium supplemented with antibiotic and 10% FCS in 150-cm^2 tissue culture flasks. Three days later, the viruses in the culture supernatant were concentrated by centrifugation at 25,000 rpm for 2 h using a JA-25.50 rotor (Beckman Coulter). The pellets were resuspended in 1 ml of culture medium and added to 29 ml of culture medium containing 5×10^7 BMMCs. After 2 days, the medium was changed to virus-free medium and the cells were cultured for an additional 2 days (recovery period). Stable selection was achieved by culturing the transduced cells for 1 week in the presence of puromycin (5 μg/ml). Cells were pooled and analyzed for PAG expression by immunoblotting. Cells with the highest reduction in the amount of PAG, obtained with shRNA14 and shRNA15, were used for further experiments. Cells transfected with empty pLKO.1 vector were used as negative controls. For rescue experiments, mouse Pag1 cDNA (RefSeq accession number BC145761; catalog number 40131064; Open Biosystems) was amplified using forward primer 5′-AAAGAATTCGCCG CCACCAT**GGGCCCTGCAGGAAGCGT**-3′ (the EcoRI restriction site is underlined, the coding sequence is in bold) and reverse primer 5′-TTTG TCGAC**GAGCCTGGTGACATCTCTGC**-3′ (the SalI restriction site is underlined, the coding sequence is in bold). The amplified DNA was cloned via the EcoRI and SalI restriction sites (upstream of Myc) into the pFLAG-CMV-5a expression vector (Sigma-Aldrich) modified to express the Myc tag (kindly provided by V. Korinek). The cassette encoding the Myc-tagged Pag1 sequence was then amplified with the same forward primer described above and reverse primer 5′-TTTGCGGCCGCTTA**CA GGTCCTCCTCTGAGA**-3′ (the NotI restriction site is underlined, the

coding sequence is in bold) and recloned via EcoRI and NotI restriction sites into the pCDH-CMV-MCS-EF1-Puro expression lentivector (pCDH; catalog number CD510B-1; System Biosciences). The construct was verified by DNA sequencing. Viruses with pCDH-Pag-myc or empty pCDH were produced as described above. Medium with virus (30 ml) was filtered through a 0.22-μm-pore-size filter and divided into two aliquots. The first aliquot was used to transduce the WT or PAG-KO BMMCs at day 0. The second aliquot was preserved at 4°C and used for the second transduction of the same cells at day 3. Stable selection was achieved by culturing the cells for 7 days in the presence of puromycin (2 μg/ml), added 5 days after the first transduction.

Flow cytometry. To determine the surface expression of FcεRI, cells were exposed to FITC-conjugated anti-FcεRI (1 μg/ml). The samples were evaluated by flow cytofluorometry using a FACSCalibur instrument (BD Biosciences). For rescue experiments, cells were sensitized with TNP-specific IgE for 20 h of incubation in culture medium without IL-3 and SCF. Then they were washed and activated by antigen (TNP-bovine serum albumin [BSA] conjugate; 15 to 25 mol of TNP/mol of BSA; 100 ng/ml) for 90 min and fixed in 4% paraformaldehyde for 10 min at 37°C. The cells were washed once in phosphate-buffered saline (PBS), and free binding sites were blocked with 5% normal donkey serum (Jackson ImmunoResearch Laboratories) in PBS. After washing, the cells were incubated for 45 min with anti-TNF antibody diluted 1:100 in PBS with 0.5% BSA. After repeated washing, the cells were incubated for 30 min with a secondary donkey anti-rabbit IgG–Alexa Fluor 488 antibody conjugate, washed, and analyzed by flow cytometry using an LSR II flow cytometer (Becton Dickinson). For analysis of peritoneal mast cells, mice were sacrificed and injected intraperitoneally with 5 ml of PBS supplemented with 1% FCS. The peritoneal cavity was gently massaged for 30 s, and the injected PBS with free peritoneal fluid cells was withdrawn. One milliliter of PBS with peritoneal cells was spun down (400 × *g*, 5 min), and the cells were washed in cold PBS and stained for FcεRI (as described above) or KIT using the anti-mouse KIT–APC conjugate.

Cell activation. Before the experiments, BMMCs were cultured for 48 h in medium without SCF, followed by incubation for 12 to 16 h in SCF- and IL-3-free medium supplemented with IgE (1 μg/ml). Sensitized cells were washed in buffered salt solution (BSS; 20 mM HEPES, pH 7.4, 135 mM NaCl, 5 mM KCl, 1.8 mM $CaCl_2$, 5.6 mM glucose, 1 mM $MgCl_2$, 0.1% BSA). To quantify degranulation, the cells (0.15×10^6) in 30-μl aliquots were transferred into the wells of a 96-well plate and challenged with 30 μl of antigen (TNP-BSA conjugate), thapsigargin, or SCF at the concentrations indicated in Results. The degree of degranulation was determined as the amount of β-glucuronidase released into the supernatant, as described previously (33). Briefly, 40-μl aliquots of the cell supernatants were mixed in white wells of a 96-well plate (Nunc) with 40 μl of β-glucuronidase substrate (40 μM 4-methylumbelliferyl-β-D-glucuronide hydrate). After incubation for 60 min at 37°C, the reaction was stopped by adding 200 μl of ice-cold 0.2 M glycine buffer, pH 10.0, and fluorescence was determined in an Infinite M200 microtiter plate reader (Tecan) with 355-nm excitation and 460-nm emission filters. The total content of the enzyme in the cells was evaluated by measuring the levels of enzyme in the supernatant from cells lysed in 1% Triton X-100.

Extracellular calcium uptake. Calcium uptake was determined by a modification of a previously described procedure (34). Briefly, IgE-sensitized BMMCs (2×10^6) were resuspended in 100 μl BSS-BSA with 1 mM Ca^{2+}, mixed with 100 μl of BSS-BSA supplemented with $^{45}Ca^{2+}$ and various concentrations of antigen or thapsigargin, and incubated for selected time intervals at 37°C. The reactions were terminated by placing the tubes on ice and then suspending 100-μl aliquots on the walls of microtest tubes to make them separated by air space from the 12% BSA in PBS (300 μl) at the bottoms. Cells with bound $^{45}Ca^{2+}$ were separated from free $^{45}Ca^{2+}$ by centrifugation through 12% BSA at 3,220 × *g* for 15 min at 4°C. The cell pellets were recovered by freezing the tubes and slicing off the tube bottoms, and the cell pellets were solubilized with 1 ml of 1% Triton X-100. The radioactivity was counted in 10 ml scintillation liquid (EcoLite; ICN Biomedicals) in a scintillation counter with QuantaSmart software (PerkinElmer).

Immunoprecipitation and immunoblotting. Cells were pelleted and solubilized in ice-cold lysis buffer for immunoprecipitation (25 mM Tris-HCl, pH 8.0, 140 mM NaCl, 1 mM Na_3VO_4, 2 mM EDTA, 1 μg/ml aprotinin, 1 μg/ml leupeptin, 1 mM phenylmethylsulfonyl fluoride) supplemented with 1% *n*-dodecyl-β-D-maltoside and 1% Nonidet P-40 (for most experiments), 0.2% Triton X-100 (for FcεRI immunoprecipitation), or 1% Brij 96 (for kinase assays). After incubation (30 min on ice), the lysates were spun down (16,000 × *g* for 5 min at 4°C) and postnuclear supernatants were immunoprecipitated with the corresponding antibodies prebound to UltraLink-immobilized protein A or G (Pierce, Thermo Scientific). The immunoprecipitates were size fractionated by sodium dodecyl sulfate-polyacrylamide gel electrophoresis (SDS-PAGE) and immunoblotted with phosphotyrosine-specific PY-20–HRP conjugate or with protein-specific antibodies, followed by HRP-conjugated anti-mouse or anti-rabbit IgG antibody. Some phosphorylated proteins were determined by direct immunoblotting with phosphoprotein-specific antibodies, followed by immunoblotting with the corresponding secondary HRP-conjugated anti-mouse or anti-rabbit IgG. The HRP signal was detected by chemiluminescence. Immunoblots were quantified by use of a luminescent image analyzer (LAS-3000; Fuji Photo Film Co., Tokyo, Japan) and further analyzed by Aida image analyzer software (Raytest). The amount of phosphorylated proteins was normalized to the amount of immunoprecipitated proteins after stripping off the membranes, followed by development with the corresponding antibodies. In some experiments, parallel immunoblots instead of stripped membranes were used.

Sucrose density gradient fractionation. Sucrose density gradient separations were performed as previously described (35), with some modifications. Briefly, BMMCs (30×10^6) were lysed with 0.8 ml ice-cold lysis buffer (20 mM Tris-HCl, pH 8.0, 100 mM NaCl, 10 mM EDTA, 1 mM Na_3VO_4, 10 mM glycerophosphate, 1 mM phenylmethylsulfonyl fluoride, 100× diluted protease inhibitor cocktail, 5 mM iodoacetamide) supplemented with 1% Brij 96. The lysates were homogenized by passing them 10 times through a 27-gauge needle and adjusted to 40% (wt/vol) using 80% stock sucrose in 25 mM Tris-HCl, pH 7.5, 125 mM NaCl, and 2 mM EDTA. The gradient was prepared by adding 0.5 ml 80% sucrose at the bottom of a polyallomer tube (11 by 60 mm; Beckman Instruments), followed by 1.5 ml of 40% sucrose containing the cell lysate, 2 ml of 30% sucrose, and 1 ml of 10% sucrose. The gradient was ultracentrifuged at 210,000 × *g* for 4 h at 4°C using an SW55 Ti rotor (Beckman Instruments), and 0.5-ml fractions were collected from the top.

Immunocomplex kinase assay. The *in vitro* kinase assays were performed as previously described (36), with some modifications. FcεRI, LYN, and FYN were immunoprecipitated from nonactivated or antigen-activated cells lysed in lysis buffer for immunoprecipitation. Proteins immobilized to antibody-armed protein A beads were washed with kinase buffer (25 mM HEPES–NaOH, pH 7.2, 3 mM $MnCl_2$, 0.1% Nonidet P-40, 100 mM Na_3VO_4, 20 mM $MgCl_2$) and then resuspended in 25 μl kinase buffer supplemented with 2.5 μCi (92.5 kBq) of [γ-^{32}P]ATP, 100 μM ATP, and 0.5 μg/μl of acid-denatured enolase as the exogenous substrate. After incubation for 30 min at 37°C, the immunoprecipitates were eluted from the beads with reducing 2×-concentrated SDS-PAGE sample buffer and boiled for 7 min. The ^{32}P-labeled proteins were size fractionated by SDS-PAGE, transferred to a nitrocellulose membrane, and visualized by autoradiography. Films were quantified with Aida image analyzer software.

Cytokine and chemokine detection. IgE-sensitized BMMCs were activated with different concentrations of antigen. One hour later, mRNA was extracted using a TurboCapture 96 mRNA kit (Qiagen). Single-stranded cDNA was synthesized with Moloney murine leukemia virus reverse transcriptase (Invitrogen) according to the manufacturer's instructions. Real-time PCR amplifications of cDNAs were performed in 10-μl reaction volumes of a quantitative PCR (qPCR) mix containing 1 M 1,2-propanediol, 0.2 M trehalose, and SYBR green 1 (37) in 384-well

plates sealed with LightCycler 480 sealing foil (Roche Diagnostics) and analyzed in a LightCycler 480 apparatus (Roche Diagnostics). The following primer sets (sense/antisense) were used for amplification of the different cDNA fragments (the sizes of the amplified fragments are indicated in parentheses): actin, 5′-GATCTGGCACCACACCTTCT-3′/5′-GGGGTG TTGAAGGTCTCAAA-3′ (138 bp); glyceraldehyde-3-phosphate dehydrogenase (GAPDH), 5′-AACTTTGGCATTGTGGAAGG-3′/5′-ATCCA CAGTCTTCTGGGTGG-3′ (69 bp); ubiquitin, 5′-ATGTGAAGGCCAA GATCCAG-3′/5′-TAATAGCCACCCCTCAGACG-3′ (160 bp); TNF-α, 5′-CCCTCACACTCAGATCATCTTCT-3′/5′-GCTACGACGTGGGCT ACAG-3′ (61 bp); IL-6, 5′-GAGGATACCACTCCCAACAGACC-3′/5′-AAGTGCATCATCGTTGTTCATACA-3′ (141 bp); IL-13, 5′-AGACCA GACTCCCCTGTGCA-3′/5′-TGGGTCCTGTAGATGGCATTG-3′ (123 bp); CCL3, 5′-CATCGTTGACTATTTTGAAACCAG-3′/5′-GCCGGTT TCTCTTAGTCAGGAA-3′ (72 bp); and CCL4, 5′-CTTGGAGTTGAAC TGAGCAGC-3′/5-AGAGGGGCAGGAAATCTGAA-3′ (126 bp). The following cycling conditions were used: 3 min at 95°C, followed by 50 cycles of 10 s at 95°C, 20 s at 60°C, and 20 s at 72°C. Threshold cycle (C_T) values were determined by automated threshold analysis of the cycler. The specificity of the PCR was evaluated by examining melting curves. The genes for actin, GAPDH, and ubiquitin were used as reference genes, and the expression levels of all mRNAs were normalized to the geometric mean level of expression of these genes. The relative increase in the expression level of a cytokine was normalized to the level of expression by nonactivated WT cells in each experiment.

For detection of cytokines, an immuno-PCR method was used as described previously (38). Briefly, anti-TNF-α (1 μg/ml), anti-IL-6 (2 μg/ml), or anti-IL-13 (1 μg/ml) in 100 mM borate buffer (pH 9.5) was dispensed in 50-μl aliquots into the wells of a real-time 96-well plate (Eppendorf). After overnight incubation at 4°C, each well was washed four times with 200 μl of Tris-buffered saline (10 mM Tris-HCl, pH 7.4, 150 mM NaCl) containing 0.05% Tween 20 (TBST), and the remaining binding sites were blocked by 2 h of incubation at 37°C with TBST supplemented with 2% BSA. After washing, 50 μl of serial dilutions (0.1 to 100 ng/ml) of recombinant TNF-α, IL-6, or IL-13 (all from PeproTech EC) or the tested samples diluted in PBS–1% BSA was added. The samples were incubated for 1 h at 37°C, and after washing with TBST, 50 μl of Au-NPs armed with thiolated DNA oligonucleotide template (5′-thiol modifier C6 S-S/18-atom hexa-ethyleneglycol spacer-CCTTGAACCT GTGCCATTTGAATATATTAAGACTATACGCGGGAACA-3′] and with the corresponding cytokine-specific antibody was applied into each well. The wells were incubated for 1 h at 37°C and washed with TBST and deionized water. Fifty-microliter aliquots of qPCR master mix solution (see above) supplemented with 60 nM oligonucleotide primers 5′-CCTTGAACCTGTGCC ATTTG-3′ and 5′-GTCCCTCCATCTTCCTACTGTTCCACATGTTC CCGCGTATAGTCTT-3′ were then dispensed into each well. The plates were sealed, and the amount of template DNA bound to antigen-anchored functionalized Au-NPs was evaluated by real-time PCR using a Realplex4 Mastercycler apparatus (Eppendorf) with the following cycling conditions: 2 min at 94°C, followed by 40 cycles of 20 s at 94°C, 20 s at 53°C, and 20 s at 72°C. For the calculation of TNF-α, IL-6, and IL-13 concentrations, the corresponding C_T values were substituted into the regression equations obtained from the calibration curves constructed from the concentration series of appropriate recombinant proteins.

Chemotaxis assay. Chemotaxis responses were assayed in 24-well Transwell chambers (Corning) with 8-μm-pore-size polycarbonate filters in the upper wells. Chemoattractants (antigen or SCF) in 0.6 ml chemotaxis medium (RPMI 1640 supplemented with 1% BSA and 20 mM HEPES, pH 7.4) were added to the lower wells. IgE-sensitized BMMCs (0.3×10^6 in 120 μl chemotactic medium) were added to the upper wells. Cells migrating into the lower wells during the 8 h of incubation (37°C, 5% CO_2) were counted using an Accuri C6 flow cytometer (BD Biosciences).

Confocal microscopy. BMMCs (3×10^5) were attached to fibronectin-coated multitest slides (MP Biomedicals). Cells were fixed with 4% paraformaldehyde for 15 min at room temperature and permeabilized in 0.3% Triton X-100 for 20 min. Free binding sites were blocked with 5% normal donkey serum, and the cells were stained with rabbit anti-Myc tag antibody, followed by labeling with secondary antibody (donkey anti-rabbit IgG–Alexa Fluor 488 conjugate). After 60 min, the cells were washed and mounted in Mowiol 4-88 mounting solution supplemented with Hoechst 33258 nucleic acid stain (1 μg/ml; Molecular Probes) to label the nuclei. Samples were examined with a confocal laser scanning microscope (Leica TCS SP5) equipped with a ×63 (numerical aperture, 1.4) oil immersion objective.

Passive systemic anaphylaxis. The systemic anaphylactic reaction is accompanied by the release of histamine from activated mast cells, leading to a decreased body temperature (39). The body temperature was measured with an accuracy of ±0.1°C using a VitalView data acquisition system with ER-4000 energizer receivers, G2 E-mitter transponders, and VitalView software (Mini Mitter). G2 probes were implanted intra-abdominally into mice while they were under systemic anesthesia with isoflurane (Abbott Laboratories). Monitoring of body temperature was initiated 9 days after the surgery. Mice aged 11 to 18 weeks were sensitized by tail vein injection of TNP-specific IgE (3 μg in 100 μl PBS per mouse), and 24 h later, anaphylaxis was induced by intravenous administration of antigen (500 μg in 100 μl PBS per mouse). The body temperature was recorded at 1-min intervals for at least 3 h after antigen challenge.

Serum IgE quantification. Ninety-six-well enzyme-linked immunosorbent assay plates (Nunc) were coated for 16 h at 4°C with rat antibody specific for mouse IgE (1 μg/ml in PBS; 50 μl/well; BD Biosciences). Wells were washed (four times with TBST) and blocked by incubation at 22°C with TBST–2% BSA. After 2 h, the plates were washed and incubated for 1 h at 22°C with various concentrations of mouse IgE standard (1.95 to 125 ng/ml in PBS–1% BSA; BD Biosciences) or mouse serum samples (diluted 1:5 in PBS–1% BSA). Then, the wells were washed and the captured IgE was detected with biotinylated rat anti-mouse IgE antibody (2 μg/ml in PBS–1% BSA; BD Bioscience), washed, and incubated for 30 min with streptavidin-HRP conjugate (diluted 1:1,000 in PBS–1% BSA; BD Biosciences). Peroxidase substrate solution (0.5 mg/ml *o*-phenylenediamine and 0.015% H_2O_2 in 0.1 M NaH_2PO_4, pH 6.0) was used for colorimetric reaction. The reaction was stopped by adding 50 μl of 4 M H_2SO_4, and the absorbance at 492 nm was determined using an Infinite M200 plate reader (Tecan).

Statistical analysis. The significance of intergroup differences was evaluated by Student's *t* test.

RESULTS

Positive regulatory role of PAG on antigen-induced degranulation. To examine the role of PAG in mast cell signaling, we isolated bone marrow cells from homozygous F1-descendant PAG-KO and PAG-WT mice and cultured them in the presence of IL-3 and SCF to obtain BMMCs. Cells with or without PAG exhibited comparable growth parameters under *in vitro* conditions (not shown), suggesting that PAG had no effect on the growth response of mast cells to IL-3 and SCF. The same PAG-WT BMMCs were used for the production of PAG-KD cells after transduction with lentiviral vectors containing PAG shRNA constructs based on a pLKO vector (shRNA14 to shRNA17), followed by selection in puromycin. PAG-WT BMMCs infected with empty lentiviral vector were used as a negative control (pLKO). PAG-KO and PAG-WT cells expressed comparable amounts of surface FcεRI, as detected by flow cytometry (Fig. 1A). Similarly, no difference in surface FcεRI was observed among various PAG-KD cells and controls (not shown). As expected, we found no detectable PAG in PAG-KO cells using immunoblotting with PAG-specific antibody (Fig. 1B). The amount of PAG in PAG-KD cells was substantially reduced compared to that in control (pLKO) cells. The strongest inhibition was observed in the cells infected with the shRNA14 and shRNA15

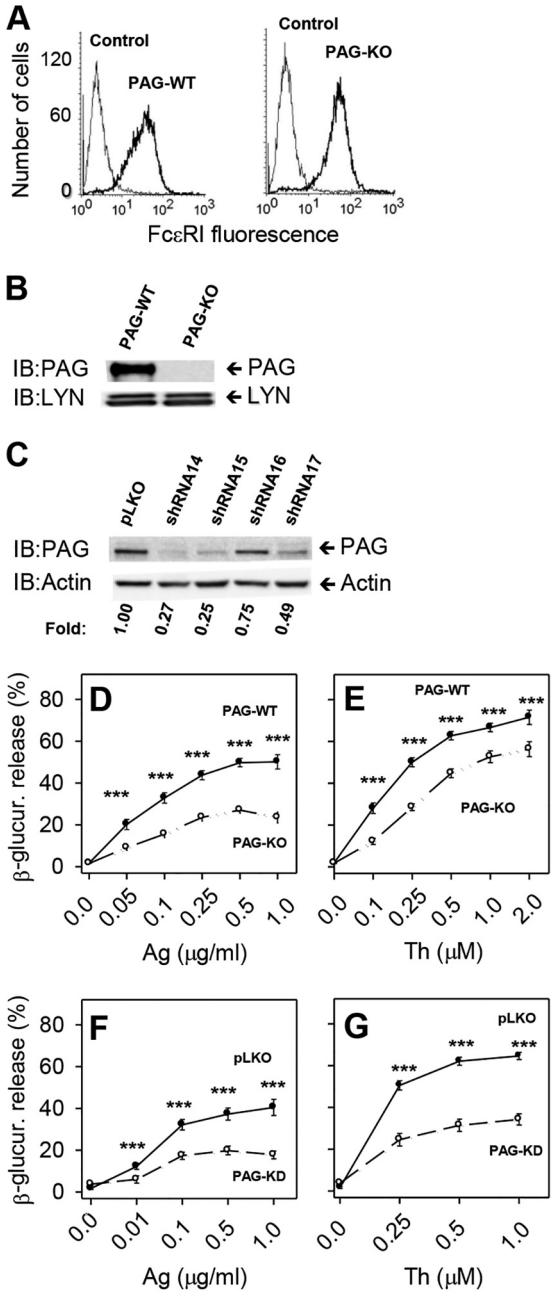

FIG 1 Positive regulatory role of PAG in antigen- or thapsigargin-induced degranulation. (A) BMMCs derived from WT mice (PAG-WT) or PAG-deficient mice (PAG-KO) were stained for surface FcεRI by use of an anti-FcεRI-FITC conjugate. Unstained WT cells were used as negative controls. Samples were analyzed by flow cytometry. (B, C) The presence of PAG in lysates from PAG-WT and PAG-KO BMMCs (B) or WT BMMCs infected with empty pLKO lentiviral vector (pLKO) or lentiviral vectors shRNA14 to shRNA17 (C) was determined by immunoblotting (IB). As loading controls, the membranes were also developed for LYN (B) or actin (C). The amount of PAG normalized to its amount in cells infected with the empty pLKO vector and actin loading control (fold) is also shown (C). For each panel, the results of one representative experiment out of a minimum of three performed are shown. (D, E) PAG-WT or PAG-KO BMMCs were sensitized (D) or not (E) with TNP-specific IgE (1 μg/ml) and then stimulated for 30 min with various concentrations of antigen (Ag) (D) or thapsigargin (Th) (E). (F, G) PAG-WT BMMCs were infected with empty pLKO lentiviral vector (pLKO) or with PAG shRNA14 and shRNA15 vectors (PAG-KD), and stable transfectants were activated with antigen (F) or thapsigargin (G), as described above. The amount of β-glucuronidase (β-glucur.) released from the cells was determined 30 min after triggering. Data represent means ± SEs calculated from 11 independent experiments performed in duplicate or triplicate in panels D and E and from 6 to 8 independent experiments performed in duplicate or triplicate in panels F and G. The statistical significance of differences between PAG-WT and PAG-KO cells or pLKO and PAG-KD cells is shown: ***, $P < 0.001$.

constructs, which reduced PAG expression by 73% and 75%, respectively (Fig. 1C). Infection with constructs containing shRNA16 and shRNA17 reduced PAG expression by 25% and 51%, respectively. Guided by these data, we used viruses containing shRNA14 and shRNA15 for further experiments with BMMCs. Because of the similar knockdown characteristics of these constructs, data from BMMCs infected with these shRNAs were combined and are presented under the common heading of PAG-KDs.

Using BMMCs with PAG-KO and PAG-KD and the corresponding controls, we first investigated whether PAG deficiency has any effect on mast cell degranulation after FcεRI triggering. Degranulation was estimated from the amount of β-glucuronidase released from activated cells. BMMCs were sensitized with TNP-specific IgE and then exposed to various concentrations of antigen. After 30 min, PAG-KO cells exhibited significantly lower levels of degranulation than WT cells at all concentrations of the antigen tested (0.05 to 1.0 μg/ml; Fig. 1D); the total amount of β-glucuronidase released from both cell types by Triton X-100 was similar (data not shown). These data indicate that the absence of PAG reduces antigen-induced degranulation but does not interfere with the production of β-glucuronidase in secretory vesicles. Significant inhibition of degranulation was also observed in PAG-KO cells activated with various concentrations of thapsigargin (0.1 to 2.0 μM; Fig. 1E). Thapsigargin induces the release of Ca^{2+} from intracellular stores by inhibiting the endoplasmic reticulum (ER) ATPase (40). The combined data suggest that PAG not only is involved in the CSK-mediated FcεRI-proximal regulation of SFKs but also could still have other functions distal to FcεRI regulation.

To test whether compensatory developmental alterations could be responsible for the unexpected properties of PAG-KO BMMCs, we examined antigen- and thapsigargin-induced degranulation in cells with PAG-KD and the corresponding controls. The data shown in Fig. 1F and G demonstrate that stimulation of PAG-KD cells with antigen or thapsigargin decreased the level of degranulation compared to that in the pLKO controls, supporting previous findings that PAG is a positive regulator of mast cell degranulation.

Positive regulatory role of PAG on Ca^{2+} response. Early events in mast cell signaling involve the release of Ca^{2+} from intracellular stores followed by the influx of extracellular Ca^{2+} through store-operated Ca^{2+} (SOC) channels in the plasma membrane (41). To determine whether PAG has a role in this process, we quantified Ca^{2+} uptake in PAG-deficient and control BMMCs. The data presented in Fig. 2A show that stimulation with antigen causes significantly lower levels of uptake of extracellular $^{45}Ca^{2+}$ in PAG-KO cells than in PAG-WT cells, reaching a peak at approximately 5 min after triggering in both cell types. Inhibition of Ca^{2+} uptake in PAG-KO cells was observed 5 min after triggering at all concentrations of the antigen tested (Fig. 2B). Significant inhibition of Ca^{2+} uptake in PAG-KO cells was also seen after stimulation for various time intervals (Fig. 2C) or with various

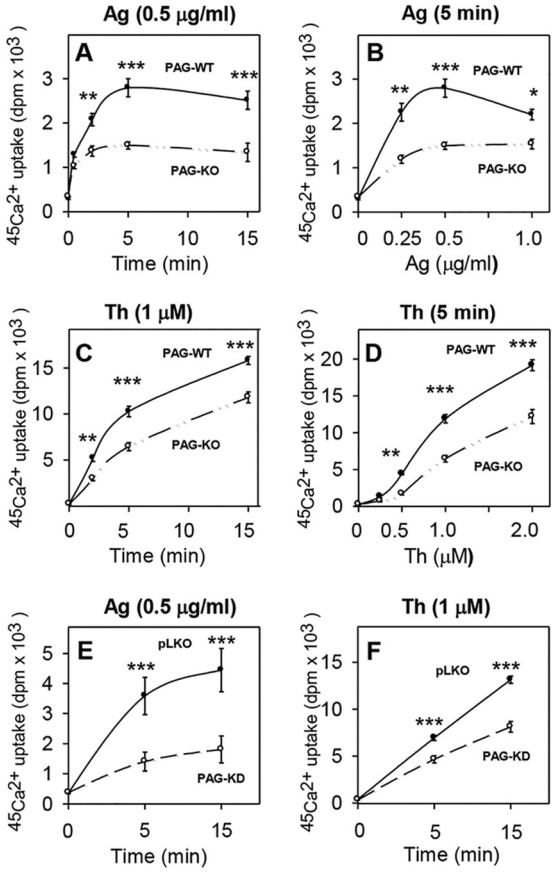

FIG 2 Positive regulatory role of PAG on antigen- or thapsigargin-induced calcium uptake. (A, B) PAG-WT and PAG-KO BMMCs were sensitized with IgE and then stimulated for various time intervals with antigen (0.5 μg/ml) (A) or with various concentrations of antigen for 5 min (B) in the presence of 1 mM extracellular $^{45}Ca^{2+}$. The reactions were terminated by centrifugation of the cells through a BSA gradient, and cell-bound radioactivity (in the sediment) was determined. (C, D) PAG-WT and PAG-KO BMMCs were activated for various time intervals with 1 μM thapsigargin (C) or with various concentrations of thapsigargin for 5 min (D), and the uptake of $^{45}Ca^{2+}$ was determined as described above. (E, F) PAG-WT BMMCs were infected with empty pLKO lentiviral vector (pLKO) or with PAG shRNA vectors (PAG-KD), and stable transfectants were activated with antigen (E) or thapsigargin (F) and analyzed as described above. Data represent means ± SEs from three to six independent experiments performed in duplicate or triplicate. *, $P < 0.05$; **, $P < 0.01$; ***, $P < 0.001$.

concentrations of thapsigargin (Fig. 2D). A positive regulatory role of PAG in calcium uptake after antigen (Fig. 2E) or thapsigargin (Fig. 2F) activation was also evident when PAG-KD cells were compared to the corresponding PAG-expressing (pLKO) controls. These data imply that the observed inhibition of degranulation in PAG-deficient cells could be at least in part attributable to decreased calcium mobilization.

Localization of CSK in lipid rafts depends on PAG. Previous studies localized PAG almost exclusively to lipid rafts, where it could interact with CSK and through this interaction negatively regulate lipid raft-associated SFKs (15). This conclusion was based on data evaluating the distribution of PAG in fractions after sucrose density gradient ultracentrifugation of lysates from cells disintegrated in nonionic detergents (11, 12) or 0.5 M $NaHCO_3$ (21). However, there are inconsistencies regarding the role of PAG in

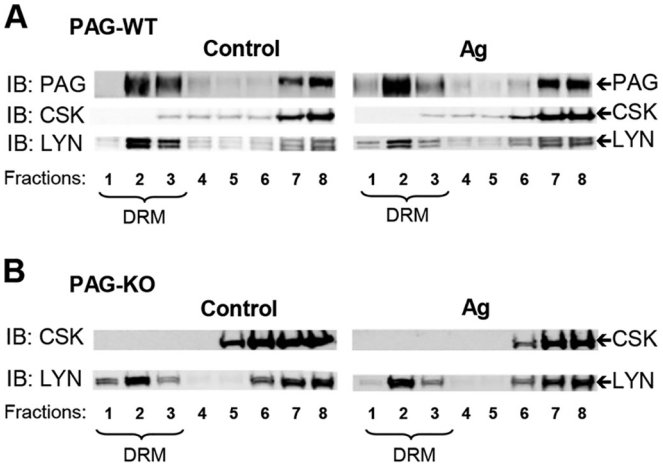

FIG 3 Localization of CSK in lipid rafts depends on PAG. IgE-sensitized PAG-WT BMMCs (A) or PAG-KO BMMCs (B) were nonactivated (Control) or activated for 5 min with antigen (250 ng/ml). After solubilization in lysis buffer containing 1% Brij 96, the whole-cell lysates were fractionated by sucrose density gradient ultracentrifugation as described in Materials and Methods. Individual fractions were collected and analyzed by immunoblotting for the presence of PAG, CSK, and LYN. Fractions containing DRMs are indicated. Representative data from three independent experiments are shown.

the localization of CSK in lipid rafts. One study found that the level of lipid raft-associated CSK in thymocytes was greatly reduced in the absence of PAG (18), whereas another concluded that PAG is dispensable for the localization of CSK in lipid rafts (17). To determine whether PAG contributes to the localization of CSK in lipid rafts in BMMCs, nonactivated or antigen-activated PAG-WT and PAG-KO BMMCs were solubilized in a buffer supplemented with 1% Brij 96 and fractionated by sucrose density gradient ultracentrifugation, and their presence in individual fractions was analyzed by immunoblotting. The distribution of LYN kinase, a well-known lipid raft marker in BMMCs, was also examined. In accordance with previous data (42), most of the LYN (88%) in nonactivated cells was associated with detergent-resistant membranes (DRM; fractions 1 to 3). Five minutes after activation with antigen, this amount was reduced by approximately half (Fig. 3A). In the same gradient fractions, less PAG was found in DRMs (55%), and no significant changes were observed after stimulation with antigen. Only a small fraction of CSK was found in DRM fractions (4%), and no significant changes were observed after activation with antigen. When lysates from PAG-KO BMMCs were analyzed, no CSK was found in DRM fractions from activated and nonactivated cells even after a longer exposure (Fig. 3B), suggesting that PAG is involved in the localization of CSK in DRMs.

PAG and tyrosine phosphorylation of signal transduction proteins. The first biochemically defined step after FcεRI triggering is tyrosine phosphorylation of the FcεRI subunits by SFK LYN, followed by engagement of other kinases and phosphorylation of a number of signal transduction proteins. To specify the role of PAG in these processes, we examined tyrosine phosphorylation of FcεRI and several selected proteins involved in early stages of antigen-induced mast cell signaling (SYK, LAT, extracellular signal-regulated kinase [ERK]) (43), as well as proteins involved in cell movement (FAK and paxillin) (44). In initial experiments, we looked for proteins phosphorylated on tyrosine in total cellular

lysates. We found that PAG-WT cells differed from PAG-KO cells in several tyrosine-phosphorylated proteins not only after antigen stimulation but also in the nonactivated state (Fig. 4A). Further analysis showed that FcεRI triggering caused an increase in tyrosine phosphorylation of FcεRI β and γ chains in WT cells and that this process was significantly reduced in PAG-KO cells (Fig. 4B). Tyrosine phosphorylation of SYK (Fig. 4C) and its substrates, LAT (Fig. 4D) and ERK (Fig. 4E), was also impaired in PAG-deficient cells. In contrast, FAK (Fig. 4F) and the focal adhesion-associated adaptor protein paxillin (Fig. 4G) showed elevated basal levels of tyrosine phosphorylation in PAG-KO cells; this difference was maintained after FcεRI triggering (Fig. 4F and G).

The observed decrease in tyrosine phosphorylation of FcεRI β and γ subunits in antigen-activated PAG-KO cells suggested an imbalance between PTKs and PTPs in the vicinity of the receptor. To examine FcεRI-associated PTK activity toward its endogenous substrate, FcεRI was immunoprecipitated from nonactivated and antigen-activated PAG-WT and PAG-KO cells, and the immunocomplexes were analyzed by *in vitro* kinase assays with [γ-^{32}P]ATP. Using PAG-WT cells, we observed a significant increase in radioactivity bound to FcεRI β and γ receptor subunits after activation with antigen (Fig. 5A and B). Surprisingly, when the receptor was precipitated from PAG-KO cells, strong phosphorylation of the receptor β and γ subunits was observed in nonactivated cells and was decreased after FcεRI triggering. These data, together with the results of immunoblotting experiments showing weak and comparable tyrosine phosphorylation of the β and γ subunits of FcεRI isolated from nonactivated PAG-WT and PAG-KO cells, suggest that the activity of PTKs bound to FcεRI isolated from PAG-KO cells is enhanced.

To determine the enzymatic activities of total LYN and FYN, the kinases were immunoprecipitated and their activities were assessed by an *in vitro* kinase assay. To overcome the problem with possible variation in the extent of nonphosphorylated residues in the target proteins, we used acid-denatured enolase as the exogenous substrate in immunocomplex kinase assays. The data in Fig. 5C to F show low but significantly higher levels of autophosphorylation of the LYN and FYN kinases immunoprecipitated from PAG-KO cells than of those immunoprecipitated from PAG-WT cells. Importantly, enolase phosphorylation was also enhanced in LYN and FYN immunoprecipitates obtained from PAG-KO cells. In contrast to the findings of previous studies (3, 19), we did not observe any increase in the activity of the kinases after FcεRI triggering, which is probably due to the different culture condition used (45).

LYN is a positive regulator of PTPs (46, 47), which could be responsible for the decreased tyrosine phosphorylation of several substrates, as shown in Fig. 4A to E. One of the phosphatases involved in the regulation of mast cell degranulation and calcium responses is SHIP1. LYN kinase phosphorylates SHIP1 and thus enhances its enzymatic activity and downregulates degranulation (47, 48). In further experiments, we therefore examined tyrosine phosphorylation of SHIP1 in BMMCs from PAG-WT and PAG-KO mice. In nonactivated WT cells, SHIP1 showed baseline phosphorylation which was enhanced after FcεRI triggering (Fig. 5G and H). Compared to PAG-WT cells, nonactivated PAG-KO cells exhibited significantly higher levels of SHIP1 tyrosine phosphorylation. After activation with antigen, the difference between PAG-WT and PAG-KO cells became insignificant.

Different regulatory roles of PAG in SCF signaling. An important surface receptor of mast cells is KIT, which binds SCF and thereby triggers mast cell activation and enhances activation induced by FcεRI (49). However, no data on the involvement of PAG in SCF-induced activation are available. To determine a possible role of PAG in KIT-mediated activation, PAG-WT and PAG-KO BMMCs were activated with different concentrations of SCF and degranulation was examined. PAG-WT cells released increasing amounts of β-glucuronidase when activated with 25 to 200 ng/ml SCF. The extent of SCF-induced degranulation was higher than that described in previous studies (50, 51) and was apparently related to the growth of bone marrow cells in the presence of both IL-3 and SCF. When BMMCs were derived from cultures containing IL-3 alone, their SCF-induced degranulation was low (45). PAG-KO cells released significantly more β-glucuronidase than PAG-WT cells at all concentrations of SCF tested (Fig. 6A). This effect was associated with higher levels of KIT tyrosine phosphorylation in PAG-KO cells (Fig. 6B and C). However, an opposite effect of PAG on FcεRI- and KIT-mediated signaling events was absent when tyrosine phosphorylation of PLCγ1 was examined. Stimulation of PAG-WT cells with antigen as well as with SCF resulted in tyrosine phosphorylation of PLCγ1, even though it was slower in SCF-activated cells. Similar findings have been previously described (50) and indicate that FcεRI-activated PTKs are more potent for the phosphorylation of PLCγ1 than that of KIT. In PAG-KO cells, the extent of PLCγ1 tyrosine phosphorylation was significantly inhibited in both antigen- and SCF-triggered cells (Fig. 6D and E). A similar effect was observed when PLCγ2 was examined (data not shown). No significant effect of PAG was observed when the tyrosine phosphorylation of several other signaling molecules (SYK, LAT, FAK, paxillin) was examined in PAG-WT and PAG-KO cells. Furthermore, no effect of PAG on the calcium response was observed in SCF-activated BMMCs (not shown).

An important aspect of mast cell physiology is chemotaxis directed by various ligands (52). Here we compared chemotaxis toward antigen or SCF in cells differing in PAG expression. In transwell migration assays, PAG-WT BMMCs exhibited faster migration toward the antigen than PAG-KO cells. The difference was almost 2-fold and was significant (Fig. 6F). When SCF was used as a chemoattractant, both cell types migrated faster and no significant difference between them was evident. To exclude possible compensatory developmental alterations in PAG-KO cells, we also compared the chemotaxis of BMMCs with PAG-KD and their corresponding controls (pLKO cells). We found significantly lower levels of migration of PAG-KD cells than of pLKO cells after exposure to antigen. Again, no significant difference between the two cell types was observed when SCF was used as a chemoattractant (Fig. 6G).

Positive regulatory role of PAG in cytokine and chemokine production. Previous studies showed that activation of mast cells resulted in the rapid tyrosine phosphorylation of several transcription factors. We selected STAT5, which has been extensively studied in FcεRI- or KIT-activated cells (53, 54), as the transcription factor. To elucidate the role of PAG in this process, we examined tyrosine phosphorylation of STAT5 in nonactivated and antigen- or SCF-activated PAG-WT and PAG-KO cells (Fig. 7A and B). Antigen-induced tyrosine phosphorylation of STAT5 was positively regulated by PAG. A significantly lower level of phosphorylation of STAT5 in PAG-KO cells was observable even without activation, but activation intensified the difference. Phosphorylation of STAT5 was also observed in cells stimulated with SCF

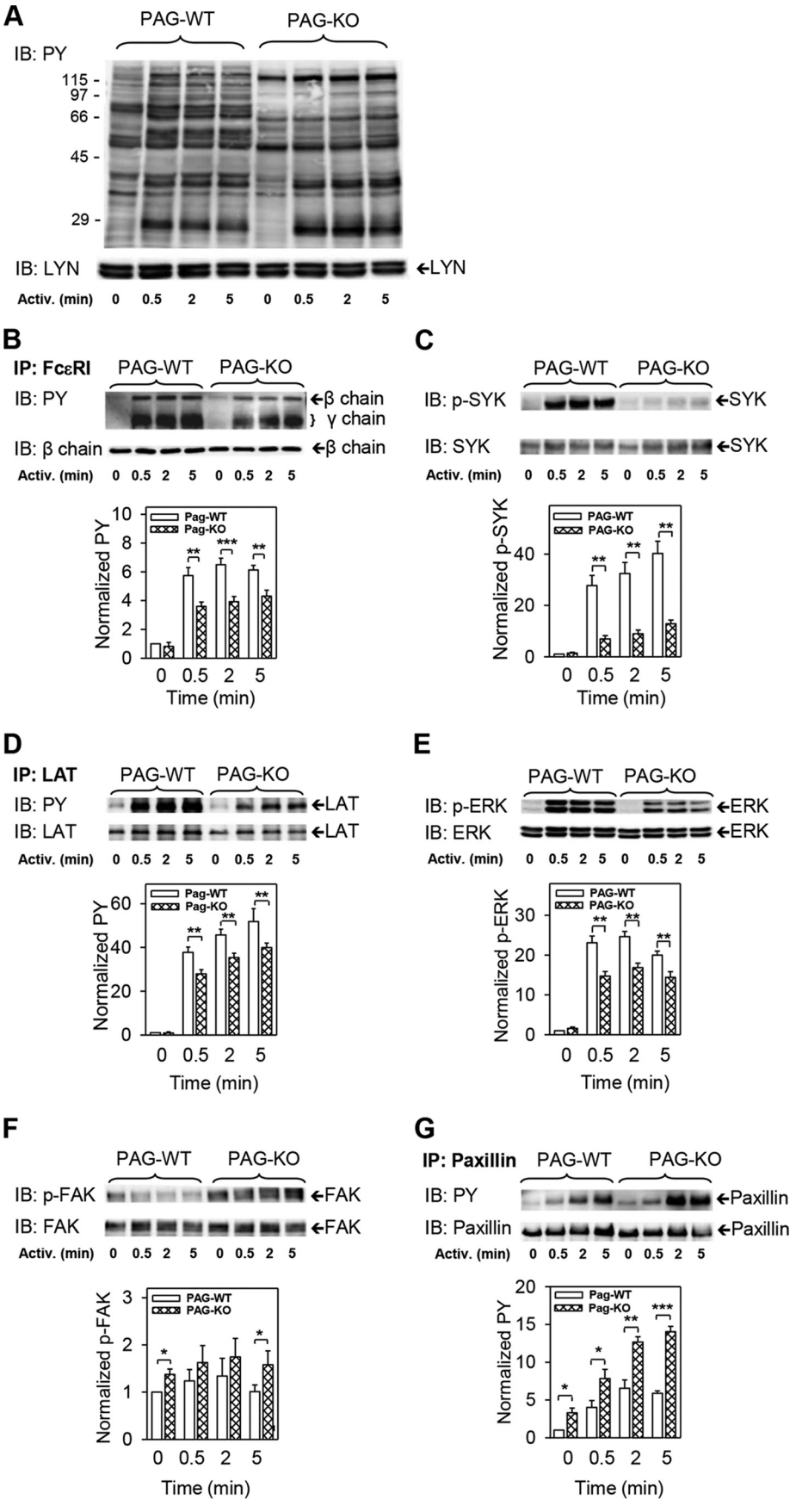
A
PAG-WT
PAG-KO
IB: PY
115 -
97 -
66 -
45 -
29 -
IB: LYN
←LYN
Activ. (min) 0 0.5 2 5 0 0.5 2 5
B
IP: FcεRI
PAG-WT
PAG-KO
IB: PY
←β chain
γ chain
IB: β chain
←β chain
Activ. (min) 0 0.5 2 5 0 0.5 2 5
Pag-WT
Pag-KO
Normalized PY
Time (min)
C
PAG-WT
PAG-KO
IB: p-SYK
←SYK
IB: SYK
←SYK
Activ. (min) 0 0.5 2 5 0 0.5 2 5
PAG-WT
PAG-KO
Normalized p-SYK
Time (min)
D
IP: LAT
PAG-WT
PAG-KO
IB: PY
←LAT
IB: LAT
←LAT
Activ. (min) 0 0.5 2 5 0 0.5 2 5
Pag-WT
Pag-KO
Normalized PY
Time (min)
E
PAG-WT
PAG-KO
IB: p-ERK
←ERK
IB: ERK
←ERK
Activ. (min) 0 0.5 2 5 0 0.5 2 5
PAG-WT
PAG-KO
Normalized p-ERK
Time (min)
F
PAG-WT
PAG-KO
IB: p-FAK
←FAK
IB: FAK
←FAK
Activ. (min) 0 0.5 2 5 0 0.5 2 5
PAG-WT
PAG-KO
Normalized p-FAK
Time (min)
G
IP: Paxillin
PAG-WT
PAG-KO
IB: PY
←Paxillin
IB: Paxillin
←Paxillin
Activ. (min) 0 0.5 2 5 0 0.5 2 5
Pag-WT
Pag-KO
Normalized PY
Time (min)

(Fig. 7A and B). However, no significant difference between PAG-WT and PAG-KO cells was observed.

The decreased phosphorylation of STAT5 in antigen-stimulated PAG-KO cells suggested the reduced production of cytokines and chemokines in such cells (55). Detailed analysis at the protein and mRNA levels showed that, indeed, the levels of three selected cytokines, TNF-α, IL-6, and IL-13, were significantly reduced in antigen-stimulated PAG-KO cells compared with their levels in PAG-WT cells at both the protein and mRNA levels (Fig. 7C). Antigen-activated PAG-KO BMMCs also exhibited significant inhibition of transcription of two chemokines, CCL3 and CCL4 (Fig. 7D).

Phenotype rescue of PAG-KO cells. Next, we attempted to confirm the role of PAG as a positive regulator of cytokine production. We prepared a PAG-myc construct in the pCDH vector and transfected it into PAG-KO BMMCs. Control cells were transfected with the empty pCDH vector, and puromycin-resistant cells were further analyzed. Staining for myc after cell permeabilization and confocal microscopy showed the association of the PAG-myc with the plasma membrane (Fig. 8A). No signal was observed in cells transduced with empty pCDH (Fig. 8B). Furthermore, immunoblotting analysis with Myc tag-specific antibody confirmed the expression of PAG-myc in cells transduced with the pCDH-PAG-myc vector but not the pCDH empty vector (Fig. 8C). These data suggest that PAG-myc was expressed as expected. Next, we examined the production of TNF-α in antigen-activated PAG-WT and PAG-KO cells transfected with empty pCDH and PAG-KO cells transfected with pCDH-PAG-myc. For this analysis we selected flow cytometry, which allowed us to evaluate TNF-α-positive cells, after gating out the cellular debris detected in forward and side scatter plots. This eliminated the problem associated with the presence of different proportions of living cells and debris in various transduction experiments. Data presented in Fig. 8D indicate that the level of production of TNF-α in cells transfected with the empty pCDH vector was significantly lower in PAG-KO cells than in PAG-WT cells. PAG-KO cells transfected with pCDH-PAG-myc produced significantly more TNF-α than pCDH transfectants. These data confirm the phenotype rescue in PAG-KO cells.

Impaired passive systemic anaphylaxis in PAG-KO mice. Finally, we examined degranulation in antigen-activated mast cells under *in vivo* conditions. We induced passive systemic anaphylaxis in PAG-KO and PAG-WT mice by sensitizing them with TNP-specific IgE MAb and subsequent challenge with antigen. In control mice, the decrease in body temperature was observable within the first 60 min and was followed by slow recovery for more than 180 min after antigen injection (Fig. 9A). In PAG-KO mice, the decrease in body temperature was less pronounced and recovery was faster, being complete 150 min after antigen administration. The difference in body temperature between PAG-WT and PAG-KO mice was significant in the interval ranging from 45 to 170 min after antigen administration. The observed decrease in systemic anaphylaxis was not likely attributable to decreased numbers of mast cells in PAG-KO mice, as inferred from comparable mast cell (KIT and FcεRI positive) counts in the peritoneal lavage fluid of PAG-WT and PAG-KO cells (Fig. 9B). Furthermore, we found no significant difference in serum IgE levels between PAG-WT and PAG-KO mice (Fig. 9C). This finding indicates that the production of IgE is not affected by the absence of PAG and that the decreased anaphylactic response in PAG-KO mice is not caused by enhanced production of IgE, which might preclude sensitization with antigen-specific IgE.

DISCUSSION

In this study, we used BMMCs derived from PAG-KO and PAG-WT mice to understand the role of PAG in FcεRI and SCF signaling. To minimize the possible effect of compensatory developmental alterations in PAG-KO cells, we also used BMMCs with PAG-KD and corresponding controls. Several lines of evidence indicate that PAG has positive as well as negative regulatory roles in FcεRI- or KIT-mediated signaling, depending on the receptor triggered and the signaling pathway involved.

First, when stimulated with antigen, mast cells derived from PAG-KO mice exhibited decreased degranulation. In view of previous results obtained with other immunoreceptors (17, 18, 26), this was an unexpected finding because phosphorylated PAG was regarded as a plasma membrane anchor of CSK, a negative regulator of SFKs. Furthermore, overexpression of PAG reportedly resulted in decreased degranulation in RBL-2H3 cells (21). The positive regulatory role of PAG in FcεRI-mediated signaling described here was not the consequence of developmental changes caused by the absence of PAG, since a similar phenotype was also observed in PAG-KD BMMCs where PAG expression was downregulated by RNA interference, nor was the decreased degranulation caused by the reduced production of β-glucuronidase or the reduced expression of FcεRI in PAG-KO and PAG-KD cells. Interestingly, a defect in degranulation was also observed in PAG-deficient cells activated by thapsigargin, a noncompetitive inhibitor of ER Ca^{2+} ATPase.

Second, antigen-activated PAG-KO cells exhibited decreased tyrosine phosphorylation of FcεRI β and γ subunits. This change implies that the reduced degranulation in PAG-deficient cells is caused at least in part by inhibition of the earliest stages of mast cell signaling, starting from reduced phosphorylation of the FcεRI β and γ subunits, followed by impaired membrane anchoring, phosphorylation, and activation of SYK. The exact molecular mechanism of the impaired phosphorylation of FcεRI in PAG-

FIG 4 Antigen-induced tyrosine phosphorylation of signal transduction proteins is dependent on PAG. (A to G) IgE-sensitized PAG-WT and PAG-KO cells were activated (Activ.) for the indicated time intervals with antigen (250 ng/ml). The cells were lysed, and total cellular lysates were analyzed by immunoblotting with the tyrosine-specific MAb PY-20–HRP conjugate (PY). Alternatively, FcεRI (B), LAT (D), and paxillin (G) were immunoprecipitated (IP) from the lysates and examined by immunoblotting with tyrosine-specific MAb as in the experiment whose results are shown in panel A. For SYK (C), ERK (E), and FAK (F), size-fractionated proteins in cell lysates were directly analyzed by immunoblotting with the corresponding phosphoprotein-specific antibodies. For loading controls, the membranes were analyzed by immunoblotting for LYN kinase (A), the FcεRI β chain (B), SYK (C), LAT (D), ERK (E), FAK (F), and paxillin (G). Panel A and the tops of panels B to G show representative immunoblots from at least three experiments. The bottoms of panels B to G show the results of densitometry analysis of the corresponding immunoblots in which signals from tyrosine-phosphorylated proteins in activated cells were normalized to the signals in nonactivated cells and loading control proteins. Means ± SEs were calculated from a minimum of four independent experiments. The statistical significance of the differences between PAG-WT and PAG-KO cells is also shown: *, $P < 0.05$; **, $P < 0.01$; ***, $P < 0.001$. p-SYK, p-ERK, and p-FAK, phosphorylated SYK, ERK, and FAK, respectively.

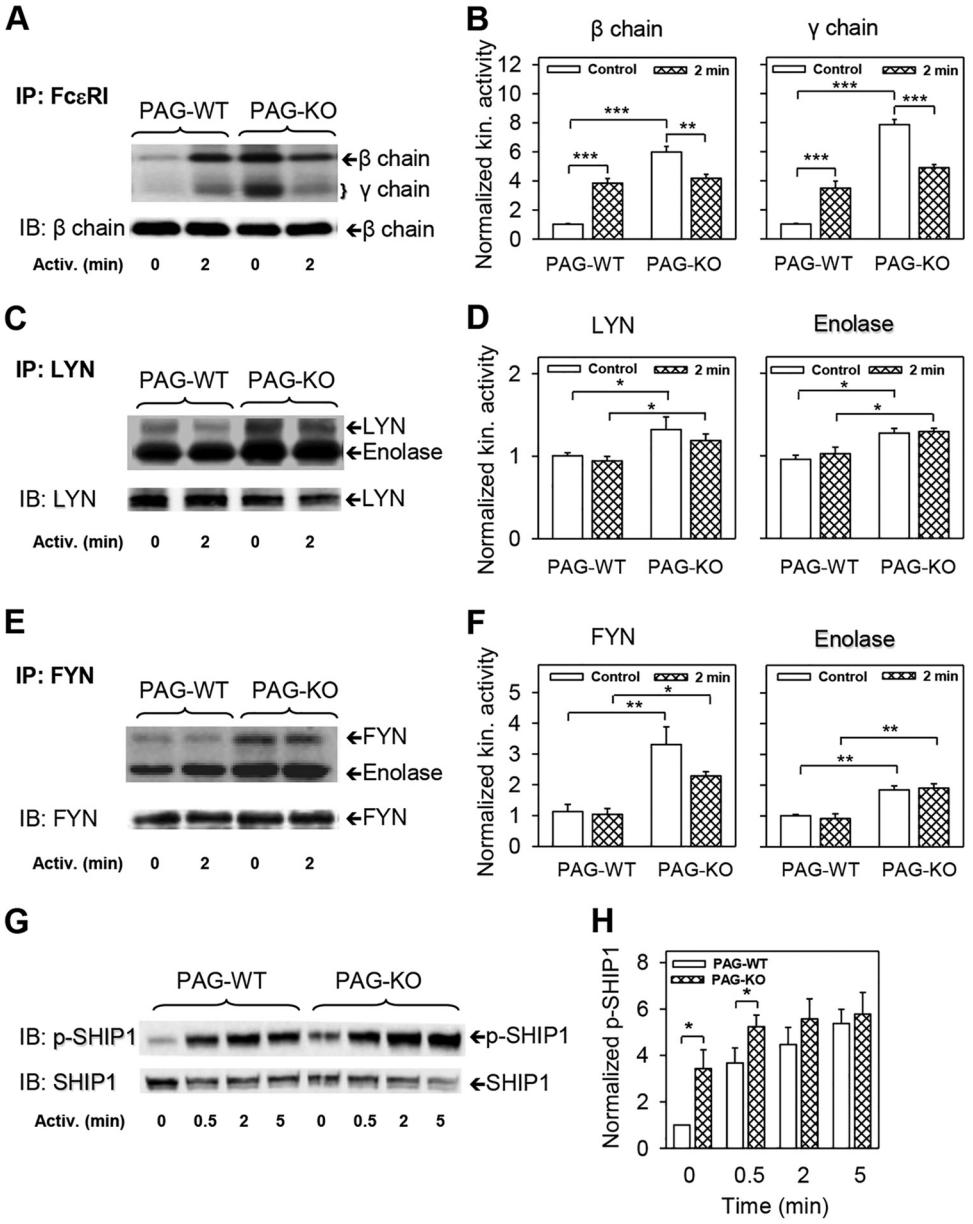

FIG 5 PAG-dependent regulation of LYN and FYN kinase (kin.) activities and SHIP1 tyrosine phosphorylation. (A) IgE-sensitized PAG-WT and PAG-KO BMMCs were activated or not for 2 min with antigen (250 ng/ml) and then solubilized with lysis buffer containing 1% Brij 96. FcεRI-IgE complexes were immunoprecipitated and incubated in a kinase buffer containing [γ-^{32}P]ATP. After the kinase assay, ^{32}P-labeled proteins were size fractionated, transferred to nitrocellulose membranes, and examined by autoradiography. The relative amounts of the FcεRI β chain were determined by immunoblotting. The positions of FcεRI β and γ chains are indicated. (B) Autoradiograms obtained as described in the legend to panel A were quantified, and the signals corresponding to the FcεRI β and γ chains were normalized to the signals in nonactivated PAG-WT cells and the amount of FcεRI β chain immunoprecipitated. (C to F) The cells were activated and solubilized as described in the legend to panel A. LYN (C and D) and FYN (E and F) were immunoprecipitated and incubated in kinase buffer supplemented with [γ-^{32}P]ATP and acid-denatured enolase, used as an exogenous substrate. Kinase assays and further analyses were performed as described in the legend to panel A. Autoradiograms were quantified, and the signals corresponding to LYN, FYN, and enolase were normalized to the signals in nonactivated PAG-WT cells and the amount of immunoprecipitated LYN (D) or FYN (F). (G and H) IgE-sensitized PAG-WT and PAG-KO BMMCs were activated for the indicated time intervals with antigen as described in the legend to panel A. The cells were lysed and analyzed by immunoblotting with phosphorylated-SHIP1 (p-SHIP1)-specific antibody. The amount of SHIP1 was used as a loading control. (H) Densitometry analysis of the immunoblots in which the signal for phospho-SHIP1 was normalized to the signal in nonactivated PAG-WT cells and the amount of SHIP1. The results of representative experiments are shown in panels A, C, E, and G. The means ± SEs in panels B, D, F, and H were calculated from three to five independent experiments. The statistical significance of intergroup differences is indicated: *, $P < 0.05$; **, $P < 0.01$; ***, $P < 0.001$.

deficient cells is unknown and is likely connected to local changes in the activity and/or the topography of SFKs and PTPs within the FcεRI signalosome. Our finding that FcεRI immunocomplexes isolated from nonionic detergent-solubilized nonactivated PAG-KO cells show kinase activity higher than those isolated from PAG-WT cells would be compatible with this hypothesis, provided that PTKs are more stably associated with isolated FcεRI immunocomplexes than PTPs. Furthermore, we found that ty-

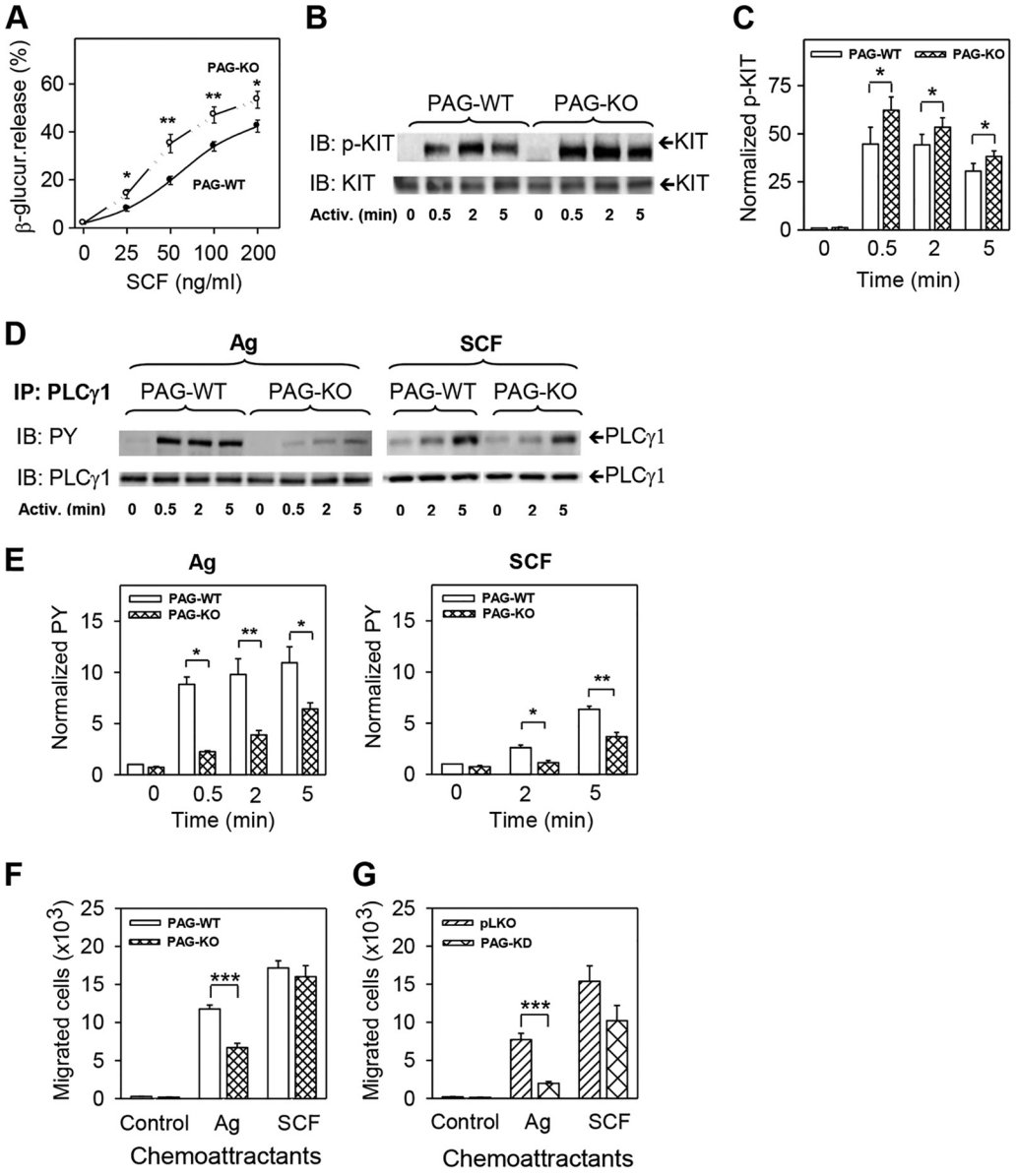

FIG 6 Different regulatory roles of PAG in KIT and FcεRI signaling. (A) PAG-WT and PAG-KO BMMCs were stimulated for 30 min with various concentrations of SCF, and the amount of β-glucuronidase released into the supernatant was determined. (B) PAG-WT and PAG-KO cells were exposed to SCF (50 ng/ml) for different time intervals and lysed, and tyrosine phosphorylation of KIT was analyzed by immunoblotting with phosphorylated-KIT (p-KIT)-specific antibody. Immunoblotting with KIT-specific antibody served as a loading control. The results of one representative experiment out of three performed are shown. (C) The immunoblots obtained as described in the legend to panel B were analyzed by densitometry, and the amounts of tyrosine-phosphorylated KIT were normalized to the amounts of tyrosine-phosphorylated KIT in nonactivated PAG-WT cells and loading controls. (D and E) PAG-WT and PAG-KO BMMCs were activated for different time intervals with antigen (250 ng/ml) or SCF (50 ng/ml) and lysed, and PLCγ1 was immunoprecipitated. The immunoprecipitates were analyzed by immunoblotting with tyrosine-specific MAb PY-20–HRP conjugate (PY) (D). As loading controls, the membranes were also analyzed by immunoblotting for PLCγ1. Representative immunoblots out of three performed are shown. The immunoblots obtained were analyzed by densitometry, and the relative amounts of tyrosine-phosphorylated proteins were normalized to the amounts of the proteins immunoprecipitated and to the amounts of tyrosine-phosphorylated proteins in nonactivated PAG-WT cells (E). (F) IgE-sensitized PAG-WT or PAG-KO BMMCs were analyzed in a chemotactic assay with chemotaxis medium alone (Control) or with chemotaxis medium supplemented with antigen (250 ng/ml) or SCF (100 ng/ml) in the lower wells. The numbers of cells migrating into the lower wells were determined after 8 h. (G) The experiments were performed as described in the legend to panel F, except that cells with PAG-KD and the corresponding controls (pLKO) were used. Means ± SEs were calculated from a minimum of nine independent experiments performed in triplicate (A), three independent experiments (C, E, and G), or six independent experiments (F). The statistical significance of differences between PAG-WT/PAG-KO cells (A, C, E, and F) and pLKO/PAG-KD cells (G) is shown: *, $P < 0.05$; **, $P < 0.01$; ***, $P < 0.001$.

rosine phosphorylation of SHIP1, a negative regulator of mast cell activation (48, 56), is increased in nonactivated PAG-KO cells. This could be caused by the enhanced enzymatic activity of LYN, which phosphorylates and activates SHIP1 (47), and in this manner could contribute to decreased calcium and degranulation responses (48, 56).

In contrast to FcεRI and several other signaling proteins involved in the calcium response (SYK, LAT, and PLCγ), FAK and at

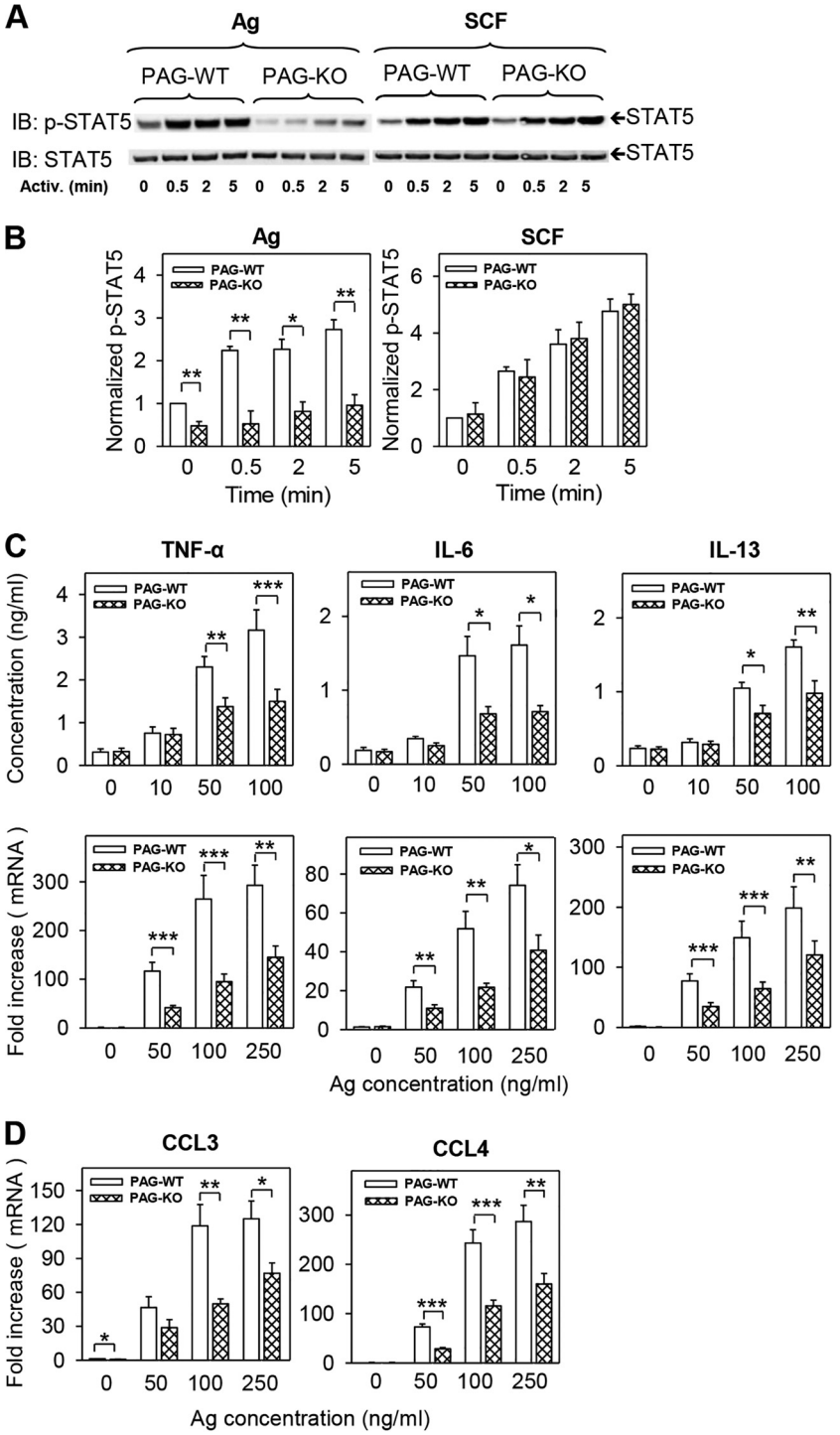

FIG 7 Decreased tyrosine phosphorylation of STAT5 and production of cytokines and chemokines in antigen-activated PAG-KO BMMCs. (A) Cells were activated for different time intervals with antigen (250 ng/ml) or SCF (50 ng/ml), lysed, and analyzed for STAT5 tyrosine 694 phosphorylation by immunoblotting. As loading controls, the membranes were also immunoblotted with STAT5-specific antibody. Representative immunoblots are shown. (B) The immunoblots were analyzed by densitometry, and the relative amount of tyrosine-phosphorylated STAT5 (p-STAT5) was normalized to its amount in nonactivated cells and the corresponding loading control. (C, D) The levels of production of cytokines (TNF-α, IL-6, and IL-13) at the protein level (C, top) and mRNA level (C, bottom) and chemokines (CCL3 and CCL4) (D) were evaluated at the mRNA level in PAG-WT and PAG-KO BMMCs activated with various concentrations of antigen for 1 h (mRNA) or 6 h (protein). Specific proteins and mRNAs were quantified by immuno-PCR and qPCR, respectively. Means ± SEs were calculated from 4 to 12 independent experiments. The statistical significance of differences between PAG-WT and PAG-KO cells is shown: *, $P < 0.05$; **, $P < 0.01$; ***, $P < 0.001$.

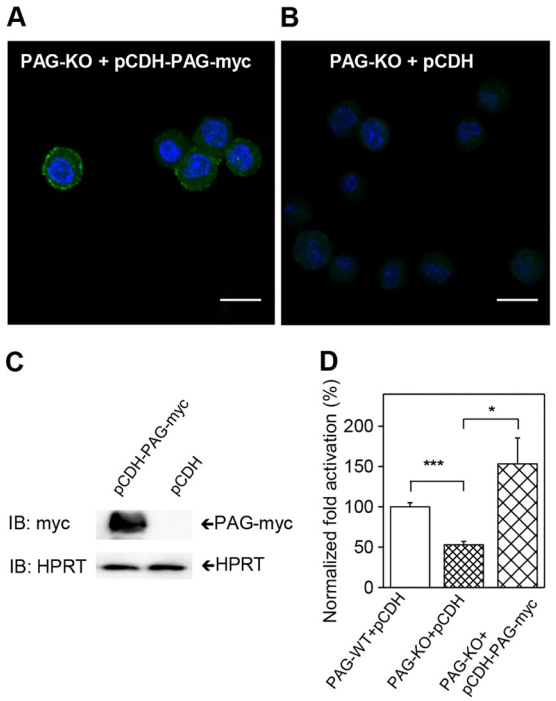

FIG 8 Phenotype rescue of PAG-KO BMMCs. (A, B) PAG-KO BMMCs were transfected with the pCDH-PAG-myc vector (A) or the control empty vector (pCDH) (B). Puromycin-resistant transfectants were isolated and attached to fibronectin-coated slides. Then, the cells were fixed, permeabilized, and labeled for PAG-myc with an anti-Myc tag/anti-IgG–Alexa Fluor 488 conjugate (green) and Hoechst 33258 (blue). Bars, 10 μm. (C) Puromycin-resistant pCDH-PAG-myc- or empty pCDH vector-transfected cells were solubilized, and the presence of PAG-myc was determined by immunoblotting with anti-Myc tag antibody. As loading controls, the membranes were developed for HPRT. (D) PAG-WT or PAG-KO BMMCs stably transfected with the pCDH vector (PAG-WT+pCDH and PAG-KO+pCDH, respectively) or PAG-KO BMMCs transfected with pCDH-PAG-myc (PAG-KO+pCDH-PAG-myc) were sensitized overnight with IgE and then activated with antigen (100 ng/ml). After 90 min the cells were fixed and stained with TNF-α specific rabbit antibody, followed by anti-rabbit IgG–Alexa Fluor 488 conjugate. The cells were analyzed by flow cytometry, and the ratios of the mean fluorescence intensity between activated and nonactivated cells were normalized to those for the pCDH-transfected PAG-WT controls. Data show means ± SEs calculated from three independent experiments. The statistical significance of the differences is indicated: *, $P < 0.05$; ***, $P < 0.001$.

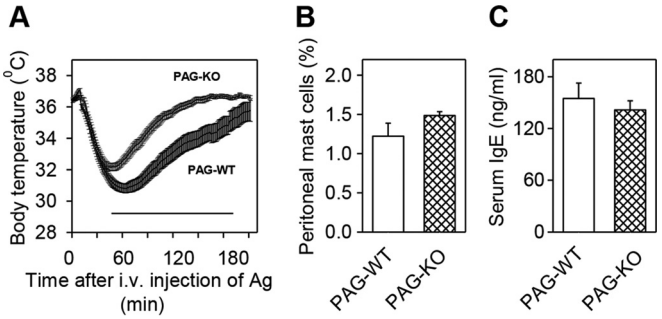

FIG 9 Decreased passive systemic anaphylaxis in PAG-KO mice. (A) PAG-WT ($n = 17$) and PAG-KO mice ($n = 16$) were passively sensitized with TNP-specific IgE (3 μg/mouse) and 24 h later were challenged with antigen (500 μg per mouse) to induce systemic anaphylaxis. Body temperature responses at various time intervals after antigen administration were recorded. Means ± SEs are shown. Statistically significant differences ($P < 0.05$) between PAG-WT and PAG-KO mice are indicated by the black line below the curves. i.v., intravenous. (B) Percentage of mast cells (KIT and FcεRI positive) in peritoneal lavage fluid of PAG-WT and PAG-KO mice. (C) Serum IgE levels in PAG-WT and PAG-KO mice. Data are means ± SEs calculated for three (B) or four (C) animals in each group.

least one of its substrates, the multidomain scaffolding adaptor protein paxillin, showed enhanced tyrosine phosphorylation in PAG-KO cells. The molecular mechanism of enhanced phosphorylation of FAK and paxillin in PAG-KO cells remains to be determined but apparently reflects changes in the activity of SFKs and PTPs which use FAK and paxillin as a substrate (57, 58).

Third, PAG-deficient BMMCs showed reduced calcium uptake after activation with antigen. This could be attributed to the reduced tyrosine phosphorylation and activity of PLCγ, which cleaves the plasma membrane-bound phosphatidylinositol 4,5-bisphosphate into diacylglycerol and inositol 1,4,5-trisphosphate; the latter binds to its receptors and regulates the release of calcium from intracellular organelles. Increases in cytoplasmic calcium lead to the influx of extracellular calcium into the cytoplasm through SOC channels. Reduced calcium uptake in PAG-KO cells was observed not only after exposure to antigen but also after activation with thapsigargin. This could be related to previous findings documenting that PLCγ is involved in thapsigargin-induced Ca^{2+} entry (59–61) and reduced phosphorylation of PLCγ in PAG-deficient cells. Furthermore, it has been shown that STIM1, which is indispensable for opening SOC channels in mast cells (62, 63), needs for its function expression and phosphorylation of SYK and LYN kinases (64). Enhanced tyrosine phosphorylation of SHIP1 and, presumably, its increased enzymatic activity (45, 46) could also contribute to decreased calcium mobilization in activated PAG-KO cells.

Fourth, PAG-KO cells exhibited higher degranulation when activated by SCF. SCF binds to KIT, a type III plasma membrane receptor tyrosine kinase. After SCF binding, the receptor forms a dimer that stimulates its intrinsic tyrosine kinase activity, creating phosphotyrosine binding sites for FYN (65) and LYN (66) kinases and many other signaling molecules, including SHIP1 and PLCγ (67). These molecules are apparently integrated into signaling circuits regulated by PAG.

Fifth, it has previously been shown that activation through FcεRI as well as KIT rapidly stimulates STAT5 tyrosine phosphorylation and that STAT5 deficiency greatly reduces early and late mast cell responses (68). PAG-KO cells exhibited lower tyrosine phosphorylation of STAT5 when activated via FcεRI but not when activated via KIT. This difference could be explained by the different kinases involved in STAT5 phosphorylation. In SCF-activated cells, KIT activates STAT5 partly through the tyrosine kinase JAK2 (69). In contrast, JAK2 is dispensable in IgE-activated cells, which use FYN for STAT5 phosphorylation (53). Phosphorylated STAT5 serves as a transcription factor for a number of inflammatory genes (55). The reduced transcription of genes for cytokines (TNF-α, IL-6, and IL-13) and chemokines (CCL3 and CCL4) and the reduced production of TNF-α, IL-6, and IL-13 in antigen-activated PAG-KO cells could be a direct consequence of impaired STAT5 tyrosine phosphorylation.

Sixth, IgE-sensitized PAG-KO cells exhibited decreased chemotaxis toward antigen. Mast cell chemotaxis is a complex process dependent on numerous signaling molecules and cell signaling pathways (52). The observed inhibition of tyrosine phosphorylation of the FcεRI β and γ subunits, SYK, and LAT in an-

tigen-activated PAG-deficient cells could partly explain the reduced antigen-induced chemotaxis (70). In contrast, PAG-KO BMMCs showed no inhibition of KIT and LAT tyrosine phosphorylation after SCF triggering, and this could be related to a normal chemotaxis response toward SCF in these cells. These findings indicate that either PAG is not involved in the regulation of KIT-mediated chemotaxis or the positive regulatory roles of PAG are compensated for by activation of other molecules, such as PTPs, which also bind to KIT (71, 72).

Seventh, experiments *in vivo* showed that PAG is a positive regulator of passive systemic anaphylaxis, manifested by a decreased body temperature after administration of antigen into IgE-sensitized mice. It is widely accepted that the anaphylactic reaction is initiated by inflammatory mediators released from mast cells (73, 74). Experiments with mice deficient in histidine decarboxylase and therefore lacking histamine suggested that the histamine released from mast cells controls body temperature (39). Our finding of impaired degranulation in PAG-KO cells could thus be directly related to the impaired anaphylactic response. A positive regulatory role of PAG in passive systemic anaphylaxis is the first well-defined *in vivo* trait that is regulated by PAG.

Although previous data from studies using other cell types have implicated the phosphorylation of PAG and PAG-CSK interactions as an important regulatory step in immunoreceptor signaling (11, 12), no dramatic changes in tyrosine phosphorylation of PAG were observed in the course of FcεRI-mediated activation of BMMCs (19; our unpublished data). Furthermore, only a small fraction of CSK colocalized with PAG in lipid raft fractions in PAG-WT BMMCs. In PAG-KO cells, CSK was not detected in lipid raft fractions, suggesting that in mast cells PAG could be a major anchor of CSK in lipid rafts. These data corroborate the results of a previous study documenting that PAG in lipid rafts from mouse thymocytes is a major anchor of CSK (18). On the other hand, they stand in contrast to the findings of another study (17) showing that the amount of lipid raft-associated CSK in thymus cells is not affected by the absence of PAG. However, we would like to point out that different detergents and cell/detergent ratios were used in these various studies and that the association of proteins with lipid rafts is sensitive to these parameters (75, 76).

In summary, the data reported in this study provide compelling evidence that PAG functions as both a positive and a negative regulator of mast cell signaling, depending on the signaling pathway involved. It seems that through interaction with CSK, PAG serves as a negative regulator of SFKs, which are involved in both positive and negative regulatory loops in mast cell activation. Furthermore, we show for the first time that PAG-deficient mice exhibit a distinct phenotype in terms of a passive systemic anaphylaxis response.

ACKNOWLEDGMENTS

We thank H. Mrazova, L. Kocanda, and R. Budovicova for technical assistance.

This work was supported by projects 301/09/1826, P302/10/1759, P302-14-09807S, P302/12/G101, P305-14-00703S, and 204/09/H084 from the Czech Science Foundation, by Action BM1007 from European Cooperation in Science and Technology, by project LD12073 COST-CZ-MAST from the Ministry of Education, Youth, and Sports of the Czech Republic, and by the Institute of Molecular Genetics of the Academy of Sciences of the Czech Republic (RVO 68378050). L.P., M.B., and I.P. were supported in part by the Faculty of Science, Charles University, Prague, Czech Republic.

We have no conflicting financial interests.

REFERENCES

1. **Galli SJ, Borregaard N, Wynn TA.** 2011. Phenotypic and functional plasticity of cells of innate immunity: macrophages, mast cells and neutrophils. Nat. Immunol. **12:**1035–1044. http://dx.doi.org/10.1038/ni.2109.
2. **Eiseman E, Bolen JB.** 1992. Engagement of the high-affinity IgE receptor activates *src* protein-related tyrosine kinases. Nature **355:**78–80. http://dx.doi.org/10.1038/355078a0.
3. **Yamashita T, Mao S-Y, Metzger H.** 1994. Aggregation of the high-affinity IgE receptor and enhanced activity of p53/p56^{lyn} protein-tyrosine kinase. Proc. Natl. Acad. Sci. U. S. A. **91:**11251–11255. http://dx.doi.org/10.1073/pnas.91.23.11251.
4. **Pribluda VS, Pribluda C, Metzger H.** 1994. Transphosphorylation as the mechanism by which the high-affinity receptor for IgE is phosphorylated upon aggregation. Proc. Natl. Acad. Sci. U. S. A. **91:**11246–11250. http://dx.doi.org/10.1073/pnas.91.23.11246.
5. **Field KA, Holowka D, Baird B.** 1995. FcεRI-mediated recruitment of p53/56^{lyn} to detergent-resistant membrane domains accompanies cellular signaling. Proc. Natl. Acad. Sci. U. S. A. **92:**9201–9205. http://dx.doi.org/10.1073/pnas.92.20.9201.
6. **Heneberg P, Dráberová L, Bambousková M, Pompach P, Dráber P.** 2010. Down-regulation of protein tyrosine phosphatases activates an immune receptor in the absence of its translocation into lipid rafts. J. Biol. Chem. **285:**12787–12802. http://dx.doi.org/10.1074/jbc.M109.052555.
7. **Tolar P, Dráberová L, Tolarová H, Dráber P.** 2004. Positive and negative regulation of Fcε receptor I-mediated signaling events by Lyn kinase C-terminal tyrosine phosphorylation. Eur. J. Immunol. **34:**1136–1145. http://dx.doi.org/10.1002/eji.200324505.
8. **Bergman M, Mustelin T, Oetken C, Partanen J, Flint NA, Amrein KA, Autero M, Burn P, Alitalo K.** 1992. The human p50 csk tyrosine kinase phosphorylates p56 lck at tyr-505 and down regulates its catalytic activity. EMBO J. **11:**2919–2924.
9. **Plas DR, Thomas ML.** 1998. Negative regulation of antigen receptor signaling in lymphocytes. J. Mol. Med. (Berl.) **76:**589–595. http://dx.doi.org/10.1007/s001090050254.
10. **Nada S, Okada M, MacAuley A, Cooper JA, Nakagawa H.** 1991. Cloning of a complementary DNA for a protein-tyrosine kinase that specifically phosphorylates a negative regulatory site for p60$^{c\text{-}src}$. Nature **351:**69–72. http://dx.doi.org/10.1038/351069a0.
11. **Brdička T, Pavlistová D, Leo A, Bruyns E, Kořínek V, Angelisová P, Scherer J, Shevchenko A, Hilgert I, Černý J, Drbal K, Kuramitsu Y, Kornacker B, Hořejší V, Schraven B.** 2000. Phosphoprotein associated with glycosphingolipid-enriched microdomains (PAG), a novel ubiquitously expressed transmembrane adaptor protein, binds the protein tyrosine kinase csk and is involved in regulation of T cell activation. J. Exp. Med. **191:**1591–1604. http://dx.doi.org/10.1084/jem.191.9.1591.
12. **Kawabuchi M, Satomi Y, Takao T, Shimonishi Y, Nada S, Nagai K, Tarakhovsky A, Okada M.** 2000. Transmembrane phosphoprotein Cbp regulates the activities of Src-family tyrosine kinases. Nature **404:**999–1003. http://dx.doi.org/10.1038/35010121.
13. **Brdičková N, Brdička T, Anděra L, Špička J, Angelisová P, Milgram SL, Hořejší V.** 2001. Interaction between two adapter proteins, PAG and EBP50: a possible link between membrane rafts and actin cytoskeleton. FEBS Lett. **507:**133–136. http://dx.doi.org/10.1016/S0014-5793(01)02955-6.
14. **Draber P, Halova I, Levi-Schaffer F, Draberova L.** 2012. Transmembrane adaptor proteins in the high-affinity IgE receptor signaling. Front. Immunol. **2:**1–11. http://dx.doi.org/10.3389/fimmu.2011.00095.
15. **Hrdinka M, Horejsi V.** 11 November 2013. PAG—a multipurpose transmembrane adaptor protein. Oncogene http://dx.doi.org/10.1038/onc.2013.485.
16. **Smida M, Cammann C, Gurbiel S, Kerstin N, Lingel H, Lindquist S, Simeoni L, Brunner-Weinzierl MC, Suchanek M, Schraven B, Lindquist JA.** 2013. PAG/Cbp suppression reveals a contribution of CTLA-4 to setting the activation threshold in T cells. Cell Commun. Signal. **11:**28. http://dx.doi.org/10.1186/1478-811X-11-28.
17. **Dobenecker MW, Schmedt C, Okada M, Tarakhovsky A.** 2005. The ubiquitously expressed Csk adaptor protein Cbp is dispensable for embryogenesis and T-cell development and function. Mol. Cell. Biol. **25:**10533–10542. http://dx.doi.org/10.1128/MCB.25.23.10533-10542.2005.

18. **Xu S, Huo J, Tan JE, Lam KP.** 2005. Cbp deficiency alters Csk localization in lipid rafts but does not affect T-cell development. Mol. Cell. Biol. **25:**8486–8495. http://dx.doi.org/10.1128/MCB.25.19.8486-8495.2005.
19. **Odom S, Gomez G, Kovarova M, Furumoto Y, Ryan JJ, Wright HV, Gonzalez-Espinosa C, Hibbs ML, Harder KW, Rivera J.** 2004. Negative regulation of immunoglobulin E-dependent allergic responses by Lyn kinase. J. Exp. Med. **199:**1491–1502. http://dx.doi.org/10.1084/jem.20040382.
20. **Kitaura J, Kawakami Y, Maeda-Yamamoto M, Horejsi V, Kawakami T.** 2007. Dysregulation of Src family kinases in mast cells from epilepsy-resistant ASK versus epilepsy-prone EL mice. J. Immunol. **178:**455–462. http://dx.doi.org/10.4049/jimmunol.178.1.455.
21. **Ohtake H, Ichikawa N, Okada M, Yamashita T.** 2002. Cutting edge: transmembrane phosphoprotein Csk-binding protein/phosphoprotein associated with glycosphingolipid-enriched microdomains as a negative feedback regulator of mast cell signaling through the FcεRI. J. Immunol. **168:**2087–2090. http://dx.doi.org/10.4049/jimmunol.168.5.2087.
22. **Nishizumi H, Horikawa K, Mlinaric-Rascan I, Yamamoto T.** 1998. A double-edged kinase Lyn: a positive and negative regulator for antigen receptor-mediated signals. J. Exp. Med. **187:**1343–1348. http://dx.doi.org/10.1084/jem.187.8.1343.
23. **Kawakami Y, Kitaura J, Satterthwaite AB, Kato RM, Asai K, Hartman SE, Maeda-Yamamoto M, Lowell CA, Rawlings DJ, Witte ON, Kawakami T.** 2000. Redundant and opposing functions of two tyrosine kinases, Btk and Lyn, in mast cell activation. J. Immunol. **165:**1210–1219. http://dx.doi.org/10.4049/jimmunol.165.3.1210.
24. **Parravicini V, Gadina M, Kovarova M, Odom S, Gonzalez-Espinosa C, Furumoto Y, Saitoh S, Samelson LE, O'Shea JJ, Rivera J.** 2002. Fyn kinase initiates complementary signals required for IgE-dependent mast cell degranulation. Nat. Immunol. **3:**741–748. http://dx.doi.org/10.1038/ni817.
25. **Yang Y, Seed B.** 2003. Site-specific gene targeting in mouse embryonic stem cells with intact bacterial artificial chromosomes. Nat. Biotechnol. **21:**447–451. http://dx.doi.org/10.1038/nbt803.
26. **Lindquist S, Karitkina D, Langnaese K, Posevitz-Fejfar A, Schraven B, Xavier R, Seed B, Lindquist JA.** 2011. Phosphoprotein associated with glycosphingolipid-enriched microdomains differentially modulates SRC kinase activity in brain maturation. PLoS One **6:**e23978. http://dx.doi.org/10.1371/journal.pone.0023978.
27. **National Research Council.** 2011. Guide for the care and use of laboratory animals, 8th ed. National Academies Press, Washington, DC.
28. **Tolar P, Tůmová M, Dráber P.** 2001. New monoclonal antibodies recognizing the adaptor protein LAT. Folia Biol. (Praha) **47:**215–217.
29. **Dráberová L, Amoui M, Dráber P.** 1996. Thy-1-mediated activation of rat mast cells: the role of Thy-1 membrane microdomains. Immunology **87:**141–148.
30. **Rivera J, Kinet J-P, Kim J, Pucillo C, Metzger H.** 1988. Studies with a monoclonal antibody to the β subunit of the receptor with high affinity for immunoglobulin E. Mol. Immunol. **25:**647–661. http://dx.doi.org/10.1016/0161-5890(88)90100-9.
31. **Rudolph AK, Burrows PD, Wabl MR.** 1981. Thirteen hybridomas secreting hapten-specific immunoglobulin E from mice with Ig^a or Ig^b heavy chain haplotype. Eur. J. Immunol. **11:**527–529. http://dx.doi.org/10.1002/eji.1830110617.
32. **Kovářová M, Tolar P, Arudchandran R, Dráberová L, Rivera J, Dráber P.** 2001. Structure-function analysis of Lyn kinase association with lipid rafts and initiation of early signaling events after Fcε receptor I aggregation. Mol. Cell. Biol. **21:**8318–8328. http://dx.doi.org/10.1128/MCB.21.24.8318-8328.2001.
33. **Surviladze Z, Dráberová L, Kovářová M, Boubelík M, Dráber P.** 2001. Differential sensitivity to acute cholesterol lowering of activation mediated via the high-affinity IgE receptor and Thy-1 glycoprotein. Eur. J. Immunol. **31:**1–10. http://dx.doi.org/10.1002/1521-4141(200101)31:1<1::AID-IMMU1>3.0.CO;2-W.
34. **Dráberová L.** 1990. Cyclosporin A inhibits rat mast cell activation. Eur. J. Immunol. **20:**1469–1473. http://dx.doi.org/10.1002/eji.1830200710.
35. **Surviladze Z, Dráberová L, Kubínová L, Dráber P.** 1998. Functional heterogeneity of Thy-1 membrane microdomains in rat basophilic leukemia cells. Eur. J. Immunol. **28:**1847–1858. http://dx.doi.org/10.1002/(SICI)1521-4141(199806)28:06<1847::AID-IMMU1847>3.0.CO;2-O.
36. **Amoui M, Dráber P, Dráberová L.** 1997. Src family-selective tyrosine kinase inhibitor, PP1, inhibits both FcεRI- and Thy-1-mediated activation of rat basophilic leukemia cells. Eur. J. Immunol. **27:**1881–1886. http://dx.doi.org/10.1002/eji.1830270810.
37. **Horáková H, Polakovičová I, Shaik GM, Eitler J, Bugajev V, Dráberová L, Dráber P.** 2011. 1,2-Propanediol-trehalose mixture as a potent quantitative real-time PCR enhancer. BMC Biotechnol. **11:**41. http://dx.doi.org/10.1186/1472-6750-11-41.
38. **Potůčková L, Franko F, Bambousková M, Dráber P.** 2011. Rapid and sensitive detection of cytokines using functionalized gold nanoparticle-based immuno-PCR, comparison with immuno-PCR and ELISA. J. Immunol. Methods **371:**38–47. http://dx.doi.org/10.1016/j.jim.2011.06.012.
39. **Makabe-Kobayashi Y, Hori Y, Adachi T, Ishigaki-Suzuki S, Kikuchi Y, Kagaya Y, Shirato K, Nagy A, Ujike A, Takai T, Watanabe T, Ohtsu H.** 2002. The control effect of histamine on body temperature and respiratory function in IgE-dependent systemic anaphylaxis. J. Allergy Clin. Immunol. **110:**298–303. http://dx.doi.org/10.1067/mai.2002.125977.
40. **Thastrup O, Dawson AP, Scharff O, Foder B, Cullen PJ, Drobak BK, Bjerrum PJ, Christensen SB, Hanley MR.** 1989. Thapsigargin, a novel molecular probe for studying intracellular calcium release and storage. Agents Actions **27:**17–23. http://dx.doi.org/10.1007/BF02222186.
41. **Putney JW, Jr.** 2005. Capacitative calcium entry: sensing the calcium stores. J. Cell Biol. **169:**381–382. http://dx.doi.org/10.1083/jcb.200503161.
42. **Volná P, Lebduška P, Dráberová L, Šímová S, Heneberg P, Boubelík M, Bugajev V, Malissen B, Wilson BS, Hořejší V, Malissen M, Dráber P.** 2004. Negative regulation of mast cell signaling and function by the adaptor LAB/NTAL. J. Exp. Med. **200:**1001–1013. http://dx.doi.org/10.1084/jem.20041213.
43. **Gilfillan AM, Rivera J.** 2009. The tyrosine kinase network regulating mast cell activation. Immunol. Rev. **228:**149–169. http://dx.doi.org/10.1111/j.1600-065X.2008.00742.x.
44. **Huang C, Jacobson K, Schaller MD.** 2004. MAP kinases and cell migration. J. Cell Sci. **117:**4619–4628. http://dx.doi.org/10.1242/jcs.01481.
45. **Nocka KH, Levine BA, Ko JL, Burch PM, Landgraf BE, Segal R, Lobell R.** 1997. Increased growth promoting but not mast cell degranulation potential of a covalent dimer of c-Kit ligand. Blood **90:**3874–3883.
46. **Heneberg P, Dráber P.** 2002. Nonreceptor protein tyrosine and lipid phosphatases in type I Fcε receptor-mediated activation of mast cells and basophils. Int. Arch. Allergy Immunol. **128:**253–263. http://dx.doi.org/10.1159/000063864.
47. **Hernandez-Hansen V, Smith AJ, Surviladze Z, Chigaev A, Mazel T, Kalesnikoff J, Lowell CA, Krystal G, Sklar LA, Wilson BS, Oliver JM.** 2004. Dysregulated FcεRI signaling and altered Fyn and SHIP activities in Lyn-deficient mast cells. J. Immunol. **173:**100–112. http://dx.doi.org/10.4049/jimmunol.173.1.100.
48. **Huber M, Helgason CD, Damen JE, Liu L, Humphries RK, Krystal G.** 1998. The src homology 2-containing inositol phosphatase (SHIP) is the gatekeeper of mast cell degranulation. Proc. Natl. Acad. Sci. U. S. A. **95:**11330–11335. http://dx.doi.org/10.1073/pnas.95.19.11330.
49. **Gilfillan AM, Tkaczyk C.** 2006. Integrated signalling pathways for mast-cell activation. Nat. Rev. Immunol. **6:**218–230. http://dx.doi.org/10.1038/nri1782.
50. **Iwaki S, Tkaczyk C, Satterthwaite AB, Halcomb K, Beaven MA, Metcalfe DD, Gilfillan AM.** 2005. Btk plays a crucial role in the amplification of FcεRI-mediated mast cell activation by kit. J. Biol. Chem. **280:**40261–40270. http://dx.doi.org/10.1074/jbc.M506063200.
51. **Iwaki S, Spicka J, Tkaczyk C, Jensen BM, Furumoto Y, Charles N, Kovarova M, Rivera J, Horejsi V, Metcalfe DD, Gilfillan AM.** 2008. Kit- and FcεRI-induced differential phosphorylation of the transmembrane adaptor molecule NTAL/LAB/LAT2 allows flexibility in its scaffolding function in mast cells. Cell. Signal. **20:**195–205. http://dx.doi.org/10.1016/j.cellsig.2007.10.013.
52. **Halova I, Draberova L, Draber P.** 2012. Mast cell chemotaxis—chemoattractants and signaling pathways. Front. Immunol. **3:**119. http://dx.doi.org/10.3389/fimmu.2012.00119.
53. **Pullen NA, Barnstein BO, Falanga YT, Wang Z, Suzuki R, Tamang TD, Khurana MC, Harry EA, Draber P, Bunting KD, Mizuno K, Wilson BS, Ryan JJ.** 2012. Novel mechanism for FcεRI-mediated signal transducer and activator of transcription 5 (STAT5) tyrosine phosphorylation and the selective influence of STAT5B over mast cell cytokine production. J. Biol. Chem. **287:**2045–2054. http://dx.doi.org/10.1074/jbc.M111.311142.
54. **Grange M, Verdeil G, Arnoux F, Griffon A, Spicuglia S, Maurizio J, Buferne M, Schmitt-Verhulst AM, Auphan-Anezin N.** 2013. Active STAT5 regulates T-bet and eomesodermin expression in CD8 T cells and imprints a T-bet-dependent Tc1 program with repressed IL-6/TGF-beta1 signaling. J. Immunol. **191:**3712–3724. http://dx.doi.org/10.4049/jimmunol.1300319.
55. **Pullen NA, Falanga YT, Morales JK, Ryan JJ.** 2012. The Fyn-STAT5

pathway: a new frontier in IgE- and IgG-mediated mast cell signaling. Front. Immunol. **3:**117. http://dx.doi.org/10.3389/fimmu.2012.00117.
56. **Huber M, Helgason CD, Scheid MP, Duronio V, Humphries RK, Krystal G.** 1998. Targeted disruption of SHIP leads to Steel factor-induced degranulation of mast cells. EMBO J. **17:**7311–7319. http://dx.doi.org/10.1093/emboj/17.24.7311.
57. **Deakin NO, Turner CE.** 2008. Paxillin comes of age. J. Cell Sci. **121:**2435–2444. http://dx.doi.org/10.1242/jcs.018044.
58. **Fang X, Lang Y, Wang Y, Mo W, Wei H, Xie J, Yu M.** 2012. Shp2 activates Fyn and Ras to regulate RBL-2H3 mast cell activation following FcεRI aggregation. PLoS One **7:**e40566. http://dx.doi.org/10.1371/journal.pone.0040566.
59. **Broad LM, Braun FJ, Lievremont JP, Bird GS, Kurosaki T, Putney JW, Jr.** 2001. Role of the phospholipase C-inositol 1,4,5-trisphosphate pathway in calcium release-activated calcium current and capacitative calcium entry. J. Biol. Chem. **276:**15945–15952. http://dx.doi.org/10.1074/jbc.M011571200.
60. **Litjens T, Nguyen T, Castro J, Aromataris EC, Jones L, Barritt GJ, Rychkov GY.** 2007. Phospholipase C-γ1 is required for the activation of store-operated Ca^{2+} channels in liver cells. Biochem. J. **405:**269–276. http://dx.doi.org/10.1042/BJ20061762.
61. **Antigny F, Jousset H, Konig S, Frieden M.** 2011. Thapsigargin activates Ca^{2+} entry both by store-dependent, STIM1/Orai1-mediated, and store-independent, TRPC3/PLC/PKC-mediated pathways in human endothelial cells. Cell Calcium **49:**115–127. http://dx.doi.org/10.1016/j.ceca.2010.12.001.
62. **Baba Y, Nishida K, Fujii Y, Hirano T, Hikida M, Kurosaki T.** 2008. Essential function for the calcium sensor STIM1 in mast cell activation and anaphylactic responses. Nat. Immunol. **9:**81–88. http://dx.doi.org/10.1038/ni1546.
63. **Hájková Z, Bugajev V, Dráberová E, Vinopal S, Dráberová L, Janáček J, Dráber P, Dráber P.** 2011. STIM1-directed reorganization of microtubules in activated mast cells. J. Immunol. **186:**913–923. http://dx.doi.org/10.4049/jimmunol.1002074.
64. **Chung SC, Limnander A, Kurosaki T, Weiss A, Korenbrot JI.** 2007. Coupling Ca^{2+} store release to Icrac channel activation in B lymphocytes requires the activity of Lyn and Syk kinases. J. Cell Biol. **177:**317–328. http://dx.doi.org/10.1083/jcb.200702050.
65. **Timokhina I, Kissel H, Stella G, Besmer P.** 1998. Kit signaling through PI 3-kinase and Src kinase pathways: an essential role for Rac1 and JNK activation in mast cell proliferation. EMBO J. **17:**6250–6262. http://dx.doi.org/10.1093/emboj/17.21.6250.
66. **Linnekin D, DeBerry CS, Mou S.** 1997. Lyn associates with the juxtamembrane region of c-Kit and is activated by stem cell factor in hematopoietic cell lines and normal progenitor cells. J. Biol. Chem. **272:**27450–27455. http://dx.doi.org/10.1074/jbc.272.43.27450.
67. **Lennartsson J, Ronnstrand L.** 2012. Stem cell factor receptor/c-Kit: from basic science to clinical implications. Physiol. Rev. **92:**1619–1649. http://dx.doi.org/10.1152/physrev.00046.2011.
68. **Barnstein BO, Li G, Wang Z, Kennedy S, Chalfant C, Nakajima H, Bunting KD, Ryan JJ.** 2006. Stat5 expression is required for IgE-mediated mast cell function. J. Immunol. **177:**3421–3426. http://dx.doi.org/10.4049/jimmunol.177.5.3421.
69. **Morales JK, Falanga YT, Depcrynski A, Fernando J, Ryan JJ.** 2010. Mast cell homeostasis and the JAK-STAT pathway. Genes Immun. **11:**599–608. http://dx.doi.org/10.1038/gene.2010.35.
70. **Hálová I, Dráberová L, Bambousková M, Machyna M, Stegurová L, Smrž D, Dráber P.** 2013. Crosstalk between tetraspanin CD9 and transmembrane adaptor protein non-T cell activation linker (NTAL) in mast cell activation and chemotaxis. J. Biol. Chem. **288:**9801–9814. http://dx.doi.org/10.1074/jbc.M112.449231.
71. **Samayawardhena LA, Hu J, Stein PL, Craig AW.** 2006. Fyn kinase acts upstream of Shp2 and p38 mitogen-activated protein kinase to promote chemotaxis of mast cells towards stem cell factor. Cell. Signal. **18:**1447–1454. http://dx.doi.org/10.1016/j.cellsig.2005.11.005.
72. **Samayawardhena LA, Kapur R, Craig AW.** 2007. Involvement of Fyn kinase in Kit and integrin-mediated Rac activation, cytoskeletal reorganization, and chemotaxis of mast cells. Blood **109:**3679–3686. http://dx.doi.org/10.1182/blood-2006-11-057315.
73. **Metcalfe DD, Baram D, Mekori YA.** 1997. Mast cells. Physiol. Rev. **77:**1033–1079.
74. **Williams CM, Galli SJ.** 2000. The diverse potential effector and immunoregulatory roles of mast cells in allergic disease. J. Allergy Clin. Immunol. **105:**847–859. http://dx.doi.org/10.1067/mai.2000.106485.
75. **Schuck S, Honsho M, Ekroos K, Shevchenko A, Simons K.** 2003. Resistance of cell membranes to different detergents. Proc. Natl. Acad. Sci. U. S. A. **100:**5795–5800. http://dx.doi.org/10.1073/pnas.0631579100.
76. **Garner AE, Smith DA, Hooper NM.** 2008. Visualization of detergent solubilization of membranes: implications for the isolation of rafts. Biophys. J. **94:**1326–1340. http://dx.doi.org/10.1529/biophysj.107.114108.

7.3 C-TERMINAL SRC KINASE REGULATES FcεRI ACTIVATION LEADING TO DEGRANULATION AND CYTOKINES/CHEMOKINES PRODUCTION IN OPPOSITE WAYS, INDEPENDENTLY OF THE TRANSMEMBRANE ADAPTOR PROTEIN PAG.

Potuckova L., Draberova L., Halova I., Paulenda T., Draber P.

Manuscript, 2017

C-terminal Src kinase regulates FcεRI activation leading to degranulation and cytokines/chemokines production in opposite ways, independently of the transmembrane adaptor protein PAG

Lucie Potuckova[a], Lubica Draberova[a], Ivana Halova[a], Tomas Paulenda[a], Petr Dráber[a#]

[a]Department of Signal Transduction, Institute of Molecular Genetics, Academy of Sciences of the Czech Republic, Prague, Czech Republic.

Running title: Different roles of CSK and PAG in FcεRI signaling

#Correspondence:
Petr Draber, PhD
Department of Signal Transduction
Institute of Molecular Genetics
Academy of Sciences of the Czech Republic
Videnska 1083
CZ-142 20 Prague 4
Czech Republic

Tel.: +420-241062468;
Fax: +420-241470339;
E-mail: draberpe@img.cas.cz

Materials and Methods: 2132 words

Introduction, Results, Discussion: 6430 words

ABSTRACT

C-terminal Src kinase (CSK) is an important negative regulator of Src family tyrosine kinases (SFKs) that play critical roles in immunoreceptor signaling. CSK is brought in contiguity to the plasma membrane-bound SFKs via binding to a transmembrane adaptor PAG (Cbp). Recent finding that PAG can function as a positive or a negative regulator of bone marrow mast cells (BMMCs) signaling suggested that PAG and CSK have some non-overlapping regulatory functions in mast cell activation. To determine regulatory roles of CSK in FcεRI activation we derived from wild-type or PAG knockout (KO) mice BMMCs with reduced or enhanced expression of CSK and analyzed their FcεRI-mediated activation events. We found that antigen-activated BMMCs with CSK knockdown (KD) exhibited, in contrast to PAG-KO cells, significantly higher degranulation, calcium response, and tyrosine phosphorylation of FcεRI, SYK, and phospholipase C. On the other hand, cells with CSK-KD showed impaired phosphorylation of the transcription factor STAT5 and production of proinflammatory cytokines/chemokines. BMMCs with CSK-KD/PAG-KO resembled those with CSK-KD. The combined data indicate that CSK and PAG are, respectively, negative and positive regulators of events leading to degranulation, whereas they are both positive regulators of cytokines/chemokines production.

INTRODUCTION

Aggregation of the high-affinity IgE receptor (FcεRI)-IgE complexes by multivalent antigen in mast cells leads to the release of variety of mediators which play important roles in innate and adaptive immunity (1). Activated mast cells release mediators pre-stored in cytoplasmic granules, such as histamine, proteases, proteoglycans, and cytokines, as well as *de novo* synthetized lipids, cytokines, and chemokines. The first biochemically well defined step in FcεRI-activated cells is tyrosine phosphorylation of the immunoreceptor tyrosine-based activation motives (ITAMs) in the cytoplasmatic domains of the FcεRI β and γ subunits by a Src family kinase (SFK) LYN, followed by recruitment of protein tyrosine kinase (PTK) SYK to the FcεRI γ and its activation. LYN and SYK, together with FYN and some other PTKs phosphorylate tyrosine motives of transmembrane adaptor proteins (TRAPs) such as linker for activation of T cells (LAT; official name LAT1; (2), non-T cell activation linker (NTAL; official name LAT2; (3) and phosphoprotein associated with glycosphingolipid-enriched microdomains (PAG; official name PHAG1, also known as CSK-binding protein (Cbp); (4-6), which serve as anchors for other signal-transduction molecules that govern the biochemical signals responsible for initiating cell degranulation and cytokines and chemokines production. How exactly phosphorylation of the FcεRI subunits by LYN kinase is initiated is not completely understood and several models have been proposed, including the transphosphorylation model (7), lipid raft model (8) and PTK-protein tyrosine phosphatase (PTP) interplay model (9, 10).

The catalytic activity of LYN kinase is tightly regulated by phosphorylation/dephosphorylation of two conserved tyrosines at position 397 (Y^{397}) and 508 (Y^{508}) (11-13). Phosphorylation of Y^{397} stabilizes the activation loop of the catalytic domain and increases LYN activity. In contrast phosphorylation of Y^{508}, at the C terminus of LYN, promotes a conformation in which intramolecular binding of the Src homology 2 (SH2) domain with phosphorylated Y^{508} stabilizes the inactive conformation of the catalytic domain. Y^{397} of LYN is autophosphorylated *in trans*, whereas Y^{508} phosphorylation is catalyzed by C-terminal Src kinase (CSK). A critical role of CSK in cell physiology has been demonstrated by phenotype of mice lacing CSK. These mice die in early embryonic stages and their tissues possess SFKs with increased enzymatic activity (14-16). When CSK was inactivated in immature thymocytes, T cell development was significantly impaired (17). Furthermore, mice possessing

granulocytes with CSK inactivated by conditional mutagenesis, developed acute inflammatory responses (18).

In contrast to SFKs, which are anchored to the plasma membrane via their N-terminal myristoyl and/or palmitate moieties, CSK lacks a transmembrane domain and fatty acyl modifications and is predominantly localized in the cytosol (16). Thus, recruitment of cytosolic CSK to the vicinity of the plasma membrane-bound SFKs is involved in CSK-SFK cross-talk. An important anchor of CSK in the plasma membrane and regulator of CSK function is PAG. PAG is ubiquitously expressed and like other TRAPs, has a short extracellular domain, a transmembrane domain followed by palmitoylation site and a cytoplasmic domain with 10 potential tyrosine phosphorylation sites. In mouse PAG, phosphorylated Y^{314} binds CSK through its SH2 domain. Based on initial studies it has been postulated that PAG in resting T cells is constitutively phosphorylated and associated with CSK, which phosphorylates C-terminal tyrosines of SFKs in the vicinity of PAG, and inactivates them in this way. Activation through the T cell receptor (TCR) leads to rapid PAG dephosphorylation, which results in the release of CSK from PAG and relief of Csk-mediated inhibition of SFKs. This leads to an increased activity of LCK SFK, tyrosine phosphorylation of CD3 ITAMs and further propagation of the signal to downstream substrates (4, 19-21)

In contrast to T cell, in mast cells FcεRI activation results in rapid tyrosine phosphorylation of PAG, peaking at 2 – 3 min after triggering and then returns to basal levels. This suggested that together with LYN and CSK, PAG initiates a negative regulatory loop contributing to signal termination (22, 23). It should be noted, however, that recent experiments showed that even in resting T cells, PAG shows a low basal level of tyrosine phosphorylation that increases upon T cell activation and that the inhibitory function of PAG on TCR is seen in effector, but not naive T cells (24, 25).

Our recent study showed that bone marrow derived mast cells (BMMCs) with PAG knockout (KO) or PAG knockdown (KD) exhibited impaired antigen-induced degranulation, calcium response, tyrosine phosphorylation of FcεRI, SYK and some other signal transduction molecules, production of several cytokines and chemokines and chemotaxis. At the same time, enzymatic activites of LYN and FYN kinases were increased in nonactivated cells, suggesting the involvement of LYN and/or FYN-dependent negative regulatory loop (26). These data, together with our finding of enhanced degranulation and c-KIT receptor phosphorylation in stem cell factor (SCF)-

activated BMMCs with PAG KO, suggested that PAG can function as a positive or negative regulator of mast cell signaling, depending on the signaling pathway involved.

To better understand contribution of CSK and PAG in FcεRI-mediated signaling we examined in this study antigen-induced activation events in BMMCs from WT and PAG-KO mice with reduced or enhanced expression of CSK and corresponding controls. We also analyzed involvement of CSK and PAG in adhesion to fibronectin and chemotaxis towards antigen and SCF. Our data indicate that CSK and PAG in mast cells are, respectively, negative and positive regulators of events leading to degranulation and chemotaxis towards antigen and SCF, whereas they are both positive regulators of FcεRI-induced production of cytokines and chemokines.

MATERIALS AND METHODS

Antibodies and reagents. The following monoclonal antibodies (mAbs) were used: mouse IgE mAb specific for 2,4,6-trinitrophenol (TNP) clone IGEL b4.1 (27), anti-FcεRI β chain JRK (28), and SYK-specific mAb (29). Polyclonal antibodies specific for NTAL, LAT and LYN were prepared in this laboratory, by immunization of rabbits with the corresponding recombinant proteins or their fragments (30). Rabbit anti-IgE was prepared by immunization with whole IGEL b4.1. Polyclonal antibodies specific for CSK [catalogue number (Cat. No.) sc-286], STAT5 (Cat. No. sc-835), SHP-1 (Cat. No. sc-287), FYN (Cat. No. sc-16), phospholipase C (PLC) γ1 (Cat. No. sc-12943) and GRB2 (Cat. No. sc-255), as well as horseradish peroxidase (HRP)-conjugated goat anti-mouse IgG (Cat. No. sc-2005), and goat anti-rabbit IgG (Cat. No. sc-2004) and donkey anti-goat IgG (Cat. No. sc-2056), were obtained from Santa Cruz Biotechnology Inc. Antibodies specific for phospho-Lyn^{Y507} (in mouse Lyn^{Y508}) (Cat. No. 2731), phospho-SFKs^{Y416} (in mouse LYN^{Y397}; Cat. No. 2101), phospho-SYK$^{Y525/Y526}$ (Cat. No. 2711), phospho-STAT5^{Y694} (Cat. No. 9351), and phospho-SHP-1^{Y564} (Cat. No. 8849) were obtained from Cell Signaling. Phospho-LAT^{Y191} (Cat. No. 07-278) was obtained from Millipore. Anti-mouse β1 integrin specific antibody HM β1-1 (Cat. No. 553837) was purchase from BD Biosciences. Secondary antibody AF488-conjugated goat Ab specific for hamster IgG (Cat. No. A-21110) was obtained from Life Technologies). HRP-conjugated anti-phosphotyrosine mAb (PY20) and V450-conjugated rat anti-

mouse CD107a (Cat. No. 560648) were obtained from BD Biosciences. Anti-mouse FcεRI-fluorescein isothiocyanate (FITC; Cat. No. 11-5898) and anti-mouse c-KIT (CD117)-allophycocyanin (APC; Cat. No. 17-1171) conjugates were obtained from eBiosciences. Polyclonal antibodies specific for mouse tumor necrosis factor (TNF)-α (Cat. No. 500-P64), interleukin (IL)-13 (Cat. No. 500-P178), recombinant (r) mouse TNF-α (Cat. No. 315-01A), rIL-13 (Cat. No. 210-13), and rIL-6 (Cat. No. 216-16) were obtained from PeproTech. Murine anti-IL-6 (Cat. No. 553414) was purchased from Becton Dickinson. Colloidal gold nanoparticles (Au-NPs; diameter, 30 nm; Cat. No. EM.GC30), consisting of approximately 2×10^{11} Au-NPs/ml, were obtained from BB International. TNP-bovine serum albumin (BSA) conjugate (15 to 25 mol TNP/mol BSA) was produced as described previously (31). ^{45}Ca (specific activity, 773 MBq/mg Ca^{2+}) and [γ-^{32}P] ATP (specific activity, 222 TBq/mmol) were purchased from the Institute of Isotopes Co., Ltd. (Budapest, Hungary). All other reagents were from Sigma-Aldrich.

Mice and cells. Mice deficient in PAG and their WT littermates of C57BL/6 genotype were used in this study. The mice were maintained according to the protocols approved by the Animal Care and Usage Committee of the Institute of Molecular Genetics (Permit number 12135/2010-17210) and national guidelines (2048/2004-1020). PAG-KO mice were generated by modified bacterial artificial chromosome (BAC) technology as previously described (32), (33). For experiments, PAG-KO mice were mated with C57BL/6 mice and their F_1 descendants were genotyped by PCR and the expression of PAG was verified at protein level as previously described (26). Bone marrow cells were isolated from the femurs and tibias of 8 - 12 week-old mice. The cells were cultured for 6 - 10 weeks in RPMI-1640 medium supplemented with 100 U/ml penicillin, 100 µg/ml streptomycin, 71 µM 2-mercaptoethanol, minimum essential medium (MEM) non-essential amino acids, 0.7 mM sodium pyruvate, 2.5 mM L-glutamine, 12 mM D-glucose, recombinant mouse stem cell factor (SCF, 15 ng/ml, PeproTech EC), mouse recombinant interleukin (IL)-3 (15 ng/ml, PeproTech EC), and 10% fetal calf serum (FCS).

Lentiviral vectors and gene transduction. Lentiviral transductions were done as described previously using HEK 293 T/17 packaging cells for virus preparation (26). A set of murine csk-specific short hairpin (sh) RNAs constructs based on pLKO.1 vector

(TRCN0000023735 [shRNA 35], TRCN0000023736 [shRNA 36], TRCN0000361164 [shRNA 64], TRCN0000321790 [shRNA 90]) were purchased from Open Biosystems. Cells were transduced with individual shRNAs or with a pool of shRNAs prepared by mixing shRNAs 35, 36, 64, and 90, in equimolar ratios. Individual constructs or pool of the constructs (14 μg) was mixed with OptiMEM (1 ml; Invitrogen), 21 μl of lentiviral packaging mix (Invitrogen), and 105 μl polyethyleneimine (PEI; Sigma) and virus was produced and transduced as described (26). The pilot degranulation experiments were performed with individual shRNAs vectors, but because the individual vectors gave similar results as the pooled shRNA vectors, further experiments were done with shRNA pool denoted in further text as CSK-KD. For experiments with stable CSK overexpression, a pMX plasmid encoding human Csk (hCsk), kindly provided by T. Brdička (Laboratory of Leukocyte Signaling, Institute of Molecular Genetics, Prague) was used for recloning casette of hCSK-mCherry into the vector pCDH-CMV-MCS-EF1-Puro (Systembio; pCDH). For PCR, the forward primer 5´-AAATCTAGAGCCACCATGTCAGCAATACAGGCC-3´ (the XbaI restriction site is underlined) and reverse primer 3´-TTTGCGGCCGCCTACTTGTACAGCTCGTCCAT-5´ (the NotI restriction site is underlined) was used. For recloning casette of hCSK-myc we used the same forward primer but different reverse primer 3´-TTTGCGGCCGCTCACAGATCCTCTTCAGAGAT-5´ (the NotI restriction site is underlined). The constructs were verified by sequencing and denoted hCSK-mCherry and hCSK-myc. In all experiments, empty pLKO.1 or empty pCDH vectors were used as controls. In some experiments related to CD107a and β-glucuronidase detection, we also used pLKO.1 vector containing nontarget (NTG) shRNA (Sigma-Aldrich) as a control.

Flow cytometry analysis. To quantify the surface expression of FcεRI and c-KIT, BMMCs were double-stained with anti-mouse FcεRI-FITC and anti-mouse c-KIT-allophycocyanin antibodies for 30 min on ice. After labeling, the cells were washed 3 times with ice-cold PBS and analyzed with an LSRII flow cytometer (BD Biosciences) and further processed using FlowJo software (Ashland, OR). For analysis of surface LAMP1, BMMCs were activated or not with various concentrations of antigen (10-100 ng/ml) for 10 min at 37°C. Activation was stopped by centrifugation at 4°C. The cells were then resuspended in 50 μl of PBS-1% BSA containing 200-fold-diluted V450-

conjugated rat anti-mouse CD107a and stained on ice for 30 min. After washing with PBS, the cells were examined as described above. For analysis of IgE internalization, IgE-sensitized cells were activated with antigen (500 ng/ml TNP-BSA) or not for various time intervals (5, 15, or 30 min) at 37°C. Activation were stoped by centrifugation at 4°C (300×g; 3min), cells were fixed by 4% paraformaldehyde for 15 minutes and washed with PBS. IgE was stained using AF488-conjugated anti-mouse IgG (cross-reacting with IgE) and analyzed as described previously (34). To quantify surface expression of β1 integrin, the cells were exposed for 30 min on ice to β1 integrin specific antibodies HM β1-1 followed by 30 min incubation with AF488-conjugated goat Ab specific for hamster IgG. After 30 min incubation, the cells were washed in ice-cold PBS and evaluated as previously described (35).

β-glucuronidase release and Ca^{2+} response. BMMCs were cultured for 4 h in SCF- and IL-3-free medium supplemented with TNP-specific IgE (1 μg/ml). The IgE-sensitized cells were washed and degranulation assay, based on evaluation of β-glucuronidase release, was performed and evaluated, as previously described (26). Fluorescence was determined by an Infinite 200M (Tecan) plate reader at 355-nm excitation and 460-nm emission wavelengths. Calcium response was analyzed using Fura-2, AM (Life Technologies) cytoplasmatic reporter, as described previously (26). Levels of intracellular Ca^{2+} were determined by spectrofluorometry using the Infinite 200 M plate reader with excitation wavelengths at 340 and 380 nm and with a constant emission at 510 nm.

Cytokines and chemokines detection. mRNA was extracted from IgE-sensitized and antigen-activated BMMCs using a TurboCapture 96 mRNA kit or RNeasy miniKit (Qiagen). Single-stranded cDNA was synthesized with M-MLV reverse transcriptase (Invitrogen) according to the manufacturer's instructions. Real-time quantitative polymerase chain reaction (RT-qPCR) amplifications of cDNAs and oligonucleotide primers used were described previously (26), (36). Actin, GAPDH and ubiquitin were used as reference genes and the expression levels of TNF-α, IL-13, IL-6, CCL3, and CCL4 mRNAs were normalized to the geometric mean of the reference genes in nonactivated control cells. For quantification of cytokines, an immuno PCR method with nangold particles armed with immobilized DNA template and cytokine specific antibodies were used as described previously (26), (37). Briefly, anti-TNF-α, anti-IL-

6, or anti-IL-13 in 100 mM borate buffer (pH 9.5) was dispensed in 50-µl aliquots into the wells of a real-time 96-well plate (Eppendorf). After overnight incubation at 4°C, each well was washed four times with 200 µl of Tris-buffered saline (10 mM Tris-HCl, pH 7.4, 150 mM NaCl) containing 0.05% Tween 20 (TBST), and the remaining binding sites were blocked by 2 h of incubation at 37°C with TBST supplemented with 2% BSA. After washing, 50 µl of serial dilutions (0.1 to 100 ng/ml) of recombinant TNF-α, IL-6, or IL-13 (used for construction of calibration curves) or the tested samples diluted in PBS–1% BSA was added. The samples were incubated for 1 h at 37°C, and after washing with TBST, 50 µl of Au-NPs armed with thiolated DNA oligonucleotide template and with the corresponding cytokine-specific antibody was applied into each well. The wells were incubated for 1 h at 37°C and washed with TBST and deionized water. Fifty-microliter aliquots of qPCR master mix solution (see above) supplemented with 60 nM of the corresponding oligonucleotide primers were then dispensed into each well. The plates were sealed, and the amount of template DNA bound to antigen-anchored functionalized Au-NPs was evaluated by real-time PCR using a Realplex4 Mastercycler apparatus (Eppendorf). For calculation of cytokines concentrations, the corresponding CT values of the cytokines were substituted into the regression equations obtained from the calibration curves constructed from the concentration series of appropriate recombinant proteins.

Cell chemotaxis and adhesion assay. Chemotaxis responses were assayed in 24-well Transwell chambers (Corning) with 8-µm-pore-size polycarbonate filters in the upper wells as previously described (26). Chemoattractants, antigen (250 ng/ml) or SCF (100 ng/ml), in 0.6 ml chemotaxis medium (RPMI 1640 supplemented with 1% BSA and 20 mM HEPES, pH 7.4) were added to the lower compartments and IgE-sensitized BMMCs (0.3×10^6 in 120 µl chemotactic medium) were added into each upper compartment. Cells migrating into the lower compartments during the 8 h of incubation (37°C, 5% CO_2) were counted using an Accuri C6 flow cytometer (BD Biosciences). Adhesion to fibronection was quantified in 96-well plates coated overnight with fibronectin (10 µg/ml in PBS), blocked with 4% BSA in PBS (1 h at 37°C) and washed twice with PBS. IgE-sensitized BMMCs were loaded with Calcein-AM (4 mM) for 30 min at 37°C, washed and transferred into the fibronectin-coated wells (10^5 cells/well). After activation with antigen (100 ng/ml, 30 min) or SCF (100 ng/ml, 30 min), unbound cells were washed out using microplate washer (HydroSpeed, TECAN) and bound cells

were determined using an Infinite 200M Fluorometer with excitation and emission filters at 485 nm and 538 nm, respectively.

Immunoprecipitation and immunoblotting. Whole-cell extracts from nonactivated or Ag-activated (250 ng/ml) cells were prepared by solubilizing cell pelletes in sodium dodecyl sulfate (SDS) sample buffer (38), followed by sonication and boiling of samples at 97°C for 5 min. Proteins were size fractionated on 10% SDS-polyacrylamide gel electrophoresis (39), electrophoretically transferred onto nitrocellulose membrane, and analyzed by immunoblotting with protein- or phosphoprotein-specific antibodies. Bound primary antibodies were detected with HRP-conjugated secondary antibodies. The HRP signal was detected with chemiluminescence reagent (40) and quantified by a Luminescent Image Analyzer LAS 3000 (Fuji Photo Film Co.). Aida software (Raytest GmbH) was used for signal quantification. Protein levels were normalized to the corresponding controls and/or GRB2 loading control protein after stripping of the membrane in stripping buffer (62.5 mM Tris-HCl, pH 6.7, 100 mM 2-mercaptoethanol, 2% SDS) at 50°C for 30 min. For FcεRI immunoprecipitation, cells were solubilized in ice-cold immunoprecipitation buffer (25 mM Tris-HCl, pH 8.0, 140 mM NaCl, 1 mM Na_3VO_4, 2 mM EDTA, 1 μg/ml aprotinin, 1 μg/ml leupeptin, 1 mM phenylmethylsulfonyl fluoride) supplemented with 0.2% Triton X-100. After incubation on ice for 30 min, the lysates were centrifuged (16,000 x g for 5 min at 4°C) and postnuclear supernatants were immunoprecipitated with rabbit anti-IgE antibody prebound to UltraLink-immobilized protein A (Pierce, Thermo Scientific). The immunoprecipitated proteins were size-fractionated by SDS-PAGE as described above, transferred to nitrocellulose membrane and immunoblotted with PY20 conjugate or with FcεRI-β chain-specific antibody followed by HRP-conjugated anti-mouse IgG.

Immunocomplex kinase assay. The *in vitro* kinase assays were performed as previously described (41), with some modifications. FcεRI, LYN, and FYN were solubilized in immunoprecipitation buffer-0.2% Triton X-100. Proteins immobilized to antibody-armed protein A beads were washed with kinase buffer (25 mM HEPES–NaOH, pH 7.2, 3 mM $MnCl_2$, 0.1% Nonidet P-40, 100 mM Na_3VO_4, 20 mM $MgCl_2$) and then resuspended in 25 μl kinase buffer supplemented with 2.5 μCi (92.5 kBq) of [γ-^{32}P]ATP, 100 μM ATP, and 0.5 μg/μl of acid-denatured enolase as the exogenous substrate. The ^{32}P-labeled proteins were size fractionated by SDS-PAGE, transferred to

a nitrocellulose membrane, and visualized by autoradiography. Films were quantified with Aida image analyzer software (Raytest).

Statistical analyses. The significance of intergroup differences was evaluated by Student's t test, except experiments evaluating calcium responses where intergroup differences were determined by one-way ANOVA with Tukey's post-test; *, $p<0.05$; **, $p<0.01$; ***, $p<0.001$. Microsoft Excel 2010 or GrafPad Prism 5 (GraphPad Software, La Jolla, CA, USA) was used for statistical analysis evaluation.

RESULTS

Production of BMMCs with reduced or enhanced expression of CSK. To determine the role of CSK in mast cell signaling we prepared BMMCs from C57BL/6 mice with reduced or enhanced expression of CSK. For CSK silencing we used four CSK-specific shRNAs (35, 36, 64, and 90) in lentiviral pLKO.1 vector. As controls, BMMCs transduced with empty pLKO.1 vector or pLKO.1 vector containing non-target sequence were used; because there were no significant differences between the results obtained with these different control vectors the data were pooled and are presented together as control pLKO.1 vector. Lentiviral-mediated delivery of individual CSK-specific shRNAs resulted in a decrease of CSK protein to 26% (shRNA 35), 18% (shRNA 36), 26% (shRNA 64), and 36% (shRNA 90) when compared to cells transduced with control pLKO.1 (Fig. 1 A, B). BMMCs were also transduced with a pool of individual CSK-specific shRNAs, which reduced the level of CSK in these cells in average to 19% of controls (Fig. 1C, D). To get enhanced expression of CSK, BMMCs were transduced with pCDH lentiviral vector containing Csk cDNA tagged with mCherry (hCSK-mCherry) or with myc (hCSK-myc). Empty pCDH vector was used as a control. Ten days after transduction and growing in media with puromycin, more than 90% of cells transduced with hCSK-mCherry construct expressed detectable mCherry (not shown). Immunoblotting analyses showed that cells transduced with hCSK-mCherry or hCSK-myc vectors, denoted as CSK overexpressors (OE) exhibited, respectively, about 2- to 3-fold higher CSK levels than cells transduced with empty pCDH vector (Fig. 1E and F). To find out whether altering CSK expression by transduction procedure and selection in puromycin has any effect on surface expression of FcεRI and c-KIT receptor we examined various cell types by flow cytometry. We found that cells transduced with individual CSK-specific shRNAs (not shown), pooled CSK-specific shRNA (CSK-KD), or hCSK-mCherry and hCSK-myc (CSK-OE; Fig. 1G) displayed surface expression of FcεRI and c-KIT receptor comparable to corresponding control cells transduced with empty vectors (pLKO.1 and pCDH; Fig. 1G and H).

Enhanced degranulation and calcium response and reduced FcεRI-IgE complexes internalization in BMMCs with CSK-KD. To find out whether reduced expression of

CSK in BMMCs affects their FcεRI-mediated degranulation, the cells transduced with individual shRNAs (35, 36, 64 and 90) or pooled shRNAs were sensitized with IgE and activated with various concentrations of antigen. Degranulation was quantified based on β-glucuronidase released from the cells upon antigen exposure or spontaneously. In non-activated cells there were no significant changes in spontaneous β-glucuronidase released from the cells transduced with various individual shRNAs vectors or empty vector (Fig. 2A). After FcεRI triggering with antigen at a concentration 100 ng/ml or 250 ng/ml, significantly increased degranulation was observed in all cell types transduced with various shRNAs when compared to pLKO.1 control cells (Fig. 2A). Significantly increased degranulation was also observed when cells transduced with pooled shRNAs were used for transduction (Fig. 2 B). It should be noted that total amount of β-glucuronidase present in all cell types was similar (not shown), indicating a negative regulatory role of CSK on FcεRI-mediated degranulation, rather than on enhanced production of β-glucuronidase. Because the results obtained with cells transduced with individual shRNAs or pooled shRNAs were similar, we decided to combine the data and present them as data from cells with CSK-KD.

Previous studies showed that mast cell degranulation is accompanied by enhanced surface expression of CD107a (LAMP1) (42). To determine whether CSK has any effect on this process, we examined levels of CD107a expression by flow cytometry in BMMC with CSK-KD and control cells before and after activation with antigen. The results showed that BMMCs with CSK-KD activated for 10 min with various concentrations of antigen exhibited significantly higher surface expression of CD107a than pLKO.1 control cells (Fig 2C). We also examined CD107a expression in BMMCs transduced with empty pCDH vector or the vectors possessing hCSK-mCherry or hCSK-myc constructs and found no significant differences in CD107a surface expression among the cell types activated with various concentrations of antigen (Fig. 2D).

FcεRI-mediated activation induces rapid Ca^{2+} mobilization, which is required for mast cell degranulation (43). To determine the role of CSK in Ca^{2+} signaling, IgE-sensitized cells with CSK-KD or CSK-OE (hCSK-mCherry and hCSK-myc) were loaded with intracellular Ca^{2+} indicator Fura-2 and mobilization of Ca^{2+} was measured upon antigen stimulation. We found that Ca^{2+} levels were significantly increased in BMMCs with CSK-KD when compared to cells transduced with empty pLKO.1 vector (Fig. 2E). On the other hand, no significant difference in antigen-mediated Ca^{2+}

mobilization was observed among BMMCs transduced with pCDH vector alone or possessing hCSK-mCherry or hCSK-myc (Fig. 2F).

To determine whether enhanced degranulation and calcium response in BMMCs with CSK KD are related to changes in the FcεRI internalization, we used flow cytometry and measured fraction of total IgE remaining on the cell surface at various time intervals after antigen-mediated aggregation of the FcεRI-IgE complexes. We found that upon antigen triggering BMMCs with CSK-KD showed significantly reduced internalization of the antigen-IgE-FcεRI complexes when compared to pLKO.1 control cells (Fig. 2G).

Negative and positive regulatory roles of CSK in tyrosine phosphorylation of early signal-transduction molecules. To contribute to understanding the molecular mechanism by which CSK regulates degranulation and Ca^{2+} response after FcεRI triggering, we first examined tyrosine phosphorylation profiles. We found no dramatic differences in global tyrosine phosphorylation between nonactivated BMMCs with CSK-KD and control cells (pLKO.1). One minute after antigen-mediated activation, control cells exhibited enhanced tyrosine phosphorylation of several substrates, which was down-regulated 5 min after triggering. Similar set of proteins showed enhanced phosphorylated in cells with CSK-KD, but the extent of phosphorylation was for most of the proteins higher than in control cells at 1 and 5 min after triggering (Fig. 3A).

Next we analyzed the role of CSK in tyrosine phosphorylation of individual proteins involved in early signal transduction events after FcεRI triggering. BMMCs with CSK KD or the corresponding control cells were sensitized with IgE, activated or not with antigen for various time intervals, solubilized, and tyrosine phosphorylation of the immunoprecipitated FcεRI chains was examined by immunoblotting (Fig. 3B) and analyzed by densitometry (Fig. 3C). Data show that after antigen-mediated activation, FcεRI β and γ chains are rapidly tyrosine phosphorylated in both cell types. However, cells with CSK KD, when compared to corresponding control cells, exhibited significantly higher phosphorylation of the FcεRI β and γ chains in nonactivated state as well as 1 min after triggering.

In further experiments we examined tyrosine phosphorylation of SYK and PLCγ in antigen-activated BMMCs using phosphotyrosine specific antibodies and found that both proteins showed higher tyrosine phosphorylation in cells with CSK-KD than control cells (Fig. 3D - F).

Previous study showed that inhibition of CSK enzymatic activity in T cells resulted in enhanced tyrosine phosphorylation of adaptor protein LAT (44). However, there are no data on the regulatory role of CSK for another adaptor protein similar to LAT, but absent in nonactivated T cells, NTAL, which is expressed together with LAT in mast cells (45). Next we therefore examined tyrosine phosphorylation of both adaptor proteins in antigen-activated BMMCs with CSK-KD and controls. In nonactivated cells, tyrosine phosphorylation of LAT and NTAL was low and comparable in both cell types. When compared to corresponding controls, antigen-activated BMMCs with CSK-KD exhibited comparable tyrosine phosphorylation of the LAT adaptor protein but significantly decreased tyrosine phosphorylation of the NTAL adaptor (Fig. 3G - I).

Tyrosine phosphorylations of the FcεRI subunits and also LAT and NTAL are mediated at least in part by LYN kinase activity (46). Enzymatic activity of LYN is regulated in positive way by auto-phosphorylation of its Y^{397} and negative way by CSK-mediated phosphorylation of its C-terminal Y^{508} (16). To determine the role of CSK in phosphorylation of these tyrosines, the cells were sensitized with IgE, activated or not with various concentration of antigen, and analyzed by immunoblotting with phosphotyrosine specific antibodies. In control BMMCs, transduced with empty pLKO.1 vector, LYN^{Y508} was phosphorylated in nonactivated cells and after activation its phosphorylation did not show significant changes (Fig. 3J and K). As expected, BMMCs with CSK-KD, when compared to controls, showed significantly reduced phosphorylation of LYN^{Y508} in nonactivated as well as activated cells. When auto-phosphorylation of LYN^{Y397} was analyzed in nonactivated cells, no significant changes were observed between BMMCs with CSK-KD and control cells. After antigen-mediated activation, both cell types exhibited significant decrease in phosphorylation of $SFKs^{Y397}$ and again no significant difference was observed between them (Fig. 3J and L).

Protein tyrosine kinases are negatively regulated by protein tyrosine phosphatases (PTPs) (47) . PTP, Src homology region 2 domain-containing phosphatase-1 (SHP-1), is involved in regulation of FcεRI signaling and directly interacts with LYN (48). To determine whether CSK is involved in SHP-1 regulation in the course of FcεRI-mediated activation, we analyzed phosphorylation of SHP-1by immunoblotting. In nonactivated cells, there was only weak tyrosine phosphorylation of this phosphatase and CSK had no significant effect on it. Upon antigen stimulation, phosphorylation of SHP-1 was significantly higher in cells with CSK-KD than pLKO.1 control cells (Fig.

3M and N). The data suggest that CSK is a negative regulator of SHP-1 tyrosine phosphorylation.

Different regulation of LYN, FYN, and FcεRI-bound kinase activity by CSK. The observed changes between BMMCs with CSK KD and corresponding controls in phosphorylation of signal transduction molecules led us to compare regulatory role of CSK on LYN kinase activity in nonactivated and antigen-activated cells. For these experiments LYN was immunoprecipitated and its auto-phosphorylation and phosphorylation of the exogenous substrate, an acid-denaturated enolase, was examined by an *in vitro* kinase assay. LYN kinases from nonactivated BMMCs with CSK-KD and control cells exhibited comparable enzymatic activities as reflected by similar autophosphorylation and enolase phosphorylation (Fig. 4A - C). However, upon antigen stimulation, immunoprecipitated LYN from cells with CSK-KD showed lower auto-phosphorylation but no significant difference in phosphorylation of enolase when compared to LYN from control cells (Fig. 4A - C).

We also analyzed in the kinase assay an enzymatic activity of FYN kinase, which is an important regulator of FcεRI-induced degranulation and found no difference in auto-phosphorylation and enolase phosphorylation between FYN immunoprecipitated from non-activated or antigen-activated BMMC with CSK-KD or control cells (Fig. 4D - F).

Finally, we examined phosphorylation of FcεRI subunits by the FcεRI-associated kinases. The FcεRI-IgE complexes were isolated by immunoprecipitation from nonactivated or antigen-activated BMMCs with CSK-KD or control cells and examined by an *in vitro* kinase assays. In non-activated cells FcεRI β and γ subunits showed significantly higher phosphorylation when derived from BMMCs with CSK-KD than from control cells. After activation there was significant increase in phosphorylation of the receptor subunits from control cells, but no significant change when the receptor was obtained from cells with CSK-KD (Fig. 4G – I). These data are in accord with tyrosine phosphorylation of the FcεRI subunits as detected by immunoblotting (Fig. 3B, C).

CSK is a positive regulator of cytokines and chemokines production, and STAT5 phosphorylation. Production and release of cytokines and chemokines is cardinal feature of the FcεRI-induced mast cell activation (1). In further experiments we

therefore compared these responses between BMMCs with CSK-KD and pLKO.1 control cells. IgE-sensitized cells were activated with antigen and mRNA levels of various cytokines (TNF-α, IL-13, IL-6) and chemokines (CCL3 and CCL4) were analyzed by RT-qPCR. Interestingly, the mRNA levels of all studied cytokines (Fig. 5A) and chemokines (Fig. 5B) were significantly reduced in BMMCs with CSK-KD when compared to control cells. Next, we measured secretion of the cytokines into the media. In nonactivated cells there were no significant differences in basal levels of secreted cytokines between BMMCs with CSK-KD and control cells. Upon 6-hr stimulation with various concentration of antigen, concentrations of secreted TNF-α (Fig. 5C), IL-13 (Fig. 5D) and IL-6 (Fig. 5E) were significantly lower in BMMCs with CSK-KD than in control cells. It is known that TNF-α is an early secreted mediator in antigen-activated cells (49, 50). Therefore, we also examined secretion of TNF-α at earlier time points. Cells with CSK-KD exhibited significantly lower TNF-α secretion into the media even 1 h and 2 h after antigen triggering (Fig. 5F).

To understand the mechanism how CSK positively regulates FcεRI-induced cytokines production, we examined tyrosine phosphorylation of transcription factor STAT5, which is one of the key regulators of cytokines production in mast cells (51). In control BMMCs antigen induced gradual increase of STAT5 tyrosine phosphorylation, but in BMMCs with CSK-KD no such increase was observed and significant difference between cells with CSK KD and controls in STAT5 phosphorylation was observed 5 min after FcεRI triggering (Fig. 5G and H).

CSK regulates adhesion to fibronectin and chemotactic responses in opposite direction. We also examined a role of CSK in adhesion of antigen- or SCF-activated BMMCs on fibronectin-coated wells. Upon activation with various concentrations of antigen, BMMCs with CSK-KD exhibited significantly lower adhesion on fibronectin than control cells at all antigen concentrations tested (Fig 5I). When the cells were activated by SCF, cells with CSK KD exhibited less dramatic reduction of adhesion to fibronectin than control cells; the difference was significant when SCF was used at a concentration giving maximum adhesion (50 ng/ml; Fig. 5J). It should be noted that reduced adhesion in cells with CSK KD was not caused by changes in expression of β1-integrine (not shown).

An important feature of mast cells is their ability to migrate towards chemoattractant, which can be simulated by an *in vitro* transwell-migration assay (52).

When compared to control cells, BMMCs with CSK-KD exhibited enhanced migration towards antigen as well as towards SCF, which is more potent chemoattractant than antigen (Fig. 5K).

Production of PAG-KO BMMCs with reduced or enhanced CSK expression. Previous studies showed that CSK is anchored to the plasma membrane by transmembrane adaptor protein PAG (4, 5, 26). Removal of PAG by gene KO caused positive or negative regulation of mast cell activation depending on the activation event analyzed. Properties of BMMC with PAG KO were in part similar to those with CSK KD described in this study. However, because PAG interacts with many other signal transduction molecules (24), we also examined properties of PAG-deficient mast cells with reduced or enhanced expression of CSK. To this end, we used BMMCs from PAG KO mice and performed CSK-KD by lentiviral-mediated delivery of CSK-specific shRNA (pool of four shRNAs), followed by selection of puromycin-resistant clones, as described above. Immunoblotting and densitometry analyses of such cells showed a decreased expression of CSK by approximately 80% when compared to control cells transduced with an empty pLKO.1 vector (Fig. 6A and B). For production of PAG-KO BMMCs with enhanced expression of CSK, we used lentiviral system for transduction of pCDH vectors containing CSK cDNA tagged with mCherry (hCSK-mCherry) or myc (hCSK-myc). As a control, empty pCDH vector was used. Immunoblotting analyses combined with densitometry showed approximately 2- or 3-fold increase of CSK expression in the cells transduced with hCSK-mCherry or hCSK-myc, respectively (Fig. 6C and D). More than 90% of PAG-KO BMMCs transduced with hCSK-mCherry or hCSK-myc expressed detectable mCherry (not shown).

To find out whether altering CSK expression in BMMCs with PAG KO has any effect of FcεRI and c-KIT expression, we examined surface expression of all transduced cell types and found that CSK-KD or CSK-OE in PAG-KO BMMCs had no significant effect on the surface expression of the FcεRI and c-KIT (Fig. 6E and F).

PAG-KO BMMCs with CSK-KD exhibit enhanced degranulation, calcium response and tyrosine phosphorylation of early signal transduction proteins. Our previous study showed that BMMCs isolated from mice with PAG-KO exhibited significantly reduced tyrosine phosphorylation of several molecules involved in early FcεRI-mediated signaling, including FcεRI chains, SYK, LAT, and pPLCγ, which

resulted in reduced degranulation and Ca^{2+} mobilization after antigen-mediated activation (26). On the other hand this study showed that degranulation and Ca^{2+} responses were enhanced in cells with CSK KD. In order to better understand regulatory roles and cross-talks between CSK and PAG during FcεRI-mediated mast cell signaling, we first compared degranulation and Ca^{2+} response in PAG-KO BMMCs with CSK-KD (labeled as CSK-KD/PAG-KO) and PAG-KO cells with normal level of CSK (pLKO.1/PAG-KO).

To determine β-glucuronidase response in BMMCs with CSK-KD/PAG-KO, the cells were sensitized with IgE and then activated with various concentrations of antigen (Fig. 7A). Results showed that even nonactivated CSK-KD/PAG-KO cells exhibited enhanced β-glucuronidase release in comparison with pLKO.1/PAG-KO control cells. Upon stimulation with various concentration of antigen, CSK-KD/PAG-KO cells exhibited significantly elevated levels of β-glucuronidase in all antigen concentration tested when compared to the control cells (Fig 7A). Next, we determined surface localization of CD107a in antigen-activated or nonactivated CSK-KD/PAG-KO cells. Consistent with the β-glucuronidase release, we observed significantly increased surface localization of CD107a after antigen activation, when compared to pLKO.1 control cells (Fig. 7B). Next, we analyzed CD107a surface localization in PAG-KO cells with enhanced expression of CSK. PAG-KO BMMCs were transduced with hCSK-mCherry or hCSK-myc constructs (CSK-OE) and CD107a was analyzed by flow cytometry. We found a moderate decreased surface expression of CD107a in CSK-OE/PAG-KO BMMCs when compared to control cells (Fig. 7C). We also analyzed Ca^{2+} response in BMMCs with CSK-KD/PAG-KO. The cells were sensitized with IgE, loaded with Fura-2 and activated with antigen. In such cells Ca^{2+} response was significantly higher when compared to Ca^{2+} response in control cells (Fig. 7D). These data indicate that CSK in BMMCs is a negative regulator of degranulation and Ca^{2+} response, regardless of the presence of PAG adaptor.

To further explore whether PAG has a role in downstream of FcεRI signaling in BMMCs with CSK-KD, we analyzed tyrosine phosphorylation of the antigen-aggregated FcεRI in CSK-KD/PAG-KO and control cells. Cells were sensitized with IgE, activated or not with antigen for various time intervals and tyrosine phosphorylation of FcεRI in immunoprecipitates were examined (Fig. 7E). Quantification of the data showed that tyrosine phosphorylation of FcεRI β and γ chains were significantly increased in BMMCs with CSK-KD/PAG-KO in comparison with

control cells (Fig. 7F). Further, we examined tyrosine phosphorylation of SYK (pSYK), LAT (pLAT) and NTAL (pNTAL) in IgE-sensitized and antigen-activated or nonactivated CSK-KD/PAG-KO BMMCs cells (Fig. 7G). Statistical evaluation of intergroup differences showed an increased tyrosine phosphorylation of SYK in CSK-KD/PAG-KO cells after antigen stimulation in comparison with control cells (Fig. 7G and H). Phosphorylation of LAT and phosphorylation of NTAL was also significantly higher in antigen-activation CSK-KD/PAG-KO cells than control BMMCs (Fig. 7G, I and J).

Collectively, these data suggested that CSK deficiency is dominant over PAG deficiency in BMMCs with respect to antigen-induced degranulation and Ca^{2+} mobilization. On the other hand, PAG-deficient BMMCs with CSK-KD exhibit different phosphorylation pattern of adaptor protein LAT and NTAL in comparison with CSK-KD cells.

PAG-KO BMMCs with CSK-KD exhibit reduced cytokines production, STAT5 phosphorylation and adhesion to fibronectin, but enhanced chemotaxis towards antigen and SCF. Our previous study showed that in antigen-activated BMMCs, PAG adaptor exhibited positive regulatory role in cytokines secretion and migration towards antigen (26). In this study we observed a positive regulatory role of CSK on cytokines and chemokines production but a negative regulatory role on antigen-mediated chemotaxis. To determine whether there is an additive effect of PAG-KO and CSK-KD in regulation of these signaling pathways, we further examined secretion of cytokines into the media in antigen-stimulated BMMCs with CSK-KD/PAG-KO and control cells, with PAG-KO alone. In nonactivated cells there were no significant differences in basal level secretions of the cytokines between BMMCs with CSK-KD/PAG-KO and pLKO.1/PAG-KO control cells. Upon stimulation with various concentration of antigen, secretion of TNF-α (Fig. 8A) and IL-13 (Fig. 8B) was significantly decreased in cells with CSK-KD/PAG-KO when compared with control cells at the highest concentration of antigen used. No significant inhibition was observed between the cells when IL-6 production was analyzed. (Fig. 8C). In agreement with this results we observed significantly decreased phosphorylation of STAT5 in CSK-KD/PAG-KO cells, which was reduced not only upon antigen activation but also in nonactivated cells (Fig. 8D and E).

Next, we examined adhesion on fibronectin-coated wells of IgE-sensitized BMMCs with CSK-KD/PAG-KO and control cells activated with antigen or SCF. Upon activation, BMMCs with CSK-KD/PAG-KO exhibited significantly reduced adhesion to fibronectin than control cells at all concentrations of antigen (Fig. 8F) and SCF (Fig 8G) tested.

To determine cross-talk between PAG and CSK in chemotaxis response, we examined in transwell-migration assay, migration of BMMCs with normal level of PAG and CSK (WT), PAG-KO and CSK-KD/PAG-KO towards antigen or SCF (Fig. 8H). There were no differences among the cell types in the absence of chemoattractant. In cells exposed to antigen, PAG-KO reduced chemotaxis, as expected (26), while cells CSK-KD/PAG-KO exhibited enhanced migration towards antigen in comparison with cells with cells with PAG-KO alone. When we analyzed chemotaxis towards SCF, the migration of cells with CSK-KD/PAG-KO was significantly higher than migration of WT cells and PAG-KO cells (Fig. 8F). It should be noted that WT cells showed similar migration as cells transduced with empty pLKO.1 vector. The data suggested, that both PAG and CSK are implicated in BMMCs chemotaxis in different pathways.

DISCUSSION

Our previous report on the biochemical activity and responses of PAG-deficient mast cells (26) has provided a glimpse of positive and negative regulatory roles of PAG in various signaling pathways. PAG serves as an anchor for CSK and in this way could negatively regulate activity of SFKs. However, PAG interacts with numerous other signal transduction proteins (24), whose contribution to FcεRI- or c-Kit-mediated mast cell activation is poorly understood. Here we explored the role of CSK-PAG cross-talk in mast cell activation by examining activation of BMMCs with CSK-KD or CSK-OE alone or in combination with PAG-KO. Summary of the data comparing properties of FcεRI-activated control BMMC and BMMCs with CSK-KD, CSK-KD/PAG-KO (this study) and PAG-KO (26) is shown in Table 1 and Figure 9. Several lines of evidence in this study indicate that CSK regulates FcεRI-mediated activation events leading to degranulation and chemotaxis versus cytokines/chemokines production in opposite ways. At least some of them seem to be regulated by CSK independently of the PAG.

First, in IgE-sensitized BMMCs with PAG-KO exposure to antigen resulted in significantly decreased degranulation when compared to antigen-activated wild-type cells (26), indicating that PAG is a positive regulator in this process. When BMMCs with CSK-KD were activated by antigen, degranulation was significantly increased as determined by measurement of β-glucuronidase release or levels of CD107a expressed on the cell surface. Furthermore, BMMCs with PAG-KO combined with CSK-KD exhibited antigen-induced degranulation higher than PAG-KO control cells, resembling to cells with CSK-KD. These data suggested that negative regulation of FcεRI-induced degranulation by CSK does not require PAG. Reduced degranulation in BMMCs with PAG-KO cells and enhanced degranulation in cells with CSK-KD and PAG-KO/CSK-KD could be explained by existence of CSK binding proteins, other than PAG, which are more relevant for the inhibitory action of CSK than PAG and by competition for the substrate between PAG and hypothetical other adaptors. Thus, in the absence of PAG, CSK could bind more to the other adaptors and inhibit more efficiently relevant SFKs. Our finding that only relative small fraction of CSK (~4%) is found in 1% Brij 96-resistant membranes, that this fraction is not changed after FcεRI triggering and that the fraction disappears in cell extracts from PAG-KO BMMCs (26), suggests that the hypothetical CSK anchor resides in detergent soluble fraction of the cell extracts. Experiments with BMMCs with LYN-KO showed that LYN is a negative regulator of

mast cell degranulation (23, 53, 54). However, increased degranulation in cells with CSK-KD and presumably increased activity of LYN kinase *in vivo*, as revealed by enhanced FcεRI phosphorylation, suggested that other SFKs with positive regulatory role in FcεRI-mediated degranulation, such as FYN (53), are also affected. It should be noted, however, that in *in vitro* kinase assay enzymatic activity of FYN kinase, was not affected by CSK-KD.

Enhanced release of β-glucuronidase was observed not only after antigen-induced stimulation, but also in resting cells with CSK-KD. This finding together with enhanced phosphorylation of FcεRI β and γ subunits in nonactivated cells indicated that CSK contributes to setting activation threshold in mast cells. This conclusion is consistent with previous finding that CSK-deficient granulocytes exhibit elevated spontaneous and ligand-induced degranulation (18). When BMMCs with PAG and two- to three-fold increased levels of CSK were examined and compared to control cells, no significant decrease in spontaneous or FcεRI-induced degranulation was observed. However, cells with CSK-OE combined with PAG-KO exhibited significant inhibition of antigen-induced degranulation, suggesting that PAG could compete for CSK binding with other more relevant CSK-binders. Negative regulatory role of CSK was previously observed in rat basophilic leukemia cells (RBL-2H3) in which enhanced expression of CSK delayed histamine release observable only a few minutes upon antigen stimulation (55).

In molecular terms, CSK in the vicinity of SFKs phosphorylates their C-terminal tyrosines and in this way inactivates their kinase activity. As expected, in cells with CSK-KD, phosphorylation of LYN-Y^{508} was significantly reduced in nonactivated cells and after activation phosphorylation of this tyrosine remained significantly lower than in controls. In control cells, FcεRI-triggering did not induce any decrease in tyrosine phosphorylation of LYN C-terminal tyrosine, which is in line with our previous study (56) indicating importance of this tyrosine for control of both proximal and distal signaling pathways in FcεRI-activated cells. On the other hand, phosphorylation of LYN positive regulatory tyrosine Y^{397} was not affected by CSK-KD and was down-regulated after antigen stimulation in both control cells and cells with CSK-KD. Although there was dramatic defect in phosphorylation of Y^{508} in Lyn from BMMCs with CSK-KD, kinase activity measured by an *in vitro* kinase assay with exogenous substrate enolase was not different when LYN was immunoprecipitated from cells with CSK-KD or control cells, and auto-phosphorylation was even significantly decreased in LYN from

cells with CSK-KD. This could be caused in part by coprecipitation of the inhibitory molecules such as phosphatases. In fact, using antibody specific for SHP-1^{Y564} we found significantly increased phosphorylation of this phosphatases, which is known to be present in complexes containing FcεRI and LYN (57), is likely to recognize LYN as a substrate via kinase tyrosine-based inhibitory motif (KTIM) located within the kinase domain of the kinase (58), and dephosphorylates LYN at Y^{396} (57).

Second, antigen-activated BMMCs with PAG-KO, exhibited significantly decreased calcium response when compared to control cells (26). In contrast, BMMCs with CSK-KD showed significantly higher calcium response. In BMMCs with CSK-KD combined with PAG-KO, calcium response was significantly higher than in cells with PAG-KO alone. Calcium response in antigen-activated cells is dependent on LYN-SYK-LAT-PLCγ-dependent signaling pathway (53). CSK-KD had stimulatory effect on this pathway as reflected by significantly increased tyrosine phosphorylation of SYK, LAT (only in cells with CSK-KD/PAG-KO), and PLC-γ. Interestingly, in BMMCs with CSK-OE no significant changes in antigen-induced calcium response were observed, which is in accord with previous studies using WEHI-231 cells in which CSK-OE was unable to alter BCR-induced signaling (59) and RBL-2H3 cells in which CSK-OE only delayed calcium response (55). Data obtained with BMMCs contrast with those showing that overexpression of CSK in T cell line resulted in significant inhibition of TCR-induced activation events (60). Our data with BMMCs are, however, in line with recent experiments showing that in TCR-activated T cells with CSK catalytic activity inhibited by a small inhibitor, phosphorylation of ZAP-70, LAT and PLCγ were significantly increased when compared to control cells (44).

Third, despite the fact that LAT and NTAL TRAPs share structural similarities (3, 61), they are differently phosphorylated depending on signaling pathway used (2, 62). When pLKO.1 control BMMCs were compared with CSK-KD cells, there was no difference in basal tyrosine phosphorylation of LAT and NTAL. However, after activation, LAT was phosphorylated to the same extent in both cell types, whereas NTAL showed significantly lower phosphorylation in cell with CSK-KD. In our previous study we found that LAT was less phosphorylated in cells with PAG-KO than control cells and therefore, we expected that combined CSK-KD/PAG-KO will deepen the defect in LAT phosphorylation. However, cells with PAG-KO/CSK-KD showed higher LAT phosphorylation than cells with PAG-KO alone. Even more dramatic

differences were observed when NTAL phosphorylation was compared in cells with CSK-KD alone, PAG-KD alone, PAG-KO/CSK-KD and corresponding controls. CSK-KD alone reduced NTAL phosphorylation significantly, PAG-KO alone had only week effect (not shown), but PAG-KO combined with CSK-KD significantly enhanced NTAL phosphorylation. Apparently, complex interactions involving SFKs modulated by CSK, TRAPs and phosphatases are involved in the processes. The observed difference in phosphorylation of LAT and NTAL in antigen-activated cells with or without CSK could be in part explained by the finding that phosphotyrosines in LAT could bind not only positive regulators but also negative regulators and that there is a competition between LAT and NTAL for binding of the phosphatases (63). Taking into account that NTAL and LAT occupy different membrane microdomains (45), removal of CSK, PAG or both these signal transduction regulators could have different effect on phosphorylation of LAT and NTAL adaptors, binding of kinases and phosphatases to the adaptors and to other target structures, and modulation of FcεRI-mediated activation as described in this study.

Fourth, FcεRI activation rapidly stimulates tyrosine phosphorylation of the transcription factor STAT5, which serves as a positive regulator of expression of genes for cytokines and chemokines (64, 65). In FcεRI-activated BMMCs with PAG-KO tyrosine phosphorylation of STAT5, transcription of cytokine genes, and production of cytokines were substantially reduced (26). Similar inhibition of STAT5 phosphorylation, transcription of cytokine genes TNF-α, IL-13 and IL-6, and production of the corresponding cytokines was observed in BMMCs with CSK-KD. Interestingly, cells with PAG-KO/CSK-KD, when compared to cells with PAG-KO alone, exhibited higher inhibition of TNF-α and IL-13, but there was no significant difference when IL-6 was examined. The observed additive effects of PAG-KO and CSK-KD suggests that CSK and PAG could regulate cytokine production by independent pathways which converge at the level of STAT5 tyrosine phosphorylation. CSK could regulate this pathway through phosphorylation of negative regulatory tyrosine in FYN, which phosphorylates STAT5 (51), whereas PAG through interaction with signal transduction molecules of the PAG interactome (24). Reduced cytokines production could by also direct consequence of enhanced phosphorylation of SHP-1, resulting in increased phosphatase activity and thereby negative regulation of STAT5 phosphorylation at Y694 (48, 57). In connection with these experiments it should be mentioned that positive

regulatory role of CSK in production of TNF-α and IL-6 has been also described in macrophage cell line RAW 264.7 (66).

Fifth, migration towards antigen is positively regulated by PAG (26) but negatively by CSK (this study). In cells with CSK-KD/PAG-KO, the positive regulatory role of PAG in chemotaxis towards antigen was neutralized by CSK-KD. When chemotaxis towards SCF was measured, cells with PAG-KO/CSK-KD exhibited significantly higher response when compared to PAG-KO cells. Our finding that PAG is a positive regulator of chemotaxis towards antigen without any effect on chemotaxis towards SCF, whereas CSK is a negative regulator of antigen- as well as SCF-mediated chemotaxis, suggest that the CSK and PAG have different regulatory role in these processes. Mast cell chemotaxis is a complex process involving numerous molecules (52) and it is not clear at which step CSK is involved. One possibility is that CSK affects integrins, which are involved in chemotaxis. However, our findings that antigen- or SCF-activated cells with CSK-KD, PAG-KO or CSK-KD/PAG-KO exhibit similarly reduced adhesion to fibronectin, which is dependent on activity of integrins, suggest that integrins are not the negative regulators of antigen- or SCF-mediated chemotaxis. In our previous study we found an important role of NTAL in chemotaxis towards antigen (67). In antigen-activated cells, NTAL was rapidly phosphorylated and served as negative regulator of degranulation and calcium response (45, 68), a positive regulator of adhesion to fibronectin, and a negative regulator of chemotaxis towards antigen (67), properties which are shared with CSK. NTAL seems to signals to mast cell cytoskeleton via the small GTPase RhoA and it is possible that this pathway is affected by CSK. In fact it has been already reported that there is a cross-talk between CSK and Rho-family GTPases, which could contribute to cell migration (69). Cytoskeleton is known to be involved in FcεRI internalization (39, 70, 71). Our finding that CSK-KD leads to reduced antigen-induced internalization of FcεRI is in line with reduced adhesion to fibronectin and reduced phosphorylation of NTAL, which is a positive regulator of cell adhesion (67). Reduced internalization is known to contribute to prolonged generation of FcεRI-induced signal and enhanced degranulation (72, 73). Thus, CSK through its negative regulation of FcεRI internalization could contribute to enhanced degranulation.

Taken together, our results support the conclusion that CSK is a negative regulator of FcεRI-mediated activation leading to degranulation, calcium response and chemotaxis, but a positive regulator of cytokines and chemokines production and

adhesion to fibronectin. At least some of these regulatory functions of CSK are not dependent on its binding to PAG, which seems to have some other not yet fully understood functions. Opposite effect of CSK-KD and PAG-KO on antigen-induced degranulation as well as enhanced degranulation in cells with PAG-KO combined with CSK-KD suggest that CSK binds not only to PAG, but also to some other anchors, which could serve better than PAG for positioning CSK in the vicinity of SFKs and thus more efficient inactivation of SFKs involved in FcεRI signaling. These alternative CSK anchor proteins remains to be identified.

ACKNOWLEDGMENTS

This work was supported by project 14-09807S from the Czech Science Foundation and Institutional project RVO 68378050 from the Academy of Sciences of the Czech Republic. L.P and T.P. were supported in part by the Faculty of Science, Charles University, Prague. The authors report no conflicting financial interests.

REFERENCES

1. **Galli SJ, Kalesnikoff J, Grimbaldeston MA, Piliponsky AM, Williams CM, Tsai M.** 2005. Mast cells as "tunable" effector and immunoregulatory cells: recent advances. Annu Rev Immunol **23:**749-786.
2. **Saitoh S, Arudchandran R, Manetz TS, Zhang W, Sommers CL, Love PE, Rivera J, Samelson LE.** 2000. LAT is essential for FcεRI-mediated mast cell activation. Immunity **12:**525-535.
3. **Brdička T, Imrich M, Angelisová P, Brdičková N, Horváth O, Špička J, Hilgert I, Lusková P, Dráber P, Novák P, Engels N, Wienands J, Simeoni L, Osterreicher J, Aguado E, Malissen M, Schraven B, Hořejší V.** 2002. Non-T cell activation linker (NTAL): a transmembrane adaptor protein involved in immunoreceptor signaling. J Exp Med **196:**1617-1626.
4. **Brdička T, Pavlištová D, Leo A, Bruyns E, Kořínek V, Angelisová P, Scherer J, Shevchenko A, Hilgert I, Černý J, Drbal K, Kuramitsu Y, Kornacker B, Hořejší V, Schraven B.** 2000. Phosphoprotein associated with glycosphingolipid-enriched microdomains (PAG), a novel ubiquitously expressed transmembrane adaptor protein, binds the protein tyrosine kinase Csk and is involved in regulation of T cell activation. J Exp Med **191:**1591-1604.
5. **Kawabuchi M, Satomi Y, Takao T, Shimonishi Y, Nada S, Nagai K, Tarakhovsky A, Okada M.** 2000. Transmembrane phosphoprotein Cbp regulates the activities of Src-family tyrosine kinases. Nature **404:**999-1003.
6. **Simeoni L, Lindquist JA, Smida M, Witte V, Arndt B, Schraven B.** 2008. Control of lymphocyte development and activation by negative regulatory transmembrane adapter proteins. Immunol Rev **224:**215-228.
7. **Pribluda VS, Pribluda C, Metzger H.** 1994. Transphosphorylation as the mechanism by which the high-affinity receptor for IgE is phosphorylated upon aggregation. Proc Natl Acad Sci U S A **91:**11246-11250.
8. **Field KA, Holowka D, Baird B.** 1997. Compartmentalized activation of the high affinity immunoglobulin E receptor within membrane domains. J Biol Chem **272:**4276-4280.
9. **Heneberg P, Dráberová L, Bambousková M, Pompach P, Dráber P.** 2010. Down-regulation of protein-tyrosine phosphatases activates an immune receptor in the absence of its translocation into lipid rafts. J Biol Chem **285:**12787-12802.
10. **Bugajev V, Bambouskova M, Draberova L, Draber P.** 2010. What precedes the initial tyrosine phosphorylation of the high affinity IgE receptor in antigen-activated mast cell? FEBS Lett **584:**4949-4955.
11. **Hibbs ML, Harder KW, Armes J, Kountouri N, Quilici C, Casagranda F, Dunn AR, Tarlinton DM.** 2002. Sustained activation of Lyn tyrosine kinase in vivo leads to autoimmunity. J Exp Med **196:**1593-1604.
12. **Harder KW, Parsons LM, Armes J, Evans N, Kountouri N, Clark R, Quilici C, Grail D, Hodgson GS, Dunn AR, Hibbs ML.** 2001. Gain- and loss-of-function Lyn mutant mice define a critical inhibitory role for Lyn in the myeloid lineage. Immunity **15:**603-615.
13. **Katagiri T, Ogimoto M, Hasegawa K, Arimura Y, Mitomo K, Okada M, Clark MR, Mizuno K, Yakura H.** 1999. CD45 negatively regulates lyn activity by dephosphorylating both positive and negative regulatory tyrosine residues in immature B cells. J Immunol **163:**1321-1326.
14. **Nada S, Yagi T, Takeda H, Tokunaga T, Nakagawa H, Ikawa Y, Okada M, Aizawa S.** 1993. Constitutive activation of Src family kinases in mouse embryos that lack Csk. Cell **73:**1125-1135.
15. **Imamoto A, Soriano P.** 1993. Disruption of the csk gene, encoding a negative regulator of Src family tyrosine kinases, leads to neural tube defects and embryonic lethality in mice. Cell **73:**1117-1124.
16. **Okada M.** 2012. Regulation of the Src family kinases by Csk. Int J Biol Sci **8:**1385-1397.

17. **Schmedt C, Saijo K, Niidome T, Kühn R, Aizawa S, Tarakhovsky A.** 1998. Csk controls antigen receptor-mediated development and selection of T-lineage cells. Nature **394:**901-904.
18. **Thomas RM, Schmedt C, Novelli M, Choi BK, Skok J, Tarakhovsky A, Roes J.** 2004. C-terminal Src kinase controls acute inflammation and granulocyte adhesion. Immunity **20:**181-191.
19. **Torgersen KM, Vang T, Abrahamsen H, Yaqub S, Hořejší V, Schraven B, Rolstad B, Mustelin T, Taskén K.** 2001. Release from tonic inhibition of T cell activation through transient displacement of C-terminal Src kinase (Csk) from lipid rafts. J Biol Chem **276:**29313-29318.
20. **Hrdinka M, Horejsi V.** 2014. PAG--a multipurpose transmembrane adaptor protein. Oncogene **33:**4881-4892.
21. **Davidson D, Bakinowski M, Thomas ML, Horejsi V, Veillette A.** 2003. Phosphorylation-dependent regulation of T-cell activation by PAG/Cbp, a lipid raft-associated transmembrane adaptor. Mol Cell Biol **23:**2017-2028.
22. **Ohtake H, Ichikawa N, Okada M, Yamashita T.** 2002. Cutting Edge: Transmembrane phosphoprotein Csk-binding protein/phosphoprotein associated with glycosphingolipid-enriched microdomains as a negative feedback regulator of mast cell signaling through the FcεRI. J Immunol **168:**2087-2090.
23. **Odom S, Gomez G, Kovarova M, Furumoto Y, Ryan JJ, Wright HV, Gonzalez-Espinosa C, Hibbs ML, Harder KW, Rivera J.** 2004. Negative regulation of immunoglobulin E-dependent allergic responses by Lyn kinase. J Exp Med **199:**1491-1502.
24. **Reginald K, Chaoui K, Roncagalli R, Beau M, Goncalves Menoita M, Monsarrat B, Burlet-Schiltz O, Malissen M, Gonzalez de Peredo A, Malissen B.** 2015. Revisiting the Timing of Action of the PAG Adaptor Using Quantitative Proteomics Analysis of Primary T Cells. **195:**5472-5481.
25. **Davidson D, Zhong MC, Pandolfi PP, Bolland S, Xavier RJ, Seed B, Li X, Gu H, Veillette A.** 2016. The Csk-Associated Adaptor PAG Inhibits Effector T Cell Activation in Cooperation with Phosphatase PTPN22 and Dok Adaptors. Cell Rep **17:**2776-2788.
26. **Draberova L, Bugajev V, Potuckova L, Halova I, Bambouskova M, Polakovicova I, Xavier RJ, Seed B, Draber P.** 2014. Transmembrane adaptor protein PAG/CBP is involved in both positive and negative regulation of mast cell signaling. Mol Cell Biol **34:**4285-4300.
27. **Rudolph AK, Burrows PD, Wabl MR.** 1981. Thirteen hybridomas secreting hapten-specific immunoglobulin E from mice with Ig^a or Ig^b heavy chain haplotype. Eur J Immunol **11:**527-529.
28. **Rivera J, Kinet JP, Kim J, Pucillo C, Metzger H.** 1988. Studies with a monoclonal antibody to the beta subunit of the receptor with high affinity for immunoglobulin E. Mol Immunol **25:**647-661.
29. **Tolar P, Dráberová L, Dráber P.** 1997. Protein tyrosine kinase Syk is involved in Thy-1 signaling in rat basophilic leukemia cells. Eur J Immunol **27:**3389-3397.
30. **Kovářová M, Tolar P, Arudchandran R, Dráberová L, Rivera J, Dráber P.** 2001. Structure-function analysis of Lyn kinase association with lipid rafts and initiation of early signaling events after Fcε receptor I aggregation. Mol Cell Biol **21:**8318-8328.
31. **Schmitt-Verhulst AM, Pettinelli CB, Henkart PA, Lunney JK, Shearer GM.** 1978. H-2-restricted cytotoxic effectors generated in vitro by the addition of trinitrophenyl-conjugated soluble proteins. J Exp Med **147:**352-368.
32. **Yang Y, Seed B.** 2003. Site-specific gene targeting in mouse embryonic stem cells with intact bacterial artificial chromosomes. Nat Biotechnol **21:**447-451.
33. **Lindquist S, Karitkina D, Langnaese K, Posevitz-Fejfar A, Schraven B, Xavier R, Seed B, Lindquist JA.** 2011. Phosphoprotein associated with glycosphingolipid-enriched microdomains differentially modulates Src kinase activity in brain maturation. PLoS One **6:**e23978.

34. **Bambouskova M, Polakovicova I, Halova I, Goel G, Draberova L, Bugajev V, Doan A, Utekal P, Gardet A, Xavier RJ, Draber P.** 2016. New Regulatory Roles of Galectin-3 in High-Affinity IgE Receptor Signaling. Mol Cell Biol **36:**1366-1382.
35. **Hálová I, Dráberová L, Bambousková M, Machyna M, Stegurová L, Smrž D, Dráber P.** 2013. Cross-talk between tetraspanin CD9 and transmembrane adaptor protein non-T cell activation linker (NTAL) in mast cell activation and chemotaxis. J Biol Chem **288:**9801-9814.
36. **Horakova H, Polakovicova I, Shaik GM, Eitler J, Bugajev V, Draberova L, Draber P.** 2011. 1,2-propanediol-trehalose mixture as a potent quantitative real-time PCR enhancer. BMC Biotechnol **11:**41.
37. **Potůčková L, Franko F, Bambousková M, Dráber P.** 2011. Rapid and sensitive detection of cytokines using functionalized gold nanoparticle-based immuno-PCR, comparison with immuno-PCR and ELISA. J Immunol Methods **371:**38-47.
38. **Laemmli UK.** 1970. Cleavage of structural proteins during the assembly of the head of bacteriophage T4. Nature **227:**680-685.
39. **Cleyrat C, Darehshouri A, Anderson KL, Page C, Lidke DS, Volkmann N, Hanein D, Wilson BS.** 2013. The architectural relationship of components controlling mast cell endocytosis. J Cell Sci **126:**4913-4925.
40. **Haan C, Behrmann I.** 2007. A cost effective non-commercial ECL-solution for Western blot detections yielding strong signals and low background. J Immunol Methods **318:**11-19.
41. **Amoui M, Dráber P, Dráberová L.** 1997. Src family-selective tyrosine kinase inhibitor, PP1, inhibits both FcεRI- and Thy-1-mediated activation of rat basophilic leukemia cells. Eur J Immunol **27:**1881-1886.
42. **Grützkau A, Smorodchenko A, Lippert U, Kirchhof L, Artuc M, Henz BM.** 2004. LAMP-1 and LAMP-2, but not LAMP-3, are reliable markers for activation-induced secretion of human mast cells. Cytometry A **61:**62-68.
43. **Ozawa K, Szallasi Z, Kazanietz MG, Blumberg PM, Mischak H, Mushinski JF, Beaven MA.** 1993. Ca^{2+}-dependent and Ca^{2+}-independent isozymes of protein kinase C mediate exocytosis in antigen-stimulated rat basophilic RBL-2H3 cells. Reconstitution of secretory responses with Ca^{2+} and purified isozymes in washed permeabilized cells. J Biol Chem **268:**1749-1756.
44. **Manz BN, Tan YX, Courtney AH, Rutaganira F, Palmer E, Shokat KM, Weiss A.** 2015. Small molecule inhibition of Csk alters affinity recognition by T cells. Elife **4**.
45. **Volná P, Lebduška P, Dráberová L, Šimová S, Heneberg P, Boubelík M, Bugajev V, Malissen B, Wilson BS, Hořejší V, Malissen M, Dráber P.** 2004. Negative regulation of mast cell signaling and function by the adaptor LAB/NTAL. J Exp Med **200:**1001-1013.
46. **Draber P, Halova I, Levi-Schaffer F, Draberova L.** 2011. Transmembrane adaptor proteins in the high-affinity IgE receptor signaling. Front Immunol **2:**95.
47. **Gilfillan AM, Rivera J.** 2009. The tyrosine kinase network regulating mast cell activation. Immunol Rev **228:**149-169.
48. **Xiao W, Ando T, Wang HY, Kawakami Y, Kawakami T.** 2010. Lyn- and PLC-β3-dependent regulation of SHP-1 phosphorylation controls Stat5 activity and myelomonocytic leukemia-like disease. Blood **116:**6003-6013.
49. **Gordon JR, Galli SJ.** 1991. Release of both preformed and newly synthesized tumor necrosis factor alpha (TNF-alpha)/cachectin by mouse mast cells stimulated via the Fc epsilon RI. A mechanism for the sustained action of mast cell-derived TNF-alpha during IgE-dependent biological responses. J Exp Med **174:**103-107.
50. **Bischoff SC, Lorentz A, Schwengberg S, Weier G, Raab R, Manns MP.** 1999. Mast cells are an important cellular source of tumour necrosis factor alpha in human intestinal tissue. Gut **44:**643-652.
51. **Pullen NA, Falanga YT, Morales JK, Ryan JJ.** 2012. The Fyn-STAT5 Pathway: A New Frontier in IgE- and IgG-Mediated Mast Cell Signaling. Front Immunol **3:**117.

52. **Halova I, Draberova L, Draber P.** 2012. Mast cell chemotaxis - chemoattractants and signaling pathways. Front Immunol **3:**119.
53. **Parravicini V, Gadina M, Kovarova M, Odom S, Gonzalez-Espinosa C, Furumoto Y, Saitoh S, Samelson LE, O'Shea JJ, Rivera J.** 2002. Fyn kinase initiates complementary signals required for IgE-dependent mast cell degranulation. Nat Immunol **3:**741-748.
54. **Nishizumi H, Yamamoto T.** 1997. Impaired tyrosine phosphorylation and Ca2+ mobilization, but not degranulation, in lyn-deficient bone marrow-derived mast cells. J Immunol **158:**2350-2355.
55. **Honda Z, Suzuki T, Hirose N, Aihara M, Shimizu T, Nada S, Okada M, Ra C, Morita Y, Ito K.** 1997. Roles of C-terminal Src kinase in the initiation and the termination of the high affinity IgE receptor-mediated signaling. J Biol Chem **272:**25753-25760.
56. **Tolar P, Dráberová L, Tolarová H, Dráber P.** 2004. Positive and negative regulation of Fcε receptor I-mediated signaling events by Lyn kinase C-terminal tyrosine phosphorylation. Eur J Immunol **34:**1136-1145.
57. **Xiao W, Kashiwakura J, Hong H, Yasudo H, Ando T, Maeda-Yamamoto M, Wu D, Kawakami Y, Kawakami T.** 2011. Phospholipase C-β3 regulates FcεRI-mediated mast cell activation by recruiting the protein phosphatase SHP-1. Immunity **34:**893-904.
58. **Abu-Dayyeh I, Ralph B, Grayfer L, Belosevic M, Cousineau B, Olivier M.** 2010. Identification of key cytosolic kinases containing evolutionarily conserved kinase tyrosine-based inhibitory motifs (KTIMs). Dev Comp Immunol **34:**481-484.
59. **Veillette A, Latour S, Davidson D.** 2002. Negative regulation of immunoreceptor signaling. Annu Rev Immunol **20:**669-707.
60. **Chow LM, Fournel M, Davidson D, Veillette A.** 1993. Negative regulation of T-cell receptor signalling by tyrosine protein kinase p50csk. Nature **365:**156-160.
61. **Janssen E, Zhu M, Zhang W, Koonpaew S, Zhang W.** 2003. LAB: a new membrane-associated adaptor molecule in B cell activation. Nat Immunol **4:**117-123.
62. **Iwaki S, Spicka J, Tkaczyk C, Jensen BM, Furumoto Y, Charles N, Kovarova M, Rivera J, Horejsi V, Metcalfe DD, Gilfillan AM.** 2008. Kit- and Fc epsilonRI-induced differential phosphorylation of the transmembrane adaptor molecule NTAL/LAB/LAT2 allows flexibility in its scaffolding function in mast cells. Cell Signal **20:**195-205.
63. **Roget K, Malissen M, Malbec O, Malissen B, Daeron M.** 2008. Non-T cell activation linker promotes mast cell survival by dampening the recruitment of SHIP1 by linker for activation of T cells. J Immunol **180:**3689-3698.
64. **Pullen NA, Barnstein BO, Falanga YT, Wang Z, Suzuki R, Tamang TD, Khurana MC, Harry EA, Draber P, Bunting KD, Mizuno K, Wilson BS, Ryan JJ.** 2012. Novel mechanism for FcεRI-mediated signal transducer and activator of transcription 5 (STAT5) tyrosine phosphorylation and the selective influence of STAT5B over mast cell cytokine production. J Biol Chem **287:**2045-2054.
65. **Barnstein BO, Li G, Wang Z, Kennedy S, Chalfant C, Nakajima H, Bunting KD, Ryan JJ.** 2006. Stat5 expression is required for IgE-mediated mast cell function. J Immunol **177:**3421-3426.
66. **Aki D, Mashima R, Saeki K, Minoda Y, Yamauchi M, Yoshimura A.** 2005. Modulation of TLR signalling by the C-terminal Src kinase (Csk) in macrophages. Genes Cells **10:**357-368.
67. **Tůmová M, Koffer A, Šimíček M, Dráberová L, Dráber P.** 2010. The transmembrane adaptor protein NTAL signals to mast cell cytoskeleton via the small GTPase Rho. Eur J Immunol **40:**3235-3245.
68. **Zhu M, Liu Y, Koonpaew S, Granillo O, Zhang W.** 2004. Positive and negative regulation of FcεRI-mediated signaling by the adaptor protein LAB/NTAL. J Exp Med **200:**991-1000.
69. **Lowry WE, Huang J, Ma YC, Ali S, Wang D, Williams DM, Okada M, Cole PA, Huang XY.** 2002. Csk, a critical link of g protein signals to actin cytoskeletal reorganization. Dev Cell **2:**733-744.

70. **Ra C, Furuichi K, Rivera J, Mullins JM, Isersky C, White KN.** 1989. Internalization of IgE receptors on rat basophilic leukemic cells by phorbol ester. Comparison with endocytosis induced by receptor aggregation. Eur J Immunol **19:**1771-1777.
71. **Xu K, Williams RM, Holowka D, Baird B.** 1998. Stimulated release of fluorescently labeled IgE fragments that efficiently accumulate in secretory granules after endocytosis in RBL-2H3 mast cells. J Cell Sci **111 (Pt 16):**2385-2396.
72. **Kalesnikoff J, Rios EJ, Chen CC, Alejandro Barbieri M, Tsai M, Tam SY, Galli SJ.** 2007. Roles of RabGEF1/Rabex-5 domains in regulating FcεRI surface expression and FcεRI-dependent responses in mast cells. Blood **109:**5308-5317.
73. **Molfetta R, Belleudi F, Peruzzi G, Morrone S, Leone L, Dikic I, Piccoli M, Frati L, Torrisi MR, Santoni A, Paolini R.** 2005. CIN85 regulates the ligand-dependent endocytosis of the IgE receptor: a new molecular mechanism to dampen mast cell function. J Immunol **175:**4208-4216.

FIGURE LEGENDS

FIG 1 Production of BMMCs with reduced or enhanced expression of CSK. (A) Determination of CSK protein by immunoblotting (IB) in whole-cell lysates from BMMCs transduced with individual CSK-specific shRNAs (35, 36, 64, and 90) or control empty vector (pLKO.1). (B) Quantification of the relative amounts of CSK normalized to the relative amounts of GRB2 used as loading controls and amount of CSK in pLKO.1 control cells. (C) Determination of CSK in whole-cell lysates from BMMCs transduced with a pool of CSK-specific shRNAs (labeled as CSK-KD) or pLKO.1 control vector. (D) Quantification of the relative amounts of CSK analyzed as in Fig. 1B. The results in B and D are shown as means ± SD from 8 - 13 independent experiments. (E) Determination of CSK by immunoblotting in whole-cell lysates from BMMCs transduced with empty vector (pCDH), pCDH vector containing hCSK-mCherry construct or hCSK-myc construct. Positions of endogenous (En.) and exogenous (Ex.) CSKs are indicated by arrows. The results are representative of 3 experiments. (F) Quantification of the relative amounts of CSK and CSK constructs normalized to the relative amounts of GRB2 used as loading controls and amount of CSK in cells transduced with pCDH control vector. (G) Flow cytometry analysis of the surface expression of FcεRI and c-KIT receptor in BMMCs with CSK-KD, CSK-OE (hCSK-mCherry or hCSK-myc) and appropriate control cells (pLKO.1 and pCDH). (H) Quantification of surface FcεRI and c-KIT receptors, obtained in experiments as in Fig. 1G. The data represent means ± SD from 7-13 independent experiments.

FIG 2 Enhanced degranulation and calcium response, but reduced FcεRI-IgE complexes internalization in BMMCs with CSK-KD. (A) β-glucuronidase release was analyzed in BMMCs transduced with individual CSK-specific shRNAs (35, 36, 64, and 90) in pLKO.1 vector or empty pLKO.1 vector (pLKO.1). The cells were sensitized with IgE and activated with various concentration of antigen (Ag; TNP-BSA). The data represents means ± SEM from 4-8 independent experiments performed in duplicates or triplicates. (B) β-glucuronidase release from BMMCs transduced with a pool of shRNAs or empty pLKO.1 vector was analyzed as in Fig. 2A. The data represent means ± SEM from 8 independent experiments performed in duplicates or triplicates. (C, D) Surface

expression of CD107a in BMMCs with CSK-KD (C) or CSK/OE (hCSK-mCherry or hCSK-myc; D). The cells were sensitized with IgE, activated with various concentration of antigen and surface expression of CD107a was analyzed by flow cytometry. The results shown are means ± SEM from 3 (C) or 4 (D) independent experiments performed in duplicates. (E, F) Calcium response examined in BMMCs with CSK-KD and corresponding controls (E) or CSK-OE and controls (F). The cells were sensitized with IgE, loaded with Fura-2 and activated with antigen added as indicated by arrows. Data represent means ± SEM calculated from 3-6 independent experiments each performed in duplicates. (G) IgE internalization in BMMCs with CSK-KD or control pLKO.1 cells. The IgE-sensitized cells were activated with antigen for various time intervals and fixed with 4% parafolmaldehyde. IgE was quantified using AF488-labeled anti-IgE antibody and flow cytometry. Means ± SEM calculated from 3 independent experiments are shown. Statistical significance of intergroup differences, determined as described in Materials and methods, is also shown.

FIG 3 Negative and positive regulatory roles of CSK in tyrosine phosphorylation of early signal-transduction molecules. (A) Total tyrosine phosphorylation of IgE-sensitized BMMCs with CSK-KD or control pLKO.1 cells activated or not with antigen for various time intervals. The cells were lysed and analyzed by immunoblotting with the tyrosine specific mAb PY20-HRP conjugate (PY20). GRB2 was used as a loading control. A representative immunoblot from 3 experiments is shown. Numbers on the right indicate positions of molecular weight standards. (B) FcεRIs were immunoprecipitated (IP) from the lysates of nonactivated or Ag-activated BMMCs with CSK-KD or control cells (pLKO.1). The immunoprecipitates were examined by immunoblotting with PY20-HRP mAb. For loading controls, FcεRI β-chain specific antibody was used. Position of FcεRI β and γ chains is marked by arrows. A representative immunoblot from 3 performed is shown. (C) Densitometry analysis of immunoblots as from panel B in which signals from tyrosine phosphorylated FcεRI β and γ subunits in activated cells were normalized to the signals from nonactivated cells and loading control protein. Means ± SEM were calculated from 3 experiments. (D - N) IgE-sensitized BMMCs with CSK-KD or control pLKO.1 cells were activated with antigen for various time intervals and whole-cell lysates were analyzed by immunoblotting for tyrosine phosphorylated SYK (pSYK; D and E), PLCγ (pPLCγ; D

and F), phosphorylated LAT (pLAT; G and H), phosphorylated NTAL (pNTAL; G and I), pLYN^{Y508} (J and K), pLYN^{Y397} (J and L), and phosphorylated SHP-1 (pSHP-1; M and N). Corresponding proteins were used as loading controls. Representative immunoblots from 4 to 7 experiments for each phosphorylated protein is shown on the left (D, G, J, and M). Densitometry analysis of the immunoblots as in left panels in which signals from tyrosine phosphorylated proteins in activated cells were normalized to the signals in nonactivated cells and loading control proteins. Means ± SEM calculated from 4 to 7 experiments are shown. Statistical significance of intergroup differences is also shown.

FIG 4 Different regulation of LYN, FYN and FcεRI-bound kinase aktivity by CSK. (A) LYN kinase was immunoprecipitated from nonactivated or Ag-activated BMMC with CSK-KD or control cells (pLKO.1) and then incubated with kinase buffer containing [γ-^{32}P]ATP and acid-denatured enolase, used as an endogenous substrate. ^{32}P-labeled proteins were size fractionated, transfered to nitrocellulose membranes, and examined by autoradiography. (B, C) Signals from autoradiograms were quantified and those corresponding to LYN (B) and enolase (C) were normalized to the amount of precipitated LYN and to the signals in nonactivated pLKO.1 BMMCs. (D) Kinase activity of immunoprecipitated FYN was determined as above, except that anti-FYN antibody was used for immunoprecipitation. (E, F) Signals from autoradiograms of FYN (E) and enolase (F) were quantified and normalized to the amount of precipitated FYN and to the signals in nonactivated control cells. (G) Kinase activity bound to immunoprecipitated FcεRI was determined as above except that anti-IgE was used for IgE-FcεRI complexes precipitation and fosforylation of FcεRI β and γ chain was examined. (H, I) Signals from autoradiograms of FcεRI β chain (H) and FcεRI γ chain (I) were quantified and normalized to the amount of precipitated FcεRI β chain and to the signals in nonactivated control cells. The means ± SEM were calculated from 5 independent experiments in each panel. The statistical significance of differences between cells with CSK-KD and control pLKO.1 cells is also shown.

FIG 5 CSK is a positive regulator of cytokines and chemokines production, STAT5 phosphorylation, and adhesion to fibronectin, but a negative regulator of chemotaxis

towards antigen and SCF. (A, B) IgE-sensitized BMMCs with CSK-KD or control cells were activated for 1 h with antigen and mRNAs encoding cytokines (TNF-α, IL-6 and IL-13; A) or chemokines (CCL3 and CCL4; B) were quantified by RT-qPCR. Means ± SEM were calculated from 4 independent experiments. (C-E) IgE-sensitized BMMCs with CSK-KD or pLKO.1 control cells were activated or not for 6 h with various concentrations of antigen and concentration of cytokines TNF-α (C), IL-13 (D) and IL-6 (E) secreted into the supernatants were determined. Means ± SEM were calculated from 4-8 independent experiments performed in duplicates or triplicates. (F) The cells were analyzed as in C except that they were activated with only one concentration of antigen (50 ng/ml) for 30 min or 120 min. Means ± SEM were calculated from 4 independent experiments performed in duplicates. (G) Representative immunoblot of whole-cell lysates from BMMCs with CSK-KD or pLKO.1 control cells activated or not with antigen and analyzed by immunoblotting with antibodies to tyrosine phosphorylated STAT5. For loading controls the membranes were analyzed by immunobloting for GRB2. (H) Densitometry analysis of the immunoblots as from panel G in which signals from pSTAT5 in activated cells were normalized to the signals from nonactivated control cells and loading control protein. Means ± SEM were calculated from 3 experiments. (I, J) Cell adhesion to fibronectin-coated surfaces. BMMCs with CSK-KD or pLKO.1 control cells were sensitized with IgE, loaded with calcein and activated with various concentration of antigen (I) or SCF (J). Fluorescence was determined before and after washing out the non-adherent cells, and percentages of adherent cells were calculated. The results indicate means ± SEM from 5 independent experiments. (K) BMMCs with CSK-KD or pLKO.1 control cells were sensitized with IgE and their migration toward antigen or SCF was determined. Means ± SEM (n = 5) are shown. Statistical significance of differences between BMMCs with CSK-KD and control cells is also shown.

FIG 6 Production of PAG-KO BMMCs with reduced or enhanced CSK expression. (A) CSK protein expression determined by immunoblotting with whole-cell lysates from PAG-KO BMMCs transduced with CSK-specific shRNAs (pooled shRNAs; CSK-KD) or empty pLKO.1 vector. GRB2 was used as a loading control. (B) Quantification of the relative amounts of CSK normalized to amounts of GRB2 used as a loading control and CSK level in pLKO.1 control cells. (C) CSK expression determined by

immunoblotting in whole-cell lysates from PAG-KO BMMCs after transduction with empty vector pCDH or pCDH vector containing hCSK-mCherry or hCSK-myc (CSK-OE). Positions of endogenous (En.) and exogenous (Ex.) CSKs are indicate by arrows. (D) Quantification of the relative amounts of CSK normalized to the amounts GRB2 used as a loading control and CSK level in pCDH control cells. The results in B and D are shown as the means ± SD from 3-5 independent experiments. (E) Flow cytometry analysis of the surface expression of FcεRI and c-KIT receptor in PAG-KO BMMCs with CSK-KD, CSK-OE (hCSK-mCherry, hCSK-myc) and corresponding controls. (F) Quantification of surface expression of FcεRI and c-KIT from experiments as in E. The data represent means ± SD from 5-8 independent experiments.

FIG 7 PAG-KO BMMCs with CSK-KD exhibit enhanced degranulation, calcium response and tyrosine phosphorylation of early signal transduction proteins. (A) β-glucuronidase release was determined in IgE-sensitized PAG-KO BMMCs with CSK-KD or pLKO.1/PAG-KO control cells activated or not with various concentrations of antigen. The data represent means ± SEM from 5 independent experiments performed in duplicates or triplicates. (B, C) Surface expression of CD107a was analyzed by flow cytometry in IgE-sensitized and Ag-activated PAG-KO BMMCs with CSK-KD or PAG-KO BMMCs with hCSK-mCherry, hCSK-myc (CSK-OE) and appropriate controls. The results shown are means ± SEM from 5-7 (B) or 3 (C) independent experiments performed in duplicates. (D) Calcium response examined in PAG-KO BMMCs with CSK-KD or control pLKO.1 cells. IgE-sensitized cells were loaded with Fura-2, exposed to antigen (arrow) and Fura-2 fluorescence was analyzed for 300 s. The data represent means ± SEM calculated from 4 independent experiments each performed in duplicates. (E) FcεRI were immunoprecipitated from the lysates of PAG-KO BMMCs with CSK-KD or control pLKO.1 cells activated with antigen or not and examined by immunoblotting with tyrosine specific mAb (PY20). For loading controls, FcεRI β-chain specific antibody was used. (F) Densitometry analysis of the immunoblots as from panel E in which combined signals from tyrosine phosphorylated FcεRI β and γ chains in activated cells were normalized to the signals from nonactivated cells and a loading control protein, FcεRI β subunit. A representative immunoblot from three obtained is shown. (G) IgE-sensitized PAG-KO BMMCs with CSK-KD or pLKO.1 controls were activated or not with antigen and whole-cell lysates were

analyzed by immunoblotting for tyrosine phosphorylated SYK (pSYK), LAT (pLAT) and NTAL (pNTAL). For loading controls, SYK-, LAT- and GRB2-specific antibodies were used. Representative immunoblots from 4-6 experiments are shown. (H - J) Densitometry analyses of the pSYK (H), pLAT (I) and pNTAL (J) from immunoblots as in panel H in which signals from tyrosine phosphorylated proteins in activated cells were normalized to the signals from nonactivated cells and corresponding loading control proteins. Means ± SEM were calculated from 4-6 independent experiments. Statistical significance of intergroup differences is also shown.

FIG 8 PAG-KO BMMCs with CSK-KD exhibit reduced cytokines production, STAT5 phosphorylation and adhesion towards fibronectin, but enhanced chemotaxis towards antigen and SCF. (A – C) IgE-sensitized PAG-KO BMMCs with CSK-KD or pLKO1 control cells were activated for 6 h with various concentration of antigen. Concentration of cytokines TNF-α (A), IL-13 (B) and IL-6 (C) secreted into the supernatants of nonactivated or activated cells were determined by immuno-iPCR. The means ± SEM were calculated from 4-8 independent experiments performed in duplicates or triplicates. (D) STAT5 phosphorylation in whole-cell lysates from PAG-KO BMMCs with CSK-KD or pLKO.1 control cells activated for various time intervals with antigen. Phosphorylation was determined by immunoblotting with antibodies to tyrosine phosphorylated STAT5 (pSTAT5). Because of poor performance of anti-STAT5 specific antibody on stripped membrane, GRB2 was used as a loading control. (E) Densitometry analysis of the immunoblots from gels as in G in which signals from tyrosine pSTAT5 in activated cells were normalized to the signals from pSTAT in nonactivated cells and loading control protein. The results are shown as the means ± SEM from 3-5 independent experiments. (F, G) Adhesion of PAG-KO BMMCs with CSK-KD or pLKO.1 controls to fibronectin-coated surfaces. The cells were sensitized with IgE, loaded with calcein and activated with various concentration of antigen (F) or SCF (G). Fluorescence was determined before and after washing out the non-adherent cells, and percentages of adherent cells were calculated. The results are means ± SEM calculated from 5 experiments. (H) Chemotaxis of BMMCs with PAG-KO, PAG-KO together with CSK-KD or wild type cells was determined in Boyden chambers. The cells were sensitized with IgE and their migration toward antigen and SCF was determined. Means

± SEM (n = 5) are shown. The statistical significance of intergroup differences is also shown.

FIG 9 Proposed models of FcεRI signaling in BMMCs with CSK-KO, PAG-KO or CSK-KD/PAG-KO. For simplicity, only one FcεRI with bound antigen (Ag)-IgE complex is shown. Activated WT cells (A) with normal signal transduction machinery and Ag-mediated responses (Ca^{2+} response, degranulation, cytokines and chemokines production, chemotaxis and adhesion to extracellular matrix proteins (EMP)) are compared to activated cells with CSK-KD (B) or cells with PAG-KO (C). Cells with CSK-KD/PAG-KO (D) are compared with cells with PAG-KO alone (C). Formation of multivalent Ag-IgE-FcεRI complexes leads to FcεRI aggregation and tyrosine phosphorylation of FcεRI β and γ subunits by the LYN kinase, followed by binding and activation of SYK and FYN kinases. (A) In activated WT cells, CSK binds to phosphorylated PAG and/or other so far not identified TRAP(s) and phosphorylates the C-terminal inhibitory tyrosine residues of LYN and other SFKs. Together with PTPs, such as SHP-1, and in cooperation with adaptor proteins, LAT and NTAL, CSK sets a treshold for mast cell activation, which involves GRB2, PLCγ, STAT5 and numerous other molecules, which are activated and/or inhibited by phosphorylation/dephosphorylation of various tyrosines. (B) In cells with CSK-KD, phosphorylation of FcεRI subunits, SYK and PLCγ is significantly increased, resulting in enhanced calcium response and degranulation. LYN kinase, which is not phosphorylated at C-terminal inhibitory tyrosine (Y508) phosphorylates more its substrate, SHP-1 at Y564, thereby increasing its phosphatase activity, which in turn leads to reduced phosphorylation of STAT5 at Y^{694}. This leads to reduced production of cytokines and chemokines. SHP-1 could also bind to NTAL, but not LAT, and in this way alters balance between signaling proteins anchored to these adaptors. Changes in NTAL tyrosine phosphorylation lead to enhanced chemotaxis and reduced adhesion to EMPs. (C) Cells with PAG-KO exhibit different changes in signaling events when compared to WT cells and cells with CSK-KD. PAG KO cells exhibit reduced tyrosine phosphorylation of FcεRI β and γ subunits, SYK, LAT, PLCγ and STAT5, resulting in reduced Ca^{2+} response, degranulation, migration, and cytokines, and chemokines production. (D) In cells with CSK-KD/PAG-KO, phosphorylation of SYK, NTAL, LAT and PLCγ is increased, resulting in enhanced calcium response, degranulation and

chemotaxis. However, phosphorylation of STAT5 is reduced and this leads in reduced production of cytokines in the cells. Cells with CSK-KD/PAG-KO resemble in properties more to cells with CSK-KD than to cells with PAG-KO.

Table 1. Summary of responses of BMMCs with CSK-KD, PAG-KO and CSK-KD/PAG-KO when compared with corresponding control cells

Parameter	CSK-KD	PAG-KO*	CSK-KD/ PAG-KO
Degranulation			
β-glucuronidase	↑	↓	↑
CD107a	↑	↓	↑
Ca^{2+} response	↑	↓	↑
Production of cytokines			
TNF-α	↓	↓	↓
IL-13	↓	↓	↓
IL-6	↓	↓	-
Production of chemokines			
CCL3	↓	↓	n.a.
CCL4	↓	↓	n.a.
Adhesion			
Ag	↓	-	↓
SCF	↓	-	↓
Chemotaxis			
Ag	↑	↓	↑
SCF	↑	-	↑
Kinase activity			
FcεRI	↑	↑	n.a.
LYN	↓	↑	n.a.
FYN	-	↑	n.a.
phospho-FcεRI	↑	↓	↑
phospho-LYN^{Y508}	↓	n.a.	n.a.
phospho-LYN^{Y397}	-	n.a.	n.a.
phospho-SYK	↑	↓	↑
phospho-PLCγ	↑	↓	↑
phospho-LAT	-	↓	↑
phospho-NTAL	↓	-	↑
phospho-STAT5	↓	↓	↓

↑ increase; ↓ decrease; – no changed; n.a. not analyzed

* Data from ref. 26.

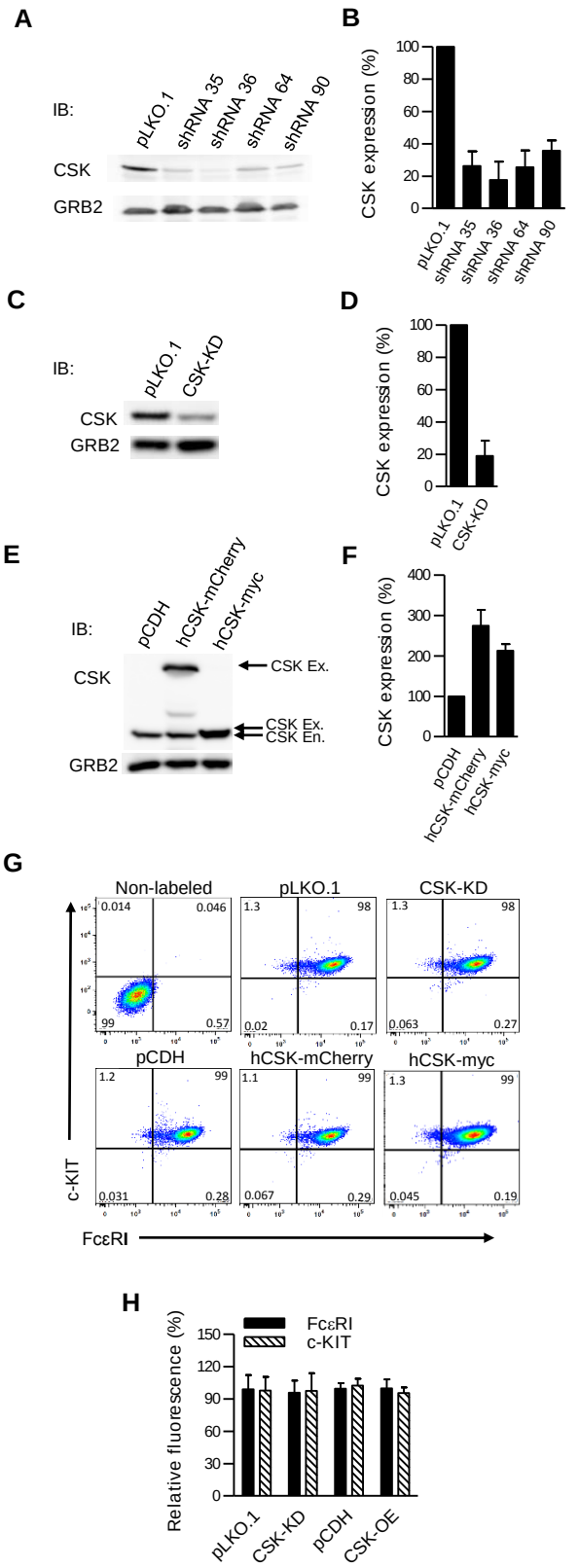

Fig. 1 Potuckova et al.

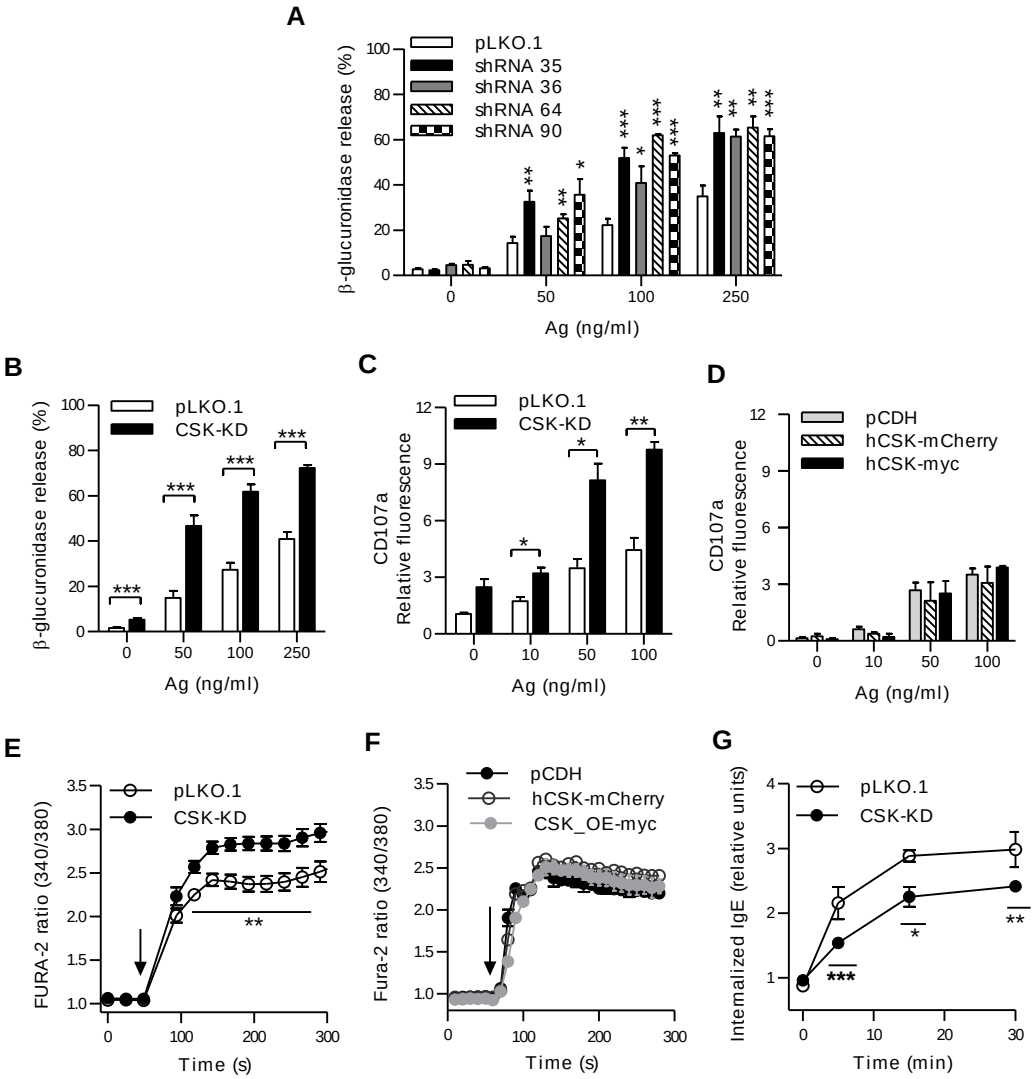

Fig. 2 Potuckova et al.

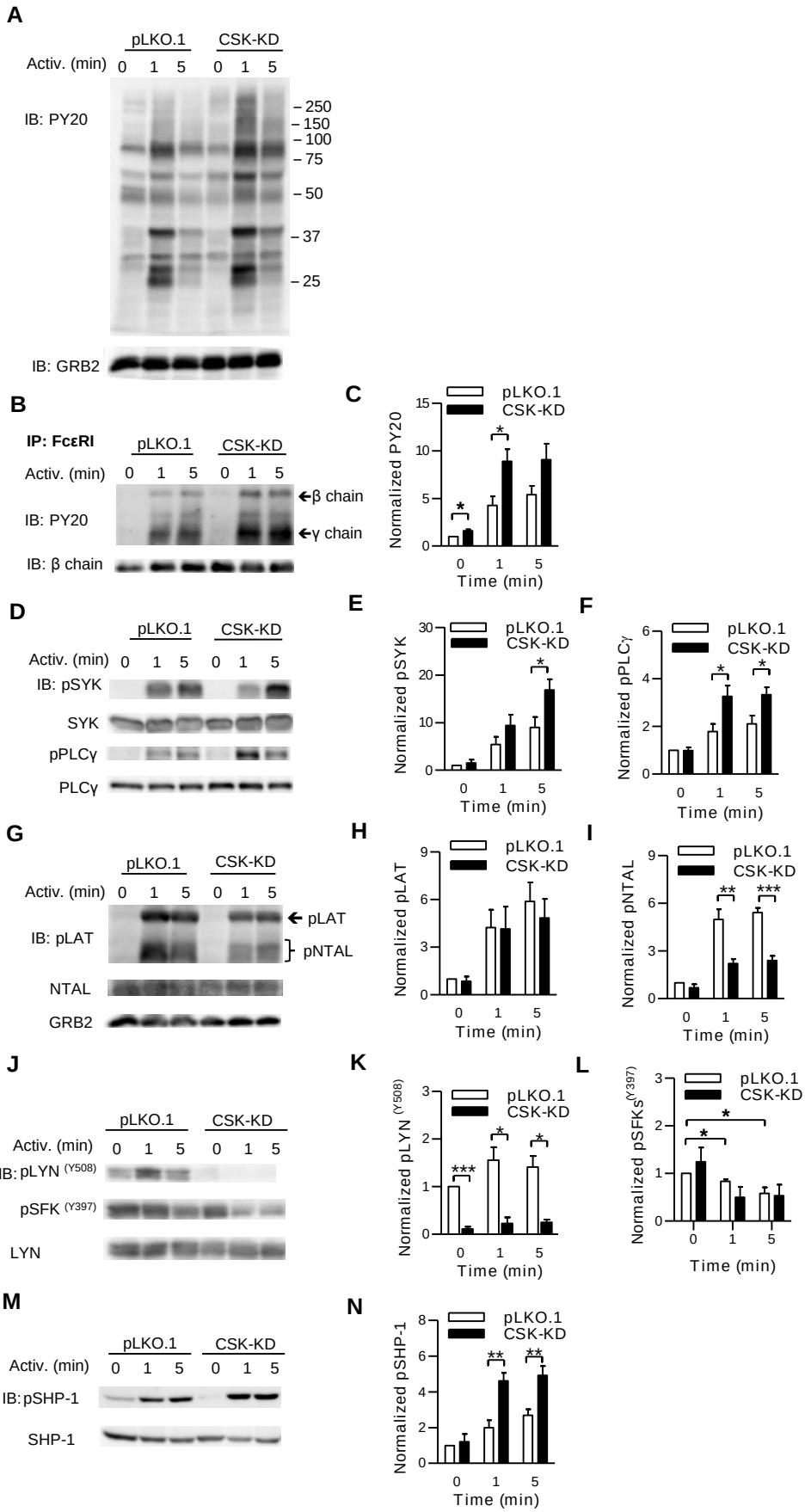

Fig.3 Potuckova et al.

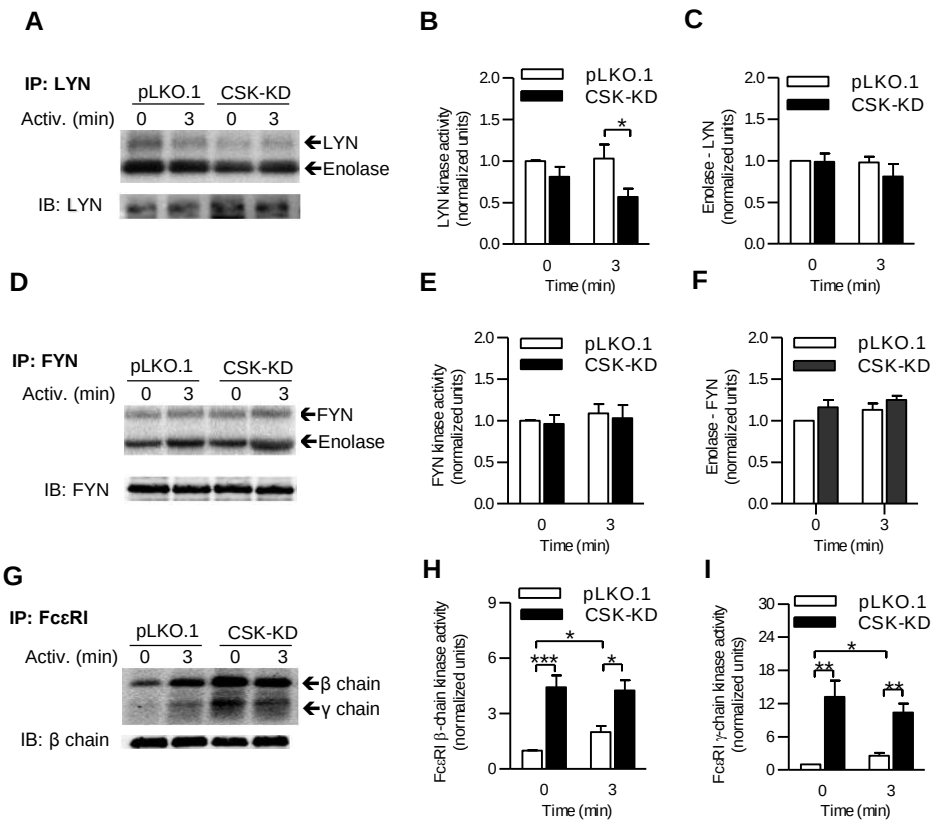

Fig. 4 Potuckova et al.

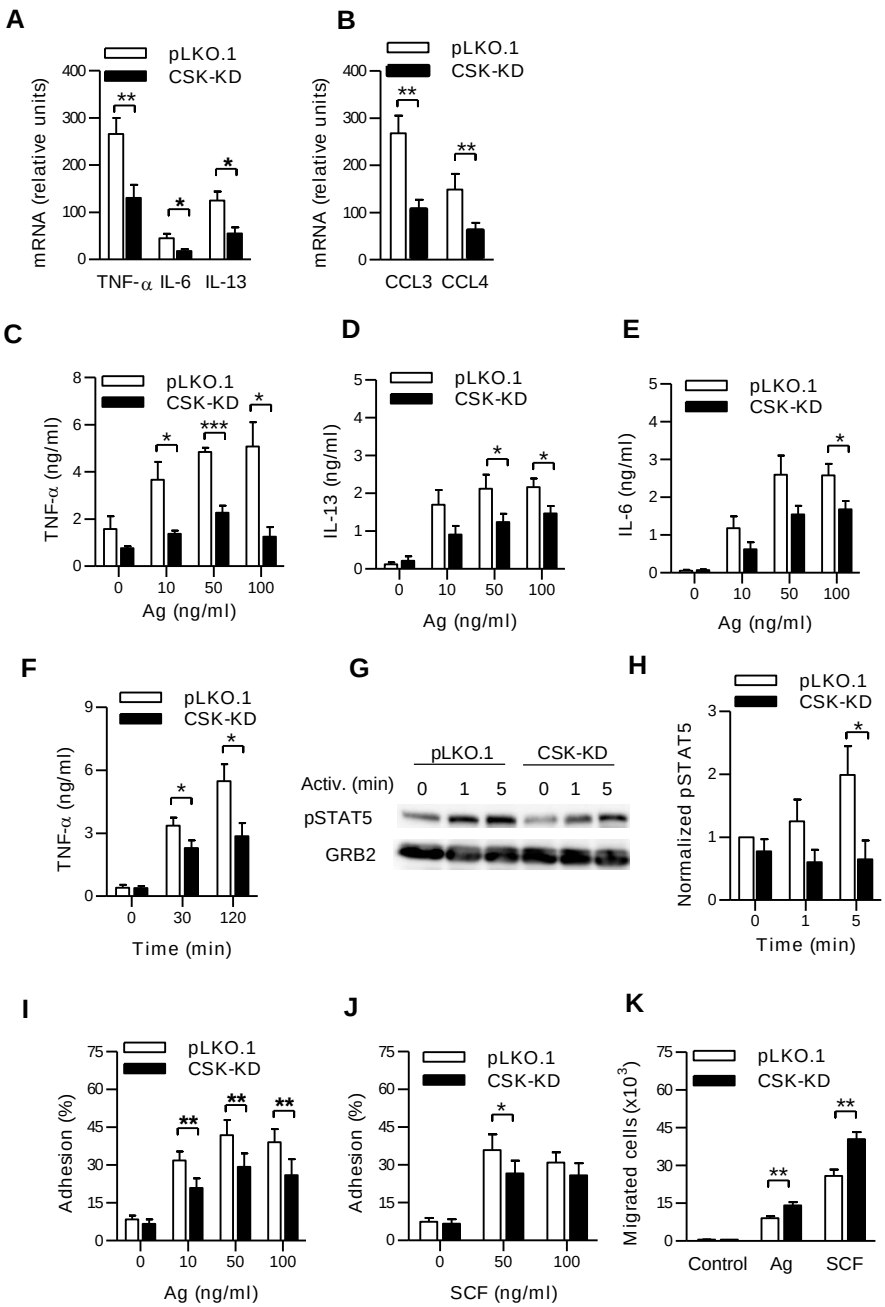

Fig. 5 Potuckova et al.

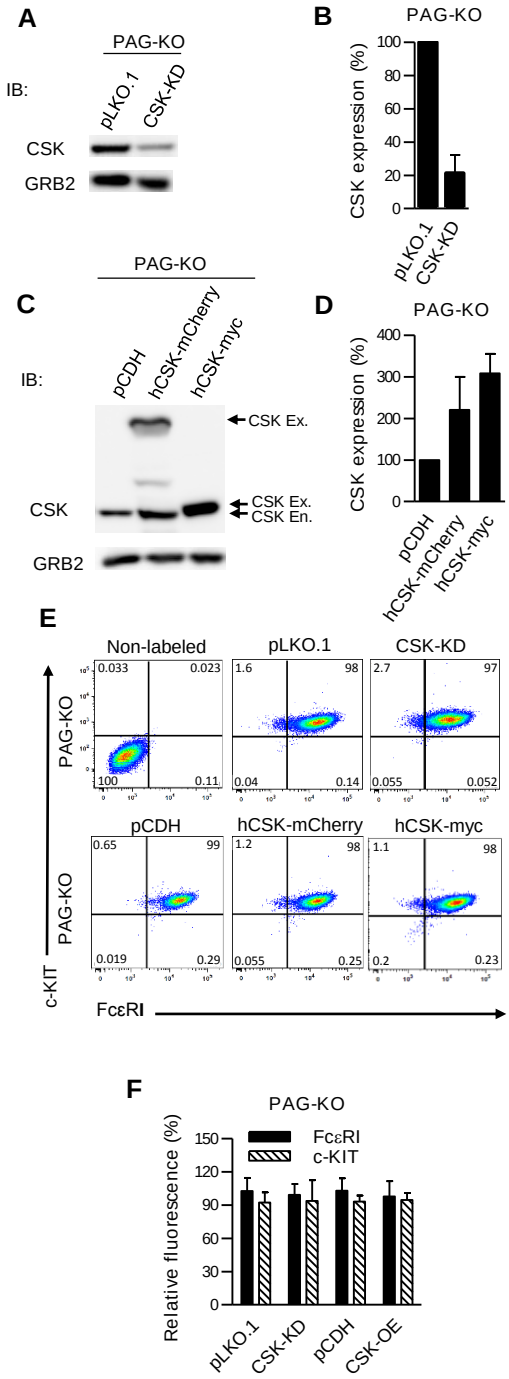

Fig.6 Potuckova et al.

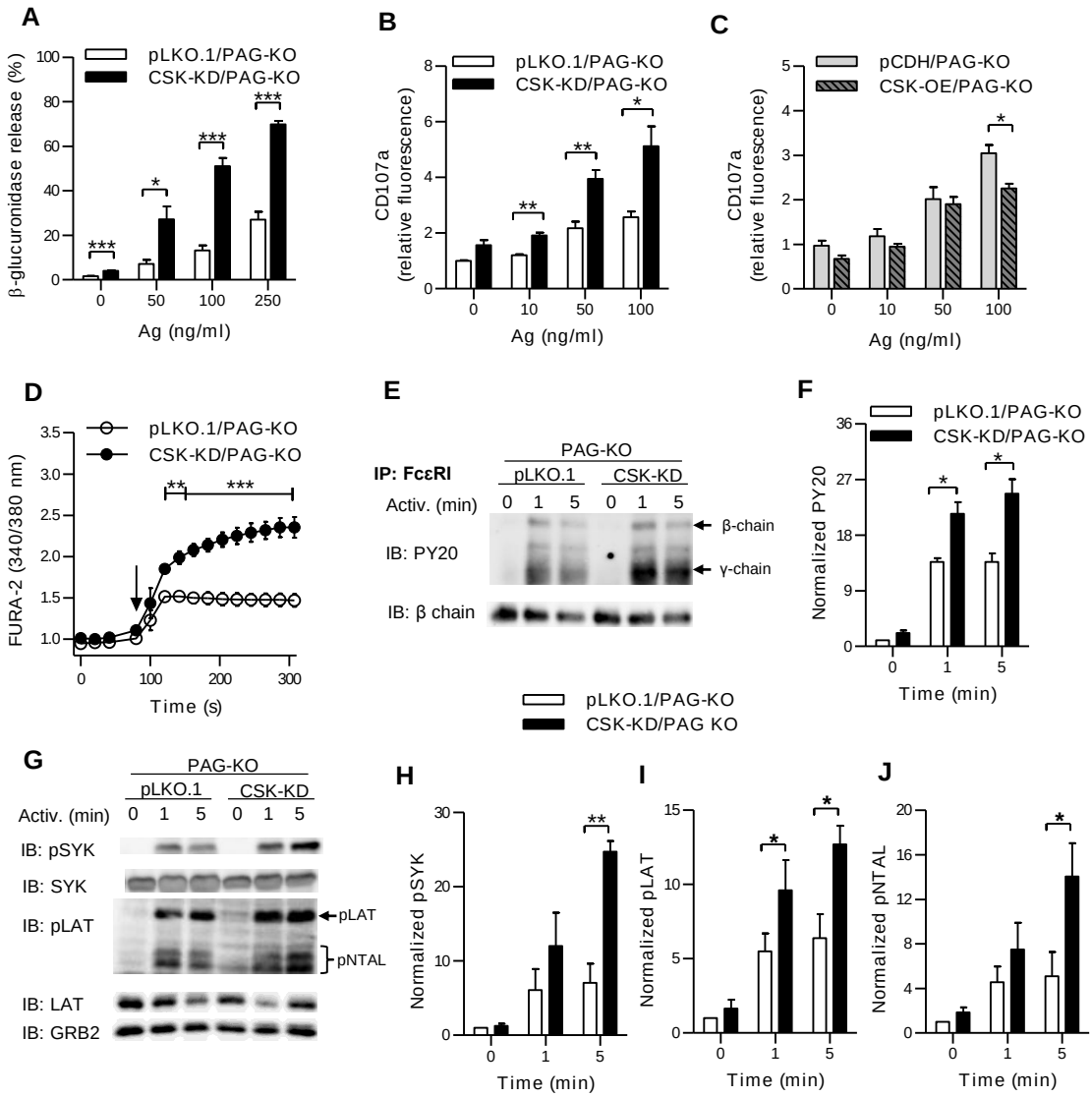

Fig.7 Potuckova et al.

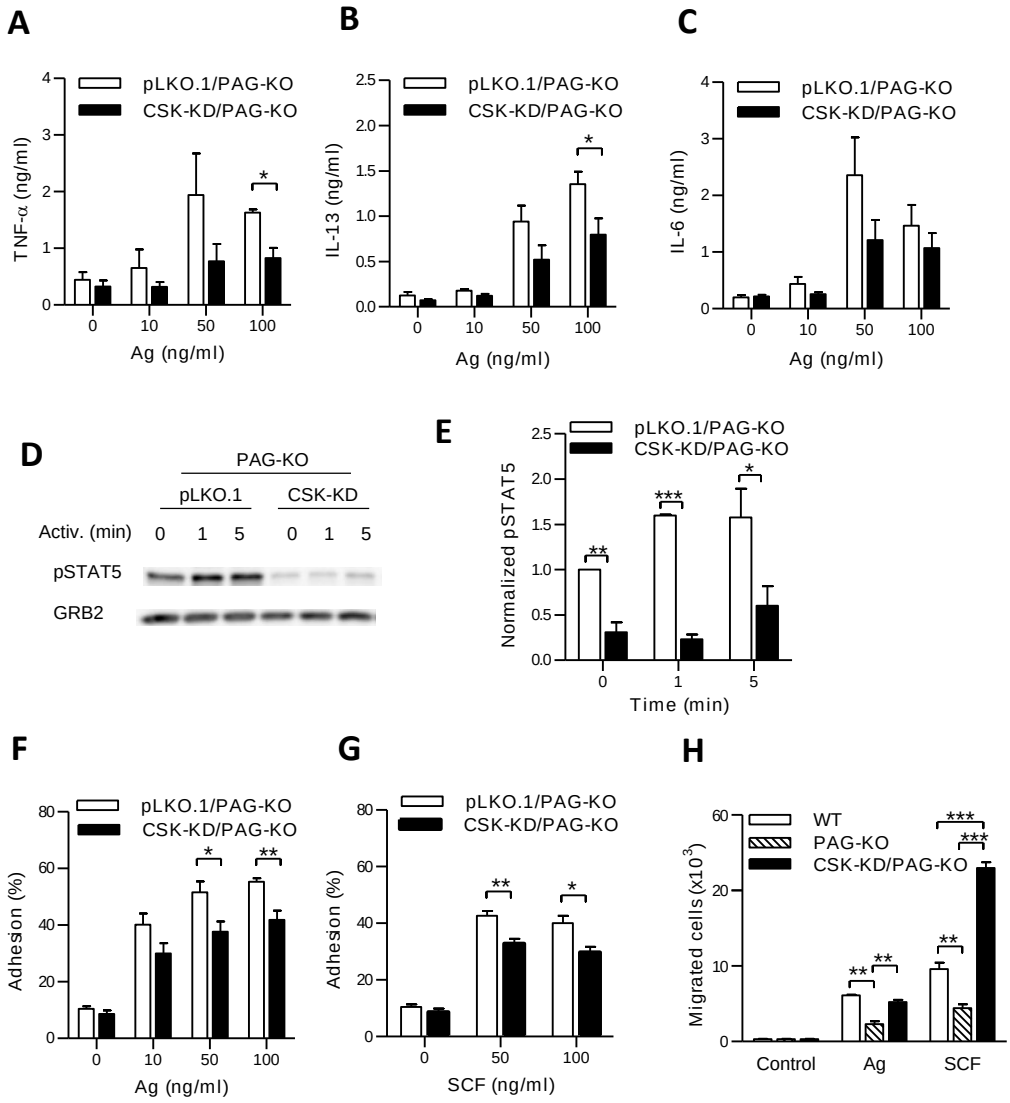

Fig. 8 Potuckova et al.

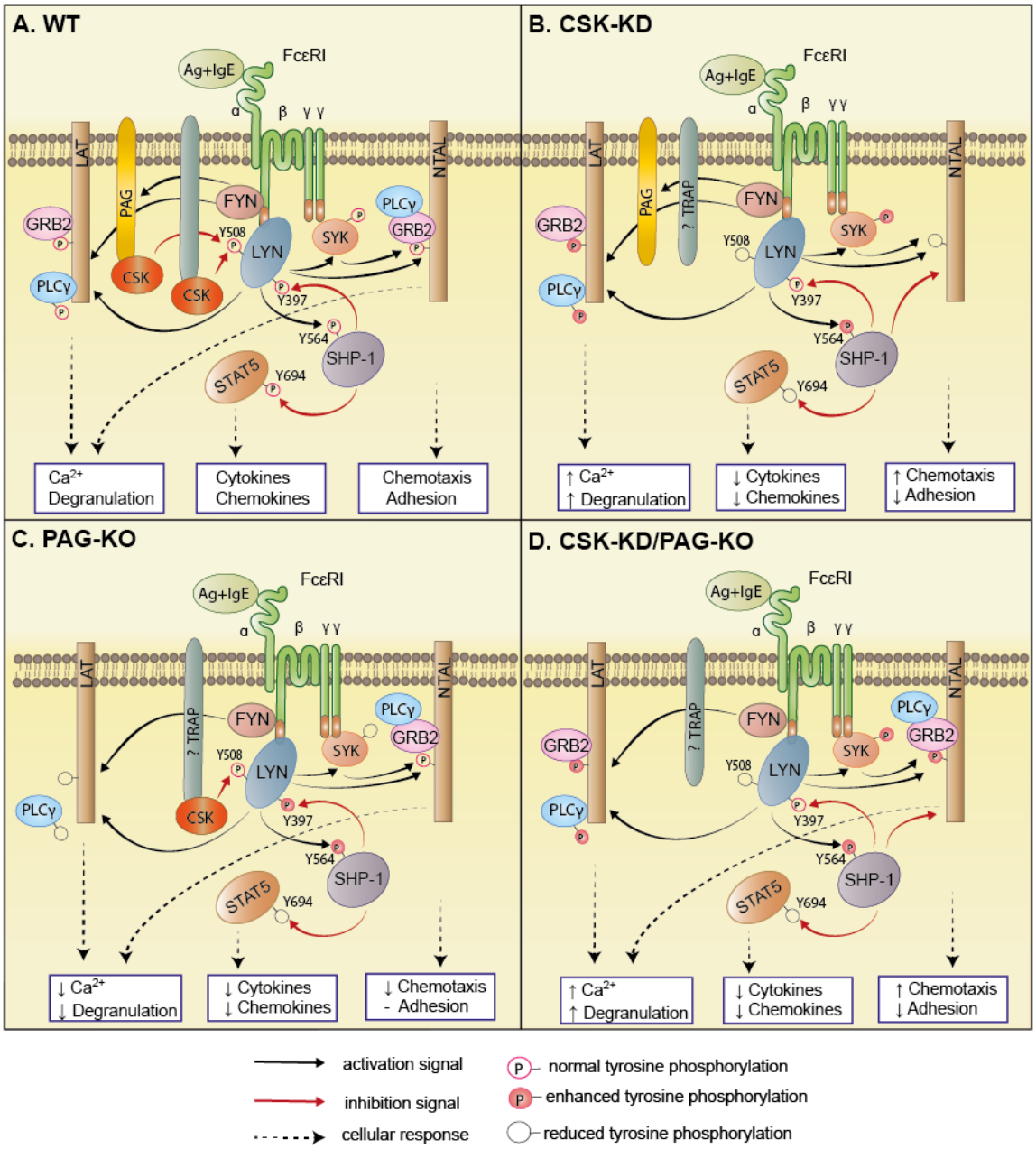

Fig. 9 Potuckova et al.

7.4 NEGATIVE REGULATORY ROLES OF ORMDL3 IN THE FcεRI-TRIGGERED EXPRESSION OF PROINFLAMMATORY MEDIATORS AND CHEMOTACTIC RESPONSE IN MURINE MAST CELLS.

Bugajev V., Hálová I., Dráberová L., Bambousková M., **Potůčková L.**,
Dráberová H., Paulenda T., Junyent S., Dráber P.

Cell Mol. Life Sci., 73(6):1265-85, 2016

Cell. Mol. Life Sci.
DOI 10.1007/s00018-015-2047-3

Cellular and Molecular Life Sciences

ORIGINAL ARTICLE

Negative regulatory roles of ORMDL3 in the FcεRI-triggered expression of proinflammatory mediators and chemotactic response in murine mast cells

Viktor Bugajev[1] · Ivana Halova[1] · Lubica Draberova[1] · Monika Bambouskova[1] · Lucie Potuckova[1] · Helena Draberova[1] · Tomas Paulenda[1] · Sergi Junyent[1] · Petr Draber[1]

Received: 16 April 2015 / Revised: 19 August 2015 / Accepted: 17 September 2015

Abstract Single-nucleotide polymorphism studies have linked the chromosome 17q12-q21 region, where the human orosomucoid-like (*ORMDL*)*3* gene is localized, to the risk of asthma and several other inflammatory diseases. Although mast cells are involved in the development of these diseases, the contribution of ORMDL3 to the mast cell physiology is unknown. In this study, we examined the role of ORMDL3 in antigen-induced activation of murine mast cells with reduced or enhanced ORMDL3 expression. Our data show that in antigen-activated mast cells, reduced expression of the ORMDL3 protein had no effect on degranulation and calcium response, but significantly enhanced phosphorylation of AKT kinase at Ser 473 followed by enhanced phosphorylation and degradation of IκBα and translocation of the NF-κB p65 subunit into the nucleus. These events were associated with an increased expression of proinflammatory cytokines (TNF-α, IL-6, and IL-13), chemokines (CCL3 and CCL4), and cyclooxygenase-2 dependent synthesis of prostaglandin D2. Antigen-mediated chemotaxis was also enhanced in ORMDL3-deficient cells, whereas spreading on fibronectin was decreased. On the other hand, increased expression of ORMDL3 had no significant effect on the studied signaling events, except for reduced antigen-mediated chemotaxis. These data were corroborated by increased IgE-antigen-dependent passive cutaneous anaphylaxis in mice with locally silenced ORMDL3 using short interfering RNAs. Our data also show that antigen triggers suppression of ORMDL3 expression in the mast cells. In summary, we provide evidence that downregulation of ORMDL3 expression in mast cells enhances AKT and NF-κB-directed signaling pathways and chemotaxis and contributes to the development of mast cell-mediated local inflammation in vivo.

Keywords Mast cell · RNA interference · ORMDL3 knockdown · Prostaglandin D2 · Degranulation · Chemotaxis · Proinflammatory cytokines

Abbreviations

Ag	Antigen
BMMC	Bone marrow-derived mast cell
BSS	Buffered saline solution
Bp	Base pairs
$[Ca^{2+}]_i$	Concentrations of free intracellular Ca^{2+}
COX	Cyclooxygenase
Ct	Threshold cycle
NT	Nontarget
O3_KD	ORMDL3 knockdown
O3_OE	ORMDL3 overexpression
ORM	Orosomucoid
ORMDL	Orosomucoid-like
PCA	Passive cutaneous anaphylaxis
pCDH	pCDH-CMV-MCS-EF1-Puro
PG	Prostaglandin
SERCA	Sarco/endoplasmic reticulum Ca^{2+} ATPase
sh	Short hairpin
siRNA	Short interfering RNA
SNP	Single-nucleotide polymorphisms
TNP	2,4,6-Trinitrophenol

Electronic supplementary material The online version of this article (doi:10.1007/s00018-015-2047-3) contains supplementary material, which is available to authorized users.

✉ Petr Draber
draberpe@img.cas.cz

[1] Department of Signal Transduction, Institute of Molecular Genetics, Academy of Sciences of the Czech Republic, v.v.i., Videnska 1083, 142 20 Prague 4, Czech Republic

Published online: 25 September 2015

WT Wild type

Introduction

Orosomucoid-like (ORMDL)3 protein has attracted increased attention since the discovery of single-nucleotide polymorphisms (SNPs) in the chromosome 17q12-q21 region that were associated with onset of asthma in childhood [1]. Further studies confirmed these data in ethnically diverse populations [2, 3]. Interestingly, SNPs associated with 17q12-q21 were also linked to chronic obstructive pulmonary disease [4], ulcerative colitis [5], primary biliary cirrhosis [6], type 1 diabetes [6], Crohn disease [6, 7] and rheumatoid arthritis [8]. It has been suggested that the risk alleles for asthma mapped in the 17q12-q21 region are linked to increased levels of the *ORMDL3* gene transcript [1, 6], but the risk alleles implicated in the predisposition to primary biliary cirrhosis, type 1 diabetes and Crohn disease are associated with decreased ORMDL3 mRNA levels [6]. Since *ORMDL3* is only one of several genes in the chromosome 17q12-q21 region, the observed data underline the complexity of inflammatory diseases [6, 9].

Human and mouse *ORMDL3* genes encode 153 aa proteins belonging to the conserved ORMDL family consisting of three members. All three members of this family (ORMDL1–3) are embedded in the endoplasmic reticulum membrane [10]. Pivotal studies of ORMDL3 yeast homologs, orosomucoid (ORM)1 and ORM2, showed that ORM proteins are negative regulators of sphingolipid synthesis [11, 12] and that knockdown of all three ORMDL isoforms resulted in increased ceramide production in distinct mammalian cell lines [11, 13, 14]. Further experiments showed that disruption of sphingolipid homeostasis in the mouse model increased bronchial reactivity in the absence of inflammatory stimulus [15]. ORMDL3 has also been found to play a role as a regulator of Ca^{2+} homeostasis in the endoplasmic reticulum [16, 17] and as a trigger of unfolded protein response [16, 18, 19].

Several studies attempted to explain the physiological role of ORMDL3 in cells and tissues relevant to asthma. Mice challenged with allergen exhibited enhanced expression of ORMDL3 in macrophages, eosinophils and lung epithelial cells [18]. Furthermore, a lung epithelial cell line transfected with ORMDL3 cDNA showed increased transcription of genes encoding metalloproteases, chemokines and oligoadenylate synthetases [18]. In addition, bone marrow-derived eosinophils transduced with ORMDL3 cDNA showed enhanced rolling and nuclear localization of the phosphorylated NF-κB p65 subunit [20]. Transgenic mice overexpressing human ORMDL3 exhibited increased levels of serum IgE and showed spontaneous development of enhanced airway responsiveness. This correlated with increased numbers of $CD4^+$ cells, macrophages, eosinophils and neutrophils, and enhanced Th2 cytokine levels in the lungs of transgenic mice [19]. Although mast cells are crucial effector cells in IgE-dependent allergic disorders [21, 22] and are critical for promoting the severity of collagen-induced arthritis, which is an autoimmune inflammatory disease [23], the involvement of ORMDL3 in FcεRI-dependent activation and mast cell-mediated inflammation has not yet been determined.

In this study, we decided to test the hypothesis that changes in the expression levels of ORMDL3 could modulate mast cell proinflammatory responses. Bone marrow-derived mast cells (BMMCs) with enhanced or reduced expression of ORMDL3 were produced and examined. We focused on the NF-κB signaling axis, which is an important player in the transcription of proinflammatory cytokines and immunoregulatory proteins [24] and is involved in the promotion of inflammation [25–27]. We found that ORMDL3-deficient cells exhibited significantly increased translocation of the NF-κB p65 subunit into the nucleus. These events were accompanied by enhanced expression of genes encoding proinflammatory cytokines, chemokines, and cyclooxygenase (COX)-2, an inducible enzyme involved in prostaglandin (PG)D2 synthesis [28]. In an attempt to identify the signaling pathway that precedes activation of NF-κB, we found that AKT kinase exhibited increased phosphorylation. We also studied the roles of ORMDL3 in the migration of mast cells toward antigen (Ag) and changes in ORMDL3 expression after high-affinity IgE receptor (FcεRI) triggering. Altogether, our data provide evidence that in mast cells, ORMDL3 functions predominantly as a negative regulator of FcεRI-mediated signaling events leading to the expression of proinflammatory mediators and chemotaxis. These data were corroborated by the finding of enhanced passive cutaneous anaphylaxis (PCA) in mice with locally silenced ORMDL3.

Materials and methods

Cells and lentiviral infection

BMMCs were derived from femurs and tibias of 8- to 10-week-old BALB/c mice bred, maintained, and used in accordance with the Institute of Molecular Genetics guidelines (Permit number 12135/2010-17210) and national guidelines (2048/2004-1020). The cells were cultured in RPMI-1640 medium supplemented with 100 U/ml penicillin, 100 μg/ml streptomycin, 71 μM 2-mercaptoethanol, MEM non-essential amino acids, 0.7 mM

sodium pyruvate, 2.5 mM L-glutamine, 12 mM D-glucose, recombinant mouse stem cell factor (15 ng/ml, PeproTech EC), mouse recombinant IL-3 (20 ng/ml, PeproTech EC) and 10 % FCS. Lentiviral transductions were done as described previously using HEK 293 T/17 packaging cells for virus preparation [29]. A set of murine ORMDL3 short hairpin (sh)RNAs cloned into the pLKO.1 vector (TRCN0000126**200**, TRCN0000126**201**, TRCN0000126**202**, TRCN0000126**203**; denoted in further text as indicated by numbers in bold) were purchased from Open Biosystems. To generate the myc-ORMDL3 vector, mouse *ORMDL3* cDNA (Open Biosystems) was first amplified using forward primer 5′-AAAGAATTCGGAATGTGGGCACAGCACAC-3′ and reverse complementary primer 5′-TTTGCGGCCGCTCAGTACTTATTGATTCCAAA-3′, introducing *EcoRI* and *NotI* restriction endonuclease sites (underlined), respectively. Amplified *ORMDL3* was then inserted into a pCMV-myc eukaryotic expression vector (Clontech). Myc-*ORMDL3* was recloned by PCR into the vector pCDH-CMV-MCS-EF1-Puro (Systembio; pCDH) using forward primer 5′-AAATCTAGAGCCGCCACCATGGAGCAGAAGCTGATCTCA-3′ and reverse complementary primer 5′-TTTGCGGCCGCTCAGTACTTATTGATTCCAAA-3′, introducing *Xba*I and *Not*I restriction endonuclease sites (underlined), respectively. The construct was verified by sequencing and denoted myc-O3. The pCDH vector Myc-ORMDL3 was also used to clone murine ORMDL1 and ORMDL2 cDNAs (OpenBiosystems). Specific primers for ORMDL1 (forward primer 5′-AAAGAATTCGGAATGTTGGAGTTGCCCAC-3′ and reverse complementary primer 5′-TTTGCGGCCGCTCAATACTTATTAATTCCAAA-3′) and ORMDL2 (forward primer 5′-AAAGAATTCGGAATGTGGGGGTGGCACAC-3′ and reverse complementary primer 5′-TTTGCGGCCGTTAGTATTTGTTGATTCCAAA-3′) were designed to be cloned into pCDH using *Eco*RI and *Not*I restriction endonuclease sites (underlined). To prepare an expression vector for ORMDL3 with C-terminal myc-tag, *ORMDL3* cDNA was amplified using forward primer 5′-AAAGAATTCGCCGCCACCATGAATGTGGGCACAGCACAC-3′ and reverse complementary primer 5′-TTTGGATCCGTACTTATTGATTCCAAA-3′, introducing *Eco*RI and *Bam*HI restriction endonuclease sites (underlined), respectively. Amplified ORMDL3 was then cloned into pCDH-myc. The construct, denoted O3-myc, was verified by sequencing. Both constructs were used to produce lentiviruses as described [29]. BMMCs were transduced with the lentiviruses and stable transfectants were obtained by culturing the transduced cells for 2 weeks in the presence of puromycin (5 μg/ml). Cells were analyzed for FcεRI and c-Kit expression using flow cytometry, while ORMDL3 expression was examined by qPCR and immunoblotting as described below. In all experiments, more than 80 % of cells were alive and the selected populations were maintained for less than 3 weeks in culture. In all experiments, empty pLKO.1 or empty pCDH vectors were used as controls. In most of the functional studies, comparison between nontransduced cells and cells transduced with pLKO.1 was performed. In some experiments related to AKT/IκB signaling, we also used as a control pLKO.1 vector containing nontarget (NT) shRNA (Sigma-Aldrich) as a control.

Antibodies and reagents

Mouse IgE mAb specific for 2,4,6-trinitrophenol (TNP), clone IGEL b4 1 [30], SYK-specific mAb [31], and Lyn-specific mAb [32] were produced in our laboratory. Anti-mouse KIT (CD117)-allophycocyanin conjugate [catalog number (#) 17-1171] and anti-mouse FcεRI α-FITC conjugate (#11-5898) were obtained from eBioscience. Rabbit anti-COX-2 (#12282), rabbit anti-pSYK (Tyr525/526; #2710), rabbit anti-p65 subunit of NF-κB (#8242), rabbit phospho-AKT (Thr 308; #2965) and mouse anti-pIκBα (Ser32/36; #9246) were obtained from Cell Signaling. Anti-HPRT mAb (#sc-376938), rabbit anti-actin polyclonal Ab (#sc-8432), rabbit anti-p65 subunit of NF-κB (#sc-372), rabbit phospho-AKT1/2/3 (#sc-7985), rabbit ERK1 (#sc-93), rabbit phospho-ERK (Tyr204; #sc-7976), goat anti-AKT1 (#sc-1618), rabbit anti-IκBα (#sc-371), mouse anti-Myc (#sc-40), rabbit anti-GRB2 (#sc-255), HRP-conjugated goat anti-mouse IgG (#sc-2005), HRP-goat anti-rabbit IgG (#sc-2004), and HRP-donkey anti-goat IgG (#sc-2056) were obtained from Santa Cruz Biotechnology, Inc. Donkey anti-rabbit-IgG Alexa Fluor 488 conjugate (#A21206) and goat anti-rabbit-IgG Alexa Fluor 568 (#A11036) were from Molecular Probes. Antibodies specific for mouse TNF-α (#500-P64), IL-13 (#500-P178), the corresponding recombinant proteins, and recombinant IL-6 were obtained from PeproTech. Murine anti-IL-6 (#553414) was purchased from Becton–Dickinson. Antibodies used for immunoblotting of ORMDL proteins were obtained after immunization of rabbits with a peptide corresponding to the middle part of ORMDL3 (TPFETPDQGKARLLTHWEQMDC) conjugated to keyhole limpet hemocyanin via an extra cysteine residue (underlined). This antibody is designated TPF. For immunofluorescence studies, rabbit polyclonal serum raised against the N-terminal ORMDL3 peptide (CNVGTAHSEVNPNTR) was used. This antibody was prepared as described above and is designated NVG. The peptides used for immunization share high similarities with ORMDL1 and ORMDL2 proteins and both polyclonal sera recognize all three members of the ORMDL family. Therefore, we refer to the 17 kDa band on immunoblots as ORMDL. The sera were affinity purified using a

SulfoLink™ Immobilization Kit for Peptides (Pierce) according to the manufacturer's instructions. Fura-2, AM was obtained from Life Technologies. All other reagents were obtained from Sigma-Aldrich.

β-Glucuronidase release and Ca^{2+} response

BMMCs were sensitized with TNP-specific IgE (IGEL b4 1 mAb, 1 μg/ml) in stem cell factor- and IL-3-free culture medium for 16 h, unless stated otherwise. Then the cells were washed in buffered saline solution (BSS; 135 mM NaCl, 5 mM KCl, 1.8 mM CaCl2, 5.6 mM glucose, 20 mM HEPES, pH 7.4) supplemented with 0.1 % BSA and activated with Ag (TNP–BSA conjugate, 15–25 mol TNP/mol BSA). The extent of degranulation was evaluated by determining β-glucuronidase concentrations as described previously [33] except that an Infinite 200 M (TECAN) plate reader was used at 355 nm excitation and 460 nm emission wavelengths. Calcium mobilization was determined using Fura-2 acetoxymethyl ester (Fura-2 AM; Life Technologies) as a reporter. Cells were incubated with Fura-2 AM (1 ng/ml) and probenecid (2.5 mM) in BSS supplemented with 0.1 % BSA and incubated in the shaker for 30 min at 37 °C. Fura-2 AM-loaded cells were washed twice with 2.5 mM probenecid in BSS-0.1 % BSA and then transferred to BSS-0.1 % BSA supplemented with 2.5 mM probenecid and incubated in Thermomixer (Eppendorf; 15 min, 37 °C, 500 rpm). Cells were pelleted by centrifugation at $500\times g$ for 3 min, resuspended in BSS-0.1 % BSA and transferred to white polysorp 96 well plate (NUNC, Thermo Scientific). After 1 min, BSS-0.1 % BSA supplemented with Ag (final concentration 100 ng/ml) was added using the TECAN injector system. Measurement continued up to 200 s. Levels of Ca^{2+} were determined by spectrofluorometry using the Infinite 200 M plate reader with excitation wavelengths at 340 and 380 nm and with a constant emission at 510 nm. To determine basal concentrations of free intracellular Ca^{2+} ($[Ca^{2+}]_i$) in various cell types, Triton X-100 (0.1 % final concentration) was added to the Fura-2-loaded cells and Fura-2 fluorescence was determined. Then, EGTA (16 mM final concentration) was added and Fura-2 fluorescence was again determined. Calcium concentrations were then calculated using the formula: $[Ca^{2+}]_i = K_d \times S_{f2}/S_{b2} \times (R - R_{min})/(R_{max} - R)$, where K_d represents the dissociation constant for Fura-2 (224 nM), S_{f2} the average fluorescence obtained at 380 nm after EGTA addition, S_{b2} the average fluorescence obtained at 380 nm after addition of Triton X-100, R_{min} the mean ratio calculated from the data acquired after EGTA addition, R_{max} the mean of ratio calculated from data acquired after addition of Triton X-100, and R the ratio of fluorescence obtained at 340/380.

Detection of ORMDL, cytokines, and chemokines at the mRNA level

IgE-sensitized BMMCs were activated with different concentrations of Ag. One hour later, mRNA was extracted using a TurboCapture 96 mRNA kit or RNeasy miniKit (Qiagen). Single-stranded cDNA was synthesized with M-MLV reverse transcriptase (Invitrogen) according to the manufacturer's instructions. Real-time PCR amplifications of cDNAs were performed in 10 μl reaction volumes of qPCR mix containing 1 M 1,2-propanediol, 0.2 M trehalose and SYBR green 1 [34] in 384-well plates sealed with LightCycler 480 sealing foil and analyzed by LightCycler 480 (Roche Diagnostics). The following cycling conditions were used: 3 min at 95 °C, followed by 50 cycles of 10 s at 95 °C, 20 s at 60 °C and 20 s at 72 °C. Threshold cycle (Ct) values were determined by automated threshold analysis of the cycler. Specificity of the PCR was evaluated by examining the melting curves. For data presented in Fig. 2a, actin, *GAPDH*, ubiquitin, *TBP*, *SDHA*, and *HPRT* were used as reference genes and the expression levels of ORMDL3 mRNA were normalized to the geometric mean of the reference genes in nonactivated control cells. In all other experiments, actin, *GAPDH*, and ubiquitin were used as the reference genes. The relative changes in the mRNA expression levels were normalized to the ones of the corresponding controls. The following primer sets were used for amplification of different cDNA fragments (sense/antisense; numbers in square brackets are sizes of the fragments in bps): actin, 5′-GATCTGGCACCACACCTTCT-3′/5′-GGGGTGTTGAAGGTCTCAAA-3′ [138]; GAPDH, 5′-AACTTTGGCATTGTGGAAGG-3′/5′-ATCCACAGTCTTCTGGGTGG-3′ [69]; ubiquitin, 5′-ATGTGAAGGCCAAGATCCAG-3′/5′-TAATAGCCACCCCTCAGACG-3′ [160]; HPRT, 5′-CTGGTGAAAAGGACCTCTCGAA-3′/5′-CTGAAGTACTCATTATAGTCAAGGGCAT-3′ [109]; TBP, 5′-GAAGAACAATCCAGACTAGCAGCA-3′/5′-CCTTATAGGGAACTTCACATCACAG-3′ [128]; SDHA, 5′-AAGGCAAATGCTGGAGAAGA-3′/5′-TGGTTCTGCATCGACTTCTG-3′ [112]; ORMDL3, 5′- CCAACCTTATCCACAACCTGG-3′/5′-GACCCCGTAGTCCATCTGC-3′ [124]; ORMDL2, 5′-CACAGCGAAGTAAACCCCAAC-3′/5′-AGGGTCCAGACAACAGGAATG-3′ [134]; ORMDL1, 5′-ACAGTGAGGTAAACCCCAATACT-3′/5′-GCAAAAACACATACATCCCCAGA-3′ [174]; TNF-α, 5′-CCCTCACACTCAGATCATCTTCT-3′/5′-GCTACGACGTGGGCTACAG-3′ [61]; IL-6, 5′-GAGGATACCACTCCCAACAGACC-3′/5′-AAGTGCATCATCGTTGTTCATACA-3′ [141]; IL-13, 5′-AGACCAGACTCCCCTGTGCA-3′/5′-TGGGTCCTGTAGATGGATTG-3′ [123]; CCL3, 5′-CATCGTTGACTATTTTGAAACCAG-3′/5′-GCCGGTTTCTCTTAGTCAGGAA-3′ [72]; CCL4, 5′-CTTGGAGTTGAACTGAGCA

GC-3′/5′-AGAGGGGCAGGAAATCTGAA-3′ [126]; SERCA2b, 5′-GAGAACGCTCACACAAAGACC-3′/5′-CAATTCGTTGGAGCCCCAT-3′ [120]; COX-2, 5′-TGAGCAACTATTCCAAACCAGC-3′/5′-GCACGTAGTCTTCGATCACTATC-3′ [74].

For detection of cytokine secretion, the nano-iPCR method was used as described [35]. Briefly, anti-TNF-α, anti-IL-13 (each at 1 μg/ml), or anti-IL-6 (2 μg/ml) in 100 mM borate buffer (pH 9.5) was dispensed in 50 μl aliquots into wells of a real-time 96-well plate (Eppendorf). After overnight incubation at 4 °C, each well was washed four times with 200 μl of TBST (10 mM Tris–HCl, pH 7.4, 150 mM NaCl, and 0.05 % Tween 20) and the remaining binding sites were blocked by 2 h incubation at 37 °C with TBST supplemented with 2 % BSA. After washing, 50 μl of serial dilutions (0.1–100 ng/ml) of recombinant TNF-α, IL-13 or IL-6, or the tested samples diluted in PBS-1 % BSA were added. The samples were incubated 1 h at 37 °C and after washing with TBST, 50 μl of gold nanoparticles armed with thiolated DNA oligonucleotide template were added and further processed as described [35]. For calculation of the cytokine concentrations, the obtained Ct values were compared with those from the corresponding calibration curves.

PGD2 measurements

IgE-sensitized mast cells were seeded at 2×10^5 cells per well in 100 μl of BSS–BSA buffer in a 96-well culture plate. Cells were stimulated by adding 100 μl of Ag to a final concentration of 100 ng/ml for 5 h. Cell-free supernatants were collected and assessed for PGD2 using competitive enzyme immunoassay based on measurement of PGD2-methoxylamine hydrochloride derivate according to the manufacturer's conditions (Cayman Chemicals). For detection, the Infinite 200 M plate reader was used. Supernatants of nonactivated and activated cells were diluted 1/10 and 1/40, respectively, to be read within the range of the respective standard curve.

Gel electrophoresis and immunoblotting

Whole-cell extracts were prepared by washing the cells in cold PBS, solubilizing them in hot SDS-sample buffer [36], sonicating, and boiling for 5 min. Proteins were size fractionated on 10 or 12.5 % SDS-PAGE gels, electrophoretically transferred onto nitrocellulose membrane, and analyzed by immunoblotting with protein- or phosphoprotein-specific Abs. Bound primary Abs were detected with HRP-conjugated secondary Abs. The HRP signal was detected with chemiluminescence reagent [37] and quantified by a Luminescent Image Analyzer LAS 3000 (Fuji Photo Film Co.). Aida software (Raytest GmbH) was used for signal quantification. Protein levels were normalized to the corresponding controls.

Flow cytometry analysis

To quantify the surface expression of FcεRI and KIT, BMMCs (3×10^5/ml) were exposed simultaneously to anti-mouse FcεRI-FITC and anti-mouse KIT-allophycocyanin for 30 min on ice. Then, the cells were washed with ice-cold PBS and evaluated using an Accuri C6 flow cytometer (BD Biosciences).

Cell adhesion and spreading

IgE-sensitized BMMCs were loaded with calcein-AM and transferred into a 96-well plate (Thermo Scientific) coated with fibronectin (10 ng/ml) diluted in PBS [38]. Cells activated for 30 min with 100 ng/ml of Ag were examined for adhesion assay using the Infinite 200 M plate reader with excitation and emission filters at 485 nm and 538 nm, respectively. For cell spreading, wells in 96-well glass-bottom plates (InVitroSci) were coated with fibronectin (50 μl; 50 μg/ml) diluted in PBS. Wells were then washed with PBS, and 30×10^3 cells in BSS-0.1 % BSA were added per well. Cells were allowed to attach for 30 min at 37 °C, washed, and activated or not with Ag. After 30 min, cells were fixed with 3 % paraformaldehyde in PBS for 30 min at room temperature. For filamentous (F)-actin staining, cells were exposed to Alexa Fluor 488-phalloidin conjugate (Invitrogen, #A12379), diluted 1:100 in PBS supplemented with L-α-lysophosphatidylcholine (80 μg/ml). After 1 h, cells were washed and kept in PBS supplemented with Hoechst 33258 stain (1 μg/ml) until measurement. Cells were then examined with the Scan^R system (Olympus).

Chemotactic response

Ag-Mediated chemotactic responses were evaluated using 24-well Transwell chambers (Corning) with 8 μm polycarbonate filters as described previously [38]. Cells migrating into lower compartments within the 8-h incubation period were counted using an Accuri C6 Flow Cytometer (Becton–Dickinson).

F-actin assay

The total amount of F-actin in nonactivated and Ag-activated cells was determined by flow cytometry. BMMCs in a 96-well plate (5×10^4 cells per well) were exposed to various stimuli at 37 °C, fixed with 3 % paraformaldehyde in phosphate-buffered saline, and then permeabilized and stained in a single step by a mixture of lysophosphatidylcholine (200 mg/ml)

and 1000× diluted Alexa Fluor 488-phalloidin (Molecular Probes) in phosphate-buffered saline. The fluorescence intensity was measured using LSRII flow cytometer (Becton–Dickinson). The acquired data were analyzed using FlowJo software (Tree Star Inc).

Confocal microscopy

IgE-sensitized BMMCs (3×10^5) were attached (60 min at 37 °C) to a fibronectin-coated multitest slide (MP Biomedicals) and then activated by Ag. After 30 min, the cells were fixed with 4 % paraformaldehyde for 15 min at room temperature and permeabilized with 0.3 % Triton X-100 for 20 min. Free binding sites were blocked with 5 % donkey serum (Jackson ImmunoResearch Laboratories) in PBS and the cells were stained with a mixture of rabbit Abs against p65 subunit of NF-κB diluted 1:400 (#8242) and 1:200 (#sc-372), followed by labeling with secondary antibody, donkey anti-rabbit-Alexa Fluor 488 conjugate, and diluted 1:200 in PBS containing 1 % BSA. ORMDL was labeled with rabbit polyclonal serum (described in Antibodies and reagents) followed by labeling with donkey anti-rabbit-Alexa Fluor 568 (1:100). After 60 min incubation, the cells were washed and mounted in Mowiol 4-88, supplemented with 1 μg/ml Hoechst 33258 to label nuclei. Samples were examined with a confocal laser scanning microscope Leica TCS SP5 equipped with an X63/1.4.N.A. oil-immersion objective. STIM1-YFP (kind gift of Dr. T. Meyer, Stanford University Medical School) was used as an endoplasmic reticulum marker. Golgi marker (YFP-GT) was from Clontech Laboratories. ORMDL3-YFP was cloned into the N1-YFP plasmid (Clontech) using forward primer 5′-AAACTCGAGGCCGCCACCATGAATGTG GGCACAGCAC-3′ and reverse complementary primer 5′-AAAGAATTCGGTACTTATTGATTCCAAAG-3′, introducing *XhoI* and *EcoRI* restriction endonuclease sites (underlined), respectively. Amaxa Nucleofector II (Lonza Cologne AG, Cologne, Germany) was used to nucleofect mast cells using a Mouse Macrophage Kit and program Y-001.

Image analysis

Image processing and analysis were performed using CellProfiler software (Broad Institute, Boston, MA) [39]. For cell spreading, areas corresponding to individual cells were identified by F-actin staining with Alexa Fluor 488-phalloidin and the mean values were calculated from 200 to 400 cells in each sample. The fraction of NF-κB p65 subunit in the nucleus was determined as the difference between NF-κB mean fluorescence in the nucleus (stained with Hoechst 332578) and NF-κB mean fluorescence in the cytoplasm as described [40]. Fifty to hundred cells were evaluated per sample and the values obtained for each cell were plotted in GraphPad Prism (San Diego, CA, USA). Other charts were done in SigmaPlot 8.0 (San Jose, CA, USA).

Short interfering RNA (siRNA)-mediated inhibition of ORMDL3 expression and measurements of PCA

To silence ORMDL3 in the mouse ear, we followed the experimental procedure described by Kanada et al. [41] with some modifications. The specificity of ORMDL3 siRNAs was first confirmed by immunoblotting analysis of lysates from BMMCs nucleofected by Amaxa Nucleofector II 48 h earlier with 1 μg of ORMDL3 siRNA pool (Accell Mouse Ormdl3 siRNA; E-049023-00-0005; Dharmacon) or 1 μg control siRNAs ORMDL3 (O3_siRNA; Accell Non-targeting Pool; D-001910-10-05; Dharmacon) using a Mouse Macrophage Kit and program Y-001 as recommended by the manufacturer (Lonza). For PCA, 20 μL of PBS containing 4 μg/ml of anti-TNP-specific IgE and 2.5 μg of ORMDL3 siRNAs pool was injected into the right ear. As a control, 20 μL of anti-TNP-specific IgE (4 μg/ml) and 2.5 μg of control siRNA was injected intradermally into the left ear. After 48 h, the mice were challenged with an intravenously injected PBS (200 μl) containing Ag (100 μg TNP–BSA) and 1 mg of Evans blue. Two hours later, the mice were killed and the ears removed for measurement of the amount of extravasated dye. Formamide (0.75 ml) was then added to each ear, which was then homogenized with the T-25 ULTRA-TURRAX Digital High-Speed Homogenizer Systems (IKA) and incubated at 80^{O}C for 2 h. The samples were centrifuged at 14,000×*g* for 15 min and supernatants were used for measurement of absorbance at 620 nm.

Statistical analyses

Unless stated otherwise, the significance of intergroup differences was evaluated by Student's *t* test; *, $P < 0.05$; **, $P < 0.01$; ***, $P < 0.001$. Microsoft Excel 2010 or GraphPad Prism was used for statistical analysis evaluation.

Results

Properties of BMMCs with reduced or enhanced expression of ORMDL3

Although ORMDL3 expression was described in various cells of the immune system [1, 18], its presence in mast cells has not yet been determined. Here, we used RT-PCR to show the expression of ORMDL3 in BMMCs. We found

that ORMDL3 as well as ORMDL1 and ORMDL2 are expressed in BMMCs (Fig. 1a). We did not observe any variations in the expression of ORMDL3 during BMMC cultivation in medium supplemented with IL-3 and SCF (data not shown). Using BMMCs transduced with markers of endoplasmic reticulum or Golgi apparatus, we confirmed previous findings [16, 18] that endogenous ORMDL proteins detected by the NVG antibody recognizing all three ORMDLs (Fig. S1a, c, d) are associated with the endoplasmic reticulum and perinuclear membrane, but not with the Golgi apparatus (Fig. 1b). Next, we examined whether the changes in ORMDL3 expression influence mast cell effector functions. To induce ORMDL3 knockdown (O3_KD), BMMCs were transduced using the pLKO.1 lentiviral vector with ORMDL3 shRNAs (200, 201, 202, and 203, Fig. 1c). As controls, BMMCs were transduced with the empty pLKO.1 vector. Quantification of ORMDL3 mRNA expression by RT-qPCR showed its 30–80 % decrease after transduction of ORMDL3 shRNAs (Fig. 1c). To find out whether silencing of ORMDL3 is accompanied by changes in expression of other ORMDL family members, we assessed the expression of all members of the ORMDL family in BMMCs with O3_KD. Data in Fig. 1d indicate that silencing with the O3_KD vector (shRNA 200) led to a significant reduction of ORMDL3 mRNA without any effect on the expression of ORMDL1 and ORMDL2 mRNA. For production of cells with enhanced expression of ORMDL3, we used pCDH vectors containing ORMDL3 cDNA tagged with myc at the N terminus (myc-O3) or C terminus (O3-myc). Cells transduced with ORMDL3 cDNAs exhibited an 8- to 12-fold increase in ORMDL3 mRNA when compared with cells transduced with the empty pCDH vector, but expression of ORMDL1 and ORMDL2 mRNAs was not significantly changed (Fig. 1e). It should be noted that orientation of the tag attached to ORMDL3 influenced the mobility of the proteins in the gel ([11]; Fig. 1f). However, because in functional assays we did not see any significant differences between cells transduced with the two constructs, the data obtained with both of them were pooled and are presented as cells with ORMDL3 overexpressors (O3_OE). The observed downregulation or upregulation of ORMDL3 mRNA in cells with O3_KD or O3_OE, respectively, resulted in the expected changes in the intensity of the band corresponding to the ORMDL family proteins as detected by immunoblotting with polyclonal serum. The amount of the band corresponding to the ORMDL proteins was reduced by 60–80 % depending on the shRNA used (Fig. 1f). The characteristics of the rabbit serum used for immunoblotting (TPF) are shown in Fig. S1b, c. Both sera (NVG and TPF) recognize other members of the ORMDL family, as determined by their reactivity with cells expressing cDNAs encoding ORMDL1 and ORMDL2 (Fig. S1c). Therefore, we refer to the corresponding band of 17 kDa as ORMDL. In BMMCs transfected with myc-O3 or O3-myc vectors, ORMDL3 protein was enhanced approximately three to fourfold (Fig. 1f), although the increase of ORMDL3 expression at the mRNA level was more prominent (Fig. 1e). BMMCs with both O3_KD (all four shRNAs) and O3_OE (myc-O3 or O3-myc vectors) had preserved expression of FcεRI and KIT receptors on the plasma membrane (Fig. S2), but statistical evaluation revealed that shRNAs 201 and 202 exhibited significant changes in the expression of c-Kit ($P < 0.05$) and shRNA 201 as well as in FcεRI expression (Fig. 1g; $P < 0.05$). Based on these results, we excluded shRNAs 201 and 202 from further work. All experiments with O3_KD are based on shRNA 200. Cells transduced with shRNA 203 exhibited similar properties to those with shRNA 200. Based on these findings, experimental data were pooled and all data are presented as O3_KD. Alcian blue staining of cytospin slides showed that the morphology of O3_KD and O3_OE mast cells was not different from that of cells transduced with appropriate controls (see examples in Fig. 1h).

Ag activation of BMMCs induces downregulation of ORMDL3

A previous study showed that challenge with allergen induced expression of ORMDL3 in mouse bronchial epithelial cells, lung macrophages, or BM-derived eosinophils, but not in peripheral blood neutrophils [18]. Moreover, increased ORMDL3 expression in bronchial airway epithelial cells was stimulated with IL-4 and IL-13 [18] and in eosinophils triggered with IL-3 and eotaxin-1 [20]. In further experiments, we therefore examined whether FcεRI activation of BMMCs would also lead to changes in ORMDL3 expression. Interestingly, in IgE-sensitized cells, activation with Ag resulted in a significant decrease of ORMDL3 mRNA expression 1, 4, and 6 h after FcεRI triggering, but ORMDL1 and ORMDL2 mRNA expression was not significantly affected (Fig. 2a). At the protein level, for detection we used polyclonal antibodies recognizing all members of the ORMDL family (Fig. S1a–c). Data presented in Fig. 2b and c indicate that there is a slight, but significant decrease in ORMDL family member expression in cells activated for 8–24 h with Ag. Attenuation of ORMDL3 transcription in activated cells was also observed in cells with O3_KD, in which the residual amount of ORMDL3 mRNA was further lowered (Fig. 2d). Thus, FcεRI-activated mast cells exhibit downregulation of ORMDL3 and in this regard differ from activated eosinophils, lung macrophages, and bronchial airway epithelial cells.

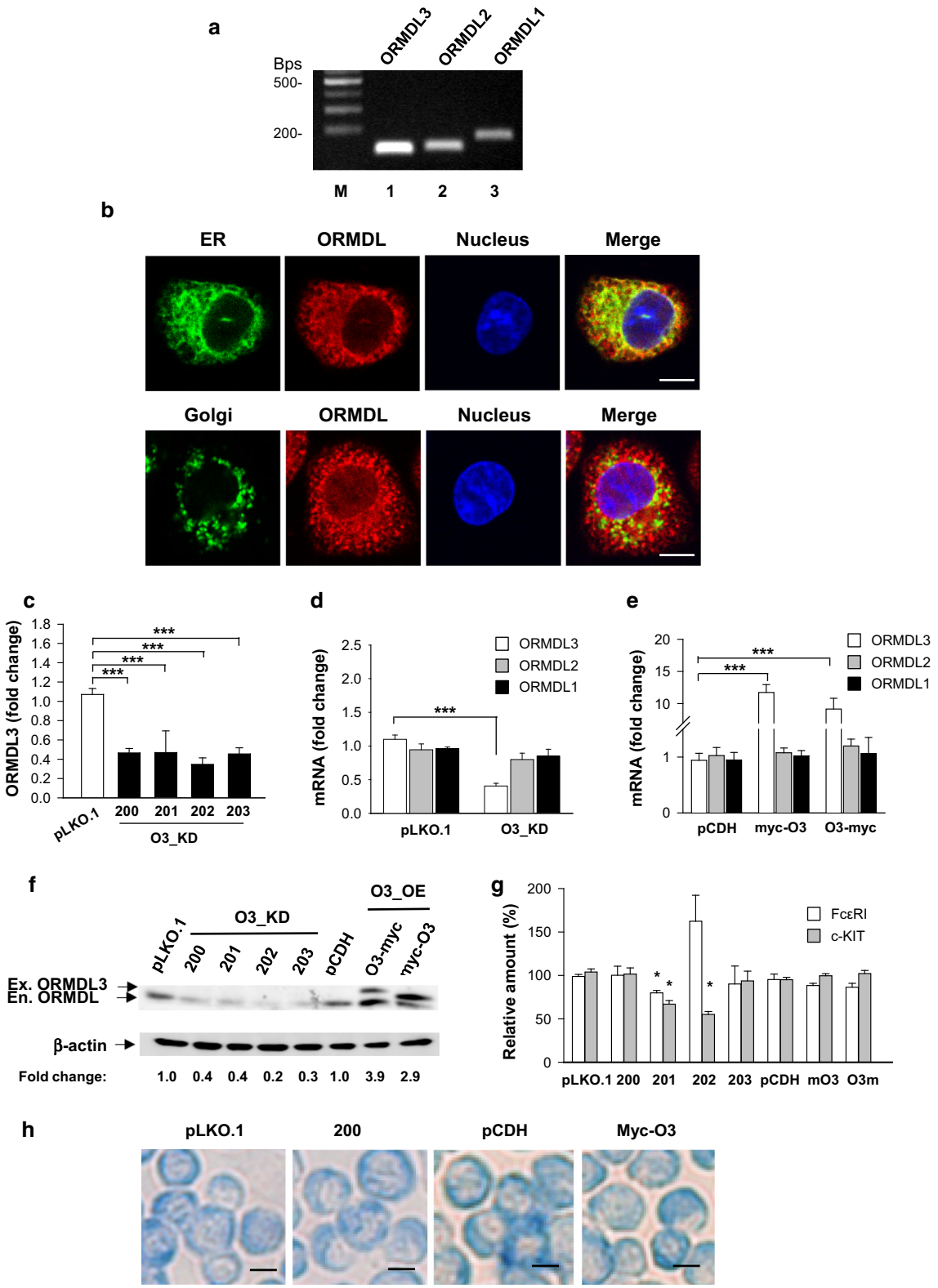
a
ORMDL3
ORMDL2
ORMDL1
Bps
500-
200-
M
1
2
3
b
ER
ORMDL
Nucleus
Merge
Golgi
ORMDL
Nucleus
Merge
c
ORMDL3 (fold change)
***
pLKO.1
200
201
202
203
O3_KD
d
mRNA (fold change)
ORMDL3
ORMDL2
ORMDL1
***
pLKO.1
O3_KD
e
mRNA (fold change)
ORMDL3
ORMDL2
ORMDL1
***
pCDH
myc-O3
O3-myc
f
O3_KD
O3_OE
pLKO.1
200
201
202
203
pCDH
O3-myc
myc-O3
Ex. ORMDL3
En. ORMDL
β-actin
Fold change:
1.0 0.4 0.4 0.2 0.3 1.0 3.9 2.9
g
Relative amount (%)
FcεRI
c-KIT
pLKO.1 200 201 202 203 pCDH mO3 O3m
h
pLKO.1
200
pCDH
Myc-O3

◀**Fig. 1** Properties of BMMCs with reduced or enhanced ORMDL3 expression. **a** Expression of ORMDL1-3 mRNAs in BMMCs as determined by RT-PCR followed by agarose gel electrophoresis and staining with ethidium bromide. DNA marker in bps is shown in *line M*. **b** Colocalization of endogenous ORMDL proteins (shown in *red pseudocolor*) with STIM1-YFP, a marker of endoplasmic reticulum (ER *upper panel*; green pseudocolor), but not with GT-YFP, a marker of Golgi (*lower panel* green pseudocolor) is shown. Nuclei were stained with Hoechst 33258 (shown in blue pseudocolor); *bars* 5 μm. **c** BMMCs with O3_KD were obtained after transduction with lentiviruses containing four shRNAs denoted 200, 201, 202, and 203. Control cells were transduced with empty pLKO.1 vector. ORMDL3 mRNAs were quantified by RT-qPCR. **d** RT-qPCR quantification of individual ORMDL family members in cells with O3_KD or in control cells transduced with empty pLKO.1 vector. **e** BMMCs with O3_OE were obtained after transduction with lentiviruses containing ORMDL3 cDNAs terminally tagged with myc at the N-(myc-O3) or C-(O3-myc) end. Control cells were transduced with empty pCDH vector. The levels of ORMDL1 and ORMDL2 mRNAs are shown. RT-qPCR data in **c**–**e** were normalized as described in "Materials and methods" and represent the means and SEMs calculated from three to seven independent experiments. **f** Quantification of ORMDL proteins (serum not specific for ORMDL3) by immunoblotting in whole-cell lysates after transduction of the cells as in **c** and **e**. *Numbers* under the immunoblots indicate the amounts of ORMDL proteins normalized to control cells transfected with pLKO.1 vector (for O3_KD) or pCDH vector (for O3_OE) and to the amount of β-actin used as a loading control (fold change). The positions of endogenous (En.) and exogenous (Ex.) ORMDL3 and β-actin are indicated by *arrows*. **g** Statistical evaluation of FcεRI and c-Kit expression in the transduced BMMCs. **h** Alcian blue staining of cytospin preparations of BMMCs transduced as above; *bars* 10 μm

BMMCs with reduced or enhanced expression of ORMDL3 do not exhibit changes in SYK tyrosine phosphorylation, degranulation, and Ca^{2+} response after FcεRI triggering

FcεRI-mediated signaling events are initiated by tyrosine phosphorylation of the FcεRI β and γ subunits by Src family kinase LYN, followed by propagation of the signal through activity of the Src family kinases and SYK kinase [22]. To examine a possible role of ORMDL3 in FcεRI signaling, we first examined phosphorylation of SYK in Ag-activated BMMCs with reduced or enhanced ORMDL3 expression. Our data indicate that cells with O3_KD (Fig. 3a) or O3_OE (Fig. 3b) show similar SYK phosphorylation as the corresponding controls.

Next, we examined Ag-induced degranulation estimated by the release of β-glucuronidase from preformed secretory lysosomes. We found that BMMCs with O3_KD (Fig. 3c) or O3_OE (Fig. 3d) exhibited similar degranulation as the control cells. We also compared cells transduced with pLKO.1 and nontransduced wild-type (WT) cells to show that mast cell degranulation is not changed by lentivirus transduction (Fig. S3a).

Previous studies have shown that ORMDL3 affects Ca^{2+} mobilization in lymphocytes and eosinophils [16, 17, 20] and regulates the expression of sarco/endoplasmic reticulum Ca^{2+} ATPase (SERCA)2b [19]. Interestingly, BMMCs with O3_KD (Fig. 3e) or O3_OE (Fig. 3f) exhibited similar Ca^{2+} mobilization to cells transduced with empty pLKO.1 or pCDH vectors. We also compared cells transduced with pLKO.1 and WT cells to show that calcium mobilization in mast cells is not changed by lentivirus transduction (Fig. S3b). We also found that expression of mRNA for SERCA2b was not significantly changed in activated and nonactivated mast cells with O3_KD (Fig. 3g) or O3_OE (Fig. 3h) when compared with the corresponding controls. The mRNA levels of SERCA2b in cells transduced with pLKO.1 were comparable to those in WT cells (Fig. S3c). In line with the SERCA2b expression, the basal levels of $[Ca^{2+}]_i$ were not changed in O3_KD (Fig. S4a) or O3_OE (Fig. S4b) when compared with the corresponding controls. We conclude that early FcεRI-induced activation events, including SYK tyrosine phosphorylation, degranulation, and calcium responses in mast cells, are not affected by enhanced or reduced expression of ORMDL3. Furthermore, we show that changes in ORMDL3 protein levels have no significant effect on SERCA2b expression.

Negative regulatory role of ORMDL3 in the expression of cytokines and chemokines

Mast cells are potent producers of various cytokines and chemokines involved in both asthma and autoimmune diseases [22, 23, 42, 43]. In further experiments, we therefore quantified the levels of mRNA encoding cytokines (TNF-α, IL-6, and IL-13; Fig. 4a) and chemokines (CCL3 and CCL4; Fig. 4b) in BMMCs with O3_KD. Using RT-qPCR, we found that all the studied transcripts for cytokines and chemokines were significantly increased in cells with O3_KD when compared with control cells transduced with empty pLKO.1 vector in both nonactivated and Ag-activated cells (Fig. 4a, b). The observed increase in cytokine mRNA levels corresponded to enhanced secretion of the cytokines TNF-α, IL-6 and IL-13 from Ag-activated BMMCs with O3_KD (Fig. 4c). In contrast, no significant changes in the transcription of TNF-α, IL-6, and IL-13 at the RNA (not shown) or protein (Fig. 4d) level were observed when BMMCs with O3_OE were compared with the corresponding controls. These data indicate that ORMDL3 in mast cells is a negative regulator of the production of proinflammatory cytokines such as TNF-α, IL-6, and IL-13 and chemokines CCL3 and CCL4.

ORMDL3 functions as a negative regulator of Ag-mediated chemotaxis

The observed changes in the expression of genes for cytokines and chemokines depending on the expression of

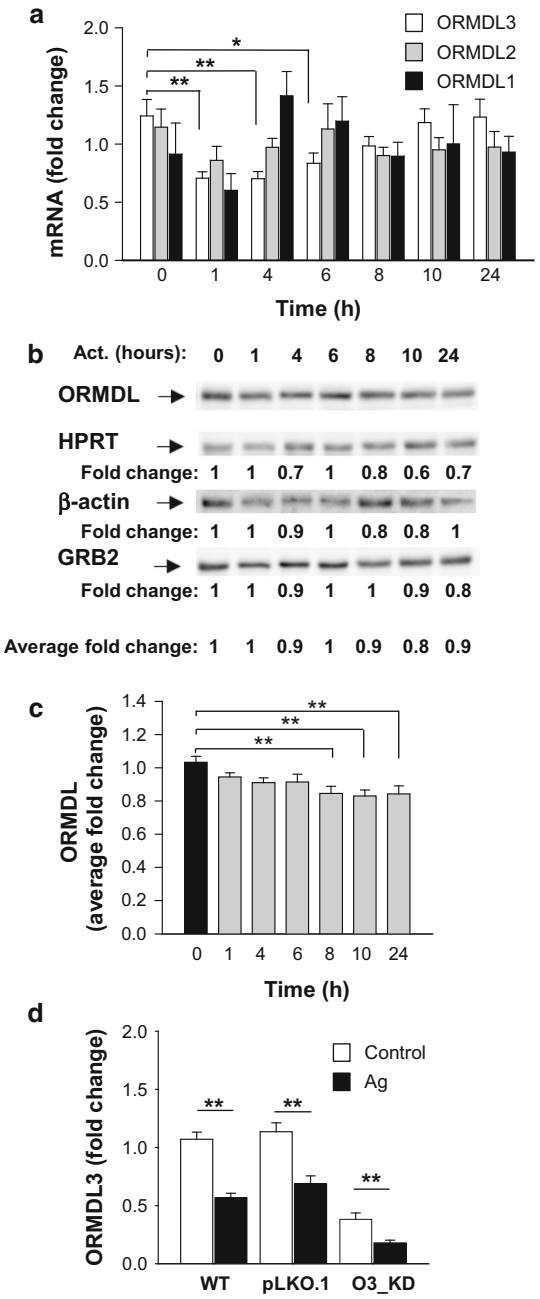

Fig. 2 Changes in ORMDL3 expression in Ag-activated BMMCs. ▶ **a** BMMCs were sensitized for 16 h with IgE and then activated with Ag (100 ng/ml) or not (0 h) for the indicated time intervals. ORMDL3, ORMDL2, and ORMDL1 mRNAs were quantified by RT-qPCR and normalized as described in "Materials and methods". The means and SEMs were calculated from three independent experiments performed in duplicate. **b** Immunoblot quantification of ORMDL proteins at various time intervals after activation of IgE-sensitized BMMCs with Ag (100 ng/ml). *Numbers* under the immunoblots indicate the relative amounts of ORMDL3 normalized to its amount in nonactivated cells and the amounts of HPRT, β-actin, and GRB2 were used as loading controls (Average fold change). A representative immunoblot from seven independent experiments with similar results is shown. **c** Statistical evaluation of ORMDL proteins expression is shown. ORMDL3 was normalized to its amount in nonactivated cells and the amount of the average fold change of three loading controls mentioned above. **d** RT-qPCR quantification of ORMDL3 in nonactivated (control) or Ag-activated (100 ng/ml; 1 h) BMMCs with the empty vector (pLKO.1) or O3_KD. Data are normalized as in **a**. The means and SEMs were calculated from six independent experiments performed in duplicate

ORMDL3 led us to examine the capability of IgE-sensitized cells to migrate toward Ag and to adhere and spread on fibronectin-coated substrates. BMMCs with O3_KD exhibited a significantly stronger chemotactic response to all tested concentrations of Ag when compared with control cells transfected with empty pLKO.1 vector (Fig. 5a). In contrast, BMMCs with O3_OE showed a less efficient chemotactic response than the corresponding control cells (Fig. 5b). We also compared cells transduced with pLKO.1 and WT cells to show that mast cell migration is not changed by lentivirus transduction (Fig. S3d). When adhesion to fibronectin was measured, cells with O3_KD (Fig. S5a) or O3_OE (Fig. S5b) exhibited adhesion similar to the corresponding control cells. In contrast, spreading on fibronectin-coated surfaces after exposure to Ag was reduced in cells with O3_KD (Fig. 5c, d). When compared to control cells, cells with O3_OE exhibited no significant difference in Ag-induced spreading (Fig. 5e, f). We also compared cells transduced with pLKO.1 and WT cells and showed that Ag-induced mast cells adhesion to and spreading on fibronectin was not changed by lentivirus transduction (Fig. S3e, f). Finally, we examined the depolymerization of F-actin in Ag-activated cells with O3_KD (Fig. S5c) or O3_OE (Fig. S5d) and corresponding controls and found that F-actin content was independent of ORMDL3 expression levels.

Upregulation of NF-κB signaling axis in mast cells with O3_KD

Previous studies with eosinophils showed that increased expression of ORMDL3 enhanced translocation of NF-κB into the nucleus and its activation [20]. Based on our findings that reduced expression of ORMDL3 upregulated the expression of cytokine and chemokine genes (Fig. 4a–d) and that these mediators were directed by transcription factor NF-κB [44–48], we decided to analyze the NF-κB signaling axis in BMMCs with enhanced or decreased ORMDL3 protein levels. First, we examined the phosphorylation of IκBα, a negative regulator of NF-κB signaling. We found that 5 min after Ag activation, BMMCs with O3_KD exhibited higher phosphorylation of IκBα than control pLKO.1 cells. Interestingly, we found that IκBα in activated BMMCs with O3_KD is more degraded than in control cells (Fig. 6a). This is in accord with the previously described observation that phosphorylation of IκBα triggers its degradation [49]. Densitometry evaluation of the data and normalization of pIκBα to LYN

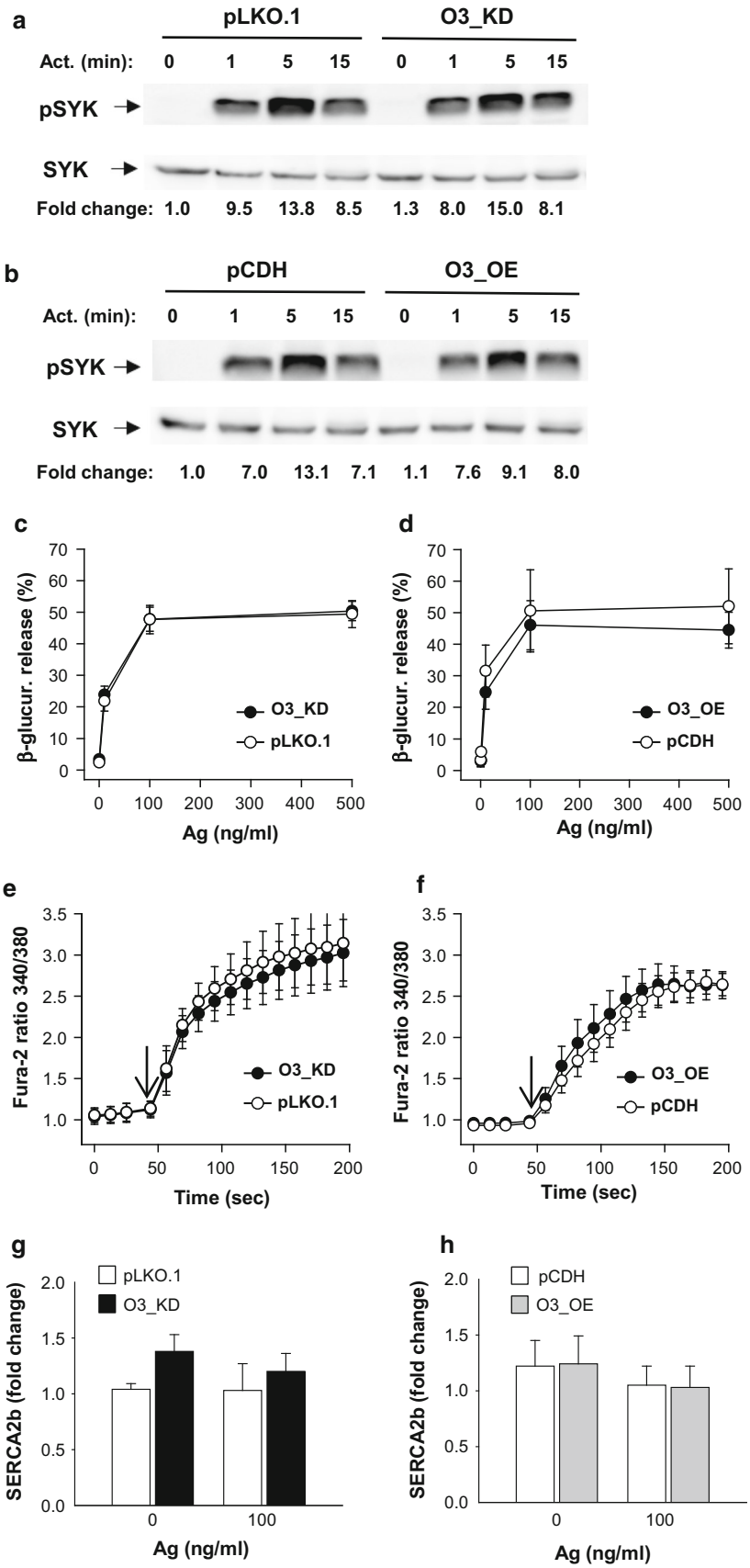

Fig. 3 Early activation events in BMMCs with enhanced or reduced ORMDL3 expression. **a** Ag-induced tyrosine phosphorylation of SYK as determined by immunoblotting of whole-cell lysates from BMMCs with O3_KD or control cells transfected with empty pLKO.1. IgE-sensitized cells were activated for various time intervals with Ag (100 ng/ml). The positions of pSYK and SYK, used as loading controls, are indicated by *arrows*. **b** Phosphorylation of SYK was examined as in **a**, except that the lysates were from cells with O3_OE or control cells transfected with empty pCDH. Representative immunoblots from at least three performed in each group are shown in **a** and **b**. Numbers under the immunoblots indicate the relative amounts of pSYK normalized to its amounts in nonactivated cells transduced with empty vectors and total amounts of SYK in individual samples (fold change). **c**, **d** β-Glucuronidase release in IgE-sensitized BMMCs. The cells were activated with various concentrations of Ag and after 30 min β-glucuronidase released into the supernatant was determined. Data presented are means and SEMs for cells with O3_KD (**c**, $n = 19$), pLKO.1 controls (**c**, $n = 19$), O3_OE (**d**, $n = 8$), and pCDH control cells (**d**, $n = 5$). **e**, **f** Calcium response in IgE-sensitized BMMCs activated with Ag (100 ng/ml) for various time intervals. *Arrows* show the time points when Ag was added. Means and SEMs were calculated for cells with O3_KD (**e**, $n = 16$), pLKO.1 controls (**e**, $n = 8$), O3_OE (**f**, $n = 3$), and pCDH controls (**f**, $n = 5$). **g**, **h** RT-qPCR quantification of SERCA2b mRNA in resting and activated BMMCs with O3_KD (**g**, $n = 4$) pLKO.1 controls (**g**, $n = 4$), O3_OE (**h**, $n = 4$) and pCDH controls (**h**, $n = 4$). Data for SERCA2b mRNA were normalized as described in "Materials and methods"

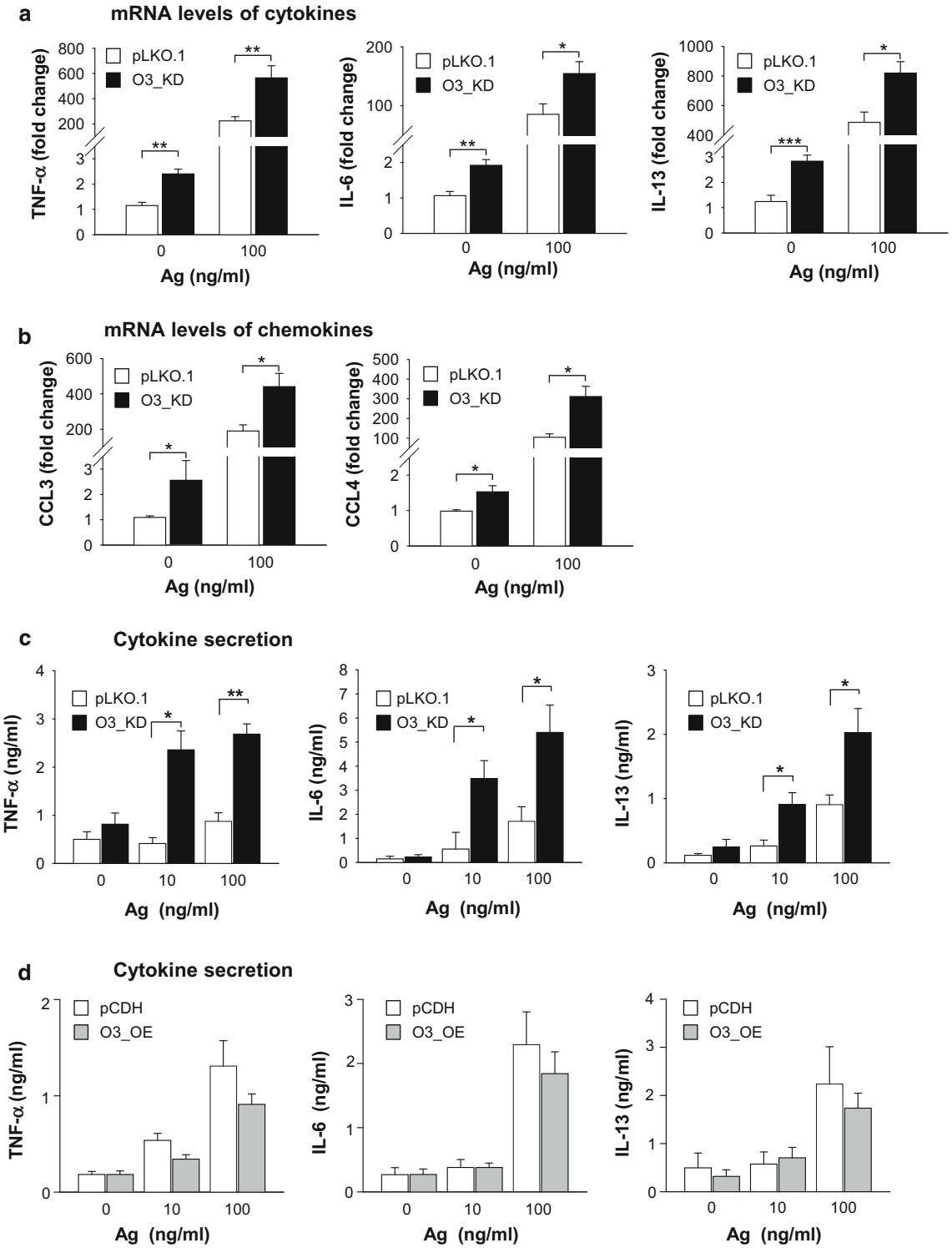

Fig. 4 Expression of cytokine and chemokine genes and production of cytokines in BMMCs with O3_KD and O3_OE. **a** RT-qPCR quantification of mRNAs encoding TNF-α, IL-6, and IL-13 in nonactivated or Ag-activated (100 ng/ml; 1 h) BMMCs with O3_KD and the corresponding control cells, pLKO.1. Means and SEMs were calculated from 13 to 16 independent experiments. **b** RT-qPCR quantification of mRNA for CCL3 and CCL4 chemokines from cells as in **a**. The means and SEMs were calculated from six to eight experiments. Data in **a** and **b** were normalized as described in "Materials and methods". **c**, **d** Quantification of cytokines TNF-α, IL-6, and IL-13 secreted into the supernatants of nonactivated or Ag-activated (100 ng/ml; 6 h) BMMCs with O3_KD or pLKO.1 control (**c**) and O3_OE or pCDH control (**d**) as determined by nano-iPCR. The means and SEMs were calculated from four to five independent experiments

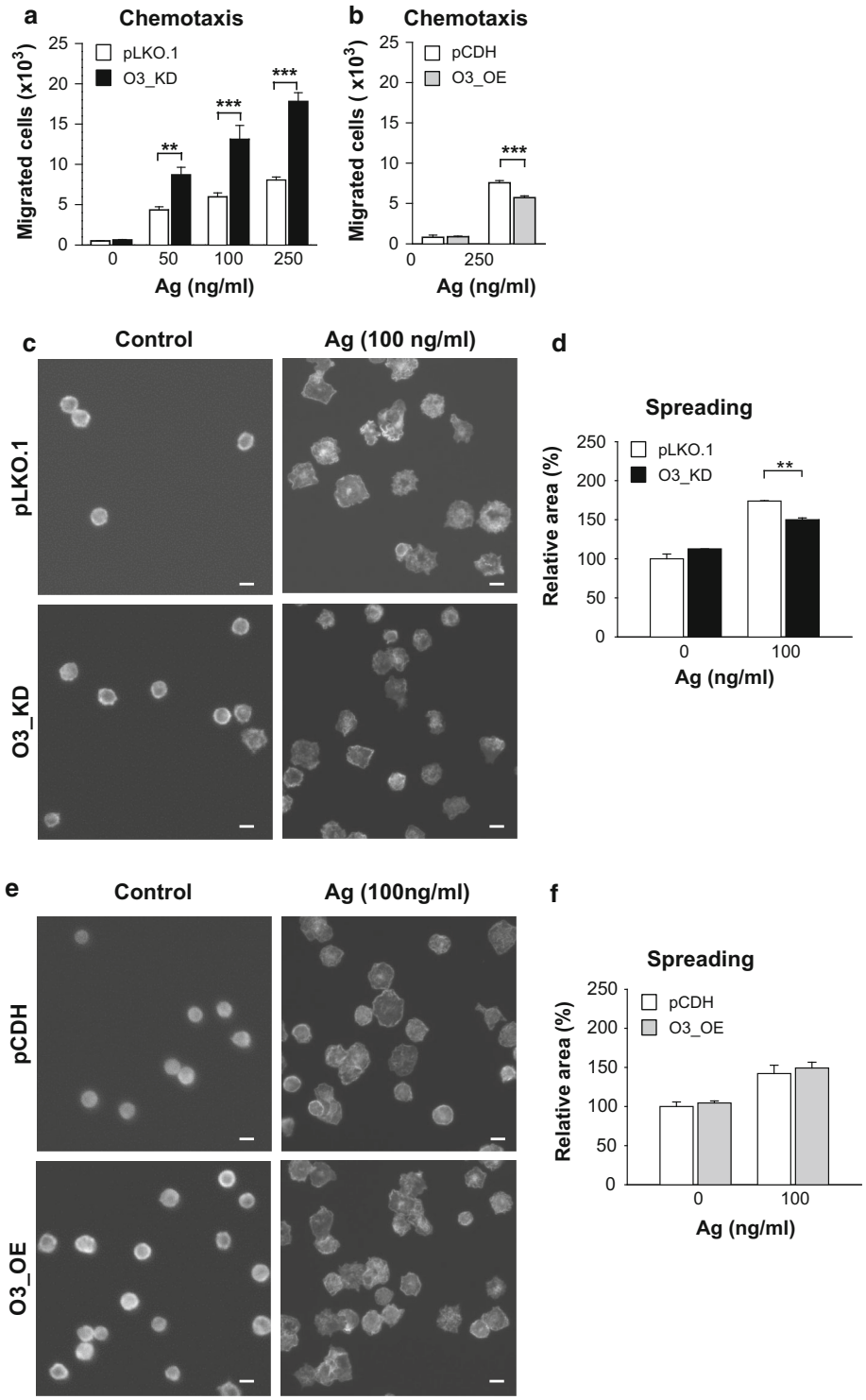

Fig. 5 Negative regulatory role of ORMDL3 in Ag-mediated chemotaxis, but not cell spreading on fibronectin. **a**, **b** Migration of BMMCs toward various concentrations of Ag was determined in IgE-sensitized BMMCs with O3_KD (**a**) or O3_OE (**b**) and the corresponding controls. The means and SEMs were calculated from four to eight independent experiments performed in duplicate. **c**–**f** Spreading of BMMCs with O3_KD (**c**, **d**), O3_OE (**e**, **f**), and the corresponding controls. The cells were attached to fibronectin-coated slides and activated with Ag (100 ng/ml) for 30 min. Representative fluorescent images are shown in **c** and **e**; *bars* 10 μm. Quantification and statistical evaluation of data obtained as in **c** and **e** are shown in **d** and **f**, respectively. The means and SEMs were calculated from five independent experiments

kinase, used as a loading control, showed significantly higher IκBα phosphorylation in O3_KD cells than control pLKO.1 cells (Fig. 6b). BMMCs with O3_OE showed a small, but nonsignificant decrease of IκBα phosphorylation (not shown). Based on these data, we next examined the consequences of reduced ORMDL3 levels on translocation of the NF-κB p65 subunit into the nucleus in BMMCs. We found that Ag-induced translocation of the p65 subunit into the nucleus was higher in BMMCs with O3_KD than in control cells (Fig. 6c). The difference was statistically significant (Fig. 6d). Interestingly, resting BMMCs with O3_KD also exhibited increased p65 nuclear localization

when compared with resting control pLKO.1 cells. These data are consistent with the findings that basal levels of mRNAs for cytokines (Fig. 4a) and chemokines (Fig. 4b) were higher in cells with O3_KD than in control cells. We also compared cells transduced with pLKO.1 and WT cells and found that p65 nuclear localization after activation was not changed by lentivirus transduction (Fig. S3g).

To determine which signaling pathways are involved in enhanced IκBα phosphorylation we examined phosphorylation of ERK kinase, which is involved in IκBα phosphorylation [50]. We found that mast cells with decreased expression of ORMDL3 exhibited similar ERK phosphorylation as pLKO.1 control cells (Fig. 6e, f). Next, we therefore tested phosphorylation of AKT kinase, which is a positive regulator of NF-κB signaling [51]. Interestingly, BMMCs with O3_KD exhibited significantly enhanced phosphorylation of AKT at Ser 473 at all examined time points, but phosphorylation of AKT at Thr 308 was not significantly affected (Fig. 6g–i). To exclude the possibility that the observed immunological responses are not specifically activated by siRNA [52], we compared the phosphorylation of IκBα and AKT (at Ser 473) in WT cells, BMMCs transduced with empty pLKO.1, or cells transduced with NT shRNA (Fig. S6a). We found that cells with O3_KD showed enhanced responses when compared with all controls. We also used the same controls in experiments with cytokines to demonstrate that lentiviral transduction had no impact on cytokine production and that cytokines were specifically increased by O3_KD (Fig. S6b–d). Collectively, these data demonstrate that decreased expression of ORMDL3 is accompanied in Ag-activated cells by enhanced phosphorylation of AKT, increased translocation of the p65 subunit into the nucleus, and enhanced production of cytokines.

ORMDL3 is a negative regulator of COX-2 expression and PGD2 synthesis

We also examined the expression of an inducible enzyme, COX-2, which is regulated by NF-κB [53, 54]. COX-2 converts arachidonic acid to PGH2, a precursor of PGD2 and PGE2 [28]. When compared with control cells (pLKO.1), BMMCs with O3_KD exhibited significantly higher levels of COX-2 mRNA than both resting and Ag-activated control cells (Fig. 7a), while cells with O3_OE showed decreased COX-2 mRNA expression when compared with the control cells (pCDH); however, the difference was not significant (Fig. 7b). These data were corroborated by studies of the COX-2 protein in Ag-activated BMMCs. After 5 h stimulation with Ag, we observed a higher increase of COX-2 levels in cells with O3_KD than in control cells (Fig. 7c); this difference was

Fig. 6 Negative regulatory role of ORMDL3 in AKT and NF-κB signaling axis in Ag-activated BMMCs. **a** Phosphorylation of IκBα and its amount was determined by immunoblotting of whole-cell lysates from BMMCs with O3_KD and control cells (pLKO.1) with the corresponding antibodies. Representative immunoblots from four independent experiments areshown. Numbers under the immunoblots indicate the relative amounts of pIκBα and IκBα normalized to their amounts in nonactivated pLKO.1 control cells and the amount of Lyn used as a loading control (Fold change). **b** Quantification and statistical evaluation of pIκBα in pLKO.1 control cells and O3_KD cells activated with Ag for 5 min as in **a**. Means and SEMs were calculated from four independent experiments. **c** Representative confocal microscopy pictures of NF-κB p65 subunit (p65) localization in the nuclei (stained with Hoechst 33258) and cytoplasm in nonactivated or Ag-activated (100 ng/ml; 30 min) BMMCs with O3_KD or pLKO.1 control; *bars* 10 μm. **d** Quantification of NF-κB p65 subunit localization in the nucleus of nonactivated or Ag-activated (100 ng/ml, 30 min) O3_KD and pLKO.1 control cells. *Values* from two independent experiments as in **c** (50–100 cells per experiment) were plotted; each *symbol* represents one cell, *red horizontal lines* indicate means. **e–i** Phosphorylation of ERK at Tyr 204 (**e**, **f**), AKT at Ser 473 (**g**, **h**), and AKT at Thr 308 (**g**, **i**) was assessed by immunoblotting with the corresponding antibodies of the whole-cell lysates from BMMCs with O3_KD or pLKO.1 controls. Representative immunoblots from at least three in each group are shown in **e** and **g**. Numbers under the immunoblots indicate the relative amounts of pERK (**e**) or pAKT (**g**) normalized to their amounts in nonactivated pLKO.1 control cells and the amount of ERK or AKT used as loading controls (fold changes). Quantification and statistical analyses of differences in fold changes between cells with O3_KD and pLKO.1 controls in $pERK^{Y204}$ (**f**), $pAKT^{S473}$ (**h**), and $pAKT^{T308}$ (**i**) are also shown. Means and SEMs were calculated from three experiments in each group

significant ($P < 0.05$; $n = 3$). On the other hand, Ag-activated cells with O3_OE showed lower COX-2 levels than the corresponding control cells (Fig. 7d); however, this difference was not significant ($P > 0.05$; $n = 3$). The stronger band of exogenous ORMDL3-myc after 5 h of activation in Fig. 7d was reproducibly observed. Ag-induced activation apparently induces enhanced transcription from the CMV promoter. We found that this enhancement was not ORMDL3 specific, rather it depended on the CMV promoter, as several other ORMDL family nonrelated proteins cloned into the same pCDH vector exhibited a similar increase (data not shown).

Supernatants collected from the experiments as depicted in Fig. 7 c, d were assessed for PGD2 levels. We found that Ag-activated mast cells with O3_KD released significantly higher amounts of PGD2 than appropriate controls (Fig. 7e). Furthermore, PGD2 expression was not significantly changed in mast cells with O3_OE (Fig. 7f). To show that COX-2 expression is independent of immunological responses toward dsRNAs, we compared COX-2 production in cells with O3_KD and controls (NT and WT). We found that in O3_KD cells activated with Ag, the levels of COX2 were more elevated than in control cells (Fig. S6e). These data support the negative regulatory role of ORMDL3 in the activation of the NF-κB signaling axis.

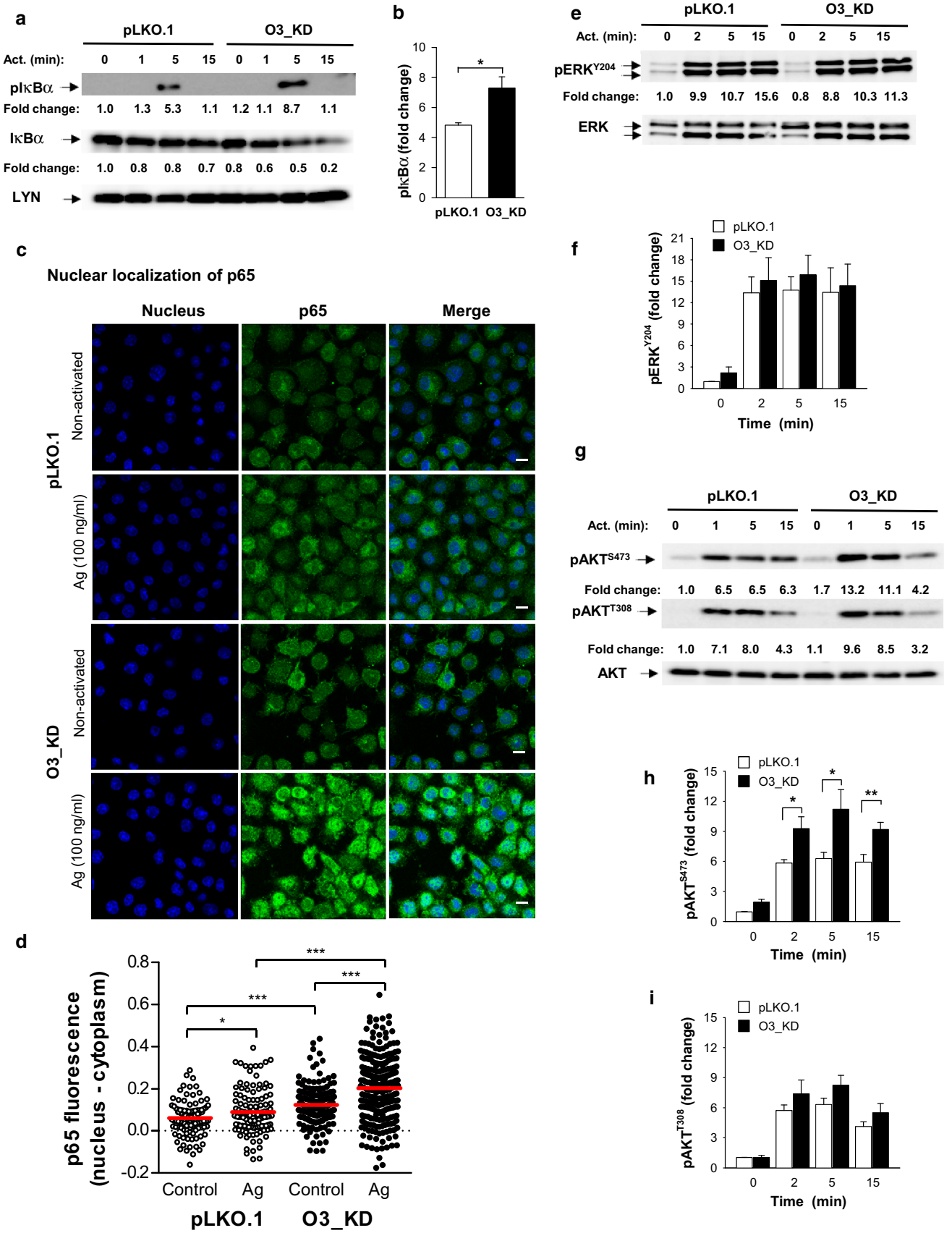
a
pLKO.1
O3_KD
Act. (min): 0 1 5 15 0 1 5 15
pIκBα
Fold change: 1.0 1.3 5.3 1.1 1.2 1.1 8.7 1.1
IκBα
Fold change: 1.0 0.8 0.8 0.7 0.8 0.6 0.5 0.2
LYN
b
pIκBα (fold change)
pLKO.1 O3_KD
e
pLKO.1
O3_KD
Act. (min): 0 2 5 15 0 2 5 15
pERK Y204
Fold change: 1.0 9.9 10.7 15.6 0.8 8.8 10.3 11.3
ERK
f
pLKO.1
O3_KD
pERK Y204 (fold change)
Time (min)
c
Nuclear localization of p65
Nucleus
p65
Merge
pLKO.1
Non-activated
Ag (100 ng/ml)
O3_KD
Non-activated
Ag (100 ng/ml)
g
pLKO.1
O3_KD
Act. (min): 0 1 5 15 0 1 5 15
pAKT S473
Fold change: 1.0 6.5 6.5 6.3 1.7 13.2 11.1 4.2
pAKT T308
Fold change: 1.0 7.1 8.0 4.3 1.1 9.6 8.5 3.2
AKT
h
pLKO.1
O3_KD
pAKT S473 (fold change)
Time (min)
d
p65 fluorescence (nucleus - cytoplasm)
Control Ag Control Ag
pLKO.1 O3_KD
i
pLKO.1
O3_KD
pAKT T308 (fold change)
Time (min)

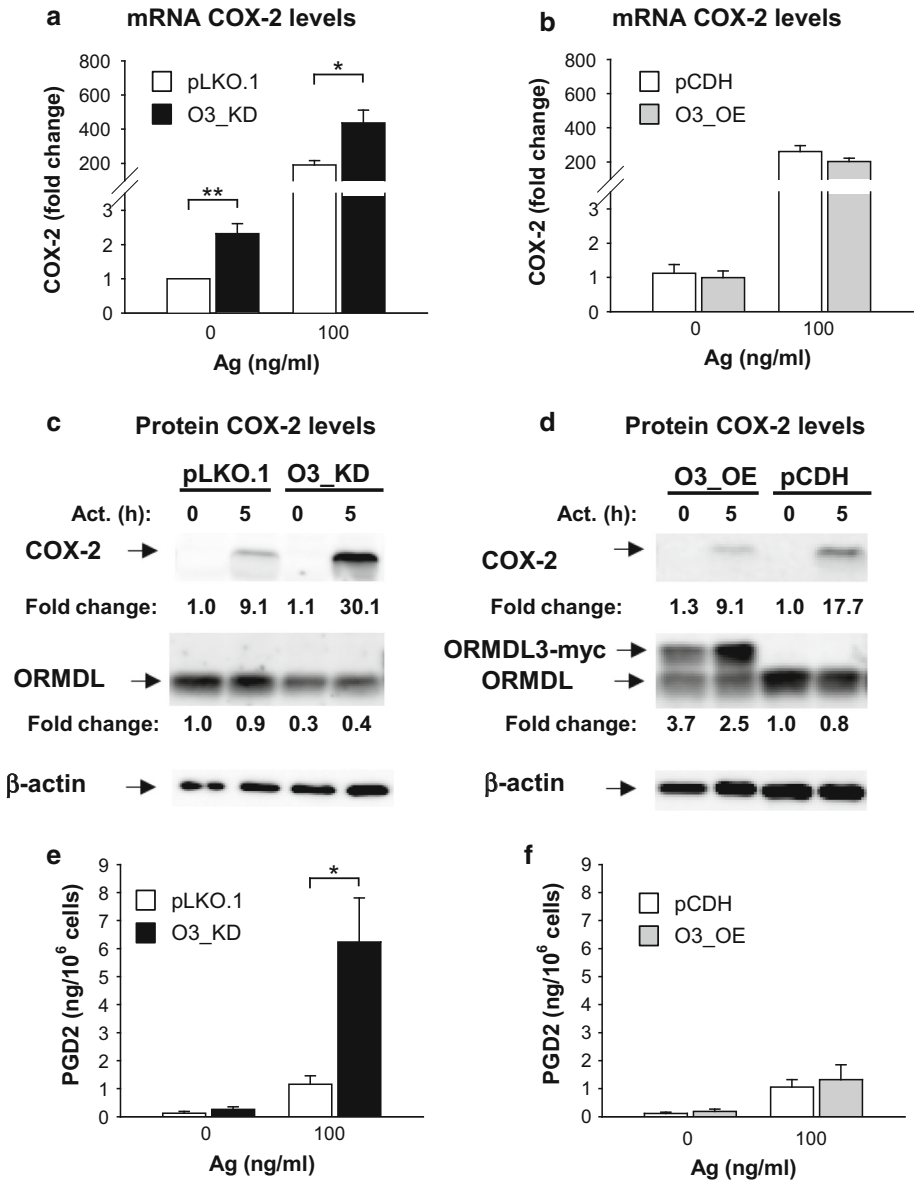

Fig. 7 Increased COX-2 expression and PGD2 synthesis in nonactivated or Ag-activated BMMCs with O3_KD. **a, b** RT-qPCR quantification of COX-2 mRNAs in nonactivated or Ag-activated (100 ng/ml; 1 h) BMMCs with O3_KD (**a**), O3_OE (**b**), and the corresponding controls, pLKO.1 (**a**) and pCDH (**b**). The means and SEMs were calculated from five independent experiments. **c**, **d** Amount of COX-2 protein in nonactivated or Ag-activated (100 ng/ml; 5 h) BMMCs with O3_KD (**c**), O3_OE (**d**), and the corresponding controls, pLKO.1 (**c**) and pCDH (**d**). Numbers under the COX-2 immunoblots indicate the relative amount of COX-2 normalized to its levels in nonactivated control cells and to the amount of β-actin, used as a loading control, in individual samples (fold change). Levels of ORMDL3 normalized as above are also shown. Representative immunoblots from three independent experiments are shown. **e**, **f** Levels of PGD2 released into supernatants of nonactivated or Ag-activated (100 ng/ml; 5 h) BMMCs with O3_KD (**e**), O3_OE (**f**), and the corresponding controls, pLKO.1 (**e**) and pCDH (**f**). The means and SEMs were calculated from three independent experiments

Silencing of ORMDL3 enhances mast cell-dependent PCA

To evaluate whether ORMDL3 has a function in mast cells in vivo, we silenced ORMDL3 locally by intradermal injection of the ORMDL3 siRNA pool. First, we examined the efficiency of ORMDL3 siRNA in vitro. When compared with BMMCs exposed to nontargeting control siRNA pool, the ORMDL3 siRNA pool reduced ORMDL expression by approximately 60 % as determined by immunoblotting (Fig. 8a, b; serum specific for all members of murine ORMDL family). For FcεRI-mediated PCA reactions, mice were intradermally injected with ORMDL3 siRNAs together with TNP-specific IgE into the right ears and control siRNAs together with TNP-specific IgE into the left ears. After 48 h, mice were challenged intravenously with Ag (TNP–BSA) and Evans blue dye and 2 h later Evans blue in both ears was quantified. Data presented in Fig. 8c show that ears injected with ORMDL3 siRNA displayed significantly higher amounts of Evans blue than ears injected with control siRNA. These data corroborate previous results obtained with BMMCs in vitro. Based on these results, we conclude that silencing of ORMDL3 in vivo leads to enhanced local inflammation triggered by mast cells.

Discussion

In this study, we examined the role of ORMDL3 protein in Ag-mediated mast cell signaling. Although enhanced or reduced expression of ORMDL3 had no effect on Ag-

induced degranulation and calcium responses, several lines of evidence presented in this study indicate that ORMDL3 is a negative regulator of proinflammatory activities of mast cells (Table 1). Increased expression of cytokines, chemokines, and COX-2 in O3_KD cells could be explained by our observation that BMMCs with O3_KD exhibited enhanced phosphorylation of IκBα, which is a regulator of transcription factor NF-κB [24]. Indeed, localization of the NF-κB p65 subunit was increased in the nuclei of Ag-activated ORMDL3-deficient mast cells. It is known that enhanced nuclear localization of the NF-κB p65 subunit leads to increased transcription of NF-κB-regulated genes encoding various cytokines, including TNF-α, IL-6 and IL-13, chemokines, CCL3 and CCL4, and COX-2 enzyme [44–48, 53–55]. Moreover, improperly regulated NF-κB causes a broad variety of inflammatory diseases [25–27]. Our findings regarding the regulatory roles of ORMDL3 are different from those obtained with other cell types, demonstrating a positive regulatory role of ORMDL3 in cell signaling. For example, eosinophils overexpressing ORMDL3 exhibited enhanced localization of the phosphorylated NF-κB p65 subunit in the nucleus [20]. Furthermore, transfection of ORMDL3 into lung epithelial cell line A549 increased the expression of several genes, including those for metalloproteases, ADAM-8 and MMP-9, chemokines CXCL-10, CXCL-11, IL-8, CCL-20, and oligoadenylate synthetases [18]. It has also been shown that the expression of several genes, including TGF-β1, ADAM8, MMP9, and CXCL-10, is enhanced in the bronchial epithelium of transgenic mice overexpressing ORMDL3 [19]. Recent studies showed that in eosinophils with O3_OE, ERK kinase played a role in regulating NF-κB signaling [20]. However, mast cells with O3_KD or O3_OE (not shown) exhibited similar ERK^{Y204} phosphorylation when compared with control cells. Although we did not exclude the possibility that phosphorylation of other targets in ERK could be affected by changing ORMDL3 levels, we focused on another potent activator of the NF-κB pathway, AKT kinase. We found that AKT kinase is more phosphorylated at the Ser 473 (but not at the Thr 308) in BMMCs with O3_KD than control cells. These data suggested a regulatory role of AKT in NF-κB signaling in mast cells with O3_KD. However, the exact molecular mechanism by which ORMDL3 activates AKT kinase remains unclear. To exclude the possibility that immunological responses toward dsRNAs could non-specifically activate IκBα/AKT phosphorylation, COX-2 expression, and cytokine production, we included cells transduced with pLKO.1 containing NT shRNA as a control. It should be mentioned that BMMCs poorly expressed toll-like receptors recognizing dsRNA, and their activation by specific ligands had little impact on TNF-α, IL-6, and IL-13 expression [56].

It has been shown that silencing of all three members of the ORMDL family potentiates de novo synthesis of sphingolipids [11]. In our study, we used shRNA to decrease the expression of ORMDL3 and found that expression of the other two members, ORMDL1 and ORMDL2, remained unchanged. Thus, we propose that in mast cells, a decrease in ORMDL3 expression alone is capable of promoting inflammation without the coordinate silencing of the ORMDL family genes. It should be noted that the NF-κB transcription factor is activated by multiple stimuli and that the multiprotein NF-kB signaling complex is subjected to extensive regulation [24]. TNF-α is known to be involved in the phosphorylation of IκBα [57, 58], and autocrine activation of NF-κB by TNF-α was observed in human mast cells [59]. Collectively, our data suggest a unique role of ORMDL3 in mast cells in the negative regulation of proinflammatory mediator synthesis. Interestingly, mast cells with O3_OE exhibited no significant inhibition of IκBα/AKT signaling and no suppression of proinflammatory mediator production. This could be explained at least in part by a recently published study, which showed that the expression levels of ORMDL3 were crucial for regulation of cell signaling in lipopolysaccharide-mediated activation of RAW264.7 macrophage cell line and A549 lung epithelial cells [60]. Thus, the relatively low overexpression of ORMDL3 in BMMCs could be under the threshold to regulate signaling pathways leading to the changes in cytokine expression. Our attempt to increase the exogenous expression of ORMDL3 in BMMCs failed because of enhanced mortality of BMMCs.

As already mentioned, no significant changes in calcium mobilization were found in Ag-activated BMMCs with O3_KD or O3_OE. These findings are different from those obtained with ORMDL3-deficient BM-derived eosinophils which, when compared with wild-type cells, showed reduced Ca^{2+} response after activation with eotaxin-1 [20]. On the other hand, Jurkat T cells with an siRNA-mediated O3_KD exhibited elevated mobilization of Ca^{2+} when activated via CD3, while a decreased Ca^{2+} response was observed in Jurkat cells with O3_OE [17]. Recent data showed that transgenic mice with elevated expression of ORMDL3 exhibited enhanced lung expression of SERCA2b, a known regulator of cytosolic calcium concentrations [19]. In contrast, our data with BMMCs showed that the expression of SERCA2b was not affected by changes in the ORMDL3 levels. These data are in line with our finding that BMMCs with decreased or enhanced expression of ORMDL3 exhibited similar levels of basal $[Ca^{2+}]_i$, and Ag-induced calcium mobilization when compared with corresponding control cells.

ORMDL3 has been described as an inducible gene upon *Alternaria* allergen challenge of mouse lung epithelial cells,

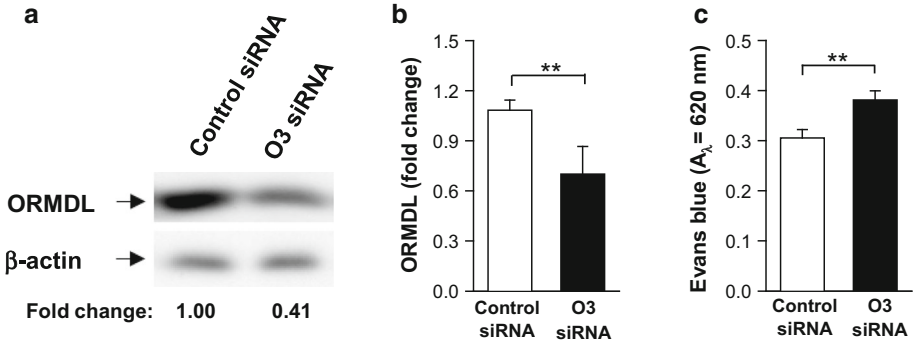

Fig. 8 Enhanced PCA in mice pretreated with ORMDL3 siRNA (O3 siRNA). **a** Specificity of the O3 siRNA. BMMCs were exposed to O3 siRNA pool or non-targeting control siRNA. 48 h later, the cells were lysed and analyzed for ORMDL3 and β-actin by immunoblotting. The position of ORMDL3 and β-actin, used as a loading control, is indicated by an *arrow*. Numbers under immunoblots indicate the relative amount of ORMDL3 normalized to its level in cells nucleofected with control siRNA and the amount of β-actin. **b** Quantification of ORMDL3 from data as in **a**. Means ± SEMs are shown ($n = 5$). **c** Role of ORMDL3 in PCA. TNP-specific IgE and O3 siRNA were injected intradermally into the right ears and TNP-specific IgE and control siRNA into the left ears. After 48 h, TNP–BSA was administered intravenously together with Evans blue dye and mice were killed 2 h later. Extravasation of Evans blue in both ears was determined. Means ± SEMs are shown ($n = 7$)

Table 1 Summary of Ag-induced responses of BMMCs with O3_KD or O3_OE when compared with control cells

Parameter	BMMCs with	
	O3_KD	O3_OE
Degranulation	–	–
Ca^{2+} response	–	–
SERCA2b (mRNA)	–	–
Chemotaxis toward Ag	↑	↓
Adhesion to fibronectin	–	–
Spreading on fibronectin	↓	–
F-actin content	–	–
Phosphorylation of IκBα (Ser 32/36)	↑	–
Phosphorylation of AKT (Ser 473)	↑	–
Phosphorylation of AKT (Thr 308)	–	–
Phosphorylation of ERK (Tyr 204)	–	–
Nuclear p65 subunit of NF-κB	↑	–
Production of cytokines (mRNA and protein)		
TNF-α	↑	–
IL-6	↑	–
IL-13	↑	–
Production of chemokines (mRNA)		
CCL3	↑	–
CCL4	↑	–
Expression of COX-2 (mRNA and protein)	↑	–
PGD2 synthesis	↑	–

BMMCs with O3_KD or O3_OE exhibited unchanged (–), decreased (↓) or increased (↑) responses when compared to control cells transduced with the corresponding empty vectors (pLKO.1 or pCDH)

lung eosinophils, and lung macrophages, but not lung neutrophils [18]. Moreover, IL-4 and IL-13 were capable of inducing ORMDL3 expression in lung epithelial cells [18]. These data were extended to mouse BM-derived eosinophils, which exhibited IL-3- and eotaxin-1-dependent induction of ORMDL3 expression [20]. In contrast to these data, our studies with mouse mast cells showed that expression of the *ORMDL3* gene was downregulated after FcεRI triggering. Interestingly, a similar decrease was observed in our previous study in which gene expression was analyzed in nonactivated and Ag-activated BMMCs (Gene Expression Omnibus repository dataset GSE40731 [61]). The data show that 2 h after FcεRI triggering, ORMDL3 was decreased to 0.6 in WT and to 0.43 in pLKO.1-transduced cells ($n = 3$ for each group, adj. P value <0.006). There were no significant changes between ORMDL1 and ORMDL2. The amounts of all ORMDL family members were not significantly changed between WT and pLKO.1 BMMCs. These data suggest a distinct regulation of *ORMDL3* gene expression in Ag-activated mast cells when compared with activated eosinophils, macrophages, and lung epithelial cells [18, 20]. Recently, it has been shown that lipopolysaccharide activation of macrophage cell line RAW267.4 induces coordinated transient suppression of expression of genes encoding the ORMDL family and in this way regulates sphingolipids homeostasis [14]. Chemotaxis is another example of distinct ORMDL3 regulatory roles in mast cells and eosinophils. ORMDL3-deficient eosinophils exhibited decreased chemotaxis toward eotaxin-1 [20], while we showed that BMMCs with O3_KD increasingly migrate toward Ag. Moreover, O3_KD exhibited decreased Ag-induced spreading on fibronectin. These data are consistent with previous observations of indirect relationship between mast cell migration and cell spreading [62]. The observed difference between mast cells and eosinophils could be caused by distinct chemoattractants and different methods

used and/or different involvement of ORMDL3 in chemotaxis of BMMCs and bone marrow-derived eosinophils.

Dysregulation of ORMDL3 expression is linked to various inflammatory diseases [1, 4–7]. It has been shown that upregulation of ORMDL3 stimulates the release of proinflammatory mediators [18, 20] and that ORMDL3 transgenic mice exhibit the proinflammatory phenotype [19]. On the other hand, decreased expression of all members of the ORMDL family led to activation of sphingolipid synthesis [11]. In this study, we showed for the first time that O3_KD alone is able to enhance the inflammatory response of mast cells. In BMMCs with O3_KD, we described a complex phenotype based on the enhanced AKT–NF-κB signaling axis, followed by increased secretion of TNF-α, IL-6, and IL-13 and enhanced expression of COX-2 associated with increased PGD2 synthesis. In addition, the chemotactic response of IgE-sensitized BMMCs to Ag was increased in cells with O3_KD and decreased in O3_OE. Moreover, we have found that ORMDL3 mRNA levels are decreased after challenge of IgE-sensitized BMMCs with Ag. These data were corroborated by an in vivo study, which showed that decreased ORMDL3 expression in mast cells was capable of inducing Ag-dependent inflammation. The opposite results obtained in mast cells versus other cell types described in the literature could be explained by formation of different functional complexes of ORMDL3 with other molecules in various cell types. Clarification of this issue and ORMDL3 properties in human mast cells requires further studies.

Collectively, our data show that ORMDL3 is predominantly a negative regulator of proinflammatory responses in Ag-activated murine mast cells, both in vitro and in vivo.

Acknowledgments This work was supported by projects P305-14-00703S, P302/12/G101, and P302-14-09807S from the Grant Agency of the Czech Republic and Institutional project RVO 68378050 from the Academy of Sciences of the Czech Republic. L.P., H.D., M.B., and T.P. were supported in part by the Faculty of Science, Charles University, Prague. We thank J. Eitler for preparation of ORMDL3-myc plasmid, H. Mrazova, and R. Budovicova for technical assistance, and Pavel Draber, Peter Draber, and S. Takacova for critical reading of the manuscript.

References

1. Moffatt MF, Kabesch M, Liang L, Dixon AL, Strachan D, Heath S, Depner M et al (2007) Genetic variants regulating ORMDL3 expression contribute to the risk of childhood asthma. Nature 448:470–473
2. Galanter J, Choudhry S, Eng C, Nazario S, Rodriguez-Santana JR, Casal J, Torres-Palacios A et al (2008) ORMDL3 gene is associated with asthma in three ethnically diverse populations. Am J Respir Crit Care Med 177:1194–1200
3. Hirota T, Harada M, Sakashita M, Doi S, Miyatake A, Fujita K, Enomoto T et al (2008) Genetic polymorphism regulating ORM1-like 3 (*Saccharomyces cerevisiae*) expression is associated with childhood atopic asthma in a Japanese population. J Allergy Clin Immunol 121:769–770
4. Balantic M, Rijavec M, Flezar M, Camlek T, Hudoklin I, Kosnik M, Korosec P, Suskovic S (2013) A polymorphism in ORMDL3 is associated not only with asthma without rhinitis but also with chronic obstructive pulmonary disease. J Investig Allergol Clin Immunol 23:256–261
5. McGovern DP, Gardet A, Torkvist L, Goyette P, Essers J, Taylor KD, Neale BM et al (2010) Genome-wide association identifies multiple ulcerative colitis susceptibility loci. Nat Genet 42:332–337
6. Verlaan DJ, Berlivet S, Hunninghake GM, Madore AM, Lariviere M, Moussette S, Grundberg E et al (2009) Allele-specific chromatin remodeling in the ZPBP2/GSDMB/ORMDL3 locus associated with the risk of asthma and autoimmune disease. Am J Hum Genet 85:377–393
7. Barrett JC, Hansoul S, Nicolae DL, Cho JH, Duerr RH, Rioux JD, Brant SR et al (2008) Genome-wide association defines more than 30 distinct susceptibility loci for Crohn's disease. Nat Genet 40:955–962
8. Kurreeman FA, Stahl EA, Okada Y, Liao K, Diogo D, Raychaudhuri S, Freudenberg J et al (2012) Use of a multiethnic approach to identify rheumatoid- arthritis-susceptibility loci, 1p36 and 17q12. Am J Hum Genet 90:524–532
9. Li X, Ampleford EJ, Howard TD, Moore WC, Torgerson DG, Li H, Busse WW et al (2012) Genome-wide association studies of asthma indicate opposite immunopathogenesis direction from autoimmune diseases. J Allergy Clin Immunol 130:861–868
10. Hjelmqvist L, Tuson M, Marfany G, Herrero E, Balcells S, Gonzalez-Duarte R (2002) ORMDL proteins are a conserved new family of endoplasmic reticulum membrane proteins. Genome Biol 3:RESEARCH0027-1-16
11. Breslow DK, Collins SR, Bodenmiller B, Aebersold R, Simons K, Shevchenko A, Ejsing CS, Weissman JS (2010) Orm family proteins mediate sphingolipid homeostasis. Nature 463:1048–1053
12. Roelants FM, Breslow DK, Muir A, Weissman JS, Thorner J (2011) Protein kinase Ypk1 phosphorylates regulatory proteins Orm1 and Orm2 to control sphingolipid homeostasis in Saccharomyces cerevisiae. Proc Natl Acad Sci USA 108:19222–19227
13. Siow DL, Wattenberg BW (2012) Mammalian ORMDL proteins mediate the feedback response in ceramide biosynthesis. J Biol Chem 287:40198–40204
14. Kiefer K, Carreras-Sureda A, Garcia-Lopez R, Rubio-Moscardo F, Casas J, Fabrias G, Vicente R (2015) Coordinated regulation of the orosomucoid-like gene family expression controls de novo ceramide synthesis in mammalian cells. J Biol Chem 290:2822–2830
15. Worgall TS, Veerappan A, Sung B, Kim BI, Weiner E, Bholah R, Silver RB, Jiang XC, Worgall S (2013) Impaired sphingolipid synthesis in the respiratory tract induces airway hyperreactivity. Sci Transl Med 5:186ra67
16. Cantero-Recasens G, Fandos C, Rubio-Moscardo F, Valverde MA, Vicente R (2010) The asthma-associated ORMDL3 gene product regulates endoplasmic reticulum-mediated calcium signaling and cellular stress. Hum Mol Genet 19:111–121
17. Carreras-Sureda A, Cantero-Recasens G, Rubio-Moscardo F, Kiefer K, Peinelt C, Niemeyer BA, Valverde MA, Vicente R (2013) ORMDL3 modulates store-operated calcium entry and lymphocyte activation. Hum Mol Genet 22:519–530
18. Miller M, Tam AB, Cho JY, Doherty TA, Pham A, Khorram N, Rosenthal P et al (2012) ORMDL3 is an inducible lung epithelial

gene regulating metalloproteases, chemokines, OAS, and ATF6. Proc Natl Acad Sci USA 109:16648–16653
19. Miller M, Rosenthal P, Beppu A, Mueller JL, Hoffman HM, Tam AB, Doherty TA et al (2014) ORMDL3 transgenic mice have increased airway remodeling and airway responsiveness characteristic of asthma. J Immunol 192:3475–3487
20. Ha SG, Ge XN, Bahaie NS, Kang BN, Rao A, Rao SP, Sriramarao P (2013) ORMDL3 promotes eosinophil trafficking and activation via regulation of integrins and CD48. Nat Commun 4:2479
21. Galli SJ (2000) Mast cells and basophils. Curr Opin Hematol 7:32–39
22. Galli SJ, Tsai M, Piliponsky AM (2008) The development of allergic inflammation. Nature 454:445–454
23. Schubert N, Dudeck J, Liu P, Karutz A, Speier S, Maurer M, Tuckermann J, Dudeck A (2015) Mast cell promotion of T cell-driven antigen-induced arthritis despite being dispensable for antibody-induced arthritis in which T cells are bypassed. Arthritis Rheumatol 67:903–913
24. Oeckinghaus A, Ghosh S (2009) The NF-κB family of transcription factors and its regulation. Cold Spring Harb Perspect Biol 1:a000034
25. Bollrath J, Greten FR (2009) IKK/NF-κB and STAT3 pathways: central signalling hubs in inflammation-mediated tumour promotion and metastasis. EMBO Rep 10:1314–1319
26. Sheller JR, Polosukhin VV, Mitchell D, Cheng DS, Peebles RS, Blackwell TS (2009) Nuclear factor κB induction in airway epithelium increases lung inflammation in allergen-challenged mice. Exp Lung Res 35:883–895
27. Wullaert A, Bonnet MC, Pasparakis M (2011) NF-κB in the regulation of epithelial homeostasis and inflammation. Cell Res 21:146–158
28. Ricciotti E, FitzGerald GA (2011) Prostaglandins and inflammation. Arterioscler Thromb Vasc Biol 31:986–1000
29. Hájková Z, Bugajev V, Dráberová E, Vinopal S, Dráberov L, Janáček J, Dráber P, Dráber P (2011) STIM1-directed reorganization of microtubules in activated mast cells. J Immunol 186:913–923
30. Rudolph AK, Burrows PD, Wabl MR (1981) Thirteen hybridomas secreting hapten-specific immunoglobulin E from mice with Ig^a or Ig^b heavy chain haplotype. Eur J Immunol 11:527–529
31. Tolar P, Dráberová L, Dráber P (1997) Protein tyrosine kinase Syk is involved in Thy-1 signaling in rat basophilic leukemia cells. Eur J Immunol 27:3389–3397
32. Dráberová L, Amoui M, Dráber P (1996) Thy-1-mediated activation of rat mast cells: the role of Thy-1 membrane microdomains. Immunology 87:141–148
33. Draberova L, Bugajev V, Potuckova L, Halova I, Bambouskova M, Polakovicova I, Xavier RJ, Seed B, Draber P (2014) Transmembrane adaptor protein PAG/CBP is involved in both positive and negative regulation of mast cell signaling. Mol Cell Biol 34:4285–4300
34. Horáková H, Polakovičová I, Shaik GM, Eitler J, Bugajev V, Dráberová L, Dráber P (2011) 1,2-propanediol-trehalose mixture as a potent quantitative real-time PCR enhancer. BMC Biotechnol 11:41
35. Potůčková L, Franko F, Bambousková M, Dráber P (2011) Rapid and sensitive detection of cytokines using functionalized gold nanoparticle-based immuno-PCR, comparison with immuno-PCR and ELISA. J Immunol Methods 371:38–47
36. Laemmli UK (1970) Cleavage of structural proteins during the assembly of the head of bacteriophage T4. Nature 227:680–685
37. Haan C, Behrmann I (2007) A cost effective non-commercial ECL-solution for Western blot detections yielding strong signals and low background. J Immunol Methods 318:11–19
38. Hálová I, Dráberová L, Bambousková M, Machyna M, Stegurová L, Smrž D, Dráber P (2013) Crosstalk between tetraspanin CD9 and transmembrane adaptor protein non-T cell activation linker (NTAL) in mast cell activation and chemotaxis. J Biol Chem 288:9801–9814
39. Carpenter AE, Jones TR, Lamprecht MR, Clarke C, Kang IH, Friman O, Guertin DA et al (2006) Cell Profiler: image analysis software for identifying and quantifying cell phenotypes. Genome Biol 7:R100
40. Ding GJ, Fischer PA, Boltz RC, Schmidt JA, Colaianne JJ, Gough A, Rubin RA, Miller DK (1998) Characterization and quantitation of NF-κB nuclear translocation induced by interleukin-1 and tumor necrosis factor-α. Development and use of a high capacity fluorescence cytometric system. J Biol Chem 273:28897–28905
41. Kanada S, Nishiyama C, Nakano N, Suzuki R, Maeda K, Hara M, Kitamura N, Ogawa H, Okumura K (2011) Critical role of transcription factor PU.1 in the expression of CD80 and CD86 on dendritic cells. Blood 117:2211–2222
42. Bradding P (2007) Mast cell regulation of airway smooth muscle function in asthma. Eur Respir J 29:827–830
43. Walker ME, Hatfield JK, Brown MA (2012) New insights into the role of mast cells in autoimmunity: evidence for a common mechanism of action? Biochim Biophys Acta 1822:57–65
44. Hinz M, Lemke P, Anagnostopoulos I, Hacker C, Krappmann D, Mathas S, Dorken B, Zenke M, Stein H, Scheidereit C (2002) Nuclear factor κB-dependent gene expression profiling of Hodgkin's disease tumor cells, pathogenetic significance, and link to constitutive signal transducer and activator of transcription 5a activity. J Exp Med 196:605–617
45. Klemm S, Gutermuth J, Hultner L, Sparwasser T, Behrendt H, Peschel C, Mak TW, Jakob T, Ruland J (2006) The Bcl10-Malt1 complex segregates FcεRI-mediated nuclear factor κB activation and cytokine production from mast cell degranulation. J Exp Med 203:337–347
46. Marquardt DL, Walker LL (2000) Dependence of mast cell IgE-mediated cytokine production on nuclear factor-κB activity. J Allergy Clin Immunol 105:500–505
47. Peng Y, Power MR, Li B, Lin TJ (2005) Inhibition of IKK down-regulates antigen + IgE-induced TNF production by mast cells: a role for the IKK-IκB-NF-κB pathway in IgE-dependent mast cell activation. J Leukoc Biol 77:975–983
48. Widmer U, Manogue KR, Cerami A, Sherry B (1993) Genomic cloning and promoter analysis of macrophage inflammatory protein (MIP)-2, MIP-1 α, and MIP-1 β, members of the chemokine superfamily of proinflammatory cytokines. J Immunol 150:4996–5012
49. Baba Y, Nishida K, Fujii Y, Hirano T, Hikida M, Kurosaki T (2008) Essential function for the calcium sensor STIM1 in mast cell activation and anaphylactic responses. Nat Immunol 9:81–88
50. Lee FS, Hagler J, Chen ZJ, Maniatis T (1997) Activation of the IκBα kinase complex by MEKK1, a kinase of the JNK pathway. Cell 88:213–222
51. Dan HC, Cooper MJ, Cogswell PC, Duncan JA, Ting JP, Baldwin AS (2008) Akt-dependent regulation of NF-κB is controlled by mTOR and Raptor in association with IKK. Genes Dev 22:1490–1500
52. Marques JT, Williams BR (2005) Activation of the mammalian immune system by siRNAs. Nat Biotechnol 23:1399–1405
53. Kaltschmidt B, Linker RA, Deng J, Kaltschmidt C (2002) Cyclooxygenase-2 is a neuronal target gene of NF-κB. BMC Mol Biol 3:16
54. Mortaz E, Redegeld FA, Nijkamp FP, Engels F (2005) Dual effects of acetylsalicylic acid on mast cell degranulation, expression of cyclooxygenase-2 and release of pro-inflammatory cytokines. Biochem Pharmacol 69:1049–1057

55. Kurumbail RG, Kiefer JR, Marnett LJ (2001) Cyclooxygenase enzymes: catalysis and inhibition. Curr Opin Struct Biol 11:752–760
56. Matsushima H, Yamada N, Matsue H, Shimada S (2004) TLR3-, TLR7-, and TLR9-mediated production of proinflammatory cytokines and chemokines from murine connective tissue type skin-derived mast cells but not from bone marrow-derived mast cells. J Immunol 173:531–541
57. Lin WJ, Yeh WC (2005) Implication of Toll-like receptor and tumor necrosis factor α signaling in septic shock. Shock 24:206–209
58. Aggarwal BB (2004) Nuclear factor-κB: the enemy within. Cancer Cell 6:203–208
59. Coward WR, Okayama Y, Sagara H, Wilson SJ, Holgate ST, Church MK (2002) NF-κB and TNF-α: a positive autocrine loop in human lung mast cells? J Immunol 169:5287–5293
60. Oyeniran C, Sturgill JL, Hait NC, Huang WC, Avni D, Maceyka M, Newton J et al (2015) Aberrant ORM (yeast)-like protein isoform 3 (ORMDL3) expression dysregulates ceramide homeostasis in cells and ceramide exacerbates allergic asthma in mice. J Allergy Clin Immunol. doi:10.1016/j.jaci.2015.02.031
61. Polakovicova I, Draberova L, Simicek M, Draber P (2014) Multiple Regulatory Roles of the Mouse Transmembrane Adaptor Protein NTAL in Gene Transcription and Mast Cell Physiology. PLoS ONE 9:e105539
62. Tůmová M, Koffer A, Šimíček M, Dráberová L, Dráber P (2010) The transmembrane adaptor protein NTAL signals to mast cell cytoskeleton via the small GTPase Rho. Eur J Immunol 40:3235–3245

7.5 ETHANOL INHIBITS HIGH-AFFINITY IMMUNOGLOBULIN E RECEPTOR (FcεRI) SIGNALING IN MAST CELLS BY SUPPRESSING THE FUNCTION OF FcεRI -CHOLESTEROL SIGNALOSOME.

Dráberová L., Paulenda T., Hálová I., **Potůčková L**., Bugajev V.,
Bambousková M., Tůmová M., Dráber P.

PLoS One, 10(12):e0144596, 2015

PLOS ONE

RESEARCH ARTICLE

Ethanol Inhibits High-Affinity Immunoglobulin E Receptor (FcεRI) Signaling in Mast Cells by Suppressing the Function of FcεRI-Cholesterol Signalosome

Lubica Draberova*, Tomas Paulenda, Ivana Halova, Lucie Potuckova, Viktor Bugajev, Monika Bambouskova, Magda Tumova, Petr Draber*

Laboratory of Signal Transduction, Institute of Molecular Genetics, Academy of Sciences of the Czech Republic, Prague, Czech Republic

* draberovalu@img.cas.cz (LD); draberpe@img.cas.cz (PD)

Citation: Draberova L, Paulenda T, Halova I, Potuckova L, Bugajev V, Bambouskova M, et al. (2015) Ethanol Inhibits High-Affinity Immunoglobulin E Receptor (FcεRI) Signaling in Mast Cells by Suppressing the Function of FcεRI-Cholesterol Signalosome. PLoS ONE 10(12): e0144596. doi:10.1371/journal.pone.0144596

Editor: David Holowka, Cornell University, UNITED STATES

Received: July 25, 2015

Accepted: November 21, 2015

Published: December 14, 2015

Data Availability Statement: All relevant data are within the manuscript.

Funding: This work was supported by Project P302/12/G101 from the Grant Agency of the Czech Republic and Project LD12073 COST-CZ-MAST from the Ministry of Education Youth and Sports of the Czech Republic. The funders had no role in study design, data collection and analysis, decision to publish, or preparation of the manuscript.

Abstract

Ethanol has multiple effects on biochemical events in a variety of cell types, including the high-affinity immunoglobulin E receptor (FcεRI) signaling in antigen-activated mast cells. However, the underlying molecular mechanism remains unknown. To get better understanding of the effect of ethanol on FcεRI-mediated signaling we examined the effect of short-term treatment with non-toxic concentrations of ethanol on FcεRI signaling events in mouse bone marrow-derived mast cells. We found that 15 min exposure to ethanol inhibited antigen-induced degranulation, calcium mobilization, expression of proinflammatory cytokine genes (tumor necrosis factor-α, interleukin-6, and interleukin-13), and formation of reactive oxygen species in a dose-dependent manner. Removal of cellular cholesterol with methyl-β-cyclodextrin had a similar effect and potentiated some of the inhibitory effects of ethanol. In contrast, exposure of the cells to cholesterol-saturated methyl-β-cyclodextrin abolished in part the inhibitory effect of ethanol on calcium response and production of reactive oxygen species, supporting lipid-centric theories of ethanol action on the earliest stages of mast cell signaling. Further studies showed that exposure to ethanol and/or removal of cholesterol inhibited early FcεRI activation events, including tyrosine phosphorylation of the FcεRI β and γ subunits, SYK kinases, LAT adaptor protein, phospholipase Cγ, STAT5, and AKT and internalization of aggregated FcεRI. Interestingly, ethanol alone, and particularly in combination with methyl-β-cyclodextrin, enhanced phosphorylation of negative regulatory tyrosine 507 of LYN kinase. Finally, we found that ethanol reduced passive cutaneous anaphylactic reaction in mice, suggesting that ethanol also inhibits FcεRI signaling under *in vivo* conditions. The combined data indicate that ethanol interferes with early antigen-induced signaling events in mast cells by suppressing the function of FcεRI-cholesterol signalosomes at the plasma membrane.

Competing Interests: The authors have declared that no competing interests exist.

Introduction

Although it is known that ethanol has multiple effects on a variety of cells types, the molecular mechanisms of its action are far from understood. There are two basic theories of ethanol action on the cells, lipid-centric and protein-centric [1]. The lipid theory of ethanol action postulates that ethanol, similarly to anesthetics [2,3], dissolves in cellular lipids and acts by non-specific mechanisms. This theory was supported by experiments showing that alcohols and anesthetics induce changes in properties of cellular membranes, including fluidity [4], lateral mobility of lipid molecules [5], phase transition temperature [6,7], and membrane permeability [8]. The protein theory of alcohol and anesthetics action proposes that the drugs interact specifically with certain proteins and in this way affect their properties [9]. This theory was mostly based on experiments suggesting that binding of alcohols and anesthetics induces conformational changes that diminish or abolish the function of some proteins, such as those forming neurotransmitter-gated ion channels [10–13]. However, concentrations of ethanol required to cause significant changes in the receptor functions were often greater than those attainable *in vivo*, and effects mediated by lower concentrations have not always been replicated [14].

Previous studies showed that alcohol modulates various components of the immune system [15–17]. Acute exposure to ethanol resulted in reduced monocyte/macrophage phagocytosis [18,19], T-cell receptor signaling [20], Toll-like receptor-mediated activation of macrophages [21,22], and reduced neutrophil migration [23]. It has also been reported that *in vitro* exposure of mast cells to ethanol for 1 hour or longer inhibited the high-affinity immunoglobulin E (IgE) receptor (FcεRI)-induced degranulation and production of tumor necrosis factor (TNF)-α and interleukin (IL)-8 [24,25]. Although these data suggested that ethanol inhibits signal transduction from the immunoreceptors, molecular mechanisms of the inhibitory action of ethanol on early steps of immunoreceptor signaling remained enigmatic.

In this study we used primary mouse bone marrow-derived mast cells (BMMCs) and examined sensitivity to ethanol of the earliest signaling events after FcεRI triggering. We also examined effect of ethanol on FcεRI activation in cells with reduced levels of cholesterol and on passive cutaneous anaphylaxis (PCA) in mice. Our data indicate that ethanol inhibits tyrosine phosphorylation of the FcεRI β and γ subunits, the first biochemically defined event after antigen-mediated aggregation of FcεRI, and support lipid-centric theory of ethanol action in mast cells.

Materials and Methods

Mice and cells

Mice were bred and maintained in specific pathogen free facility of the Institute of Molecular Genetics and used in compliance with the Institute guidelines. All protocols, including killing mice by decapitation, was approved by the Animal Care and Use Committee of the Institute of Molecular Genetics (Permit number 12135/2010-17210) and was in compliance with the EU Directive 2010/63/EU for animal experiments. All efforts were made to minimize suffering of the mice.

Bone marrow mast cells were isolated from femurs and tibias of C57BL/6 mice (females, 6–8 weeks old). The cells were cultured in RPMI-1640 medium supplemented with 100 U/ml penicillin, 100 μg/ml streptomycin, 71 μM 2-mercaptoethanol, minimum essential medium non-essential amino acids, 0.7 mM sodium pyruvate, 2.5 mM L-glutamine, 12 mM D-glucose, recombinant mouse stem cell factor (SCF; 20 ng/ml, ProSpec), mouse recombinant IL-3 (20 ng/ml, ProSpec) and 10% fetal calf serum (FCS). For PCA experiments, BALB/c male mice aged 8–12 weeks were used.

Antibodies and reagents

The following monoclonal antibodies (mAbs) were used: anti-FcεRI β chain [26], trinitrophenol (TNP)-specific IgE mAb (IGEL b4 1) [27], anti-LAT [28], anti-LYN [29], and anti-NTAL [30]. Polyclonal antibodies specific for LYN and LAT were prepared by immunization of rabbits with the corresponding recombinant proteins or their fragments [31]. Rabbit anti-IgE was prepared by immunization with whole IGEL b4.1. Polyclonal antibodies specific for phospholipase C (PLC)γ1, phospho(p)PLCγ1 (Tyr 783), STAT5, ERK, pERK (Tyr 783), AKT, pAKT (Ser 473) as well as horseradish peroxidase (HRP)-conjugated goat anti-mouse IgG, and goat anti-rabbit IgG, were obtained from Santa Cruz Biotechnology Inc. Antibodies specific for pSYK (Tyr 525/Tyr 526), pSTAT5 (Tyr 694), pLYN (Tyr 507), and pLYN (Tyr 416) were obtained from Cell Signaling. Antibody specific for pLAT (Tyr 191) cross-reacting with pNTAL was obtained from Merc-Millipore. PAG-specific rabbit polyclonal antibody was from Exbio. V450-conjugated rat anti-mouse CD107a (LAMP1) and HRP-conjugated anti- phosphotyrosine mAb (PY-20) were obtained from BD Biosciences. Anti-mouse FcεRI labeled with fluorescein isothiocyanate (FITC) and anti-mouse KIT-allophycocyanin conjugates were obtained from eBiosciences. Donkey anti-mouse Ig-Alexa Fluor 568 conjugate was obtained from Invitrogen. All other reagents were from Sigma-Aldrich.

Flow cytometry

For flow cytometry measurements, BMMCs (10^5/sample) were used. To analyze the surface levels of FcεRI and Kit receptor, the labeling proceeded as described previously [32]. For analysis of surface CD107a (LAMP1), BMMCs were activated with various concentrations of antigen for 10 min at 37°C. Activation was stopped by pelleting the cells at 4°C. Cells were then resuspended in 50 μl of phosphate-buffered saline (PBS) containing 1% bovine serum albumin (BSA) and 1:200 diluted V450-conjugated rat anti-mouse CD107a (LAMP1). After 30 min on ice, the cells were washed with ice-cold PBS and analyzed by an LSRII flow cytometer (BD Biosciences). Median fluorescence intensities were determined and further processed using FlowJo software (Ashland).

Cell activation

BMMCs were cultured for 48 hours in medium without SCF, followed by incubation in SCF- and IL-3-free medium supplemented with TNP-specific IgE (1 μg/ml). After 14 hours the cells were washed in buffered salt solution (BSS; 20 mM HEPES, pH 7.4, 135 mM NaCl, 5 mM KCl, 1.8 mM $CaCl_2$, 5.6 mM glucose, 1 mM $MgCl_2$) supplemented with 0.1% BSA and incubated with or without ethanol and/or other drugs. After 15 min, antigen was added and the cells were activated in the presence or absence of the drugs. The degree of degranulation was determined as the amount of β-glucuronidase released into the supernatant as described [32].

Measurement of free intracellular calcium

Changes in concentrations of free intracellular calcium were determined using cell permeant Fura-2 acetoxymetyl ester (Fura-2 AM; Life Technologies) as a reporter. IgE-sensitized cells were harvested, washed in BSS-0.1% BSA and transferred to BSS-0.1% BSA supplemented with Fura-2 AM (1 ng/ml) and probenecid (2.5 mM) used to prevent dye leakage [33], and incubated in the shaker for 30 min at 37°C, 500 rpm. Fura-2 loaded cells were washed twice with 2.5 mM probenecid in BSS-0.1% BSA and then transferred to BSS-0.1% BSA supplemented with 2.5 mM probenecid and various drugs as specified in the Results. Cells were then incubated in Thermomixer (Eppendorf; 10 min, 37°C, 500 rpm). For measurement in the presence

of extracellular calcium, cells were pelleted by centrifugation 500 x g for 3 min, resuspended in BSS-0.1% BSA and transferred to white polysorp 96 well plate (NUNC, Thermo Scientific). To determine free intracellular Ca^{2+} levels in the absence of extracellular Ca^{2+}, cells were pelleted by centrifugation, washed in Ca^{2+}-free BSS-0.1% BSA and transferred to the plate. Free intracellular Ca^{2+} was measured on INFINITE M200 (Tecan) as Fura-2 emission at 510 nm after excitation with 340 nm and 380 nm. Basal level of calcium was usually measured in the first 60 sec, followed by addition of antigen (TNP-BSA, final concentration 100 ng/ml) in BSS-0.1% BSA. Measurement continued up to 350 s. In the absence of extracellular calcium the cells were activated with antigen for 5 min followed by addition of $CaCl_2$ to final concentration 1 mM and measurement continued up to 600 s.

Immunoprecipitation and immunoblotting

Activated or nonactivated cells were solubilized in ice-cold lysis buffer (25 mM Tris-HCl, pH 8.0, 140 mM NaCl, 1 mM Na_3VO_4, 2 mM EDTA, 1 μg/ml aprotinin, 1 μg/ml leupeptin, 1 mM phenylmethylsulfonyl fluoride) supplemented with 0.2% Triton X-100 (for FcεRI immunoprecipitation). After incubation on ice for 30 min, the lysates were centrifuged (16,000 x g for 5 min at 4°C) and postnuclear supernatants were immunoprecipitated with rabbit anti-IgE antibody prebound to UltraLink-immobilized protein A (Pierce, Thermo Scientific). The immunoprecipitated proteins were size-fractionated by sodium dodecyl sulfate-polyacrylamide gel electrophoresis (SDS-PAGE), transferred to nitrocellulose membrane and immunoblotted with PY-20-HRP conjugate or with FcεRI-β chain-specific antibody followed by HRP-conjugated anti-mouse IgG. For immunoblotting analysis of other proteins, the cells were solubilized in lysis buffer supplemented with 1% n-dodecyl β-D-maltoside and 1% Nonidet P-40 and postnuclear supernatants were directly analyzed by SDS-PAGE followed by immunoblotting with phospho-protein-specific or the corresponding protein-specific antibodies and HRP-conjugated secondary antibodies. The HRP signals were detected by chemiluminescence, quantified by luminescent image analyzer LAS-3000 (Fuji Photo Film Co), and further analyzed by Aida image analyzer software (Raytest). The amount of phosphorylated proteins was normalized to the loading controls, run in parallel experiments [32]. We found that this approach gave more reliable data than normalization towards specific proteins after stripping of the membranes.

Sucrose density gradient fractionation and expression of cytokine genes

Sucrose density gradient separations were performed as previously described [32] and individual fractions were analyzed by SDS-PAGE followed by immunoblotting with PY-20-HRP and protein-specific antibodies. Expression of cytokine genes was examined by quantitative polymerase chain reaction (qPCR) as described [32].

Confocal microscopy

The wells of microscopy slides (CN Biomedicals) were coated with CellTak (BD Biosciences; 8 μl in 1 ml PBS). IgE-sensitized cells were left to attach to the coated wells for 15 min in BSS-0.1% BSA and then activated or not with Ag. After 15 min, the cells were fixed for 30 min with 3% paraformaldehyde in PBS and then permeabilized with 0.1% Triton X-100 in PBS for 30 min. After washing with PBS, the samples were blocked in PBS-1% BSA, and subsequently IgE was detected with Alexa Fluor 568-labeled donkey anti-mouse Ig. After labeling, the cells were washed and mounted in glycerol mounting solution supplemented with Hoechst 33258 stain to label nuclei. Samples were examined with a confocal laser scanning microscope Leica TCS SP5 equipped with an X63/1.4.N.A. oil-immersion objective. The image analysis was performed using a pipeline generated in CellProfiler software (Broad Institute, Boston) [34].

ROS measurements

Reactive oxygen species (ROS) were examined with cell-permeant 2',7'-dichlorodihydrofluorescein diacetate (H_2DCFDA; Life Technologies) as a reporter. Cells were sensitized for 16 hours with anti-TNP IgE (1 μg/ml) at 37°C in culture medium supplemented with 10% FCS, but devoid of SCF and IL-3. Then, the cells were washed and loaded into the wells of a 96-well plate (0.25 x 10^6 cells/well) in 100 μl of the same medium supplemented with H_2DCFDA (5 μg/ml) in the presence of probenecid (2.5 mM) and various concentrations of ethanol. After 15 min, the cells were centrifuged and resuspended in 50 μl BSS-BSA. Activation was triggered by adding 50 μl of 500 ng/ml TNP-BSA (final concentration 250 ng/ml) in the absence or presence of different concentrations of ethanol. Alternatively, in the experiment with methyl-β-cyclodextrin (Mβ) and cholesterol-saturated Mβ (sMβ), the cells were stained with H_2DCFDA as above, washed and incubated 15 min in BSS-BSA supplemented or not with 0.5% (v/v) ethanol, 2 mM Mβ, and/or 2 mM sMβ. The activation was triggered by antigen (TNP-BSA; 250 ng/ml final concentrations) in the presence of the drugs; sMβ was prepared as previously described [35]. After 10 min, changes in fluorescence intensity were monitored in an LSRII flow cytometer (BD Biosciences; Ex/Em 488/505-535 nm).

PCA

Mice were anesthetized by intraperitoneal injection of a cocktail containing ketamine (Narketan 10; 40 mg/kg, final concentration), xylazine (Xylapan; 10 mg/kg), and atropine (Atropin Biotika; 0.1 mg/kg) and then sensitized by intradermal injection of 20 μl of anti-TNP-specific IgE (50 μg/ml) in PBS into the left ear; the right ear was injected with 20 μl of PBS alone. Twenty-four hours later, 5% (v/v), 10% or 20% absolute ethanol in PBS was injected intraperitoneally (0.5 ml per mouse weighing 20 g). Mice injected with 0.5 ml of 10% or 20% ethanol exhibited reduced motoric activity, which lasted for 30 min or 90 min, respectively. Mice challenged with 0.5 ml of 5% ethanol were without any clinical signs. One hour after ethanol in PBS or PBS alone injection, each mouse was challenged with an intravenous injection of antigen (TNP-BSA, 100 μg) in 200 μl of PBS containing 1% Evans blue. The mice were killed 30 min later and their ears were removed for measurement of the amount of the Evans blue extravasated. The dye was extracted by adding 1 ml of formamide to each ear, followed by homogenization with the IKA T-25 ULTRA-TURRAX digital high-speed homogenizer systems (IKA) and incubation at 80°C. After 2 h, the formamide solution was centrifuged for 15 min at 13.000 x g and absorbance at 620 nm was determined in the supernatants.

Statistical analysis

Statistical significance of intergroup differences was determined by one-way ANOVA with Tukey's post-test using the Prism version 5.04 graphics and statistics software package (GraphPad); *, $P<0.05$; **, $P<0.01$, ***, $P<0.001$.

Results

Short-term exposure to ethanol inhibits FcεRI-induced degranulation and calcium response

To examine the inhibitory effect of ethanol on antigen-induced activation of mast cells, we isolated bone marrow cells from C57BL/6 mice and cultured them for 6–12 weeks in culture media supplemented with SCF and IL-3. More than 98% of the cells were mast cells as deduced from expression of both FcεRI and KIT receptors (see below). Exposure of BMMCs for 15 min– 2 hours with ethanol at concentrations up to 2% had no toxic effect, as determined by

trypan blue dye exclusion test (not shown). Pretreatment of IgE-sensitized BMMCs for 15 min with ethanol at concentrations 0.2–1%, inhibited degranulation induced by multivalent antigen in a dose-dependent way. Significant inhibition was observed at all concentrations of ethanol tested when the cells were activated with antigen (50 ng/ml or 100 ng/ml) for 5 min or 15 min, except for cells treated with 0.2% ethanol and stimulated with antigen (50 ng/ml) for 5 min (Fig 1A and 1B).

Ethanol at all concentrations used also inhibited, in a dose-dependent way, the calcium response after stimulation of IgE-sensitized cells with antigen in the presence of extracellular calcium (Fig 1C). When the cells were stimulated with antigen in the absence of extracellular calcium, the calcium response was significantly inhibited by 0.5% and 1% ethanol. Addition of extracellular calcium resulted in increased calcium response, which was significantly lower in cells exposed to 0.2%, 0.5% or 1% ethanol (Fig 1D). These data suggested that ethanol could act on early signaling events leading to the release of calcium from internal stores as well as on calcium channels directing influx of calcium from the extracellular space. When the cells were pretreated with 4-methylpyrazole (4-MP; 0.1 or 1 mM), a known inhibitor of alcohol dehydrogenase [36], the inhibitory effect of ethanol was not affected (Fig 2), suggesting that ethanol itself, rather than its metabolite product, is responsible for the inhibitory effect.

Involvement of cholesterol in the inhibitory effect of ethanol on FcεRI-mediated activation

Recently, Setiawan and Blanchard showed that ethanol interferes with the size and distribution of cholesterol domains in planar lipid bilayer structures [37]. To determine whether plasma membrane cholesterol could be involved in the inhibitory effect of ethanol, we evaluated the effect of Mβ alone or together with ethanol on FcεRI-mediated degranulation. Mβ is a water-soluble cyclic heptasaccharide that binds cholesterol and can extract cholesterol from the exoplasmic leaflet of the plasma membrane by harboring cholesterol in a hydrophobic cavity [35,38,39]. Exposure of cells for 15 min to 2 mM Mβ alone or in combination with 0.5% ethanol had no significant effect on spontaneous release of β-glucuronidase (Fig 3A–3C). In cells activated with antigen at a concentration 50 ng/ml or 100 ng/ml for 5 (Fig 3A) or 15 min (Fig 3B), degranulation was significantly reduced by both Mβ and ethanol. When ethanol and Mβ were used together, the inhibition of degranulation was higher than in cells treated with ethanol or Mβ alone. Mβ is not specific for cholesterol, but has pleiotropic effects on the level and distribution of various membrane components [40]. Next, we therefore evaluated antigen-induced degranulation in cells pretreated with cholesterol-saturated Mβ (sMβ), which increases plasma membrane cholesterol [35]. We found that sMβ, in contrast to Mβ, had no significant inhibitory effect on degranulation (Fig 3C). Interestingly, sMβ-treatment did not protect the cells from the inhibitory effect of ethanol (Fig 3B and 3C). We also found that exposure of cells to 2 mM Mβ or sMβ with or without ethanol for 15 min had no effect on the FcεRI expression as determined by flow cytometry (not shown).

Degranulation is accompanied by enhanced surface expression of CD107a (LAMP1), a secretory granule/lysosomal marker detectable by flow cytometry [41]. In agreement with antigen-induced β-glucuronidase release, 2 mM Mβ and 0.5% ethanol alone inhibited CD107a (LAMP1) surface expression, even though ethanol was less potent. An additive effect of the drugs was observed when the cells were activated with antigen at optimal (100 ng/ml) and supra-optimal (500 ng/ml) concentrations (Fig 3D).

We also analyzed the combined effect of Mβ and/or ethanol pretreatment on antigen-induced calcium response. The data indicate that pretreatment with Mβ did not intensify the inhibitory effect of ethanol (Fig 4A). When the cells were activated in the absence of extracellular calcium,

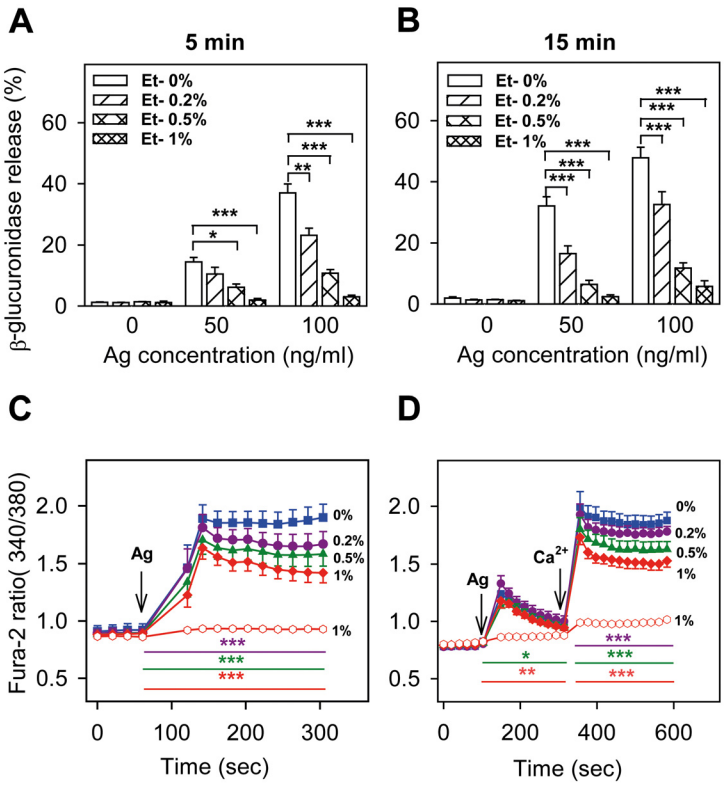

Fig 1. Short-term exposure to ethanol inhibits antigen-induced degranulation and calcium response in BMMCs. IgE-sensitized cells were preincubated for 15 min with various concentrations of ethanol (0–1%), which was also present during antigen-mediated activation. (A, B) Degranulation (release of β-glucuronidase) was measured 5 min (A) or 15 min (B) after exposure of the cells to the indicated concentrations of antigen. (C, D) Calcium response after addition of antigen (arrow, Ag, 100 ng/ml) was measured in the presence of 1 mM extracellular calcium (C), or in its absence (D), followed by addition of 1 mM calcium (arrow, Ca^{2+} in D). Calcium levels in the absence of antigen activation but in the presence of 1% ethanol is also shown in C and D (empty circles). Data are means ± SEs (n = 6–8). Statistical significance of intergroup differences is shown in A and B. In C and D, statistical significance of differences between control cells (0% ethanol) and cells exposed to 0.2% ethanol (violet line), 0.5% ethanol (green line) or 1% ethanol (red line) calculated for the corresponding time intervals (coloured lines) are also indicated.

doi:10.1371/journal.pone.0144596.g001

the inhibitory effect of ethanol was abrogated by Mβ. After addition of calcium, both ethanol and ethanol+Mβ showed comparable responses (Fig 4B). Cells pretreated with sMβ showed increased calcium response and were more resistant to the inhibitory effect of ethanol (Fig 4C). When the difference between sMβ + ethanol and ethanol was calculated, it was lower than the difference between sMβ and controls (Fig 4D). The data suggest that manipulation with the cellular cholesterol modulates sensitivity of antigen-induced calcium response to ethanol, and thus support the lipid-centric hypothesis of ethanol action in this system.

Ethanol exposure or cholesterol removal inhibit expression of cytokine genes in antigen-activated BMMCs

Next we examined the effect of short-term pretreatment of BMMCs with various concentrations of ethanol (0–1%) on antigen-induced expression of cytokines. Data presented in Fig 5A indicate dose-dependent inhibition of antigen-induced mRNA production of TNF-α, IL-6 and IL-13, as determined by qPCR. Transcriptional inhibition of cytokines was also observed in cells with reduced levels of cholesterol after pretreatment with Mβ. When the cells were

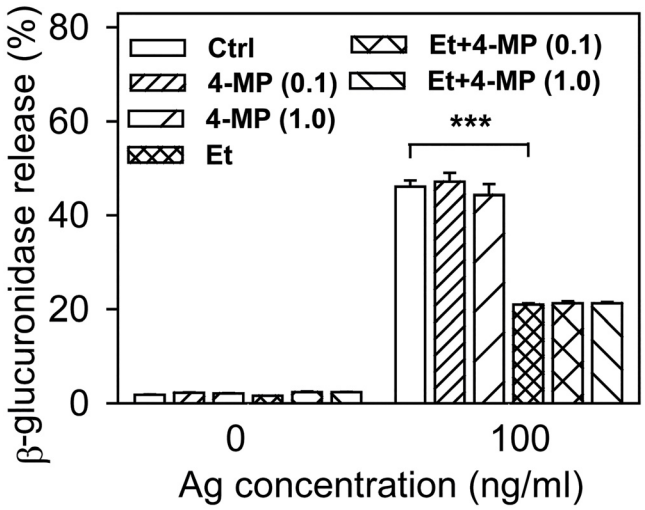

Fig 2. The inhibitory effect of ethanol on antigen-induced degranulation is not affected by blocking alcohol dehydrogenase. IgE-sensitized cells were pretreated or not (Ctrl) for 15 min with ethanol (0.5%) and/or 4-MP (0.1 or 1.0 mM). The cells were non-activated or activated with antigen (100 ng/ml) in the presence of ethanol and/or 4-MP for 15 min and degranulation was determined. Data are means ± SEs (n = 6). Statistical significance of differences between antigen-activated control cells and ethanol-treated cells is also shown. 4-

doi:10.1371/journal.pone.0144596.g002

pretreated simultaneously with both Mβ and ethanol, less-than-additive effects were observed (Fig 5B). These data suggest that both drugs could inhibit a similar signaling pathway.

Protective effect of cholesterol against ethanol-mediated inhibition of ROS in antigen-activated BMMCs

Recent studies indicated that exposure of macrophages to ethanol promoted generation of ROS [42–44]. To determine whether ROS could also be generated by ethanol in BMMCs, we first measured ROS production in cells exposed to various concentrations of ethanol. Our data show that short-term exposure to ethanol had no effect on production of ROS in non-activated cells (Fig 6A). In cells activated with antigen, in accord with previous studies [45,46], ROSs were increased. Pretreatment with ethanol resulted in a dose-dependent decrease of ROS after activation with antigen (Fig 6A). Next we examined whether cholesterol could be involved in ROS production (Fig 6B). IgE-sensitized cells were pretreated or not with ethanol, Mβ, and/or sMβ. In non-activated cells, ethanol had no significant effect on ROS, but pretreatment with Mβ reduced baseline ROS production. sMβ had a lower inhibitory effect on ROS levels than Mβ. In antigen-activated cells, ROS production was more inhibited by Mβ than by ethanol. In contrast, pretreatment with sMβ followed by antigen activation resulted in higher ROS production than in control cells. When ethanol was combined with Mβ, strong inhibition of antigen-induced ROS production was observed, whereas ethanol had no inhibitory effect in cells exposed to sMβ. These data suggest that cholesterol has a dramatic effect on ROS production and its sensitivity to ethanol.

Inhibitory effect of ethanol on tyrosine phosphorylation of FcεRI-related signal transduction proteins

The first biochemically well-defined step in FcεRI signaling is tyrosine phosphorylation of the receptor subunits, followed by formation of the FcεRI signalosome and phosphorylation of

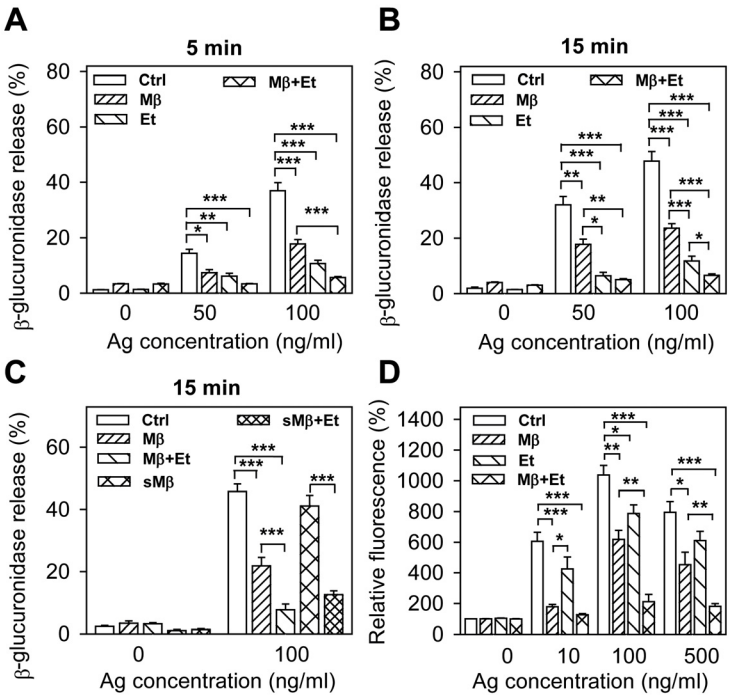

Fig 3. Involvement of cholesterol in the inhibitory effect of ethanol on FcεRI-mediated degranulation. (A, B) IgE-sensitized BMMCs were preincubated for 15 min without (Ctrl) or with Mβ (2 mM), and/or ethanol (0.5%), followed by exposure to the indicated concentrations of antigen in the presence of the drugs. Degranulation was measured 5 min (A) or 15 min (B) after triggering. (C) IgE-sensitized cells were preincubated for 15 min without (Ctrl) or with Mβ (2 mM), sMβ (2 mM), and/or ethanol (0.5%) and then activated (Ag; 100 ng/ml) or not in the presence of the drugs. Degranulation was determined 15 min after triggering. (D) IgE-sensitized cells were preincubated with various drugs as above, then exposed to various concentrations of antigen and cell activation, measured by CD107a (LAMP1) expression, was determined by flow cytometry. Data are means ± SEs (n = 4–12). Statistical significance of the intergroup differences is also shown.

doi:10.1371/journal.pone.0144596.g003

other substrates [47]. Next, we therefore investigated global tyrosine phosphorylation of proteins in non-activated or antigen-activated cells pretreated or not with various concentrations of ethanol. To determine whether there are any changes in association of the tyrosine phosphorylated proteins with membrane domains, the cells were solubilized in solubilization buffer containing 1% Brij-96 and fractionated on sucrose density gradient to separate cellular components according to their solubility in detergents and density. Data presented in Fig 7A indicate distribution of tyrosine phosphorylated proteins in non-activated control cells, not exposed to ethanol. In low-density detergent-resistant membranes (DRM, fractions 1–3), the key tyrosine phosphorylated proteins were transmembrane adaptor proteins PAG and NTAL and SRC family kinase LYN, as determined by immunoblotting with protein-specific antibodies. A number of other tyrosine phosphorylated proteins were observed in detergent-soluble fractions (fractions 6–9). In cells pretreated with various concentrations of ethanol (Fig 7B–7D), there were dose-dependent changes in the distribution of some tyrosine phosphorylated proteins in the low-density and high-density fractions. Densitometry analysis of the immunoblots showed a significant increase in the percentage of tyrosine phosphorylated PAG (Fig 7G) and LYN (Fig 7H) in DRMs from cells exposed to low concentrations of ethanol (0.2%). However, when ethanol was used at a higher concentration (1%), percentage of tyrosine phosphorylated LYN (Fig 7H) and NTAL (Fig 7I) in DRMs was significantly reduced (Fig 7D). In antigen-activated cells, some proteins were more tyrosine phosphorylated in both low- and high-density fractions

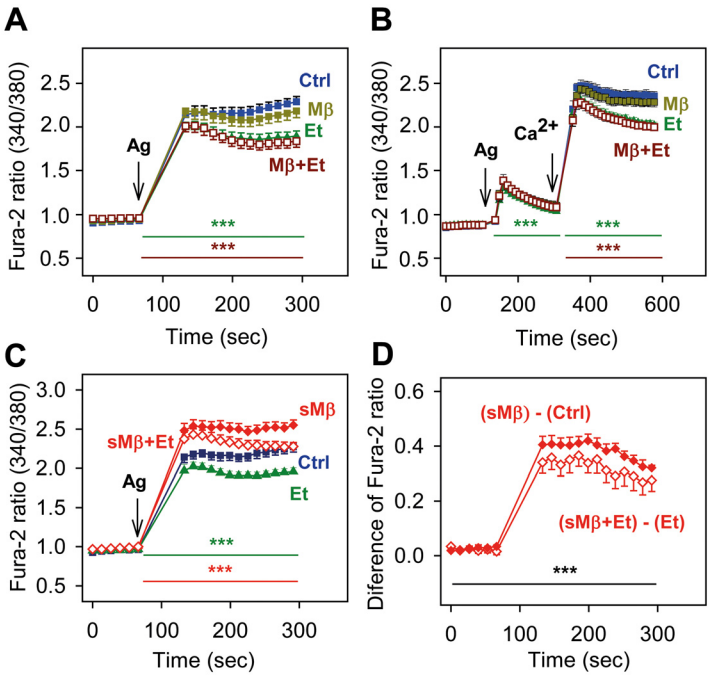

Fig 4. Involvement of cholesterol in the inhibitory effect of ethanol on FcεRI-mediated calcium response. (A, B) IgE-sensitized BMMCs were incubated for 15 min without (Ctrl) or with ethanol (Et, 0.5%) and/or Mβ (2 mM). Calcium response after adding antigen (arrow, Ag; 100 ng/ml) was measured in the presence of the drugs as indicated. The cells were activated in the presence of extracellular calcium (A) or in its absence, followed by addition of 1 mM calcium (B, Ca^{2+}, arrow). (C) IgE-sensitized cells were incubated for 15 min in medium alone (Ctrl) or medium supplemented with ethanol (Et; 0.5%), Mβ saturated with cholesterol (sMβ; 2 mM), or sMβ (2mM) and ethanol (0.5%). The cells were activated in the presence of the drugs with antigen (arrow, Ag; 100 ng/ml) and calcium response was determined. (D) Data from Fig 4C were used to calculate the difference between calcium response in cells exposed to sMβ or Ctrl and sMβ+Et or Et. Data are means ± SEs (n = 6–12). Statistical significance of differences in A and B [Ctrl versus Et-treated cells (green line) and Ctrl versus Mβ+Et-treated cells (brown line)], C [sMβ versus Ctrl (green line) and sMβ+Et versus Et (red line)], and D [sMβ—Ctrl versus sMβ+Et—Et (black line)] calculated for the corresponding time intervals (coloured lines) are also indicated.

doi:10.1371/journal.pone.0144596.g004

(compare Fig 7A and 7E). After activation, the percentage of tyrosine phosphorylated LYN in DRMs was increased by ethanol (Fig 7H). When PAG-, LYN-, or NTAL-specific antibodies were used, no significant differences in the distribution of proteins in DRMs from control and ethanol-pretreated cells were observed (Fig 7G–7H). These data suggest that ethanol at the concentrations used caused fine changes in the cross-talk between signaling molecules rather than global changes in the detergent solubility of plasma membrane proteins.

To determine changes in tyrosine phosphorylation of FcεRI, the receptor was immunoprecipitated and analyzed by immunoblotting with phosphotyrosine-specific antibody, PY-20-HRP conjugate. In non-activated cells, the receptor β and γ subunits exhibited weak tyrosine phosphorylation, and ethanol (0.5%) with or without Mβ had no significant effect on their phosphorylation (Fig 8A). In cells exposed to Mβ alone, a significant increase in tyrosine phosphorylation of FcεRI β and γ subunits was observed, which is in line with our previous studies indicating that cholesterol removal enhances phosphorylation of various substrates in mast cells [48]. Tyrosine phosphorylation of FcεRI β and γ subunits was increased after FcεRI triggering, as expected [47], and pretreatment with Mβ, ethanol, and especially Mβ+ethanol, significantly reduced this phosphorylation (Fig 7A).

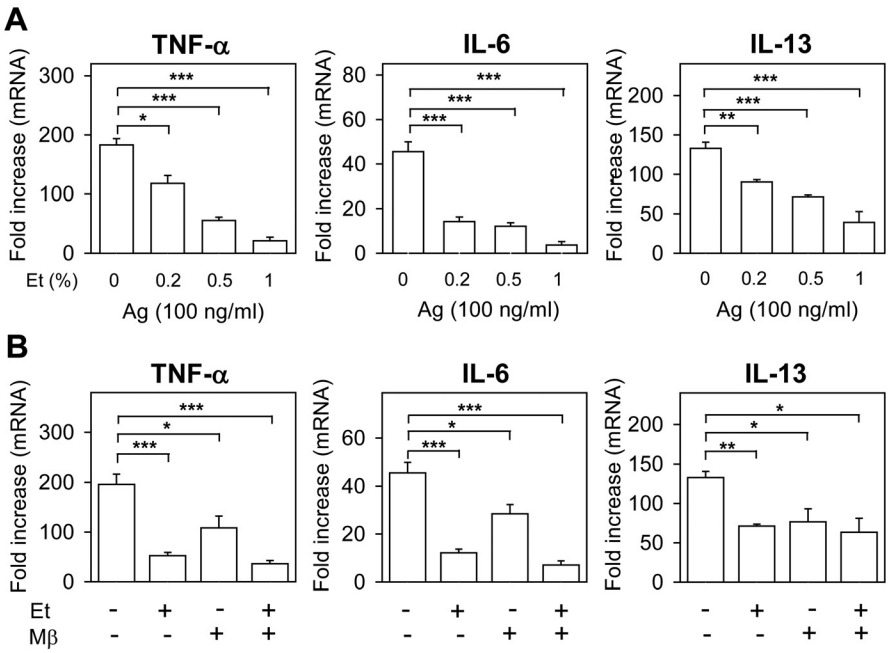

Fig 5. Ethanol or cholesterol removal inhibit expression of cytokine genes in antigen-activated BMMCs. (A) IgE-sensitized cells were preincubated for 15 min with the indicated concentrations of ethanol, which were also present during activation with antigen (100 ng/ml). mRNAs for TNF-α, IL-6, and IL-13 were isolated one hour after triggering and quantified by qPCR. (B) The cells were exposed to medium alone (-), ethanol (0.5%) and/or Mβ (2 mM) and mRNAs for TNF-α, IL-6, and IL-13 were quantified as above. Data are means ± SEs (n = 6–8). The statistical significance of the intergroup differences is also shown.

doi:10.1371/journal.pone.0144596.g005

Tyrosine phosphorylation of several other proteins involved in FcεRI signaling was examined by direct immunoblotting of size-fractionated cell lysates with phosphotyrosine protein-specific antibodies. For these experiments we used IgE-sensitized cells pretreated or not with Mβ and/or ethanol (Fig 8B and 8C). The cells were either non-activated or activated with

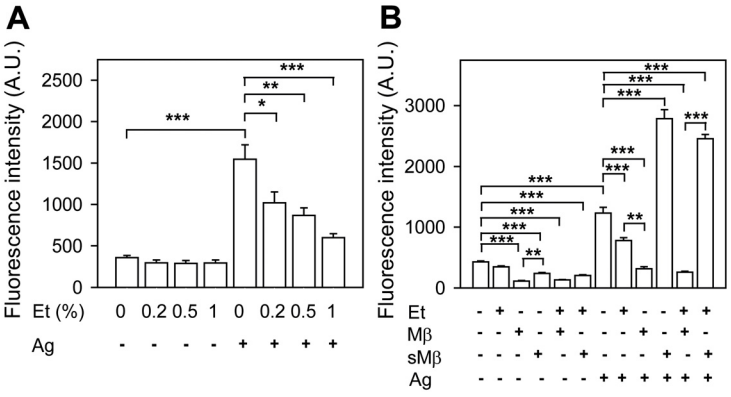

Fig 6. Protective effect of cholesterol against ethanol-mediated inhibition of ROS production in antigen-activated BMMCs. (A) IgE-sensitized cells were incubated for 15 min with the indicated concentrations of ethanol, which was also present during the activation. Then the cells were activated or not with antigen (250 ng/ml) and ROSs were determined using H_2DCFDA as a substrate. The values on y-axes indicate fluorescence intensities observed 10 min after triggering. (B) The cells were exposed to BSS-BSA supplemented or not with ethanol (0.5%), Mβ (2 mM) and/or sMβ (2 mM), and after 20 min activated or not with antigen (250 ng/ml). ROSs were determined as above. Data are means ± SEs (n = 6–8). The statistical significance of the intergroup differences is also shown.

doi:10.1371/journal.pone.0144596.g006

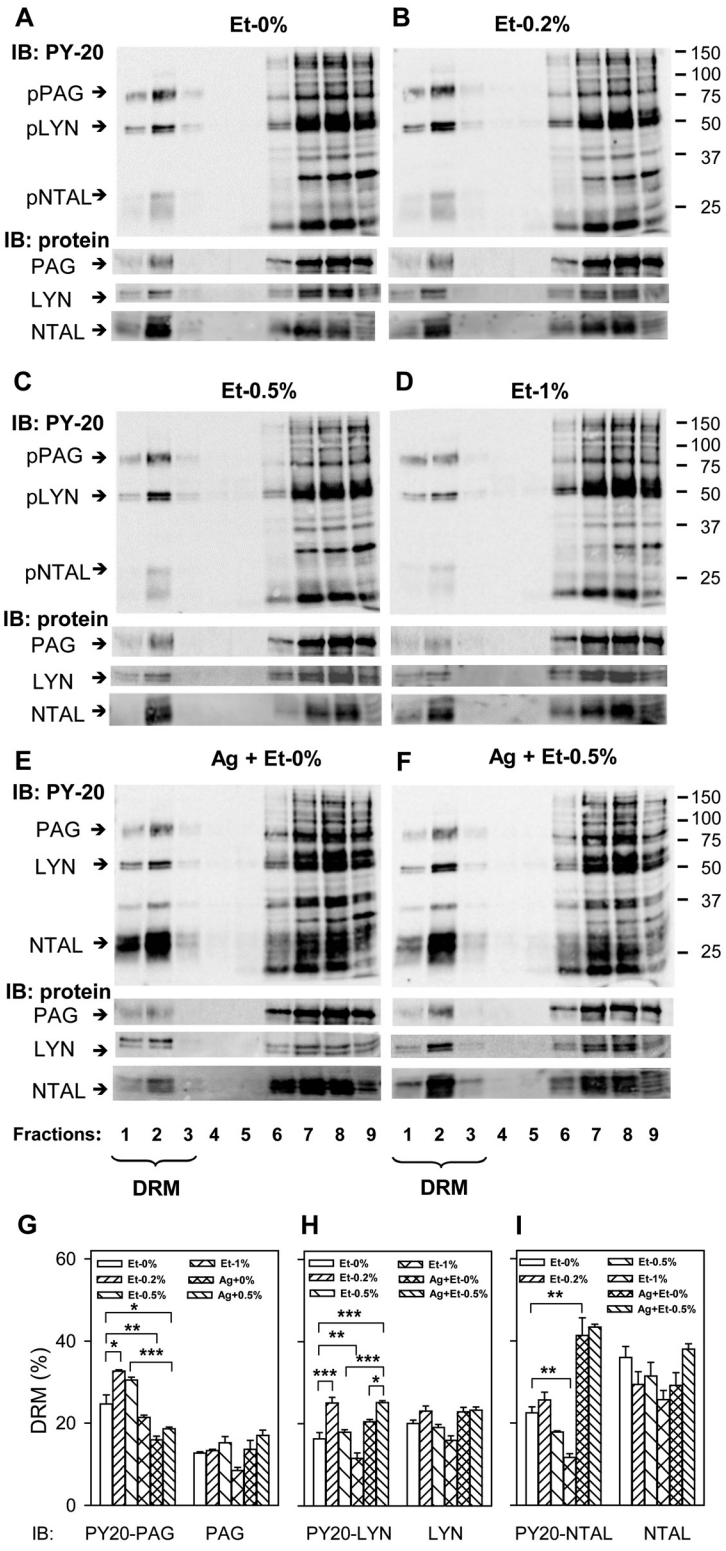

Fig 7. Ethanol-induced changes in protein tyrosine phosphorylation in the plasma membrane domains. (A–F) IgE-sensitized BMMCs were pretreated or not with the indicated concentrations of ethanol for 15 min and then non-activated (A–D) or activated with antigen (E and F; 100 ng/ml) for 5 min. Then the cells were solubilized in 1% Brij-96-containing lysis buffer and fractionated on sucrose density gradient. Individual fractions were collected from the top of the gradient (fraction 1), size fractionated by SDS-PAGE

and examined for tyrosine phosphoproteins by immunoblotting (IB) with PY-20-HRP conjugate (PY-20) or with antibodies specific for PAG, LYN, and NTAL). Positions of PAG, LYN, and NTAL are indicated by arrows on the left. Fractions (1–3) containing detergent-resistant membranes are marked (DRM). Numbers on the right indicate positions of molecular weight markers in kDa. Representative immunoblots from three to four independent experiments are shown. (G–I) All immunoblots were analyzed by densitometry, and the relative amounts of PAG (G), LYN (H), and NTAL (I) and their tyrosine phosphorylated forms (PY-20) in DRMs were determined. Means ± S.E. were calculated and the statistical significance of intergroup differences was determined.

doi:10.1371/journal.pone.0144596.g007

antigen for 5 min. For these studies we selected proteins involved in tyrosine phosphorylation of the FcεRI subunits (LYN and SYK), regulation of calcium response (LAT and PLCγ), and transcriptional regulation of cytokines (STAT5, ERK, AKT). We found that in non-activated cells, Mβ alone and/or ethanol either had no effect (SYK, LAT, pLCγ1, STAT5, and AKT) or slightly but significantly increased phosphorylation of the target (ERK). In antigen-activated cells, pretreatment with Mβ alone and/or ethanol reduced tyrosine phosphorylation of several target proteins (SYK, LAT, STAT5, and AKT). When pPLCγ1 was analyzed, only ethanol and Mβ+ethanol showed inhibitory effects, whereas in the case of pERK, only ethanol alone was inhibitory.

Activity of mouse LYN kinase is regulated by tyrosine phosphorylation of Tyr 507 (a negative regulator; Fig 8D) and Tyr 416 (a positive regulator; Fig 8E). To determine whether Mβ and/or ethanol interfere with phosphorylation of these tyrosines, we performed immunoblotting with LYN-tyrosine-specific antibodies. We found that pretreatment of cells with 0.5% ethanol enhanced phosphorylation at LYN-Tyr 507 15 min after FcεRI triggering. Mβ together with ethanol increased phosphorylation of LYN-Tyr 507 at all intervals. In contrast, LYN-Tyr 416 did not exhibit any significant changes in phosphorylation after Mβ and/or ethanol exposure and antigen activation. These data suggest that ethanol could inhibit FcεRI activation by enhancing tyrosine phosphorylation of LYN-Tyr 507.

Pretreatment with ethanol and/or cholesterol removal does not interfere with FcεRI expression but affects its internalization

Previous studies with other cell types showed that ethanol interferes with internalization of plasma membrane receptors, their trafficking, endocytosis, and recycling [49–51]. FcεRI is rapidly internalized upon antigen triggering [52,53]. Next, we therefore compared internalization of antigen-aggregated FcεRI in BMMCs pretreated or not with ethanol and/or Mβ. Data presented in Fig 9A indicate that 15 min pretreatment with 0.5% ethanol and/or 2 mM Mβ had no effect on the surface expression of the FcεRI and KIT. When the cells were pretreated with ethanol and/or Mβ and then permeabilized and stained for total IgE, no significant differences in the amount of internalized IgE were determined in non-activated cells. In cells activated with antigen for 15 min, IgE was internalized, and pretreatment with ethanol together with Mβ significantly reduced the internalization. Pretreatment with ethanol or Mβ alone had no significant effect on internalization of the antigen-IgE-receptor complexes (Fig 9B and 9C).

Ethanol suppresses IgE-mediated PCA in mice

Finally, we examined whether ethanol could have an inhibitory effect on mast cells under *in vivo* conditions. We used PCA in which local activation of mast cells results in increased vascular permeability, as visibly manifested by leakage of the Evans blue dye into the reaction site of the ear. This leakage was not affected by intraperitoneal administration of 0.5 ml PBS containing 5% ethanol (Fig 10A and 10B; compare 0% and 5%) 30 min before the antigen. In contrast, in mice that were injected with 10% or 20% ethanol in PBS, the vascular permeability of the

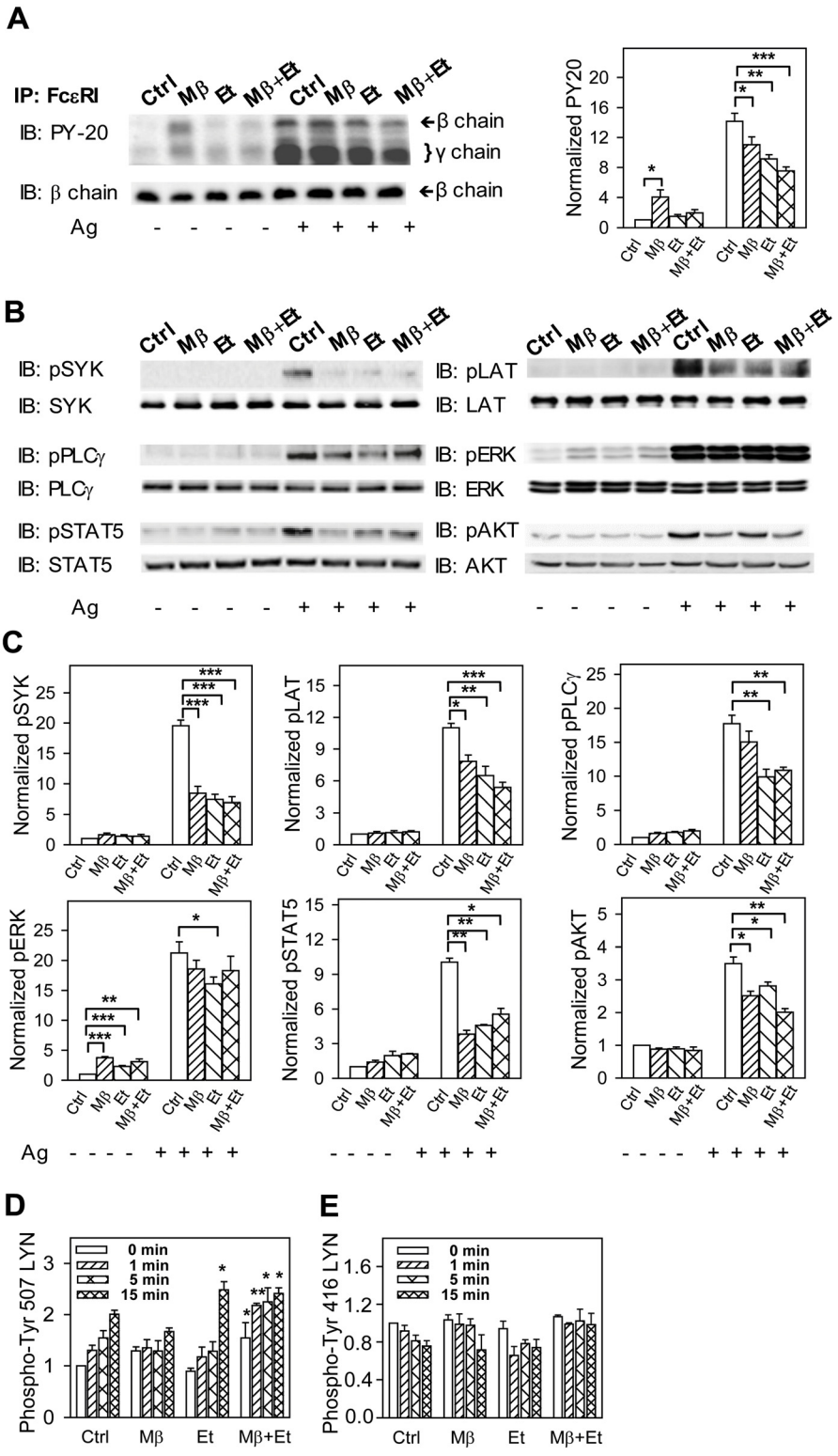

Fig 8. Pretreatment with ethanol inhibits tyrosine phosphorylation of FcεRI β and γ subunits and some other proteins involved in FcεRI signaling. (A) IgE-sensitized cells were preincubated for 15 min with BSS-BSA alone (Ctrl) or supplemented with ethanol (0.5%) and/or Mβ and then activated or not with antigen (100 ng/ml) in the presence or absence of the compounds. After 5 min the cells were solubilized in 0.2% Triton X-100 and FcεRI was immunoprecipitated (IP) from postnuclear supernatants. The

immunoprecipitates were resolved by SDS-PAGE and analyzed by immunoblotting with PY-20-HRP conjugate. For loading controls, the same membrane was stripped and re-blotted with FcεRI-β-chain-specific antibody. Representative immunoblots from three to five independent experiments are shown on the left. The immunoblots were analyzed by densitometry and the fold increase in tyrosine FcεRI-β and -γ chain phosphorylation, normalized to non-activated cells and the amount of FcεRI-β chain, is also shown on the right. (B) IgE-sensitized cells were incubated and activated as above. Five min after triggering the cells were solubilized, size fractionated, and tyrosine phosphorylated proteins were detected by immunoblotting with the phosphoprotein-specific antibodies. Antibodies for the corresponding proteins were used for detection of loading controls. Representative immunoblots from three to four independent experiments are shown. (C) The immunoblots were analyzed by densitometry. Fold increases of protein tyrosine phosphorylation, normalized to control (Ctrl) non-activated cells and the corresponding protein loads are shown. (D and E) IgE-sensitized cells were incubated with the drugs as in A and then activated with antigen (100 ng/ml) in the presence of the drugs for the indicated time intervals. The cells were solubilized, size fractionated, and LYN phosphorylated on Tyr 507 (D) or Tyr 416 (E) was detected by immunoblotting with the corresponding antibodies. After stripping, the membranes were developed for LYN used as a loading control. Fold increase in protein tyrosine phosphorylation, normalized to non-activated cells (Ctrl) and protein load, is also shown. Means ± SEs and the statistical significance of differences in A, C, E, and D were calculated from three to five independent experiments.

doi:10.1371/journal.pone.0144596.g008

ears was attenuated, as evaluated by the extent of Eva blue staining (Fig 10A, 10% and 20%) and amounts of Evans blue extracted from the ears (Fig 10B). The difference in PCA between mice injected with 0.5 ml PBS alone or 0.5 ml PBS containing 10% or 20% ethanol was significant (Fig 10B). No significant intergroup differences were noticed when control ears (not sensitized with IgE) were evaluated. The data suggest that ethanol inhibits FcεRI-induced mast cell activation *in vivo*.

Discussion

Data presented in this study show that short-term exposure of BMMCs to nontoxic concentrations of ethanol inhibits FcεRI-mediated degranulation, calcium response, and production of several cytokines (TNF-α, IL-6, and IL-13) in a dose-dependent manner. To understand the molecular mechanism of the inhibitory effect of ethanol on these activation events we examined various candidate targets. Several lines of evidence suggest that ethanol interferes with the function of FcεRI-cholesterol signalosomes and support the lipid-centric theory of ethanol action in this system, at least at the early stages of cell activation

First, pretreatment of the cells with 4-MP, an inhibitor of alcohol dehydrogenase, together with ethanol had no effect on the inhibitory action of ethanol on degranulation. Thus, inhibition of mast cell activation seems to be caused by ethanol itself and not its metabolites. This conclusion is supported by the finding that up to 2 hours exposure to 2% ethanol in BSS-BSA at 37°C was not toxic to BMMCs. It should also be noted that the cells in this study were pretreated with ethanol only for 15 min before activation, which makes less likely that metabolites are formed and affect signaling pathways.

Second, antigen-mediated degranulation, calcium response, and production of cytokines were also inhibited by Mβ. In cells treated with Mβ, the inhibitory effect of ethanol on degranulation, and IgE receptor internalization was potentiated. Interestingly, when the cells were pretreated with Mβ saturated with cholesterol, the inhibitory effect of ethanol on calcium response was reduced. These data suggest that cholesterol is involved in the inhibitory effect of ethanol.

Third, production of ROS after FcεRI triggering was also inhibited by ethanol in a dose-dependent manner and treatment together with Mβ potentiated the inhibitory effect of ethanol. These findings are in accord with previous data showing that lowering cellular cholesterol by Mβ in hepatocytes inhibits ROS production [54]. Interestingly, exposure of the cells to sMβ enhanced ROS production, and the inhibitory effect of ethanol was abolished, confirming that cholesterol interferes with the inhibitory activity of ethanol.

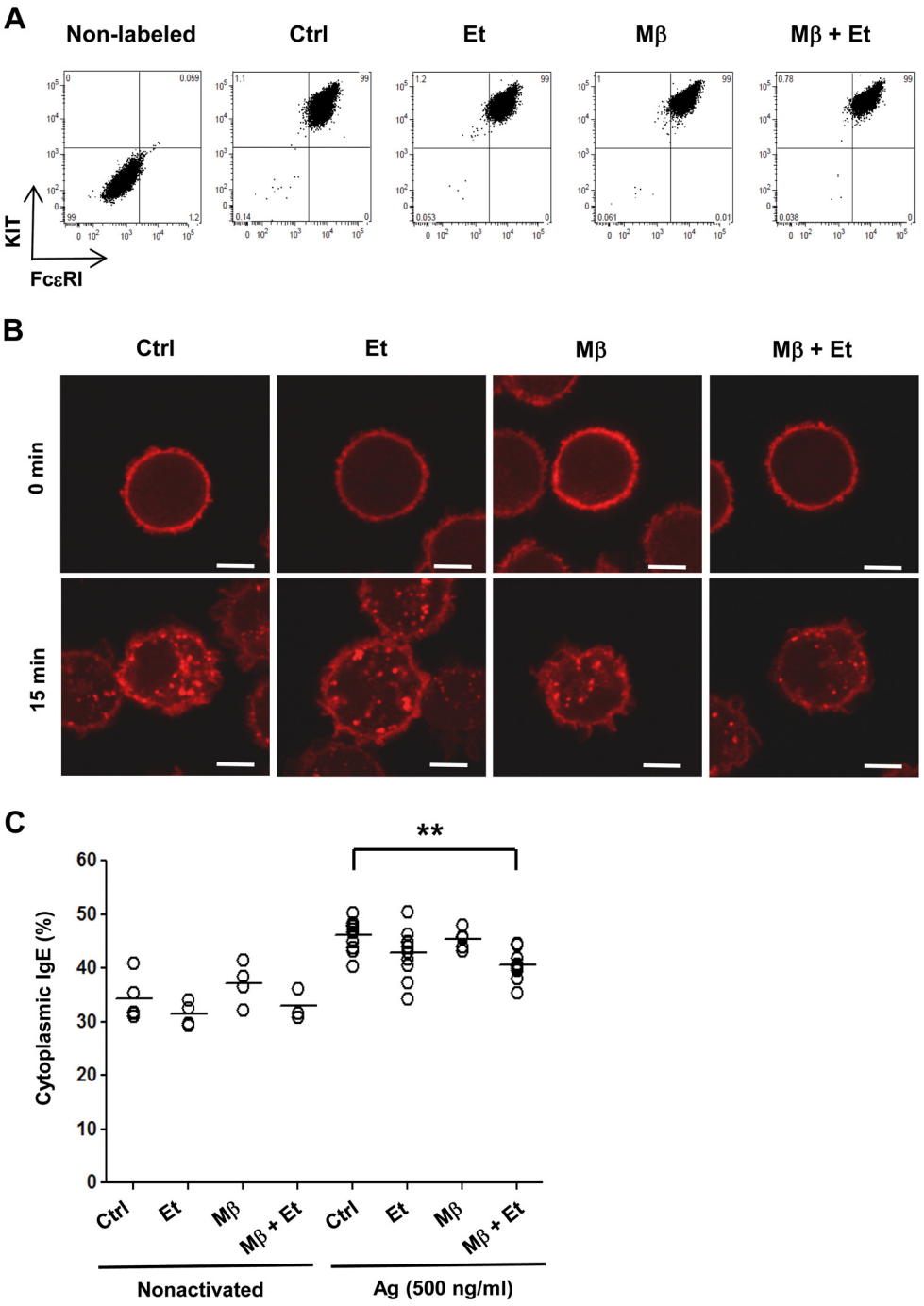

Fig 9. Pretreatment with ethanol and cholesterol removal do not interfere with the FcεRI expression but affect its internalization. (A) The cells were incubated or not for 15 min with BSS-BSA alone (Ctrl) or supplemented with ethanol (0.5%) and/or Mβ (2 mM) and then stained for surface KIT and FcεRI by direct immunofluorescence followed by flow cytometry analysis. (B) IgE-sensitized cells were incubated with the drugs as above and activated or not with antigen (500 ng/ml). After 15 min the cells were fixed, permeabilized, labeled for IgE and analyzed by confocal microscopy. Bars = 5 μm. (C) Distribution of IgE in individual cells was evaluated and the fraction of IgE detected in the cytoplasm was determined. Each spot represents one cell, bars indicate means. Statistical significance of intergroup differences is also indicated.

doi:10.1371/journal.pone.0144596.g009

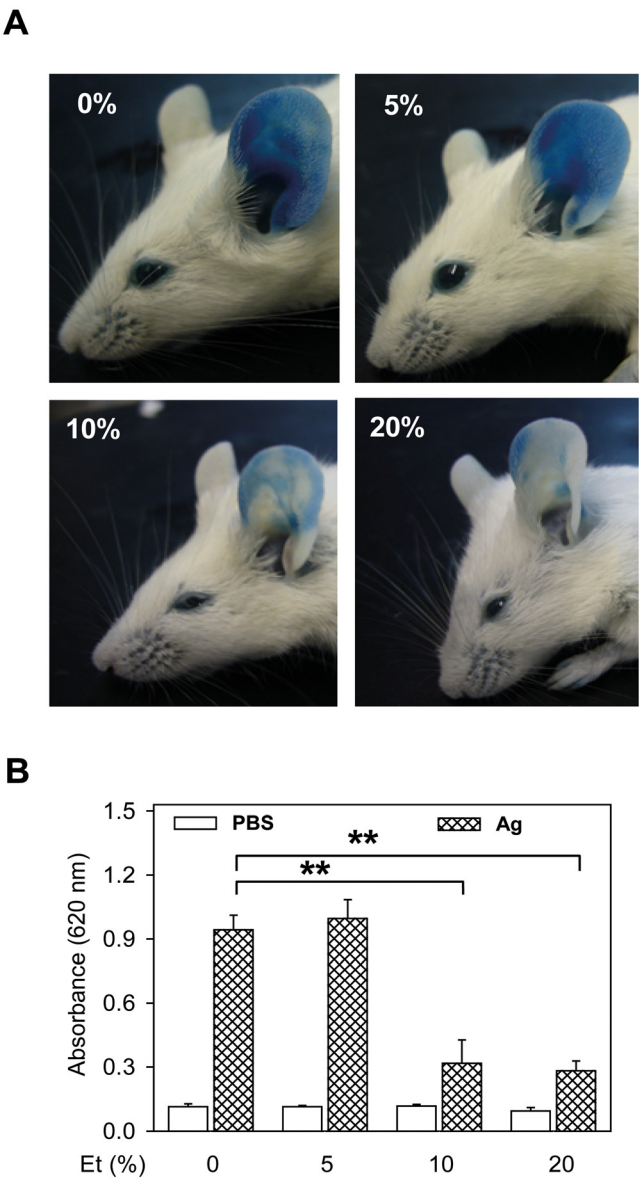

Fig 10. Inhibitory effect of ethanol on mast cell-mediated PCA. PCA was performed as described in Materials and methods. Sensitizing IgE in PBS and PBS alone were injected into left and right ears, respectively. (A) Representative photographs of ears of the mice injected intraperitoneally with 0.5 ml (per mouse weighing 20 g) PBS alone (0%) or with 0.5 ml of PBS containing 5%, 10%, or 20% ethanol, followed by intravenous administration of Evans blue and antigen in PBS. (B) Quantitative data for ear-tissue extracted Evans blue from left (IgE) and right (PBS) ears in mice treated as above. Means ± SEs were calculated from 3–4 animals in each group. Statistically significant differences between control mice injected with PBS alone and mice injected with 10% or 20% ethanol in PBS are shown.

doi:10.1371/journal.pone.0144596.g010

Fourth, immunoprecipitation and immunoblotting analyses showed that ethanol inhibits tyrosine phosphorylation of FcεRI β and γ subunits in antigen-activated cells. Phosphorylation of these targets is the first biochemically well-defined step after FcεRI triggering and depends on the topography and activity of protein tyrosine kinase LYN and protein tyrosine phosphatases in the vicinity of the FcεRI [55,56]. The impaired tyrosine phosphorylation of the FcεRI β and γ subunits could explain reduced tyrosine phosphorylation of the downstream substrates,

including SYK, LAT, PLCγ, AKT, and STAT5 in ethanol-treated cells. Tyrosine phosphorylation of these substrates was also inhibited by Mβ, but no clear additive effect of ethanol and Mβ was observed. This could be related to a similar mechanism of inhibition of both drugs. The reduced phosphorylation of FcεRI by ethanol was neither caused by reduced phosphorylation of the positive regulatory Tyr 416 of LYN nor by enhanced phosphorylation of the negative regulatory Tyr 507 of LYN, which showed enhanced phosphorylation only 15 min after activation. Surprisingly, when Mβ and ethanol were used together, enhanced Tyr 507 phosphorylation was observed at all time intervals after activation and even in non-activated cells. Tyr 507 is phosphorylated by CSK, which is presumably anchored to the plasma membrane via phosphorylated PAG [32]. However, our study did not show enhanced tyrosine phosphorylation of PAG in the cells pretreated with ethanol. The enhanced phosphorylation of Tyr 507 of LYN could be related to our recent findings that PAG is both a positive and negative regulator of FcεRI signaling and that in mast cells there are some other not yet discovered anchors of CSK [32]. Enhanced phosphorylation of LYN Tyr 507 in cells pretreated with ethanol alone, but not in cells treated with Mβ alone, was not accompanied by the corresponding inhibition of SYK phosphorylation, which was observed in cells pretreated with both ethanol alone and Mβ alone. Thus, rather than changes in activity of the LYN kinase, ethanol and Mβ could interfere with formation of the FcεRI signalosome in which cholesterol could play a key role and in which kinases and phosphatases are at equilibrium in nonactivated cells [55]. Nanoscale changes in lateral organization of proteins and lipids in the plasma membrane and enhanced actin polymerization have recently been described in ethanol-pretreated cells [57]. In fact, there could be a direct cross-talk between ethanol and cholesterol, as was noticed in other systems. For example, Furlow and Diamond showed that the interplay between membrane cholesterol and ethanol contributes to alterations of the membrane fluidity, viscosity, and redistribution of surface molecules, which affects neutrophil adhesion, rolling, and tethering behavior [58].

Fifth, internalization of antigen-aggregated FcεRI was significantly inhibited by 15 min pretreatment with Mβ and ethanol. In our previous study we found that cholesterol removal by Mβ enhanced antigen-mediated clustering of the FcεRI [48]. These findings, together with a previous report that aggregated FcεRI can be endocytosed by a clathrin-independent mechanism that appears to be mediated by membrane structures enriched in cholesterol [52], suggest that Mβ and ethanol prevent internalization of the receptor aggregates, which remain for prolonged time intervals on the cell surface.

The capacity of externally added cholesterol to reduce the inhibitory effect of ethanol on calcium and ROS responses are more compatible with the lipid-centric theory than the protein-centric theory of the inhibitory effect of ethanol. How exactly ethanol interacts with lipids and/or how it affects lipid-protein interactions is not known but could involve direct interaction of ethanol with cholesterol [59] and the ability of ethanol to mediate and modify organization of the lipid bilayer structures [7,37]. However, our data do not rule out the possibility that ethanol-protein interactions are also involved in the inhibitory effect of ethanol as was observed in other systems [12,60–62]. This could explain different effects of enhanced cholesterol levels on the inhibitory action of ethanol in various signaling pathways. For example, the observed decrease in the inhibitory effect of ethanol on calcium or ROS responses in cells with enhanced cholesterol levels could reflect the reduced penetration of ethanol through lipid bilayers with increased rigidity caused by cholesterol [63]. On the other hand, ethanol could act directly as an inhibitor of some enzymes involved at later stages of degranulation; this could be an explanation of our finding that degranulation was not protected from the inhibitory effect of ethanol in cells pretreated with sMβ. In this context, Lisboa et al showed that phosphatidic acid produced by phospholipase D (PLD) plays an important role in promoting IgE-dependent

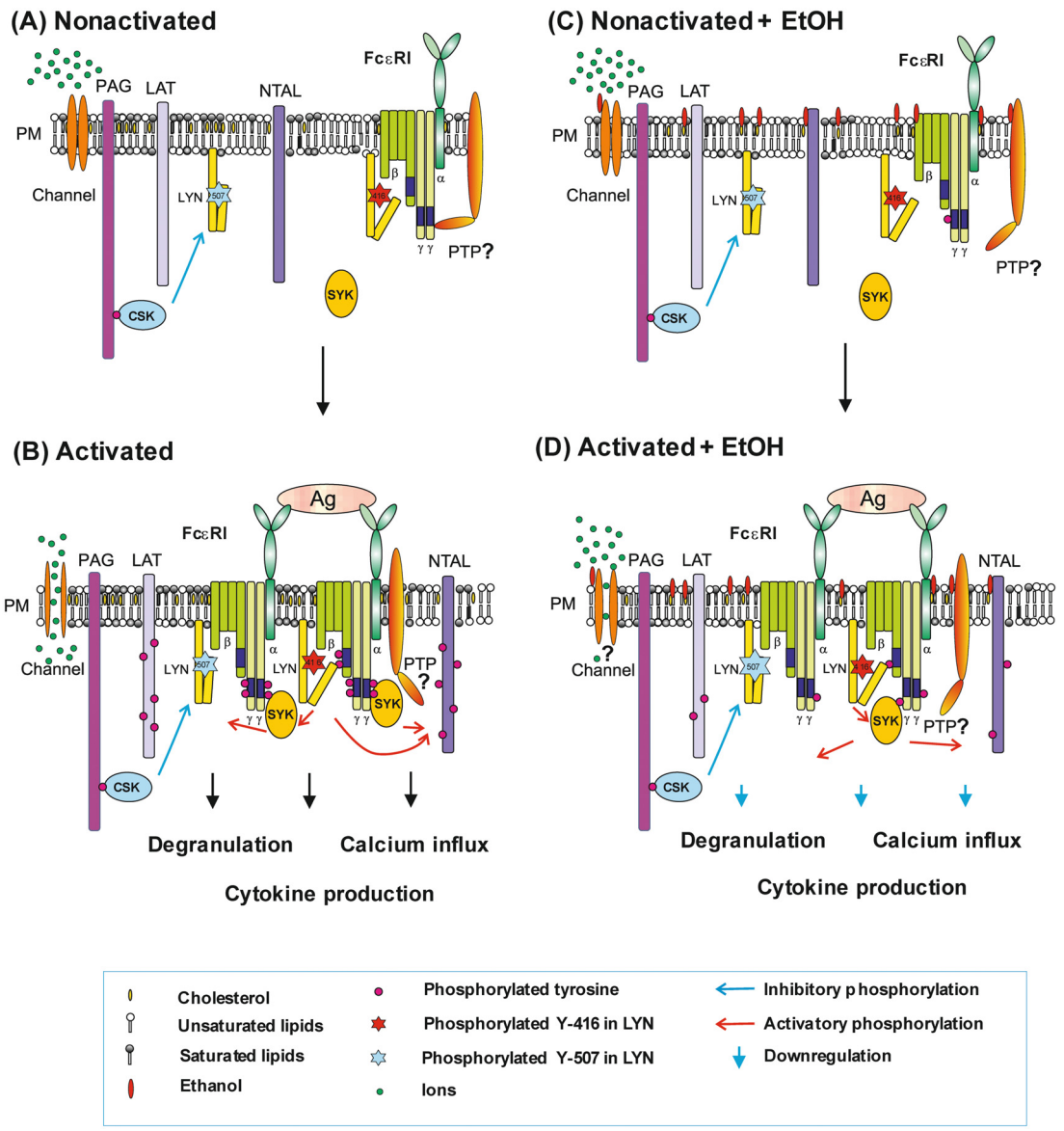

Fig 11. Model of FcεRI-mediated activation in ethanol-pretreated mast cells. In nonactivated cells (A), the topography of FcεRI and other signaling molecules, such as SRC family kinase LYN, protein tyrosine phosphatase (PTP), and adaptor proteins (LAT, PAG, and NTAL), prevents signaling. An important role in this process is played by the plasma membrane cholesterol. Aggregation of the FcεRI-IgE complexes by multivalent antigen (B) induces topographical changes that lead to formation of the FcεRI signalosome and enhanced tyrosine phosphorylation of the FcεRI β and γ subunits by LYN and SYK kinases. This results in enhanced degranulation, calcium response, cytokine production and numerous other events. In the cells exposed to ethanol and/or with reduced amount of cholesterol (C), the topography of plasma membrane molecules is slightly modified, resulting in increased tyrosine phosphorylation of some signaling molecules even in nonactivated cells. Aggregation of the receptor in ethanol-treated cells leads to suboptimal topographical changes resulting in reduced tyrosine phosphorylation of the FcεRI β and γ subunits by LYN and SYK kinases and/or enhanced activity of the corresponding phosphatases (D). This leads to reduced degranulation, calcium response, cytokine production and other events. Ethanol could also bind directly to some cytoplasmic or plasma membrane proteins, such as ion channel proteins, and in this way inhibit the cell signaling.

doi:10.1371/journal.pone.0144596.g011

signaling events within lipid microdomains in mast cells [64]. As a tool they used 1-butanol, which subverts production of phosphatidic acid to the biologically inert phosphatidyl butanol. Similarly, the presence of ethanol could lead to production of phosphatidyl ethanol instead of phosphatidic acid [65] and in this way inhibit FcεRI signaling. However, our and others' data

suggest that ethanol inhibits FcεRI signaling by another mechanism. We found that the inhibitory effect of ethanol on calcium response and ROS production was blocked by exposure of the cells to sMβ, which is unlikely to change production of PA and/or activity of PLD. Furthermore, it has been recently found that mice deficient in PLD1 and PLD2, which do not produce any PA, show no changes in early signaling events after FcεRI triggering [66].

Model of ethanol action on mast cells and their activation by antigen is shown in Fig 11. Exposure of the cells to ethanol leads to changes in properties of plasma membrane and topography of plasma membrane components, resulting in the observed increase in basal tyrosine phosphorylation of some membrane proteins, including FcεRI. When IgE-sensitized and ethanol-treated cells are activated by antigen, tyrosine phosphorylation of the FcεRI β and γ subunits is reduced reflecting suboptimal topography and/or reduced activity of LYN and SYK kinases and/or enhanced activity of protein tyrosine phosphatases in the vicinity of the receptor. Ethanol could also bind to ion channels or some other plasma membrane or cytoplasmic proteins and in this way inhibit various signaling events, including degranulation, calcium response and production of cytokines.

The inhibitory effect of ethanol on mast cell activation was confirmed by experiments *in vivo* in which mast cells were sensitized locally by IgE, and ethanol and antigen was administered intraperitoneally and intravenously, respectively. The results of PCA assays, which reflect the activity of mast cells [67] support previous findings indicating that excessive ethanol consumption is associated with increased risk of infection [68]. Experimental studies with animal and human subjects given ethanol in a controlled setting showed suppression of the innate immunity and inflammation [69–71]. Attention was focused mainly on the inhibitory effect of ethanol on activation of macrophages [72,73], monocytes [74] and T cells [20,75–77]. Although previous studies also indicated that mast cells could be the target of ethanol [24,25], this is the first study showing that ethanol inhibits the earliest events in FcεRI signaling and demonstrate the inhibitory effect of ethanol on mast cells *in vivo*.

Conclusions

In this study we found that 15 min treatment with non-toxic concentrations of ethanol *in vitro* inhibited antigen-induced tyrosine phosphorylation of the FcεRI β and γ subunits, SYK kinase, NTAL adaptor protein, PLCγ, calcium response, production of ROS, degranulation, and expression of cytokine genes in a dose-dependent manner. Early activation events were also inhibited by Mβ, suggesting that cholesterol could be involved. The role of cholesterol in the inhibitory effect of ethanol was supported by the finding that sMβ reduced the inhibitory effect of ethanol on calcium and ROS responses. The data support the lipid-centric theory of ethanol action on the initial stages of FcεRI signaling. The inhibitory effect of ethanol on mast cell activation was also observed in a mouse PCA model *in vivo*, explaining previous findings of the reduced inflammatory response associated with enhanced consumption of ethanol.

Acknowledgments

The authors thank Hana Mrazova and Romana Budovicova for technical and secretary assistance.

Author Contributions

Conceived and designed the experiments: LD MB PD. Performed the experiments: LD TP IH LP VB MB MT. Analyzed the data: LD TP IH LP VB MB MT PD. Contributed reagents/materials/analysis tools: LD PD. Wrote the paper: LD VB IH PD.

References

1. Peoples RW, Li C, Weight FF. Lipid vs protein theories of alcohol action in the nervous system. Annu Rev Pharmacol Toxicol. 1996; 36: 185–201. doi: 10.1146/annurev.pa.36.040196.001153 PMID: 8725387
2. Meyer HH. Zur theorie der alkoholnarkose. I. Mitt. welche eigenschaft der anästhetika bedingt ihre narkotische wirkung? Arch Exp Pathol Pharmakol. 1899; 42: 109–108.
3. Meyer KH. Contribution to the theory of narcosis. Trans Faraday Soc. 1937; 33: 1062–1068.
4. Chin JH, Goldstein DB. Effects of low concentrations of ethanol on the fluidity of spin-labeled erythrocyte and brain membranes. Mol Pharmacol. 1977; 13: 435–441. PMID: 876032
5. Chen SY, Yang B, Jacobson K, Sulik KK. The membrane disordering effect of ethanol on neural crest cells in vitro and the protective role of GM1 ganglioside. Alcohol. 1996; 13: 589–595. S0741832996000730. PMID: 8949954
6. Rowe ES. Thermodynamic reversibility of phase transitions. Specific effects of alcohols on phosphatidylcholines. Biochim Biophys Acta. 1985; 813: 321–330. PMID: 3970925
7. Gray E, Karslake J, Machta BB, Veatch SL. Liquid general anesthetics lower critical temperatures in plasma membrane vesicles. Biophys J. 2013; 105: 2751–2759. S0006-3495(13)01233-2. doi: 10.1016/j.bpj.2013.11.005 PMID: 24359747
8. Ly HV, Longo ML. The influence of short-chain alcohols on interfacial tension, mechanical properties, area/molecule, and permeability of fluid lipid bilayers. Biophys J. 2004; 87: 1013–1033. doi: 10.1529/biophysj.103.034280 PMID: 15298907
9. Seeman P. The membrane actions of anesthetics and tranquilizers. Pharmacol Rev. 1972; 24: 583–655. PMID: 4565956
10. Franks NP, Lieb WR. Molecular mechanisms of general anaesthesia. Nature. 1982; 300: 487–493. PMID: 6755267
11. Franks NP, Lieb WR. Partitioning of long-chain alcohols into lipid bilayers: implications for mechanisms of general anesthesia. Proc Natl Acad Sci U S A. 1986; 83: 5116–5120. PMID: 3460084
12. Ronald KM, Mirshahi T, Woodward JJ. Ethanol inhibition of N-methyl-D-aspartate receptors is reduced by site-directed mutagenesis of a transmembrane domain phenylalanine residue. J Biol Chem. 2001; 276: 44729–44735. doi: 10.1074/jbc.M102800200 PMID: 11572853
13. Ren H, Zhao Y, Dwyer DS, Peoples RW. Interactions among positions in the third and fourth membrane-associated domains at the intersubunit interface of the N-methyl-D-aspartate receptor forming sites of alcohol action. J Biol Chem. 2012; 287: 27302–27312. doi: 10.1074/jbc.M111.338921 PMID: 22715100
14. Borghese CM, Storustovu S, Ebert B, Herd MB, Belelli D, Lambert JJ, et al. The δ subunit of γ-aminobutyric acid type A receptors does not confer sensitivity to low concentrations of ethanol. J Pharmacol Exp Ther. 2006; 316: 1360–1368. doi: 10.1124/jpet.105.092452 PMID: 16272217
15. Brayton RG, Stokes PE, Schwartz MS, Louria DB. Effect of alcohol and various diseases on leukocyte mobilization, phagocytosis and intracellular bacterial killing. N Engl J Med. 1970; 282: 123–128. doi: 10.1056/NEJM197001152820303 PMID: 4982606
16. Gluckman SJ, MacGregor RR. Effect of acute alcohol intoxication on granulocyte mobilization and kinetics. Blood. 1978; 52: 551–559. PMID: 678671
17. Szabo G, Dolganiuc A, Dai Q, Pruett SB. TLR4, ethanol, and lipid rafts: a new mechanism of ethanol action with implications for other receptor-mediated effects. J Immunol. 2007; 178: 1243–1249. 178/3/1243. PMID: 17237368
18. Rimland D, Hand WL. The effect of ethanol on adherence and phagocytosis by rabbit alveolar macrophages. J Lab Clin Med. 1980; 95: 918–926. PMID: 7381298
19. Karavitis J, Murdoch EL, Deburghgraeve C, Ramirez L, Kovacs EJ. Ethanol suppresses phagosomal adhesion maturation, Rac activation, and subsequent actin polymerization during FcγR-mediated phagocytosis. Cell Immunol. 2012; 274: 61–71. doi: 10.1016/j.cellimm.2012.02.002 PMID: 22381996
20. Ghare S, Patil M, Hote P, Suttles J, McClain C, Barve S, et al. Ethanol inhibits lipid raft-mediated TCR signaling and IL-2 expression: potential mechanism of alcohol-induced immune suppression. Alcohol Clin Exp Res. 2011; 35: 1435–1444. doi: 10.1111/j.1530-0277.2011.01479.x PMID: 21463338
21. Pruett SB, Schwab C, Zheng Q, Fan R. Suppression of innate immunity by acute ethanol administration: a global perspective and a new mechanism beginning with inhibition of signaling through TLR3. J Immunol. 2004; 173: 2715–2724. 173/4/2715 [pii]. PMID: 15294990
22. Mandrekar P, Dolganiuc A, Bellerose G, Kodys K, Romics L, Nizamani R, et al. Acute alcohol inhibits the induction of nuclear regulatory factor κ B activation through CD14/toll-like receptor 4, interleukin-1, and tumor necrosis factor receptors: a common mechanism independent of inhibitory κ B α

degradation? Alcohol Clin Exp Res. 2002; 26: 1609–1614. doi: 10.1097/01.ALC.0000036926.46632.57 PMID: 12436048

23. Patel M, Keshavarzian A, Kottapalli V, Badie B, Winship D, Fields JZ. Human neutrophil functions are inhibited in vitro by clinically relevant ethanol concentrations. Alcohol Clin Exp Res. 1996; 20: 275–283. PMID: 8730218

24. Toivari M, Maki T, Suutarla S, Eklund KK. Ethanol inhibits IgE-induced degranulation and cytokine production in cultured mouse and human mast cells. Life Sci. 2000; 67: 2795–2806. S0024320500008638. PMID: 11105996

25. Kennedy RH, Pelletier JH, Tupper EJ, Hutchinson LM, Gosse JA. Estrogen mimetic 4-tert-octylphenol enhances IgE-mediated degranulation of RBL-2H3 mast cells. J Toxicol Environ Health A. 2012; 75: 1451–1455. doi: 10.1080/15287394.2012.722184 PMID: 23116450

26. Rivera J, Kinet J-P, Kim J, Pucillo C, Metzger H. Studies with a monoclonal antibody to the β subunit of the receptor with high affinity for immunoglobulin E. Mol Immunol. 1988; 25: 647–661. PMID: 2971137

27. Rudolph AK, Burrows PD, Wabl MR. Thirteen hybridomas secreting hapten-specific immunoglobulin E from mice with Ig^a or Ig^b heavy chain haplotype. Eur J Immunol. 1981; 11: 527–529. PMID: 6790293

28. Tolar P, Tumová M, Dráber P. New monoclonal antibodies recognizing the adaptor protein LAT. Folia Biol (Praha). 2001; 47: 215–217.

29. Dráberová L, Amoui M, Dráber P. Thy-1-mediated activation of rat mast cells: the role of Thy-1 membrane microdomains. Immunology. 1996; 87: 141–148. PMID: 8666426

30. Volná P, Lebduška P, Dráberová L, Šímová S, Heneberg P, Boubelík M, et al. Negative regulation of mast cell signaling and function by the adaptor LAB/NTAL. J Exp Med. 2004; 200: 1001–1013. PMID: 15477348

31. Kovárová M, Tolar P, Arudchandran R, Dráberová L, Rivera J, Dráber P. Structure-function analysis of Lyn kinase association with lipid rafts and initiation of early signaling events after Fcε receptor I aggregation. Mol Cell Biol. 2001; 21: 8318–8328. PMID: 11713268

32. Draberova L, Bugajev V, Potuckova L, Halova I, Bambouskova M, Polakovicova I, et al. Transmembrane adaptor protein PAG/CBP is involved in both positive and negative regulation of mast cell signaling. Mol Cell Biol. 2014; 34: 4285–4300. doi: 10.1128/MCB.00983-14 PMID: 25246632

33. DiVirgilio F, Steinberg TH, Swanson JA, Silverstein SC. Fura-2 secretion and sequestration in macrophages. A blocker of organic anion transport reveals that these processes occur via a membrane transport system for organic anions. J Immunol. 1988; 140: 915–920. PMID: 3339244

34. Carpenter AE, Jones TR, Lamprecht MR, Clarke C, Kang IH, Friman O, et al. CellProfiler: image analysis software for identifying and quantifying cell phenotypes. Genome Biol. 2006; 7: R100. doi: 10.1186/gb-2006-7-10-r100 PMID: 17076895

35. Christian AE, Haynes MP, Phillips MC, Rothblat GH. Use od cyclodextrins for manipulating cellular cholesterol content. J Lipid Res. 1997; 38: 2264–2272. PMID: 9392424

36. Li TK, Theorell H. Human liver alcohol dehydrogenase: inhibition by pyrazole and pyrazole analogs. Acta Chem Scand. 1969; 23: 892–902. PMID: 4308830

37. Setiawan I, Blanchard GJ. Ethanol-induced perturbations to planar lipid bilayer structures. J Phys Chem B. 2014; 118: 537–546. doi: 10.1021/jp410305m PMID: 24372563

38. Loftsson T, Magnusdottir A, Masson M, Sigurjonsdottir JF. Self-association and cyclodextrin solubilization of drugs. J Pharm Sci. 2002; 91: 2307–2316. doi: 10.1002/jps.10226 PMID: 12379916

39. Nishijo J, Moriyama S, Shiota S. Interactions of cholesterol with cyclodextrins in aqueous solution. Chem Pharm Bull (Tokyo). 2003; 51: 1253–1257.

40. Zidovetzki R, Levitan I. Use of cyclodextrins to manipulate plasma membrane cholesterol content: evidence, misconceptions and control strategies. Biochim Biophys Acta. 2007; 1768: 1311–1324. doi: 10.1016/j.bbamem.2007.03.026 PMID: 17493580

41. Grutzkau A, Smorodchenko A, Lippert U, Kirchhof L, Artuc M, Henz BM. LAMP-1 and LAMP-2, but not LAMP-3, are reliable markers for activation-induced secretion of human mast cells. Cytometry A. 2004; 61: 62–68. doi: 10.1002/cyto.a.20068 PMID: 15351990

42. Yeligar SM, Harris FL, Hart CM, Brown LA. Ethanol induces oxidative stress in alveolar macrophages via upregulation of NADPH oxidases. J Immunol. 2012; 188: 3648–3657. doi: 10.4049/jimmunol.1101278 PMID: 22412195

43. Kim MJ, Nepal S, Lee ES, Jeong TC, Kim SH, Park PH. Ethanol increases matrix metalloproteinase-12 expression via NADPH oxidase-dependent ROS production in macrophages. Toxicol Appl Pharmacol. 2013; 273: 77–89. doi: 10.1016/j.taap.2013.08.005 PMID: 23978445

44. Kim MJ, Nagy LE, Park PH. Globular adiponectin inhibits ethanol-induced reactive oxygen species production through modulation of NADPH oxidase in macrophages: involvement of liver kinase B1/AMP-

activated protein kinase pathway. Mol Pharmacol. 2014; 86: 284–296. doi: 10.1124/mol.114.093039 PMID: 24850909

45. Swindle EJ, Coleman JW, DeLeo FR, Metcalfe DD. FcεRI- and Fcγ receptor-mediated production of reactive oxygen species by mast cells is lipoxygenase- and cyclooxygenase-dependent and NADPH oxidase-independent. J Immunol. 2007; 179: 7059–7071. PMID: 17982097

46. Kuehn HS, Swindle EJ, Kim MS, Beaven MA, Metcalfe DD, Gilfillan AM. The phosphoinositide 3-kinase-dependent activation of Btk is required for optimal eicosanoid production and generation of reactive oxygen species in antigen-stimulated mast cells. J Immunol. 2008; 181: 7706–7712. 181/11/7706. PMID: 19017959

47. Kraft S, Kinet JP. New developments in FcεRI regulation, function and inhibition. Nat Rev Immunol. 2007; 7: 365–378. PMID: 17438574

48. Surviladze Z, Dráberová L, Kovárová M, Boubelík M, Dráber P. Differential sensitivity to acute cholesterol lowering of activation mediated via the high-affinity IgE receptor and Thy-1 glycoprotein. Eur J Immunol. 2001; 31: 1–10. PMID: 11169432

49. Dalton SR, Wiegert RL, Casey CA. Receptor-mediated endocytosis by the asialoglycoprotein receptor: effect of ethanol administration on endosomal distribution of receptor and ligand. Liver Int. 2003; 23: 484–491. PMID: 14986823

50. Methner DN, Mayfield RD. Ethanol alters endosomal recycling of human dopamine transporters. J Biol Chem. 2010; 285: 10310–10317. doi: 10.1074/jbc.M109.029561 PMID: 20133946

51. Pascual-Lucas M, Fernandez-Lizarbe S, Montesinos J, Guerri C. LPS or ethanol triggers clathrin- and rafts/caveolae-dependent endocytosis of TLR4 in cortical astrocytes. J Neurochem. 2014; 129: 448–462. doi: 10.1111/jnc.12639 PMID: 24345077

52. Fattakhova G, Masilamani M, Borrego F, Gilfillan AM, Metcalfe DD, Coligan JE. The high-affinity immunoglobulin-E receptor FcεRI is endocytosed by an AP-2/clathrin-independent, dynamin-dependent mechanism. Traffic. 2006; 7: 673–685. PMID: 16637889

53. Cleyrat C, Darehshouri A, Anderson KL, Page C, Lidke DS, Volkmann N, et al. The architectural relationship of components controlling mast cell endocytosis. J Cell Sci. 2013; 126: 4913–4925. doi: 10.1242/jcs.128876 PMID: 23986485

54. Nourissat P, Travert M, Chevanne M, Tekpli X, Rebillard A, Le Moigne-Muller G, et al. Ethanol induces oxidative stress in primary rat hepatocytes through the early involvement of lipid raft clustering. Hepatology. 2008; 47: 59–70. doi: 10.1002/hep.21958 PMID: 18038449

55. Heneberg P, Draberova L, Bambouskova M, Pompach P, Draber P. Down-regulation of protein tyrosine phosphatases activates an immune receptor in the absence of its translocation into lipid rafts. J Biol Chem. 2010; 285: 12787–12802. doi: 10.1074/jbc.M109.052555 PMID: 20157115

56. Bugajev V, Bambousková M, Dráberová L, Dráber P. What precedes the initial tyrosine phosphorylation of the high affinity IgE receptor in antigen-activated mast cell? FEBS Lett. 2010; 584: 4949–4955. doi: 10.1016/j.febslet.2010.08.045 PMID: 20828563

57. Tobin SJ, Cacao EE, Hong DW, Terenius L, Vukojevic V, Jovanovic-Talisman T. Nanoscale effects of ethanol and naltrexone on protein organization in the plasma membrane studied by photoactivated localization microscopy (PALM). PLoS One. 2014; 9: e87225. doi: 10.1371/journal.pone.0087225 PMID: 24503624

58. Furlow M, Diamond SL. Interplay between membrane cholesterol and ethanol differentially regulates neutrophil tether mechanics and rolling dynamics. Biorheology. 2011; 48: 49–64. doi: 10.3233/BIR-2011-0583 PMID: 21515936

59. Daragan VA, Voloshin AM, Chochina SV, Khazanovich TN, Wood WG, Avdulov NA, et al. Specific binding of ethanol to cholesterol in organic solvents. Biophys J. 2000; 79: 406–415. doi: 10.1016/S0006-3495(00)76302-8 PMID: 10866966

60. Salous AK, Ren H, Lamb KA, Hu XQ, Lipsky RH, Peoples RW. Differential actions of ethanol and trichloroethanol at sites in the M3 and M4 domains of the NMDA receptor GluN2A (NR2A) subunit. Br J Pharmacol. 2009; 158: 1395–1404. doi: 10.1111/j.1476-5381.2009.00397.x PMID: 19788495

61. Das J, Pany S, Rahman GM, Slater SJ. PKC ε has an alcohol-binding site in its second cysteine-rich regulatory domain. Biochem J. 2009; 421: 405–413. doi: 10.1042/BJ20082271 PMID: 19432558

62. Olsen RW, Li GD, Wallner M, Trudell JR, Bertaccini EJ, Lindahl E, et al. Structural models of ligand-gated ion channels: sites of action for anesthetics and ethanol. Alcohol Clin Exp Res. 2014; 38: 595–603. doi: 10.1111/acer.12283 PMID: 24164436

63. Polley A, Vemparala S. Partitioning of ethanol in multi-component membranes: effects on membrane structure. Chem Phys Lipids. 2013; 166: 1–11. doi: 10.1016/j.chemphyslip.2012.11.005 PMID: 23220048

64. Lisboa FA, Peng Z, Combs CA, Beaven MA. Phospholipase d promotes lipid microdomain-associated signaling events in mast cells. J Immunol. 2009; 183: 5104–5112. doi: 10.4049/jimmunol.0802728 PMID: 19794068

65. Jenkins GM, Frohman MA. Phospholipase D: a lipid centric review. Cell Mol Life Sci. 2005; 62: 2305–2316. doi: 10.1007/s00018-005-5195-z PMID: 16143829

66. Zhu M, Zou J, Li T, O'Brien SA, Zhang Y, Ogden S, et al. Differential Roles of Phospholipase D Proteins in FcεRI-Mediated Signaling and Mast Cell Function. J Immunol. 2015. doi: 10.4049/jimmunol.1500665

67. Zhou JS, Xing W, Friend DS, Austen KF, Katz HR. Mast cell deficiency in Kit(W-sh) mice does not impair antibody-mediated arthritis. J Exp Med. 2007; 204: 2797–2802. doi: 10.1084/jem.20071391 PMID: 17998392

68. Happel KI, Nelson S. Alcohol, immunosuppression, and the lung. Proc Am Thorac Soc. 2005; 2: 428–432. doi: 10.1513/pats.200507-065JS PMID: 16322595

69. Gluckman SJ, Dvorak VC, MacGregor RR. Host defenses during prolonged alcohol consumption in a controlled environment. Arch Intern Med. 1977; 137: 1539–1543. PMID: 921440

70. Szabo G, Chavan S, Mandrekar P, Catalano D. Acute alcohol consumption attenuates interleukin-8 (IL-8) and monocyte chemoattractant peptide-1 (MCP-1) induction in response to ex vivo stimulation. J Clin Immunol. 1999; 19: 67–76. PMID: 10080106

71. Boe DM, Nelson S, Zhang P, Bagby GJ. Acute ethanol intoxication suppresses lung chemokine production following infection with Streptococcus pneumoniae. J Infect Dis. 2001; 184: 1134–1142. doi: 10.1086/323661 PMID: 11598836

72. Dolganiuc A, Bakis G, Kodys K, Mandrekar P, Szabo G. Acute ethanol treatment modulates Toll-like receptor-4 association with lipid rafts. Alcohol Clin Exp Res. 2006; 30: 76–85. doi: 10.1111/j.1530-0277.2006.00003.x PMID: 16433734

73. Dai Q, Pruett SB. Ethanol suppresses LPS-induced Toll-like receptor 4 clustering, reorganization of the actin cytoskeleton, and associated TNF-α production. Alcohol Clin Exp Res. 2006; 30: 1436–1444. doi: 10.1111/j.1530-0277.2006.00172.x PMID: 16899048

74. Mandrekar P, Catalano D, Szabo G. Inhibition of lipopolysaccharide-mediated NFκB activation by ethanol in human monocytes. Int Immunol. 1999; 11: 1781–1790. PMID: 10545482

75. Bagasra O, Howeedy A, Dorio R, Kajdacsy-Balla A. Functional analysis of T-cell subsets in chronic experimental alcoholism. Immunology. 1987; 61: 63–69. PMID: 2953674

76. Glassman AB, Bennett CE, Randall CL. Effects of ethyl alcohol on human peripheral lymphocytes. Arch Pathol Lab Med. 1985; 109: 540–542. PMID: 3838884

77. Brodie C, Domenico J, Gelfand EW. Ethanol inhibits early events in T-lymphocyte activation. Clin Immunol Immunopathol. 1994; 70: 129–136. S0090122984710208 [pii]. PMID: 8299228

7.6 CROSS-TALK BETWEEN TETRASPANIN CD9 AND TRANSMEMBRANE ADAPTOR PROTEIN NON-T CELL ACTIVATION LINKER (NTAL) IN MAST CELL ACTIVATION AND CHEMOTAXIS.

Hálová I., Dráberová L., Bambousková M., Machyna M., **Stegurová L**., Smrž D., Dráber P.

J. Biol. Chem., 288(14):9801-14, 2013

THE JOURNAL OF BIOLOGICAL CHEMISTRY VOL. 288, NO. 14, pp. 9801–9814, April 5, 2013

Cross-talk between Tetraspanin CD9 and Transmembrane Adaptor Protein Non-T Cell Activation Linker (NTAL) in Mast Cell Activation and Chemotaxis*

Received for publication, December 27, 2012, and in revised form, February 21, 2013 Published, JBC Papers in Press, February 26, 2013, DOI 10.1074/jbc.M112.449231

Ivana Hálová, Lubica Dráberová, Monika Bambousková[1], Martin Machyna[2], Lucie Stegurová[1], Daniel Smrž[3], and Petr Dráber[4]

From the Department of Signal Transduction, Institute of Molecular Genetics, Academy of Sciences of the Czech Republic, CZ 14220 Prague, Czech Republic

Background: Chemotaxis is regulated by chemoattractants and poorly understood intrinsic regulators.
Results: Aggregation of tetraspanin CD9 leads to activation of mast cells and inhibition of their antigen-driven chemotaxis.
Conclusion: Chemotaxis toward antigen involves cross-talk between immunoreceptor, CD9, transmembrane adaptor proteins, and cytoskeleton-regulatory proteins.
Significance: Tetraspanin CD9 is defined as a novel regulator of mast cell chemotaxis.

Chemotaxis, a process leading to movement of cells toward increasing concentrations of chemoattractants, is essential, among others, for recruitment of mast cells within target tissues where they play an important role in innate and adaptive immunity. Chemotaxis is driven by chemoattractants, produced by various cell types, as well as by intrinsic cellular regulators, which are poorly understood. In this study we prepared a new mAb specific for the tetraspanin CD9. Binding of the antibody to bone marrow-derived mast cells triggered activation events that included cell degranulation, Ca^{2+} response, dephosphorylation of ezrin/radixin/moesin (ERM) family proteins, and potent tyrosine phosphorylation of the non-T cell activation linker (NTAL) but only weak phosphorylation of the linker for activation of T cells (LAT). Phosphorylation of the NTAL was observed with whole antibody but not with its $F(ab)_2$ or Fab fragments. This indicated involvement of the Fcγ receptors. As documented by electron microscopy of isolated plasma membrane sheets, CD9 colocalized with the high-affinity IgE receptor (FcϵRI) and NTAL but not with LAT. Further tests showed that both anti-CD9 antibody and its $F(ab)_2$ fragment inhibited mast cell chemotaxis toward antigen. Experiments with bone marrow-derived mast cells deficient in NTAL and/or LAT revealed different roles of these two adaptors in antigen-driven chemotaxis. The combined data indicate that chemotaxis toward antigen is controlled in mast cells by a cross-talk among FcϵRI, tetraspanin CD9, transmembrane adaptor proteins NTAL and LAT, and cytoskeleton-regulatory proteins of the ERM family.

Mast cells are derived from progenitors that are released from bone marrow into circulation, and subsequently migrate to peripheral tissues where they undergo differentiation and maturation (1). The process plays a vital role in innate and/or adaptive immune response and is controlled by a plethora of different chemoattractants, which require sophisticated mechanisms for their recognition and proper cellular responses (2–4). It is obvious that such mechanisms must involve efficient cross-talk between surface receptors, plasma membrane component organizers, such as tetraspanin, signal transducers, cytoskeletal effectors, and others. Signal transduction mediated by two important mast cell receptors, the high-affinity IgE receptor (FcϵRI)[5] and the stem cell factor (SCF) receptor (KIT), is dependent on the presence of two transmembrane adaptor proteins (TRAPs), the linker for activated T cells (LAT) and the non-T cell activation linker (NTAL, also called LAB or LAT2) (5–8). Both adaptors are structurally similar and serve as plasma membrane docking sites for cytoplasmic signal transduction molecules. TRAPs are characterized by a short extracellular domain, a single transmembrane domain, and a cytoplasmic tail, which has no intrinsic enzymatic activity but possesses various tyrosine-containing motifs and domains. The properties of transmembrane domains and the presence of palmitoylation sites determine the solubility of LAT and NTAL in non-ionic detergents, distribution in the plasma membrane, and some other functional properties (9–11). Despite their

* This work was supported in part by the Projects 301/09/1826, P302/10/1759 and P302/12/G101, 204/09/H084 from Grant Agency of the Czech Republic, Action BM1007 from the European Cooperation in Science and Technology. Project LD12073 COST-CZ-MAST, Project TA01010436 of the Technology Agency of the Czech Republic, Project FR-TI3/067 of the Ministry of Industry and Trade of the Czech Republic, and Institutional Support Grant RVO 68378050.
[1] Supported in part by the Faculty of Science, Charles University, Prague, Czech Republic.
[2] Present address: Max Planck Institute of Molecular Cell Biology and Genetics, Dresden, Germany.
[3] Present address: Institute of Immunology, 2nd Medical School and University Hospital Motol, Charles University, V Úvalu 84, Prague, Czech Republic.
[4] To whom correspondence should be addressed: Laboratory of Signal Transduction, Institute of Molecular Genetics, Academy of Sciences of the Czech Republic, Vídeňská 1083, CZ-14220 Prague 4, Czech Republic. Tel.: 420-241062468; Fax: 420-241062214; E-mail: draberpe@img.cas.cz.

[5] The abbreviations used are: FcϵRI, high-affinity IgE receptor; SCF, stem cell factor; TRAP, transmembrane adaptor protein; LAT, linker for activation of T cells; NTAL, non-T cell activation linker; KD, knockdown; BMMC, bone marrow-derived mast cell; Ag, antigen; ERM, ezrin/radixin/moesin; TNP, 2,4,6-trinitrophenol; 2KO, $Ntal^{-/-}/Lat^{-/-}$ double KO; BSS, buffered saline solution; BSSA, BSS supplemented with 0.1% BSA; $[Ca^{2+}]_i$, concentrations of intracellular Ca^{2+}; 2-PCCF, pair cross-correlation function; F-actin, filamentous actin.

structural similarity, NTAL and LAT were found in different microdomains in plasma membrane (5, 11). Studies with mast cells generated from NTAL or LAT KO mice (5, 6), human mast cells with NTAL knockdown (KD) (7), or rat basophilic leukemia cells with enhanced or reduced NTAL levels (12) showed that NTAL could act either as positive or negative regulator of FcεRI signaling, whereas LAT acts as positive regulator (4, 13). Although the role of these two adaptors in immunoreceptor signaling has been extensively studied, their function in mast cell migration is not fully understood. We have previously shown that NTAL serves as a negative regulator of bone marrow-derived mast cells (BMMCs) migration toward antigen (Ag) but has no apparent role in migration toward SCF (14). However, the role of LAT ablation either alone or together with NTAL on Ag-mediated chemotactic response is unknown.

Tetraspanins, similarly as TRAPs, have no enzymatic activity and regulate signaling events by cross-talk with other plasma membrane-associated protein molecules, including integrins (15–21), G-protein-coupled receptors (21–23), several immunoglobulin superfamily members (24, 25), and PKC (26). Although tetraspanins are involved in a variety of biological and pathological processes (27, 28), it is not clear whether tetraspanins interact with TRAPs and what are consequences of such interactions.

In this study we aggregated tetraspanin CD9 on the surface of mast cells and investigated signaling events elicited by such treatment. We also analyzed the effect of CD9 aggregation on cell activation events induced by Ag-mediated aggregation of the FcεRI, including degranulation, calcium response, phosphorylation of cytoskeleton-regulatory proteins of the ezrin/radixin/moesin (ERM) family, and chemotaxis. Using mast cells derived from NTAL- and/or LAT-deficient mice we studied a cross-talk of these adaptors with CD9 and its impact on mast cell chemotaxis. Finally, we investigated the role of CD9 in activation through the FcεRI and membrane topography of CD9 with respect to NTAL, LAT, and FcεRI. Our data indicate that chemotaxis toward Ag in mast cells is regulated by a cross-talk among CD9, FcεRI, TRAPs, and cytoskeleton-regulatory ERM family proteins.

EXPERIMENTAL PROCEDURES

Antibodies and Reagents—Anti-CD9 mAb (clone 2H9, IgG_1 type) was generated by immunizing a rat (Wistar strain) with BMMCs permeabilized with 0.1% saponin and washed. Hybridoma production and mAb selection was done as described previously (29) with the exception that rat spleen cells instead of mouse spleen cells were used. Specificity of the 2H9 antibody was verified by immunoprecipitation followed by mass spectrometry analysis as described (30) and by cross-immunoprecipitation using commercially available anti-CD9 antibody (KMC8.8, Santa Cruz Biotechnology, Inc.). Isotyping was performed with the IsoStrip Isotyping kit (Roche Diagnostics) following the manufacturer's protocol. $F(ab)_2$ and Fab fragments of the 2H9 antibody were generated using, respectively, $F(ab)_2$ and Fab Preparation Kits (Pierce) according to the manufacturer's protocol. Functionality of both types of the fragments was verified by FACS analysis and SDS-PAGE electrophoresis.

The following mAbs were used: 2,4,6-trinitrophenol (TNP)-specific IgE, clone IGEL b4 1 (31), anti-FcεRI β-subunit (JRK) (32), anti-NTAL (NAP-07) (33), anti-LAT (34), anti-Lyn (35), and anti-CD16/CD32 (2.4G2; directed against extracellular domains of mouse receptors FcγRIIB and FcγRIII; a gift from V. Horejsi). Polyclonal antibodies specific for LAT, NTAL, and IgE have been prepared in this laboratory after immunizing rabbits with the corresponding recombinant proteins or their fragments (36). Polyclonal antibodies specific for phospho-ERK (phospho-Y^{204}), phospho-Akt (phospho-S^{473}), phospho-c-Kit (phospho-$Y^{568/570}$), anti-integrin β1 (CD29), as well as HRP-conjugated goat anti-mouse IgG, and goat anti-rabbit IgG were obtained from Santa Cruz Biotechnology, Inc.; antibodies against phospho-p38 (Y^{182}/T^{180}; $pp38^{Y/T}$), phospho-Ezrin (T^{567})/Radixin (T^{564})/Moesin (T^{558}) ($pERM^{T}$), phospho-Syk (Y^{525}/Y^{526}; $pSyk^{Y}$), phospho-Akt (T^{308}; $pAkt^{T}$), and HRP-conjugated goat anti-rat IgG were obtained from Cell Signaling. Phospho-Tyr-specific mAb (PY-20) conjugated to HRP, anti-CD9 (KMC8), and anti-integrin β1 (HM β1–1) were purchased from BD Biosciences. Anti-mouse FcεRI-FITC conjugate and anti-mouse CD117 (KIT)-APC conjugate were obtained from eBioscience; anti-mouse integrin β1-FITC was from Millipore. Recombinant mouse IL-16 was obtained from Prospec. All other chemicals were obtained from Sigma.

Cells and Lentiviral Infection—BMMCs were derived from C57BL.6 mice of WT ($Ntal^{+/+}$ or $Lat^{+/+}$) or from $Ntal^{-/-}$, $Lat^{-/-}$ or $Ntal^{-/-}/Lat^{-/-}$ double KO (2KO) mice (5). In some experiments, Balb/c mice were also used as indicated in the text. All work with animals was conducted in accordance with institutional (33/2008) and national (2048/2004–1020) guidelines. Bone marrow cells were isolated and cultured as previously described (5). BMMCs deficient in Lyn ($Lyn^{-/-}$) and their WT controls ($Lyn^{+/+}$) were kindly provided by M. Hibbs (Ludwig Institute for Cancer Research, Melbourne, Australia) (37). HEK 293 T/17 packaging cells were purchased from American Type Culture Collection. The cells were grown as adherent monolayer culture in DMEM containing 10% FCS, 100 units/ml of penicillin, and 100 μg/ml of streptomycin. Cultures were passaged regularly every 4–5 days and kept at 37 °C in an atmosphere of 5% CO_2. The cells used for lentivirus production were at passage 4–15. Lentiviral infection was done as described previously (38). A set of murine CD9 shRNAs cloned into the pLKO.1 vector (TRCN0000066393, TRCN0000066394, TRCN0000066395, TRCN0000066396, and TRCN0000066397) were purchased from Open Biosystems. Stable selection was achieved by culturing the transfected cells for 2 weeks in the presence of puromycin (5 μg/ml). Cells were analyzed for CD9 expression by immunoblotting and FACS. Cells with the highest reduction of CD9 protein, obtained with TRCN0000066393 and TRCN0000066395, were selected for further experiments. Cells transfected with empty pLKO.1 vector were used as negative controls.

β-Glucuronidase Release, Ca^{2+} Response, Protein Phosphorylation, and Immunoprecipitation—BMMCs were sensitized in SCF- and IL-3-free culture medium supplemented with IGEL b4 1 mAb (1 μg/ml) for 16 h, unless stated otherwise. Then the cells were washed in buffered saline solution (BSS) supplemented with 0.1% BSA (BSSA), and activated with Ag (TNP-

BSA conjugate, 15–25 mol of TNP/mol of BSA; 100–500 ng/ml, depending on batch), SCF (20–100 ng/ml, depending on batch), or anti-CD9 (0.04–20 μg/ml) at concentrations and times giving maximum degranulation or protein phosphorylation, respectively. For inhibition experiments cells were pretreated with different concentrations of anti-CD9 mAb for 15 min. The extent of secretion was determined by determining the concentration of β-glucuronidase as described previously (39) except that the Infinite 200M (TECAN) plate reader instrument at excitation and emission wavelengths of 355 and 460 nm, respectively, was used. Cells used in calcium response assays were loaded with Fura-2AM as described previously (40) and changes in concentrations of intracellular Ca^{2+} ($[Ca^{2+}]_i$) were determined by spectrofluorometry as the changes in ratios of emissions at 510 nm when the cells were excited at 340 and 380 nm; selected cell activators were added automatically using the injector system (TECAN).

Protein phosphorylation was analyzed by immunoblotting of size-fractionated cell lysates. Cells were centrifuged and resuspended in sample buffer containing 10% SDS with or without 2-mercaptoethanol (2-ME) and then sonicated (3 × 10 s), resolved by SDS-PAGE, and immunoblotted with PY-20-HRP conjugate or with protein-specific antibodies followed by the corresponding secondary antibodies: HRP-conjugated anti-mouse, anti-rat, or anti-rabbit IgG. HRP signal was detected by the ECL reagent (Amersham Biosciences) and quantified by Luminescent Image Analyzer LAS 3000 (Fuji Photo Film Co.). Aida software (Raytest GmbH) was used for analysis.

For immunoprecipitation, postnuclear supernatants were prepared from 10–50 × 10^6 cells lysed in ice-cold lysis buffer (40) supplemented with 1% Nonidet P-40 and 1% *n*-dodecyl-β-D-maltoside (for LAT and NTAL immunoprecipitation), 1% CHAPS (for CD9 immunoprecipitation), or 0.2% Triton X-100 (for FcεRI immunoprecipitation). Target proteins were immunoprecipitated with appropriate antibodies attached to protein A/G PLUS-agarose (Santa Cruz) or Protein A UltraLink Resin (ThermoScientific).

Flow Cytometry Analysis—To quantify surface expression of CD9, BMMCs (3 × 10^5/ml) were exposed for 30 min on ice to 1–10 μg/ml of anti-CD9 followed by a 30-min incubation with FITC-conjugated anti-rat antibody. For detection of other membrane proteins, the cells were directly labeled with anti-mouse FcεRI-FITC, anti-mouse CD117-APC, or anti-mouse integrin β1-FITC conjugate. After a 30-min incubation on ice the cells were washed in ice-cold PBS and evaluated with LSRII flow cytometer (BD Biosciences). Median fluorescence intensities were determined in the FITC or APC channel and further processed using FlowJo software (Ashland, OR). For inhibition experiments, cells were pretreated with anti-CD9 mAb (10 μg/ml) for 15 min.

Chemotactic Response—Chemotactic responses were assayed using 24-well Transwell chambers (Corning) with 8-μm polycarbonate filters in the upper wells. Chemoattractants were added to the lower wells in 0.6 ml of chemotactic medium (RPMI 1640 supplemented with 1% BSA and 20 mM HEPES, pH 7.4). BMMCs (0.3 × 10^6 cells in 120 μl of chemotactic media) were added into each upper well. In experiments with Ag-mediated chemotaxis the cells were sensitized with IgE before the assay. Cells migrating into lower wells within the 8-h incubation period (37 °C, 5% CO_2 in air) were counted using Accuri C6 Flow Cytometer (BD Biosciences).

Electron Microscopy of Immunogold-labeled Membrane Sheets—Ultraclean glass coverslips (15 mm in diameter) were prepared as previously described (11). The coverslips in 24-well plates were coated by overnight incubation at 4 °C with fibronectin (50 μg/ml in PBS), followed by washing with distilled water, and used immediately. BMMCs (1.5 × 10^6) were washed twice with BSSA and then incubated on fibronectin-coated glass coverslips. After 1 h the cells were washed with BSSA and incubated with anti-CD9 antibody (15 μg/ml) in BSSA at room temperature. After 10 min the cells were washed 3 times in PBS and subsequently incubated with the secondary antibody conjugated with 12-nm gold particles. Alternatively, the cells were prefixed in 2% paraformaldehyde for 7 min, washed 3 times in PBS, and immersed in ice-cold HEPES buffer (25 mM HEPES, pH 7.0, 25 mM KCl, 2.5 mM magnesium acetate). Plasma membrane sheets were isolated and fixed in 2% paraformaldehyde in HEPES buffer for 10 min. After fixation, electron microscopy grids were transferred to PBS and target epitopes located on the cytoplasmic side of the plasma membrane were labeled with specific primary antibodies in 0.1% BSA in PBS (rabbit anti-NTAL, 1:200; rabbit anti-LAT, 1:200; mouse anti-FcεRI-β subunit mAb, clone JKR, 4 μg/ml) washed 4 times and subsequently labeled with goat anti-rabbit or anti-mouse secondary antibodies conjugated to gold nanoparticles. After extensive washing the membrane sheets were fixed in 2.5% glutaraldehyde in PBS for 10 min and the grids were transferred to PBS. After 10 min the membranes were stained with 1% OsO_4 in PBS, washed three times for 5 min in water, incubated for 10 min with 1% aqueous tannic acid, washed again in water, and stained for 10 min with 1% aqueous uranyl acetate. Finally, samples were washed twice with water for 5 min, air-dried, and observed with FEI Morgagni 268 electron microscope (FEI Czech Republic) operating at 80 kV. Typically, 10 micrographs covering 22.2 μm^2 of the cell surface were obtained from each grid; at least three independent experiments were made for each condition tested. The coordinates of gold particles were determined by ImageJ (National Institutes of Health). Statistical evaluation of colocalization of two types of particles was based on the program Gold using pair cross-correlation function (PCCF) (41).

Cell Adhesion and Spreading—IgE-sensitized BMMCs were loaded with Calcein-AM and incubated or not with anti-CD9 mAb (10 μg/ml) and/or anti-β1 integrin antibody (20 μg/ml) for 15 min before their transfer into fibronectin-coated wells. Cell adhesion was determined after a 30-min activation of the cells with Ag (50 ng/ml of TNP-BSA) using a TECAN fluorometer with excitation at 485 nm and emission at 538 nm. For cell spreading, wells of 96-well glass-bottom plates (InVitroSci) were coated with 50 μl of fibronectin in PBS (50 μg/ml). After 1 h at 22 °C the wells were washed with PBS, and 30 × 10^3 cells in BSSA were added into each well. Cells were allowed to attach for 30 min at 37 °C, gently washed, and then activated or not with Ag. After 20 min the cells were fixed for 30 min at room temperature with 3% paraformaldehyde in PBS. For filamentous (F)-actin staining, the cells were washed with 50 mM gly-

cine in PBS and then exposed to Alexa Fluor 488-phalloidin conjugate diluted 1:100 in PBS supplemented with L-α-lysophosphatidylcholine (120 μg/ml). After 1 h, the cells were washed in PBS, fixed, and kept in PBS supplemented with Hoechst 33258 stain. They were then examined with the Olympus Scan® system. Image processing and analysis were completed by means of CellProfiler software (Broad Institute, Boston, MA) (42).

Statistical Analysis—Unless specified otherwise, the significance of intergroup differences was evaluated by Student's *t* test.

RESULTS

Aggregation of CD9 Causes Activation of Mast Cells and Tyrosine Phosphorylation of NTAL but Not LAT—In an attempt to contribute to elucidating the role of membrane glycoproteins in mast cell signaling and chemotaxis we studied the properties of a new mAb prepared after immunization of a rat with cellular ghosts obtained after permeabilization of BMMCs with saponin. Previously we (30, 35, 40) and others (43, 44) showed that such ghosts are deprived of soluble cytoplasmic proteins, but possess plasma membrane proteins, cytoskeletal proteins, and nucleus. One of the mAbs prepared against such ghosts, the 2H9, was found to bind to the plasma membrane target (see below) and activate mast cells in a manner different from that known for other mast cell activators, the SCF and IgE-Ag complexes. When BMMCs were exposed to the 2H9 mAb, an increased degranulation (Fig. 1*A*) and calcium response (Fig. 1*B*) were noticed. The responses were comparable with those induced by SCF and lower than those observed in cells activated by Ag. The 2H9 mAb-induced tyrosine phosphorylation of several protein substrates in whole cell lysates was determined by immunoblotting with PY-20-HRP conjugate (Fig. 1*C*). The phosphorylation profile was, however, different from that induced by SCF or Ag (Fig. 1*C*). To identify the proteins that are phosphorylated in cells activated by 2H9 we analyzed several signaling targets using phosphospecific antibodies. For comparison we also quantified the extent of phosphorylation in cells activated by SCF and Ag. Data presented in Fig. 1*D* show that binding of 2H9 mAb had no effect on phosphorylation of Akt on Thr^{308} or Ser^{473}, and induced a weak phosphorylation of ERK and p38. Tyrosine phosphorylation profile of the whole cell lysate (Fig. 1*C*) suggested that NTAL (25–30 kDa) and LAT (36–38 kDa) could be among the proteins phosphorylated in 2H9-activated cells. To verify this, NTAL and LAT were immunoprecipitated from nonactivated or activated cells and tyrosine phosphorylation was determined using PY-20-HRP conjugate. Data in Fig. 1*E* show that tyrosine phosphorylation of NTAL in 2H9-activated cells was more pronounced than in SCF-activated cells but weaker than in Ag-activated cells. Similar analysis of LAT immunoprecipitates showed that 2H9 triggering caused only a weak LAT phosphorylation, comparable with that observed in SCF-activated cells. This was in sharp contrast to Ag-induced activation, which induced a strong phosphorylation of LAT.

Next, we attempted to identify which kinases are involved in NTAL phosphorylation in 2H9-activated cells. Previous studies showed that NTAL in Ag-activated mast cells is phosphory-

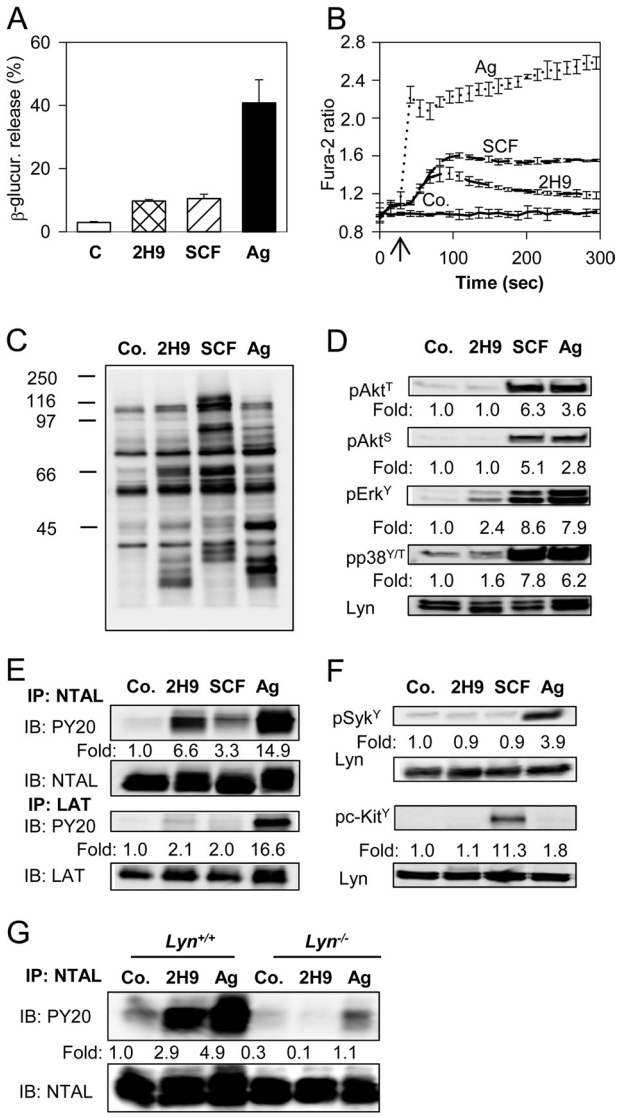

FIGURE 1. **Activation events in mast cells caused by 2H9 mAb.** BMMCs derived from WT C57BL.6 mice were sensitized overnight with TNP-specific IgE. *A,* the cells were exposed to BSSA (nonactivated control, *C*) or activated with 2H9 mAb (10 μg/ml), SCF (100 ng/ml), or Ag (500 ng/ml TNP-BSA) for 30 min. β-Glucuronidase released into supernatant was determined as described under "Experimental Procedures." Mean ± S.D. were calculated from 3 independent experiments performed in triplicates. *B,* IgE-sensitized BMMCs were loaded with Fura-2AM and exposed (*arrow*) to BSSA (*Co.*), 2H9 mAb (10 μg/ml), SCF (100 ng/ml), or Ag (500 ng/ml of TNP-BSA). Changes in $[Ca^{2+}]_i$ were determined by spectrofluorometry as the ratio of emissions at 510 nm when the cells were excited at 340 and 380 nm. *C, D,* and *F,* IgE-sensitized BMMCs were exposed to BSSA (*Co.*) or activated for 3 min with 2H9 mAb (1 μg/ml), SCF (100 ng/ml), or Ag (100 ng/ml TNP-BSA). Whole cell lysates were fractionated by SDS-PAGE and analyzed by immunoblotting with phosphotyrosine-specific mAb PY-20-HRP conjugate (*C*), antibodies specific for the indicated phosphotyrosines, pAkt-T^{308} ($pAkt^T$), pAkt-S^{473} ($pAkt^S$), pErk-Y^{204} ($pErk^Y$), and pp38-Y^{182}/T^{180} ($pp38^{Y/T}$) (*D*), or antibodies specific for pSyk-$Y^{525/526}$ ($pSyk^Y$), or pc-Kit-$Y^{568/570}$ ($pc\text{-}Kit^Y$) (*F*). In *D and F*, anti-Lyn mAb (*Lyn*) was used as a loading control. *E* and *G,* IgE-sensitized BMMCs derived from C57BL.6 mice (*E*) or $Lyn^{+/+}$ or $Lyn^{-/-}$ (*G*) were nonactivated (*Co.*) or activated with 2H9 mAb, SCF (*E* only), or Ag as above. The cells were solubilized in lysis buffer containing 1% Nonidet P-40 and 1% *n*-dodecyl-β-D-maltoside and postnuclear supernatants were immunoprecipitated *(IP)* with NTAL- or LAT-specific rabbit antibodies immobilized on protein A. The immunoprecipitates were analyzed by immunoblotting (*IB*) with phosphotyrosine-specific PY-20-HRP conjugate (PY20). Protein loading was determined by LAT- or NTAL-specific mAbs. In *D-G*, fold-increase in protein phosphorylation normalized to phosphorylation in nonactivated cells and protein loading is also shown. Typical results from at least 4 experiments performed are shown.

A

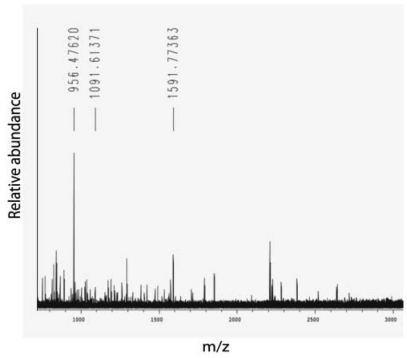

B

Identified peptides	MH+
MicroHPLC-ESI-MS/MS	
K.QLLESFQVK.P	1092.2
K.ELQEFYKDTYQK.L	1592.7
K.QLLESFQVKPC(+57)PEAISEVFNNK.F	2578.8
MALDI/FTMS	
ELQEFYK	956.4762
QLLESFQVK	1091.6137
ELQEFYKDTYQK	1591.7736

C

1 MPVKGGSKCI KYLLFGFNFI FWLAGIAVLA IGLWLRFDSQ TKSIFEQENN HSSFYTGVYI
61 LIGAGALMML VGFLGCCGAV QESQCMLGLF FGFLLVIFAI EIAAAVWGYT HKDEVIKELQ
121 EFYKDTYQKL RSKDEPQRET LKAIHMALDC CGIAGPLEQF ISDTCPKKQL LESFQVKPCP
181 EAISEVFNNK FHIIGAVGIG IAVVMIFGMI FSMILCCAIR RSREMV

D

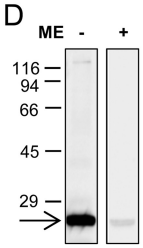

E

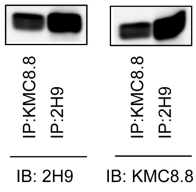

FIGURE 2. **Identification of CD9 as the target protein of 2H9 mAb.** 2H9 mAb covalently bound to protein G resin by dimethylpimelimidate was used to pulldown the target Ag from postnuclear supernatant of BMMCs lysed in a lysis buffer containing 1% Triton X-100. Bound material was eluted from the resin by SDS-PAGE sample buffer, size-fractionated on 12% SDS-PAGE, and stained with Coomassie Brilliant Blue. The major band was excised and analyzed with HPLC in combination with electrospray ionization tandem mass spectrometry (*microHPLC-ESI-MS/MS*) and MALDI-Fourier transform mass spectrometry (*MALDI/FTMS*). *A*, the chart represents the spectrum of detected peptides from trypsin-digested immunoprecipitated protein. Masses of identified peptides (*MH+*) and their corresponding peaks are indicated. *B*, table shows sequences identified by MS analysis with mass of their appropriate MH^+ ions. *C*, positions of the identified sequences (*underlined*) in the whole CD9 protein (NCBI Reference Sequence NP_031683.1). *D*, lysates from BMMCs were diluted with SDS-PAGE sample buffer supplemented with (+) or without (−) 2-mercaptoethanol (*ME*), size fractionated by SDS-PAGE, and analyzed by immunoblotting with 2H9 mAb followed by anti-rat IgG HRP conjugate. The *arrow* indicates the migration of the 2H9 target protein and *numbers on the left* represent the position of the molecular mass markers in kDa. *E*, BMMCs were lysed as in *A* and postnuclear supernatants were immunoprecipitated (*IP*) with 2H9 or KMC8.8 antibodies immobilized to protein G resin. Material released from the resin was fractionated on a 12% SDS-PAGE gel and analyzed by immunoblotting (*IB*) with 2H9 or KMC8.8 Abs. The data presented in *D* and *E* are typical results from at least 3 experiments performed.

lated by the Src family kinase Lyn, Syk kinase, and/or by KIT (45). Proper kinase activity of Syk and KIT is associated with their increased tyrosine phosphorylation (46, 47); we therefore first analyzed changes in phosphorylation of Syk and KIT. We found that these two kinases do not exhibit enhanced phosphorylation after 2H9 treatment (Fig. 1*F*). Control experiments showed, as expected, that Syk and KIT were phosphorylated in cells activated by Ag or SCF, respectively. To determine whether Lyn kinase is involved in 2H9-induced NTAL phosphorylation, NTAL was immunoprecipitated from BMMCs derived from $Lyn^{-/-}$ mice or WT ($Lyn^{+/+}$) mice. Data in Fig. 1*G* show that the absence of Lyn caused no increase in NTAL phosphorylation in 2H9-treated cells. The data suggest that Lyn is the kinase required for phosphorylation of NTAL after exposure of the cells to 2H9 mAb.

To identify the target recognized by the 2H9 mAb, we immunoprecipitated the target Ag from the lysate of resting BMMCs. The isolated material was digested with trypsin and analyzed by peptide mass mapping and peptide sequencing. Both analyses showed that 2H9 mAb binds to mouse CD9 (Fig. 2, *A-C*). The identity of the target was confirmed by decreased binding of the antibody to the cells with decreased expression of CD9 (see below). Furthermore, as determined by immunoblotting experiments, 2H9 mAb recognized a protein with a molecular mass of 22 kDa, corresponding to CD9; only unreduced samples were reactive (Fig. 2*D*). Finally, CD9 immunoprecipitated with commercially available CD9-specific antibody (KMC8.8) reacted by immunoblotting with 2H9 and vice versa (Fig. 2*E*). The combined data indicate that binding of anti-CD9 2H9 mAb induces mast cell signaling events that are different from those induced by Ag or SCF.

CD9 Colocalizes with NTAL—Previous studies showed that despite their similarity in structure and resistance to solubilization in nonionic detergents, NTAL and LAT occupy different membrane microdomains (5, 11). Tetraspanins are known to be present in both raft and nonraft regions of the plasma membrane and therefore it was of interest to determine whether CD9 colocalizes with NTAL and/or LAT. For co-localization experiments we used plasma membrane sheets isolated from BMMCs and probed them with immunogold labeling on the cytoplasmic (NTAL and LAT) or extracellular (CD9) side. Plasma membrane sheets isolated from BMMCs were fixed (i) before anti-CD9 (2H9) mAb exposure, (ii) 5 min after incubation with 2H9 mAb at 37 °C to induced CD9 dimerization, or (iii) after extensive aggregation of CD9–2H9 complexes with secondary anti-rat antibody (Fig. 3). As inferred from representative figures and PCCF analysis, NTAL exhibited some colocalization with CD9 in membranes obtained from cells

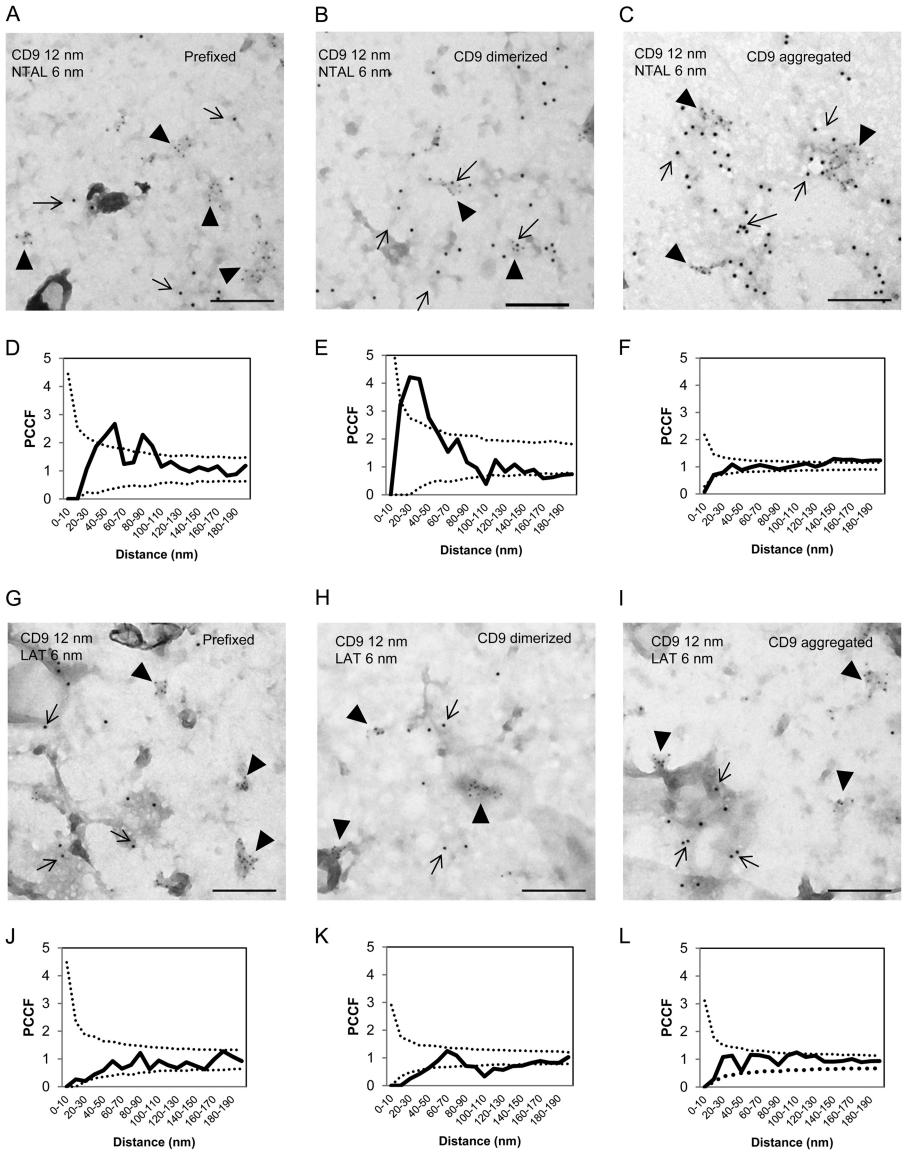

FIGURE 3. **Different colocalization of CD9 with NTAL or LAT.** BMMCs were prefixed in 2% paraformaldehyde and then stained with 2H9 mAb followed by secondary antibody conjugated to 12 nm of gold (*A, D, G,* and *J*). Alternatively, the cells were first treated with 2H9 mAb and then fixed and stained (*B, E, H,* and *K*) or the cells were first treated with 2H9 mAb followed by its aggregation with secondary antibody followed by fixation (*C, F, I,* and *L*). Plasma membrane sheets were then isolated and NTAL (*A-F*) or LAT (*G-L*) on the cytoplasmic side of the plasma membrane were labeled with primary antibodies followed by secondary antibodies conjugated to 6-nm gold particles. Topography of gold particles was evaluated by electron microscopy. Representatives from 3 independent experiments performed are shown (*A-C* and *G-I*). Evaluation of colocalization of 6- and 12-nm gold particles is represented as PCCF analysis for CD9/NTAL labeling (*D-F*) and CD9/LAT labeling (*J-L*). For calculation of PCCF, 20 μm^2 of the plasma membrane sheets was used in each experiment. PCCF indicates colocalization when experimental values (*solid line*) are higher than random distribution of particles presented by a *dotted line*. *Bars*, 200 nm.

fixed before labeling (Fig. 3, *A* and *D*). Antibody-mediated dimerization of CD9 before fixation promoted this colocalization (Fig. 3, *B* and *E*) and extensive CD9 aggregation with secondary antibody led to localization of both CD9 and NTAL in large separated clusters (Fig. 3, *C* and *F*). In contrast, LAT showed no significant colocalization with CD9 at any condition tested (Fig. 3, *G-L*). These data suggest that NTAL (unlike LAT) is located together with CD9 in membrane microdomains; this could form a mechanistical basis for their functional cross-talk.

Inhibitory Effect of Anti-CD9 on Ag-mediated Chemotaxis—Previous studies showed that tetraspanins are involved in regulation of chemotaxis in several cell types, including mast cells (48, 49). In further experiments we therefore tested the effect of the 2H9 anti-CD9 mAb on chemotaxis driven by Ag. We found that pretreatment of IgE-sensitized BMMCs with anti-CD9 mAb inhibited migration toward Ag even at low concentrations of the mAb (Fig. 4*A*). Visual microscopic inspection showed that exposure of the cells to all concentrations of the 2H9 mAb tested in the chemotaxis assays did not induce aggregation of BMMCs (not shown), which could be responsible to the observed inhibitory effect. When commercially available CD9-specific mAb, KMC8, was used, the binding to BMMCs was comparable with 2H9, but no inhibition of Ag-driven chemotaxis was observed (not shown). This suggests unique binding properties of 2H9 mAb. Previous studies showed that mast cells use tetraspanin CD9 as an alternate IL-16 receptor (48). Next we therefore examined whether anti-CD9 antibodies will interfere with IL-16-driven chemotaxis. Data presented in Fig.

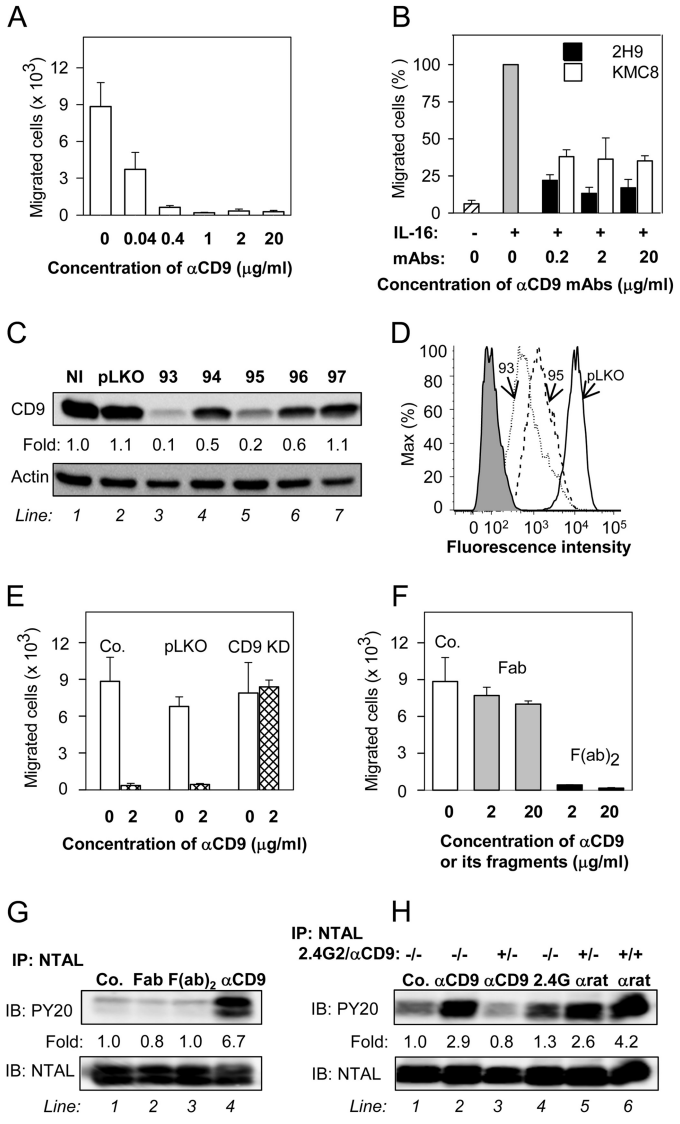

FIGURE 4. **Anti-CD9 mAb inhibits chemotaxis toward Ag and induces tyrosine phosphorylation of NTAL by different mechanism.** *A,* IgE-sensitized BMMCs were pretreated with the indicated concentrations of anti-CD9 mAb 2H9 for 15 min and their chemotactic response toward Ag (250 ng/ml of TNP-BSA in the lower chamber) was determined in the Transwell system. *B,* BMMCs were pretreated or not with the indicated concentrations of anti-CD9 antibodies (2H9 or KMC8) for 15 min and their chemotactic response toward IL-16 (50 ng/ml) was determined as above. Data were normalized toward the maximum response attained in the absence of antibody pretreatment. Migration in the absence of IL-16 is also shown. *C* and *D*, a set of murine CD9 shRNAs cloned into the pLKO.1 vector (TRCN0000066393 (*93*), TRCN0000066394 (*94*), TRCN0000066395 (*95*), TRCN0000066396 (*96*), TRCN0000066397 (*97*)) was used for lentiviral infection of BMMCs. After selection in puromycin, the cellular proteins were size fractionated by SDS-PAGE and analyzed by immunoblotting (*IB*) with anti-CD9 mAb 2H9. Actin was used as a loading control. Immunoblots were evaluated by densitometry and data were normalized to noninfected controls (*NI*) and actin amount. Similar results were obtained in at least three independent experiments. *D*, flow cytometry analysis of surface expression of CD9 in clones selected for further studies, 93 (*dotted line*) and 95 (*dashed line*). *Gray filled region* represents control cells exposed to secondary anti-rat Alexa 488 antibody alone. *Thick line* indicates cells infected with empty vector (pLKO). *E*, BMMCs were deprived of CD9 after infection with CD9 shRNA-containing vector (*CD9 KD*), uninfected cells (*Co.*), or cells infected with empty vector (*pLKO*) served as controls. Ag-mediated chemotaxis in the cells was measured as in *A*. *F*, BMMCs were not exposed (*Co.*) or exposed for 15 min to 2H9 mAb Fab or $F(ab)_2$ fragments, each at a concentration 2 or 20 μg/ml. Their chemotaxis was determined as in *A*. *G,* BMMCs were exposed to BSSA (negative control, Co., *line 1*), 2H9 mAb Fab fragment (*line 2*), 2H9 mAb $F(ab)_2$ fragment (*line 3*), or 2H9 whole molecule (αCD9; *line 4*); each at a concentration of 10 μg/ml. After 5 min the cells were solubilized in lysis buffer containing 1% Nonidet P-40 and 1% *n*-dodecyl-β-D-maltoside and postnuclear supernatants were immunoprecipitated (*IP*) with rabbit anti-NTAL antibody. The immunoprecipitates were analyzed by immunoblotting (*IB*) with phosphotyrosine-specific antibody PY-20-HRP conjugate (*PY20*) or NTAL-specific antibody as a loading control. Fold-increase in protein tyrosine phosphorylation, normalized to phosphorylation in nonactivated cells and NTAL amount is also indicated. A typical experiment from 4 performed is shown. *H,* BMMCs were pretreated or not with anti-CD16/CD32 (2.4G2; 1:50 diluted supernatant) and/or anti-CD9 mAb 2H9 (1 μg/ml, αCD9) for 15 min and then exposed to control BSSA (*Co.*, line *1*), anti-CD9 (1 μg/ml, *lines 2* and *3*), 2.4G2 antibody (1:50 diluted supernatant, *line 4*), or anti-rat IgG (1 μg/ml, *lines 5* and *6*). After 3 min the cells were lysed and NTAL was immunoprecipitated and analyzed as in *G*. Typical results from at least 3 experiments performed are shown. Mean ± S.D. in *A*, *B*, *E*, and *F* were calculated from 3 to 5 independent experiments.

4*B* indicate that both 2H9 and KMC8 inhibited chemotaxis toward IL-16; 2H9 was more potent than KMC8 at all concentrations tested.

To find out whether binding of 2H9 mAb to CD9 is indeed involved in chemotaxis inhibition, we prepared BMMCs with CD9 KD after infection of the cells with lentiviral vectors containing CD9 shRNA. From the 5 vectors used, two of them (TRCN0000066393 (*93*) and TRCN0000066395 (*95*)) strongly inhibited CD9 expression as detected by immunoblotting (Fig. 4*C*) and flow cytometry analysis (Fig. 4*D*) and were used in further experiments. Both vectors gave comparable results and therefore experimental data were pooled for presentation. Data shown in Fig. 4*E* indicate that chemotaxis toward Ag was not reduced by anti-CD9 in cells with CD9 KD, but was inhibited in control cells with empty pLKO vector. Interestingly, cells with reduced expression of CD9 showed normal migration toward Ag. These data indicate that reduced expression of CD9 is compatible with chemotaxis but not with the inhibitory effect of anti-CD9.

In macrophages (50) and platelets (51–53) anti-CD9 induced changes in signaling pathways that were caused by co-cross-linking of CD9 with FcγRs. Next we therefore studied the role of FcγRs in anti-CD9 mAb-mediated inhibition of chemotaxis. We prepared Fab and $F(ab)_2$ fragments of 2H9 mAb and compared their effects on Ag-driven chemotaxis. Pretreatment of BMMCs with anti-CD9 $F(ab)_2$ fragments had a similar inhibitory effect on chemotaxis toward Ag as caused by the whole IgG (compare Fig. 4, *A* and *F*). However, when Fab fragments were used only minimal effects were observed (Fig. 4*F*). These findings suggest that inhibition of chemotaxis is caused by aggregation of CD9 and does not require co-cross-linking of CD9 with FcγR. It should be noted that the binding capacity of the whole 2H9 IgG or its $F(ab)_2$ and Fab fragments to BMMCs was comparable as determined by flow cytometry (not shown).

CD9, Fcγ Receptors, and NTAL Phosphorylation—As shown in Fig. 1, *E* and *G*, NTAL becomes tyrosine phosphorylated after exposure of the cells to anti-CD9 mAb 2H9. The logical next step was therefore to find out whether FcγRs are involved in the process. Whereas intact 2H9 mAb induced strong tyrosine phosphorylation of NTAL (Fig. 4*G*, *line 4*), $F(ab)_2$ as well as Fab fragments of the mAb were without any effect (Fig. 4*G*, *lines 2* and *3*). In this context it should be mentioned that phosphorylation of NTAL was observed when $F(ab)_2$ or Fab fragments of the 2H9 mAb were aggregated by anti-rat IgG antibodies (not shown). These data together with the finding that 2H9 $F(ab)_2$

fragments inhibit Ag-directed chemotaxis indicate that there is no simple connection between 2H9-induced chemotaxis inhibition and NTAL tyrosine phosphorylation. It should be also mentioned that 2H9 mAb was able to induce a weak tyrosine phosphorylation of NTAL in CD9 KD cells (not shown). This indicates that aggregation of residual CD9 on cells with CD9 KD (Fig. 4*D*) is still capable to induce NTAL phosphorylation, but is no longer capable of inhibiting chemotaxis (Fig. 4*E*).

To confirm the role of Fcγ receptors in NTAL phosphorylation induced by 2H9 mAb we used rat 2.4G2 antibody, which is specific for mouse FcγRIIB/FcγRIII. BMMCs pretreated or not with a saturating concentration of 2.4G2 mAb and/or anti-CD9 mAb (1st step) was followed by exposure to anti-CD9 mAb, 2.4G2 mAb, or anti-rat IgG antibody (2nd step). The results show that the 2.4G2 antibody alone caused weak phosphorylation of NTAL (Fig. 4*H*, compare *line 1* with *line 4*). Phosphorylation of NTAL was enhanced when 2.4G2 mAb was aggregated in the 2nd step by anti-rat IgG (Fig. 4*H*, *line 5*). Pretreatment of the cells with 2.4G2 mAb followed by exposure to anti-CD9 mAb resulted in lower phosphorylation of NTAL (Fig. 4*H*, *line 3*) than after exposure of the cells to anti-CD9 alone (Fig. 4*H*, *line 2*). Maximum NTAL phosphorylation was observed when both FcγR and CD9 were extensively aggregated with the first and second layer of antibodies (Fig. 4*H*, *line 6*).

CD9 Aggregation Does Not Interfere with Early FcϵRI-mediated Signaling Events—Because 2H9 binding inhibited chemotaxis toward Ag, we were curious to know whether other Ag-induced signaling pathways are affected and whether CD9 colocalizes with FcϵRI. Our data show that FcϵRI exhibited colocalization with CD9 after CD9 dimerization or a more extensive aggregation (Fig. 5, *A-F*). Furthermore, we could demonstrate that Ag-induced degranulation (Fig. 5*G*), Ca^{2+} release (Fig. 5*H*), and tyrosine phosphorylation of Akt, ERK, and pp38 (Fig. 5*I*) were not affected by anti-CD9 mAb binding. We also found that phosphorylation of the FcϵRI-β subunit was not changed (Fig. 5*J*). These data thus indicate that signaling pathways leading to degranulation after FcϵRI triggering were not affected by anti-CD9. The experiments presented in Fig. 5 were performed with BMMCs from Balb/c mice, but similar results were obtained with BMMCs derived from C57BL/6 mice (not shown).

Different Roles of LAT and NTAL in Mast Cell Chemotaxis and Cross-talk with CD9—Data presented above show that anti-CD9 inhibits chemotaxis toward Ag and induces disparate phosphorylation of NTAL and LAT. Next we investigated the role of NTAL and LAT in mast cell chemotaxis and their sensitivity to the inhibitory effect of anti-CD9. For such experiments, BMMCs were obtained by growing progenitors from bone marrow of $Ntal^{-/-}$, $Lat^{-/-}$, 2KO mice, and corresponding controls. The cells were sensitized with TNP-specific IgE overnight and their migration toward Ag was investigated. Surprisingly, LAT-deficient cells ($Lat^{-/-}$) showed similar Ag-mediated chemotaxis as WT ($Lat^{+/+}$) cells (Fig. 6*A*). In accordance with our previous findings (14), BMMCs derived from $Ntal^{-/-}$ mice exhibited significantly higher migration toward Ag than the corresponding WT ($Ntal^{+/+}$) cells (Fig. 6*A*). These data confirm that NTAL is a negative regulator of Ag-driven chemotaxis. Interestingly, 2KO cells exhibited higher migration toward Ag than WT ($Ntal^{+/+}$ or $Lat^{+/+}$) cells or $Lat^{-/-}$ cells, but lower migration than $Ntal^{-/-}$ cells. This suggests that in the absence of NTAL even LAT negatively regulates chemotaxis. To verify that LAT and NTAL had the anticipated regulatory roles in Ag-induced degranulation, we also tested the release of β-glucuronidase after activation of the cells with Ag. Data shown in Fig. 6*B* indicate, as expected, decreased degranulation in $Lat^{-/-}$ and even more in 2KO cells and an enhanced response in $Ntal^{-/-}$ cells, when compared with the corresponding WT ($Ntal^{+/+}$ or $Lat^{+/+}$) controls.

To examine a functional regulatory cross-talk between NTAL and CD9 in chemotaxis, we compared the effect of anti-CD9 on Ag-driven chemotaxis of $Ntal^{-/-}$ and WT $Ntal^{+/+}$ cells. Data presented in Fig. 6*C* show that treatment with anti-CD9 mAb inhibited chemotaxis toward Ag in both $Ntal^{+/+}$ cells and $Ntal^{-/-}$ cells. However, $Ntal^{-/-}$ cells were more perceptive to the inhibitory effect of anti-CD9 than $Ntal^{+/+}$ cells.

CD9 Forms Complex with β1-Integrin but Anti-CD9 Does Not Interfere with β1-Integrin Function—The most prominent partners of tetraspanins are integrins (15–17, 20, 21). Next, we therefore investigated the effect of anti-CD9 mAb on integrin-mediated signaling pathways. Pretreatment of BMMCs with anti-CD9 mAb inhibited the binding of β1-integrin antibody to the cells (Fig. 7, *A* and *D*). The inhibitory effect was not affected by pretreatment with F-actin disrupting drugs, latrunculin B (0.4 μM, 30 min) or cytochalasin D (1 μM, 30 min; data not shown). This suggests that F-actin-dependent events, such as internalization, are not responsible for the observed inhibitory effect. On the other hand, pretreatment of the cells with anti-CD9 mAb had no effect on the binding of antibodies against FcϵRI and KIT (Fig. 7, *B-D*); these data support the concept that integrin is in close proximity to CD9. Immunoprecipitation data indicated that CD9 and β1-integrin are physically associated in complexes after solubilization of the cells in lysis buffer containing 1% CHAPS (Fig. 7*E*). To investigate the functional cross-talk between CD9 and β1-integrin, we tested the effect of anti-CD9 on Ag-induced adhesion of mast cells to fibronectin. It is remarkable that although anti-CD9 mAb blocked the binding of anti-β1 integrin antibody to the cells, no significant inhibition of anti-CD9 on adhesion to fibronectin was observed. As a control we used antibody against β1-integrin and found that it significantly inhibited adhesion of BMMCs to the fibronectin (Fig. 7*F*). We also tested the effect of anti-CD9 on Ag-induced spreading of mast cell on surfaces coated with fibronectin. Data presented in Fig. 7, *G* and *H*, indicate that binding of anti-CD9 at saturation concentrations to BMMCs had no significant effect on Ag-induced spreading of the cells to fibronectin. The combined data indicate that although CD9 forms complexes with β1-integrin, binding of anti-CD9 mAb does not interfere with the studied β1-integrin functions.

Cross-talk between CD9 and Cytoskeleton-regulatory Proteins of the ERM Family—An important feature of cell activation and chemotaxis is a rapid and extensive communication between plasma membrane components and cellular cytoskeleton. This process is regulated by conformational changes in ERM family proteins caused by transient dephosphorylation of their regulatory threonines. Although such changes have been documented in immunoreceptor-activated B cells, T cells, and

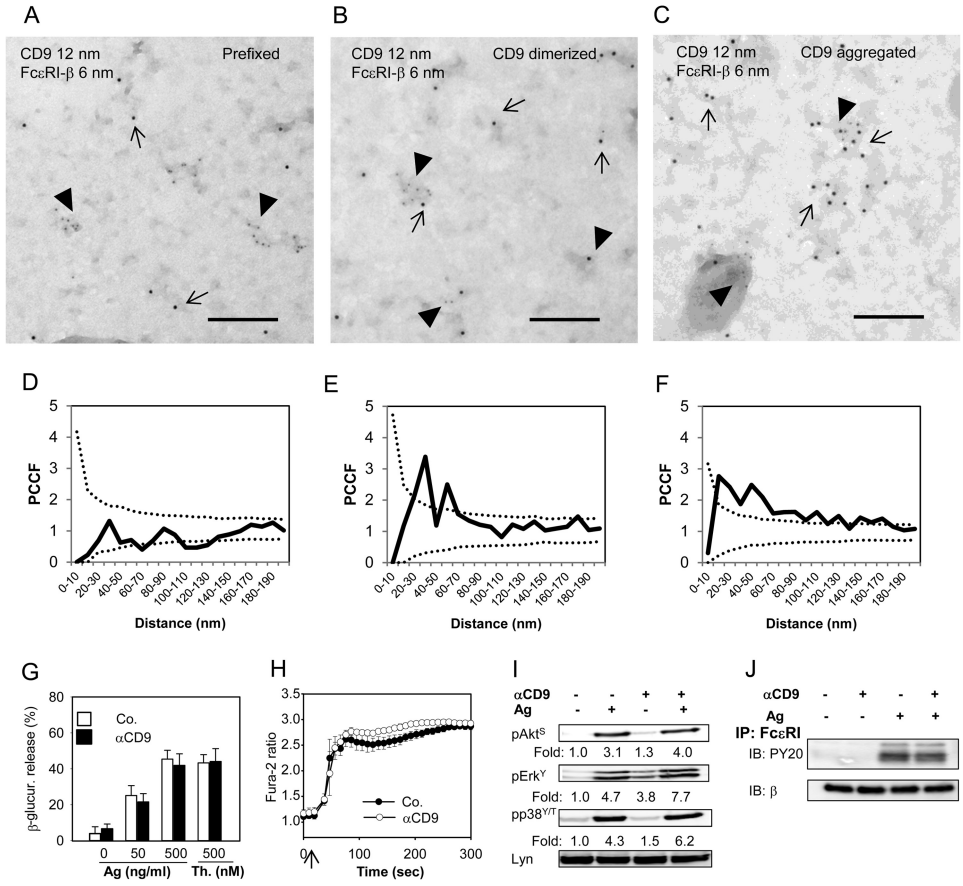

FIGURE 5. **CD9 colocalizes with FcεRI on the plasma membrane but CD9 aggregation does not interfere with early Ag-induced activation events.** *A* and *D*, BMMCs derived from Balb/c mice were prefixed with paraformaldehyde and then labeled with anti-CD9 mAb 2H9 followed by secondary anti-rat antibody-12 nm gold conjugate. Plasma membrane sheets were then isolated and the FcεRI-β subunit was labeled on the cytoplasmic side of the membrane with JRK mAb followed by secondary anti-mouse antibody-6 nm gold conjugate. Colocalization of CD9 (12 nm gold particles) and FcεRI-β (6-nm gold particles) was analyzed by electron microscopy (*A*) and evaluated by PCCF (*D*) as described in the legend to Fig. 3. *B* and *E*, BMMCs were exposed to 2H9 mAb (CD9 dimerized) before fixation and labeling for CD9; other procedures and evaluations were as in *A* and *D*. *C* and *F*, the cells were exposed to 2H9 mAb followed by the secondary anti-mouse antibody (CD9 aggregation) and then fixed and further processed as in *A* and *D*. In *A-C* representatives from 3 independent experiments are shown. *Bars*, 200 nm. *G-J*, IgE-sensitized BMMCs derived from Balb/c mice were pretreated (αCD9) or not (*Co.*; −) with anti-CD9 mAb 2H9 (10 μg/ml) for 15 min before activation. *G*, the cells were exposed to various concentrations of Ag (0–500 ng/ml TNP-BSA) or 500 nM thapsigargin (*Th.*) and 30 min later amounts of β-glucuronidase released into the cell supernatants were determined. Mean ± S.D. were calculated from at least 3 independent experiments performed in triplicates. *H*, the cells were loaded with Fura-2AM at the time of exposure to anti-CD9 and stimulated (*arrow*) with Ag (500 ng/ml of TNP-BSA). $[Ca^{2+}]_i$ was measured as described in the legend to Fig. 1*B*. Mean ± S.D. were calculated from 3 independent experiments performed in triplicates. *I*, IgE-sensitized BMMCs were exposed (+) or not (−) to anti-CD9 mAb 2H9 and then activated (+) or not (−) with Ag (100 ng/ml of TNP-BSA) for 3 min. Whole cell lysates were prepared and analyzed by immunoblotting with antibodies specific for pAkt-S^{473} (pAkt^S), pErk-Y^{204} (pErk^Y) or pp38-Y^{182}/T^{180} (pp38$^{Y/T}$); anti-Lyn mAb (*Lyn*) was used as a loading control. Fold-increase in protein phosphorylation, normalized to phosphorylation in nonactivated cells and protein loading is also shown. Typical results from at least 4 experiments performed are shown. *J*, IgE-sensitized BMMCs were exposed (+) or not (−) to anti-CD9 mAb and then activated by Ag (+; 250 ng/ml of TNP-BSA) or not (−). After 5 min the cells (15×10^6 per sample) were solubilized in lysis buffer containing 0.2% Triton X-100 and FcεRI was immunoprecipitated from postnuclear supernatants by anti-IgE antibody immobilized to Protein A beads. Tyrosine phosphorylation of the receptor subunits was evaluated with PY-20-HRP conjugate (PY-20). The amount of immunoprecipitated receptor was estimated by immunoblotting (after stripping of the membrane) with JRK mAb recognizing FcεRI β subunit. A typical experiment from 3 performed is shown.

mast cells (54–58), whether aggregation of CD9 could also induce such dephosphorylations is unknown. We have examined the phosphorylation status of the regulatory threonine after exposure of BMMCs to anti-CD9 mAb 2H9, SCF, or Ag and found that all 3 activators significantly reduced phosphorylation of the regulatory threonine (Fig. 7, *I* and *J*).

DISCUSSION

Migration of mast cell progenitors from bone marrow to connective tissues and subsequent movement of mature mast cells to the sites of inflammation is crucial for proper functioning of innate and adaptive immunity. Mast cell migration is directed by chemoattractants, which are produced by a variety of cells localized in different target tissues, as well as by intrinsic mast cell regulators that are still poorly understood (2). This study was initiated by functional screening of mAbs prepared after immunization of rats with cellular ghosts obtained by treatment of BMMCs with saponin. One of the antibodies, 2H9, recognizing tetraspanin CD9, was found capable to induce cell activation and inhibit Ag-driven mast cell chemotaxis. Several lines of evidence presented in this study indicate that 2H9-mediated CD9 aggregation triggers signaling pathways, which are different from those activated through FcεRI or KIT, and have impact on mast cell chemotaxis.

First, exposure of BMMCs to CD9-specific mAb 2H9 resulted in phosphorylation of several signal transduction proteins. Importantly, the phosphorylation profile of the target proteins differed from that produced by SCF- or Ag-mediated

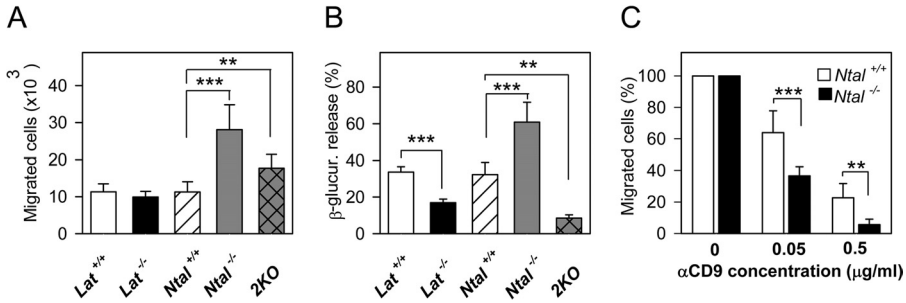

FIGURE 6. **Different roles of LAT and NTAL in mast cell chemotaxis and cross-talk with CD9.** *A*, BMMCs derived from $Lat^{-/-}$, $Ntal^{-/-}$, 2KO, and corresponding littermate ($Lat^{+/+}$, $Ntal^{+/+}$) control mice were sensitized overnight with TNP-specific IgE and their migration toward Ag (250 ng/ml of TNP-BSA) was tested in the Transwell system. *B*, the same IgE-sensitized BMMCs as in *A* were activated with Ag (250 ng/ml TNP-BSA) for 30 min and β-glucuronidase released into the supernatant was determined as described under "Experimental Procedures." *C*, BMMCs from $Ntal^{+/+}$ and $Ntal^{-/-}$ mice were sensitized with IgE and treated with the indicated concentrations of anti-CD9 mAb 2H9. Chemotaxis toward Ag was determined as in *A*. Numbers of cells migrating toward Ag were normalized to controls, 2H9 nontreated cells. Mean ± S.D. were calculated from 3 to 5 independent experiments performed in duplicates. **, $p < 0.01$; ***, $p < 0.001$.

activation (Table 1). Specifically, 2H9 mAb induced stronger phosphorylation of NTAL than activation through KIT but weaker than activation via FcεRI. On the other hand, several proteins, which were phosphorylated in KIT- and FcεRI-activated cells, were either not at all or only weakly phosphorylated after CD9 triggering (Akt, Erk, and p38). Other proteins, which were strongly phosphorylated after Ag-induced activation (Syk and LAT), showed no or only weak tyrosine phosphorylation after CD9 triggering. Enhanced phosphorylation of NTAL in anti-CD9-treated cells was only observed when whole IgG was used; Fab and $F(ab)_2$ fragments had no effect. This suggested that co-cross-linking of CD9 and Fcγ receptor(s) is required for tyrosine phosphorylation of NTAL and other targets. This conclusion was corroborated by experiments where antibody specific for FcγRIIB/FcγRIII induced tyrosine phosphorylation of NTAL, on the one hand, and, on the other, partially inhibited NTAL phosphorylation after exposure to anti-CD9. Involvement of Fcγ receptors in CD9 signaling was also described in CD9-dependent activation of platelets (53, 59) and macrophages (50).

Second, binding of anti-CD9 to target structures on the surface of mast cells resulted in weak calcium and degranulation responses, comparable with those observed in SCF-activated cells (Table 1). However, because tyrosine phosphorylation of LAT was lower in cells activated through CD9 than through KIT and because phosphorylated NTAL is unable to bind phospholipase γ and thus substitute for phosphorylated LAT in calcium metabolism (5, 6), it is evident that activation through CD9 or KIT is initiated by different activation pathways. In this connection it should be noted that pretreatment with anti-CD9 had no significant effect on subsequent binding of IgE to FcεRI and on Ag-induced degranulation, Ca^{2+} responses, and tyrosine phosphorylation of numerous substrates. In this respect, CD9 seems to differ from CD81, another tetraspanin, whose Ab-mediated aggregation inhibited Ag-induced degranulation in rat basophilic leukemia cells without affecting the Ca^{2+} response or protein tyrosine phosphorylation (60).

Third, electron microscopy studies on isolated plasma membrane sheets disclosed colocalization of CD9 with NTAL, but not with LAT, in quiescent cells. After CD9 dimerization the colocalization of CD9 with NTAL became even more prominent. This finding and the potent phosphorylation of NTAL after CD9 triggering suggest that these two molecules are physically and functionally coupled. This could explain our previous findings that although NTAL and LAT are very similar TRAPs, they, nevertheless, occupy different membrane domains (5). CD9 also colocalized with FcεRI. However, this colocalization was clearly seen only after Ab-mediated dimerization or extensive aggregation of CD9.

Fourth, pretreatment of BMMCs with anti-CD9 mAb abolished chemotaxis toward Ag. The inhibitory effect was observed not only with intact mAb but also with the corresponding $F(ab)_2$ fragment. These data suggest that the inhibitory effect is caused by CD9 aggregation and is not dependent on signals derived from cross-linking of CD9 with FcγR. This conclusion is further supported by findings that chemotaxis was not affected by Fab fragments of the anti-CD9 mAb. When another CD9-specific mAb, KMC8, was tested, no inhibition of chemotaxis was observed. This finding could be related to different epitopes recognized by 2H9 and KMC8 antibodies and/or other differences between the antibodies, such as configurational constraints (61). On the other hand, both antibodies inhibited IL-16-mediated chemotaxis by a mechanism, which seems to involve blocking binding of IL-16 to its alternate receptor, CD9 (48). We have also noticed that chemotaxis toward Ag was not affected in BMMCs with CD9 KD. This suggests that CD9 is dispensable for Ag-driven chemotaxis or that the remaining CD9 is sufficient for signal processing. Alternatively, it is possible that antibody-mediated aggregation of CD9 and CD9-bound proteins leads to uncoupling of key elements important for chemotaxis (see below).

The molecular mechanism of the inhibitory effect of anti-CD9 on Ag-induced chemotaxis seems to be complex and involves TRAPs. We found that anti-CD9 mAb was more potent in inhibiting Ag-induced chemotaxis in NTAL-deficient cells than in WT cells. This could be related to the multiple regulatory roles of NTAL and its cross-talk with CD9 and LAT (Fig. 8).

Fifth, extensive communication between plasma membrane components and the cellular cytoskeleton is crucial for immunoreceptor activation and chemotaxis. This process is regulated by conformational changes in ERM family proteins reflecting the phosphorylation status of their regulatory threonine. Our finding of increased dephosphorylation of ERM pro-

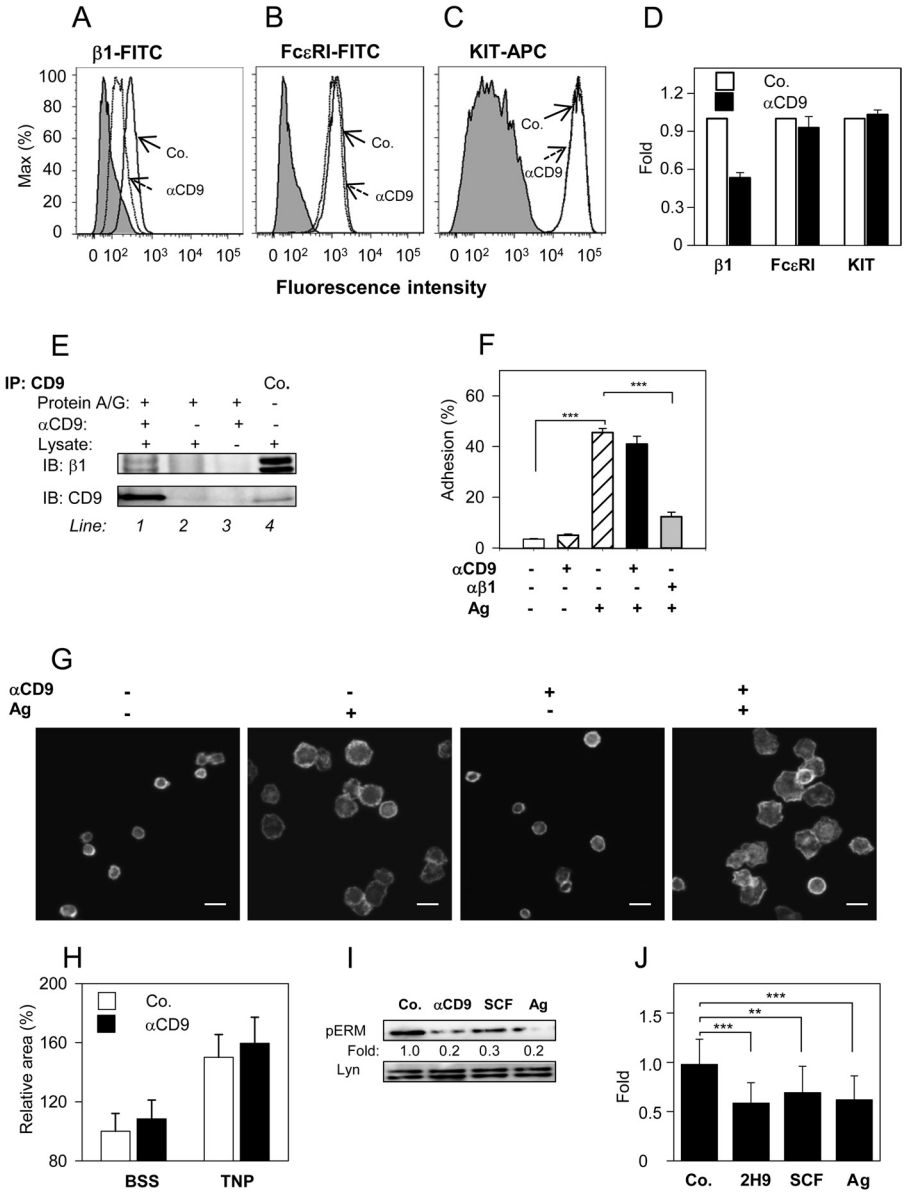

FIGURE 7. **CD9 aggregation does not interfere with β1-integrin function, but induces dephosphorylation of ERM proteins.** *A-D*, BMMCs were pretreated or not with anti-CD9 mAb 2H9 (1 μg/ml) for 15 min and the binding anti-integrin-β1-FITC conjugate (*A*), anti-FcεRI-FITC conjugate (*B*), and anti-c-Kit-APC conjugate (*C*) were estimated by flow cytometry. *Gray filled regions* represent control cells not exposed to antibodies; *dashed* and *thick lines* indicate antibody binding to anti-CD9 treated (*dashed*; αCD9) or nontreated cells (*thick*; *Co.*). *D*, data obtained as in *A-C* were normalized to maximal values obtained in the absence of anti-CD9; mean ± S.D. were determined from at least 3 independent experiments. *E*, BMMCs (10^7 per sample) were solubilized in lysis buffer supplemented with 1% CHAPS. CD9 was immunoprecipitated from postnuclear supernatants by 2H9 mAb immobilized on protein A/G beads (*line 1*). Material bound to protein A/G beads without 2H9 mAb (*line 2*) or 2H9 mAb armed protein A/G beads without cell lysate (*line 3*) served as negative controls. Whole lysates from 2.5×10^5 cells were used as positive controls (*Co.*; *line 4*). Immunoprecipitated material and controls were recovered in SDS-PAGE sample buffer with or without 2-mrecaptoethanol. Reduced and unreduced samples were immunoblotted with anti-β1 integrin (β1) or anti-CD9 (CD9), respectively. *F*, cell adhesion to fibronectin. IgE-sensitized and Calcein-loaded BMMCs were incubated with (+) or without (−) anti-CD9 mAb 2H9 and/or anti-β1 integrin antibody for 15 min before their transfer into fibronectin-coated wells. Adherence to fibronectin was determined by fluorometry after a 30-min exposure of the cells to Ag (+) or BSSA alone (−). Fluorescence was evaluated before (100%) and after washing out the non-adherent cells and percentages of adherent cells were calculated. *G*, cell spreading on fibronectin. IgE-sensitized BMMCs were pretreated (+) or not (−) with anti-CD9 mAb 2H9 and allowed to attach to fibronectin immobilized on glass surface. Then the cells were exposed (+) or not (−) to Ag for 20 min, fixed, permeabilized, and stained for actin with Alexa Fluor 488-phalloidin conjugate. Examples of the cells are shown. *Bars*, 20 μm. *H*, average areas of the cells processed as in *G* were calculated using automated CellProfiller software. Mean ± S.D. from three independent experiments, each involving ~500 cells, are shown. *I*, IgE-sensitized BMMCs were nonactivated (*Co.*) or activated with 2H9 mAb (*αCD9*), SCF, or Ag for 3 min. Whole cell lysates were prepared and analyzed by immunoblotting with *p*-ERM^T-specific Ab; anti-Lyn was used as a loading control. *Numbers* correspond to the fold-increase in phosphorylation after normalization to the total amount of protein and phosphorylation in nonactivated cells. Typical results are shown. *J*, mean ± S.D. were calculated from 10 to 18 independent experiments performed as in *I*. **, $p < 0.01$; ***, $p < 0.001$.

teins in cells exposed to anti-CD9 suggested that anti-CD9 interferes with the process of phosphorylation/dephosphorylation of ERM family members, and in this way could interfere with chemotaxis. The molecular mechanism of the cross-talk between CD9 and ERM family members is unknown. Recent studies imply an important role of the phosphorylation state of threonine in actin-binding domains of ERM proteins in cell chemotaxis (54–57). The proteins exist in an open (active) conformation with regulatory threonine phosphorylated, or closed (inactive) conformation with the regulatory threonine dephos-

TABLE 1

Comparison of anti-CD9 mAb, SCF, and Ag in their ability to induce signaling events in mast cells

Parameter[a]	Anti-CD9	SCF	Ag
Protein phosphorylation			
Akt-S^{473}	−[b]	+++	+++
Akt-T^{308}	−	+++	+++
Erk-Y^{204}	+	+++	+++
p38-T^{180}/Y^{182}	+	+++	+++
Syk	−	−	+++
NTAL	++	+	+++
LAT	−/+	−	+++
Protein dephosphorylation			
ERM-$T^{567/564/558}$	++	++	++
Degranulation (β-glucuronidase)	+	+	+++
Ca^{2+} mobilization	+	+	+++
Adhesion	−	++[c]	++
Spreading	−	+++[c]	+++
Chemotaxis	−	+++[c]	++

[a] Specific protein phosphorylation or dephosphorylation, degranulation, Ca^{2+} mobilization, adhesion, and chemotactic potential of CD9-specific mAb 2H9, SCF and Ag were measured using appropriate methods as indicated under "Experimental Procedures" and "Results."

[b] −, No signal; +, weak signal; ++, medium signal; +++, strong signal.

[c] See Ref. 14.

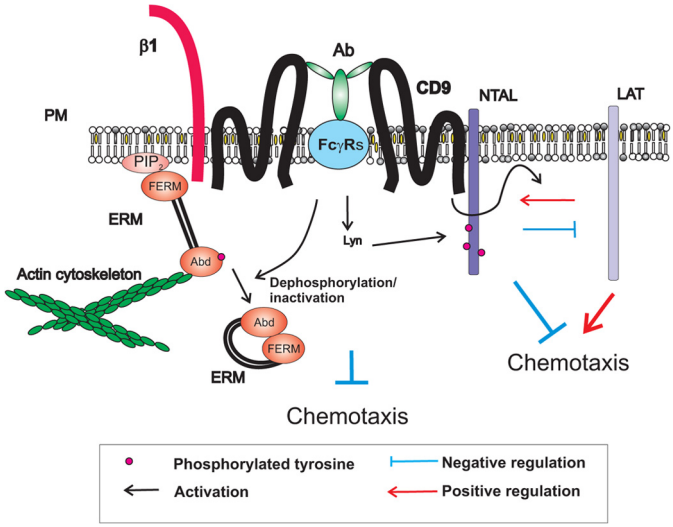

FIGURE 8. **A model of chemotaxis regulators involving CD9 and NTAL-LAT cross-talk.** Tetraspanin CD9 resides in the plasma membrane (*PM*) in close proximity to β1-integrin (β1) and NTAL. CD9-specific antibody 2H9 (*Ab*) binds to CD9 and FcγR through its Ag-binding site and Fc region, respectively. This leads to tyrosine phosphorylation of NTAL and other proteins. CD9 cross-linking also results in dephosphorylation of the regulatory threonine of ERM family proteins leading to changes in their conformation and subsequent disconnection from binding to phosphatidylinositol 4,5-bisphosphate (*PIP2*) and/or other membrane components (throughout N-terminal FERM domain) and actin cytoskeleton (through actin-binding domain, *Abd*). These and other events under certain conditions inhibit mast cell chemotaxis. Chemotaxis is also regulated by cross-talk between NTAL, LAT, and CD9. LAT and NTAL seem to be, respectively, predominantly positive and negative regulators of chemotaxis. Binding of the anti-CD9 mAb 2H9 interferes with NTAL-LAT cross-talk.

phorylated (62, 63). In the case of ezrin, the open conformation enables its binding through the actin-binding domain to F-actin and through the FERM domain to phosphatidylinositol 4,5-biphosphate on the plasma membrane, to adapter proteins or directly to cytoplasmic portions of the transmembrane molecules (59, 64). Transient dephosphorylation of the regulatory threonine disrupts this binding and has been shown to be crucial for migration of lymphocytes (54–57). A recent study with mast cells showed that dephosphorylation of the regulatory tyrosine is mediated by activity of the protein phosphatase 2A after interaction with the p21-activated kinase 1 (58). Based on our own findings and published data we propose that aggregation of CD9 leads to dephosphorylation of ERM proteins leading to their dissociation from the membrane and restrictions in communication of membrane proteins with actin cytoskeleton. This in combination with some other events involving NTAL and/or LAT contributes to inhibition of Ag-driven chemotaxis (Fig. 8). As shown in experiments with $F(ab)_2$ fragments, tyrosine phosphorylation of NTAL is not required for the inhibitory effect of anti-CD9 mAb. Nevertheless, it is possible that NTAL functions in chemotaxis even in the absence of its phosphorylation, similarly to its role in phospholipase Cγ-independent calcium uptake (12).

The combined data support the view that chemotaxis and early activation events leading to degranulation and cytokine production are processes that use different signaling pathways. The differences could be important for switching between the migratory and secretory phases depending on the concentrations of Ag and/or other chemoattractant mast cell encounters (65). At low concentrations of the Ag, mast cells migrate toward its higher concentrations. When regions of higher concentrations of the Ag are attained, the cells stop moving and activate the signaling pathways leading to secretion of the preformed allergy mediators and production and release of cytokines, leukotrienes, and other inflammatory mediators that then act as chemoattractants for other cells and/or orchestrate local immune responses. Tetraspanin CD9 and NTAL are important regulators of these events. CD9 could regulate chemotaxis through direct or indirect interactions with FcεRI, other plasma membrane receptors, and cytoskeletal components. On the other hand NTAL, which acts as a negative regulator of chemotaxis, could contribute to fine tuning of chemotaxis by competing with LAT, as suggested for its negative role in mast cell degranulation (5).

REFERENCES

1. Okayama, Y., and Kawakami, T. (2006) Development, migration, and survival of mast cells. *Immunol. Res.* **34,** 97–115
2. Halova, I., Draberova, L., and Draber, P. (2012) Mast cell chemotaxis-chemoattractants and signaling pathways. *Front Immunol.* **3,** 119
3. Wedemeyer, J., and Galli, S. J. (2000) Mast cells and basophils in acquired immunity. *Br. Med. Bull.* **56,** 936–955
4. Saitoh, S., Arudchandran, R., Manetz, T. S., Zhang, W., Sommers, C. L., Love, P. E., Rivera, J., and Samelson, L. E. (2000) LAT is essential for FcεRI-mediated mast cell activation. *Immunity* **12,** 525–535
5. Volná, P., Lebduška, P., Dráberová, L., Šímová, Š., Heneberg, P., Boubelík, M., Bugajev, V., Malissen, B., Wilson, B. S., Hořejší, V., Malissen, M., and Dráber, P. (2004) Negative regulation of mast cell signaling and function by the adaptor LAB/NTAL. *J. Exp. Med.* **200,** 1001–1013
6. Zhu, M., Liu, Y., Koonpaew, S., Granillo, O., and Zhang, W. (2004) Positive and negative regulation of FcεRI-mediated signaling by the adaptor protein LAB/NTAL. *J. Exp. Med.* **200,** 991–1000
7. Tkaczyk, C., Horejsi, V., Iwaki, S., Draber, P., Samelson, L. E., Satterthwaite, A. B., Nahm, D. H., Metcalfe, D. D., and Gilfillan, A. M. (2004) NTAL phosphorylation is a pivotal link between the signaling cascades leading to human mast cell degranulation following Kit activation and FcεRI aggregation. *Blood* **104,** 207–214
8. Draber, P., Halova, I., Levi-Schaffer, F., and Draberova, L. (2011) Transmembrane adaptor proteins in the high-affinity IgE receptor signaling. *Front. Immunol.* **2,** 95
9. Rivera, J. (2005) NTAL/LAB and LAT. A balancing act in mast-cell acti-

vation and function. *Trends Immunol.* **26,** 119–122
10. Simeoni, L., Lindquist, J. A., Smida, M., Witte, V., Arndt, B., and Schraven, B. (2008) Control of lymphocyte development and activation by negative regulatory transmembrane adapter proteins. *Immunol. Rev.* **224,** 215–228
11. Lebduška, P., Korb, J., Tůmová, M., Heneberg, P., and Dráber, P. (2007) Topography of signaling molecules as detected by electron microscopy on plasma membrane sheets isolated from non-adherent mast cells. *J. Immunol. Methods* **328,** 139–151
12. Dráberová, L., Shaik, G. M., Volná, P., Heneberg, P., Tůmová, M., Lebduska, P., Korb, J., and Dráber, P. (2007) Regulation of Ca^{2+} signaling in mast cells by tyrosine-phosphorylated and unphosphorylated non-T cell activation linker. *J. Immunol.* **179,** 5169–5180
13. Kimura, T., Hisano, M., Inoue, Y., and Adachi, M. (2001) Tyrosine phosphorylation of the linker for activator of T cells in mast cells by stimulation with the high affinity IgE receptor. *Immunol. Lett.* **75,** 123–129
14. Tůmová, M., Koffer, A., Šimíček, M., Dráberová, L., and Dráber, P. (2010) The transmembrane adaptor protein NTAL signals to mast cell cytoskeleton via the small GTPase Rho. *Eur. J. Immunol.* **40,** 3235–3245
15. Charrin, S., Le Naour, F., Oualid, M., Billard, M., Faure, G., Hanash, S. M., Boucheix, C., and Rubinstein, E. (2001) The major CD9 and CD81 molecular partner. Identification and characterization of the complexes. *J. Biol. Chem.* **276,** 14329–14337
16. Kotha, J., Longhurst, C., Appling, W., and Jennings, L. K. (2008) Tetraspanin CD9 regulates β_1 integrin activation and enhances cell motility to fibronectin via a PI-3 kinase-dependent pathway. *Exp. Cell Res.* **314,** 1811–1822
17. Levy, S., and Shoham, T. (2005) Protein-protein interactions in the tetraspanin web. *Physiology* **20,** 218–224
18. Hemler, M. E., Mannion, B. A., and Berditchevski, F. (1996) Association of TM4SF proteins with integrins. Relevance to cancer. *Biochim. Biophys. Acta* **1287,** 67–71
19. Xu, D., Sharma, C., and Hemler, M. E. (2009) Tetraspanin12 regulates ADAM10-dependent cleavage of amyloid precursor protein. *FASEB J.* **23,** 3674–3681
20. Berditchevski, F., and Odintsova, E. (1999) Characterization of integrin-tetraspanin adhesion complexes. Role of tetraspanins in integrin signaling. *J. Cell Biol.* **146,** 477–492
21. Berditchevski, F. (2001) Complexes of tetraspanins with integrins. More than meets the eye. *J. Cell Sci.* **114,** 4143–4151
22. Little, K. D., Hemler, M. E., and Stipp, C. S. (2004) Dynamic regulation of a GPCR-tetraspanin-G protein complex on intact cells: central role of CD81 in facilitating GPR56-$G\alpha_{q/11}$ association. *Mol. Biol. Cell* **15,** 2375–2387
23. Murayama, Y., Shinomura, Y., Oritani, K., Miyagawa, J., Yoshida, H., Nishida, M., Katsube, F., Shiraga, M., Miyazaki, T., Nakamoto, T., Tsutsui, S., Tamura, S., Higashiyama, S., Shimomura, I., and Hayashi, N. (2008) The tetraspanin CD9 modulates epidermal growth factor receptor signaling in cancer cells. *J. Cell Physiol.* **216,** 135–143
24. Sala-Valdés, M., Ursa, A., Charrin, S., Rubinstein, E., Hemler, M. E., Sánchez-Madrid, F., and Yáñez-Mó, M. (2006) EWI-2 and EWI-F link the tetraspanin web to the actin cytoskeleton through their direct association with ezrin-radixin-moesin proteins. *J. Biol. Chem.* **281,** 19665–19675
25. Stipp, C. S., Kolesnikova, T. V., and Hemler, M. E. (2001) EWI-2 is a major CD9 and CD81 partner and member of a novel Ig protein subfamily. *J. Biol. Chem.* **276,** 40545–40554
26. Zhang, X. A., Bontrager, A. L., and Hemler, M. E. (2001) Transmembrane-4 superfamily proteins associate with activated protein kinase C (PKC) and link PKC to specific β_1-integrins. *J. Biol. Chem.* **276,** 25005–25013
27. Hemler, M. E. (2005) Tetraspanin functions and associated microdomains. *Nat. Rev. Mol. Cell Biol.* **6,** 801–811
28. Rubinstein, E. (2011) The complexity of tetraspanins. *Biochem. Soc. Trans.* **39,** 501–505
29. Dráber, P., Zikán, J., and Vojtíšková, M. (1980) Establishment and characterization of permanent murine hybridomas secreting monoclonal anti-thy-1 antibodies. *J. Immunogenet.* **7,** 455–474
30. Smrž, D., Lebduška, P., Dráberová, L., Korb, J., and Dráber, P. (2008) Engagement of phospholipid scramblase 1 in activated cells. Implication for phosphatidylserine externalization and exocytosis. *J. Biol. Chem.* **283,** 10904–10918
31. Rudolph, A. K., Burrows, P. D., and Wabl, M. R. (1981) Thirteen hybridomas secreting hapten-specific immunoglobulin E from mice with Iga or Igb heavy chain haplotype. *Eur. J. Immunol.* **11,** 527–529
32. Rivera, J., Kinet, J. P., Kim, J., Pucillo, C., and Metzger, H. (1988) Studies with a monoclonal antibody to the β subunit of the receptor with high affinity for immunoglobulin E. *Mol. Immunol.* **25,** 647–661
33. Brdička, T., Imrich, M., Angelisová, P., Brdičková, N., Horváth, O., Špička, J., Hilgert, I., Lusková, P., Dráber, P., Novák, P., Engels, N., Wienands, J., Simeoni, L., Osterreicher, J., Aguado, E., Malissen, M., Schraven, B., and Hořejší, V. (2002) Non-T cell activation linker (NTAL). A transmembrane adaptor protein involved in immunoreceptor signaling. *J. Exp. Med.* **196,** 1617–1626
34. Tolar, P., Tůmová, M., and Dráber, P. (2001) *Folia Biol.* **47,** 215–217
35. Dráberová, L., Amoui, M., and Dráber, P. (1996) Thy-1-mediated activation of rat mast cells. The role of Thy-1 membrane microdomains. *Immunology* **87,** 141–148
36. Kovářová, M., Tolar, P., Arudchandran, R., Dráberová, L., Rivera, J., and Dráber, P. (2001) Structure-function analysis of Lyn kinase association with lipid rafts and initiation of early signaling events after Fcϵ receptor I aggregation. *Mol. Cell Biol.* **21,** 8318–8328
37. Hibbs, M. L., Tarlinton, D. M., Armes, J., Grail, D., Hodgson, G., Maglitto, R., Stacker, S. A., and Dunn, A. R. (1995) Multiple defects in the immune system of Lyn-deficient mice, culminating in autoimmune disease. *Cell* **83,** 301–311
38. Hájková, Z., Bugajev, V., Dráberová, E., Vinopal, S., Dráberová, L., Janáček, J., Dráber, P., and Dráber, P. (2011) STIM1-directed reorganization of microtubules in activated mast cells. *J. Immunol.* **186,** 913–923
39. Surviladze, Z., Dráberová, L., Kovářová, M., Boubelík, M., and Dráber, P. (2001) Differential sensitivity to acute cholesterol lowering of activation mediated via the high-affinity IgE receptor and Thy-1 glycoprotein. *Eur. J. Immunol.* **31,** 1–10
40. Hálová, I., Dráberová, L., and Dráber, P. (2002) A novel lipid raft-associated glycoprotein, TEC-21, activates rat basophilic leukemia cells independently of the type 1 Fcϵ receptor. *Int. Immunol.* **14,** 213–223
41. Philimonenko, A. A., Janáček, J., and Hozák, P. (2000) Statistical evaluation of colocalization patterns in immunogold labeling experiments. *J. Struct. Biol.* **132,** 201–210
42. Carpenter, A. E., Jones, T. R., Lamprecht, M. R., Clarke, C., Kang, I. H., Friman, O., Guertin, D. A., Chang, J. H., Lindquist, R. A., Moffat, J., Golland, P., and Sabatini, D. M. (2006) CellProfiler. Image analysis software for identifying and quantifying cell phenotypes. *Genome Biol.* **7,** R100
43. Fiskum, G., Craig, S. W., Decker, G. L., and Lehninger, A. L. (1980) The cytoskeleton of digitonin-treated rat hepatocytes. *Proc. Natl. Acad. Sci. U.S.A.* **77,** 3430–3434
44. Bangham, A. D., Horne, R. W., Glauert, A. M., Dingle, J. T., and Lucy, J. A. (1962) Action of saponin on biological cell membranes. *Nature* **196,** 952–955
45. Iwaki, S., Spicka, J., Tkaczyk, C., Jensen, B. M., Furumoto, Y., Charles, N., Kovarova, M., Rivera, J., Horejsi, V., Metcalfe, D. D., and Gilfillan, A. M. (2008) Kit- and FcϵRI-induced differential phosphorylation of the transmembrane adaptor molecule NTAL/LAB/LAT2 allows flexibility in its scaffolding function in mast cells. *Cell Signal* **20,** 195–205
46. Zhang, J., Billingsley, M. L., Kincaid, R. L., and Siraganian, R. P. (2000) Phosphorylation of Syk activation loop tyrosines is essential for Syk function. An *in vivo* study using a specific anti-Syk activation loop phosphotyrosine antibody. *J. Biol. Chem.* **275,** 35442–35447
47. Linnekin, D. (1999) Early signaling pathways activated by c-Kit in hematopoietic cells. *Int. J. Biochem. Cell Biol.* **31,** 1053–1074
48. Qi, J. C., Wang, J., Mandadi, S., Tanaka, K., Roufogalis, B. D., Madigan, M. C., Lai, K., Yan, F., Chong, B. H., Stevens, R. L., and Krilis, S. A. (2006) Human and mouse mast cells use the tetraspanin CD9 as an alternate interleukin-16 receptor. *Blood* **107,** 135–142
49. Krämer, B., Schulte, D., Körner, C., Zwank, C., Hartmann, A., Michalk, M., Söhne, J., Langhans, B., Nischalke, H. D., Coenen, M., Möhl, C., Vogt, A., Hennenberg, M., Sauerbruch, T., Spengler, U., and Nattermann, J. (2009) Regulation of NK cell trafficking by CD81. *Eur. J. Immunol.* **39,** 3447–3458

50. Kaji, K., Takeshita, S., Miyake, K., Takai, T., and Kudo, A. (2001) Functional association of CD9 with the Fcγ receptors in macrophages. *J. Immunol.* **166,** 3256–3265
51. Kuroda, K., Ozaki, Y., Qi, R., Asazuma, N., Yatomi, Y., Satoh, K., Nomura, S., Suzuki, M., and Kume, S. (1995) FcγII receptor-mediated platelet activation induced by anti-CD9 monoclonal antibody opens Ca^{2+} channels which are distinct from those associated with Ca^{2+} store depletion. *J. Immunol.* **155,** 4427–4436
52. Qi, R., Ozaki, Y., Kuroda, K., Asazuma, N., Yatomi, Y., Satoh, K., Nomura, S., and Kume, S. (1996) Differential activation of human platelets induced by Fcγ receptor II cross-linking and by anti-CD9 monoclonal antibody. *J. Immunol.* **157,** 5638–5645
53. Worthington, R. E., Carroll, R. C., and Boucheix, C. (1990) Platelet activation by CD9 monoclonal antibodies is mediated by the Fcγ II receptor. *Br. J. Haematol.* **74,** 216–222
54. Gupta, N., Wollscheid, B., Watts, J. D., Scheer, B., Aebersold, R., and DeFranco, A. L. (2006) Quantitative proteomic analysis of B cell lipid rafts reveals that ezrin regulates antigen receptor-mediated lipid raft dynamics. *Nat. Immunol.* **7,** 625–633
55. Liu, Y., Belkina, N. V., Park, C., Nambiar, R., Loughhead, S. M., Patino-Lopez, G., Ben-Aissa, K., Hao, J. J., Kruhlak, M. J., Qi, H., von Andrian, U. H., Kehrl, J. H., Tyska, M. J., and Shaw, S. (2012) Constitutively active ezrin increases membrane tension, slows migration, and impedes endothelial transmigration of lymphocytes *in vivo* in mice. *Blood* **119,** 445–453
56. Parameswaran, N., Matsui, K., and Gupta, N. (2011) Conformational switching in ezrin regulates morphological and cytoskeletal changes required for B cell chemotaxis. *J. Immunol.* **186,** 4088–4097
57. Treanor, B., Depoil, D., Bruckbauer, A., and Batista, F. D. (2011) Dynamic cortical actin remodeling by ERM proteins controls BCR microcluster organization and integrity. *J. Exp. Med.* **208,** 1055–1068
58. Staser, K., Shew, M. A., Michels, E. G., Mwanthi, M. M., Yang, F. C., Clapp, D. W., and Park, S. J. (2013) A Pak1-PP2A-ERM signaling axis mediates F-actin rearrangement and degranulation in mast cells. *Exp. Hematol.* **41,** 56–66
59. Yonemura, S., Hirao, M., Doi, Y., Takahashi, N., Kondo, T., Tsukita, S., and Tsukita, S. (1998) Ezrin/radixin/moesin (ERM) proteins bind to a positively charged amino acid cluster in the juxta-membrane cytoplasmic domain of CD44, CD43, and ICAM-2. *J. Cell Biol.* **140,** 885–895
60. Fleming, T. J., Donnadieu, E., Song, C. H., Laethem, F. V., Galli, S. J., and Kinet, J. P. (1997) Negative regulation of FcεRI-mediated degranulation by CD81. *J. Exp. Med.* **186,** 1307–1314
61. Ortega, E., Schweitzer-Stenner, R., and Pecht, I. (1988) Possible orientational constraints determine secretory signals induced by aggregation of IgE receptors on mast cells. *EMBO J.* **7,** 4101–4109
62. Gary, R., and Bretscher, A. (1995) Ezrin self-association involves binding of an N-terminal domain to a normally masked C-terminal domain that includes the F-actin binding site. *Mol. Biol. Cell* **6,** 1061–1075
63. Reczek, D., and Bretscher, A. (1998) The carboxyl-terminal region of EBP50 binds to a site in the amino-terminal domain of ezrin that is masked in the dormant molecule. *J. Biol. Chem.* **273,** 18452–18458
64. Hirao, M., Sato, N., Kondo, T., Yonemura, S., Monden, M., Sasaki, T., Takai, Y., Tsukita, S., and Tsukita, S. (1996) Regulation mechanism of ERM (ezrin/radixin/moesin) protein/plasma membrane association. Possible involvement of phosphatidylinositol turnover and Rho-dependent signaling pathway. *J. Cell Biol.* **135,** 37–51
65. Gonzalez-Espinosa, C., Odom, S., Olivera, A., Hobson, J. P., Martinez, M. E., Oliveira-Dos-Santos, A., Barra, L., Spiegel, S., Penninger, J. M., and Rivera, J. (2003) Preferential signaling and induction of allergy-promoting lymphokines upon weak stimulation of the high affinity IgE receptor on mast cells. *J. Exp. Med.* **197,** 1453–1465

7.7 GOLD NANOPARTICLE-BASED IMMUNO-PCR FOR DETECTION OF TAU PROTEIN IN CEREBROSPINAL FLUID.

Stegurová L., Dráberová E., Bartos A., Dráber P., Rípová D., Dráber P.

J. Immunol. Methods, 406:137-42, 2014

Journal of Immunological Methods 406 (2014) 137–142

Contents lists available at ScienceDirect

Journal of Immunological Methods

journal homepage: www.elsevier.com/locate/jim

Technical note

Gold nanoparticle-based immuno-PCR for detection of tau protein in cerebrospinal fluid

Lucie Stegurová [a,1], Eduarda Dráberová [b,1], Ales Bartos [c,d,e], Pavel Dráber [b], Daniela Řípová [c,d], Petr Dráber [a,*]

[a] Laboratory of Signal Transduction, Institute of Molecular Genetics, Academy of Sciences of the Czech Republic, CZ-142 20, Prague 4, Czech Republic
[b] Laboratory of Biology of Cytoskeleton, Institute of Molecular Genetics, Academy of Sciences of the Czech Republic, CZ-142 20, Prague 4, Czech Republic
[c] Laboratory of Biochemistry and Brain Pathophysiology, Prague Psychiatric Center, National Institute of Mental Health, CZ-181 03, Prague 8, Czech Republic
[d] AD Center, Prague Psychiatric Center, National Institute of Mental Health, CZ-181 03, Prague 8, Czech Republic
[e] Department of Neurology, Third Faculty of Medicine, Charles University in Prague, University Hospital Královské Vinohrady, CZ-100 34, Prague 10, Czech Republic

ARTICLE INFO

Article history:
Received 24 August 2013
Received in revised form 6 March 2014
Accepted 6 March 2014
Available online 15 March 2014

Keywords:
Gold nanoparticles
PCR
ELISA
Tau protein

ABSTRACT

Tau protein in cerebrospinal fluid (CSF) is an important biomarker of Alzheimer's disease and some other brain diseases. Enzyme-linked immunosorbent assays (ELISAs) have been mostly used for quantification of tau and other biomarkers in CSF. However, these assays do not have sufficient sensitivity and dynamic range. In this study we tested the suitability of gold nanoparticles functionalized with tau-specific monoclonal antibody and oligonucleotide template for immuno-polymerase chain reaction (Nano-iPCR) quantification of tau protein in human CSF samples and compared it with ELISA, either commercial or newly developed with tyramide signal amplification. Our data indicate that Nano-iPCR is superior in sensitivity and detection range to ELISA in tau protein detection.

1. Introduction

Cerebrospinal fluid (CSF) is an important source of protein biomarkers that reflect pathological changes in the brain and provide information necessary for diagnosis and treatment of various brain-associated diseases. One of the meaningful CSF biomarkers of neuronal and axonal degeneration is the tau protein. Very high levels of tau are characteristic for patients with extensive neuronal degeneration, such as Creutzfeldt–Jacob disease (Otto et al., 1997). Enhanced levels of total and phosphorylated tau associated with decreased levels of the 42 amino acid form of β-amyloid in CSF have been used for diagnosis of Alzheimer's disease (AD), the most frequent form of dementia (Dubois et al., 2007). Quantification of total tau and other CSF markers of AD is mostly done with commercial enzyme-linked immunosorbent assays (ELISAs). However, these assays are expensive and do not have the desirable dynamic range. New low-cost methods for simultaneous detection of samples with both low and high levels of tau proteins are therefore needed.

We and others have recently introduced the polymerase chain reaction (PCR) combined with sandwich ELISA-like strategy where the target antigen is immobilized by antibodies to PCR plate wells and subsequently detected by immuno-PCR using gold nanoparticles (Au-NPs) functionalized with both antigen-specific antibody and PCR oligonucleotide template. This assay, called Nano-iPCR, proved superior in detection of cytokines and viral proteins to standard ELISAs (Potůčková et al., 2011; Chen et al., 2009; Perez et al., 2011). Here we present data confirming the utility of Nano-iPCR for quantification of tau protein in CSF samples. Compared to commercial or newly

* Corresponding author at: Laboratory of Signal Transduction, Institute of Molecular Genetics, Academy of Sciences of the Czech Republic, Vídeňská 1083, CZ-14220, Prague 4, Czech Republic. Tel.: +420 241062468; fax: +420 241062214.
E-mail address: draberpe@img.cas.cz (P. Dráber).
[1] L. S. and E. D. contributed equally to this work.

http://dx.doi.org/10.1016/j.jim.2014.03.007
0022-1759/

developed ELISAs, quantification of tau protein with Nano-iPCR is superior in sensitivity and detection range.

2. Materials and methods

2.1. Materials and reagents

Purified mouse monoclonal antibody specific for tau protein, HT7 (IgG1), and its biotinylated form were purchased from Autogen Bioclear (Calne, UK; Cat. No. 90222 and 90214). The antibody recognizes an epitope located in amino acid region 159–163, according to the human full-length four-repeat tau, tau 40 (Goedert et al., 1989). Purified mouse monoclonal antibody, TAU-5 (IgG1), which recognizes an epitope located in amino acid region 210–230 in tau 40 (Carmel et al., 1996), was obtained from Abcam (Cambridge, UK; Cat. No. ab80579). The kit for determination of total tau (INNOTEST hTAU Ag) was from Innogenetics (Gent, Belgium). Recombinant human Tau-441 protein (2N4R variant) was purchased from Enzo Life Sciences (Farmingdale, NY, USA). Colloidal Au-NPs (30 nm in diameter) at a concentration of approximately 2×10^{11} particles/ml were obtained from BBInternational (Cardiff, UK). 5′-thiol-modified oligonucleotide primer 1 [5′-(5ThioMC6-D//iSp18)CCTTGAACC TGTGCCATTTGAATATATTAAGACTATACGCGGGAACA-3′], where iSp18 is an 18-atom hexa-ethyleneglycol spacer connecting the thiol reactive group and the DNA sequence, primer 2 (5′-CCTTGAACCTGTGCCATTTG-3′) and primer 3 (5′-GTCCCTCC ATCTTCCTACTGTTCCACATGTTCCCGCGTATAGTCTT-3′) were obtained from IDT (Coralville, IA, USA). Other chemical were from Sigma-Aldrich (St. Louis, MO, USA). Lumbar CSFs from 32 individuals were collected, centrifuged, aliquoted in 1 ml polypropylene tubes and stored at −80 °C in accordance with established guidelines (Teunissen et al., 2009) until analysis. All participants signed an informed consent form. The study was approved by the Ethics Committees of the University Hospital, Královské Vinohrady and Prague Psychiatric Center.

2.2. Preparation of functionalized gold nanoparticles

Au-NPs functionalized with antibodies and oligonucleotides were prepared as described previously (Hill and Mirkin, 2006; Potůčková et al., 2011) with some modifications. Briefly, 1 ml of colloidal Au-NPs (30 nm in diameter) was incubated for 30 min at room temperature with HT7 antibody at optimal concentration (10 μg/ml), determined by Au-NP-antibody loading test (Hill and Mirkin, 2006); suboptimal concentration of the antibody resulted in rapid aggregation of the particles, whereas excess antibody prevented binding of the thiolated oligonucleotides in a later step. Then, 10% Tween 20 (10 μl) and 2 M NaCl in PBS (10 mM phosphate, 150 mM NaCl, pH 7.4; 100 μl) were added, followed by 5′-thiol-modified oligonucleotide primer 1 at final concentration 4 nmol/ml. After overnight incubation at 4 °C with gentle stirring, the samples were salted by adding 50 μl aliquots of 2 M NaCl in PBS in four 1-h steps. The armed Au-NPs were further stabilized by adding 20 μl of 10% bovine serum albumin (BSA) and incubating for 30 min at room temperature. Free oligonucleotides were removed by three centrifugation steps through discontinuous glycerol gradient (Potůčková et al., 2011); the pellet was finally resuspended in 1 ml of PBS containing 20% glycerol, 1% BSA, 0.05% Tween 20, and 0.02% NaN_3.

2.3. Nano-iPCR

Fifty microliter aliquots of capture antibody (2.5 μg/ml TAU-5) in 50 mM borate buffer (pH 9.5) were dispensed into wells of a real-time 96-well plate (Eppendorf, Hamburg, Germany). After overnight incubation at 4 °C the wells were washed (200 μl/well; four times per washing step, if not specified otherwise) with TBS (10 mM Tris–HCl, pH 7.4, 150 mM NaCl) containing 0.05% Tween 20 (TBST) and the remaining binding sites were blocked by 6-h incubation at 4 °C with TBST supplemented with 1% BSA and 1% casein. The wells were then washed with TBST followed by addition of 50 μl serially diluted recombinant human tau protein (Tau-441; 1–100,000 pg/ml in PBS-0.1% casein), PBS-0.1% casein alone (negative control) or undiluted human CSF samples. After overnight incubation at 4 °C, the wells were washed with TBST, followed by addition of 50 μl aliquots of Au-NPs armed with thiolated DNA oligonucleotide and HT7 monoclonal antibody, diluted 1:10,000 in PBS-0.1% casein. The wells were incubated for 1 h at 37 °C, washed with 200 μl TBST and finally with 200 μl MilliQ water. Next, 50 μl aliquots of PCR master mix solution containing Taq DNA polymerase, nucleotides, SYBR green I, 1,2-propanediol, and trehalose (Horáková et al., 2011) and supplemented with 60 nM oligonucleotide primers 2 and 3 were dispensed into each well. The plates were then sealed with Light cycler 480 sealing foil (Roche, Mannheim, Germany) and the amount of template DNA bound to antigen-anchored functionalized Au-NPs was evaluated by real-time PCR using Realplex^4 Mastercycler (Eppendorf, Hamburg, Germany) with the following cycling parameters: denaturation at 94 °C for 1 min, followed by 40 cycles at 94 °C for 20 s, 53 °C for 20 s, and 72 °C for 20 s. The samples without template DNA were used in each run as negative controls.

2.4. Sandwich ELISAs

Newly developed sandwich ELISA with tyramide signal amplification (TSA) was routinely performed in high-binding 96-well half-area plates (Costar Corning Inc., Corning, NY, USA) or TopYield Strips (Nunc, Roskilde Site, Denmark). Capture anti-tau antibody, TAU-5, was coated at a concentration of 2.5 μg/ml in borate buffer pH 9.5 (30 μl/well) by overnight incubation at 4 °C. The plates were washed with TBST and free binding sites were blocked by adding TBS with 2% BSA (TBS-2% BSA; 185 μl/well). After 6 h at room temperature the plates were washed again with TBST and incubated overnight at 4 °C with recombinant human tau standard (Tau-441) diluted in PBS-1% BSA or tested samples (30 μl/well). Similar results were obtained when the samples were diluted in PBS-0.1% casein. Wells washed with TBST were then incubated for 1 h at room temperature with biotinylated anti-tau antibody HT7 at concentration 0.5 μg/ml in TBST-1% BSA (30 μl/well). After washing, the plates were incubated for 45 min at room temperature with extravidin-peroxidase diluted 1:5000 in TBST-1% BSA (30 μl/well). Sensitivity of the assay was increased by biotinyl-tyramide signal amplification (TSA) using the ELAST ELISA Amplification System (tyramide; PerkinElmer Life Sciences, Boston) as previously described (Dráberová et al., 2013). Absorption was measured at 450 nm

with a Sunrise plate Reader (TECAN). Background of the negative control was subtracted from the determined values.

The Innotest hTAU Ag (Innogenetics, Gent, Belgium, Cat. No. 80323) commercial kit for tau protein quantification was used according to the manufacturer's directions.

2.5. Statistics

Calibration curves were constructed after plotting the quantification cycle (C_q) values or absorbance against tau concentrations using a four-parameter logistic regression model function (variable slope) and linear regression showing the regression correlation coefficient (R^2). The limit of detection (LOD) was calculated as the mean of the negative control (NC; sample diluent) plus 3× standard deviations of NC. Correlation analyses were performed using Pearson's coefficient for normally distributed and Spearman's coefficient for non-Gaussian data. Bland–Altman curves were constructed for comparison between different methods for detection of the tau protein level. Precision profiles, reproducibility, and accuracy were expressed by the intra- and inter-assay coefficients of variation (CV). Mean of individual CVs was calculated for each standard and sample as standard deviation divided by the mean. The results were then multiplied by 100 for expression as a percentage. For recovery experiments, high (4000 pg/ml), medium (800 pg/ml) and low (100 pg/ml) concentrations of recombinant tau were spiked into validated samples and analyzed in Nano-iPCR. The results are expressed as a percentage of analyte recovered. Linearity of dilution was determined in CSF samples diluted 2–16-fold and expressed as percent linearity for all samples in the dilution series.

All statistical analyses were performed using program Prism 5 (GraphPad Software, La Jolla, CA, USA).

3. Results and discussion

3.1. Quantification of recombinant tau protein by Nano-iPCR and comparison with ELISA

The Nano-iPCR method for quantification of tau protein is based on immobilization of the protein on TAU-5 antibody directly in PCR wells and its detection by real-time PCR with the Au-NPs functionalized with tau-specific monoclonal antibody HT7 and a single-stranded thiolated oligonucleotide. In pilot experiments, the Au-NP-antibody loading test was used to determine the optimum concentration of the HT7 antibody for Au-NP loading. From a range of HT7 antibody concentrations (1–16 μg/ml), 10 μg/ml was found optimal for antibody and oligonucleotide arming as determined by sensitivity of tau detection and real-time PCR analysis (Potůčková et al., 2011), respectively. Moreover, Au-NPs functionalized with HT7 at the optimal concentration showed the best performance during storage for up to eight months. PCR amplification is extremely sensitive to the presence of very low amounts of antibody/oligonucleotide-functionalized Au-NPs bound nonspecifically to the walls of PCR wells, which can enhance the background signal. This problem was solved by optimizing the washing and blocking conditions, and using a routine protocol for tau analysis as described in Section 2.3.

Sensitivity of the Nano-iPCR for quantification of tau protein was tested by immobilizing recombinant tau at a concentration range from 1 to 100,000 pg/ml in TAU-5 antibody-coated wells of the PCR plate and then exposing the wells to Au-NPs functionalized with HT7 antibody and oligonucleotide primer 1. Detection by real-time PCR followed after washing off unbound particles. Fig. 1A shows a standard curve in the range of C_q values from 17.9 (at the tau concentration of 100,000 pg/ml) to 32.6 (at 1 pg/ml). Negative control (without tau protein) showed C_q values of about 33. The curve was linear from 10 to 10,000 pg/ml of recombinant tau protein with regression correlation coefficient (R^2) equal to 0.9918 (Fig. 1B). The LOD was found to be 5 pg/ml.

For comparison, recombinant tau protein was also quantified by ELISA-TSA using the same tau-specific antibody set (TAU-5 and HT7). Different concentrations of recombinant tau protein were added into wells with immobilized TAU-5. After incubation and washing off unbound tau, the wells were exposed sequentially to biotinylated anti-tau specific antibody HT7 and extravidin-peroxidase conjugates. The signal was enhanced by biotinyl-TSA. Absorbance values corresponding to different concentrations of tau protein (0–1200 pg/ml) are shown in Fig. 1C. The curve was linear in the range from 75 to 600 pg/ml of tau protein with regression correlation coefficient 0.9653 and LOD 140 pg/ml (Fig. 1D). The data clearly show that Nano-iPCR has a broader detection range and more than 30-fold higher sensitivity than ELISA-TSA. The broad detection range of Nano-iPCR was also demonstrated by precision profiles (Fig. 2E).

3.2. Quantification of tau protein in CSF by Nano-iPCR and comparison with ELISA

Next the amount of tau protein in 32 human CSF samples was examined by Nano-iPCR, ELISA-TSA and/or commercial ELISA. First we compared two ELISAs, ELISA-TSA and a commercial ELISA kit. Data presented in Fig. 2A show good correlation between tau concentrations as determined by ELISA-TSA (based on TAU-5 and HT7 antibodies) and the commercial kit with correlation coefficient $r = 0.636$ and $p < 0.0001$. This conclusion was corroborated by Bland–Altman plot (Fig. 2B). Precision, reproducibility and accuracy of ELISA-TSA was characterized by intra- and inter-assay CVs. The average of the intra-assay CV was 8.9% (range, 1.5-12%) for tau standards and 5.4% (range, 0–15%) for CSF samples. The average of inter-assay CV for ELISA-TSA based on CSF samples was 18% (range, 4–31%). Coefficient of variation between ELISA-TSA and ELISA kit based on CSF samples was 30.6% (range, 1–65%). The higher CV values could be caused by different standards used in the commercial ELISA kit and ELISA-TSA and different conditions for performing the assays.

Next, we compared the performance of Nano-iPCR and ELISA kit. Data presented in Fig. 2C show good correlation between tau concentrations as determined by Nano-iPCR and ELISA kit; correlation coefficient $r = 0.730$ and $p < 0.0001$. This finding was supported by the Bland–Altman plot (Fig. 2D). Precision, reproducibility and accuracy of Nano-iPCR were again characterized by intra- and inter-coefficients of variability. The average of intra-assay CV was 2.1% (range, 1–4%) for tau standards and 12.6% (range, 1–36%) for CSF samples. The inter-assay CV of Nano-iPCR based on CSF was 12.2% (range, 1.5–42%). Coefficient of variation between Nano-iPCR and ELISA kit was 23.4% (range, 2–63%). Again, the high CV

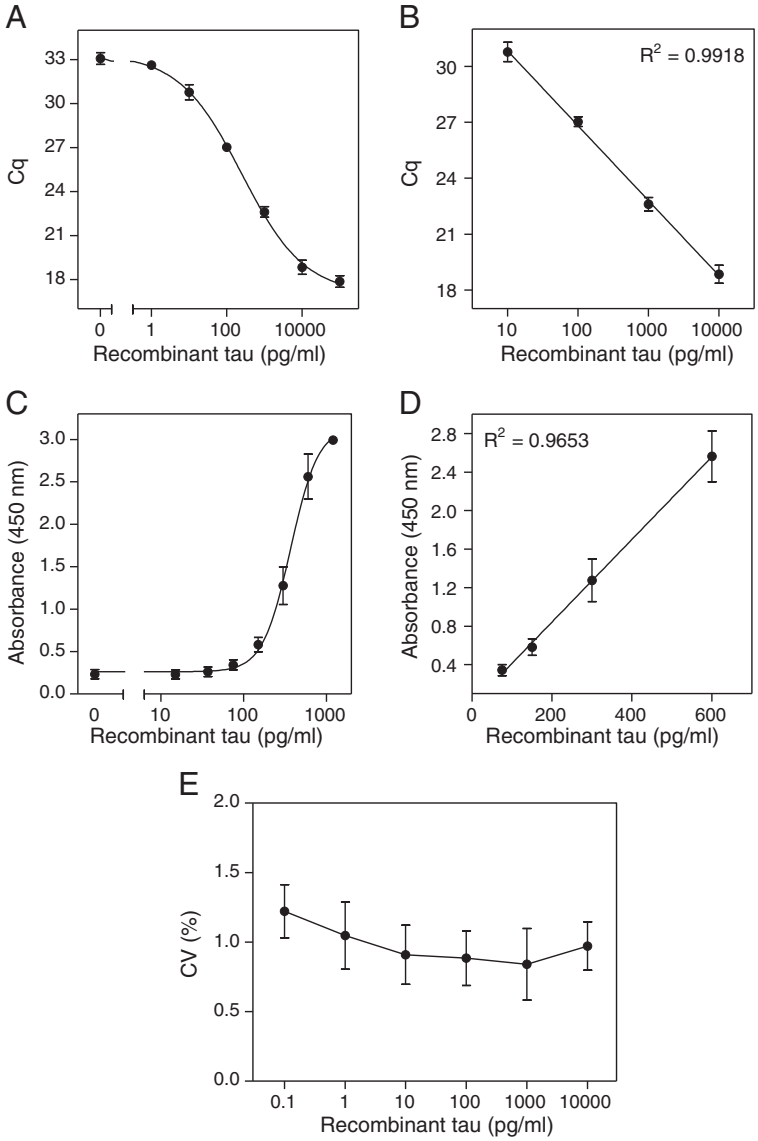

Fig. 1. Calibration curves of recombinant tau protein as determined by Nano-iPCR and ELISA-TSA. (A, B) Tau protein was detected by Nano-iPCR at concentrations ranging from 1 to 100,000 pg/ml (A); the curve was linear between 10 and 10,000 pg/ml (B). (C, D) Tau protein was detected by ELISA-TSA at a concentration range 15–1200 pg/ml (C); the curve was linear between 75 and 600 pg/ml (D). (E) Precision profile for Nano-iPCR. Estimated errors (expressed as % CVs) at various doses of recombinant tau protein were determined in each experiment from triplicates. Means ± SD were calculated from two independent experiments performed in triplicate (A, B) or duplicate (C, D), or six independent experiments (E).

between these two assays is probably caused by different standards and different assay conditions. For recovery experiments, high (4000 pg/ml), medium (800 pg/ml), and low (100 pg/ml) concentrations of recombinant tau protein were spiked into CSF samples. Tau levels were determined with Nano-iPCR with recovery (89%–113%). Finally, we attempted to determine the contribution of interfering factors present in CSF on linearity of the assay. We diluted CSF samples 2–16-fold and analyzed the amount of tau protein in the samples by Nano-iPCR. The observed mean value 107% (range, 91%–136%) indicated good linearity of the assay. These data indicate that Nano-iPCR gives results that could be used for determination of tau protein in clinical studies.

In conclusion, Nano-iPCR where Au-NPs functionalized with anti-tau monoclonal antibody and template oligonucleotide are used for real-time PCR detection of tau protein immobilized in wells of a PCR plate is fully suitable for tau protein detection. The assay is superior in sensitivity and detection range to ELISA-TSA based on the same set of anti-tau monoclonal antibodies or to a commercial ELISA kit. Nano-iPCR could be of importance for simplified determination of excessively high concentrations of tau protein in patients with Creutzfeldt–Jakob disease. The commercial availability of monoclonal antibodies suitable for tau protein detection by Nano-iPCR and the easy preparation of functionalized Au-NPs reduce the expenses for tau protein quantification at

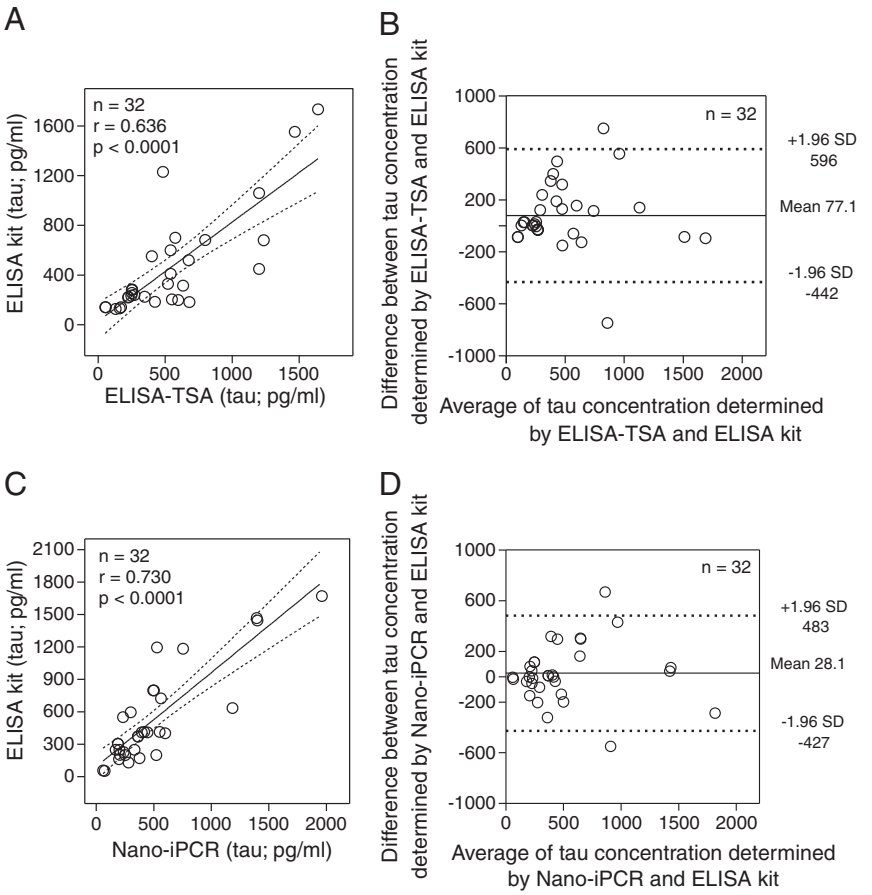

Fig. 2. Quantification of tau protein in CSF by various assays. (A, B) Comparison of ELISA-TSA and ELISA kit for tau protein level determination; (A) correlation plot and (B) Bland–Altman plot. (C, D) Comparison of Nano-iPCR and ELISA kit for tau protein level determination; correlation plot (C) and Bland–Altman plot (D). In correlation plots, the dashed line represents 95% line of identity; r means correlation coefficient; n means the number of samples analyzed. In Bland–Altman plots, the averages of the two methods of rating are shown along the horizontal axis and their difference along the vertical axis. The solid line represents the mean difference, and the upper and lower dotted lines represent 95% limits of agreement (±1.96 times the standard deviation of the differences).

least 10 times when compared to assays based on commercial kits.

Acknowledgments

We thank I. Mlchová for excellent technical assistance and Dr. J. Říčný for tau measurements using a commercial ELISA kit and for careful reading of the manuscript. This work was supported in part by project KAN200520701 from the Academy of Sciences of the Czech Republic, TA01010436 of the Technology Agency of the Czech Republic, project FR-TI3/067 of the Ministry of Industry and Trade of the Czech Republic, projects P302/12/1673 and P302/12/G101 from the Grant Agency of the Czech Republic, and Institutional Support RVO 68378050. L.S. was supported in part by the Faculty of Science, Charles University, Prague, Czech Republic.

References

Carmel, G., Mager, E.M., Binder, L.I., Kuret, J., 1996. The structural basis of monoclonal antibody Alz50's selectivity for Alzheimer's disease pathology. J. Biol. Chem. 271, 32789.

Chen, L., Wei, H., Guo, Y., Cui, Z., Zhang, Z., Zhang, X.E., 2009. Gold nanoparticle enhanced immuno-PCR for ultrasensitive detection of Hantaan virus nucleocapsid protein. J. Immunol. Methods 346, 64.

Dráberová, E., Stegurová, L., Sulimenko, V., Hájková, Z., Dráber, P., Dráber, P., 2013. Quantification of α-tubulin isotypes by sandwich ELISA with signal amplification through biotinyl-tyramide or immuno-PCR. J. Immunol. Methods 395, 63.

Dubois, B., Feldman, H.H., Jacova, C., Dekosky, S.T., Barberger-Gateau, P., Cummings, J., Delacourte, A., Galasko, D., Gauthier, S., Jicha, G., Meguro, K., O'brien, J., Pasquier, F., Robert, P., Rossor, M., Salloway, S., Stern, Y., Visser, P.J., Scheltens, P., 2007. Research criteria for the diagnosis of Alzheimer's disease: revising the NINCDS-ADRDA criteria. Lancet Neurol. 6, 734.

Goedert, M., Spillantini, M.G., Jakes, R., Rutherford, D., Crowther, R.A., 1989. Multiple isoforms of human microtubule-associated protein tau: sequences and localization in neurofibrillary tangles of Alzheimer's disease. Neuron 3, 519.

Hill, H.D., Mirkin, C.A., 2006. The bio-barcode assay for the detection of protein and nucleic acid targets using DTT-induced ligand exchange. Nat. Protoc. 1, 324.

Horáková, H., Polakovičová, I., Shaik, G.M., Eitler, J., Bugajev, V., Dráberová, L., Dráber, P., 2011. 1,2-propanediol-trehalose mixture as a potent quantitative real-time PCR enhancer. BMC Biotechnol. 11, 41.

Otto, M., Wiltfang, J., Tumani, H., Zerr, I., Lantsch, M., Kornhuber, J., Weber, T., Kretzschmar, H.A., Poser, S., 1997. Elevated levels of tau-protein in cerebrospinal fluid of patients with Creutzfeldt–Jakob disease. Neurosci. Lett. 225, 210.

Perez, J.W., Vargis, E.A., Russ, P.K., Haselton, F.R., Wright, D.W., 2011. Detection of respiratory syncytial virus using nanoparticle amplified immuno-polymerase chain reaction. Anal. Biochem. 410, 141.

Potúčková, L., Franko, F., Bambousková, M., Dráber, P., 2011. Rapid and sensitive detection of cytokines using functionalized gold nanoparticle-based immuno-PCR, comparison with immuno-PCR and ELISA. J. Immunol. Methods 371, 38.

Teunissen, C.E., Petzold, A., Bennett, J.L., Berven, F.S., Brundin, L., Comabella, M., Franciotta, D., Frederiksen, J.L., Fleming, J.O., Furlan, R., Hintzen, R.Q., Hughes, S.G., Johnson, M.H., Krasulova, E., Kuhle, J., Magnone, M.C., Rajda, C., Rejdak, K., Schmidt, H.K., P. V., van, Waubant, E., Wolf, C., Giovannoni, G., Hemmer, B., Tumani, H., Deisenhammer, F., 2009. A consensus protocol for the standardization of cerebrospinal fluid collection and biobanking. Neurology 73, 1914.

7.8 QUANTIFICATION OF α-TUBULIN ISOTYPES BY SANDWICH ELISA WITH SIGNAL AMPLIFICATION THROUGH BIOTINYL-TYRAMIDE OR IMMUNO-PCR.

Dráberová E., **Stegurová L**., Sulimenko V., Hájková Z., Dráber P., Dráber P.

J. Immunol. Methods, 395(1-2):63-70, 2013

Journal of Immunological Methods 395 (2013) 63–70

Contents lists available at SciVerse ScienceDirect

Journal of Immunological Methods

journal homepage: www.elsevier.com/locate/jim

Research paper

Quantification of α-tubulin isotypes by sandwich ELISA with signal amplification through biotinyl-tyramide or immuno-PCR

Eduarda Dráberová [a,1], Lucie Stegurová [b,1], Vadym Sulimenko [a], Zuzana Hájková [a], Petr Dráber [b], Pavel Dráber [a,*]

[a] Laboratory of Biology of Cytoskeleton, Institute of Molecular Genetics, Academy of Sciences of the Czech Republic, CZ-142 20 Prague 4, Czech Republic
[b] Laboratory of Signal Transduction, Institute of Molecular Genetics, Academy of Sciences of the Czech Republic, CZ-142 20 Prague 4, Czech Republic

ARTICLE INFO

Article history:
Received 25 April 2013
Received in revised form 2 July 2013
Accepted 2 July 2013
Available online 10 July 2013

Keywords:
α-Tubulin isotypes
Biotinyl-tyramide
ELISA
Immuno-PCR
Mast cells

ABSTRACT

Microtubules formed by αβ-tubulin dimers represent cellular structures that are indispensable for the maintenance of cell morphology and for cell motility generation. Microtubules in intact cells are in highly regulated equilibrium with cellular pools of soluble tubulin dimers. Sensitive, reproducible and rapid assays are necessary to monitor tubulin changes in cytosolic pools after treatment with anti-mitotic drugs, during the cell cycle or activation and differentiation events. Here we describe new assays for α-tubulin quantification. The assays are based on sandwich ELISA, and the signal is amplified with biotinyl-tyramide or immuno-PCR. Matching monoclonal antibody pair recognizes phylogenetically highly conserved epitopes localized outside the C-terminal isotype-defining region. This makes it possible to detect α-tubulin isotypes in different cell types of various species. Biotinyl-tyramide amplification and immuno-PCR amplification enable detection of tubulin at concentrations 2.5 ng/ml and 0.086 ng/ml, respectively. Immuno-PCR detection shows enhanced sensitivity and wider dynamic range when compared to ELISA with biotinyl-tyramide detection. Our results on taxol-treated and activated bone marrow-derived mast cells demonstrate, that the assays allow sensitive quantification of tubulin in complex biological fluids.

1. Introduction

Microtubules are highly dynamic structures vital for numerous cellular processes, including cellular organization, intracellular trafficking, migration, and cell division. Microtubules can rapidly reorganize their arrangements depending on external signals. They usually consist of 13 laterally associated protofilaments made up of αβ-tubulin dimers. In vertebrates tubulins are encoded by multiple genes and their products, tubulin isotypes, differ mainly in their C-terminal regions. Certain isotypes are tissue specific, and the isotype composition affects microtubule properties (Ludueña and Banerjee, 2008). Multiple α- and β-tubulin isotypes can be present in the same cell, and tubulin heterogeneity is further enhanced by various posttranslational modifications (Linhartová et al., 1992). In intact cells a highly regulated equilibrium exists between microtubules and the pools of soluble tubulin dimers. Tubulin binds to tubulin-binding agents, small molecule inhibitors, such as anti-mitotic drugs (e.g. taxol, vinblastin, nocodazole, colchicine) that can change the ratio between polymeric and soluble tubulin pools (Katsetos and Dráber, 2012).

Abbreviations: BMMC, bone marrow-derived mast cell; BSA, bovine serum albumin; BSS, buffered saline solution; C_q, quantification cycle; ELISA, enzyme-linked immunosorbent assay; PCR, polymerase chain reaction; PBS, phosphate buffer solution; TBS, Tris buffer solution; TBST, TBS containing 0.05% Tween 20; TMB, 3,3′,5,5′-tetramethylbenzidine.

* Corresponding author at: Laboratory of Biology of Cytoskeleton, Institute of Molecular Genetics, Academy of Sciences of the Czech Republic, Vídeňská 1083, 142 20 Prague 4, Czech Republic. Tel.: +420 241 062 632; fax: +420 241 062 758.
E-mail address: paveldra@img.cas.cz (P. Dráber).

[1] E.D. and L.S. contributed equally to this work.

0022-1759/$ – see front matter © 2013 Elsevier B.V. All rights reserved.
http://dx.doi.org/10.1016/j.jim.2013.07.001

Sensitive, reproducible and rapid assays are needed for monitoring tubulin changes in cytosolic pools after treatment with anti-mitotic drugs, during the cell cycle, and activation or differentiation events. Several methods have been described for quantification of total tubulin in cells or tissue extracts, including colchicine binding (Pipeleers et al., 1977; Wilson, 1970) or radioimmunoassay (Bulinski et al., 1980; Das et al., 1989). However, both the colchicine binding assay and radioimmunoassay use radioactive compounds. Competitive enzyme-linked immunosorbent assay (ELISA) was alternatively elaborated for quantification of tubulin pools (Thrower et al., 1991) or β-tubulin isotypes (Dozier et al., 2003); the detection limit is around 1 μg/ml.

Mast cells play an essential role in innate immunity, allergy and inflammation. When activated they release mediators that are pivotal for initiation of inflammatory reactions associated with allergic disorders (Rivera et al., 2008). In the course of mouse bone marrow-derived mast cell (BMMC) activation, substantial changes in reorganization of microtubules take place (Hájková et al., 2011). However, it is not known whether or not activation-induced changes, degranulation and/or exosome release also lead to the release of tubulin into extracellular space. Such process has been documented for some other cellular components (Valadi et al., 2007).

Here we report on the development of new sensitive assays for tubulin quantification. The assays are based on sandwich ELISA, and the signal is amplified with biotinyl-tyramide or immuno-polymerase chain reaction (PCR). The key component of the system is a matching antibody pair recognizing phylogenetically highly conserved epitopes localized outside the C-terminal isotype-defining region. This makes it possible to detect α-tubulin isotypes in different cell types of various species. The results on taxol-treated and activated BMMCs confirm, that the techniques offer sensitive alternative of quantification of tubulin in complex biological fluids.

2. Material and methods

2.1. Tubulin preparation

Microtubule protein was purified from porcine brain by two temperature-dependent cycles of assembly and disassembly (Shelanski et al., 1973), followed by subsequent purification by phosphocellulose chromatography (Weingarten et al., 1975). The eluted tubulin in column buffer (100 mM PIPES pH 6.9, 1 mM EGTA, 1 mM $MgCl_2$, 1 mM DTT, 0.5 mM GTP) was supplemented with GTP to 1 mM and polymerized by sodium glutamate added to final concentration 1.0 M. Pelleted microtubules were resuspended in BRB80 buffer (80 mM PIPES pH 6.8, 1 mM EGTA, 1 mM $MgCl_2$) supplemented with 0.1 mM GTP (BRB80-GTP) and depolymerized by cold. Tubulin concentration in supernatant was checked by measuring the absorbance at 280 nm using an extinction coefficient at 280 nm of 115,000 M^{-1} cm^{-1}. Recycled tubulin was more than 98% pure as determined by SDS-PAGE, and it was stored in liquid nitrogen in aliquots at ~200 μM concentration. Alternatively, tubulin at concentration ~200 μM was freeze-dried in small aliquots in the presence of trehalose and stored at ambient temperature (Dráberová et al., 2010). Freeze-dried tubulin was rehydrated with cold Millipore water at 4 °C to the original aliquot volume and incubated on ice for 20 min. Concentrated tubulin samples were diluted in precooled BRB80-GTP to the concentration ~50 μM and centrifuged at 300,000 ×*g* for 5 min at 4 °C; to remove any aggregates. Tubulin concentration in supernatants was determined by absorbance at 280 nm.

2.2. Cells

Mouse cell line of BMMCs, which grow in the absence of stem cell factor, was provided by M. Hibbs (Ludwig Institute for Cancer Research, Melbourne, Australia) (Hibbs et al., 1995). The cells were incubated in suspension cultures in freshly prepared culture medium (RPMI 1640 supplemented with 20 mM HEPES, pH 7.5, 100 U/ml penicillin, 100 μg/ml streptomycin, 100 μM MEM nonessential amino acids, 1 mM sodium pyruvate) supplemented with 10% fetal calf serum (FCS) and 10% WEHI-3 cell supernatant as a source of interleukin 3. Mouse embryonal fibroblasts NIH 3T3 were obtained from the American Type Culture Collection. Cells were cultured in Dulbecco's modified Eagle's medium (DMEM) containing 10% FCS, penicillin (100 U/ml), and streptomycin (0.1 mg/ml). Cells were grown at 37 °C in 5% CO_2 in air and passaged every 2 days.

To compare tubulin concentration in extracts prepared from control and taxol-treated cells, BMMCs in culture media were incubated for 2.5 h in the absence or presence of taxol at final concentration 10 μM. Cells were pelleted by centrifugation (240 ×*g*, 5 min, 25 °C), washed in ice-cold HEPES buffer (50 mM HEPES adjusted to pH 7.6 with KOH, 75 mM KCl, 1 mM EGTA, 1 mM $MgCl_2$), pelleted and counted after resuspension. Samples of 10×10^6 cells were resuspended in 1 ml of ice-cold HEPES buffer supplemented with protease (Protease inhibitor cocktail tablets; Roche) and phosphatase (1 mM Na_3VO_4 and 1 mM NaF) inhibitors and 1% NP-40. After 10 min incubation at 4 °C, cell extracts were centrifuged (20,000 ×*g*, 15 min, 4 °C) and collected supernatants were used for determination of tubulin concentration.

To quantify the release of tubulin from thapsigargin-activated cells into the culture medium, BMMCs (44×10^6 cells) were resuspended in 1 ml of buffered saline solution (BSS; 20 mM HEPES, pH 7.4, 135 mM NaCl, 5 mM KCl, 1.8 mM $CaCl_2$, 5.6 mM glucose, 2 mM $MgCl_2$) supplemented with 0.1% BSA (Sigma-Aldrich, Cat. No. A7030) (BSS-BSA) and incubated for 20 min at 37 °C in the absence or presence of thapsigargin (Sigma-Aldrich; Cat. No. 79033) at final concentration 2 μM. Cells were pelleted by centrifugation (240 ×*g*, 5 min, 25 °C) and the collected supernatant was further centrifuged (200,000 ×*g*, 4 min, 4 °C) to remove any cellular debris. Collected supernatants were used for determination of tubulin concentration.

2.3. Antibodies

Purified mouse monoclonal antibody DM1A (IgG1) to α-tubulin (Blose et al., 1984) at 1 mg/ml concentration was bought from Abcam (Cat. No. ab7291). The antibody recognizes epitope located in the C-terminal region of α-tubulin (a.a. 426–451) of various species; amino acids within the positions 426 and 430 are particularly important for antibody reactivity (Breitling and Little, 1986). The mouse monoclonal antibody TU-07 (IgM) against α-tubulin of various species (Dráber et al., 1986), recognizes the epitope exposed on the surface

of polymerized microtubules (Dráber et al., 1990; Smertenko et al., 1997).

TU-07 was purified from ascitic fluid by ammonium sulfate precipitation followed by gel chromatography on the column of Sepharose 6B. Purity verified by SDS-PAGE exceeded 85% as TU-07 antibody was biotinylated using EZ-Link Sulfo-NHS-LC-biotin from Pierce according to manufacturer's recommendation. Conjugated antibody was dialyzed against phosphate buffer solution (PBS; 10 mM phosphate, 150 mM NaCl, pH 7.4) and stored in 50% glycerol at −20 °C (final antibody concentration = 0.6 mg/ml). The capability of biotinylated antibody to bind tubulin was verified by immunoblotting on total 3T3 lysate, by staining of microtubules in fixed 3T3 cells (Dráber et al., 1989) and by indirect ELISA on immobilized tubulin. The antibody reacted on immunoblots with protein band corresponding to tubulin, stained interphase and mitotic microtubules, and bound to purified tubulin in ELISA (not shown).

Mouse monoclonal antibody TUB 2.1 (IgG_1) to β-tubulin labeled with indocarbocyanate (Cy3) was from Sigma-Aldrich. Anti-mouse antibody conjugated with horseradish peroxidase was purchased from Promega Biotec.

2.4. Epitope mapping

Synthetic overlapping peptides (15-meric peptides with 5 amino acid overlaps) were prepared by SPOT synthesis (Jerini Peptide Technologies, Berlin, Germany). Each spot carried approximately 5-nmol peptide covalently bound to cellulose-β-alanine membrane. Peptide scans (45 peptides) covered the sequences 1–451 of porcine (*Sus scrofa*) α-tubulin 1A (TUBA1A, accession number P02550 in the UniProtKB/Swiss-Prot database). Epitope mapping was performed using horseradish-conjugated anti-mouse antibody and chemiluminescent detection of bound antibodies as described (Blume et al., 2010).

2.5. Gel electrophoresis and immunoblotting

SDS-PAGE on 12% polyacrylamide gel and immunoblotting were performed using standard protocols (Sulimenko et al., 2002). Protein quantifications in cell lysates were performed with bicinchoninic acid assay (Thermo Scientific, Cat. No. 23227). DM1A and purified TU-07 were diluted 1:5000 and 1:1000, respectively. Peroxidase-conjugated secondary anti-mouse antibody (Promega, Cat. No. W4028) was diluted 1:10,000. Bound antibodies were detected by Super-Signal WestPico Chemiluminescent reagents (Pierce).

2.6. Sandwich ELISA

The assay was routinely performed in high binding 96-well half-area polystyrene plates (Corning Inc.; Cat. No. 3690). Alternatively, polycarbonate TopYield Strips (Nunc; Cat. No. 248917) were used. Washings throughout the assay (200 μl/well, four times per washing step, if not specified otherwise) were carried out by means of automatic washing device HydroFlex Platform (TECAN) with Tris buffer solution (TBS; 10 mM Tris–Cl, pH 7.4, 150 mM NaCl) containing 0.05% Tween 20 (TBST). Anti-tubulin antibody DM1A was coated at a concentration of 5 μg/ml in PBS (30 μl/well) overnight (~16 h) at 4 °C. After washing, the plates were blocked by adding 2% BSA in TBS (BSA/TBS) (185 μl/well) for 6 h at room temperature. The plates were then washed and incubated overnight (~16 h) at 4 °C with tubulin standards or tested samples diluted in 1% BSA in PBS (30 μl/well). The sample diluent served as negative control. Washed plates were then incubated for 1 h at room temperature with biotinylated anti-tubulin antibody TU-07 at concentration 1 μg/ml in 1% bovine serum albumin (BSA) in TBST (BSA/TBST) (30 μl/well). Washed plates were incubated for 45 min at room temperature with extravidin-horseradish peroxidase (Sigma-Aldrich, Cat. No. E2886) diluted 1:5000 in BSA/TBST (30 μl/well). After repeated washing, the sensitivity of the assay was augmented by biotinyl-tyramide signal amplification using the ELAST ELISA Amplification System (PerkinElmer, Cat. No. NEP116001EA) according to the manufacturer's directions. Shortly, plates were incubated with biotinyl-tyramide, diluted 1:500 in amplification diluent (30 μl/well) for 15 min at room temperature in dark, washed (5 times) and incubated with streptavidin-peroxidase diluted 1:1000 in BSA/TBST (30 μl/well) for 30 min at room temperature in dark. The plates were washed (5 times) and incubated with 3,3′,5,5′-tetramethylbenzidine (TMB) Liquid Substrate (Sigma-Aldrich, Cat. No. T8665) (30 μl/well). Reaction was stopped after 13 min by adding Stop Reagent for TMB Substrate (Sigma-Aldrich) (30 μl/well). Absorption was determined at 450 nm on Sunrise plate Reader (TECAN). Background values of negative controls were subtracted from the readings.

For long-term storage, TopYield Strips were coated with DM1A antibody and blocked with BSA; excess blocking solution was removed before air-drying. Precoated strips were stored at 4 °C in the presence of desiccant. Wells were rehydrated by adding BSA/TBS for 30 min at room temperature. The strips were then washed and incubated with samples.

2.7. Immuno-PCR

The immuno-PCR was performed as described (Niemeyer et al., 2005; Potůčková et al., 2011) with some modifications. Twenty-five microliter aliquots of capture anti-tubulin antibody DM1A (5 μg/ml) in 100 mM borate buffer (pH 9.5) were dispensed into each well of TopYield strips. The wells were incubated for 2 h at 37 °C and washed four times with 200 μl of TBST. Free binding sites were blocked with BSA/TBS. After 2 h at 37 °C, the strips were washed again four times, followed by adding 25 μl of tubulin standards or tested samples diluted in 1% BSA in PBS. The strips were further incubated for 1 h at 37 °C and then overnight at 4 °C, followed by four washings. Subsequently, 25 μl aliquots of biotinylated anti-tubulin antibody TU-07 (1 μg/ml in TBS–1% BSA) were added and the samples were incubated for 1 h at 37 °C. After washing four times, the wells were filled with 25 μl aliquots of extravidin (0.1 μg/ml, Sigma-Aldrich, Cat. No. E2511) in TBS–1% BSA, incubated for 1 h at 37 °C and then washed as before. The next step consists in the addition of 25 μl of biotinylated DNA template (0.27 pg/ml). The template was prepared by amplification of a DNA fragment corresponding to nucleotides 989–1209 of human tyrosine-protein kinase ABL1 (GenBank accession no. M14752) with biotinylated primer 5B-HRM1-F, 5′-biotin-AAACTCATCACCACGCTCCATTA-3′, and HRM1-R, 5′-TCTTCCACCTCCATGGTGTC-3′ (Generi Biotech, Czech Republic). The strips were then incubated for 1 h at 37 °C followed by washing four times with TBST and twice

with MilliQ water. Template DNA immobilized on antigen in the wells was quantified by real-time PCR. An aliquot of 25 μl of master mix solution was added into each well containing 75 mM Tris–HCl (pH 8.8), 20 mM $(NH_4)_2SO_4$, 2.5 mM $MgCl_2$, 200 μM dATP, 200 μM dGTP, 200 μM dCTP, 200 μM dTTP, Taq DNA polymerase (25 U/ml; TopBio, Czech Republic), 2 μM SYTO-9 (Invitrogen) and primers (200 nM each); forward HRM1-F (5′-CTCATCACCACGCTCCATTA-3′) and reverse HRM1-R (see above). Finally, each well was overlaid with 5 μl of light mineral oil (TopBio) and sealed with Light cycler sealing foil (Roche). The cycling conditions were as follows: 2 min at 95 °C as an initial denaturation step and 40 cycles consisting of 15 s at 95 °C, 60 s at 60 °C, and elongation step for 60 s at 72 °C using Realplex^4 Mastercycler (Eppendorf, Hamburg, Germany). The C_q (quantification cycle) values were determined using the software of the cycler.

2.8. Degranulation assay

The degree of degranulation was quantified as the release of β-glucuronidase from control or thapsigargin-activated cells, using 4-methylumbelliferyl β-D-glucuronide as a substrate (Surviladze et al., 2001). The total content of the enzyme was evaluated in supernatants from cells lysed by 0.1% Triton X-100.

2.9. Microscopy and FACS

Immunofluorescence microscopy was performed on fixed cells as described (Dráberová and Dráber, 1993). Shortly, cells were rinsed with microtubule-stabilizing buffer (0.1 M MES, pH 6.9, 2 mM EGTA, 2 mM $MgCl_2$, 4% polyethylene glycol 6000), fixed for 20 min in 3% formaldehyde in microtubule-stabilizing buffer and extracted for 4 min with 0.5% Triton X-100 in microtubule-stabilizing buffer. TUB 2.1 mAb conjugated with Cy3 was diluted 1:600. The preparations were examined with Olympus A70 Provis microscope.

Data obtained with Accuri cytometer (BD Accuri Cytometers Inc.) were employed to compare the total numbers and the viability of cells before and after activation with thapsigargin.

2.10. Data analysis

Calibration curves were constructed after plotting the absorbance or C_q values against tubulin concentrations and using a four-parameter logistic regression model function (variable slope) within GrafPad Prism 5 (GraphPad Software). The limit of detection (LOD) was calculated as the mean of the sample diluent plus 3 standard deviations of the sample diluent. Statistical analysis made use of the Student's two-tailed unpaired *t*-test.

3. Results

3.1. Epitope mapping

Sandwich ELISA requires a matched pair of antibodies recognizing non-overlapping native epitopes on the same target. Previously we have shown that some monoclonal antibodies to C-terminal domain of α-tubulin, including the TU-07 antibody, recognize epitopes exposed on the surface of tubulin molecule (Dráber et al., 1989). Peptide scan of immobilized overlapping peptides covering porcine α-tubulin (a.a. 1–451; 45 linear 15-meric peptides with 5 amino acid overlaps) was used for a more accurate epitope location of TU-07. Results of immunostaining with antibody TU-07 and with another anti-α-tubulin antibody, DM1A, are shown in Fig. 1. Epitope mapping revealed the localization of TU-07 epitope to the a.a. region 406–410 (sequence HWYVG). The epitope recognized by DM1A antibody was located to the a.a. region 426–430 (sequence AALEK); this is in accordance with previous data inferred from reactivity of the antibody with tryptic and cyanogen bromide peptides of pig brain α-tubulin (Breitling and Little, 1986). Antibodies TU-07 and DM1A thus recognize non-overlapping epitopes on α-tubulin molecule. Immunoblotting analysis revealed that the two antibodies are capable of reacting with full length tubulin isolated from porcine brain as well as with full length tubulins in cells as demonstrated on 1% NP-40 lysates from mouse BMMCs (Fig. 2). Moreover, the antibodies react with α-tubulins of various species (human, rat, chicken, plant *Nicotiana tabacum*) and do not bind to β- or γ-tubulins (not shown).

3.2. ELISA with biotinyl-tyramide signal amplification

To set up sandwich ELISA for quantification of α-tubulin, we used 96-well half-area plates (Corning) or TopYield Strips (Nunc). Antibodies, tested samples and reagents amounted to a volume of 30 μl/well. DM1A antibody was used as the capture antibody and biotinylated TU-07 antibody was applied for detection of bound tubulin. Immobilized biotinylated antibody was detected by extravidin-horseradish peroxidase and the enzyme signal was augmented by biotinyl-tyramide amplification. TMB was used as chromogen. Reaction was stopped, and absorption determined at 450 nm. Highly purified polymerization-competent porcine brain tubulin stored either in liquid nitrogen or at room temperature after freeze-drying in the presence of trehalose (Dráberová et al., 2010) was used to generate calibration curves. Concentrated tubulin samples were prediluted to ~50 μM, and any aggregates originating from the thawing and/or rehydrating process were removed by centrifugation. Actual concentration of tubulin in supernatant was checked spectrophotometrically and tubulin was then diluted to the required concentration. A typical calibration curve obtained by sandwich ELISA with biotinyl-tyramide amplification is shown in Fig. 3. Absorbance at 450 nm was measured at different tubulin concentrations ranging from 0.5 to 250 ng/ml (Fig. 3A), the curve was linear in the range of 5 to 100 ng/ml (Fig. 3B). The LOD was found to be 2.5 ng/ml. No difference was

Fig. 1. Epitope mapping. Immunostaining of peptide scans covering porcine α-tubulin 1A sequence with monoclonal antibodies TU-07 and DM1A. Peptide scans were prepared by immobilization of 45 linear 15-meric peptides with 5 amino acid overlaps. Numbers at the left and right denote positions of peptide spots in the upper, middle and lower rows of the scan; 1, a.a. 1–15 from the N-terminal end.

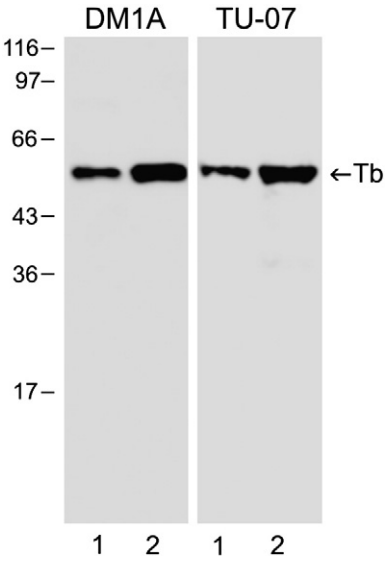

Fig. 2. Immunoblot analysis of BMMC cell extracts with monoclonal antibodies DM1A and TU-07. Porcine brain tubulin (lane 1) or 1% NP40 cell lysate from BMMCs (lane 2) was separated on 12% SDS-PAGE. Aliquots of tubulin (20 ng) were loaded in lane 1 and 4 μg of protein in lane 2. Bars on the left margin denote position of molecular weight markers in kilodaltons. Tb denotes position of tubulin.

observed when tubulin was stored in liquid nitrogen or in freeze-dried form. Very similar results were obtained when rehydrated strips, precoated with capture antibody and blocking BSA, were used after 6 months of storage at 4 °C. Usage of precoated strips can significantly save time of the assay.

3.3. Quantification of tubulin by immuno-PCR

The assay was carried out on polycarbonate TopYield strips fitting into the wells of the 96-well real-time PCR cyclers. Biotinylated TU-07 antibody was detected after incubation with extravidin followed by incubation with biotinylated DNA template. Template DNA immobilized on tubulin was quantified by real-time PCR. Compared to the widely used polypropylene PCR wells, wells of TopYield strips have a large diameter and possess a higher protein binding capacity. To prevent evaporation of PCR mixes from the wells during PCR cycling, it is essential to cover the surface of each well with light mineral oil before they are sealed (Potůčková et al., 2011). Detection of tubulin by sandwich ELISA with PCR amplification is shown in Fig. 4. Standard curves were produced with different concentrations of tubulin in the range of 0.01 to 1000 ng/ml (Fig. 4A), and the curve was linear from 0.1 to 1000 ng/ml of isolated tubulin (Fig. 4B). The LOD was found to be 0.086 ng/ml. Compared to biotinyl-tyramide signal amplification assay, the immuno-PCR amplification is characterized by broader range of detectable tubulin concentrations and higher sensitivity.

3.4. Tubulin detection in cell lysates and culture media

To prove the capability of the sandwich ELISA for monitoring the amount of tubulin, its concentrations were determined in BMMC extracts prepared from untreated and taxol-treated cells. Taxol treatment makes more tubulin in cell to polymerize

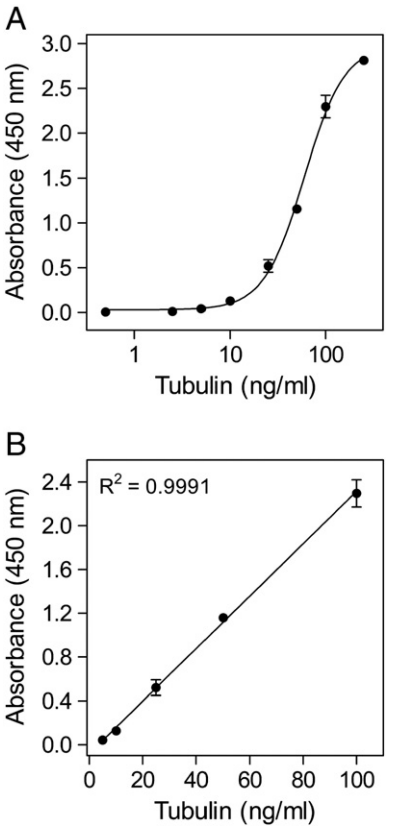

Fig. 3. Detection of tubulin at various concentrations by ELISA with biotinyl-tyramide amplification. (A) Tubulin concentration range from 0.5 to 250 ng/ml. (B) Tubulin concentration range from 5 to 100 ng/ml; R denotes correlation coefficient. Data represent mean ± SD (n = 2).

into microtubules that remain stable at 4 °C (Schiff and Horwitz, 1980). In taxol-treated BMMCs typical microtubule bundles are formed and can be detected by immunofluorescence microscopy (Fig. 5). BMMCs were solubilized in 1% NP-40 at 4 °C, and supernatants were analyzed after spinning-down the cell debris. Tubulin concentration in control cells, determined by sandwich ELISA with biotinyl-tyramide signal amplification, was 2331 ± 74.6 ng/ml (mean ± SEM, n = 3). However, preincubation of the cells for 2.5 h with 10 μM taxol reduced free tubulin concentrations to 478 ± 14.1 ng/ml (mean ± SEM, n = 3). These data document that exposure of cells to taxol leads to a substantial depletion of soluble tubulin (Fig. 6A).

Substantial changes in cell morphology and reorganization of microtubules occur during activation of BMMCs with thapsigargin (Hájková et al., 2011). Furthermore, the cells release granules containing various mediators (Dráberová et al., 2007). To find out whether thapsigargin-induced changes are accompanied by the release of tubulin into culture medium, tubulin concentrations were determined by immuno-PCR in media from resting and activated cells. While the tubulin concentration in resting cells medium was 5.3 ± 1.2 ng/ml (mean ± SEM, n = 3), it increased to 18.7 ± 5.5 ng/ml (mean ± SEM, n = 3) after thapsigargin-activation (Fig. 6B). To rule out that the increase is due to changes in cell viability, FACS measurements were performed in control and thapsigargin-activated BMMCs. The results revealed

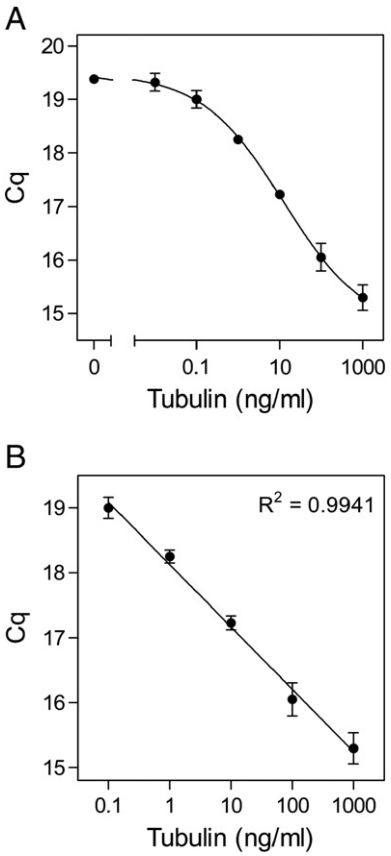

Fig. 4. Detection of various tubulin concentrations by immuno-PCR. (A) Tubulin concentration range from 0.01 to 1000 ng/ml. (B) Tubulin concentration range from 0.1 to 1000 ng/ml; R denotes correlation coefficient. Data represent mean ± SD (n = 2).

that the numbers of living cells were comparable in both samples (not shown). Activation of cells was confirmed by degranulation assay checking the level of β-glucuronidase. In control cells β-glucuronidase reached 1 ± 0.4% (mean ± SEM, n = 3) of total content of the enzyme, whereas in thapsigargin-activated cells it reached 58.4 ± 3.8% (mean ± SD, n = 3) of total enzyme content. The data thus confirm that activation of BMMCs is accompanied by release of cytosolic tubulin into medium.

4. Discussion

We have developed a new sensitive sandwich ELISA with biotinyl-tyramide or PCR signal amplification for quantification of α-tubulin isotypes in various cell types of different species. While biotinyl-tyramide amplification enhances the signal from an analyte-dependent reporter enzyme (horseradish peroxidase) (Bobrow et al., 1989), the PCR signal amplification uses analyte-dependent biotinylated DNA template for quantification by real-time PCR (Adler et al., 2003; Potůčková et al., 2011).

The components of critical importance in immunoassays are antibodies, since they can differ in their specificity, affinity to target antigen as well as non-specific binding to solid phase (Niemeyer et al., 2007). In search for biotinylated antibodies suitable for sandwich ELISA to quantify α-tubulin, we tested several commercially available conjugated antibodies as well as our own monoclonal antibodies of the TU-series (Dráber et al., 1989). Biotinylated mouse monoclonal antibody TU-07 showed the lowest nonspecific binding to "blocked" solid phase, and was therefore combined with mouse monoclonal antibody DM1A to form a matching antibody pair.

Compared to commercial PathScan Total α-Tubulin Sandwich ELISA kit (Cell Signaling), reported assays are more sensitive. Using the commercial kit, we were able to detect purified tubulin at the lowest concentration limit of 100 ng/ml (Dráberová, unpublished result), while the range of detectability was 5 to 100 ng/ml and 0.1 to 1000 ng/ml, respectively, for ELISA with biotinyl-tyramide signal amplification (Fig. 3B) and immuno-PCR (Fig. 4B). Immuno-PCR shows a >4 log dynamic range and femtomolar detection limit for tubulin dimer. The immuno-PCR thus enables to assess tubulin concentration in lysates prepared from cells, which are available only in limited amounts, e.g. cells in primary culture. Specifically in case of BMMCs, 200 cells are sufficient for determination of tubulin concentration (30 μl sample in triplicate). Performing the assays in half-area polystyrene plates or polycarbonate strips saves precious samples and reagents that are applied at volumes of only 25–30 μl. When precoated strips are used the whole assay can be performed during a single day.

Antibodies specific for α-tubulin, DM1A and TU-07, recognize amino acid sequences AALEK and HWYVG, respectively, that are evolutionarily highly conserved and are preserved from human to plants. The epitopes are located outside the C-terminal isotype-defining regions, beyond a.a. residue 430 (Khodiyar et al., 2007), and are identical in a great majority of

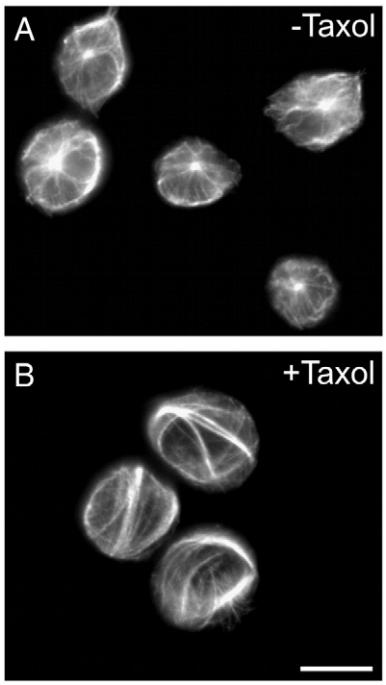

Fig. 5. Bundling of microtubules in BMMCs pretreated with anti-mitotic drug taxol. Immunofluorescence staining of control (A, −Taxol) and taxol-treated cells (B, +Taxol) with anti-tubulin antibody. Bar, 10 μm.

α-tubulin isotypes in human (*Homo sapiens* genes TUBA1A, TUBA1B, TUBA1C, TUBA3C, TUBA3D, TUBA3E, TUBA4A, TUBA8; nomenclature according to HGNC [HUGO Gene Nomenclature Committee]), mouse (*Mus musculus* genes Tuba1a, Tuba1b, Tuba1c, Tuba3a, Tuba3b, Tuba4a, Tuba8; nomenclature according to MGNC [Mouse Genomic Nomenclature Committee]) or mouse-ear cress (*Arabidopsis thaliana* genes TUA1, TUA2, TUA3, TUA4, TUA5, TUA6; nomenclature according to The Arabidopsis Information Resource [TAIR]). The matching antibody pair thus enables quantification of α-tubulin isotypes in phylogenetically distant species. Moreover, porcine brain tubulin, on which epitope mapping for antibodies DM1A and TU-07 was performed, can be utilized for the preparation of calibration curves, and controls using tubulins isolated from the same species are therefore unnecessary. Although the epitopes are located in the C-terminal region of tubulin molecule, that might potentially be cleaved off. Immunoblotting analysis revealed that antibodies recognize full-length tubulins and proteolytic fragments of tubulin were not generated during sample preparation (Fig. 2).

Epitopes recognized by DM1A and TU-07 antibodies are located outside the very C-terminal regions of α-tubulin molecules where multiple posttranslational modifications including polyglycylation and polyglutamylation were identified (Janke and Bulinski, 2011). Thus, binding of antibodies to target epitopes should not be affected by posttranslational modifications. On the other hand one cannot rule out that epitopes might in cells be masked by microtubule-associated proteins or by formation of tubulin oligomers (Mozziconacci et al., 2008). For these reasons, the assays described in this study are primarily intended for relative profiling of tubulin concentrations in lysates from different cell types and for monitoring tubulin changes after pretreatment of the cells with agents affecting equilibrium between polymeric and soluble tubulin pools. This is evident e.g. in the case of taxol that generates microtubule bundles (Fig. 5B) and depletes cytosolic tubulin from BMMCs (Fig. 6A). On the other hand, pretreatment of BMMCs with nocodazole at a concentration that depolymerizes microtubules (10 μM for 1 h) resulted in an increase of tubulin concentration in cytosolic pool (Dráberová, unpublished results).

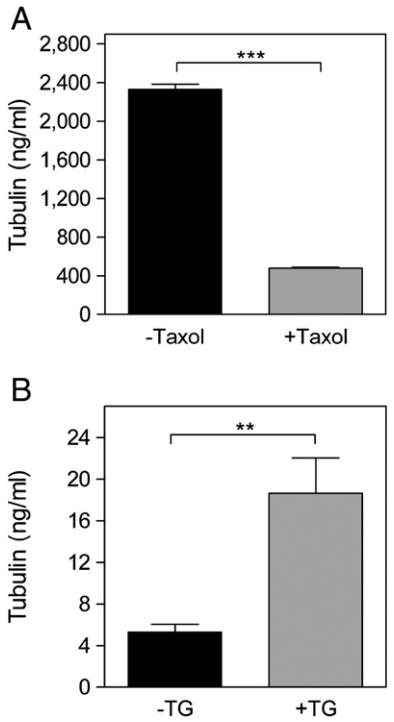

Fig. 6. Determination of tubulin concentration changes. (A) Concentration of cytosolic tubulin in untreated (−Taxol) or taxol-treated (+Taxol) BMMCs determined by ELISA with biotinyl-tyramide amplification. Bundling of microtubules by taxol leads to depletion of cytosolic tubulin. (B) Concentration of tubulin in BMMC culture media from untreated (−TG) or thapsigargin-treated (+TG) cells determined by immuno-PCR. Activation of BMMCs with thapsigargin leads to release of tubulin into media. Data are presented as the means ± SEM obtained from three independent experiments with duplicate samples. $^{**}p < 0.01$; $^{***}p < 0.001$.

Activation of mouse BMMCs, leading to the release of various mediators into extracellular space, is accompanied by dramatic changes in cell morphology and reorganization of microtubules (Dráber et al., 2012). Our data indicate, for the first time, that a small amount of tubulin during this process is also released into the culture medium (Fig. 6B). An association of tubulin with plasma membrane and detergent-resistant membranes was reported in various systems (Wolff, 2009; Macurek et al., 2008), and membrane-bound tubulin might be released into extracellular space during degranulation. Alternatively, tubulin could originate from damaged exosomes, secreted microvesicles, where tubulin subunits were also identified (Valadi et al., 2007).

It has been reported that patients with progressive multiple sclerosis, unlike healthy people, have increased tubulin concentration in cerebrospinal fluid (Semra et al., 2002; Madeddu et al., 2013). It has also been shown that evaluation of βIII-tubulin isotype levels in sera from patients with advanced gastric cancer, receiving paclitaxel treatment, is relevant prognostically for evaluation of clinical outcome (Yu et al., 2012). Due to high sensitivity of new sandwich ELISA-based assays we described here, changes in tubulin levels might be easier to detect in human body fluids.

In conclusion, sandwich ELISA assays for detection of α-tubulin isotypes make it possible to profile tubulin concentration in lysates of various cell types of different species, as well as monitor changes in tubulin concentration after treatment of cells with microtubule stabilizing or destabilizing agents. Immuno-PCR detection shows enhanced sensitivity and wider dynamic range than ELISA with biotinyl-tyramide detection. Detection of tubulin concentration at subnanogram levels might advance application of the new immunoassay for monitoring changes in tubulin concentration in body fluids during neurological or oncological diseases.

Acknowledgments

We thank T. Sulimenko for the help with epitope mapping and I. Mlchová for the excellent technical assistance. This work was supported in part by the Grant KAN200520701 from Academy of Sciences of the Czech Republic, Grants P302/12/1673, P302/11/P709, P302/10/1759, and 301/09/1826 from the Czech Science Foundation, Grants LD13015 and LD12073 from Ministry of Education, Youth and Sport of the Czech Republic to support COST Action BM1007 Mast Cells and Basophils — Targets for Innovative Therapies, and by the

Institutional Research Support (RVO 68378050). Z. Hájková and L. Stegurová were supported in part by the Faculty of Science, Charles University, Prague, Czech Republic.

References

Adler, M., Wacker, R., Niemeyer, C.M., 2003. A real-time immuno-PCR assay for routine ultrasensitive quantification of proteins. Biochem. Biophys. Res. Commun. 308, 240.

Blose, S.H., Meltzer, D.I., Feramisco, J.R., 1984. 10-nm filaments are induced to collapse in living cells microinjected with monoclonal and polyclonal antibodies against tubulin. J. Cell Biol. 98, 847.

Blume, Y., Yemets, A., Sheremet, Y., Nyporko, A., Sulimenko, V., Sulimenko, T., Dráber, P., 2010. Exposure of beta-tubulin regions defined by antibodies on an *Arabidopsis thaliana* microtubule protofilament model and in the cells. BMC Plant Biol. 10, 29.

Bobrow, M.N., Harris, T.D., Shaughnessy, K.J., Litt, G.J., 1989. Catalyzed reporter deposition, a novel method of signal amplification. Application to immunoassays. J. Immunol. Methods 125, 279.

Breitling, F., Little, M., 1986. Carboxyl-terminal regions on the surface of tubulin and microtubules. Epitope locations of YOL 1/34, DM1A and DM1B. J. Mol. Biol. 189, 367.

Bulinski, J.C., Morgan, J.L., Borisy, G.G., Spooner, B.S., 1980. Comparison of methods for tubulin quantitation in HeLa cell and brain tissue extracts. Anal. Biochem. 104, 432.

Das, S., Banerjee, S.K., Sil, M., Sarkar, P.K., 1989. An ELISA method for quantitation of tubulin using poly-1-lysine coated microtiter plates. Indian J. Exp. Biol. 27, 972.

Dozier, J.H., Hiser, L., Davis, J.A., Thomas, N.S., Tucci, M.A., Benghuzzi, H.A., Frankfurter, A., Correia, J.J., Lobert, S., 2003. β class II tubulin predominates in normal and tumor breast tissues. Breast Cancer Res. 5, R157.

Dráber, P., Dráberová, E., Zicconi, D., Sellito, C., Viklický, V., Cappuccinelli, P., 1986. Heterogeneity of microtubules recognized by monoclonal antibodies to alpha-tubulin. Eur. J. Cell Biol. 41, 82.

Dráber, P., Dráberová, E., Linhartová, I., Viklický, V., 1989. Differences in the exposure of C- and N-terminal tubulin domains in cytoplasmic microtubules detected with domain-specific monoclonal antibodies. J. Cell Sci. 92, 519.

Dráber, P., Vater, W., Böhm, K., Kuklová, E., Unger, E., 1990. Inhibition of microtubule assembly in vitro by anti-tubulin monoclonal antibodies. FEBS Lett. 262, 209.

Dráber, P., Sulimenko, V., Dráberová, E., 2012. Cytoskeleton in mast cell signaling. Front. Immunol. 3, 130.

Dráberová, E., Dráber, P., 1993. A microtubule-interacting protein involved in coalignment of vimentin intermediate filaments with microtubules. J. Cell Sci. 106, 1263.

Dráberová, L., Shaik, G.M., Volná, P., Heneberg, P., Tůmová, M., Lebduška, P., Korb, J., Dráber, P., 2007. Regulation of Ca^{2+} signaling in mast cells by tyrosine-phosphorylated and unphosphorylated non-T cell activation linker. J. Immunol. 179, 5169.

Dráberová, E., Sulimenko, V., Sulimenko, T., Böhm, K.J., Dráber, P., 2010. Recovery of tubulin functions after freeze-drying in the presence of trehalose. Anal. Biochem. 397, 67.

Hájková, Z., Bugajev, V., Dráberová, E., Vinopal, S., Dráberová, L., Janáček, J., Dráber, Pe, Dráber, P., 2011. STIM1-directed reorganization of microtubules in activated cells. J. Immunol. 186, 913.

Hibbs, M.L., Tarlinton, D.M., Armes, J., Grail, D., Hodgson, G., Maglitto, R., Stacker, S.A., Dunn, A.R.R., 1995. Multiple defects in the immune-system of Lyn-deficient mice, culminating in autoimmune-disease. Cell 83, 301.

Janke, C., Bulinski, J.C., 2011. Post-translational regulation of the microtubule cytoskeleton: mechanisms and functions. Nat. Rev. Mol. Cell Biol. 12, 773.

Katsetos, C.D., Dráber, P., 2012. Tubulins as therapeutic targets in cancer: from bench to bedside. Curr. Pharm. Des. 18, 2778.

Khodiyar, V.K., Maltais, L.J., Ruef, B.J., Sneddon, K.M., Smith, J.R., Shimoyama, M., Cabral, F., Dumontet, C., Dutcher, S.K., Harvey, R.J., Lafanechere, L., Murray, J.M., Nogales, E., Piquemal, D., Stanchi, F., Povey, S., Lovering, R.C., 2007. A revised nomenclature for the human and rodent α-tubulin gene family. Genomics 90, 285.

Linhartová, I., Dráber, P., Dráberová, E., Viklický, V., 1992. Immunological discrimination of β-tubulin isoforms in developing mouse brain. Posttranslational modification of non-class III β-tubulins. Biochem. J. 288, 919.

Ludueña, R.F., Banerjee, A., 2008. The isotypes of tubulin: distribution and functional significance. In: Fojo, T. (Ed.), The Role of Microtubules in Cell Biology, Neurobiology and Oncology. Humana Press, Totowa, NJ, p. 123.

Macurek, L., Dráberová, E., Richterová, V., Sulimenko, V., Sulimenko, T., Dráberová, L., Marková, V., Dráber, P., 2008. Regulation of microtubule nucleation in differentiating embryonal carcinoma cells by complexes of membrane-bound γ-tubulin with Fyn kinase and phosphoinositide 3-kinase. Biochem. J. 416, 421.

Madeddu, R., Farace, C., Tolu, P., Solinas, G., Asara, Y., Sotgiu, M.A., Delogu, L.G., Prados, J.C., Sotgiu, S., Montella, A., 2013. Cytoskeletal proteins in the cerebrospinal fluid as biomarker of multiple sclerosis. Neurol. Sci. 34, 181.

Mozziconacci, J., Sandblad, L., Wachsmuth, M., Brunner, D., Karsenti, E., 2008. Tubulin dimers oligomerize before their incorporation into microtubules. PLoS One 3, e3821.

Niemeyer, C.M., Adler, M., Wacker, R., 2005. Immuno-PCR: high sensitivity detection of proteins by nucleic acid amplification. Trends Biotechnol. 23, 208.

Niemeyer, C.M., Adler, M., Wacker, R., 2007. Detecting antigens by quantitative immuno-PCR. Nat. Protoc. 2, 1918.

Pipeleers, D.G., Pipeleers-Marichal, M.A., Sherline, P., Kipnis, D.M., 1977. A sensitive method for measuring polymerized and depolymerized forms of tubulin in tissues. J. Cell Biol. 74, 341.

Potůčková, L., Franko, F., Bambousková, M., Dráber, P., 2011. Rapid and sensitive detection of cytokines using functionalized gold nanoparticle-based immuno-PCR, comparison with immuno-PCR and ELISA. J. Immunol. Methods 371, 38.

Rivera, J., Fierro, N.A., Olivera, A., Suzuki, R., 2008. New insights on mast cell activation via the high affinity receptor for IgE. Adv. Immunol. 98, 85.

Schiff, P.B., Horwitz, S.B., 1980. Taxol stabilizes microtubules in mouse fibroblast cells. Proc. Natl. Acad. Sci. U. S. A. 77, 1561.

Semra, Y.K., Seidi, O.A., Sharief, M.K., 2002. Heightened intrathecal release of axonal cytoskeletal proteins in multiple sclerosis is associated with progressive disease and clinical disability. J. Neuroimmunol. 122, 132.

Shelanski, M.L., Gaskin, F., Cantor, C.R., 1973. Microtubule assembly in the absence of added nucleotides. Proc. Natl. Acad. Sci. U. S. A. 70, 765.

Smertenko, A., Blume, Y., Viklický, V., Dráber, P., 1997. Exposure of tubulin structural domains in *Nicotiana tabacum* microtubules probed by monoclonal antibodies. Eur. J. Cell Biol. 72, 104.

Sulimenko, V., Sulimenko, T., Poznanovic, S., Nechiporuk-Zloy, V., Böhm, J.K., Macůrek, L., Unger, E., Dráber, P., 2002. Association of brain γ-tubulins with αβ-tubulin dimers. Biochem. J. 365, 889.

Surviladze, Z., Dráberová, L., Kovářová, M., Boubelík, M., Dráber, P., 2001. Differential sensitivity to acute cholesterol lowering of activation mediated via the high-affinity IgE receptor and Thy-1 glycoprotein. Eur. J. Immunol. 31, 1.

Thrower, D., Jordan, M.A., Wilson, L., 1991. Quantitation of cellular tubulin in microtubules and tubulin pools by a competitive ELISA. J. Immunol. Methods 136, 45.

Valadi, H., Ekström, K., Bossios, A., Sjöstrand, M., Lee, J.J., Lötvall, J.O., 2007. Exosome-mediated transfer of mRNAs and microRNAs is a novel mechanism of genetic exchange between cells. Nat. Cell Biol. 9, 654.

Weingarten, M.D., Lockwood, A.H., Hwo, S.Y., Kirschner, M.W., 1975. A protein factor essential for microtubule assembly. Proc. Natl. Acad. Sci. U. S. A. 72, 1858.

Wilson, L., 1970. Properties of colchicine binding protein from chick embryo brain. Interactions with vinca alkaloids and podophyllotoxin. Biochemistry 9, 4999.

Wolff, J., 2009. Plasma membrane tubulin. Biochim. Biophys. Acta 1788, 1415.

Yu, J., Gao, J., Lu, Z., Li, Y., Shen, L., 2012. Serum levels of TUBB3 correlate with clinical outcome in Chinese patients with advanced gastric cancer receiving first-line paclitaxel plus capecitabine. Med. Oncol. 29, 3029.

7.9 RAPID AND SENSITIVE DETECTION OF CYTOKINES USING FUNCTIONALIZED GOLD NANOPARTICLE-BASED IMMUNO-PCR, COMPARISON WITH IMMUNO-PCR AND ELISA.

Potůčková L., Franko F., Bambousková M., Dráber P.

J. Immunol. Methods, 371(1-2):38-47, 2011

Journal of Immunological Methods 371 (2011) 38–47

Contents lists available at ScienceDirect

Journal of Immunological Methods

journal homepage: www.elsevier.com/locate/jim

Research paper

Rapid and sensitive detection of cytokines using functionalized gold nanoparticle-based immuno-PCR, comparison with immuno-PCR and ELISA

Lucie Potůčková, Filip Franko, Monika Bambousková, Petr Dráber *

Laboratory of Signal Transduction, Institute of Molecular Genetics, Academy of Sciences of the Czech Republic, CZ-14220 Prague 4, Czech Republic

ARTICLE INFO

Article history:
Received 7 March 2011
Received in revised form 9 June 2011
Accepted 13 June 2011
Available online 24 June 2011

Keywords:
Cytokine detection
Gold nanoparticle
Immuno-PCR
ELISA
Real-time PCR
Mast cell

ABSTRACT

Reliable and simple methods are required for detection of low concentrations of cytokines and some other proteins in complex biological fluids. This is especially important when monitoring the immune responses under various physiological and pathophysiological conditions *in vivo* or following production of these compounds in *in vitro* systems. Cytokines and other immunologically active molecules are being predominantly detected by enzyme-linked immunosorbent assays (ELISA) and newly also by immuno-polymerase chain reactions (iPCR). New simplified variants of iPCR have recently been described where antibodies are connected with multiple DNA templates through gold nanoparticles (Au-NPs) to form a new class of detection reagents. In this study we compared functionalized Au-NP-based iPCR (Nano-iPCR) with standard ELISA and iPCR for the detection of interleukin (IL)-3 and stem cell factor (SCF). The same immunoreagents (IL-3- and SCF-specific polyclonal antibodies and their biotinylated forms) were used throughout the assays. The obtained data indicate that both Nano-iPCR and iPCR are superior in sensitivity and detection range than ELISA. Furthermore, Nano-iPCR is easier to perform than the other two methods. Nano-iPCR was used for monitoring changes in concentration of free SCF during growth of mast cells in SCF-conditioned media. The results show that growing cultures gradually reduce the amount of SCF in supernatant to 25% after 5 days. The combined data indicate that Nano-iPCR assays may be preferable for rapid detection of low concentrations of cytokines in complex biological fluids.

1. Introduction

Cytokines are small signaling protein molecules that are produced by cells of diverse embryonic origin and serve as important mediators of the immune system. Abnormal activities of several cytokines, including interleukin (IL)-3, have been reported in schizophrenia (Chen and Kendler, 2008), and elevated levels of stem cell factor (SCF) have been detected in asthmatic patients (Lei et al., 2008). Sensitive, simple and robust methods are required for diagnostic purposes to determine low concentrations of cytokines in complex biological fluids. They are needed for monitoring immune responses *in vivo* as well as for rapid analysis of the quality of conditioned media used in culturing cytokine-dependent cells. Growth of mouse bone marrow-derived mast cells (BMMCs) *in vitro*, is promoted by two cytokines, IL-3 and SCF (Tsuji et al., 1991). Concentrations of these and other cytokines are being determined by several methods, such as bioassays employing cytokine-dependent freshly isolated cells or cell lines (Chen et al., 1993). Although very useful, these assays are time consuming and inaccurate.

Abbreviations: IL, interleukin; SCF, stem cell factor; BMMC, bone marrow-derived mast cell; ELISA, enzyme-linked immunosorbent assay; RT, reverse-transcription; PCR, polymerase chain reaction; iPCR, immuno-PCR; Au-NP, gold nanoparticle; Nano-iPCR, functionalized Au-NP-based iPCR; r, recombinant; FBS, fetal bovine serum; DMEM, Dulbecco's modified Eagle medium; PBS, phosphate buffer solution; BSA, bovine serum albumin; TPBS, PBS containing 0.05% Tween 20; HRP, horseradish peroxidase; OPD, o-phenylenediamine; C_q, quantification cycle.

* Corresponding author at: Laboratory of Signal Transduction, Institute of Molecular Genetics, Academy of Sciences of the Czech Republic, Videňská 1083, Prague 4, CZ-142 20, Czech Republic. Tel.: +420 241062468; fax: +420 241062214.
E-mail address: draberpe@img.cas.cz (P. Dráber).

0022-1759 © 2011 Elsevier B.V. Open access under CC BY-NC-ND license.
doi:10.1016/j.jim.2011.06.012

Widespread methods used for detection of cytokines are enzyme-linked immunosorbent assays (ELISA) utilizing antibodies specific for the target proteins (Silman and Katchalski, 1966; Engvall and Perlmann, 1971). However, the sensitivity of these assays is not always sufficient. It has been shown that the amount of cytokine produced by cells correlates with the expression of cytokine-specific mRNA; reverse-transcription (RT) polymerase chain reactions (PCR) have therefore also been widely used. Although RT-PCRs are fast, sensitive and simple methods to detect the expression levels of cytokine genes, the results do not always agree with those of bioassays and ELISA, and do not allow exact determination of cytokine concentrations. Other assays have therefore been explored. In 1992 a new technique was described, combining molecular specificity of antibodies with the amplification power and sensitivity of PCR (Sano et al., 1992). In this technique, called immuno-PCR (iPCR), the antibody used for detection of target compound is combined with the DNA which serves as a template in PCR. Different strategies have been applied for linking antibodies with DNA templates, like streptavidin bridge combined with biotinylated antibody and biotinylated DNA template, or chemically conjugated antibody-DNA complexes (Lind and Kubista, 2005; Niemeyer et al., 2007). The amount of DNA amplified during PCR corresponds to the amount of target structure recognized by the antibody, and can be detected by electrophoresis (Zhou et al., 1993) or by ELISA, utilizing digoxigenin- or biotin-labeled PCR products (Niemeyer et al., 1997; Smrž and Dráber, 2003). Later, immunodetection was combined with real-time PCR and used for quantification of vascular endothelial grow factor (Sims et al., 2000). The method was further modified in such a way that both protein detection and real-time PCR were performed in the same well of the TopYield strip (Niemeyer et al., 2007). Furthermore, a gold nanoparticle (Au-NP)-based bio-bar code assay for ultrasensitive detection of proteins has been developed. The assay utilizes Au-NPs functionalized with both thiolated single-strand DNA oligonucleotide and an antibody to the target antigen (Nam et al., 2003, 2004; Georganopoulou et al., 2005). Finally, PCR assays based on antibody- and oligonucleotide-functionalized Au-NPs were used for detection of Hantaan virus nucleocapsid protein (Chen et al., 2009) and respiratory syncytial viruses (Perez et al., 2011). Although the assays showed high sensitivity for virus detection, they required two sets of wells (for immunodetection and PCR) and therefore were not suitable for high throughput screening and were fraught with high risk of contamination.

Here we tested the suitability of functionalized Au-NPs-based iPCR (Nano-iPCR) for detection of low concentrations of cytokines in cell culture supernatants, and changes in cytokine concentration in aging cultures of BMMCs. We defined the conditions for simplified detection of cytokines by Nano-iPCR, and compared the performance of assays based on antibodies anchored either directly on the plastic surface or through extravidin. The assays were carried out in PCR polypropylene wells or wells of TopYield polycarbonate strips which allow more efficient binding of antibodies. We further compared Nano-iPCR with iPCR and ELISA; outline of the assays is shown in Fig. 1. For these comparisons we utilized identical immunoreagents in all assays. The data indicate that Nano-iPCR offers a sensitive, rapid and robust assay for detection of low concentrations of cytokines in complex biological fluids. Advantages and drawbacks of different assays are discussed.

2. Materials and methods

2.1. Materials

Rabbit anti-murine IL-3 and rabbit anti-murine SCF polyclonal antibodies and their biotinylated forms, recombinant (r) murine IL-3 and rSCF were all obtained from PeproTech (London, UK). Colloidal Au-NPs (30 nm), containing approximately 2×10^{11} Au-NPs/ml, were obtained from BBInternational (Cardiff, UK). Au-NPs (5 nm) conjugated with goat anti-rabbit IgG were bought from Jackson ImmunoResearch Lab., Inc. (West Grove, PA, USA). 5′thiol-modified oligonucleotide primer (Pri)1 [5′-(5ThioMC6-D//iSp18)CCTTGAACCTGTGCCATTTGAATATATTAAGACTATACGCGGGAACA-3′] where iSp18 is an 18-atom hexa-ethyleneglycol spacer connecting the thiol reactive group and the DNA sequence, Pri2 (5′-CCTTGAACCTGTGCCATTTG-3′) and Pri3 (5′-GTCCCTCCATCTTCCTACTGTTCCACATGTTCCCGCGTATAGTCTT-3′) were obtained from IDT, (Coralville, IA, USA). Biotinylated forward primer 5B-HRM1-F (5′-CTCATCACCACGCTCCATTA-3′) and its non-biotinylated form (HRM1-F) and reverse primer HRM1-R (5′-TCTTCCACCTCCATGGTGTC-3′) were obtained from Generi Biotech (Hradec Králove, Czech Republic). SYTO-9 and geneticin (G418) were obtained from Invitrogen (Eugene, OR, USA). Glutaraldehyde was bought from Fluka, Chemie GmbH (Buchs, Switzerland). All other chemicals were from Sigma-Aldrich (St. Louis, MO, USA).

2.2. Cells

BMMCs were isolated from C57BL/6 mice according to the previously reported protocol (Volná et al., 2004). All mice were maintained and used in accordance with the Institute of Molecular Genetics guidelines. The cells were seeded in complete culture medium RPMI-1640 containing 10% heat inactivated (56 °C, 30 min) fetal bovine serum (FBS), 50 μM 2-mercaptoethanol, antibiotics (100 U/ml penicillin and 100 μg/ml streptomycin) and further supplemented with fresh rSCF (15 ng/ml) and 10% culture supernatant of confluent D11 cells as a source of IL-3 (Cao et al., 2007). BMMCs were cultured at 37 °C in an atmosphere of 5% CO_2 in air. D11 cells were grown adherent in tissue culture flasks in Dulbecco's modified Eagle medium (DMEM) supplemented with 10% heat inactivated FBS, antibiotics and 0.3 mg/ml of geneticin. The cells were detached from the flasks by incubation for 5–10 min at room temperature with 0.05% trypsin in phosphate buffered saline (PBS; 10 mM phosphate, pH 7.4, 150 mM NaCl) supplemented with 0.02% EDTA. After centrifugation at 280 ×*g* for 5 min, cells were resuspended in DMEM-10% FCS with geneticin. After 3 days of culturing, the medium was aspirated and fresh DMEM medium without geneticin was added. Cells were cultured for additional week. Supernatant containing IL-3 was then collected, centrifuged at 5500 ×*g* for 15 min, filtered through a 0.22 μm membrane and stored in aliquotes at −20 °C. For determination of SCF, supernatant from cultured BMMCs was collected daily for 5 days.

2.3. Au-NPs functionalized with DNA and antibodies

Functionalized Au-NPs were prepared as previously described (Hill and Mirkin, 2006) with some modifications. One milliliter of 30 nm Au-NPs solution was incubated for 30 min at room temperature with 4 μg of polyclonal antibody (anti-IL-3 or anti-SCF) under gentle shaking. Ten microliters of 10% Tween 20 was then added, followed after 5 min by 50 μl of 2 M NaCl in 10 mM PBS (Hurst et al., 2008). The particles were then modified with 5′-thiolated oligonucleotide (final concentration 4 nmol/ml) under gentle shaking at 4 °C. After overnight incubation the samples were further salted by adding 50 μl aliquotes of 2 M NaCl in 10 mM PBS in 4 subsequent steps, each for 1 h. Functionalized Au-NPs were stabilized by adding 20 μl of 10% bovine serum albumin (BSA), followed by gentle shaking for 30 min at room temperature. Unbound oligonucleotides were removed by three times centrifugation (9.300 ×*g* for 10 min) through a discontinuous glycerol gradient in 2 ml Eppendorf tubes. The gradient consisted of 800 μl PBS containing 30% glycerol (w/v) and 1% BSA (w/v), overlaid with 1 ml of functionalized Au-NPs. The pellet was finally resuspended in 1 ml of PBS containing 1% BSA, 0.05% Tween 20, 20% glycerol and 0.02% NaN_3. In some experiments Au-NPs were functionalized with BSA instead of antibody. Absorption spectra were recorded with a UV-1601 spectrophotometer (Shimadzu Corporation, Kyoto, Japan) equipped with software package UVProbe (Shimadzu) and quartz cells (200 μl) with 10 mm path length.

2.4. Electron microscopy

Nickel electron microscopy grids coated with pioloform were glow discharged and coated with poly-L-lysine. Au-NPs functionalized with antibodies or with BSA were allowed to settle on the coated grids. After 10 min, the grids were washed in PBS and free protein-binding sites were blocked for 15 min with 0.1% BSA in PBS. Grids with bound Au-NPs were then incubated with the secondary antibody (goat anti-rabbit IgG, conjugated with 5 nm Au-NPs), diluted 1:10 in PBS-0.1% BSA. After 30 min the grids were washed three times for 5 min each with PBS. The grids were fixed in 2.5% glutaraldehyde in PBS for 10 min. Finally, samples were washed twice with MilliQ water (Millipore, Billerica, MA, USA) for 1 min, air-dried and examined with a JEOL JEM-1200EX transmission electron microscope (JEOL, Tokyo, Japan) operating at 60 kV.

2.5. Nano-iPCR

For detection of cytokines by Nano-iPCR, two methods were used differing in the mode of anchoring the antibodies to plastic surface. In Nano-iPCR I biotinylated antibody was attached to immobilized extravidin, whereas in Nano-iPCR II the antibody was directly bound to the plate.

2.5.1. Nano-iPCR I

One hundred microliter aliquotes of extravidin (1–2 μg/ml in 100 mM borate buffer, pH 9.5) were added into each well of real-time 96-well plate or real-time tube strip (Eppendorf, Hamburg, Germany) and incubated for 1 h at 37 °C. After adsorption of the protein, the wells were washed with PBS containing 0.05% Tween 20 (TPBS) and the remaining binding sites were blocked by 2 h incubation at 37 °C with TPBS supplemented with 2% BSA. The wells were then washed three times with 200 μl of TPBS, followed by addition of 100 μl biotinylated anti-SCF or anti-IL-3 antibody (1 μg/ml in TPBS-1% BSA). After incubation for 1 h at 37 °C, unbound antibody was rinsed out and 100 μl sample aliquotes were probed for the presence of SCF or IL-3. The samples were incubated overnight at 4 °C, and after washing four times with TPBS, 100 μl of Au-NPs armed with thiolated DNA oligonucleotide and anti-SCF or anti-IL-3 (diluted 1/10,000 in TPBS-1% BSA) were applied into each well. The wells were incubated for 1 h at 37 °C, washed 4 times with 200 μl TPBS followed by double washing with MilliQ water. Next, aliquotes of 25 μl of master mix solution containing 75 mM Tris–HCl (pH 8.8), 20 mM $(NH_4)_2SO_4$, 2.5 mM $MgCl_2$, 200 μM dATP, 200 μM dGTP, 200 μM dCTP, 200 μM dTTP, Taq DNA polymerase (25 U/ml), 2 μM SYTO-9 and 60 nM oligonucleotide primers Pri2 and Pri3 were dispensed into each well. Plates were sealed with Light cycler 480 sealing foil (Roche, Mannheim, Germany) and PCR strips with Masterclear cap strips (Eppendorf). The amount of template DNA bound to antigen-anchored functionalized Au-NPs was evaluated by real-time PCR using Realplex^4 Mastercycler (Eppendorf, Hamburg, Germany) with the following cycling conditions: 1 min at 94 °C, followed by 40 cycles of 20 s at 94 °C, 20 s at 53 °C and 20 s at 72 °C. The control without template DNA was used for PCR mix in every run to check for contamination.

2.5.2. Nano-iPCR II

Twenty-five microliter aliquotes of capture antibody (5 μg/ml anti-IL-3 or anti-SCF; Peprotech) in 100 mM borate buffer (pH 9.5) were distributed into each well of TopYield strips (NUNC, Roskilde, Denmark). After 1 h incubation at 37 °C and overnight incubation at 4 °C each well was washed four times with 200 μl of TPBS, and free binding sites were blocked with TPBS-2% BSA for 2 h at 37 °C. Each well was washed four times with TPBS, followed by addition of 25 μl of the tested sample containing IL-3 or SCF and incubation for 1 h at 37 °C. Other steps were the same as in Nano-iPCR I. Cycling conditions were as follows: 2 min at 95 °C, 40 cycles of 15 s at 95 °C, 60 s at 60 °C and 60 s at 72 °C.

Fig. 1. Schematic illustration of the immunoassays used in this study. In Nano-iPCR I method, wells of real-time 96-well plate or real-time tube strips were coated with extravidin (ExAv) to which biotinylated antigen-specific antibody (Ab-Bt) was anchored. BSA was used to block free binding sites. Antigen (Ag) was then added and bound to the immobilized antibody. The antibody anchored antigen was detected by Au-NPs functionalized by antigen-specific antibody and thiolated oligonucleotide which served as a template in subsequent real-time PCR with a set of template-specific primers. DNA amplicons were detected by fluorometry using DNA binding dye SYTO-9. In Nano-iPCR II method, the antibody (Ab) was bound directly to the TopYield strip wells followed by blocking free protein-binding sites with BSA; all other steps were the same as in Nano-iPCR I. In iPCR and ELISA, the Ag-specific antibody was adsorbed directly onto the surface of the well, followed by BSA block. Antigen was then added and detected by biotinylated antibody. In iPCR, extravidin was supplied to form a bridge between the biotinylated antibody and biotinylated DNA template (DNA-Bt) added during the next step. Template DNA was then amplified by real-time PCR (using a set of template-specific primers), and the amplicons were detected by means of SYTO-9 DNA dye. In ELISA, biotinylated antibody immobilized on Ag reacted with streptavidin-HRP conjugate (S-HRP). The enzymatic activity was detected using a colorimetric reaction with OPD as a substrate. The colored end-product (P) was quantified by spectrophotometery.

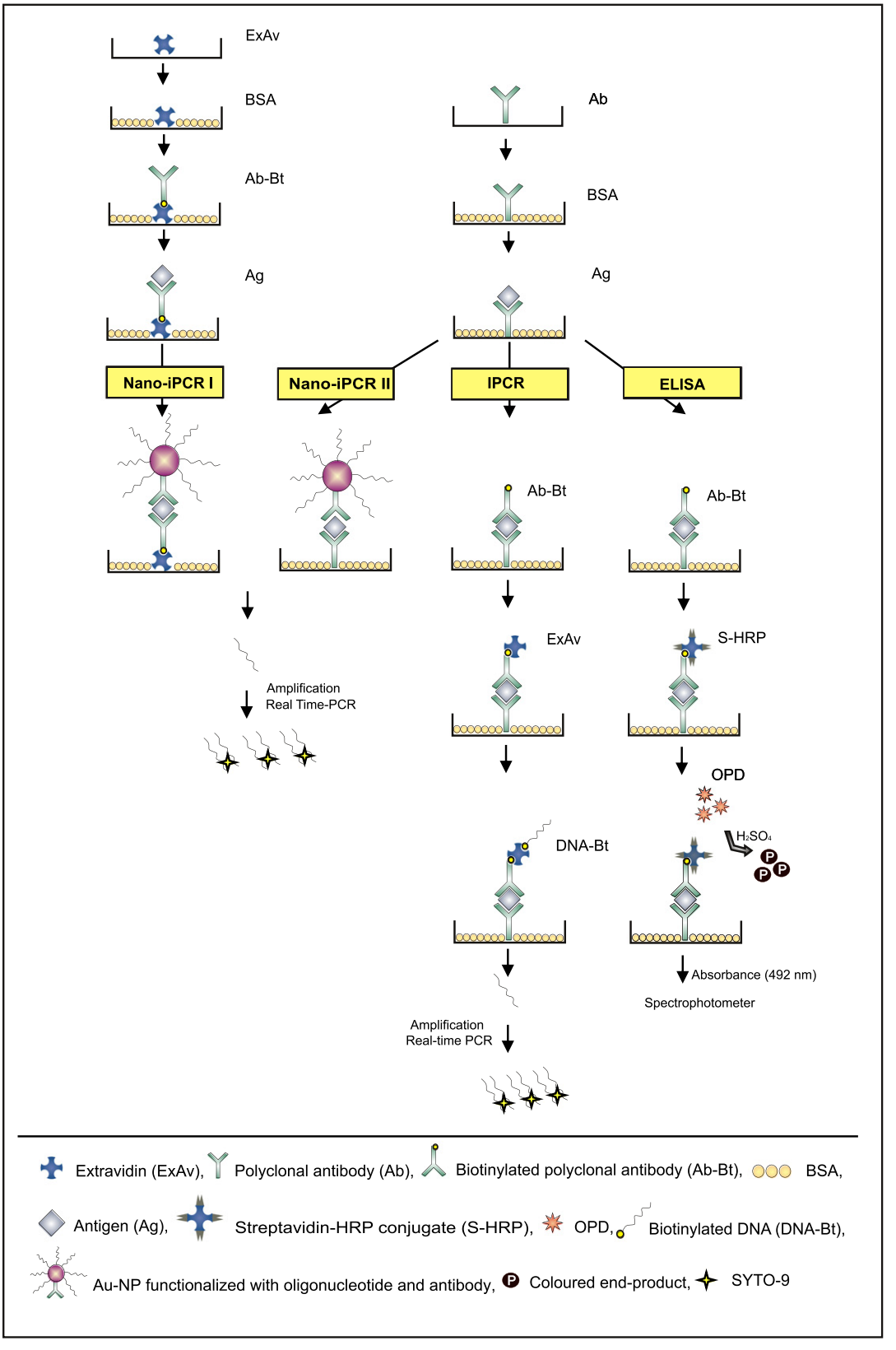
ExAv
BSA
Ab-Bt
Ag
Nano-iPCR I
Nano-iPCR II
IPCR
ELISA
Ab
BSA
Ag
Ab-Bt
Ab-Bt
Amplification
Real Time-PCR
ExAv
S-HRP
OPD
H2SO4
DNA-Bt
Absorbance (492 nm)
Spectrophotometer
Amplification
Real-time PCR
Extravidin (ExAv),
Polyclonal antibody (Ab),
Biotinylated polyclonal antibody (Ab-Bt),
BSA,
Antigen (Ag),
Streptavidin-HRP conjugate (S-HRP),
OPD,
Biotinylated DNA (DNA-Bt),
Au-NP functionalized with oligonucleotide and antibody,
Coloured end-product,
SYTO-9

2.6. iPCR

The method was performed as previously described (Niemeyer et al., 2007) with some modifications. Biotinylated DNA template (221 bps) was obtained by PCR using biotinylated forward primer 5B-HRM1-F (200 nM), reverse primer HRM1-R (800 nM) and amplified template DNA (0.1 ng; GenBank accession no. M14752). The following cycling conditions were used: 2 min at 95 °C, followed by 30 cycles of 15 s at 95 °C, 30 s at 58 °C and 20 s at 72 °C. Each well of the TopYield strip contained 25 μl polyclonal antibody specific for IL-3 or SCF (5 μg/ml, in 100 mM borate buffer pH 9.5). The wells were incubated for 1 h at 37 °C and overnight at 4 °C, followed by washing four times with 200 μl of TPBS. Free binding sites were blocked by incubation with TPBS-2% BSA. After 2 h at 37 °C, the wells were again washed four times and overlaid with 25 μl of tested samples containing various concentrations of IL-3 or SCF. The wells were further incubated for 1 h 37 °C and then washed 4 times with TPBS. Subsequently, 25 μl aliquotes of biotinylated antibody specific for IL-3 or SCF (1 μg/ml in TPBS-1% BSA) were dispensed and the samples were incubated for 1 h at 37 °C. After washing four times, the wells were covered with 25 μl of extravidin (0.1 μg/ml) in TPBS-1% BSA, incubated for 1 h at 37 °C and washed as before. After this step, biotinylated DNA template (25 μl; 0.27 pg/ml) was added and the strips were incubated for 1 h at 37 °C. Next, the wells were washed four times with TPBS and twice with MilliQ water. The amount of biotinylated DNA template immobilized in individual wells was quantified by real-time PCR using master mix supplemented with HRM1-F and HRM1-R primer set (200 nM each). The following cycling conditions were used: 2 min at 95 °C as an initial denaturation step and 40 cycles consisting of 15 s at 95 °C, 60 s at 60 °C and elongation for 60 s at 72 °C.

2.7. ELISA

ELISA was performed as previously described (Engvall and Perlmann, 1971) with some modifications. Wells of the TopYield strips were coated with Ag-specific polyclonal antibody, blocked with TPBS-2% BSA and then mixed with antigen as described above for iPCR. The wells were then washed three times with TPBS, followed by addition of 100 μl biotinylated antibody (1 μg/ml, in TPBS-1% BSA), incubation for 1 h at 37 °C and washing three times with TPBS. One hundred microliters of streptavidin-horseradish peroxidase (HRP) conjugate (0.1 μg/ml) was then added. After incubation for 1 h at 37 °C the wells were washed three times with TPBS. Finally, 100 μl PBS containing o-phenylenediamine (OPD; 0.5 mg/ml) and H_2O_2 (0.015%) was dispensed into each well. After 10 min at 37 °C, the reaction was stopped by adding 100 μl of H_2SO_4 (4 M). The absorbance was determined at 492 nm using Infinite M200 plate reader (TECAN, Männedorf, Switzerland).

2.8. Data analysis

For calibration curves, absorbance or quantification cycle (C_q) values were plotted against SCF or IL-3 concentrations using a four-parameter logistic regression model function (variable slope) within GrafPad Prism 5 (GraphPad Software, La Jolla, CA, USA). For calculation of IL-3 or SCF concentrations in the tested samples, the same mathematical model was used, using MasterPlex ReaderFit software (Hitachi Solutions America, Ltd, MiraiBio Group, South San Francisco, CA, USA).

3. Results

3.1. Characterization of functionalized Au-NPs

Au-NPs functionalized with thiolated oligonucleotides and antibodies were initially characterized by two methods. The presence of antibodies bound to 30 nm Au-NPs was verified by means of secondary anti-immunoglobulin-specific antibodies conjugated to 5 nm Au-NPs. Formation of rosettes of 30 nm Au-NPs surrounded by 5 nm-Au-NPs detectable by electron microscopy was taken as an evidence of the presence of antibodies on 30 nm Au-NPs. As shown in Fig. 2A, all 30 nm Au-NPs formed rosettes with 5 nm particles. The binding was specific as indicated by the absence of rosettes in samples containing 30 nm Au-NPs covered with BSA instead of antibodies (Fig. 2B) or with thiolated oligonucleotides alone (not shown). A typical distribution pattern of 30 nm Au-NPs associated with 1–7 gold 5 nm particles is shown in Fig. 2C. It should be noted that the number of 5 nm particles bound to 30 nm Au-NPs is underestimated because a fraction of 5 nm particles is overshadowed by the dense bodies of 30 nm particles.

Concentrations and physical properties of functionalized Au-NPs were characterized by means of UV–vis spectrophotometry (Fig. 2D). Unconjugated 30 nm Au-NPs showed an absorption peak at 525 nm. This changed to higher wavelength values by 5–10 nm if the particles were functionalized by antibodies and oligonucleotides. Absorption maxima at values >535 nm were indicative of suboptimal performance of the particles in Nano-iPCR. The actual values of the 525–535 nm peak and calculated extinction coefficient [$\varepsilon_{528\ nm} = 3.7 \times 10^9\ cm^{-1}\ M^{-1}$ (Jin et al., 2003)] made it possible to determine the number of particles present in the sample.

The number of single-stranded oligonucleotides bound to 30 nm Au-NPs was evaluated by a modified real-time PCR-based method (Kim et al., 2006) where DNA binding dye SYTO-9 was used instead of a fluorescence probe. Au-NPs with bound thiolated Pri1 oligonucleotide were directly diluted into SYTO-9-containing PCR master mix supplemented with primers (Pri2 and Pri3), and analyzed by real-time PCR (Fig. 3A). Linearity of the data and regression coefficients close to 1 indicated that the presence of 30 nm Au-NPs did not interfere with the assay and therefore was not necessary to dissociate oligonucleotide template from Au-NPs before the PCR. Similar good linearity and reasonable regression coefficients were observed in assays containing a defined amount of free Pri1 oligonucleotide (Fig. 3B). Based on the results of such assays and estimated number of gold particles in stock solutions of functionalized Au-NPs it was possible to calculate the number of oligonucleotides per one oligonucleotide- and antibody-functionalized particle as 83 ± 26 (mean ± S.D.; $n = 5$). The $1/10^4$ dilution of functionalized Au-NPs in Nano-PCR assays corresponds to approximately 1.4 pmol/l of Pri1 oligonucleotide.

3.2. Optimization of the Nano-iPCR

The sensitivity of immunoassays is limited by background signal caused by nonspecific binding of assay components (primary and secondary antibodies, antigen, extravidin, biotinylated

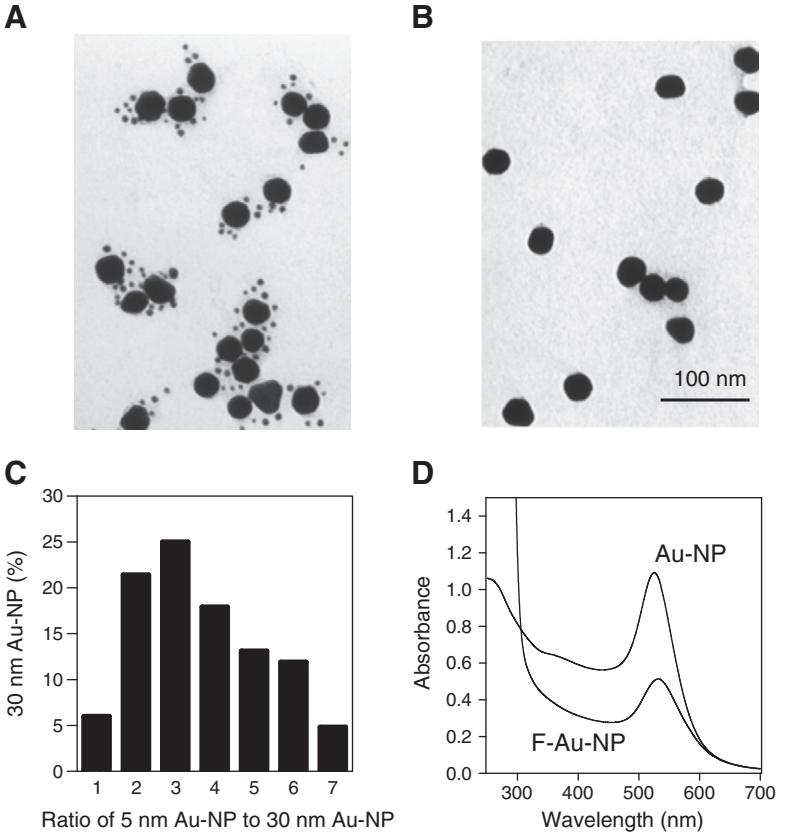

Fig. 2. Characterization of antibody-functionalized Au-NPs. (A, B) Electron microscopy visualization of polyclonal antibody bound to Au-NPs. (A) 30 nm Au-NPs were conjugated with polyclonal antibody followed by an exposure to secondary 5 nm Au-NP labeled with anti-IgG. After washing the particles were observed by electron microscopy. (B) Control 30 nm Au-NPs were conjugated with BSA, followed by an exposure to 5 nm Au-NP-labeled anti-IgG antibody. (C) Distribution of 5 nm Au-NPs (armed with anti-rabbit IgG) bound to 30 nm Au-NPs functionalized with polyclonal rabbit antibody. In total, 84 particles of 30 nm size were evaluated. (D) UV–vis spectrophotometry of control (Au-NP) and oligonucleotide- and antibody-functionalized particles (F-Au-NP).

DNA templates and/or functionalized Au-NPs) to both each other and plastic surfaces of the wells. In pilot experiments we therefore tried to define the optimal conditions for iPCR. We compared the performance of two buffers (PBS or HEPES) supplemented with several blocking agents at different concentrations (2–5% BSA, 2% ovalbumin or 2% casein) and two different detergents at various concentrations (0.01–0.2% Tween 20 or 0.1–2% Pluronic F68). A series of optimization experiments showed that the most effective agents for blocking and washing were TPBS-2% BSA and TPBS, respectively.

In initial experiments with TopYield strips we noticed, in accordance with previous studies (Barletta et al., 2004, 2005;

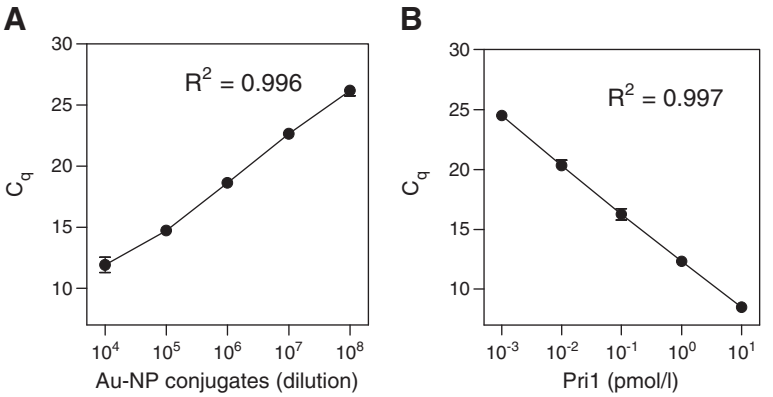

Fig. 3. Characterization of oligonucleotide-functionalized Au-NPs. (A) Real-time PCR performance of various dilutions of Au-NPs functionalized with Pri1 oligonucleotide. (B) Real-time PCR detection of various concentrations of oligonucleotide Pri1 alone. Correlation coefficients (R), means and S.D. were calculated from 3 independent experiments performed in triplicates.

Barletta, 2006) that there is a relatively high variability in the results and poor sensitivity. One possible cause was inferior heat transfer in wells of the TopYield strips during PCR. This was solved by extending the synthesis phase of the PCR cycles. Another problem was that larger surface area caused higher evaporation of PCR mixes, even though the wells were sealed with light cycler 480 sealing foil. We therefore added 5 µl of mineral oil into each well before they were sealed. Mineral oil prevented evaporation and improved the performance of detection of various concentrations of rIL-3 (Fig. 4) and rSCF (not shown).

3.3. Comparison of various immunoassays

To compare various immunoassays for detecting cytokines, we tested the performance of Nano-iPCR I and II, iPCR and ELISA for detection of rIL-3 and rSCF at various concentrations. For IL-3, polypropylene wells of the 96-well PCR plate (Eppendorf) were coated with extravidin, followed by anti-IL-3 polyclonal antibody (Nano-iPCR I). Alternatively, wells of TopYield strips (NUNC) were coated directly with anti-IL-3 antibody (Nano-iPCR II, iPCR and ELISA). Next, free binding sites were blocked with TPBS-2% BSA and rIL-3 at various concentrations was added. After incubation, unbound IL-3 was removed by washing with TPBS. Further course of the procedures differed depending on the method used (see Section 2 and Fig. 1). Analysis of data obtained showed that Nano-iPCR I (Fig. 5A) exhibited clear concentration-dependent differences in the range of 0.01–100 ng/ml of IL-3 with C_q values from ~35 (at 100 ng/ml) to ~46 (at 0.01 ng/ml). These relatively high values probably reflect low protein binding capacity of PCR polypropylene wells. Nano-iPCR II (Fig. 5C) performed in polycarbonate TopYiled strips showed lower C_q values in the range from ~19 (at 100 ng/ml) to ~32 (at 0.01 ng/ml). With iPCR (Fig. 5E), the dose–response curve was similar to that of Nano-iPCR II assay, except for even lower C_q values, from ~15 (at 100 ng/ml) to ~24 (at 0.01 ng/ml). This was in part caused by lower C_q values in negative controls (without IL-3) in iPCR compared to Nano-iPCR, and could be related to higher nonspecific binding of the biotinylated template used for iPCR. In contrast to Nano-iPCR and iPCR, ELISA assay (Fig. 5G) was less sensitive and the range of IL-3 concentrations detectable by the assay was narrower (between 0.1 and 10 ng/ml).

Similar data were obtained when various assays were used for detection of rSCF. Thus, Nano-iPCR I (Fig. 5B), compared to Nano-iPCR II (Fig. 5D) and iPCR (Fig. 5F), was characterized by relatively high C_q values (including negative controls without rSCF) and higher sensitivity at low concentration of rSCF. ELISA assay (Fig. 5H) was again less sensitive, and also the range of rSCF concentrations detectable by the assay was reduced (0.1–10 ng/ml). The data indicate that Nano-iPCRs and iPCRs are superior in sensitivity and exhibit broader range of detectable concentrations than ELISA.

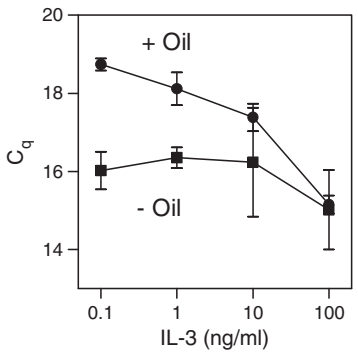

Fig. 4. The effect of mineral oil overlay on iPCR detection of IL-3 in wells of TopYield strips. Various concentrations of IL-3 were detected by iPCR in wells of TopYield strips overlaid (+) or not (−) with 5 µl of light mineral oil and sealed with real-time PCR transparent foil. Means and S.D. were calculated from 3 independent experiments performed in triplicates.

3.4. Cytokine detection in cell culture supernatants

To prove the convenience of Nano-iPCR we attempted to determine changes in the amount of rSCF during growth of BMMCs in RPMI-1640 medium supplemented with 10% FCS and SCF. Cell-free samples from cell cultures were collected at 24 h intervals for 5 days. In parallel, samples were also collected from cultures containing medium alone to determine the rate of degradation of SCF during incubated at 37 °C. Data in Fig. 6A show that growing cells gradually deplete the amount of rSCF. At the beginning of the experiment, samples contained SCF at concentration 15 ng/ml, but after 5 days, only about 3.7 ng SCF/ml remained (75% reduction). Similar data were obtained with ELISA. Degradation of rSCF in cell-free culture media had little effect, since the slight decrease there (9.5%) was only observed after 24 h of incubation and then remained constant. Binding of rSCF to the plasma membrane receptor (c-kit) and its internalization and subsequent degradation seems to be main cause of the observed depletion of rSCF from culture medium.

Next, we compared the efficiencies of various immunoassays for detection of IL-3 released into culture supernatant by growing D11 fibroblasts. Concentration of IL-3 was determined by Nano-iPCR II, iPCR and ELISA. Data presented in Fig. 6B indicate that D11 supernatant diluted 1:16 with TPBS-1% BSA contained 21.6 ± 2.0 ng/ml IL-3 (mean ± S.D.; $n = 3$), corresponding to 346 ± 32 ng/ml of undiluted supernatant. Higher dilutions of the supernatant had no effect on calculated concentration of IL-3. Similar data were obtained with iPCR (359 ± 90 ng/ml) or ELISA (384 ± 58 ng/ml).

4. Discussion

We compared three different immunoassays (Nano-iPCR, iPCR and ELISA) for detection of low concentrations of cytokines. Nano-iPCR was used in two formats differing in the mode how the antigen-specific antibodies were anchored to the reaction wells. In Nano-iPCR I, biotinylated antibody was anchored to immobilized extravidin, whereas in Nano-iPCR II the antibody was bound directly to the plastic surface. Both modifications used Au-NPs functionalized with single-stranded oligonucleotides and polyclonal antibodies specific for the cytokine in question. The assays gave reasonable concentration-dependent C_q values, although Nano-iPCR II showed higher nonspecific binding reflected by lower C_q values even in the absence of antigen. The components of the critical importance and limiting factors in all immunoassays are the antibodies, since they can differ in specificity and affinity for the target antigen, as well as nonspecific binding to the solid phase (McKie et al., 2002; Lind and Kubista, 2005; Niemeyer et al., 2007). It is therefore essential

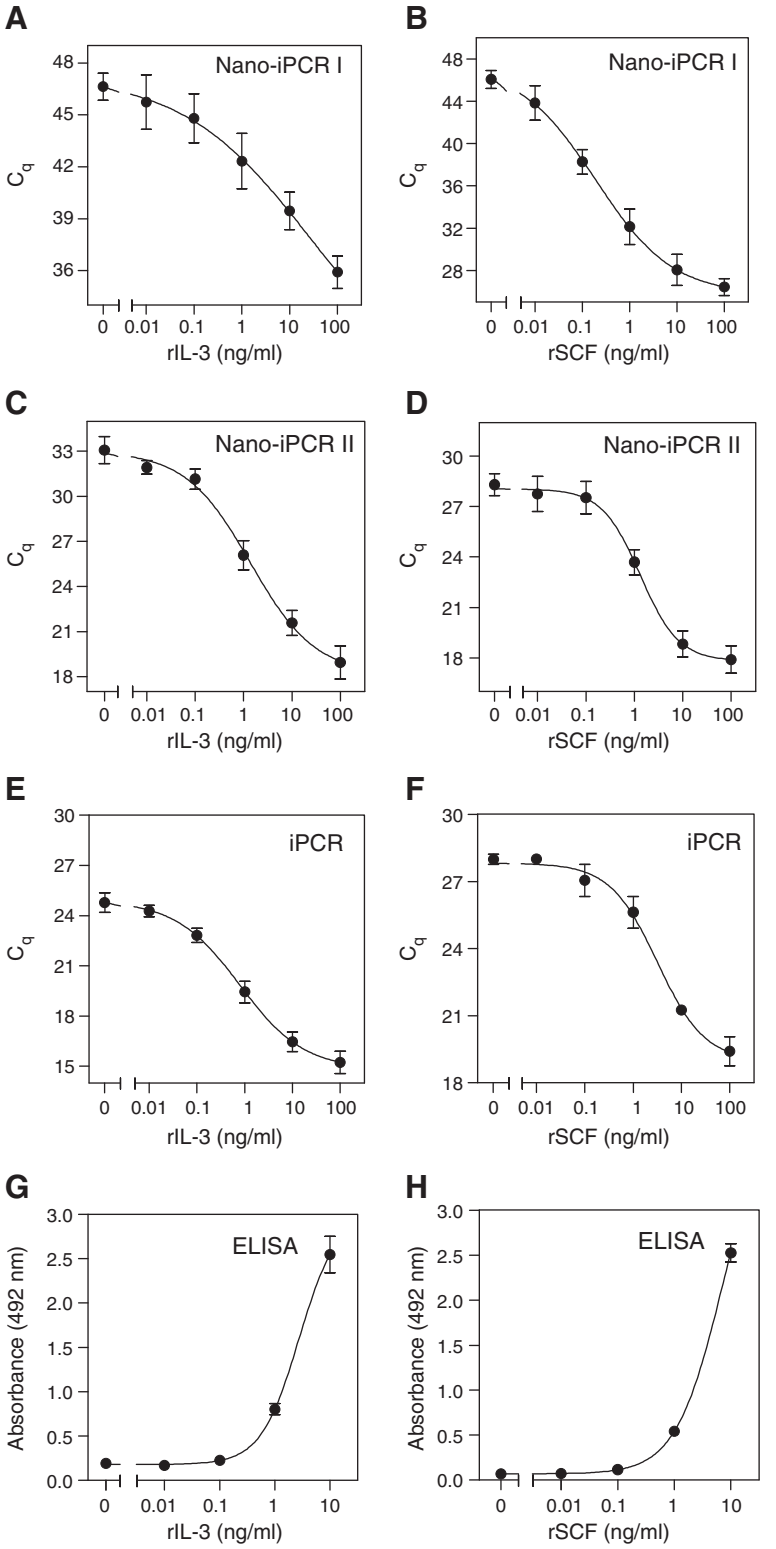

Fig. 5. Detection of various concentrations of rIL-3 and rSCF in particular immunoassays. Nano-iPCR I (A and B), Nano-iPCR II (C and D), iPCR (E and F) and ELISA (G and H) were used for detection of various concentrations of rIL-3 (A, C, E, G) or rSCF (B, D, F, H) in TPBS-1% BSA. Results are means ± S.D. from 3 to 6 independent experiment performed in triplicates or duplicates.

that in all the assays we employed the same sets of antibodies specific for IL-3 or SCF. The observed differences are thus attributable to the characteristics of the assays rather than antibodies.

The particular assays differed in a number of features which are summarized in Table 1. First, Nano-iPCR assays utilize functionalized Au-NPs. Production of such particles possessing both antibody and single-stranded oligonucleotides is more time consuming than preparation of biotinylated antibodies for ELISA and iPCR, or biotinylated double stranded oligonucleotides for iPCR. On the other hand, preparation of Au-NP conjugates is substantially easier than direct conjugation of antibodies with oligonucleotide templates (Lind and Kubista, 2005). As shown in this study, binding of the antibody to Au-NPs can be quantified by electron microscopy. The analysis proved that almost all Au-NPs bound several antibody molecules. The number of oligonucleotides bound to a particle was determined by real-time PCR using functionalized Au-NPs diluted directly into PCR mixes. Interestingly, even though each functionalized Au-NP possessed in average 80 oligonucleotides, performance of Nano-iPCR was comparable to the detection range of iPCR. This can be related to a higher background reflected in lower C_q values in iPCR calibration curves, including negative controls.

Second, an important parameter of immunoassays is the type of wells or tubes in which the assays are performed. An extensive array of various tubes, strips and plates fitting to different real-time PCR cyclers is available for PCR. However, these tubes and wells are often made of polypropylene and therefore exhibit a relatively low protein-binding capacity. At present, only the TopYield polycarbonate strips have antibody binding capacity comparable to polystyrene strips or plates widely used for ELISA, and have a shape compatible with heating blocks of various PCR cyclers. Our initial experiments showed that real-time PCR performance of TopYield strips was poor even in cyclers with heated lid. This was however improved by changing the cycling conditions and covering PCR master mixes with mineral oil. This obviously reduced evaporation from relatively large surface area of TopYield wells.

Third, both Nano-iPCR and iPCR detected the antigen with higher sensitivity than ELISA. This reflects the ability of PCR to amplify even a very small number of template DNA molecules. Initial studies indeed demonstrated a dramatic enhancement (approximately five orders of magnitude) in detection sensitivity when iPCR was used instead of ELISA (Sano et al., 1992). However, these assays were performed under optimal conditions where antigen (BSA) was directly immobilized to wells and a potent monoclonal antibody specific for BSA was available. When the antigen is present in a complex protein mix, such as in serum-containing culture medium or in crude body fluids, and analyzed in a sandwich assay, Nano-iPCR and iPCR usually detect the antigen with 1–3 orders higher sensitivity than ELISA (Adler et al., 2003; Lind and Kubista, 2005; Chen et al., 2009; Perez et al., 2011). In a study aimed at detecting mumps-specific IgG in serum samples, sensitivity of the iPCR did not exceed that of conventional ELISA. It should be kept in mind that Nano-iPCR and iPCR assays are substantially less sensitive for quantification of antigenic molecules when compared to real-time PCR for quantification of DNA templates. This is attributable to high specificity of PCR and zero amplification in the absence of DNA template.

Fourth, another important factor is the variability of the assays and the range of detectable concentrations of antigen. It is known that real-time PCR gives exponential signal amplification and real-time detection. Under optimal conditions (100% efficiency) a 10-fold increase in the amount of DNA template is associated with a decrease in C_q value by a factor of 3.4. IPCR-based assays are therefore especially useful for detection of target antigens at large quantitative differences. In contrast, standard ELISA gives linear signal amplification and end point detection and, therefore, suits better for detection of smaller differences at lower range of concentrations; meaningful calibration curves for ELISA span usually two orders of magnitude or less.

Fifth, the labor requirement of the assays must also be taken into consideration. As shown in Fig. 1, Nano-iPCR based assays are less laborious because they have fever steps than iPCR or ELISA. Once the probes (functionalized Au-NPs) are prepared they can be stored for several months and used immediately for easy quantification of the antigen.

Our primary intention was to develop an assay for detection of cytokines in serum-supplemented cell culture media. Nano-

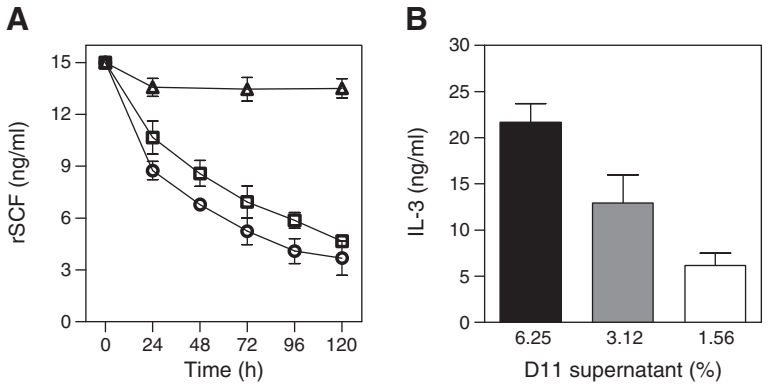

Fig. 6. Determination of SCF and IL-3 in culture media used for growth of BMMCs. (A) Changes in concentration of rSCF in culture medium with the length of time. The cells (1.0×10^6/ml) were cultured in complete RPMI-1640 medium supplemented with 15 ng/ml rSCF (0 h). Cell culture supernatants were collected at 24-h intervals for 120 h. The amount of rSCF was determined with Nano-iPCR I (circles) or ELISA (squares) using the corresponding calibration curves. As a positive control, supernatants from cell-free cultures were also analyzed in parallel by ELISA (triangles). (B) Quantification of IL-3 in supernatant from cultured D11 cells. Supernatant was diluted 16-fold, 32-fold or 64-fold in TPBS-1% BSA and the amount of IL-3 was determined with Nano-iPCR II using the corresponding calibration curves. Means and S.D. were calculated from 3 independent experiments.

Table 1
Comparison of the immunoassays used.

Parameter	Nano-iPCR	iPCR	ELISA
Reagents preparation	+	++	++
Tolerance for matrix	+	++	++
Sensitivity	+++	+++	++
Quantification range	+++	+++	+
Linearity	+++	+++	++
Variability	++	++	+++
Robustness	++	++	+++
Assay time	+++	+	++

+++, the best attribute; ++, the medium attribute; +, the worst attribute.

iPCR performed in TopYield strips with master mixes covered with oil film and transparent foil offers a simple and robust assay for rapid detection of IL-3 and SCF using commercially available antibodies and their biotinylated forms. The binding of antibody and thiolated oligonucleotide template to Au-NPs is an easy method of how to combine antibodies and oligonucleotides into a complex suitable for the assays. The assay can be used for quantification of other ligands, provided good monoclonal or polyclonal antibodies and their biotinylated forms are available.

In conclusion, Nano-iPCR assay shows enhanced sensitivity and wider dynamic range than ELISA and is easier to perform than iPCR. It can be expected that further improvement of the Nano-iPCR assays, namely introduction of better detection probes with higher ligand specificity and lower nonspecific binding will advance the application of these tests for routine detection of cytokines as well as other ligands. Synthetically prepared tailored DNA or RNA aptamers (Jayasena, 1999; Khati, 2010) and tailored recombinant binding proteins (Binz et al., 2005) could provide such probes.

Conflict of interest

The authors do not have a commercial or other association that might pose a conflict of interest.

Acknowledgments

This work was supported by project KAN200520701 and M200520901 from Academy of Sciences of the Czech Republic, 1M6837805001 (Center of Molecular and Cellular Immunology) and LC-545 from Ministry of Education, Youth and Sports of the Czech Republic, grants 204/05/H023, 301/09/1826 and P302/10/1759 from the Grant Agency of the Czech Republic, and Institutional projectAVOZ50520514.

References

Adler, M., Wacker, R., Niemeyer, C.M., 2003. A real-time immuno-PCR assay for routine ultrasensitive quantification of proteins. Biochem. Biophys. Res. Commun. 308, 240–250.
Barletta, J., 2006. Applications of real-time immuno-polymerase chain reaction (rt-IPCR) for the rapid diagnoses of viral antigens and pathologic proteins. Mol. Aspects Med. 27, 224–253.
Barletta, J.M., Edelman, D.C., Constantine, N.T., 2004. Lowering the detection limits of HIV-1 viral load using real-time immuno-PCR for HIV-1 p24 antigen. Am. J. Clin. Pathol. 122, 20–27.
Barletta, J.M., Edelman, D.C., Highsmith, W.E., Constantine, N.T., 2005. Detection of ultra-low levels of pathologic prion protein in scrapie infected hamster brain homogenates using real-time immuno-PCR. J. Virol. Methods 127, 154–164.
Binz, H.K., Amstutz, P., Pluckthun, A., 2005. Engineering novel binding proteins from nonimmunoglobulin domains. Nat. Biotechnol. 23, 1257–1268.
Cao, L., Yu, K., Banh, C., Nguyen, V., Ritz, A., Raphael, B.J., Kawakami, Y., Kawakami, T., Salomon, A.R., 2007. Quantitative time-resolved phosphoproteomic analysis of mast cell signaling. J. Immunol. 179, 5864–5876.
Chen, X., Kendler, K.S., 2008. Interleukin 3 and schizophrenia. Am. J. Psychiatry 165, 13–14.
Chen, Y.R., Hsu, M.L., Ho, C.K., Wang, S.Y., 1993. Cell source and biological characteristics of murine bone marrow-derived colony-promoting activity. Exp. Hematol. 21, 1219–1226.
Chen, L., Wei, H., Guo, Y., Cui, Z., Zhang, Z., Zhang, X.E., 2009. Gold nanoparticle enhanced immuno-PCR for ultrasensitive detection of Hantaan virus nucleocapsid protein. J. Immunol. Methods 346, 64–70.
Engvall, E., Perlmann, P., 1971. Enzyme-linked immunosorbent assay (ELISA). Quantitative assay of immunoglobulin G. Immunochemistry 8, 871–874.
Georganopoulou, D.G., Chang, L., Nam, J.M., Thaxton, C.S., Mufson, E.J., Klein, W.L., Mirkin, C.A., 2005. Nanoparticle-based detection in cerebral spinal fluid of a soluble pathogenic biomarker for Alzheimer's disease. Proc. Natl. Acad. Sci. U. S. A 102, 2273–2276.
Hill, H.D., Mirkin, C.A., 2006. The bio-barcode assay for the detection of protein and nucleic acid targets using DTT-induced ligand exchange. Nat. Protoc. 1, 324–336.
Hurst, S.J., Hill, H.D., Mirkin, C.A., 2008. "Three-dimensional hybridization" with polyvalent DNA-gold nanoparticle conjugates. J. Am. Chem. Soc. 130, 12192–12200.
Jayasena, S.D., 1999. Aptamers: an emerging class of molecules that rival antibodies in diagnostics. Clin. Chem. 45, 1628–1650.
Jin, R., Wu, G., Li, Z., Mirkin, C.A., Schatz, G.C., 2003. What controls the melting properties of DNA-linked gold nanoparticle assemblies? J. Am. Chem. Soc. 125, 1643–1654.
Khati, M., 2010. The future of aptamers in medicine. J. Clin. Pathol. 63, 480–487.
Kim, E.Y., Stanton, J., Vega, R.A., Kunstman, K.J., Mirkin, C.A., Wolinsky, S.M., 2006. A real-time PCR-based method for determining the surface coverage of thiol-capped oligonucleotides bound onto gold nanoparticles. Nucleic Acids Res. 34, e54.
Lei, Z., Liu, G., Huang, Q., Lv, M., Zu, R., Zhang, G.M., Feng, Z.H., Huang, B., 2008. SCF and IL-31 rather than IL-17 and BAFF are potential indicators in patients with allergic asthma. Allergy 63, 327–332.
Lind, K., Kubista, M., 2005. Development and evaluation of three real-time immuno-PCR assemblages for quantification of PSA. J. Immunol. Methods 304, 107–116.
McKie, A., Samuel, D., Cohen, B., Saunders, N.A., 2002. Development of a quantitative immuno-PCR assay and its use to detect mumps-specific IgG in serum. J. Immunol. Methods 261, 167–175.
Nam, J.M., Thaxton, C.S., Mirkin, C.A., 2003. Nanoparticle-based bio-bar codes for the ultrasensitive detection of proteins. Science 301, 1884–1886.
Nam, J.M., Stoeva, S.I., Mirkin, C.A., 2004. Bio-bar-code-based DNA detection with PCR-like sensitivity. J. Am. Chem. Soc. 126, 5932–5933.
Niemeyer, C.M., Adler, M., Blohm, D., 1997. Fluorometric polymerase chain reaction (PCR) enzyme-linked immunosorbent assay for quantification of immuno-PCR products in microplates. Anal. Biochem. 246, 140–145.
Niemeyer, C.M., Adler, M., Wacker, R., 2007. Detecting antigens by quantitative immuno-PCR. Nat. Protoc. 2, 1918–1930.
Perez, J.W., Vargis, E.A., Russ, P.K., Haselton, F.R., Wright, D.W., 2011. Detection of respiratory syncytial virus using nanoparticle amplified immuno-polymerase chain reaction. Anal. Biochem. 410, 141–148.
Sano, T., Smith, C.L., Cantor, C.R., 1992. Immuno-PCR: very sensitive antigen detection by means of specific antibody-DNA conjugates. Science 258, 120–122.
Silman, I., Katchalski, E., 1966. Water-insoluble derivatives of enzymes, antigens, and antibodies. Annu. Rev. Biochem. 35, 873–908.
Sims, P.W., Vasser, M., Wong, W.L., Williams, P.M., Meng, Y.G., 2000. Immunopolymerase chain reaction using real-time polymerase chain reaction for detection. Anal. Biochem. 281, 230–232.
Smrž, D., Dráber, P., 2003. One-tube semi-nested PCR-ELISA for the detection of human cytomegalovirus DNA sequences: comparison with hybridization-based and semi-nested-based PCR-ELISA procedures. J. Immunol. Methods 283, 163–172.
Tsuji, K., Zsebo, K.M., Ogawa, M., 1991. Murine mast cell colony formation supported by IL-3, IL-4, and recombinant rat stem cell factor, ligand for c-kit. J. Cell. Physiol. 148, 362–369.
Volná, P., Lebduška, P., Dráberová, L., Šímová, Š., Heneberg, P., Boubelík, M., Bugajev, V., Malissen, B., Wilson, B.S., Hořejší, V., Malissen, M., Dráber, P., 2004. Negative regulation of mast cell signaling and function by the adaptor LAB/NTAL. J. Exp. Med. 200, 1001–1013.
Zhou, H., Fisher, R.J., Papas, T.S., 1993. Universal immuno-PCR for ultra-sensitive target protein detection. Nucleic Acids Res. 21, 6038–6039.

8 GENERAL DISCUSSION

Understanding molecular mechanisms leading to allergy and other inflammatory responses is a fundamental question in mast cell signaling research. Activation of mast cells through the FcεRI, results in release of biologically active proinflammatory mediators which are responsible for variety of mast cells-mediated diseases [15]. Current research focuses on searching for master signaling molecules, which drive mast cell degranulation and cytokines production and potentially serve as therapeutic targets to dampen mast cell responses at initial stages of FcεRI activation. It has been shown that inhibitor of SYK can be successfully used for treatment of patients with rheumatoid arthritis [120]. Also, inhibitors targeting PI3K pathway have a clinical potential in allergic rhinitis [121] and asthma [122]. However, number of targets used clinically is rather limited. Thus, searching for a new signaling molecules and pathways which regulate mast cell degranulation is required.

PAG in mast cell signaling

A key role of TRAPs in immune cells is diversification of downstream signaling after immunoreceptor triggering [50]. In this thesis we focused on understanding function of one of them, the adaptor protein PAG. Our results showed that activation of mast cell derived from PAG-KO mice led to decreased antigen-mediated calcium mobilization and degranulation, although activity of SFKs was increased. This finding was unexpected because phosphorylated PAG has been proposed to mediate membrane recruitment of CSK, playing a major role in inactivation of SFKs [55, 56]. Several previous studies using primary T cells and T cell lines showed that PAG acts as a negative regulator of TCR signaling [57]. It has been shown that phosphorylated PAG together with associated CSK set an activation threshold of TCR signaling [57]. In line with these findings it has been shown that T cells with mutant PAG, which are unable to bind CSK, have impaired response to TCR stimulation [123]. Furthermore, T cells isolated from transgenic mouse, in which PAG is overexpressed, showed impaired TCR signaling as well [124]. However, in a more recent study it was shown, that effector T cells from PAG-KO mice showed enhanced TRC-mediated activation demonstrated by increase in cell proliferation and cytokine production; surprisingly, in naive T cells PAG has no appreciable role [59]. It has been shown that overexpression of PAG resulted in

reduced degranulation in RBL-2H3 cell line [125]. It should be noted, that the different role of PAG in mast cells is unlikely to be a consequence of the compensatory developmental alterations in PAG-KO mice used in our study, because we observed similar phenotype in PAG-KD cells where PAG expression was down regulated by RNA interference.

It is widely excepted that passive systemic anaphylaxis (PSA) is initiated by inflammatory mediators released from activated mast cells during degranulation [126]. A key role in this process has histamine which is known to reduce body temperature [127] and thus control anaphylactic reaction in mice [35]. Thus, our finding of impaired PSA in PAG-KO mice could be directly related to decreased degranulation in PAG-KO cells. Furhermore, in this study we demonstrated for the first time that PAG-KO mice exhibit distinct phenotype when compared to WT mice.

Our data showed that reduced calcium response and degranulation in PAG-KO mast cells are caused at least in part by inhibition of the earlies stages of FcεRI signaling, including phosphorylation of the FcεRI β and γ subunits, phosphorylation of SYK kinase, adaptor protein LAT, and PLCγ. Reduced calcium response in PAG-KO cells could be attributed to the reduced tyrosine phosphorylation and activity of PLCγ, which cleaves the plasma membrane-bound phosphatidylinositol 4,5-bisphosphate into diacylglycerol and inositol 1,4,5-trisphosphate; that the latter binds to its receptors and regulates the release of calcium from cytoplasmic stores. An increase in cytoplasmic calcium leads to the influx of extracellular calcium into the cytoplasm through SOC channels [128]. Our hypothesis that PAG is a positive regulator of antigen-induced calcium mobilization and degranulation, is supported by enhanced phosphorylation of phosphatase SHIP1 and LYN kinase, the negative regulators of FcεRI-mediated signaling [52].

It should be noted, that important differencies has been described between early regulatory events induced by stimulation of TCR and FcεRI in term of PAG. It has been shown that in resting T cells, PAG is constitutively phosphorylated via association with FYN [129]. Upon TCR engagement, PAG is rapidly dephosphorylated following release of CSK and this leads to increase in activity of LCK [81, 130]. In contrast, in mast cells, PAG is phosphorylated by LYN and FcεRI triggering results in increased phosphorylation of PAG and binding of CSK [123]. However, we observed no daramatic changes in tyrosine phosphorylation of PAG in the course of FcεRI-induce

activation (data not shown). This could reflect different methods used for mast cell activation.

An important result of this study is a finding of a positive regulatory role of PAG in production of proinflammatory cytokines and chemokines upon FcεRI-induced mast cell activation. Present data indicate that changes in transcription of genes for cytokines and chemokines as well as changes at the protein levels could be a direct consequece of impaired phosphorylation of STAT5, as publication in Mol. Cell. Biol., 2014 showed. The results are in line with the previous findings that phosphorylated STAT5 serves as a transcription factor for a number of proinflammatory genes [131] and that STAT5 defficiency leads to impaired responses in FcεRI activated mast cells [132]. Molecular mechanism, which controls STAT5-dependent cytokines production upon FcεRI triggering is not completely understood. It has been shown that IgE-mediated STAT5 phosphorylation is dependent on FYN kinase which is enhanced in context of LYN deficiency, but is independent of SYK and PI3K-AKT pathway [117]. Other study, however, showed that FYN has no effect on activation of MAPK ERK and production of TNF-α, while SYK and GAB2 seems to be a potent regulator of FcεRI-induced degranulation and activation of NFAT and NF-κB pathways [133]. Related to these results, we observed impaired phosphorylation of SYK kinase and ERK in PAG-KO cells, which could support the hypothesis that reduced activity of transcription factor STAT5 could be rather a consequence of impaired SYK and STAT5 pathway.

CSK in regulation of mast cell signaling

One of the key finding of this study was contribution to elucidation of the role of CSK in mast cell degranulation and cytokine production. Our primary goal was to examine whether widely accepted view of CSK as a negative regulator of various cell responses, and as a major interaction partner of PAG, anchoring CSK to plasma membrane, applies also to mast cells. In accord with previous studies our data showed that mast cells with CSK-KD exhibited elevated degranulation, not only upon FcεRI-induced activation, but also in nonactivated state, spontaneous degranulation. The finding that CSK acts in setting of mast cell activation threshold is supported by the observations in T cells [134] and granulocytes [85], which pointed out that CSK is a major regulator of early signaling events after triggering of MIRRs and other surface receptors. Despite of intensive studies of CSK, there has been only one study carried out in mast cell-related line (RBL) in FcεRI-mediated signaling [86]. Our data are in

agreement with this study, which showed that RBL cells with overexpressed CSK, exhibited delayed early stages of FcεRI degranulation [86]. Similarly, it has been shown that CSK-deficient granulocytes exhibit elevated ligand-induced degranulation [85]. We confirmed a negative regulatory role of CSK in mast cell degranulation by analysis of surface expression of CD107a, a lysosomal marker of degranulation. However, we were not able to detect reduced degranulation in mast cells overexpressing myc-hCSK or mCherry-hCSK. Our attempt to increase exogenous expression of CSK in BMMCs failed because of enhanced mortality of such mast cells. Collectively, these data, together with those from the previously published studies on CSK, support the concept that CSK is a negative regulator of mast cell degranulation.

Enhanced concentration of free cytoplasmic calcium is essential for degranulation and optimal production of cytokines in mast cells [128]. Our data showed enhanced calcium response in mast cells with CSK-KD upon FcεRI-induced activation. It has been shown, that calcium response in antigen-activated mast cells is dependent on LYN-SYK-LAT-PLCγ-dependent signaling pathway [135]. CSK-KD had stimulatory effect on this pathway as reflected by significantly increased tyrosine phosphorylation of SYK, LAT and PLC-γ. Our data are thus in line with previously published data showing that in T cells with reduced catalytic activity of CSK, whose catalytic activity was inhibited by a small inhibitor, exhibited significantly enhanced phosphorylation of SYK (ZAP-70 in T cell), LAT and PLCγ when compared to control cells [134]. Interestingly, in BMMCs with CSK-OE, no significant changes in antigen-induced calcium response were observed. This observation is in accord with previous studies using WEHI-231 cells in which CSK-OE was unable to alter BCR-induced signaling [136] and RBL cells in which CSK-OE displayed only delayed calcium response [86]. Data obtained with BMMCs contrast with those showing that overexpression of CSK in T cell line resulted in significant inhibition of TCR-induced activation events [137]. Our data also suggest that the downstream signal following FcεRI crosslinking in mast cells with CSK-KD is distinctly diversified signal and thereby represents unique modulation of mast cell responses, such as chemotaxis. This hypothesis is supported by another study in which we found unique mechanism of chemotaxis controlled by complexes of tetraspanin CD9 and NTAL where NTAL adaptor served as negative regulator of this process, but LAT had no effect. Similarly, we found unchanged tyrosine phosphorylation of LAT, but significantly decreased tyrosine phosphorylation of NTAL

in cells with CSK-KD, which could explain enhanced chemotaxis towards antigen and SCF.

CSK is generally considered as a major negative regulator of SFKs through phosphorylation of its regulatory C-terminal tyrosine [66]. The importance of this tyrosine for control of both proximal and distal signaling pathways in FcεRI-activated cells was shown [86]. Our data showed that although mast cells with CSK-KD revealed dramatic defect in tyrosine phosphorylation of LYN at Y^{508}, tyrosine phosphorylation of LYN at Y^{397} was unchanged and even kinase activity of LYN was reduced in such cells. Interestingly, FYN kinase activity was unaffected by CSK-KD. It has been shown that LYN negatively regulates mast cell activation *in vitro* and *in vivo* [138, 139]. In addition, considerably different molecular mechanism of various immunoreceptor signaling uderlines the fact that in mast cells upon FcεRI triggering, LYN kinase is transiently hyperphosphorylated on its inhibitory C-terminal tyrosine (Y^{487}) resulting in decrease of LYN kinase activity [108]. In contrast, studies on LCK in T cells showed decreased phosphorylation of C-terminal regulatory trosine and thus enhanced kinase activity of LCK [81].

Unexpected was our finding of positive regulatory role of CSK on production of proinflammatory cytokines (TNF-α, IL-13, IL-6) and chemokines (CCL-3, CCL-4) in FcεRI-activated cells. This finding is different from those observed in LPS-activated macrophage cell line in which CSK-OE resulted in reduced production of TNF-α, IL-1a and IL-6 [140]. Furthermore it has been reported that conditionally reduced CSK in keratinocytes resulted in elevated levels of TNF-α [84]. In addition, recent study using mice with conditionally abolished CSK in granulocytes and macrophages, showed increased TNF-α in serum; however, *in vitro* analyses showed no changes [85]. It should be mentioned that positive regulatory role of CSK in production of TNF-α and IL-6 has been also described in macrophage cell line RAW 264.7 [141]. Based on the data obtained in this study we propose that silencing of CSK in BMMCs leads to alteration of the balance between PTPs and PTKs in early stages of FcεRI-induced signaling. In cells with CSK-KD, SHP-1 phosphatase becomes more active and probably recognizes its substrate LYN via recently described unique inhibitory motif, KTIM, only found in LYN [103], and thus repress its activity. Activated SHP-1 is in turn able to dephosphorylate Y^{694} at STAT5 and thereby negatively regulate production of cytokines in cells with CSK-KD. Our results are in accord with previous reports that SHP-1-

defficient cells exhibit increased cytokine production, but reduced calcium response and degranulation, implying that SHP-1 has both positive and negative regulatory role in mast cells [94].

Our finding that CSK-mediated regulation of FcεRI signaling does not require adaptor protein PAG supports our hypothesis about existence of CSK binding proteins, other than PAG, which are more relevant for the inhibitory action of CSK in mast cells.

Firstly, we observed significantly elevated degranulation, calcium response and chemotaxis in PAG-KO cells in which CSK-KD was introduced in comparison with PAG-KO alone, resembling to phenotype cells with CSK-KD. These aspects are discussed in more detail in manuscript presented at pages 67-116 in this thesis.

Second, our data published in Mol. Cell. Biol., 2014, revealed that only a very small fraction of CSK (~4%) colocalized with PAG in lipid raft fraction in WT cells and that this fraction was not changed upon FcεRI-induced activation.

Third, there are discrepancies between the data considering role of PAG as a major CSK adaptor protein. It has been shown that PAG is major anchor of CSK in lipid raft from mouse thymocytes [142]. Another study showed, however, that amount of lipid raft associates-CSK in thymus is not affected by the absence of PAG [143]. Based on our data we suggest that the hypothetical CSK anchor could resides in detergent soluble fraction of the cell extracts.

Fourth, we determined several aspect of mast cells signaling carried out in CSK-KD, PAG-KD, PAG-KO and double-deficient CSK-KD/PAG-KO cells and observed distinct or even opposite roles of PAG and CSK in regulation of individual signaling events including, degranulation, calcium response, adhesion to fibronectin, chemotaxis towards antigen and SCF, and tyrosine phosphorylation of several signaling molecules. As was mentioned above, reduced expression of CSK is accompanied by decreased phosphorylation of NTAL, however LAT is unchanged, while PAG has opposite effect on phosphorylation of these TRAPs.

Fifth, the observed additive effect of double-deficient cells (CSK-KD/PAG-KO) on cytokine production suggests that CSK and PAG could regulate this event by independent pathways which converge at the level of STAT5 tyrosine phosphorylation.

Finally, the results obtained in our studies allowed us to propose a new model (at page 105 and 116 in this thesis) suggesting that in mast cells CSK binds not only to PAG, but also to some other anchors, which could serve better than PAG for positioning

CSK in the vicinity of SFKs and thus more efficiently contribute to inactivation of SFKs involved in FcεRI signaling. These alternative CSK anchor proteins remains to be identified.

Other FcεRI signaling regulators

In the course of the studies on this project we noticed that FcεRI-mediated activation is strongly affected by short-term treatment of mast cells with low concentrations of ethanol, which suppressed phosphorylation of FcεRI β and γ subunits and all other downstream signal transduction events, including phosphorylation of SYK, LAT, PLCγ, STAT5, and AKT, calcium response, degranulation and production of proinflammatory cytokines. Based on various experiments and literature data we proposed hypothesis that cholesterol, rather than proteins, could be the target of ethanol. This hypothesis was supported by findings that MβCD, a cholesterol sequestering drug, had similar effect as ethanol on properties of mast cells and that MβCD saturated with cholesterol, which is known to increase amount of cholesterol in the plasma membrane, reversed at least in part the inhibitory effect of ethanol. This finding is in line with the observation on neutrophiles, in which ethanol inhibits production of TNF-α and modulates redistribution of surface molecules on the plasma membrane [144], membrane fluidity [145], and membrane viscosity, resulting in changes in cell adhesion, rolling, lateral mobility of lipid molecules and tethering behaviour [144]. The inhibitory effect of ethanol on mast cell degranulation and cytokines release was corroborated by *in vivo* PCA experiments, in which mice were localy senzitized by IgE, peritoneally treated by ethanol and finally intravenously challanged by antigen, as shown in our publication in Plos One. How exactly ethanol interacts with lipids and/or how it affects lipid-protein interactions is not known but could involve direct interaction of ethanol with cholesterol [146] and the ability of ethanol to mediate and modify organization of the lipid bilayer structures [147]. The amphiphilic character of ethanol gives it the capability to be attracted simultaneously to both hydrophobic and hydrophilic targets in the plasma membrane.

Another molecule we touched in the course of these studies is ORMDL3, which in mast cells serve as a negative regulator of cytokine and chemokine production. Interestingly, our data concurrently indicated that reduced or enhanced expression of ORMDL3 had no effect on antigen-induced degranulation and calcium mobilization.

Based on previously published studies, involvement of ORMDL3 in regulation of calcium response seems to vary depending on the cell type examined. For instance, it has been shown that reduced expression of ORMDL3 in T cells led to increased calcium response [148]. In contrast, eosinophils with reduced expression of ORMDL3, displayed reduced calcium mobilization even at basal level [149]. Moreover, enhanced localization of phosphorylated NF-κB p65 subunit in the nucleus has been shown in such cells [149].

It is known that enhanced nuclear localization of NF-κB p65 subunit is a step followed by increased transcription of NF-κB regulated genes encoding various cytokines and chemokines [150]. Therefore, we focused in detail on analyses of these events and observed enhanced localization of NF-κB in the nucleus, which was driven by increased phosphorylation of AKT at Ser^{473}. This molecular mechanism could explain elevated level of cytokines (TNF-α, IL-13 and IL-6) and chemokines (CCL3, CCL4) in mast cells with ORMDL3-KD. Interestingly, no significant inhibition of IκBα/AKT signaling and unchanged release of cytokines were observed in mast cells with ORMDL3-OE. However, the direct connection between AKT- and ORMDL3-mediated regulations are not yet solved. These data support an important role of ORMDL3 in mast cell mediated inflammation.

Detection of proinflammatory cytokines

Therapeutics against mast cells related diseases target variety of substances released during mast cells degranulation, such as histamine, leukotrienes or numerous cytokines [118]. Impact of cytokines *de novo* synthetized and released by mast cells, including TNF-α, IL-13, IL-10, IL-6, and IL-4 has been demonstrated in allergy and numerous inflammatory disorders, such as pollen and food allergy, asthma, allergic rhinitis, and various autoimmune disorders [151]. For this purpose, sensitive and simple detection methods for quantification of mast cell mediators are required [152].

Widespread methods for detection of cytokines are ELISAs, which are based on a highly specific antibody-antigen interaction. However, some protein biomarkes are under the detection limit of ELISAs and therefore here a new methods have been developed. Previous studies showed that iPCR method by combining versatility of ELISAs with the amplification power and sensitivity of PCR, allows sensitive detection of target proteins [153-155]. One of the initial methodological aims of this project was

to use gold nanoparticles conjugated with both antibodies and short oligonucleotides and in this way to increase simplicity of iPCR methods [156, 157].

The results presented in this disertation show that when the same antibodies were used throughout the individual assays, newly developed iPCR method based on armed gold nanoparticles, called nano-iPCR, offers enhaced sensitivity, wider dynamic range, is easier to perform and is more cost-efficient than ELISA and classical iPCR. In our approach, several modifications of this metod were introduced allowing detection of variety of cytokines and other molecules released or utilized by mast cells. Using nano-iPCR we showed that both IL-3 and SCF are critical growth factors for BMMCs *in vitro*, which have regulatory roles on certain mast cell signaling pathways and thereby modulates mast cells responsivenes to stimuli [158]. For these reasons, we used nano-iPCR method and monitor routinely IL-3 and SCF levels in supernatants from WEHI and CHO cells. Routine measurement of IL-3 and SCF levels in the supernatants allowed us to avoid buying expensive recombinant proteins.

Besides measuring levels of IL-3 and SCF in cell supernatants used for growth of BMMCs, we used our newly nano-iPCR method extensively for quantification of proinflammatory cytokines (TNF-α, IL-13 and IL-6) released from mast cells in the course of activation [34]. In our study published in J. of Immunol. Methods 2014, we showed that Nano-iPCR method is suitable not only for basic research aplications, but also for sensitive detection of clinically relevant markers present in complex biological fluids, such as cerebrospinal fluid. Nano-iPCR assays have been rutinely used in several projects in our laboratory and the results have been presented in six publications comprising this thesis.

9 CONCLUSIONS

1. Our results showed that adaptor protein PAG plays a role as a positive or negative regulator of BMMCs signaling, depending on the signaling pathway involved. For the first time, we showed the physiological impact of PAG in immune cells under *in vivo* condition.

    a. Interestingly, PAG-KO cells exhibited decrease in several aspects of mast cell signaling, such as degranulation and pro-inflammatory cytokines (TNF-α, IL-13 and IL-6) production upon antigen activation.
    b. In vivo experiments showed, that PAG is a positive regulator of IgE-mediated PSA, however PAG-KO mice exhibited normal level of IgE.

2. Our results support the notion that CSK in mast cells is a negative regulator of calcium response, degranulation and migration, whereas in production of cytokines and adhesion to fibronectin CSK plays a positive regulatory role. Obtained data also indicated that, some of these events could be regulated by CSK independently of the PAG.
    a. BMMCs with CSK-KD exhibited elevated degranulation, calcium mobilization and migration toward antigen and SCF, accompanied by altered phosphorylation of FcεRI β and γ subunits, LYN, SYK, NTAL, and PLCγ.
    b. In contrast to CSK-KD, BMMCs with CSK-OE showed CD107a surface expression and calcium mobilization at normal levels.
    c. Surprisingly, production of cytokines and chemokines was reduced in antigen-activated BMMCs with CSK-KD by a mechanism dependent on transcription factor STAT5.
    d. We observed altered balance between PTKs and PTPs in cells with CSK-KD, where increased phosphatase activity of SHP-1 in turn negatively regulated LYN and STAT5 activity.
    e. Based on the results obtained, we proposed a model of FcεRI-mediated signaling in WT, CSK-KD, PAG-KO and CSK-KD/PAG-KO BMMCs.

3. We found out that ORMDL3 is involved in development of local inflammation initialized by FcεRI triggering under *in vitro* and *in vivo* conditions.
    a. Downregulation of ORMDL3 was associated with an increased expression of proinflammatory cytokines, chemokines, and cyclooxygenase-2 dependent synthesis of prostaglandin D_2 regulated via AKT and NF-κB signaling pathways. In contrast, degranulation was unchanged.
    b. On the other hand, enhanced expression of ORMDL3 in BMMCs leads to unchanged production of proinflammatory cytokines.
    c. Mice with locally silenced ORMDL3 by siRNA exhibited enhanced IgE-antigen-dependent PCA.

4. Results obtained in studies investigating effect of ethanol helped us to better understand early signaling events mediated by triggering of FcεRI. Our data showed that ethanol interferes with early antigen-induced signaling events in mast cells by suppressing the function of FcεRI-cholesterol signalosomes at the plasma membrane. These data were corroborated by reduced PCA reaction in mice, suggesting inhibitory role of ethanol under *in vivo* conditions.

5. Data based on studying CD9 revealed that chemotaxis toward antigen is controlled by a cross-talk between FcεRI, CD9, NTAL, and proteins of the ERM family. Newly prepared mAb specific for the tetraspanin CD9 induced activation of several signaling pathways, including mast cell chemotaxis. Moreover, NTAL and LAT showed non-overlapping role in antigen-mediated chemotaxis.

6. We developed a nano-iPCR method for detection of proteins in complex biological fluid. Our data indicate that this assay is suitable for detection of immune responses under physiological and pathophysiological conditions.

a. Nano-iPCR was optimized and implemented for detection of SCF, IL-3, TNF- α, IL-6, IL-13, tau protein, and α-tubulin.
b. This assay served as a helpful approach for monitoring changes in concentration of grow factors in culture media during mast cell cultivation.
c. The method was widely used for rapid detection of pro-inflammatory cytokines in numerous BMMC mouse models comprised in this thesis.

10 REFERENCES

1. Metcalfe DD. Mast cells and mastocytosis. Blood, 2008, **112:**946-956.
2. Moon TC, St Laurent CD, Morris KE, Marcet C, Yoshimura T, Sekar Y, Befus AD. Advances in mast cell biology: new understanding of heterogeneity and function. Mucosal Immunol, 2010, **3:**111-128.
3. Arinobu Y, Iwasaki H, Akashi K. Origin of basophils and mast cells. Allergol Int, 2009, **58:**21-28.
4. Arinobu Y, Iwasaki H, Gurish MF, Mizuno S, Shigematsu H, Ozawa H, Tenen DG, Austen KF, Akashi K. Developmental checkpoints of the basophil/mast cell lineages in adult murine hematopoiesis. Proc Natl Acad Sci U S A, 2005, **102:**18105-18110.
5. Qi X, Hong J, Chaves L, Zhuang Y, Chen Y, Wang D, Chabon J, Graham B, Ohmori K, Li Y, Huang H. Antagonistic regulation by the transcription factors C/EBPα and MITF specifies basophil and mast cell fates. Immunity, 2013, **39:**97-110.
6. Schmetzer O, Valentin P, Church MK, Maurer M, Siebenhaar F. Murine and human mast cell progenitors. Eur J Pharmacol, 2016, **778:**2-10.
7. Chen CC, Grimbaldeston MA, Tsai M, Weissman IL, Galli SJ. Identification of mast cell progenitors in adult mice. Proc Natl Acad Sci U S A, 2005, **102:**11408-11413.
8. Franco CB, Chen CC, Drukker M, Weissman IL, Galli SJ. Distinguishing mast cell and granulocyte differentiation at the single-cell level. Cell Stem Cell, 2010, **6:**361-368.
9. Mukai K, BenBarak MJ, Tachibana M, Nishida K, Karasuyama H, Taniuchi I, Galli SJ. Critical role of P1-Runx1 in mouse basophil development. Blood, 2012, **120:**76-85.
10. Arock M. Mast cell differentiation: still open questions? Blood, 2016, **127:**373-374.
11. Dahlin JS, Malinovschi A, Ohrvik H, Sandelin M. Lin- $CD34^{hi}$ $CD117^{int/hi}$ $Fc\varepsilon RI^{+}$ cells in human blood constitute a rare population of mast cell progenitors. 2016, **127:**383-391.
12. Iwasaki H, Mizuno S, Arinobu Y, Ozawa H, Mori Y, Shigematsu H, Takatsu K, Tenen DG, Akashi K. The order of expression of transcription factors directs hierarchical specification of hematopoietic lineages. Genes Dev, 2006, **20:**3010-3021.
13. Dahlin JS, Hallgren J. Mast cell progenitors: origin, development and migration to tissues. Mol Immunol, 2015, **63:**9-17.
14. Wedemeyer J, Galli SJ. Mast cells and basophils in acquired immunity. Br Med Bull, 2000, **56:**936-955.
15. Galli SJ, Kalesnikoff J, Grimbaldeston MA, Piliponsky AM, Williams CM, Tsai M. Mast cells as "tunable" effector and immunoregulatory cells: recent advances. Annu Rev Immunol, 2005, **23:**749-786.
16. Bienenstock J, Befus AD, Pearce F, Denburg J, Goodacre R. Mast cell heterogeneity: derivation and function, with emphasis on the intestine. J Allergy Clin Immunol, 1982, **70:**407-412.
17. Krishnaswamy G, Ajitawi O, Chi DS. The human mast cell: an overview. Methods Mol Biol, 2006, **315:**13-34.
18. Arock M, Le Nours A, Malbec O, Daeron M. Ex vivo and in vitro primary mast cells. Methods Mol Biol, 2008, **415:**241-254.
19. Salari H, Takei F, Miller R, Chan-Yeung M. Novel technique for isolation of human lung mast cells. J Immunol Methods, 1987, **100:**91-97.
20. Hachisuka H, Kusuhara M, Higuchi M, Okubo K, Sasai Y. Purification of rat cutaneous mast cells with Percoll density centrifugation. Arch Dermatol Res, 1988, **280:**358-362.

21. He D, Esquenazi-Behar S, Soter NA, Lim HW. Mast-cell heterogeneity: functional comparison of purified mouse cutaneous and peritoneal mast cells. J Invest Dermatol, 1990, **95:**178-185.
22. Blank U, Ra C, Miller L, White K, Metzger H, Kinet JP. Complete structure and expression in transfected cells of high affinity IgE receptor. Nature, 1989, **337:**187-189.
23. Turner H, Kinet JP. Signalling through the high-affinity IgE receptor FcεRI. Nature, 1999, **402:**B24-30.
24. Hill PB, MacDonald AJ, Thornton EM, Newlands GF, Galli SJ, Miller HR. Stem cell factor enhances immunoglobulin E-dependent mediator release from cultured rat bone marrow-derived mast cells: activation of previously unresponsive cells demonstrated by a novel ELISPOT assay. Immunology, 1996, **87:**326-333.
25. Hundley TR, Gilfillan AM, Tkaczyk C, Andrade MV, Metcalfe DD, Beaven MA. Kit and FcεRI mediate unique and convergent signals for release of inflammatory mediators from human mast cells. Blood, 2004, **104:**2410-2417.
26. Duttlinger R, Manova K, Chu TY, Gyssler C, Zelenetz AD, Bachvarova RF, Besmer P. W-sash affects positive and negative elements controlling c-kit expression: ectopic c-kit expression at sites of kit-ligand expression affects melanogenesis. Development, 1993, **118:**705-717.
27. Lantz CS, Boesiger J, Song CH, Mach N, Kobayashi T, Mulligan RC, Nawa Y, Dranoff G, Galli SJ. Role for interleukin-3 in mast-cell and basophil development and in immunity to parasites. Nature, 1998, **392:**90-93.
28. Harada M, Sumichika H, Hamano S, Ito O, Tamada K, Takenoyama M, Kimura G, Nomoto K. IL-3 derived from CD4+ T cells is essential for the in vitro expansion of mast cells from the normal adult mouse spleen. Clin Exp Immunol, 1996, **106:**149-155.
29. Booth RJ, Prestidge RL, Watson JD. Constitutive production by the WEHI-3 cell line of B cell growth and differentiation factor that co-purifies with interleukin 1. J Immunol, 1983, **131:**1289-1293.
30. Broudy VC. Stem cell factor and hematopoiesis. Blood, 1997, **90:**1345-1364.
31. Voehringer D. Protective and pathological roles of mast cells and basophils. Nat Rev Immunol, 2013, **13:**362-375.
32. Metz M, Maurer M. Mast cells-key effector cells in immune responses. Trends Immunol, 2007, **28:**234-241.
33. Galli SJ, Grimbaldeston M, Tsai M. Immunomodulatory mast cells: negative, as well as positive, regulators of immunity. Nat Rev Immunol, 2008, **8:**478-486.
34. Moon TC, Befus AD, Kulka M. Mast cell mediators: their differential release and the secretory pathways involved. Front Immunol, 2014, **5:**569.
35. Peavy RD, Metcalfe DD. Understanding the mechanisms of anaphylaxis. Curr Opin Allergy Clin Immunol, 2008, **8:**310-315.
36. Abraham SN, St John AL. Mast cell-orchestrated immunity to pathogens. Nat Rev Immunol, 2010, **10:**440-452.
37. Amin K. The role of mast cells in allergic inflammation. Respir Med, 2012, **106:**9-14.
38. Galli SJ, Nakae S, Tsai M. Mast cells in the development of adaptive immune responses. Nat Immunol, 2005, **6:**135-142.
39. Halova I, Draberova L, Draber P. Mast cell chemotaxis - chemoattractants and signaling pathways. Front Immunol, 2012, **3:**119.
40. Kinet JP. The high-affinity IgE receptor (FcεRI): from physiology to pathology. Annu Rev Immunol, 1999, **17:**931-972.
41. Metzger H. The receptor with high affinity for IgE. Immunol Rev, 1992, **125:**37-48.
42. Rivera J, Cordero JR, Furumoto Y, Luciano-Montalvo C, Gonzalez-Espinosa C, Kovarova M, Odom S, Parravicini V. Macromolecular protein signaling complexes and

mast cell responses: a view of the organization of IgE-dependent mast cell signaling. Mol Immunol, 2002, **38:**1253-1258.
43. Ronnstrand L. Signal transduction via the stem cell factor receptor/c-Kit. Cell Mol Life Sci, 2004, **61:**2535-2548.
44. Roskoski R, Jr. Structure and regulation of Kit protein-tyrosine kinase-the stem cell factor receptor. Biochem Biophys Res Commun, 2005, **338:**1307-1315.
45. Gilfillan AM, Rivera J. The tyrosine kinase network regulating mast cell activation. Immunol Rev, 2009, **228:**149-169.
46. Metcalfe DD, Mekori JA, Rottem M. Mast cell ontogeny and apoptosis. Exp Dermatol, 1995, **4:**227-230.
47. Tono T, Tsujimura T, Koshimizu U, Kasugai T, Adachi S, Isozaki K, Nishikawa S, Morimoto M, Nishimune Y, Nomura S, et al. c-kit gene was not transcribed in cultured mast cells of mast cell-deficient W^{sh}/W^{sh} mice that have a normal number of erythrocytes and a normal c-kit coding region. Blood, 1992, **80:**1448-1453.
48. Kitamura Y, Go S, Hatanaka K. Decrease of mast cells in W/Wv mice and their increase by bone marrow transplantation. Blood, 1978, **52:**447-452.
49. Lindquist JA, Simeoni L, Schraven B. Transmembrane adapters: attractants for cytoplasmic effectors. Immunol Rev, 2003, **191:**165-182.
50. Draber P, Halova I, Levi-Schaffer F, Draberova L. Transmembrane adaptor proteins in the high-affinity IgE receptor signaling. Front Immunol, 2011, **2:**95.
51. Horejsi V, Zhang W, Schraven B. Transmembrane adaptor proteins: organizers of immunoreceptor signalling. Nat Rev Immunol, 2004, **4:**603-616.
52. Gilfillan AM, Tkaczyk C. Integrated signalling pathways for mast-cell activation. Nat Rev Immunol, 2006, **6:**218-230.
53. Simeoni L, Lindquist JA, Smida M, Witte V, Arndt B, Schraven B. Control of lymphocyte development and activation by negative regulatory transmembrane adapter proteins. Immunol Rev, 2008, **224:**215-228.
54. Iwaki S, Spicka J, Tkaczyk C, Jensen BM, Furumoto Y, Charles N, Kovarova M, Rivera J, Horejsi V, Metcalfe DD, Gilfillan AM. Kit- and FcεRI-induced differential phosphorylation of the transmembrane adaptor molecule NTAL/LAB/LAT2 allows flexibility in its scaffolding function in mast cells. Cell Signal, 2008, **20:**195-205.
55. Brdička T, Pavlištová D, Leo A, Bruyns E, Kořínek V, Angelisová P, Scherer J, Shevchenko A, Hilgert I, Černý J, Drbal K, Kuramitsu Y, Kornacker B, Hořejší V, Schraven B. Phosphoprotein associated with glycosphingolipid-enriched microdomains (PAG), a novel ubiquitously expressed transmembrane adaptor protein, binds the protein tyrosine kinase Csk and is involved in regulation of T cell activation. J Exp Med, 2000, **191:**1591-1604.
56. Kawabuchi M, Satomi Y, Takao T, Shimonishi Y, Nada S, Nagai K, Tarakhovsky A, Okada M. Transmembrane phosphoprotein Cbp regulates the activities of Src-family tyrosine kinases. Nature, 2000, **404:**999-1003.
57. Hrdinka M, Horejsi V. PAG-a multipurpose transmembrane adaptor protein. Oncogene, 2014, **33:**4881-4892.
58. Smida M, Cammann C, Gurbiel S, Kerstin N, Lingel H, Lindquist S, Simeoni L, Brunner-Weinzierl MC, Suchanek M, Schraven B, Lindquist JA. PAG/Cbp suppression reveals a contribution of CTLA-4 to setting the activation threshold in T cells. Cell Commun Signal, 2013, **11:**28.
59. Davidson D, Zhong MC, Pandolfi PP, Bolland S, Xavier RJ, Seed B, Li X, Gu H, Veillette A. The Csk-Associated Adaptor PAG Inhibits Effector T Cell Activation in Cooperation with Phosphatase PTPN22 and Dok Adaptors. Cell Rep, 2016, **17:**2776-2788.

60. Cohen P. The role of protein phosphorylation in human health and disease. The Sir Hans Krebs Medal Lecture. Eur J Biochem, 2001, **268:**5001-5010.
61. Rivera J, Olivera A. Src family kinases and lipid mediators in control of allergic inflammation. Immunol Rev, 2007, **217:**255-268.
62. Hunter T. Tyrosine phosphorylation: thirty years and counting. Curr Opin Cell Biol, 2009, **21:**140-146.
63. Blume-Jensen P, Hunter T. Oncogenic kinase signalling. Nature, 2001, **411:**355-365.
64. Brown MT, Cooper JA. Regulation, substrates and functions of src. Biochim Biophys Acta, 1996, **1287:**121-149.
65. Thomas SM, Brugge JS. Cellular functions regulated by Src family kinases. Annu Rev Cell Dev Biol, 1997, **13:**513-609.
66. Okada M. Regulation of the Src family kinases by Csk. Int J Biol Sci, 2012, **8:**1385-1397.
67. Bolen JB, Brugge JS. Leukocyte protein tyrosine kinases: potential targets for drug discovery. Annu Rev Immunol, 1997, **15:**371-404.
68. Ingley E. Src family kinases: regulation of their activities, levels and identification of new pathways. Biochim Biophys Acta, 2008, **1784:**56-65.
69. Koegl M, Zlatkine P, Ley SC, Courtneidge SA, Magee AI. Palmitoylation of multiple Src-family kinases at a homologous N-terminal motif. Biochem J, 1994, **303 (Pt 3):**749-753.
70. Resh MD. Fatty acylation of proteins: new insights into membrane targeting of myristoylated and palmitoylated proteins. Biochim Biophys Acta, 1999, **1451:**1-16.
71. Sato I, Obata Y, Kasahara K, Nakayama Y, Fukumoto Y, Yamasaki T, Yokoyama KK, Saito T, Yamaguchi N. Differential trafficking of Src, Lyn, Yes and Fyn is specified by the state of palmitoylation in the SH4 domain. J Cell Sci, 2009, **122:**965-975.
72. Kasahara K, Nakayama Y, Kihara A, Matsuda D, Ikeda K, Kuga T, Fukumoto Y, Igarashi Y, Yamaguchi N. Rapid trafficking of c-Src, a non-palmitoylated Src-family kinase, between the plasma membrane and late endosomes/lysosomes. Exp Cell Res, 2007, **313:**2651-2666.
73. Oneyama C, Iino T, Saito K, Suzuki K, Ogawa A, Okada M. Transforming potential of Src family kinases is limited by the cholesterol-enriched membrane microdomain. Mol Cell Biol, 2009, **29:**6462-6472.
74. Sen B, Johnson FM. Regulation of SRC family kinases in human cancers. J Signal Transduct, 2011, **2011:**865819.
75. Cooper JA, Gould KL, Cartwright CA, Hunter T. Tyr527 is phosphorylated in pp60c-src: implications for regulation. Science, 1986, **231:**1431-1434.
76. Hubbard SR, Till JH. Protein tyrosine kinase structure and function. Annu Rev Biochem, 2000, **69:**373-398.
77. Takeya T, Hanafusa H. Structure and sequence of the cellular gene homologous to the RSV src gene and the mechanism for generating the transforming virus. Cell, 1983, **32:**881-890.
78. Okada M, Nakagawa H. Identification of a novel protein tyrosine kinase that phosphorylates pp60c-src and regulates its activity in neonatal rat brain. Biochem Biophys Res Commun, 1988, **154:**796-802.
79. Okada M, Nada S, Yamanashi Y, Yamamoto T, Nakagawa H. CSK: a protein-tyrosine kinase involved in regulation of src family kinases. J Biol Chem, 1991, **266:**24249-24252.
80. Nada S, Okada M, MacAuley A, Cooper JA, Nakagawa H. Cloning of a complementary DNA for a protein-tyrosine kinase that specifically phosphorylates a negative regulatory site of p60c-src. Nature, 1991, **351:**69-72.

81. Bergman M, Mustelin T, Oetken C, Partanen J, Flint NA, Amrein KE, Autero M, Burn P, Alitalo K. The human p50csk tyrosine kinase phosphorylates p56lck at Tyr-505 and down regulates its catalytic activity. Embo j, 1992, **11:**2919-2924.
82. Nada S, Yagi T, Takeda H, Tokunaga T, Nakagawa H, Ikawa Y, Okada M, Aizawa S. Constitutive activation of Src family kinases in mouse embryos that lack Csk. Cell, 1993, **73:**1125-1135.
83. Schmedt C, Saijo K, Niidome T, Kühn R, Aizawa S, Tarakhovsky A. Csk controls antigen receptor-mediated development and selection of T-lineage cells. Nature, 1998, **394:**901-904.
84. Yagi R, Waguri S, Sumikawa Y, Nada S, Oneyama C, Itami S, Schmedt C, Uchiyama Y, Okada M. C-terminal Src kinase controls development and maintenance of mouse squamous epithelia. Embo j, 2007, **26:**1234-1244.
85. Thomas RM, Schmedt C, Novelli M, Choi BK, Skok J, Tarakhovsky A, Roes J. C-terminal Src kinase controls acute inflammation and granulocyte adhesion. Immunity, 2004, **20:**181-191.
86. Honda Z, Suzuki T, Hirose N, Aihara M, Shimizu T, Nada S, Okada M, Ra C, Morita Y, Ito K. Roles of C-terminal Src kinase in the initiation and the termination of the high affinity IgE receptor-mediated signaling. J Biol Chem, 1997, **272:**25753-25760.
87. Oneyama C, Hikita T, Enya K, Dobenecker MW, Saito K, Nada S, Tarakhovsky A, Okada M. The lipid raft-anchored adaptor protein Cbp controls the oncogenic potential of c-Src. Mol Cell, 2008, **30:**426-436.
88. Pao LI, Badour K, Siminovitch KA, Neel BG. Nonreceptor protein-tyrosine phosphatases in immune cell signaling. Annu Rev Immunol, 2007, **25:**473-523.
89. Christophi GP, Panos M, Hudson CA, Christophi RL, Gruber RC, Mersich AT, Blystone SD, Jubelt B, Massa PT. Macrophages of multiple sclerosis patients display deficient SHP-1 expression and enhanced inflammatory phenotype. Lab Invest, 2009, **89:**742-759.
90. Krystal G. Lipid phosphatases in the immune system. Semin Immunol, 2000, **12:**397-403.
91. Tsui FW, Martin A, Wang J, Tsui HW. Investigations into the regulation and function of the SH2 domain-containing protein-tyrosine phosphatase, SHP-1. Immunol Res, 2006, **35:**127-136.
92. Tsui HW, Siminovitch KA, de Souza L, Tsui FW. Motheaten and viable motheaten mice have mutations in the haematopoietic cell phosphatase gene. Nat Genet, 1993, **4:**124-129.
93. Shultz LD, Schweitzer PA, Rajan TV, Yi T, Ihle JN, Matthews RJ, Thomas ML, Beier DR. Mutations at the murine motheaten locus are within the hematopoietic cell protein-tyrosine phosphatase (Hcph) gene. Cell, 1993, **73:**1445-1454.
94. Nakata K, Yoshimaru T, Suzuki Y, Inoue T, Ra C, Yakura H, Mizuno K. Positive and negative regulation of high affinity IgE receptor signaling by Src homology region 2 domain-containing phosphatase 1. J Immunol, 2008, **181:**5414-5424.
95. Zhu Z, Oh SY, Cho YS, Zhang L, Kim YK, Zheng T. Tyrosine phosphatase SHP-1 in allergic and anaphylactic inflammation. Immunol Res, 2010, **47:**3-13.
96. Zhou L, Oh SY, Zhou Y, Yuan B, Wu F, Oh MH, Wang Y, Takemoto C, Van Rooijen N, Zheng T, Zhu Z. SHP-1 regulation of mast cell function in allergic inflammation and anaphylaxis. PLoS One, 2013, **8:**e55763.
97. Lorenz U, Ravichandran KS, Burakoff SJ, Neel BG. Lack of SHPTP1 results in src-family kinase hyperactivation and thymocyte hyperresponsiveness. Proc Natl Acad Sci U S A, 1996, **93:**9624-9629.
98. Van Vactor D, O'Reilly AM, Neel BG. Genetic analysis of protein tyrosine phosphatases. Curr Opin Genet Dev, 1998, **8:**112-126.

99. Tonks NK, Neel BG. From form to function: signaling by protein tyrosine phosphatases. Cell, 1996, **87:**365-368.
100. Zhang J, Somani AK, Siminovitch KA. Roles of the SHP-1 tyrosine phosphatase in the negative regulation of cell signalling. Semin Immunol, 2000, **12:**361-378.
101. Tamir I, Dal Porto JM, Cambier JC. Cytoplasmic protein tyrosine phosphatases SHP-1 and SHP-2: regulators of B cell signal transduction. Curr Opin Immunol, 2000, **12:**307-315.
102. Xiao W, Ando T, Wang HY, Kawakami Y, Kawakami T. Lyn- and PLC-β3-dependent regulation of SHP-1 phosphorylation controls Stat5 activity and myelomonocytic leukemia-like disease. Blood, 2010, **116:**6003-6013.
103. Abu-Dayyeh I, Ralph B, Grayfer L, Belosevic M, Cousineau B, Olivier M. Identification of key cytosolic kinases containing evolutionarily conserved kinase tyrosine-based inhibitory motifs (KTIMs). Dev Comp Immunol, 2010, **34:**481-484.
104. Xiao W, Kashiwakura J, Hong H, Yasudo H, Ando T, Maeda-Yamamoto M, Wu D, Kawakami Y, Kawakami T. Phospholipase C-β3 regulates FcεRI-mediated mast cell activation by recruiting the protein phosphatase SHP-1. Immunity, 2011, **34:**893-904.
105. Rohrschneider LR, Fuller JF, Wolf I, Liu Y, Lucas DM. Structure, function, and biology of SHIP proteins. Genes Dev, 2000, **14:**505-520.
106. Heneberg P, Draber P. Nonreceptor protein tyrosine and lipid phosphatases in type I Fcε receptor-mediated activation of mast cells and basophils. Int Arch Allergy Immunol, 2002, **128:**253-263.
107. Pribluda VS, Pribluda C, Metzger H. Transphosphorylation as the mechanism by which the high-affinity receptor for IgE is phosphorylated upon aggregation. Proc Natl Acad Sci U S A, 1994, **91:**11246-11250.
108. Tolar P, Dráberová L, Tolarová H, Dráber P. Positive and negative regulation of Fcε receptor I-mediated signaling events by Lyn kinase C-terminal tyrosine phosphorylation. Eur J Immunol, 2004, **34:**1136-1145.
109. Tamir I, Cambier JC. Antigen receptor signaling: integration of protein tyrosine kinase functions. Oncogene, 1998, **17:**1353-1364.
110. Vonakis BM, Gibbons SP, Jr., Rotte MJ, Brothers EA, Kim SC, Chichester K, MacDonald SM. Regulation of rat basophilic leukemia-2H3 mast cell secretion by a constitutive Lyn kinase interaction with the high affinity IgE receptor (FcεRI). J Immunol, 2005, **175:**4543-4554.
111. Lin S, Cicala C, Scharenberg AM, Kinet JP. The FcεRIβ subunit functions as an amplifier of FcεRIγ-mediated cell activation signals. Cell, 1996, **85:**985-995.
112. Eiseman E, Bolen JB. Signal transduction by the cytoplasmic domains of FcεRI-γ and TCR-ζ in rat basophilic leukemia cells. J Biol Chem, 1992, **267:**21027-21032.
113. Bugajev V, Bambouskova M, Draberova L, Draber P. What precedes the initial tyrosine phosphorylation of the high affinity IgE receptor in antigen-activated mast cell? FEBS Lett, 2010, **584:**4949-4955.
114. Volná P, Lebduška P, Dráberová L, Šimová S, Heneberg P, Boubelík M, Bugajev V, Malissen B, Wilson BS, Hořejší V, Malissen M, Dráber P. Negative regulation of mast cell signaling and function by the adaptor LAB/NTAL. J Exp Med, 2004, **200:**1001-1013.
115. Zhu M, Liu Y, Koonpaew S, Granillo O, Zhang W. Positive and negative regulation of FcεRI-mediated signaling by the adaptor protein LAB/NTAL. J Exp Med, 2004, **200:**991-1000.
116. Kitaura J, Asai K, Maeda-Yamamoto M, Kawakami Y, Kikkawa U, Kawakami T. Akt-dependent cytokine production in mast cells. J Exp Med, 2000, **192:**729-740.

117. Pullen NA, Barnstein BO, Falanga YT, Wang Z, Suzuki R, Tamang TD, Khurana MC, Harry EA, Draber P, Bunting KD, Mizuno K, Wilson BS, Ryan JJ. Novel mechanism for FcεRI-mediated signal transducer and activator of transcription 5 (STAT5) tyrosine phosphorylation and the selective influence of STAT5B over mast cell cytokine production. J Biol Chem, 2012, **287:**2045-2054.
118. Galli SJ, Tsai M, Piliponsky AM. The development of allergic inflammation. Nature, 2008, **454:**445-454.
119. Draber P, Halova I, Polakovicova I, Kawakami T. Signal transduction and chemotaxis in mast cells. Eur J Pharmacol, 2016, **778:**11-23.
120. Weinblatt ME, Kavanaugh A, Genovese MC, Jones DA, Musser TK, Grossbard EB, Magilavy DB. Effects of fostamatinib (R788), an oral spleen tyrosine kinase inhibitor, on health-related quality of life in patients with active rheumatoid arthritis: analyses of patient-reported outcomes from a randomized, double-blind, placebo-controlled trial. J Rheumatol, 2013, **40:**369-378.
121. Blunt MD, Ward SG. Pharmacological targeting of phosphoinositide lipid kinases and phosphatases in the immune system: success, disappointment, and new opportunities. Front Immunol, 2012, **3:**226.
122. Lee KS, Lee HK, Hayflick JS, Lee YC, Puri KD. Inhibition of phosphoinositide 3-kinase δ attenuates allergic airway inflammation and hyperresponsiveness in murine asthma model. Faseb j, 2006, **20:**455-465.
123. Odom S, Gomez G, Kovarova M, Furumoto Y, Ryan JJ, Wright HV, Gonzalez-Espinosa C, Hibbs ML, Harder KW, Rivera J. Negative regulation of immunoglobulin E-dependent allergic responses by Lyn kinase. J Exp Med, 2004, **199:**1491-1502.
124. Itoh K, Sakakibara M, Yamasaki S, Takeuchi A, Arase H, Miyazaki M, Nakajima N, Okada M, Saito T. Cutting edge: negative regulation of immune synapse formation by anchoring lipid raft to cytoskeleton through Cbp-EBP50-ERM assembly. J Immunol, 2002, **168:**541-544.
125. Ohtake H, Ichikawa N, Okada M, Yamashita T. Cutting Edge: Transmembrane phosphoprotein Csk-binding protein/phosphoprotein associated with glycosphingolipid-enriched microdomains as a negative feedback regulator of mast cell signaling through the FcεRI. J Immunol, 2002, **168:**2087-2090.
126. Kalesnikoff J, Galli SJ. Antiinflammatory and immunosuppressive functions of mast cells. Methods Mol Biol, 2011, **677:**207-220.
127. Lagunoff D, Wan H. Temperature dependence of mast cell histamine secretion. J Cell Biol, 1974, **61:**809-811.
128. Holowka D, Wilkes M, Stefan C, Baird B. Roles for Ca^{2+} mobilization and its regulation in mast cell functions: recent progress. Biochem Soc Trans, 2016, **44:**505-509.
129. Yasuda K, Nagafuku M, Shima T, Okada M, Yagi T, Yamada T, Minaki Y, Kato A, Tani-Ichi S, Hamaoka T, Kosugi A. Cutting edge: Fyn is essential for tyrosine phosphorylation of Csk-binding protein/phosphoprotein associated with glycolipid-enriched microdomains in lipid rafts in resting T cells. J Immunol, 2002, **169:**2813-2817.
130. Plas DR, Thomas ML. Negative regulation of antigen receptor signaling in lymphocytes. J Mol Med (Berl), 1998, **76:**589-595.
131. Pullen NA, Falanga YT, Morales JK, Ryan JJ. The Fyn-STAT5 Pathway: A New Frontier in IgE- and IgG-Mediated Mast Cell Signaling. Front Immunol, 2012, **3:**117.
132. Barnstein BO, Li G, Wang Z, Kennedy S, Chalfant C, Nakajima H, Bunting KD, Ryan JJ. Stat5 expression is required for IgE-mediated mast cell function. J Immunol, 2006, **177:**3421-3426.
133. Barbu EA, Zhang J, Siraganian RP. The limited contribution of Fyn and Gab2 to the high affinity IgE receptor signaling in mast cells. J Biol Chem, 2010, **285:**15761-15768.

134. Manz BN, Tan YX, Courtney AH, Rutaganira F, Palmer E, Shokat KM, Weiss A. Small molecule inhibition of Csk alters affinity recognition by T cells. Elife, 2015, **4**.
135. Parravicini V, Gadina M, Kovarova M, Odom S, Gonzalez-Espinosa C, Furumoto Y, Saitoh S, Samelson LE, O'Shea JJ, Rivera J. Fyn kinase initiates complementary signals required for IgE-dependent mast cell degranulation. Nat Immunol, 2002, **3:**741-748.
136. Veillette A, Latour S, Davidson D. Negative regulation of immunoreceptor signaling. Annu Rev Immunol, 2002, **20:**669-707.
137. Chow LM, Fournel M, Davidson D, Veillette A. Negative regulation of T-cell receptor signalling by tyrosine protein kinase p50csk. Nature, 1993, **365:**156-160.
138. Hibbs ML, Harder KW, Armes J, Kountouri N, Quilici C, Casagranda F, Dunn AR, Tarlinton DM. Sustained activation of Lyn tyrosine kinase in vivo leads to autoimmunity. J Exp Med, 2002, **196:**1593-1604.
139. Hernandez-Hansen V, Mackay GA, Lowell CA, Wilson BS, Oliver JM. The Src kinase Lyn is a negative regulator of mast cell proliferation. J Leukoc Biol, 2004, **75:**143-151.
140. Iwabuchi K, Hatakeyama S, Takahashi A, Ato M, Okada M, Kajino Y, Kajino K, Ogasawara K, Takami K, Nakagawa H, Onoe K. Csk overexpression reduces several monokines and nitric oxide productions but enhances prostaglandin E_2 production in response to lipopolysaccharide in the macrophage cell line J774A.1. Eur J Immunol, 1997, **27:**742-749.
141. Aki D, Mashima R, Saeki K, Minoda Y, Yamauchi M, Yoshimura A. Modulation of TLR signalling by the C-terminal Src kinase (Csk) in macrophages. Genes Cells, 2005, **10:**357-368.
142. Xu S, Huo J, Tan JE, Lam KP. Cbp deficiency alters Csk localization in lipid rafts but does not affect T-cell development. Mol Cell Biol, 2005, **25:**8486-8495.
143. Dobenecker MW, Schmedt C, Okada M, Tarakhovsky A. The ubiquitously expressed Csk adaptor protein Cbp is dispensable for embryogenesis and T-cell development and function. Mol Cell Biol, 2005, **25:**10533-10542.
144. Oh H, Diamond SL. Ethanol enhances neutrophil membrane tether growth and slows rolling on P-selectin but reduces capture from flow and firm arrest on IL-1-treated endothelium. J Immunol, 2008, **181:**2472-2482.
145. Chin JH, Goldstein DB. Effects of low concentrations of ethanol on the fluidity of spin-labeled erythrocyte and brain membranes. Mol Pharmacol, 1977, **13:**435-441.
146. Daragan VA, Voloshin AM, Chochina SV, Khazanovich TN, Wood WG, Avdulov NA, Mayo KH. Specific binding of ethanol to cholesterol in organic solvents. Biophys J, 2000, **79:**406-415.
147. Setiawan I, Blanchard GJ. Ethanol-induced perturbations to planar lipid bilayer structures. J Phys Chem B, 2014, **118:**537-546.
148. Carreras-Sureda A, Cantero-Recasens G, Rubio-Moscardo F, Kiefer K, Peinelt C, Niemeyer BA, Valverde MA, Vicente R. ORMDL3 modulates store-operated calcium entry and lymphocyte activation. Hum Mol Genet, 2013, **22:**519-530.
149. Ha SG, Ge XN, Bahaie NS, Kang BN, Rao A, Rao SP, Sriramarao P. ORMDL3 promotes eosinophil trafficking and activation via regulation of integrins and CD48. Nat Commun, 2013, **4:**2479.
150. Marquardt DL, Walker LL. Dependence of mast cell IgE-mediated cytokine production on nuclear factor-κB activity. J Allergy Clin Immunol, 2000, **105:**500-505.
151. Benoist C, Mathis D. Mast cells in autoimmune disease. Nature, 2002, **420:**875-878.
152. Kuehn HS, Radinger M, Gilfillan AM. Measuring mast cell mediator release. Curr Protoc Immunol, 2010, **Chapter 7:**Unit7.38.
153. Barletta J, Bartolome A, Constantine NT. Immunomagnetic quantitative immuno-PCR for detection of less than one HIV-1 virion. J Virol Methods, 2009, **157:**122-132.

154. Sano T, Smith CL, Cantor CR. Immuno-PCR: very sensitive antigen detection by means of specific antibody-DNA conjugates. Science, 1992, **258:**120-122.
155. Niemeyer CM, Adler M, Wacker R. Immuno-PCR: high sensitivity detection of proteins by nucleic acid amplification. Trends Biotechnol, 2005, **23:**208-216.
156. Chen L, Wei H, Guo Y, Cui Z, Zhang Z, Zhang XE. Gold nanoparticle enhanced immuno-PCR for ultrasensitive detection of Hantaan virus nucleocapsid protein. J Immunol Methods, 2009, **346:**64-70.
157. Georganopoulou DG, Chang L, Nam JM, Thaxton CS, Mufson EJ, Klein WL, Mirkin CA. Nanoparticle-based detection in cerebral spinal fluid of a soluble pathogenic biomarker for Alzheimer's disease. Proc Natl Acad Sci U S A, 2005, **102:**2273-2276.
158. Wright HV, Bailey D, Kashyap M, Kepley CL, Drutskaya MS, Nedospasov SA, Ryan JJ. IL-3-mediated TNF production is necessary for mast cell development. J Immunol, 2006, **176:**2114-2121.